REMARKS

Claims 41-63 were pending in the present application. Claims 41-44, and 53-61 have been amended herein, claims 51-52 have been canceled herein, and new claims 64-71 have been added herein. Support for amended claim 41 can be found throughout the specification and original claims such as, for example, at page 4, lines 15-25 of the specification. Support for amended claim 42 can be found throughout the specification and original claims, such as for example, at page 9, lines 11-13 of the specification. Support for amended claims 43-44 can be found throughout the specification and original claims. Support for amended claim 53 can be found throughout the specification and original claims, such as for example, at page 7, lines 19-22 and page 13, lines 16-19 of the specification. Support for amended claim 54 can be found throughout the specification and original claims, such as for example, at page 14, lines 1-6 of the specification. Support for amended claims 55-56 can be found throughout the specification and original claims. Support for amended claim 57 can be found throughout the specification and original claims, such as for example, at page 39, lines 15-18 of the specification. Support for amended claims 58-61 can be found throughout the specification and original claims, such as for example, at page 38, lines 9-22 of the specification. Support for new claims 64-71 can be found throughout the specification and original claims. No new matter has been added. Upon entry of the present amendments, claims 41-50 and 53-71 will be pending.

I. The Claimed Invention is Novel

Claim 57 stands rejected under 35 U.S.C. § 102(b), as being anticipated by Ma et al. (*Synthetic Communications* (1997) 27(14): 2445-2453) or Montedison (GB 2,101,600) or Cass et al. (*J. Chem. Soc.* (1991) No. 11, 2683-2686) or Gourdie et al. (*J. Med. Chem.* (1990) 33(4): 1177-1186) or Flemming et al. (*Tetrahedron Letters* (1979) No. 34, 3205-3208) or Cai et al. (*J. Am. Chem. Soc.* (1993) 115(16): 7192-7198) or Barrett et al. (*J. Org. Chem.* (1986) 51(25): 4840-4856) or Bunce et al. (*J. Org. Chem.* (1993) 58(25): 7143-7148) or Lafon et al. (U.S. Patent No. 4,013,776) or Kalgutkar et al. (*J. Med. Chem.* (1998) 41(24): 4800-4818) or Cowart et al. (*J. Med. Chem.* (1998) 41(14): 2636-2642) or Danhardt et al. (*Die Pharmazie* (1997) 52(6): 428-436). The Action alleges that each of the cited references describe at least one compound

falling within the scope of claim 57 and Kalgutkar et al., Cowart et al., and Dannhardt et al. also indicate the relevant compounds therein have pharmaceutical use. Applicants respectfully request reconsideration in light of the amendments made herein.

Claim 57 has been amended to recite a method of inhibiting HDAC activity in an individual suffering from a disease or condition related to aberrant HDAC activity. The cited references do not report a method of inhibiting HDAC activity as claimed by Applicants. Accordingly, Applicants respectfully assert that the claimed invention is novel, and request that the claim rejection be withdrawn.

II. The Claimed Invention is Enabled

Claims 58-63 stand rejected under 35 U.S.C. § 112, first paragraph, for failing to meet the enablement requirement. The Action alleges that the specification does not reasonably provide enablement for the disease conditions recited in claims 58 and 59, because there is no evidence that histone deacetylase (HDAC) inhibitory activity extrapolates to the treatment of all of the recited diseases and/or conditions. The Action also alleges that the claimed invention is not enabled, because HDAC inhibitory activity is only described for two compounds. *See* Action at pages 4-5. Applicants respectfully disagree.

The claimed methods can be practiced without undue experimentation. Significantly, the Action acknowledges that: (1) the specification is enabling for inhibiting HDAC activity; and (2) ailments caused by the presence of HDAC should be treated by the inhibition of HDAC. *See* Action at page 5. Tables 1 and 2 on pages 67 and 68 (respectively) of the specification, demonstrate that compounds of the present invention possess HDAC inhibitory activity. In addition, Applicants have attached hereto, references which demonstrate a nexus between aberrant HDAC activity and the diseases and/or conditions recited in claims 58 to 63.

Moreover, Applicants have disclosed methods for preparing compounds of the instant application and assays for evaluating the HDAC inhibitory activity of the same. Armed with this disclosure, one skilled in the art would need only routine experimentation to confirm that the claimed compounds possess HDAC inhibitory activity. Even voluminous experimentation is not undue so long as it is of a routine nature. *See Ex parte Forman*, 230 U.S.P.Q. 546, 547 (Pat. Off.

Bd. App. 1986). Further, Applicants have enclosed herewith a reference demonstrating the HDAC inhibitory activity of several ***additional*** compounds which are within the scope of Applicants' invention.

In light of the foregoing discussion, one skilled in the art armed with Applicants' disclosure would be able to practice the claimed invention without undue experimentation. Accordingly, Applicants respectfully assert that the claimed invention meets the enablement requirement and request that the claim rejection be withdrawn.

III. The Claimed Invention is Not Indefinite

Claims 41-63 stand rejected under 35 U.S.C. § 112, second paragraph, as being indefinite for failing to particularly point out and distinctly claim the subject matter which Applicants regard as the invention. The rejection is based on several allegations, each of which is addressed individually below.

The Action alleges that claim 41 is indefinite because R_4 is not defined in the body of the claim. Applicants have amended claim 41 herein, and respectfully assert that amended claim 41 meets the requirements of 35 U.S.C. §112.

The Action also alleges that claim 56 is indefinite because it contains compounds that read on moieties not disclosed in the bodies of claims 41-44. Pending claim 56 is dependent upon claims 41-44, but does not read on moieties outside the scope of claims 41-44. Applicants believe that pending claim 55, which was also dependent on claims 41-44, is the claim to which the rejection is directed. Although Applicants believe that the rejection is improper, solely to expedite prosecution, claims 55 and 56 have been amended herein.

The Action next alleges that claims 51-55 are indefinite because they recite the limitation R_1 in line 1, without having antecedent basis. Applicants respectfully request reconsideration in light of the amendments made herein. Claims 51-52 have been canceled herein, rendering their rejection moot. Claims 53 and 54 have been amended herein and now recite compounds having structures which possess an R_1 substituent. In regards to claim 55, an R_1 limitation is not recited therein.

In light of the foregoing discussion and the amendments made herein, Applicants

respectfully assert that the claimed invention is not indefinite, and request that the claim rejection be withdrawn.

IV. Conclusion

Applicants respectfully submit that the claims are in condition for allowance. An early notice of the same is earnestly solicited. The Examiner is invited to contact Applicants' undersigned representative at (610) 640-7851 to resolve any remaining issues.

Respectfully submitted,

/Nikhil A. Heble, Reg.#61,347/
Nikhil A. Heble, Pharm.D

Date: **February 4, 2008**

Pepper Hamilton LLP
400 Berwyn Park
899 Cassatt Road
Berwyn, PA 19312-1183
Telephone: 610.640.7851
Facsimile: 215.827.5279

Induction of fetal hemoglobin expression by the histone deacetylase inhibitor apicidin

Olaf Witt, Sven Mönkemeyer, Gabi Rönndahl, Bernhard Erdlenbruch, Dirk Reinhardt, Katrin Kanbach, and Arnulf Pekrun

Pharmacologic stimulation of fetal hemoglobin (HbF) expression may be a promising approach for the treatment of β-thalassemia. In this study, we have investigated the HbF-inducing activity and molecular mechanisms of specific histone deacetylase (HDAC) inhibitors in human K562 erythroleukemia cells. Apicidin was the most potent agent compared with other HDAC inhibitors (trichostatin A, MS-275, HC-toxin, suberoylanilide hydroxamic acid [SAHA]) and previously tested compounds (butyrate, phenylbutyrate, isobutyramide, hydroxyurea, 5-aza-cytidine), leading to a 10-fold stimulation of HbF expression at nanomolar to micromolar concentrations. Hyperacetylation of histones correlated with the ability of HDAC inhibitors to stimulate HbF synthesis. Furthermore, analysis of different mitogen-activated protein (MAP) kinase signaling pathways revealed that p38 signaling was activated following apicidin treatment of cells and that inhibition of this pathway abolished the HbF-inducing effect of apicidin. Additionally, activation of the Aγ-globin promoter by apicidin could be inhibited by p38 inhibitor SB203580. In summary, the novel HDAC inhibitor apicidin was found to be a potent inducer of HbF synthesis in K562 cells. The present data outline the role of histone hyperacetylation and p38 MAP kinase signaling as molecular targets for pharmacologic stimulation of HbF production in erythroid cells. (Blood. 2003;101:2001-2007)

Introduction

Severe β-thalassemia (thalassemia major, Cooley anemia) is characterized by insufficient production of adult β-globin chains with subsequent excess of α-globin chains leading to ineffective erythropoiesis, intramedullar degradation of erythroid cells, and lifelong transfusion requirement of affected patients.[1] One molecular treatment strategy of this disease comprises the reactivation of fetal γ-globin production to substitute for the lack of β-globin chains and to correct the imbalance of α/non-α chains.[2] Several pharmacologic agents such as 5-azacytidine, hydroxyurea, erythropoietin, butyrate derivatives and combinations of these drugs have been shown to possess γ-globin chain–inducing activity.[3]

Among these compounds, butyrate analogues have been studied over many years now, and clinical benefit in some patients with β-thalassemia has been reported.[4-8] However, several pharmacologic problems are associated with these substances. First, many analogues have a very short half-life, requiring continuous intravenous application. Second, butyrate derivatives need a plasma concentration in the millimolar range to be effective, requiring large amounts of drugs to be applied. Third, induction of γ-globin chain is relatively weak, which might account for the inconsistent clinical effects observed. Fourth, many derivatives have an offensive odor, making these compounds less suitable for a long-term patient compliance. Therefore, identification of new agents that might be able to stimulate γ-globin chain via similar molecular mechanisms as butyrates but are more efficient at lower concentrations is warranted. A reasonable approach would be to investigate compounds that mimic the molecular effects of butyrate on erythroid cells.

Butyrate has been found to possess inhibitory activity on histone deacetylases, leading to hyperacetylation of ε-amino groups of lysine residues in histones.[9-11] This in turn causes a decreased association of basic core histone proteins with the DNA, rendering certain genes more accessible to the transcriptional machinery. In fact, trichostatin A, a specific histone deacetylase (HDAC) inhibitor was found to possess some fetal hemoglobulin (HbF)–inducing activity in human and mouse erythroleukemia cells,[12,13] suggesting that the histone deacetylase–inhibiting properties of butyrate contribute to its mode of action.

In this report, we have investigated several specific HDAC inhibitors with respect to their HbF-inducing activity in K562 cells. Apicidin was by far the most efficient HbF-inducing agent at nanomolar to micromolar concentrations. Our data further demonstrate that, in addition to HDAC inhibition, p38 mitogen-activated protein (MAP) kinase signaling appears to be involved in apicidin-mediated stimulation of HbF synthesis.

Materials and methods

Cell culture

The human leukemia cell line K562 was obtained from American Type Culture Collection (ATCC), Philadelphia, PA (CCL-243). Cells were cultured in RPMI containing 10% fetal calf serum with addition of penicillin/streptomycin. For experiments, cells were seeded at a density of 4×10^5 cells/4 mL in 35-mm dishes and cultured for 4 days in the presence or absence of the inducing/inhibiting agents as indicated. Viable cell counts

From the Laboratory for Hematological and Cancer Research, Children's Hospital, University of Goettingen, Goettingen, Germany.

Submitted September 8, 2002; accepted October 1, 2002. Prepublished online as *Blood* First Edition Paper, October 17, 2002; DOI 10.1182/blood-2002-08-2617.

Supported by a grant from the Deutsche Forschungsgemeinschaft (Wi 1461/3) and by the B. Braun-Stiftung, Melsungen.

Reprints: Olaf Witt, Laboratory for Hematological and Cancer Research, Children's Hospital, University of Göttingen, Robert-Koch-Str. 40; D-37075 Göttingen, Germany; e-mail: owitt@gwdg.de.

The publication costs of this article were defrayed in part by page charge payment. Therefore, and solely to indicate this fact, this article is hereby marked "advertisement" in accordance with 18 U.S.C. section 1734.

were determined by using trypan-blue dye exclusion test. For measurement of fetal hemoglobin and total hemoglobin, cells were centrifuged and washed with phosphate-buffered saline (PBS), and the cell pellet was resuspended in lysis buffer (100 mM potassium phosphate, pH 7.8, 0.2% Triton X-100) and incubated 10 minutes at room temperature. After pelleting cellular debris, the supernatant was collected and stored at −20°C until further use. For MAP kinase immunoblot analysis, cell pellets were directly lysed in sodium dodecyl sulfate (SDS) sample buffer (62.5 mM Tris [tris(hydroxymethyl)aminomethane]–HCl, pH 6.8, 2% SDS, 10% glycerol, 50 mM DTT [dithiothreitol], 0.1% bromophenol blue), incubated for 5 minutes at 95°C, cooled on ice for 5 minutes, and stored at −20°C until further use.

Reporter gene experiments

A 1436-bp fragment of the human Aγ-globin promoter (+64 to −1372 relative to the start site of transcription) was amplified from human genomic DNA using standard polymerase chain reaction (PCR) methods. The promoter fragment was cloned into the *Nhe*I/*Xho*I site of the reporter gene plasmid pGL3 basic (Promega, Madison, WI). The correct sequence of the construct was verified by automated DNA sequencing. Transient transfection of K562 cells was done by lipofection using 3 μL lipofectamine 2000 (Gibco-Life Technologies, Karlsruhe, Germany) per microgram DNA. A stock suspension of 6×10^6 K562 cells/6 mL was transfected with 12 μg DNA according to the manufacturer's protocol. After 24 hours of transfection, the transfected stock suspension was divided into 500-μL aliquots, diluted 1:4 with RPMI medium containing 10% fetal calf serum (FCS), and cultured in the presence or absence of 0.5 μM apicidin for the various times indicated. Apicidin-treated and untreated control cells were harvested in parallel at the different time points indicated; luciferase activity was determined by the luciferase assay kit (Promega) as described previously[14] and normalized by protein concentration of lysates. Normalized luciferase activity from apicidin-treated cells was corrected by the activity of untreated control cells harvested at the same time points to take into account basal, unstimulated reporter gene transcription. Because transfection was carried out in a stock suspension of cells before splitting into aliquots, there was no need to correct for different transfection efficacies by cotransfection of a constitutively expressed plasmid. To rule out direct activation of the luciferase gene or enzyme by apicidin, we performed control experiments by transfecting cells with the promoterless pGL3basic luciferase plasmid. Apicidin-treated cells did not show significant increase of luciferase activity compared with untreated control cells exhibiting a basal luciferase activity. Furthermore, direct incubation of luciferase activity containing cell lysates with apicidin did not stimulate enzyme activity.

Determination of total hemoglobin and HbF

Hemoglobin concentration was determined by using the plasma hemoglobin kit from Sigma (St Louis, MO) according to the manufacturer's instructions. This assay is based on the catalytic action of any hemoglobin on the oxidation of benzidine by hydrogen peroxide. After measurement of protein concentration of the lysate by the Coomassie method, nanogram hemoglobin per microgram total cellular protein was calculated.

Concentration of fetal hemoglobin was measured by enzyme-linked immunosorbent assay (ELISA) based on a 2-antibody sandwich principle as follows: microtiter plates were coated at 37°C for 1 hour with 100 μL sheep antihemoglobin F antibody (1 mg/mL; Bethyl Laboratories, Montgomery, TX) diluted 1:1000 in 100 mM Na_2CO_3/$NaHCO_3$, pH 9.6. After washing 4 times with Tris-buffered saline containing 0.02% (vol/vol) Tween-20 (TBS-T), unspecific binding sites were blocked with 200 μL 40 mM Tris/HCl, pH 7.6, 137 mM NaCl, 0.02% (vol/vol) Tween-20, 3% (wt/vol) bovine serum albumin at 4°C for 12 hours. After washing 4 times with TBS-T, 100 μL K562 cell lysate, diluted 1:10.000 with lysate buffer (40 mM Tris/HCl, pH 7.6, 137 mM NaCl, 0.02% [vol/vol] Tween-20, 0.5% [wt/vol] bovine serum albumin) was applied to each well and incubated at room temperature for 1 hour. After washing 4 times with TBS-T, 100 μL mouse-antihuman hemoglobin γ-chain antibody (Accurate Chemical, New York) diluted 1:10 000 with lysate buffer was added at room temperature for 1 hour. After washing 4 times with TBS-T, wells were incubated with 100 μL peroxidase-linked sheep-antimouse immunoglobulin (Amersham-Pharmacia, Piscataway, NJ) and diluted 1:1000 with lysate buffer at room temperature for 1 hour. After washing 4 times with TBS-T, bound antibody was detected by addition of 100 μL substrate solution (BM Blue POD [peroxidase] substrate; Boehringer Mannheim, Mannheim, Germany). Substrate reaction was stopped by addition of 25 μL 1 M H_2SO_4, and color reaction was determined at 450 nm (690 nm as reference) in an ELISA reader. As HbF standards, we used erythrocyte lysates obtained from a premature newborn shown to consist of pure HbF by cellulose acetate electrophoresis. The ELISA was linear at HbF concentrations ranging from 125 pg/mL to 2.5 ng/mL and was about 1000-fold more sensitive for detection of HbF than of adult hemoglobin (HbA).

Quantitative RT-PCR

Quantification of mRNA expression was done by real-time reverse transcription (RT)–PCR with Sybr Green using an ABI Prism 7700 thermal cycler (Perkin-Elmer Applied Biosystems, Foster City, CA). Total RNA was prepared from 10^6 cells with the RNeasy-kit from Quiagen (Chatsworth, CA) according to the manufacturer's instructions. For reverse transcription (RT), 1 μg total RNA was randomly primed for 10 minutes at 60°C and then subjected to reverse transcription for 1 hour at 37°C by using Moloney murine leukemia virus (MMLV)–RT from Invitrogen (Karlsruhe, Germany). For PCR: cDNA aliquots were quantified for globin gene expression by using the threshold cycle (Ct) method normalized for the house keeping gene β-actin. The following exon-spanning primer sequences were used (5′-3′ orientation): β-actin (cDNA amplicon length 151 bp), GCATCCCCCAAAGTTCACAA (forward) and AGGACTGGGCCATTCTCCTT (reverse); α-globin (cDNA amplicon length 372 bp), GACAAGACCAACGTCAAGGCCGCC (forward) and CAGGAACTTGTCCAGGGAGGC (reverse); γ-globin (cDNA amplicon length 489 bp), ACTCGCTTCTGGAACGTCTGA (forward) and GTATCTGGAGGACAGGGCACT (reverse). PCR was performed in triplicates using the qPCR Mastermix for Sybr Green I kit from Eurogentic (Seraing, Belgium) with the following protocol: after initial denaturing of the cDNA (10 minutes at 95°C), a 2-step PCR was performed (15 seconds at 95°C, 1 minute at 60°C, 40 cycles). Dilution experiments were performed to ensure similar efficiency of the PCRs, and standard curves were calculated referring the Ct (the PCR cycle at which a specific fluorescence becomes detectable) to the log of each cDNA dilution step. Specific amplification was verified by generation of a melting curve as well as agarose gel electrophoresis. Threshold cycle (Ct) values obtained for γ- and α-globin were normalized by corresponding Ct values of β-actin. Results from apicidin-treated cells were expressed relative to untreated control cells.

Materials

The following HDAC inhibitors were used: TSA (trichostatin A; Calbiochem, San Diego, CA), SAHA (suberoylanilide hydroxamic acid; Calbiochem), MS-275 (N-(2-aminophenyl)-4-[pyridine-3-ylmethoxycarbonyl)aminomethyl]benzamide; Calbiochem), HC-toxin (cyclo-D-Pro-L-Ala-D-L-2-amino-8-oxo-9, 10-epoxydecanoic acid; Sigma), apicidin (cyclo-[L-(2-amino-8-oxodecanoyl)-L-(N-methoxytryptophan)-L-isoleucyl-D-pipecolinyl); Calbiochem). The substances were dissolved in dimethyl sulfoxide (DMSO) or ethanol as recommended by the supplier and added to the culture medium to give the final concentrations as indicated. The final concentration of DMSO and ethanol in the culture medium was kept below 0.1% (vol/vol). At this concentration, the solvents did not influence hemoglobin synthesis of K562 cells. Furthermore, the respective volume of solvent was used in all control experiments. Sodium butyrate, isobutyramide, sodium valproate, hemin, hydroxyurea, 5-aza-cytidine, and sodium phenylacetate were purchased from Sigma. Sheep antihemoglobin F antibody was purchased from Bethyl Laboratories, and mouse antihuman-hemoglobin-γ chain antibody was from Accurate Chemical. The following antibodies were obtained from Calbiochem: anti-ERK1/2 (extracellular signal-related kinase 1/2) phosphorylated, anti-Jun N-terminal kinase (JNK)1/2 phosphorylated, and anti-p38 total. Antibodies obtained from Sigma were anti-p38 phosphorylated, anti-ERK1/2 total, and JNK1/2 total. The p38-specific inhibitor SB203580 was from Calbiochem, and the ERK

pathway inhibitor UO126 was from Promega. Antiacetyl H4 histone antibodies were from Upstate Biotechnology (Lake Placid, NY).

Immunoblot analysis

Detection of phosphorylated MAP kinase proteins. Cell lysates were subjected to SDS-polyacrylamide gel electrophoresis (PAGE) using 10% polyacrylamide gels and transferred to polyvinylidene fluoride (PVDF) membranes (Millipore, Bedford, MA) by using a semidry electroblot chamber. Transfer of proteins was assessed by ponceau-red staining. Membranes were blocked in tris-buffered saline, pH 7.4, containing 0.1% Tween-20 and 5% bovine serum albumin for 1 hour at room temperature. Incubations with primary antibodies were carried out at 4°C overnight by using antibody dilutions as recommended by the manufacturer in tris-buffered saline, pH 7.4, 0.1% Tween-20. Following 1 hour of incubation with goat-antirabbit peroxidase-conjugated antibody (Promega) at room temperature, proteins were detected by the electrogenerated chemiluminescence (ECL) method (Amersham-Pharmacia) according to the manufacturer's instructions. Blots were stripped at 50°C for 30 minutes in 100 mM 2-mercaptoethanol, 2% SDS, 62.5 mM Tris-HCl, pH 6.7, and reprobed as indicated.

Detection of acetylated H4 histone proteins. Histones were purified from nuclear proteins by acid extraction as described.[15] Briefly, 2×10^6 K562 cells were collected by centrifugation, washed with phosphate-buffered saline, and resuspended in 1 mL ice-cold lysis buffer (10 mM Tris/HCl, pH 6.5, 50 mM sodium bisulfite, 1% [vol/vol] Triton X-100, 10 mM $MgCl_2$, 8.6% sucrose). Cells were disrupted by using a dounce homogenizer, and nuclei were pelleted by centrifugation for 10 minutes at 1000*g*. Pellets were washed 3 times with lysis buffer and once with 10 mM Tris/HCl, pH 7.4, 13 mM EDTA (ethylenediaminetetraacetic acid). Pellets were then dissolved in 100 μL ice-cold water by vortexing. Acid extraction of nuclear histone proteins was carried out by adding 7 μL 6 N H_2SO_4 to give a final concentration of 0.4 N H_2SO_4 and incubated at 4°C for at least 1 hour. After pelleting acid-insoluble proteins (5 minutes full speed, microfuge), supernatants were collected and 1 mL ice-cold acetone was added, and acid-soluble proteins were precipitated at −20°C overnight. After pelleting for 5 minutes at full speed in a microfuge, proteins were air dried for 5 to 10 minutes and dissolved in 50 μL water. For detection of acetylated histones, acid-extracted nuclear proteins were separated by 15% SDS-polyacrylamide gel electrophoresis and transferred to a nitrocellulose membrane by electroblotting. The blotted membrane was blocked with freshly prepared TBS containing 3% nonfat dry milk (TBS-milk) for 1 hour at room temperature. The nitrocellulose membrane was incubated with 1:2000 dilution of antiacetyl histone H4, chromatin immunoprecipitation (ChIP) grade (Upstate Biotechnology) in TBS-milk, overnight at 4°C. The membrane was washed 3 times with water and incubated with donkey antirabbit immunoglobulin G (IgG) 1:10 000 in TBS-milk for 1.5 hours at room temperature. Blots were washed 3 times with water and once with TBS-0.05% Tween 20 for 5 minutes. After rinsing the membrane with 4 changes of water, detection of bound antibodies was carried out by using the ECL detection Kit (Amersham-Pharmacia) according to the manufacturer's instructions.

Results

Stimulation of fetal hemoglobin production by HDAC inhibitors

We have investigated the HbF-stimulating potential of the HDAC inhibitors trichostatin A, SAHA, HC-toxin, MS-275, and apicidin in human K562 erythroleukemia cells. These cells are widely used as an in vitro model system for the investigation of compounds with HbF-inducing activity. Cells were cultured with increasing concentrations of the respective HDAC inhibitor for 4 days. HbF concentrations in total cellular extracts were determined by ELISA as described. Figure 1 shows that the HbF-inducing potential of the HDAC inhibitors varied significantly. Whereas trichostatin A, SAHA, and HC-toxin showed relatively weak stimulation, apicidin increased HbF synthesis up to 10-fold compared with untreated control cells at a concentration of 0.1 to 1 μM (Figure 1, black bars). At the concentrations effective in stimulating HbF synthesis, inhibition of cell proliferation also varied significantly (Figure 1, white bars). Apicidin showed relative low cytotoxicity in this regard.

At the cellular level, apicidin increased the number of benzidine-positive (ie, hemoglobin-containing) cells from 3% up to 70% after 4 days of treatment (Figure 2). Butyrate, a compound with well-documented hemoglobin-inducing activity in K562 cells, leads to detectable hemoglobin in 20% of cells in the same time. After removal of the compounds, apicidin-treated K562 cells remained benzidine positive for at least another 8 days, whereas benzidine-positivity reverted back to untreated control levels in butyrate-induced cells. This finding suggests that apicidin, in contrast to butyrate, is an irreversible inhibitor of HDAC in vivo, as has been found in HeLa cells.[16] Alternatively, the compound may persist in cells much longer than butyrate, resulting in continuous blockage of HDAC activity.

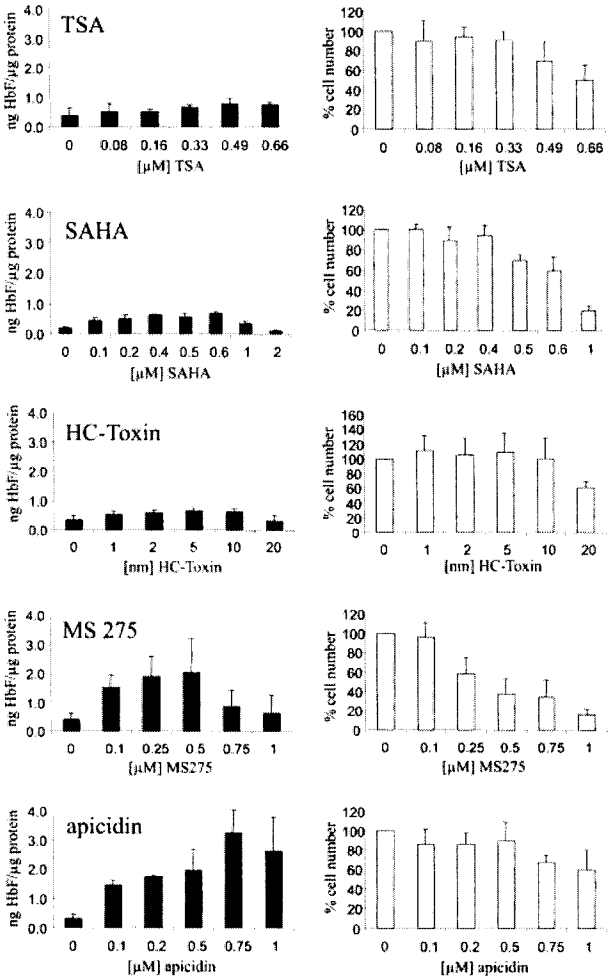

Figure 1. Induction of HbF synthesis in K562 cells by HDAC inhibitors. Cells were treated with increasing concentrations of the HDAC inhibitors TSA, SAHA, HC-toxin, MS-275, apicidin, or solvent only (0 value) for 4 days. HbF was determined from total cellular extracts by ELISA, normalized by total protein concentrations of extracts, and expressed as nanogram HbF per microgram protein (black bars). Cytotoxicity was assessed by counting cell numbers (white bars). Cell numbers were expressed relative to untreated cells (100%). Each experiment was performed at least 4 times, and standard errors were calculated as indicated.

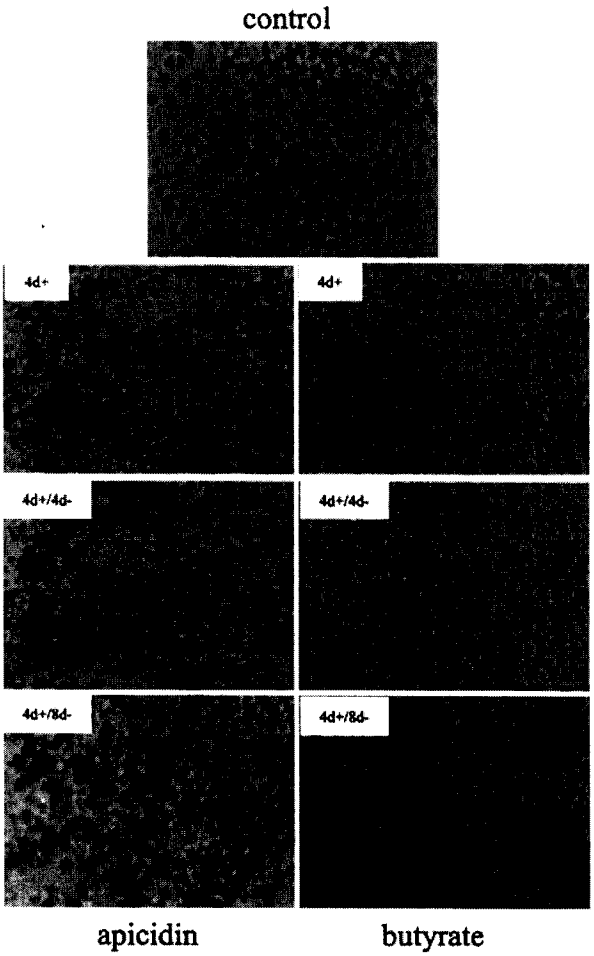

Figure 2. Benzidine staining of K562 cells treated with butyrate and apicidin. Cells were cultured in the absence (control) or presence of 0.5 μM apicidin (left panels) or 0.6 mM butyrate (right panels) for 4 days (4 d+). Thereafter, the compounds were removed from medium and cultured for another 4 days (4 d+/4 d−) or 8 days (4 d+/8 d−), respectively. After harvesting, intracellular hemoglobin was detected by benzidine staining, and cell smears were subjected to microscopy using × 400 magnification.

Comparison of the HDAC inhibitors (Figure 3A, black bars) with previously tested agents (Figure 3A, gray bars) at concentrations with maximum HbF-inducing activity revealed that apicidin was much more effective in stimulating HbF-production than butyrate, hydroxyurea, 5-azacytidine, phenylacetate, isobutyramide, and valproic acid. At the concentrations used, the inhibitory action on cell proliferation varied among the different compounds tested (Figure 3B). Again, apicidin revealed relatively low cytotoxicity at a concentration with maximum HbF-inducing activity. To investigate the specificity of HDAC inhibitors on fetal hemoglobin stimulation, we determined the HbF/total hemoglobin ratio (Figure 3C). All HDAC inhibitors investigated increased the proportion of HbF relative to total hemoglobin in K562 cells. Apicidin caused a 3-fold increase of the HbF/Hb ratio compared with untreated control cells.

Because the HbF-inducing activity of apicidin is expected to be related to increased transcription of the γ-globin genes, we measured γ-globin mRNA levels by quantitative real-time RT-PCR. As shown in Figure 3D, apicidin induced a 16-fold increase of γ-globin mRNA expression, but only a 2- to 3-fold increase of α-globin mRNA expression compared with untreated control cells. Similar results were obtained for butyrate (not shown). Thus, apicidin appears to exhibit relative specificity for γ-globin mRNA expression as the protein data suggested (Figure 3C).

Induction of histone hyperacetylation correlates with stimulation of HbF synthesis

The difference of the HbF-stimulating potential of the HDAC inhibitors tested might be due to their different ability to induce hyperacetylation of histones in K562 cells. To address this question, we have treated cells with a weak (TSA), a medium (MS-275), and a strong HbF inducer (apicidin), respectively, and compared the degree of histone H4 hyperacetylation by Western blot analysis using antiacetyl histone H4 antibodies (Figure 4). The immunoblot indicates that the degree of H4 acetylation correlated well with the potential of the compounds to stimulate HbF synthesis, ie, TSA less than MS-275 less than apicidin.

Apicidin modulates MAP kinase signal transduction pathways

We have previously reported that inhibition of ERK and activation of p38 kinase of the MAP kinase signal transduction system are

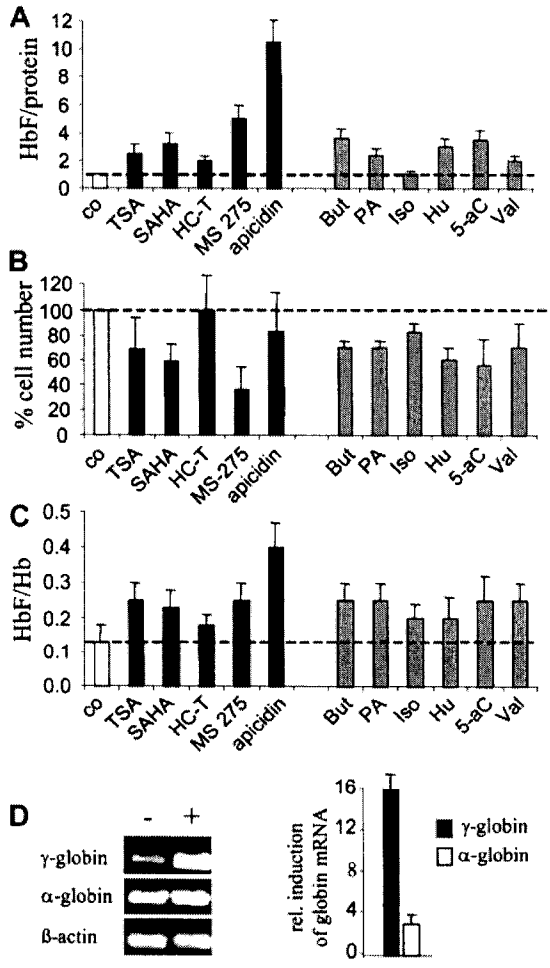

Figure 3. Comparison of various HbF-inducing compounds on HbF synthesis and globin mRNA expression in K562 cells. Cells were treated with HDAC inhibitors (black bars) and different HbF-inducing compounds (gray bars) by using concentrations with maximum HbF-inducing activity or solvent only (white bars) for 4 days. HbF per total protein (A) and cell numbers (B) were expressed relative to untreated control cells. (C) HbF per total Hb. Each experiment was performed 4 times, and standard errors were calculated as indicated. Co indicates untreated control cells; But, 0.6 mM butyrate; PA, 2 mM phenylacetate; Iso, 2 mM isobutyramide; Hu, 100 μM hydroxyurea; 5-aC, 5 μM 5-aza-cytidine; and Val, 2 mM valproate. (D) Analysis of globin mRNA expression in untreated (−) and apicidin-treated (+) K562 cells by quantitative real-time RT-PCR. mRNA expression of untreated and apicidin-treated cells was quantified by real-time RT-PCR, values were normalized by β-actin mRNA, and data expressed relative to untreated control cells. Experiments were repeated 3 times and standard errors were calculated.

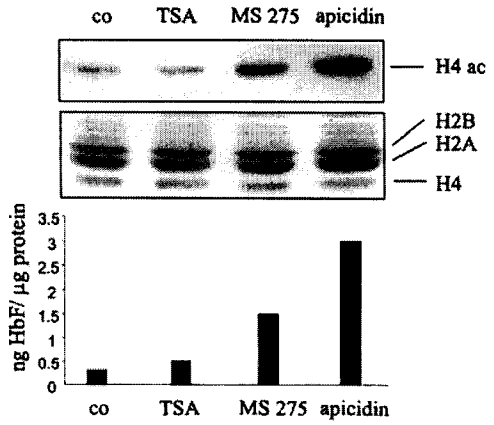

Figure 4. Induction of histone hyperacetylation correlates with stimulation of HbF synthesis. K562 cells were treated with the HDAC inhibitors TSA, MS-275, apicidin, or DMSO (co) for 1 hour, respectively. Histone proteins were prepared by acid extraction, and acetylation of histone H4 was determined by Western blot analysis by using a specific antiacetyl H4 histone antibody (top panel). Coomassie staining of the corresponding gel shows equal loading (20 µg) of histone proteins (H2A, H2B, H4) on each lane (middle panel). Bottom panel shows stimulation of HbF synthesis by the respective HDAC inhibitor after 4 days of treatment. H4 ac indicates acetylated histone H4; H2A, H2B, H4; histone proteins H2A, H2B, H4.

involved in butyrate-mediated erythroid differentiation of K562 cells.[17] If these modulations are associated with the HDAC inhibitory activity of butyrate, apicidin treatment of cells should lead to a similar change in the phosphorylation pattern of MAP kinases. Figure 5 shows that phosphorylation of p38 kinase started to increase 3 hours after addition of apicidin to cells and remained activated for the entire experimental period of 4 days. In contrast, phosphorylation of ERK did not change significantly during the experimental period. Phosphorylation of JNK was not detected, and changes in phosphorylation patterns were not observed. Thus, apicidin activates p38 signaling but has no effect on ERK- or JNK-MAP kinase pathways.

To further investigate the role of p38 signaling, we next examined the influence of the specific p38 inhibitor SB203580[18-20] on HbF stimulation by apicidin. Previously, we found that SB203580 inhibited butyrate- but not hemin-induced stimulation of hemoglobin synthesis in K562 cells.[17] This finding indicated that this p38 MAP kinase inhibitor is not a general inhibitor of erythroid differentiation in K562 cells. SB203580 inhibited the HbF-inducing effect of apicidin in a concentration-dependent manner (Figure 6A, black bars). At a concentration of 5 to 10 µM, SB203580 completely abolished the HbF-inducing effect of apicidin. In contrast, ERK pathway inhibitor UO126[21] rather increased apicidin-induced HbF synthesis in K562 cells (Figure 6A, gray bars). Interestingly, p38 inhibitor SB203580 also reverted the apicidin-induced increment of the HbF/total Hb ratio back to untreated control level (Figure 6B, black bars), whereas ERK inhibitor UO126 did not significantly influence the HbF/Hb ratio (Figure 6B, gray bars), indicating that activation of p38 signaling might be specific for induction of γ-globin gene expression. At the concentrations used, SB203580 did not influence cell proliferation (Figure 6C). UO126 decreased cell numbers by 40% to 50% but was not toxic for K562 cells as evidenced by trypan blue staining (not shown).

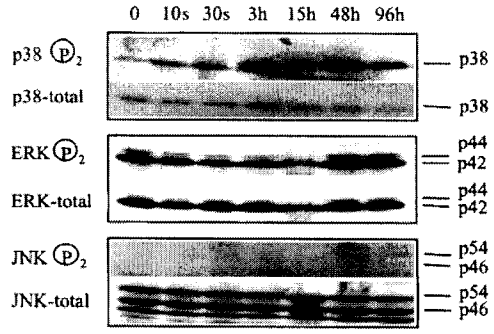

Figure 5. Changes in MAP kinase phosphorylation patterns following apicidin treatment of K562 cells. Cells were treated with 0.5 µM apicidin for the various times indicated and harvested, and 20 µg cell lysate was subjected to Western blot analysis by using specific antibodies against phosphorylated p38, ERK1/2, and JNK1/2, respectively. Blots were stripped and reprobed with pan antibodies against p38, ERK1/2, and JNK1/2, referred to as total in the figure. Lower panel shows HbF synthesis during the course of the experiment. Similar results were obtained in a second series of experiments.

Apicidin activates Aγ-globin gene promoter

To investigate the influence of apicidin on Aγ-globin promoter activity, we conducted reporter gene experiments. The −1436-bp

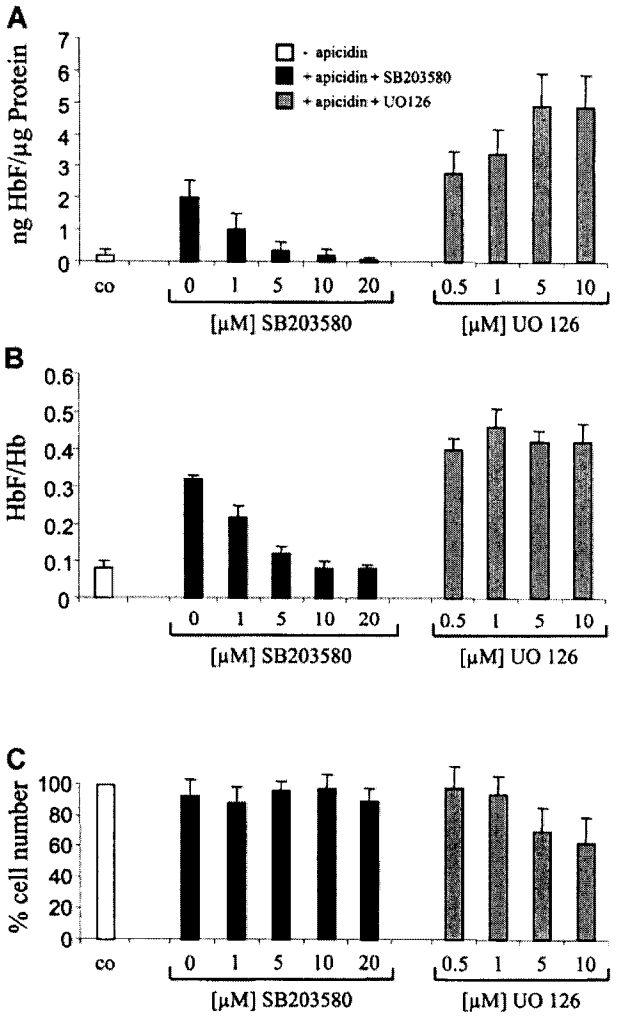

Figure 6. Effect of p38 inhibitor SB203580 and ERK inhibitor UO126 on apicidin-mediated induction of HbF synthesis in K562 cells. Cells were cultured for 4 days in the presence of 0.5 µM apicidin (gray and black bars) or 0.1% (vol/vol) DMSO (white bars). p38-specific inhibitor SB203580 (black bars) or ERK pathway inhibitor UO126 (gray bars) were added in increasing concentrations 1 hour prior to apicidin. After harvesting, cells were lysed, and HbF, total Hb, and total protein concentrations were determined. HbF per total protein (A) and HbF per total hemoglobin (B) were calculated as indicated. Cell numbers relative to untreated control cells (100%) are depicted in (C). Each experiment was performed 4 times, and standard errors were calculated as shown in the figure.

Aγ-globin promoter fragment was cloned into a luciferase reporter gene plasmid, and the construct was transiently transfected into K562 cells by lipofection. The time course of Aγ-globin promoter activity following apicidin treatment of cells is depicted in Figure 7. Apicidin stimulated promoter activity as early as 3 hours after addition to culture medium, and promoter activity peaked after 24 hours of treatment (Figure 7, white bars). Again, inhibition of p38 signaling by SB203580 resulted in inhibition of Aγ-globin promoter activation by apicidin (Figure 7, hatched bars), suggesting that p38 signaling is involved in apicidin-induced activation of the Aγ-globin promoter.

To investigate the influence of p38 signaling on histone hyperacetylation, we have pretreated K562 cells with SB203580 and then looked for induction of H4 hyperacetylation by apicidin. We observed no influence of inhibition of p38 signaling on histone acetylation (data not shown).

Discussion

Butyrate analogues have long been recognized as inducers of fetal hemoglobin expression in erythroid cells; therefore, these compounds have been used in small clinical trials for the treatment of β-thalassemia.[4-8] However, because of rapid metabolism, inconvenient mode of application, and relatively weak HbF-inducing activity of butyrate analogues, alternative substances with HbF-inducing activity are warranted. One approach would be to search for compounds that mimic the molecular action of butyrate. In this regard, butyrate has been shown to inhibit histone deacetylases (HDACs), leading to hyperacetylation of nuclear histones.[9-11] Acetylation neutralizes the positively charged histones and subsequently weakens interactions with DNA, resulting in an open nucleosomal configuration.[22,23] Such a conformation facilitates access for transcriptional regulators,[24,25] and histone acetylation patterns have recently been shown to play a role in the developmental control of murine β-globin gene expression.[26] Furthermore, the specific HDAC inhibitors trichostatin A, trapoxin, and HC-toxin have been found to induce γ-globin gene expression in erythroid cells.[12,27] However, the HbF-inducing potential of these compounds is relatively weak, being in the order of 1.5- to 2-fold over HbF production in untreated control cells. The hemoglobin-inducing potential of these specific HDAC inhibitors is even lower compared with arginine butyrate in K562 cells.[12]

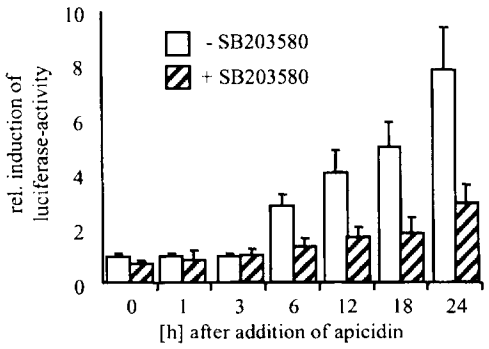

Figure 7. Activation of Aγ-globin gene promoter by apicidin in K562 cells. Cells were transiently transfected with a 1435-bp Aγ-promoter/luciferase reporter gene construct and subsequently treated with 0.5 μM apicidin for the various times indicated. After determination of luciferase activity from cell lysates as described in "Materials and methods," values were expressed relative to the activity of the 0 [h] value. Hatched bars show results of transfected cells that have been treated with p38 inhibitor SB203580 prior to addition of apicidin. Each experiment was performed 3 times, and standard errors were calculated as indicated.

In the present paper, we show that a recently identified HDAC inhibitor, apicidin, is a very potent HbF-inducing compound. Apicidin was originally isolated as a fungal metabolite from *Fusarium* species that exhibits broad spectrum antiprotozoal activity by inhibiting parasite histone deacetylases.[28] It has been shown to induce morphologic changes in tumor cells and to induce expression of the cell cycle–regulating proteins $p21^{WAF1}$ and gelsolin.[16] Compared with other HDAC inhibitors, apicidin has a relative low IC_{50} (concentration that inhibits 50%) of 0.7 nM[28] and 5 nM,[16] indicative of a high HDAC affinity. We found that apicidin strongly induced hyperacetylation of H4 histones in K562 erythroid cells and was the most potent inducer of HbF synthesis compared with the HDAC inhibitors TSA, HC-toxin, SAHA, MS-275, and butyrate. Furthermore, apicidin caused a 3-fold increase in HbF/total Hb ratio at the protein level and induced γ-globin mRNA expression 16-fold, whereas α-globin mRNA was stimulated only 2- to 3-fold. This finding was indicative of specific action on γ-globin gene expression. At the concentration with maximum HbF-inducing activity, apicidin showed relatively low cytotoxicity. Taken together, these data suggest that apicidin could be an effective HbF inducer in vivo, and further investigations using murine models of thalassemia are required.

The different HbF-inducing potencies of the investigated HDAC inhibitors might be due to their different affinities for the respective histone deacetylases associated with the fetal globin genes or other involved target genes. For example TSA exhibits much lower IC_{50} values for HDAC1 compared with HDAC4, and trapoxin B has a 3000-fold higher IC_{50} value for HDAC6 compared with HDAC1.[29]

In addition to affecting chromatin structure by histone hyperacetylation, HDAC inhibitors may induce other biologic responses in cells as well. We have observed that the MAP kinase signal transduction system contributes to the molecular action of butyrate, a compound with HDAC-inhibiting activity, during erythroid differentiation of K562 cells.[17] In the present report, we found that activation of p38 MAP kinase is also involved in the HbF-inducing activity of apicidin. P38 belongs to a group of kinases known to be activated by cellular stress such as heat, hyperosmolarity, x-radiation, and heavy metal ions,[30,31] and, thus, we were able to show in a previous report that heat shock and hyperosmolarity can induce hemoglobin production in K562 cells.[32] Additionally, p38 has been shown to be involved in erythropoietin-induced erythroid differentiation of mouse erythroleukemia cells,[33,34] demonstrating that HDAC inhibitors and cytokines might share the same signaling pathways with respect to induction of globin gene expression. In contrast to butyrate, apicidin did not affect ERK signaling, but ERK pathway inhibitor UO126 acted synergistically with both butyrate and apicidin on stimulation of hemoglobin production in K562 cells. The molecular link between inhibition of histone deacetylase activity and p38 MAP kinase signaling needs further investigation.

In summary, we have identified the HDAC inhibitor apicidin as a compound with strong HbF-inducing potential at nanomolar to micromolar concentrations. Our data outline the role of HDAC inhibition and p38 MAP kinase signaling as molecular targets for pharmacologic stimulation of HbF production in erythroid cells. Further studies need to investigate the in vivo potential of apicidin in the treatment of β-thalassemia.

References

1. Olivieri NF. The beta-thalassemias. N Engl J Med. 1999;341:99-109.
2. Atweh GF, Loukopoulos D. Pharmacological induction of fetal hemoglobin in sickle cell disease and beta-thalassemia. Semin Hematol. 2001;38: 367-373.
3. Rodgers GP, Saunthárajah Y. Advances in experimental treatment of beta-thalassaemia. Exp Opin Invest Drugs. 2001;10:925-934.
4. Perrine SP, Ginder GD, Faller DV, et al. A short-term trial of butyrate to stimulate fetal-globin-gene expression in the beta-globin disorders. N Engl J Med. 1993;328:81-86.
5. Blau CA, Constantoulakis P, Shaw CM, Stamatoyannopoulos G. Fetal hemoglobin induction with butyric acid: efficacy and toxicity. Blood. 1993;81:529-537.
6. Dover GJ, Brusilow S, Charache S. Induction of fetal hemoglobin production in subjects with sickle cell anemia by oral sodium phenylbutyrate. Blood. 1994;84:339-343.
7. Sher GD, Ginder GD, Little J, Yang S, Dover GJ, Olivieri NF. Extended therapy with intravenous arginine butyrate in patients with beta-hemoglobinopathies. N Engl J Med. 1995;332:1606-1610.
8. Reich S, Bührer C, Henze G, et al. Oral isobutyramide reduces transfusion requirements in some patients with homozygous beta-thalassemia. Blood. 2000;96:3357-3363.
9. Cousens LS, Gallwitz D, Alberts BM. Different accessibilities in chromatin to histone acetylase. J Biol Chem. 1978;254:1716-1723.
10. Candido EMP, Reeves R, Davie JR. Sodium butyrate inhibits histone deacetylation in cultured cells. Cell. 1978;14:105-113.
11. Doenecke D, Gallwitz D. Acetylation of histones in nucleosomes. Mol Cell Biochem. 1982;44:113-128.
12. McCaffrey PG, Newsome DA, Fibach E, Yoshida M, Su MSS. Induction of gamma-globin by histone deacetylase inhibitors. Blood. 1997;5:2075-2083.
13. Yoshida M, Nomura S, Beppu T. Effects of trichostatins on differentiation of murine erythroleukemia cells. Cancer Res. 1987;47:3688-3691.
14. Witt O, Albig W, Doenecke D. Transcriptional regulation of the human replacement histone gene H3.3B. FEBS Lett. 1997;408:255-260.
15. Yoshida M, Kijima M, Akita M, Beppu T. Potent and specific inhibition of mammalian histone deacetylase both in vivo and in vitro by trichostatin A. J Biol Chem. 1990;265:17174-17179.
16. Han JW, Ahn SH, Park SH, et al. Apicidin, a histone deacetylase inhibitor, inhibits proliferation of tumor cells via induction of p21 WAF1/Cip1 and gelsolin. Cancer Res. 2000;60:6068-6074.
17. Witt O, Sand K, Pekrun A. Butyrate induced erythroid differentiation of human K562 cells involves inhibition of ERK and activation of p38 MAP kinase-pathways. Blood. 2000;95:2391-2396.
18. Lee JC, Laydon JT, McDonnell PC, et al. A protein kinase involved in the regulation of inflammatory cytokine biosynthesis. Nature. 1994;372:739-746.
19. Cuenda A, Rouse J, Doza YN, et al. SB 203580 is a specific inhibitor of a MAP kinase homologue which is stimulated by cellular stresses and interleukin-1. FEBS Lett. 1995;364:229-233.
20. Badger AM, Bradbeer JN, Votta B, Lee JC, Adams JL, Griswold DE. Pharmacological profile of SB 203580, a selective inhibitor of cytokine suppressive binding protein/p38 kinase, in animal models of arthritis, bone resorption, endotoxin shock and immune function. J Pharmacol Exp Ther. 1996;279:1453-1461.
21. Favata M, Horiuchi KY, Manos EJ, et al. Identification of a novel inhibitor of mitogen activated protein kinase kinase. J Biol Chem. 1998;273: 18623-18632.
22. Hansen JC, Tse C, Wolffe AP. Structure and function of the core histone N-termini: more than meets the eye. Biochemistry. 1998;37:17637-17641.
23. Walia H, Chen HY, Sun JM, Holth LT, Davie JR. Histone acetylation is required to maintain the unfolded nucleosome structure associated with transcribing DNA. J Biol Chem. 1998;273:14516-14522.
24. Nightinghale KP, Wellinger RE, Sogo JM, Becker PB. Histone acetylation facilitates RNA polymerase II transcription of the Drosophila hsp26 gene in chromatin. EMBO J. 1998;17:2865-2876.
25. Tse C, Sera T, Wolffe AP, Hansen JC. Disruption of higher order folding by core histone acetylation dramatically enhances transcription of nucleosomal arrays by RNA polymerase III. Mol Cell Biol. 1998;18:4629-4638.
26. Forsberg EC, Downs KM, Christensen HM, Im H, Nuzzi PA, Bresnick EH. Developmentally dynamic histone acetylation pattern of a tissue-specific chromatin domain. Proc Natl Acad Sci U S A. 2000;97:14494-14499.
27. Smith RD, Li J, Noguchi CT, Schechter AN. Quantitative PCR analysis of HbF inducers in primary human adult erythroid cells. Blood. 2000;95: 863-869.
28. Darkin-Rattray SJ, Gurnett AM, Myers RW, et al. Apicidin: a novel antiprotozoal agent that inhibits parasite histone deacetylase. Proc Natl Acad Sci U S A. 1996;93:13143-13147.
29. Yoshida M, Furumai R, Nishiyama M, Komatsu Y Nishino N, Horinouchi S. Histone deacetylase as a new target for cancer chemotherapy. Cancer Chemother Pharmacol. 2001;48(suppl 1):S20-S26.
30. Lewis TS, Shapiro PS, Ahn NG. Signal transduction through MAP kinase cascades. Adv Cancer Res. 1998;74:49-139.
31. Seger R, Krebs EG. The MAPK signaling cascade. FASEB J. 1995;9:726-735.
32. Witt O, Schulze S, Kanbach K, Roth C, Pekrun A. Tumor cell differentiation by butyrate and environmental stress. Cancer Lett. 2001;171:173-182.
33. Nagata Y, Takahashi N, Davis RJ, Todokoro K. Activation of p38 MAP kinase and JNK but not ERK is required for erythropoietin-induced erythroid differentiation. Blood. 1998;92:1859-1869.
34. Nagata Y, Todokoro K. Requirement of activation of JNK and p38 for environmental stress-induced erythroid differentiation and apoptosis and of inhibition of ERK for apoptosis. Blood. 1999;94:853-863.

Circulation
JOURNAL OF THE AMERICAN HEART ASSOCIATION

American Heart Association®
Learn and Live℠

Suppression of Class I and II Histone Deacetylases Blunts Pressure-Overload Cardiac Hypertrophy

Yongli Kong, Paul Tannous, Guangrong Lu, Kambeez Berenji, Beverly A. Rothermel, Eric N. Olson and Joseph A. Hill

Circulation 2006;113;2579-2588; originally published online May 30, 2006;
DOI: 10.1161/CIRCULATIONAHA.106.625467
Circulation is published by the American Heart Association. 7272 Greenville Avenue, Dallas, TX 72514
 Print ISSN: 0009-7322. Online ISSN: 1524-4539

Suppression of Class I and II Histone Deacetylases Blunts Pressure-Overload Cardiac Hypertrophy

Yongli Kong, MD, PhD; Paul Tannous, BS; Guangrong Lu, MD; Kambeez Berenji, MD; Beverly A. Rothermel, PhD; Eric N. Olson, PhD; Joseph A. Hill, MD, PhD

Background—Recent work has demonstrated the importance of chromatin remodeling, especially histone acetylation, in the control of gene expression in the heart. In cell culture models of cardiac hypertrophy, pharmacological suppression of histone deacetylases (HDACs) can either blunt or amplify cell growth. Thus, HDAC inhibitors hold promise as potential therapeutic agents in hypertrophic heart disease.

Methods and Results—In the present investigation, we studied 2 broad-spectrum HDAC inhibitors in a physiologically relevant banding model of hypertrophy, observing dose-responsive suppression of ventricular growth that was well tolerated in terms of both clinical outcome and cardiac performance measures. In both short-term (3-week) and long-term (9-week) trials, cardiomyocyte growth was blocked by HDAC inhibition, with no evidence of cell death or apoptosis. Fibrotic change was diminished in hearts treated with HDAC inhibitors, and collagen synthesis in isolated cardiac fibroblasts was blocked. Preservation of systolic function in the setting of blunted hypertrophic growth was documented by echocardiography and by invasive pressure measurements. The hypertrophy-associated switch of adult and fetal isoforms of myosin heavy chain expression was attenuated, which likely contributed to the observed preservation of systolic function in HDAC inhibitor–treated hearts.

Conclusions—Together, these data suggest that HDAC inhibition is a viable therapeutic strategy that holds promise in the treatment of load-induced heart disease. **(*Circulation*. 2006;113:2579-2588.)**

Key Words: hypertrophy ■ signal transduction ■ chromatin remodeling ■ histone deacetylases

In response to the stress of neurohumoral activation, hypertension, or myocardial injury, the heart initially compensates with an adaptive hypertrophic increase in mass. Under prolonged stress, the heart undergoes apparently irreversible decompensation that results in dilation of the failing heart. During stress-induced hypertrophy, postnatal cardiac muscle cells increase in size and activate a set of fetal genes that encode proteins involved in contractility, calcium handling, and myocardial energetics.

Clinical Perspective p 2588

Recent work has uncovered the importance of chromatin remodeling, especially histone acetylation, in the control of gene expression in heart disease. The structure of chromatin is governed by the acetylation state of nucleosomal histones,[1] which, in turn, participates in regulating the expression of numerous genes. Histone acetyltransferases (HATs) transfer acetyl groups from acetyl coenzyme A to ϵ-amino groups of conserved lysine residues within nucleosomal histone tails, resulting in charge neutralization of the amino acid. The altered charge of the histone tail promotes chromatin relaxation and thus creates a local environment that accommodates transcriptional machinery.[1] HAT activity is antagonized by histone deacetylases (HDACs), which promote nucleosomal condensation and consequent transcriptional repression.[2] Recent studies have shown that both HAT and HDAC activities participate in regulating the hypertrophic response of the heart.[3–5]

A complex network of signaling cascades is activated during cardiac remodeling.[6] Recent studies point to HDACs as integrators of these divergent stress-response pathways.[7] Among the best characterized examples are class II HDACs; in the absence of stress signals, these enzymes interact with the MEF2 transcription factor to repress the fetal gene program and cardiac growth.[4] Paradoxically, recent studies in vitro indicate that pharmacological inhibition of HDAC enzymatic (deacetylase) activity blunts hypertrophic growth.[8] These surprising results suggest a potential role for HDAC inhibitors as therapy to control cardiac hypertrophy.

In the present study, we set out to explore the efficacy of HDAC inhibition (HDACi) in a surgical model of pressure overload-induced cardiac hypertrophy. Using 2 broad-spectrum HDAC inhibitors, we observed dose-responsive

Received November 21, 2005; de novo received March 7, 2006; revision received April 1, 2006; accepted April 7, 2006.

From the Donald W. Reynolds Cardiovascular Clinical Research Center (E.N.O., J.A.H.) and the Departments of Internal Medicine (Y.K., P.T., G.L., K.B., B.A.R., J.A.H.) and Molecular Biology (E.N.O., J.A.H.), University of Texas Southwestern Medical Center, Dallas.

The online-only Data Supplement can be found at http://circ.ahajournals.org/cgi/content/full/CIRCULATIONAHA.106.625467/DC1.

Correspondence to Joseph A. Hill, MD, PhD, Division of Cardiology, UT Southwestern Medical Center, NB11.200, 6000 Harry Hines Blvd, Dallas, TX 75390–8573. E-mail joseph.hill@UTSouthwestern.edu

Circulation **is available at http://www.circulationaha.org** **DOI: 10.1161/CIRCULATIONAHA.106.625467**

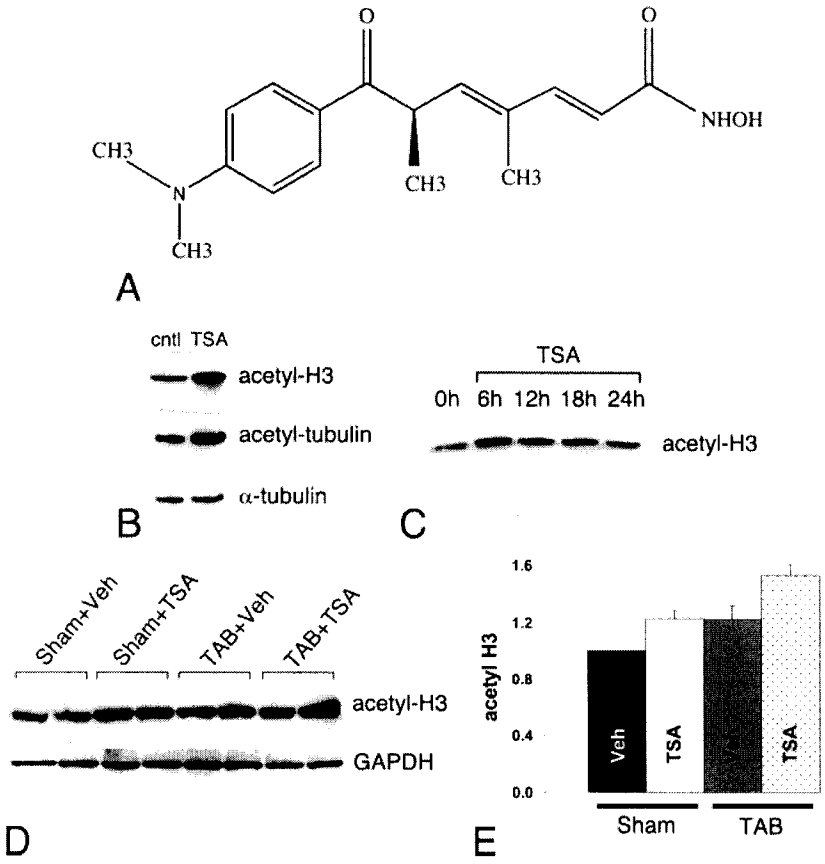

Figure 1. TSA provokes histone acetylation in vitro and in vivo. A, Chemical structure of TSA. B, Neonatal cardiomyocytes in culture were exposed to 100 nmol/L TSA (48 hours) followed by immunoblot analysis for acetyl-histone H3 and acetyl-tubulin. C, Mice were exposed to TSA 1 mg/kg, and then LV lysates were subjected to immunoblot analysis for histone H3. TSA caused a significant increase in acetylation of histone H3. D, LV lysates from hearts treated as listed (3 weeks) were subjected to immunoblot analysis. Both TSA and TAB triggered histone H3 acetylation. E, Densitometric quantification of acetyl-H3 abundance, normalized to glyceraldehyde-3-phosphate dehydrogenase. * $P<0.05$ versus Veh.

suppression of ventricular growth that was well tolerated in terms of clinical outcome and cardiac performance measures. In both short-term and long-term trials, cardiomyocyte growth was blocked by HDACi with no evidence of cell death or apoptosis. Fibrotic change was diminished in hearts treated with HDAC inhibitors, and collagen synthesis in isolated cardiac fibroblasts was blocked. Preservation of systolic function in the setting of blunted hypertrophic growth was documented by echocardiography and by invasive pressure measurements. Attenuation of the hypertrophy-associated switch of adult and fetal isoforms of myosin heavy chain (MHC) expression was detected, which likely contributed to the preservation of systolic function in HDAC inhibitor–treated hearts. Together, these data suggest that HDACi is a viable therapeutic strategy that holds promise in the treatment of load-induced heart disease.

Methods

Pressure-Overload Hypertrophy Model

Male C57BL6 mice (6 to 8 weeks old; Charles River, Wilmington, Mass) were subjected to pressure overload by thoracic aortic banding (TAB).[9] We have shown previously that constriction to a 27G stenosis induces moderate hypertrophy (≈40% increases in heart mass) without clinical signs of heart failure or malignant ventricular arrhythmia.[10] At 3 weeks, when the hypertrophic response reaches steady state,[10] integrity of aortic banding was confirmed by inspection of the surgical constriction and by visualization of marked differences in caliber of the right and left carotid arteries.

Cardiomyocyte Cross-Sectional Area

Hearts were rapidly excised and retrograde perfused (4°C) with Carson's Modified Buffered Formalin (Richard-Allan Scientific, Kalamazoo, Mich). Hematoxylin & eosin-stained tissue sections from 3 hearts in each treatment group were studied at 200× magnification. In each field, all myocytes cut in short axis with a visible nucleus were counted (≈20 cells), and 6 to 8 randomly selected fields spanning the septum, apex, and free wall were studied per tissue section. Cell borders were planimetered manually by an operator who was blinded to treatment group. ImageJ software (NIH) was used to calculate 2-dimensional cross-sectional areas.

Echocardiography

Transthoracic echocardiograms were recorded in conscious-sedated mice as described.[10,11] Details are provided in the online Data Supplement.

Invasive Hemodynamics

Left ventricular pressure volume and systemic blood pressure measurements were performed as previously described.[12] Details are provided in the online Data Supplement.

Statistical Analysis

Averaged data are reported as mean±SEM. Statistical significance was analyzed using a Student unpaired t test or 1-way ANOVA followed by Bonferroni method for post hoc pairwise multiple comparisons. Additional methodological details are provided in the online Data Supplement.

The authors had full access to the data and take full responsibility for its integrity. All authors have read and agree to the manuscript as written.

Results

HDAC Suppression Augments Histone Acetylation In Vivo

To explore the effects of HDAC inhibitors in cardiac myocytes, we examined the acetylation state of known HDAC

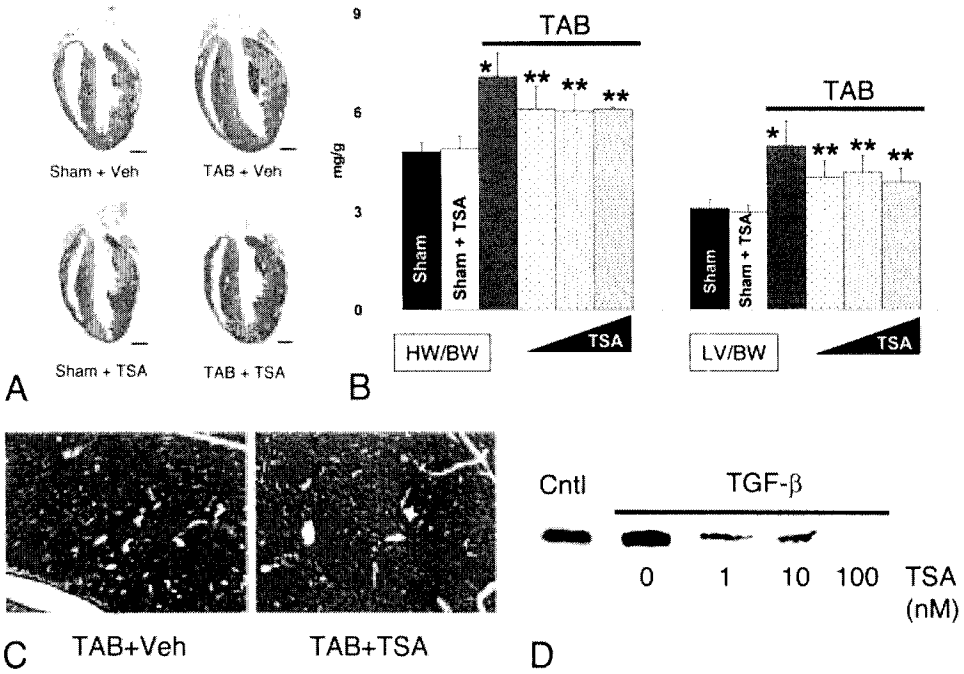

Figure 2. TSA blunts pressure-overload hypertrophy. A, Representative 4-chamber histological sections of hearts treated as listed. B, Heart mass (HW) or LV mass normalized to body mass (BW) in hearts treated as listed. Sham+Veh (n=30, black bar); sham+TSA (n=28); TAB+Veh (n=19, solid gray bar); TAB+TSA (0.5 mg/kg, n=5, lightly stippled bar); TAB+TSA (1 mg/kg, n=18, stippled bar); TAB+TSA (2 mg/kg, n=5, heavily stippled bar). *$P<0.05$ versus sham; ** $P<0.05$ versus TAB+Veh. C, Representative fields of Masson's trichrome–stained tissue sections reveal interstitial fibrosis typical of pressure-overload–induced hypertrophy (left) is nearly abolished by TSA (right). D, Fibroblasts were isolated from adult murine left ventricle and exposed to TGF-β (5 ng/mL) for 24 hours in the presence/absence of TSA. A representative immunoblot probed for type I collagen is shown, revealing dose-responsive suppression of collagen biosynthesis. Cntl indicates control.

targets. HDAC suppression would be expected to induce histone hyperacetylation due to unopposed HAT activity. To test this, we exposed neonatal cardiomyocytes in culture to 50 nmol/L Trichostatin A (TSA; Biomol, Plymouth Meeting, Pa; Figure 1A), an inhibitor of class I and II HDACs,[13] and measured acetyl-histone-3 (H3) levels by immunoblot. As expected, TSA induced significant increases in H3 acetylation confirming the efficacy of deacetylase suppression (Figure 1B). TSA also induced increases in the acetylation of α-tubulin, another HDAC substrate[14,15] (Figure 1B).

To test for efficacy in vivo, mice were treated with TSA (1 mg/kg for 3 days) and euthanized at different time points after the last injection. H3 hyperacetylation was observed for 24 hours after the final injection with the drug (Figure 1C), suggesting that once daily dosing was suitable for further testing in vivo. Similar findings were observed with Scriptaid (6-[1,3-Dioxo-1H,3H-benzo(de)isoquinolin-2-yl]-N-hydroxyhexanamide) (SA; Biomol), another broad-spectrum HDAC inhibitor (data not shown).

TSA Blunts Pressure-Overload Hypertrophy

To test the effects of HDAC inhibitors on load-induced cardiac hypertrophy, mice were subjected to TAB. On the first postoperative day, mice were randomized to daily subcutaneous injections of either TSA or vehicle. A parallel group of animals was subjected to a sham operation and treated with once-daily injections of TSA or vehicle. Animals were followed for 3 weeks, a time frame similar to the HDAC inhibitor trials presently underway in clinical oncology. In these experiments, we observed that pressure overload induced by TAB was sufficient to induce H3 acetylation (Figure 1D and 1E), suggesting that chromatin remodeling is an important mechanism governing the cardiac response to stress.

Administration of TSA (2 mg/kg) resulted in a statistically significant suppression ($P<0.05$) of hypertrophic growth measured as heart mass or left ventricular (LV) mass normalized to either body mass or tibia length (Figure 2A and 2B). Treatment with lower doses of TSA (1 mg/kg and 0.5 mg/kg) resulted in similar degrees of blunted growth, suggesting that maximal antihypertrophic efficacy had been achieved at 0.5 mg/kg. TSA had no apparent effect in sham-operated mice.

TSA treatment of skin fibroblasts has been shown to suppress collagen synthesis and fibrogenesis.[16] As pathological hypertrophy is typically associated with interstitial and perivascular fibrosis, we examined the effects of HDAC inhibition on TAB-induced fibrosis. Masson's trichrome staining of hearts from TAB+TSA animals revealed significantly less fibrosis compared with TAB+vehicle (Veh) animals (Figure 2C). These data, then, lend further credence to the notion that TSA targets pathological aspects of the hypertrophic process.

To test for effects of HDACi on collagen synthesis, fibroblasts were isolated from adult murine left ventricle and exposed to transforming growth factor-β (TGF-β; 5 ng/mL, 24 hours). Immunoblot for collagen type I revealed that TGF-β–triggered synthesis of collagen was abolished by TSA (Figure 2D). As reported previously, no cytotoxicity was observed with TSA at these concentrations.[8] Thus, these data point to blunted collagen biosynthesis as a potential

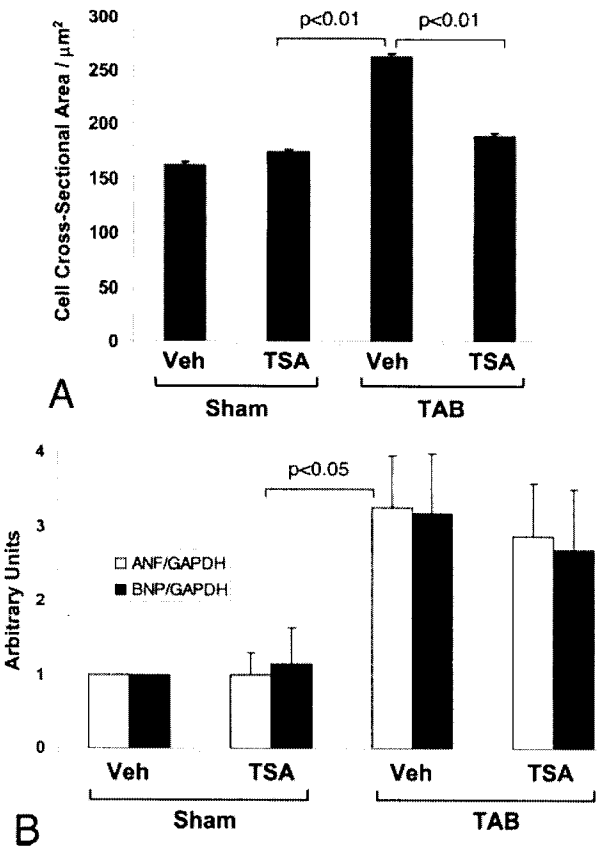

Figure 3. TSA blunts cardiomyocyte growth and preserves natriuretic peptide expression. A, Two-dimensional cardiomyocyte cross-sectional area measured as described. Sham+Veh (n=470 cells/5 hearts); sham−TSA (n=460/4); TAB+Veh (n=560/4); TAB+TSA (n=500/4). B, Transcript abundance was quantified by Northern dot blot analysis (n=3 independent experiments), revealing persistently elevated level of ANF and BNP transcript in TAB+TSA ventricle.

mechanism underlying the antifibrogenic effects of HDACi and point to cardiac fibroblasts as novel targets of HDACi therapy.

HDAC inhibitors are capable of triggering tumor cell death, and several of these compounds have shown efficacy as anticancer therapy. To determine whether the diminished heart growth seen in animals treated with TSA was due to blunted cardiomyocyte growth as opposed to apoptosis-induced cell dropout, we quantified cell cross-sectional area in sections of LV tissue (Figure 3A). As expected, cell cross-sectional area was significantly increased in TAB ventricle. In TAB+TSA ventricles, however, cardiomyocyte cell size was significantly blunted. In situ DNA nick end labeling staining and DNA laddering analysis for apoptosis revealed no significant changes in TSA-exposed heart (data not shown). Together, these data suggest that the effects of TSA derive from diminished hypertrophic cell growth rather than from TSA-triggered death of a population of cells in the heart.

A second, broad-spectrum HDAC inhibitor, Scriptaid, was tested in another series of short-term trials. Similar to the findings with TSA, banded animals treated with Scriptaid manifested statistically significantly less hypertrophic growth compared with vehicle-treated controls (Figure 4). Here, a dose-response relation was observed with greater degrees of hypertrophy suppression manifest at higher Scriptaid doses, suggesting that the serum concentrations achieved at these doses are situated on the vertical part of the dose-response curve.

Natriuretic Peptide Expression

Given that the transcriptional effects of HDAC inhibitors would be expected to augment gene expression and yet HDAC inhibitors blocked hypertrophy, we hypothesized that countervailing antigrowth pathways may be activated by these drugs. Enhanced expression of natriuretic peptides, such as atrial natriuretic factor (ANF) and brain natriuretic peptide (BNP), is a characteristic feature of the pressure-stressed heart, and it has been postulated that they may function as part of a counterregulatory mechanism that limits growth. To test whether HDAC inhibitors altered the expression of natriuretic peptides in our model of load-induced hypertrophy, we measured steady-state levels of ANF and BNP transcript in ventricle subjected to TAB+TSA (Figure 3B). Despite significant blunting of hypertrophic growth in TAB+TSA animals, ANF and BNP transcript levels were increased to a similar extent (P=NS) compared with TAB+Veh animals.

Functional Effects of HDAC Therapy

In numerous animal models, suppression of hypertrophic growth is well tolerated, with preservation of ventricular size and performance, despite persistence of the inciting stimulus (recently reviewed[6]). Our data demonstrate that HDAC inhibitors can blunt hypertrophic growth, and yet nothing is known about the tolerability of HDAC inhibitors in load-induced cardiac hypertrophy. It was therefore important to assess the impact of HDAC inhibitor therapy on cardiac function and the overall health of the mice.

TSA and Scriptaid were each well tolerated in both TAB- and sham-operated animals. Animals subjected to TAB or sham operation and subsequently randomized to TSA or vehicle injections were clinically healthy without evidence of cardiovascular insufficiency (lethargy, edema, etc). Three-week mortality was similar in all 4 treatment arms (P=NS) and less than 25% (Figure 5A).

Ventricular function was assessed by echocardiography under conditions of light sedation. We observed preservation of ventricular size and systolic function despite the presence of persistent afterload stress (Figure 5B and 5C), suggesting that under these conditions, HDAC suppression may be a viable treatment strategy.

Although ejection fraction by echocardiography is technically easy to measure, and hence frequently used as a surrogate for systolic function, it is not a true measure of intrinsic contractility because it varies with myocardial loading conditions. Additionally, ejection fraction overestimates contractility in the setting of hypertrophy because of changes in LV geometry during contraction.[17,18] Thus, we also evaluated ventricular performance by means of invasive hemodynamic pressure recordings (Figure 6A). Using this sensitive method, we uncovered evidence of diminished contractile performance in TAB hearts (Table in the online Data Supplement). For example, the end-systolic pressure-volume relation (ESPVR), a load-independent measure of ventricular

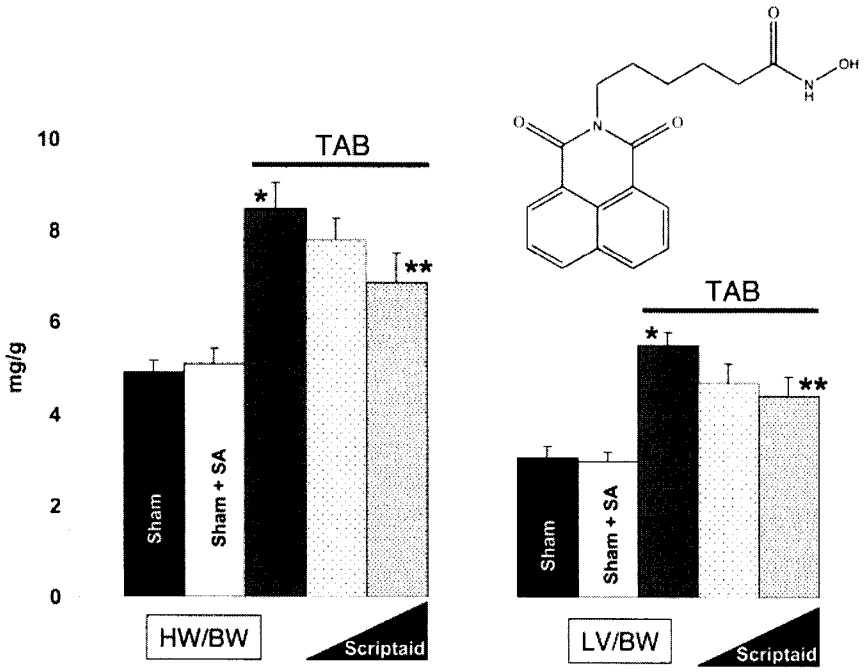

Figure 4. Scriptaid (SA) blunts pressure-overload hypertrophy. Heart mass (HW) or LV mass normalized to body mass (BW). Sham+Veh (n=7, black bar); sham+SA (n=8); TAB+Veh (n=7, solid gray bar); TAB+SA (2.5 mg/kg, n=4, lightly stippled bar); TAB+SA (5 mg/kg, n=6, heavily stippled bar). Inset, SA chemical structure. * $P<0.05$ versus sham; ** $P<0.05$ versus TAB+Veh.

performance, was significantly decreased ($P<0.01$) in TAB hearts (Figure 6B). Remarkably, this measure of systolic function was preserved in TAB+TSA hearts. In sham-operated animals, TSA had no significant effect on ventricular function. Similar results were obtained when we examined maximum and minimum dP/dt. Again, evidence of diminished ventricular function was observed in TAB hearts, which was nearly completely abolished by TSA (Figure 6C).

Myosin Heavy Chain Isoform Switching

During hypertrophic growth of the heart, expression of the fetal isoform of MHC (β-MHC) is enhanced, and expression of the adult isoform (α-MHC) is diminished. Some evidence suggests that this stress-triggered switching of sarcomeric protein isoforms contributes to the diminution of contractile performance typically seen in hypertrophy.[19,20] To determine whether the positive inotropic actions of TSA might be a consequence of preserved balance of MHC isoforms, we quantified the abundance of β-MHC and α-MHC proteins. As expected, we observed a robust increase in β-MHC protein and a decrease in α-MHC protein in TAB ventricle (Figure 7A). The increase in β-MHC protein levels was significantly blunted by TSA. Similarly, the TAB-induced decrease in α-MHC abundance was attenuated by TSA (Figure 7B). Also, TAB-induced increases in α-tubulin abundance were blocked by TSA (Figure 7C). Together, these data suggest that the dramatic effects of TSA on cardiac contractile performance may result, at least in part, from attenuated switching of contractile protein isoforms.

Long-Term TSA Trials

To envision HDAC inhibitors in clinical use, it is important to evaluate their long-term efficacy and tolerability. To begin to explore this, we studied animals subjected to TAB or sham operation and treated with TSA (1 mg/kg QD) for 9 weeks, a period roughly corresponding to 10 to 12 years in humans. In 2 independent trials, treatment with TSA was clinically well tolerated throughout the 9-week trial and did not alter survival: sham+Veh, 100% (n=7); sham+TSA, 100% (n=7); TAB+Veh, 71% (n=11); and TAB+TSA, 67% (n=13). On necropsy, statistically significant blunting of hypertrophic growth similar to that seen in short-term trials was observed in TSA-treated animals (Figure 8A).

To test for effects on cardiac performance, animals in all 4 treatment arms underwent echocardiography 1 day before euthanasia. Here, we observed modest declines in systolic function in TAB+Veh animals, consistent with pressure overload-induced pathological remodeling (Figure 8B). In TAB+TSA mice, declines in ventricular performance were significantly attenuated compared with TAB+Veh mice ($P<0.05$), despite the presence of a blunted compensatory hypertrophic response. After 9 weeks of pressure overload, marked accumulation of interstitial fibrosis was observed, which was dramatically attenuated by TSA (Figure 8C). Finally, quantification of myocyte cross-sectional area revealed the expected increases in cell growth in TAB+Veh hearts ($P<0.01$) that was significantly ($P<0.01$) blunted by HDACi (Figure 8D). No evidence of increased apoptosis was detected by in situ DNA nick end labeling staining or by DNA laddering analysis in any of the 4 long-term treatment arms (data not shown). Together, these data suggest that TSA is capable of suppressing hypertrophic growth long term. These findings also suggest that this blunted remodeling response is associated with salutary effects on ventricular performance and pathological fibrogenesis despite persistence of increased afterload.

Discussion

Recent studies point to the importance of enzymes that control histone acetylation as stress-responsive regulators of gene expression in the heart.[21] Pharmacological inhibition of HDACs blocks hypertrophic growth of cardiac myocytes in

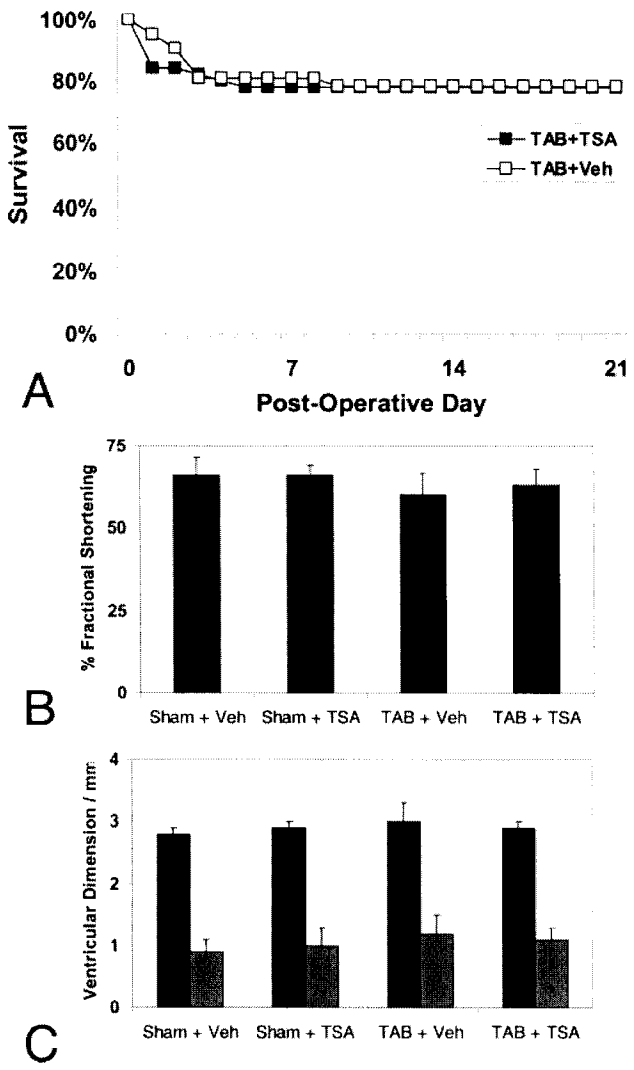

Figure 5. A, Kaplan-Meier analysis demonstrated similar survival in TAB animals treated with vehicle (open squares, n=42) or TSA (filled squares, n=50). Echocardiographic measures of systolic performance (B) and ventricular size (C) reveal preservation of cardiac function in TSA-treated animals. C, Black bars depict diastolic dimensions and gray bars depict systolic dimensions.

vitro,[8] and some evidence suggests they block agonist-induced hypertrophy in vivo.[22] Before the present study, nothing was known about whether these compounds impact hypertrophic growth of the heart in a physiologically relevant model of pressure overload in vivo. Here, we demonstrate that (1) 2 broad-spectrum HDAC inhibitors are capable of blunting hypertrophic growth in a model of load-induced cardiac hypertrophy, (2) HDAC inhibitors are clinically well tolerated, (3) suppression of pressure-overload hypertrophy by HDACi is not associated with circulatory insufficiency, (4) HDAC inhibitors preserve systolic function, (5) HDAC inhibitors blunt stress-induced fibrogenesis and inhibit collagen biosynthesis in cardiac fibroblasts, and (6) HDAC inhibitors blunt pathological switching of MHC isoforms, which may contribute to their actions to preserve ventricular performance.

HDAC Inhibitors and Transcriptional Control of Cardiac Growth

Pharmacological inhibition of HDAC activity alters gene expression in a complex manner, with both increases and decreases in expression of specific genes observed.[23,24] The end result, however, is often blockade of growth and proliferation. In the case of both TSA and Scriptaid, hypertrophic growth was not completely abolished, suggesting that a component of the growth response is not governed by HDAC-dependent mechanisms. Dose-dependent attenuation of hypertrophy was observed with Scriptaid but not with TSA, suggesting that the doses of TSA we studied were on the upper plateau of the pharmacodynamic response curve.

Class II HDACs block expression of progrowth genes through their interaction with MEF2,[25] a transcription factor that integrates multiple Ca^{2+}/calmodulin-dependent signals. On the basis of what is known about the interaction of class II HDACs with MEF2, however, one would predict that compounds inhibiting HDAC activity would induce hypertrophy rather than inhibiting hypertrophy as we and others[8,22] have observed. The key to this paradox may lie in the fact that class II HDAC isoforms that lack deacetylase activity are also capable of blocking MEF2 transcription both in vitro and in vivo.[4] The crystal structure of MEF2 bound to DNA was recently solved and showed that association of MEF2 with p300 and class II HDACs is mutually exclusive, as these proteins target an overlapping site on the transcription factor.[26] Under normal circumstances, the presence of HDAC (whether active or not) is sufficient to prevent access of HAT. In response to hypertrophic stress signals, HDAC is phosphorylated and released from MEF2 and moves to the cytoplasm. Inhibition of HDAC activity at this point would have no effect on genes regulated by class II HDACs because the class II HDACs are no longer bound to chromatin. Because of this, it is likely that within the context of a hypertrophic heart, inhibition of HDAC activity has no direct effect on MEF2 transcription and therefore does not directly derepress expression of the prohypertrophic genes under MEF2 control.

In cultured neonatal myocytes, HDAC inhibition by TSA has been reported to either induce[27] or blunt[8] agonist-induced ANF expression. Working with a model of load-induced hypertrophy in vivo, we observed that activation of ANF and BNP expression was preserved in TSA-exposed hearts even though hypertrophic growth was blunted. Thus, TSA treatment dissociated activation of expression of this set of fetal genes from a progrowth response. Our finding that ANF transcription remains elevated in TSA-treated TAB hearts despite attenuation of hypertrophic growth is consistent with studies where calcineurin was inhibited by transgenic expression of glycogen synthase kinase-3[28] or modulatory calcineurin interacting protein-1.[11] Indeed, it is tempting to speculate that the preservation of increased ANF expression in TSA-treated TAB hearts may participate in the antihypertrophic effects of deacetylase inhibitors. The observation that TSA diminished pathological remodeling measured as fibrotic change in the myocardium suggests that the sum of the effects of broad-spectrum HDAC inhibition is salutary and beneficial.

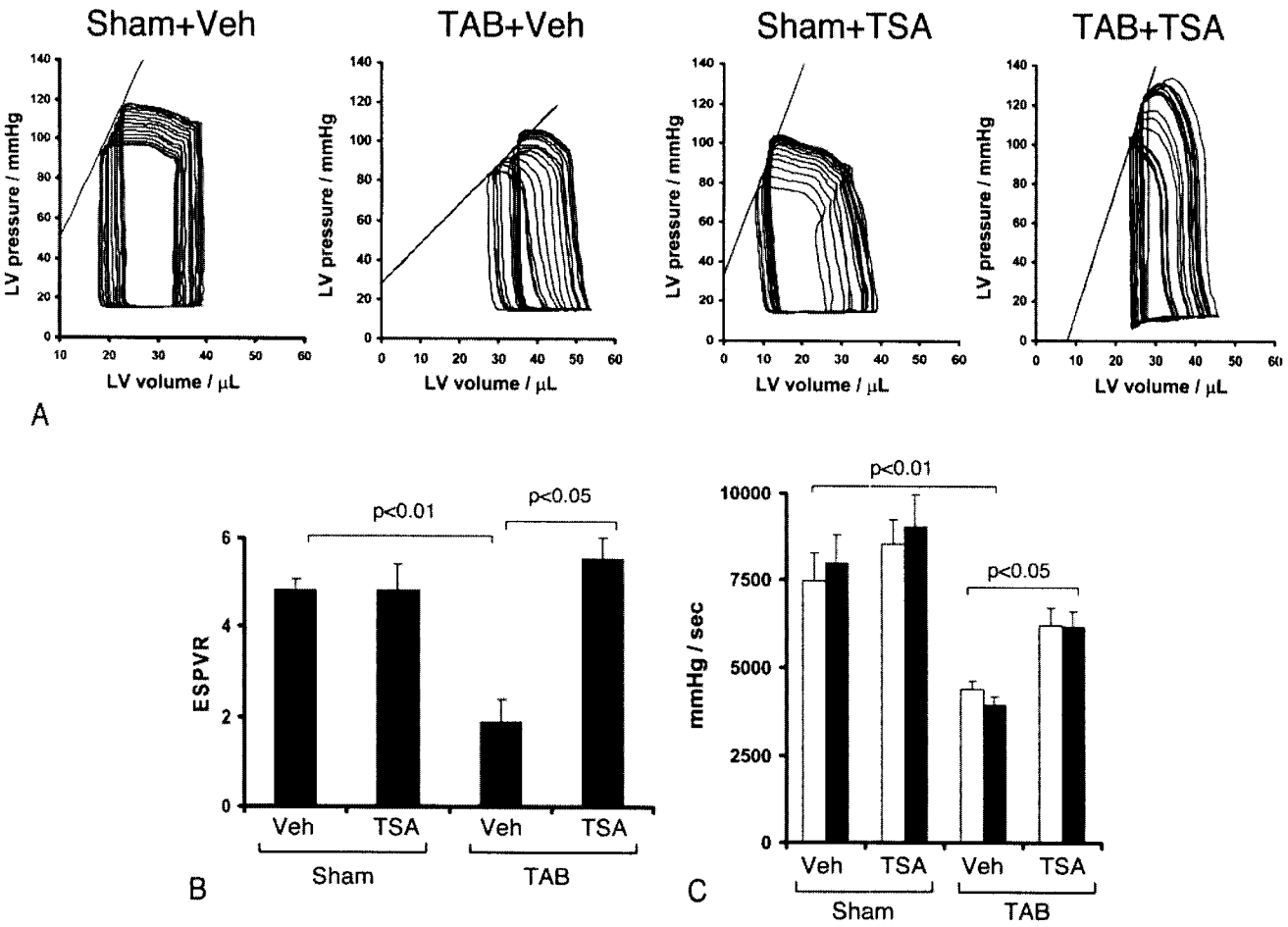

Figure 6. TSA abolished hypertrophy-associated decreases in LV performance. A, Representative pressure-volume loop recordings from mice treated as listed (3 weeks). ESPVRs were calculated using a computerized algorithm. B, Mean ESPVR data. Sham+Veh (n=4); sham+TSA (n=6); TAB+Veh (n=8); TAB+TSA (n=8). C, Mean data from maximal (white bars) and minimal (black bars) dP/dt measurements.

HDAC Targets in Hypertrophy

Despite their nomenclature, which implicates histones as a major substrate, the molecular targets of HDACs relevant to cardiac hypertrophy are unknown. Indeed, many proteins in the cell are acetylated and deacetylated by HATs and HDACs. Similar to phosphorylation, acetylation of a protein can have a wide range of effects including altering stability of the protein, changing its enzymatic activity, or facilitating new protein–protein interactions. A number of transcription factors are acetylated, as well as nuclear import factors, cell cycle regulators, and structural proteins.[29] The attenuation of hypertrophy by HDACi that we have observed could be due to increased acetylation of one or a combination of these protein substrates.

We observed that TAB-induced afterload stress, a robust trigger of hypertrophic growth, induced histone acetylation, suggesting that chromatin remodeling is a mechanism through which transcription could be regulated in response to hypertrophic stimuli. This is consistent with a recent report demonstrating that the hypertrophic agonist cardiotrophin-1 triggers histone H3 acetylation in H9c2 cells in culture.[24] Paradoxically, however, HDAC inhibition, which was similarly capable of provoking histone acetylation, blunted hypertrophic growth in our studies. Together, these data suggest that there are antigrowth targets suppressed by HDACs that, when released, are dominant over the progrowth genes controlled by class II HDACs. Consistent with this, recent evidence suggests that chromatin-modifying enzymes are capable of regulating both progrowth and antigrowth arms of the complex network that governs cardiac growth. Homeodomain-only protein (HOP) represses the transcriptional activity of serum response factor through its association with HDAC2, a class I HDAC.[22] HOP overexpression induces hypertrophy, but overexpression of a mutant HOP, unable to interact with HDAC2, does not. This suggests that in this context, and in contrast to class II HDACs, this class I HDAC facilitates prohypertrophic growth. Exactly which genes are regulated by this system is not clear. However, we have conducted preliminary studies evaluating effects of TSA on the abundance and activation of ERK, JNK, p38, Akt, phospholamban, and SERCA2a, and these experiments so far have failed to reveal robust treatment effects (Y.K., J.A.H., unpublished observations).

Blunted Hypertrophic Growth

In a study designed to evaluate antihypertrophic therapy, it is critical that the imposed hemodynamic load be equivalent

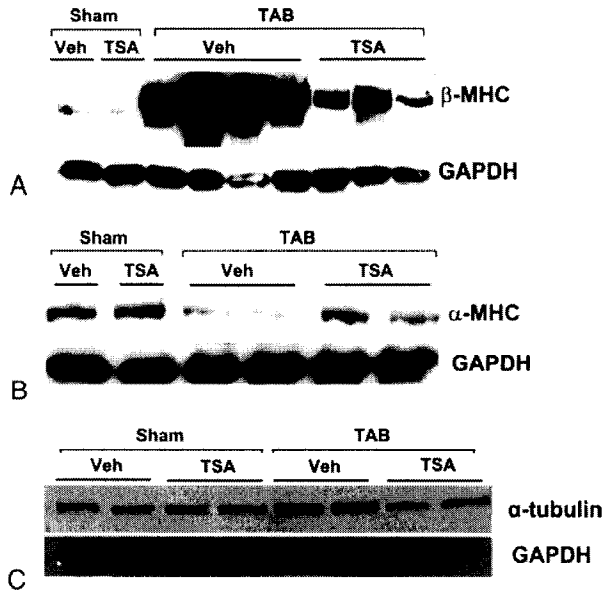

Figure 7. Blunted hypertrophy-associated switching of MHC isoforms in hearts exposed to TSA. Representative immunoblots from individual left ventricles treated as listed and probed for β-MHC (A), α-MHC (B), or α-tubulin (C).

across treatment groups. To assure that all animals were exposed to equivalent banding-induced stress, mice were randomized to 2 treatment groups the day after TAB surgery. For 2 important reasons, we did not measure transstenotic pressure gradients. First, transstenotic pressure gradients are a function of both the degree of vessel stenosis and the pressure generated by the left ventricle; hence, they provide an indirect measure of arterial resistance. To infer that transstenotic pressure gradients are indicative of TAB-induced stenosis, one must assume that cardiac output is unchanged by drug treatment. (As an analogy, to compare electrical resistance [R] in 2 circuits by measuring the voltage-drop [V] across each circuit, one must assume that current [I] is the same in both circuits; V=IR.) Our findings reveal improved systolic performance in TSA-treated animals. Thus, it was clearly inappropriate to assume that cardiac outputs are equivalent in all treatment groups. Second, measurements of simultaneous transstenotic pressures are complicated by inevitable and variable declines in blood pressure from anesthesia, which renders these indirect measures of vascular resistance yet more unreliable. As a result, we adopted a previously validated strategy[10] of banding animals by a surgeon who was blinded to treatment group followed by randomization between treatment arms.

Our findings are consistent with prior work in vitro demonstrating an antihypertrophic effect of TSA in cultured cardiac myocytes.[8] One study, however, reported that TSA was capable of provoking cardiomyocyte growth in vitro.[30] Although an explanation for the different observations in cell culture models is not apparent at this time, we report in the present study that both TSA and Scriptaid blunt hypertrophic growth of the heart triggered by pressure stress in vivo.

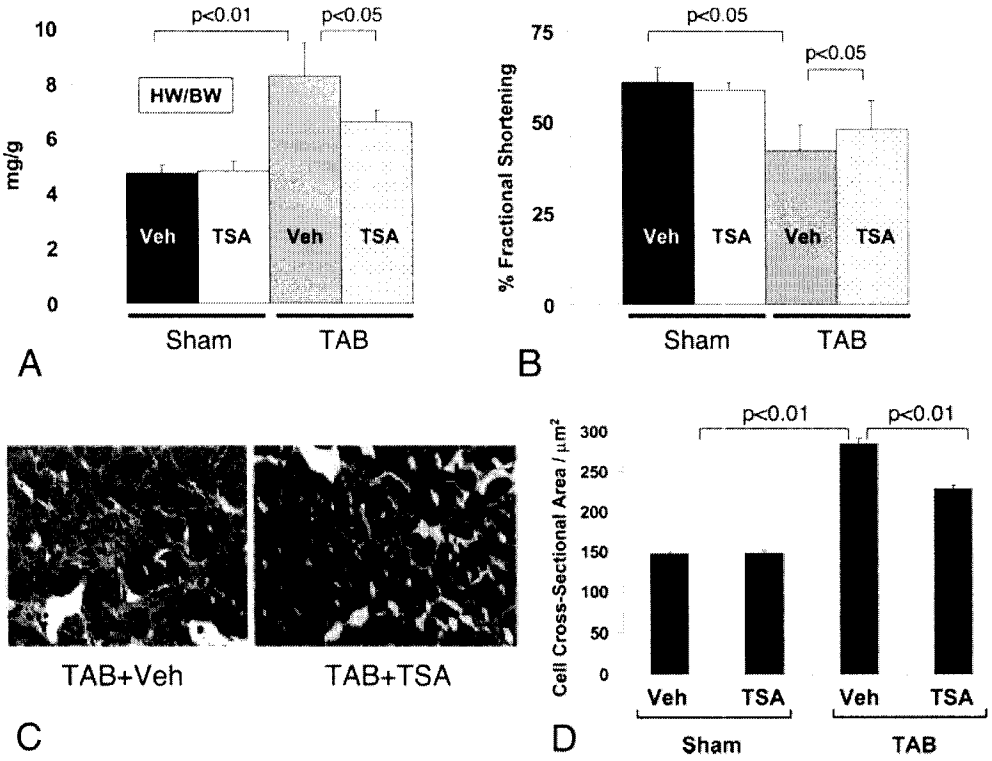

Figure 8. Long-term treatment with TSA is well tolerated. A, HW/BW ratios in hearts treated for 9 weeks as listed. Sham+Veh, n=7; sham+TSA, n=7; TAB+Veh, n=11; TAB+TSA, n=13. B, Percent fractional shortening measured at the end of the 9-week trial reveals statistically significant attenuation of pressure overload-induced systolic dysfunction in TAB hearts treated with TSA or vehicle. C, Representative fields of Masson's trichrome–stained tissue sections reveal marked accumulation of interstitial fibrosis (left) which is nearly abolished by TSA (right). D, Two-dimensional cardiomyocyte cross-sectional area measured as described. Sham+Veh (n=552 cells/3 hearts); sham+TSA (n=580/3); TAB+Veh (n=634/3); TAB+TSA (n=658/3).

Importantly, despite blunted hypertrophic growth in the setting of persistent afterload stress, ventricular size and performance were preserved, consistent with a growing literature pointing to suppression of pathological hypertrophy as a viable therapeutic strategy.[6]

The efficacy of HDAC inhibitors in cancer trials stems, in part, from their ability to induce tumor cell death. In the case of pathological cardiac growth, the HDAC inhibitors TSA and Na butyrate block myocyte hypertrophic growth and histone deacetylation at doses 10-fold lower than those capable of inducing cytotoxicity.[8] In experiments reported here, we found no evidence of drug-induced cell dropout or myocyte apoptosis.

Preserved Ventricular Function

We tested HDAC inhibitor therapy in both short-term (comparable in duration to the anticancer clinical trials presently underway) and long-term trials (as might be envisioned for antihypertrophy therapy). In both cases, we observed preservation of ventricular size and performance despite blunting of "compensatory" hypertrophy. This finding, in the presence of persistently elevated afterload, suggested a positive inotropic effect. This was confirmed in invasive hemodynamic studies where ESPVR, a measure of the intrinsic contractility of the left ventricle, was maintained in banded animals treated with TSA. One contributor to this action of TSA to preserve ventricular function may be its ability to blunt the pathological switch between MHC isoforms in stressed myocardium. This switch, where the adult isoform declines and the fetal isoform increases, is thought to contribute to the contractile dysfunction typically seen in hypertrophy.[19,20,31] It is of interest to elucidate mechanisms whereby HDAC inhibitors attenuate hypertrophy-associated switching of sarcomeric proteins, as this property holds promise as a strategy to increase myocardial performance.

Limitations of the Study

A precedent exists in the field of clinical oncology for the therapeutic application of drugs that suppress HDAC activity. In this setting, HDAC inhibitors have been shown to upregulate cell-cycle inhibitors (eg, p21), blocking both growth and proliferation of a wide variety of cell types. Indeed, numerous clinical trials are underway to test the use of HDAC inhibitors in cancer patients, and development of new HDAC inhibitors is a high priority in the pharmaceutical industry.[32] However, little is known about the effect of HDAC inhibitors on the hearts of these patients.

Aortic banding induces an abrupt increase in ventricular afterload. As such, it may not faithfully model the processes that occur in hypertension or aortic stenosis, where increased afterload typically develops gradually. Further, this study was designed as a hypertrophy-suppression trial; we did not study hypertrophy regression, which is the more typical clinical context in which antihypertrophic therapy would be envisioned. The fact that ventricular function was preserved when hypertrophy was blunted, however, even in the face of abrupt afterload increases, exceeding those observed clinically, suggests that these findings may have relevance to the clinical state.

Hypertension-induced cardiac hypertrophy is a common disease phenotype in our society, predisposing patients to ventricular dysfunction and circulatory failure. A growing body of evidence in rodent models indicates that inhibiting pathological hypertrophy in the face of hemodynamic stress maintains cardiac performance and enhances survival, pointing to the potential therapeutic benefit of strategies that suppress the hypertrophic process.[6] Indeed, while our paper was in review, Kee et al[33] reported similar hypertrophy-blocking effects of HDACi in animal models of cardiac hypertrophy. On the basis of these findings, HDAC inhibition may emerge as a promising antihypertrophic therapeutic strategy.

Acknowledgments

We thank Janet Johnstone for expert technical assistance.

Sources of Funding

This work was supported by grants from the Donald W. Reynolds Cardiovascular Clinical Research Center, the National Institutes of Health (HL-075173, HL-072016), and the American Heart Association (EI 0640084N).

Disclosures

None.

References

1. Jenuwein T, Allis CD. Translating the histone code. *Science*. 2001;293:1074–1080.
2. Johnson CA, Turner BM. Histone deacetylases: complex transducers of nuclear signals. *Semin Cell Dev Biol*. 1999;10:179–188.
3. Lu JR, McKinsey TA, Nicol RL, Olson EN. Signal-dependent activation of the MEF2 transcription factor by dissociation from histone deacetylases. *Proc Natl Acad Sci U S A*. 2000;97:4070–4075.
4. Zhang CL, McKinsey TA, Chang S, Antos CL, Hill JA, Olson EN. Class II histone deacetylases act as signal-responsive repressors of cardiac hypertrophy. *Cell*. 2002;110:479–488.
5. Gusterson RJ, Jazrawi E, Adcock IM, Latchman DS. The transcriptional co-activators CREB-binding protein (CBP) and p300 play a critical role in cardiac hypertrophy that is dependent on their histone acetyltransferase activity. *J Biol Chem*. 2003;278:6838–6847.
6. Frey N, Katus HA, Olson EN, Hill JA. Hypertrophy of the heart: a new therapeutic target? *Circulation*. 2004;109:1580–1589.
7. McKinsey TA, Olson EN. Cardiac histone acetylation: therapeutic opportunities abound. *Trends Genet*. 2004;20:206–213.
8. Antos CL, McKinsey TA, Dreitz M, Hollingsworth LM, Zhang CL, Schreiber K, Rindt H, Gorczynski RJ, Olson EN. Dose-dependent blockade to cardiomyocyte hypertrophy by histone deacetylase inhibitors. *J Biol Chem*. 2003;278:28930–28937.
9. Rockman HA, Ross RS, Harris AN, Knowlton KU, Steinhelper ME, Field LJ, Ross J Jr, Chien KR. Segregation of atrial-specific and inducible expression of an atrial natriuretic factor transgene in an in vivo murine model of cardiac hypertrophy [published correction appears in *Proc Natl Acad Sci U S A*. 1991;88:9907]. *Proc Natl Acad Sci U S A*. 1991;88:8277–8281.
10. Hill JA, Karimi M, Kutschke W, Davisson RL, Zimmerman K, Wang Z, Kerber RE, Weiss RM. Cardiac hypertrophy is not a required compensatory response to short-term pressure overload. *Circulation*. 2000;101:2863–2869.
11. Hill JA, Rothermel B, Yoo KD, Cabuay B, Demetroulis E, Weiss RM, Kutschke W, Bassel-Duby R, Williams RS. Targeted inhibition of calcineurin in pressure-overload cardiac hypertrophy: preservation of systolic function. *J Biol Chem*. 2002;277:10251–10255.
12. Tao W, Sherwood ER. Beta 2-microglobulin knockout mice treated with anti-asialoGM1 exhibit improved hemodynamics and cardiac contractile function during acute intra-abdominal sepsis. *Am J Physiol Regul Integr Comp Physiol*.. 2004;286:R569–R575.
13. Johnstone RW. Histone-deacetylase inhibitors: novel drugs for the treatment of cancer. *Nat Rev Drug Discov*. 2002;1:287–299.

14. Hubbert C, Guardiola A, Shao R, Kawaguchi Y, Ito A, Nixon A, Yoshida M, Wang XF, Yao TP. HDAC6 is a microtubule-associated deacetylase. *Nature*. 2002;417:455–458.
15. Brush MH, Guardiola A, Connor JH, Yao TP, Shenolikar S. Deactylase inhibitors disrupt cellular complexes containing protein phosphatases and deacetylases. *J Biol Chem*. 2004;279:7685–7691.
16. Rombouts K, Niki T, Greenwel P, Vandermonde A, Wielant A, Hellemans K, De Bleser P, Yoshida M, Schuppan D, Rojkind M, Geerts A. Trichostatin A, a histone deacetylase inhibitor, suppresses collagen synthesis and prevents TGF-beta(1)-induced fibrogenesis in skin fibroblasts. *Exp Cell Res*. 2002;278:184–197.
17. Carabello BA. Concentric versus eccentric remodeling. *J Card Fail*. 2002;8:S258–S263.
18. Shimizu G, Zile MR, Blaustein AS, Gaasch WH. Left ventricular chamber filling and midwall fiber lengthening in patients with left ventricular hypertrophy: overestimation of fiber velocities by conventional midwall measurements. *Circulation*. 1985;71:266–272.
19. Nakao K, Minobe W, Roden R, Bristow MR, Leinwand LA. Myosin heavy chain gene expression in human heart failure. *J Clin Invest*. 1997; 100:2362–2370.
20. Herron TJ, McDonald KS. Small amounts of alpha-myosin heavy chain isoform expression significantly increase power output of rat cardiac myocyte fragments. *Circ Res*. 2002;90:1150–1152.
21. McKinsey TA, Olson EN. Toward transcriptional therapies for the failing heart: chemical screens to modulate genes. *J Clin Invest*. 2005;115: 538–546.
22. Kook H, Lepore JJ, Gitler AD, Lu MM, Wing-Man Yung W, Mackay J, Zhou R, Ferrari V, Gruber P, Epstein JA. Cardiac hypertrophy and histone deacetylase-dependent transcriptional repression mediated by the atypical homeodomain protein Hop. *J Clin Invest*. 2003;112: 863–871.
23. Vogelauer M, Wu JS, Suka N, Grunstein M. Global histone acetylation and deacetylation in yeast. *Nature*. 2000;408:495–498.
24. Kaneda R, Ueno S, Yamashita Y, Choi YL, Koinuma K, Takada S, Wada T, Shimada K, Mano H. Genome-wide screening for target regions of histone deacetylases in cardiomyocytes. *Circ Res*. 2005;97:210–218.
25. McKinsey TA, Zhang CL, Olson EN. MEF2: a calcium-dependent regulator of cell division, differentiation and death. *Trends Biochem Sci*. 2002;27:40–47.
26. Han A, Pan F, Stroud JC, Youn HD, Liu JO, Chen L. Sequence-specific recruitment of transcriptional co-repressor Cabin1 by myocyte enhancer factor-2. *Nature*. 2003;422:730–734.
27. Kuwahara K, Saito Y, Ogawa E, Takahashi N, Nakagawa Y, Naruse Y, Harada M, Hamanaka I, Izumi T, Miyamoto Y, Kishimoto I, Kawakami R, Nakanishi M, Mori N, Nakao K. The neuron-restrictive silencer element-neuron-restrictive silencer factor system regulates basal and endothelin 1-inducible atrial natriuretic peptide gene expression in ventricular myocytes. *Mol Cell Biol*. 2001;21:2085–2097.
28. Antos CL, McKinsey TA, Frey N, Kutschke W, McAnally J, Shelton JM, Richardson JA, Hill JA, Olson EN. Activated glycogen synthase-3 beta suppresses cardiac hypertrophy in vivo. *Proc Natl Acad Sci U S A*. 2002; 99:907–912.
29. Kouzarides T. Acetylation: a regulatory modification to rival phosphorylation? *EMBO J*. 2000;19:1176–1179.
30. Alcendor RR, Kirshenbaum LA, Imai S, Vatner SF, Sadoshima J. Silent information regulator 2alpha, a longevity factor and class III histone deacetylase, is an essential endogenous apoptosis inhibitor in cardiac myocytes. *Circ Res*. 2004;95:971–980.
31. Miyata S, Minobe W, Bristow MR, Leinwand LA. Myosin heavy chain isoform expression in the failing and nonfailing human heart. *Circ Res*. 2000;86:386–390.
32. Villar-Garea A, Esteller M. Histone deacetylase inhibitors: understanding a new wave of anticancer agents. *Int J Cancer*. 2004;112:171–178.
33. Kee HJ, Sohn IS, Nam KI, Park JE, Qian YR, Yin Z, Ahn Y, Jeong MH, Bang YJ, Kim N, Kim JK, Kim KK, Epstein JA, Kook H. Inhibition of histone deacetylation blocks cardiac hypertrophy induced by angiotensin II infusion and aortic banding. *Circulation*. 2006;113:51–59.

CLINICAL PERSPECTIVE

In response to stress, the heart initially compensates with an adaptive hypertrophic increase in mass. Under prolonged stress, the heart undergoes apparently irreversible decompensation that results in dilation of the failing heart. Thus, there is great interest in developing novel treatment strategies to block hypertrophy and prevent heart failure. In the present study, we evaluated drugs that inhibit the activity of histone deacetylase (HDAC), a molecular regulator of gene transcription. Using 2 broad-spectrum HDAC inhibitors in a surgical model of pressure-overload–induced cardiac hypertrophy, we observed dose-responsive suppression of ventricular growth that was well tolerated in terms of clinical outcome and cardiac performance measures. In both short-term and long-term trials, cardiomyocyte growth was blocked, with no evidence of cell death or apoptosis. Fibrotic change was diminished in hearts treated with HDAC inhibitors, and collagen synthesis in isolated cardiac fibroblasts was blocked. Preservation of systolic function in the setting of blunted hypertrophic growth was documented by echocardiography and by invasive pressure measurements. Attenuation of the hypertrophy-associated switch of adult and fetal isoforms of myosin heavy chain expression was detected, which likely contributed to the preservation of systolic function in HDAC inhibitor–treated hearts. Together, these data suggest that HDAC inhibition is a viable therapeutic strategy that holds promise in the treatment of load-induced heart disease. Also, as HDAC inhibition is emerging as a potentially important therapy for a number of malignant tumors, our findings have relevance regarding cardiovascular effects of these drugs in cancer patients.

Suberoylanilide hydroxamic acid, a histone deacetylase inhibitor, ameliorates motor deficits in a mouse model of Huntington's disease

Emma Hockly*, Victoria M. Richon†, Benjamin Woodman*, Donna L. Smith*, Xianbo Zhou†, Eddie Rosa†, Kirupa Sathasivam*, Shabnam Ghazi-Noori*, Amarbirpal Mahal*, Philip A. S. Lowden‡, Joan S. Steffan§, J. Lawrence Marsh¶, Leslie M. Thompson§, Cathryn M. Lewis*, Paul A. Marks‖, and Gillian P. Bates*,**

*Medical and Molecular Genetics, Guy's, King's and St. Thomas' School of Medicine, King's College London, Eighth Floor Guy's Tower, Guy's Hospital, London SE1 9RT, United Kingdom; †Aton Pharma, Inc., 777 Old Saw Mill River Road, Tarrytown, NY 10591-6717; ‡School of Chemistry, University of Exeter, Stocker Road, Exeter EX4 4QD, United Kingdom; §Department of Psychiatry and Human Behavior, University of California, Gillespie 2121, Irvine, CA 92697-4260; ¶Department of Developmental and Cell Biology, University of California, 4244 McGaugh Hall, Irvine, CA 92697-2300; and ‖Cell Biology Program, Memorial Sloan-Kettering Cancer Center, 1275 York Avenue, New York, NY 10021

Contributed by Paul A. Marks, December 20, 2002

Huntington's disease (HD) is an inherited, progressive neurological disorder that is caused by a CAG/polyglutamine repeat expansion and for which there is no effective therapy. Recent evidence indicates that transcriptional dysregulation may contribute to the molecular pathogenesis of this disease. Supporting this view, administration of histone deacetylase (HDAC) inhibitors has been shown to rescue lethality and photoreceptor neurodegeneration in a *Drosophila* model of polyglutamine disease. To further explore the therapeutic potential of HDAC inhibitors, we have conducted preclinical trials with suberoylanilide hydroxamic acid (SAHA), a potent HDAC inhibitor, in the R6/2 HD mouse model. We show that SAHA crosses the blood–brain barrier and increases histone acetylation in the brain. We found that SAHA could be administered orally in drinking water when complexed with cyclodextrins. SAHA dramatically improved the motor impairment in R6/2 mice, clearly validating the pursuit of this class of compounds as HD therapeutics.

Huntington's disease (HD) is an inherited progressive neurological disorder caused by a CAG/polyglutamine (polyQ) expansion and is associated with selective cell death and the deposition of polyQ aggregates in the brain (1). Recent studies suggest that transcriptional dysregulation might play a role in HD pathogenesis (2–4) by decreasing several functions including histone acetyltransferase and Sp1 and TAFII130 activity (5–13). Although the molecular basis of transcriptional dysfunction in HD requires further dissection, transcriptional repression is the predominant result of dysregulation.

Histone deacetylases (HDACs) work in concert with histone acetyl transferases to modify chromatin and regulate transcription (14). HDAC inhibitors such as trichostatin A and suberoylanilide hydroxamic acid (SAHA) have been shown to act selectively on gene expression and are potent inducers of growth arrest, differentiation, and/or apoptotic cell death of transformed cells *in vitro* and *in vivo* (15–18). Recent studies in cell culture, yeast, and *Drosophila* models of polyQ disease have indicated that HDAC inhibitors might provide a useful class of agents to ameliorate the transcriptional changes in HD (9–11). For example, alleviation of transcriptional repression in *Drosophila* models either by genetic reduction of *Sin3A* corepressor activity or through administration of HDAC inhibitors was shown to rescue lethality and photoreceptor neurodegeneration (11).

Therapeutic trials in humans are challenging, because of the late onset, variability, and slow progression of HD. Therefore, before testing novel therapeutics in clinical trials, compounds must be rigorously and extensively evaluated in genetic HD mouse models, a wide range of which are now available (19). The R6/2 line (20, 21) has been used the most extensively for preclinical trials (22–25). The early onset of impairment (5–6 weeks), rapid progression of the disease (severely impaired at 12–14 weeks), and reproducibility of the phenotype makes it particularly suitable for this type of study.

Here we ask whether the beneficial effects of HDAC inhibitors in *Drosophila* models of polyQ disease can be reproduced in preclinical mouse trials. We show that SAHA can cross the blood–brain barrier and demonstrate bioactivity in brain tissue. SAHA has an effective concentration of $\approx$2.5 μM and is relatively insoluble in aqueous solution. We show that when complexed with 2-hydroxypropyl-β-cyclodextrin (HOP-β-CD), we are able to administer SAHA in drinking water and dramatically improve motor impairment in the R6/2 mouse model.

Methods

Drug Formulation. SAHA (Aton Pharma) was solubilized in 5 molar equivalents of HOP-β-CD (ICN) in water. In the main trial, 0.67 g of SAHA was added to a solution of 18 g of HOP-β-CD in 1 liter of water, heated until fully dissolved, and rapidly cooled on ice to room temperature. This solution was administered to the mice in place of drinking water and replaced weekly. SAHA solutions of various concentrations were prepared by maintaining the molar ratio between SAHA and HOP-β-CD. Placebo was an equivalent concentration of HOP-β-CD without SAHA.

Animals. Affected mice were hemizygous R6/2 females (20) [available from the Induced Mutant Resource, The Jackson Laboratory, code B6CBA-TgN (HDexon1)62] bred and reared in our colony by backcrossing R6/2 males to C57BL/6 $\times$ CBA F_1 females. Transgenic animals were identified before weaning by PCR of tail-tip DNA, and CAG repeat size was determined (26). Control mice were WT female littermates. Mice were weaned into their treatment groups at 4 weeks of age. All animals had unlimited access to rodent breeding chow (Special Diet Services, Witham, U.K.) from a food hopper and placebo or drug solution. From age 12 weeks, all animals were additionally given mash consisting of powdered chow mixed with the drug solution as given in the drinking bottle. The mice were subject to a 12-h light (08:00–20:00), 12-h dark (20:00–08:00) cycle. Living conditions and baseline characteristics of study groupings were rigorously standardized.

Organotypic Slice Culture Assay. Organotypic hippocampal slice cultures were established as described (27). SAHA in HOP-

Abbreviations: HD, Huntington's disease; SAHA, suberoylanilide hydroxamic acid; HDAC, histone deacetylase; polyQ, polyglutamine; HOP-β-CD, 2-hydroxypropyl-β-cyclodextrin.

**To whom correspondence should be addressed. E-mail: gillian.bates@kcl.ac.uk.

NEUROSCIENCE

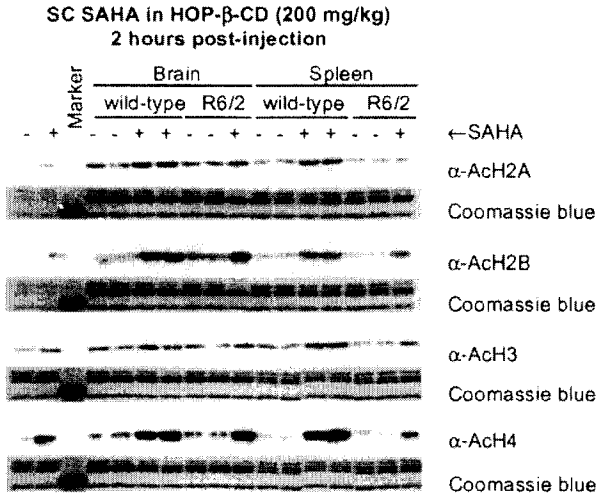

Fig. 1. SAHA crosses the blood–brain barrier and increases histone acetylation. Histones H2B and H4 are dramatically hyperacetylated 2 h post-s.c. administration of the SAHA HOP-β-CD complex in both brain and spleen. There is no difference in acetylation between genotypes.

β-CD solution was added to the culture medium from day 1 until the termination of the experiment at concentrations from 0.025 to 250 μM, and HOP-β-CD and media controls were included. We established that HOP-β-CD has no effect on polyQ aggregation over a 5-log concentration range (data not shown), and therefore the HOP-β-CD concentration required to complex 250 μM was used as the vehicle in this experiment. The medium was changed twice weekly, and slices were fixed at weekly intervals from 2 weeks in culture. The huntingtin aggregate load was assessed by quantitative indirect immunofluorescence (27), and results were analyzed by using the general linear model ANOVA with false discovery rate correction (28).

Behavioral Analysis. Rotarod impairment was assessed on a Ugo Basile 7650 accelerating Rotarod (Linton Instrumentation, Diss, U.K.), modified as described (29). Animals (R6/2: $n = 13$, WT: $n = 12$ per treatment group) were tested at 4 weeks of age to establish their baseline performance and again at 8, 10, and 12 weeks of age. Grip strength was measured once per fortnight (29), and animals were weighed weekly to the nearest 0.1 g. Statistical analysis of grip strength used ANOVA on the mean grip strength. Rotarod data were analyzed at each time point by using repeated measures in a linear mixed effects model (in S-plus).

Antibodies, Western Blotting, Histology, and Immunohistochemistry. Antibodies were as follows: huntingtin exon 1 protein (S830) (30); ubiquitin (DAKO); acetylated histone H2A (Lys-5) and acetylated histone H2B (Serotec); and acetylated histone H3 and acetylated histone H4 (Upstate Biotechnology, Lake Placid, NY). Histones were isolated from whole brain, and Western blots for histone acetylation (31) were as published. Brains for histology and immunohistochemistry were frozen in isopentane and stored at −80°C until required, and 15-μm sections were cut by using a cryostat (Bright Instrument, Huntingdon, U.K.). Immunohistochemistry was performed as described (27). Nissl staining was carried out by standard protocols (32), with the exception that frozen sections were postfixed in 4% paraformaldehyde for 30 min and washed in TBS (50 mM Tris·HCl, pH 7.5/0.9% NaCl) before staining.

Real-Time RT-PCR Analysis. RNA was prepared from whole brain by using the RNeasy mini kit (Qiagen, Crawley, U.K.) according

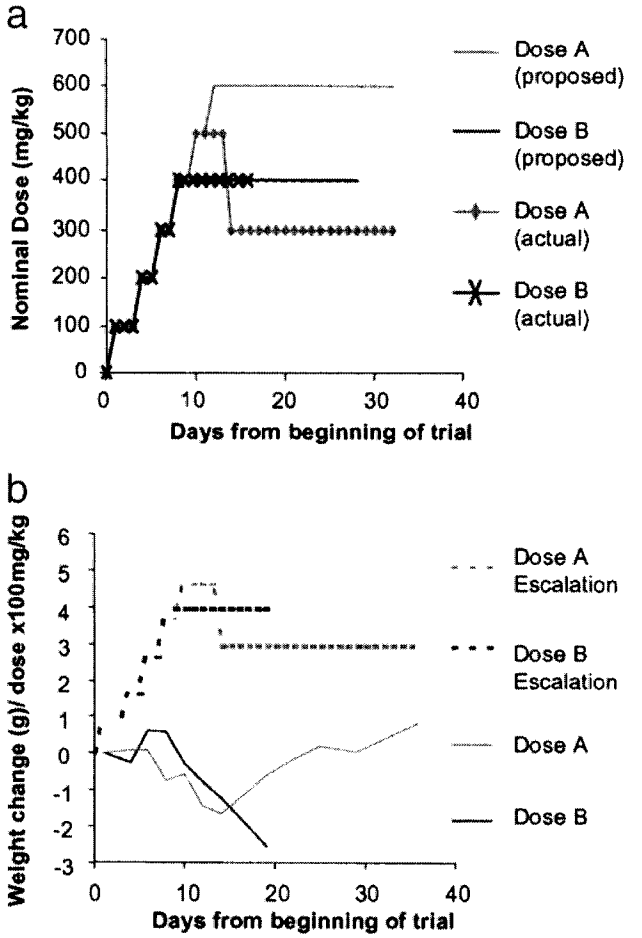

Fig. 2. Dose escalation strategy for oral SAHA administration in WT mice. (*a*) To determine the maximum dose of SAHA, which when complexed with HOP-β-CD could be administered to WT mice in drinking water, a dose escalation strategy was used (Table 1). Our initial intention was to assess the tolerability of 2.67 g/liter (400 mg/kg) and 4 g/liter (600 mg/kg). (*b*) Doses of 2.67 g/liter SAHA and above caused dramatic weight loss. On lowering the dose from 3.33 g/liter to 2 g/liter (300 mg/kg), the formulation was well tolerated.

to the manufacturer's recommendations. Real-time PCR was performed as described (33) by using the ABI Prism 7700 (Perkin–Elmer-Applied Biosystems). R6/2 transgene primers were: GCTGCACCGACCGTGAGT (forward), CAGGCTGCAGGGTTAC (reverse), and CAGCTCCCTGTCCCGGCGG (probe). Abl primers were: CAAATCCAAGAAGGGGCTCTCT (forward), TCGAGCTGCTTCGCTGAGA (reverse), and CCCTGCAGAGGCCAGTGGCATCT (probe).

Results

SAHA Crosses the Blood–Brain Barrier and Increases Histone Acetylation in Brain. Our initial experiments sought to determine whether SAHA crosses the blood–brain barrier. SAHA is relatively insoluble in aqueous solutions, and in previous mouse efficacy studies (31), it had been administered at doses up to 100 mg/kg i.p. in 100% DMSO or orally in the diet (34). The parenteral mode of administration was likely to be impractical in an efficacy study that required daily dosing, as DMSO is not well tolerated on repeated injection. Therefore, alternative vehicles for SAHA delivery were investigated and we found that SAHA is capable of forming a complex with HOP-β-CD with greatly enhanced aqueous solubility.

Increased levels of histone acetylation resulting from i.p.

Table 1. Strategy used to establish dosing regime for SAHA

Dosage	Genotype	Treatment	Route	Duration	Outcome
200 mg/kg	WT and R6/2	SAHA and placebo	s.c.	5 days	Irritation at injection site and death; study arm terminated
0.67 g/liter	WT and R6/2	SAHA and placebo	Oral	3 weeks	Mice survived; no significant weight loss
1.33 g/liter	WT and R6/2	SAHA and placebo	Oral	3 weeks	Mice survived; no significant weight loss
DE to 2 g/liter	WT	SAHA and placebo	Oral	3 weeks	Mice survived; no significant weight loss
DE to 2 g/liter	R6/2	SAHA and placebo	Oral	1 week	Mice lost weight; death occurred; study arm terminated
DE to 2 g/liter	R6/2	Placebo	Oral	1 week	Mice survived; no significant weight loss; study arm terminated
DE to 2.67 g/liter	WT	SAHA and placebo	Oral	3 weeks	Mice lost weight; study arm terminated

Summary of tolerability studies used to determine optimum dosing regime of SAHA. DE, dose escalation.

injection of 50 mg/kg SAHA are readily detected in tumor tissue (31). To determine whether comparable levels of acetylation are apparent in brain, either 100 mg/kg or 200 mg/kg SAHA in HOP-β-CD was administered to WT and R6/2 mice by a single s.c. injection, and brain and spleen samples were taken 2, 3, and 6 h after drug administration. For comparison, 100 mg/kg SAHA in either HOP-β-CD or DMSO was administered to WT and R6/2 by single i.p. injection. We found no difference in the degree of histone acetylation between untreated WT and R6/2 mice. Significant increases in histone acetylation could be detected only on s.c. administration of 200 mg/kg (Fig. 1). Administration of SAHA dramatically increased acetylation of histones H2B and H4 2 h postinjection (Fig. 1); this increase was maintained at 3 h and had diminished by 6 h (data not shown). With this regimen, increases in histone acetylation were similar in the brain and spleen and comparable between WT and R6/2 mice. Therefore, SAHA is able to cross the blood–brain barrier and mount a biological response.

SAHA Can Be Administered in Drinking Water. We had observed increases in histone acetylation in brain tissue after s.c. administration of 200 mg/kg SAHA in HOP-β-CD. However, at the

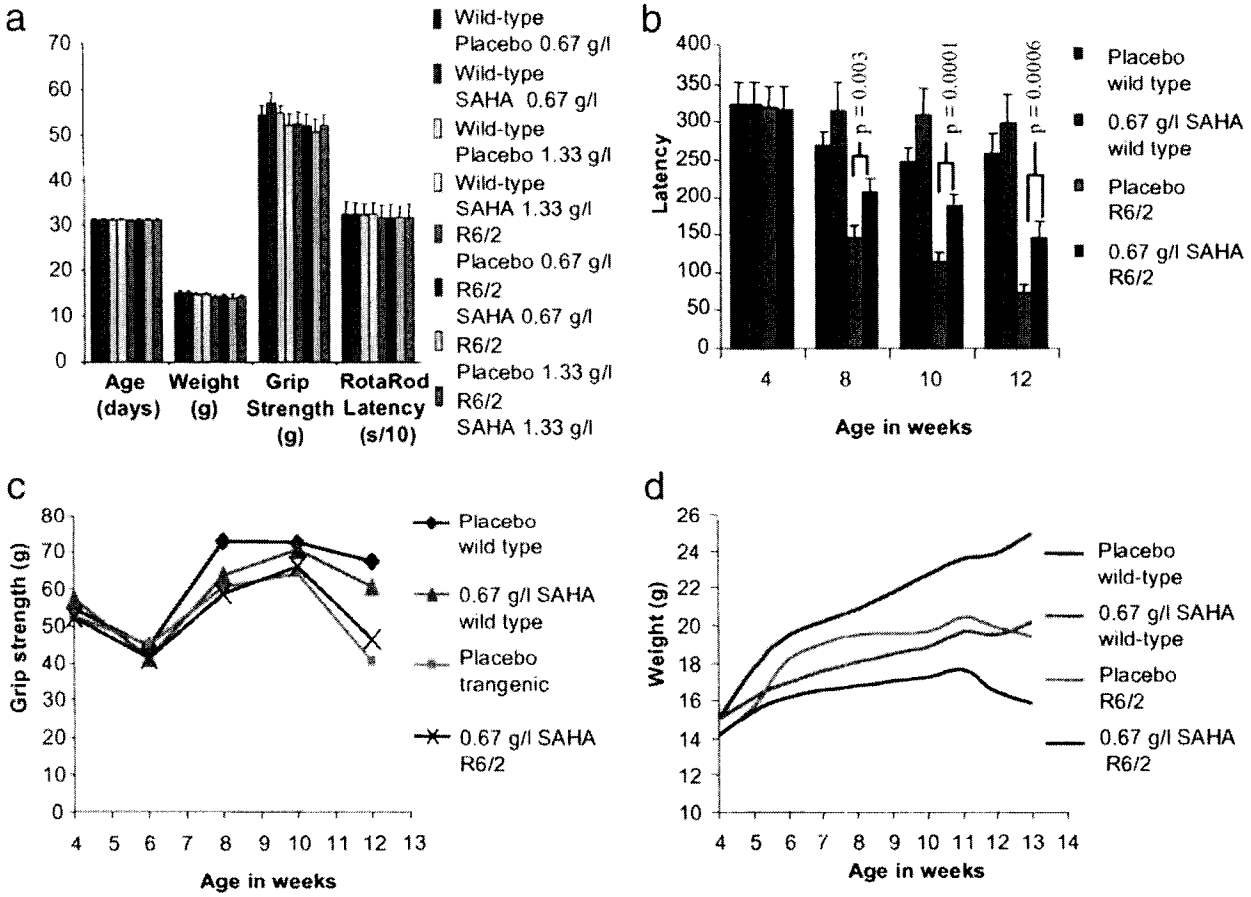

Fig. 3. Study design and outcome measures for the SAHA preclinical trial. (*a*) Comparison of the variation in age, weight, grip strength, and Rotarod performance between treatment groups and before SAHA or placebo administration. (*b*) R6/2 mice treated with 0.67 g/liter SAHA show a highly significant improvement in Rotarod performance. Latency to fall at 8 weeks of age was 207 versus 144 s ($P = 0.003$), at 10 weeks was 187 versus 113 s ($P = 0.0001$), and at 12 weeks was 144 versus 72 s ($P = 0.0006$). There was no significant difference in the performance of SAHA- and placebo-treated WT mice ($P = 0.28$ at 8 weeks, $P = 0.14$ at 10 weeks, $P = 0.38$ at 12 weeks). (*c*) Administration of SAHA does not improve mean grip strength in either WT or R6/2 mice. However, correction for weight revealed a relative improvement in grip strength in the R6/2 mice treated with SAHA ($P = 0.012$). (*d*) Both WT and R6/2 mice treated with SAHA failed to gain weight to the same extent as compared with their littermates taking the placebo control. Also, we found no treatment-related difference in the magnitude of weight loss of R6/2 mice compared with WT.

concentration required to achieve SAHA dosages of 100–200 mg/kg by injection, the cyclodextrin vehicle was viscous and difficult to handle. Therefore, we aimed to administer 200 mg/kg SAHA in HOP-β-CD in drinking water. Assuming that a 20-g mouse drinks 3 ml/day (35), this corresponds to a dose of 1.33 g/liter. Using a dose escalation strategy (Fig. 2*a*, Table 1), we found that we could administer oral doses of up to 2 g/liter in WT mice for up to 3 weeks starting at 6–7 weeks of age without significant weight loss or other adverse effects (Fig. 2*b*). However, application of this dosing regime to R6/2 mice resulted in weight loss, and one mouse (of four) died within 1 week. R6/2 mice on the HOP-β-CD placebo concentration corresponding to the 2 g/liter SAHA dose suffered no adverse effects, and R6/2 mice receiving up to 1.33 g/liter SAHA also showed no adverse symptoms (data not shown).

We therefore initiated an eight-arm efficacy trial comprising two drug (0.67 g/liter and 1.33 g/liter SAHA in HOP-β-CD) and two placebo arms (the corresponding HOP-β-CD concentrations) for WT and R6/2 mice. Drug administration commenced at 30 days of age after an initial testing week, which was used to sort the mice into well-matched treatment groups (Fig. 3a). Similarly, the CAG repeat size of the R6/2 mice was well matched at 200 ± 4 (SD). Unexpectedly, given the results of our pilot studies, both WT and R6/2 mice on 1.33 g/liter SAHA failed to gain weight, and after 2 weeks, weighed >20% less than mice on the corresponding placebo (data not shown). In addition, 2/12 WT and 2/13 R6/2 mice in this study arm died at ≈6 weeks of age. Therefore, we terminated the 1.33 g/liter SAHA and placebo arms of the experiment and proceeded only with the 0.67 g/liter and corresponding placebo groups.

SAHA Improves Motor Impairment in R6/2 Mice. The effect of SAHA administration on the R6/2 phenotype was assessed by Rotarod analysis of motor impairment, grip strength, and failure to gain weight. R6/2 mice treated with 0.67 g/liter SAHA showed a strong and consistent improvement in Rotarod performance as compared with those on placebo (Fig. 3*b*). The regression of mean latency times at weeks 8, 10, and 12 showed a highly significant difference between R6/2 mice on placebo and R6/2 mice on SAHA ($P = 0.0009$). There were no significant differences in performance of SAHA-treated WT mice compared with WT mice on placebo (Fig. 3*b*). The performance of both WT and R6/2 mice on placebo was consistent with findings from recent experiments by using the same protocol at all time points (R6/2: 8 weeks, 141–148 s; 12 weeks, 55–77 s) (WT: 8 weeks, 250–288 s; 12 weeks, 230–262 s). In contrast, the mean performance of R6/2 mice on SAHA from 8 weeks was well above the upper limit from all previous tests.

We found no significant difference in mean grip strength (Fig. 3*c*) between treated and placebo mice of either genotype at any age. WT mice in both treatment arms performed significantly better than R6/2 mice at 12 weeks of age (placebo: $P < 10^{-5}$; SAHA, $P < 0.02$). SAHA did not prevent the failure of R6/2 mice to gain weight (Fig. 3*d*). R6/2 mice were ≈20% lighter than WT mice at 13 weeks in both treatment groups. However, both WT and R6/2 mice treated with SAHA failed to gain weight to the same extent as their littermates taking the placebo control (both ≈18% at 13 weeks compared with appropriate placebo group). If this additional weight loss is caused by marginal toxicity of SAHA, it seems that there is no interaction with genotype: WT and R6/2 mice are equally affected. By regression analysis, weight was a significant positive predictor of mean grip strength in R6/2 ($P = 0.015$), but not in WT ($P = 0.229$) mice at 12 weeks of age. Entering both weight and treatment received into a multiple regression model revealed an improvement in grip strength at 12 weeks in R6/2 ($P = 0.012$) but not in WT ($P = 0.810$) mice treated with SAHA.

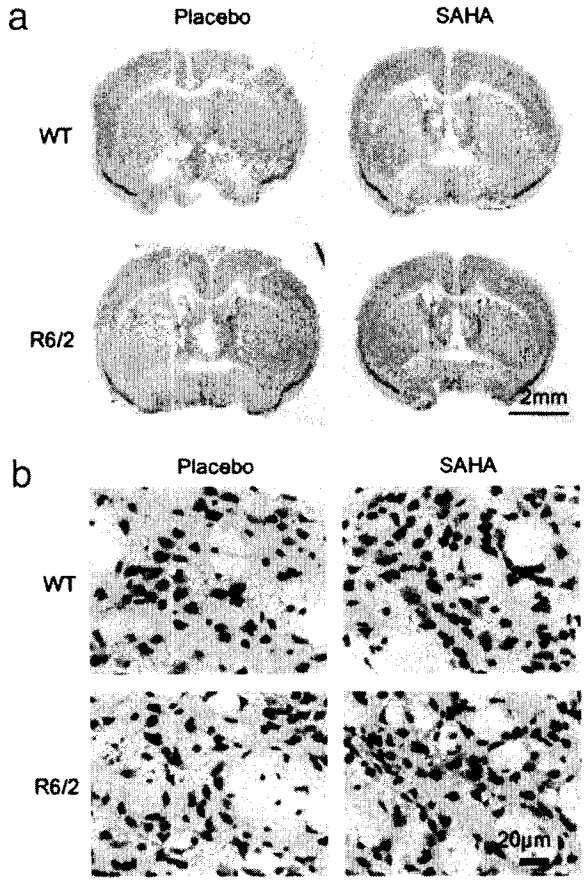

Fig. 4. Effect of SAHA on gross and cellular brain morphology. Frozen brain sections were cut from mice at 13 weeks of age, between Bregma 0 and 0.5 mm in the region of 0.26 mm and stained for Nissl substance with cresyl violet. (*a*) There is no marked change in gross morphology between R6/2 and WT mice in either treatment group. (*b*) Cellular atrophy is apparent in Nissl-stained sections from R6/2 brains. Treatment of R6/2 mice with SAHA resulted in Nissl staining more closely resembling that seen in WT mice.

Effects of SAHA on Gross and Cellular Brain Morphology. Examination of Nissl-stained brain sections revealed no overt difference in gross morphology between WT and R6/2 mice treated with either SAHA or placebo (Fig. 4*a*). Although the R6/2 mean brain weight was significantly less than WT (Student's *t* test: R6/2, 0.396 g; WT, 0.447 g; $P = 0.01$), there was no difference by regression analysis between mice treated with SAHA or placebo ($P = 0.777$). Similarly, there was no correlation with body weight within each genotype ($P = 0.243$).

Examination of the Nissl-stained sections under higher power revealed cellular atrophy in the R6/2 striatum as compared with WT (Fig. 4*b*) as documented (22). Treatment of R6/2 mice with SAHA resulted in Nissl staining more closely resembling that in WT mice.

SAHA Does Not Inhibit PolyQ Aggregation. To rule out that SAHA might exert its effects through the inhibition of polyQ aggregation, its ability to act as an aggregation inhibitor was tested in an organotypic slice culture assay (27). We have developed this technique to bridge the gap between wholly *in vitro* aggregation assays and preclinical trials and allow us to quantify aggregate formation in a system in which aggregates form at the same rate and in the same sequence as they do *in vivo*. Hippocampal slices were established from R6/2 neonates at P7 and cultured in the presence of SAHA complexed with HOP-β-CD at concentrations ranging from 0.025 to 250 μM over a period of 4 weeks.

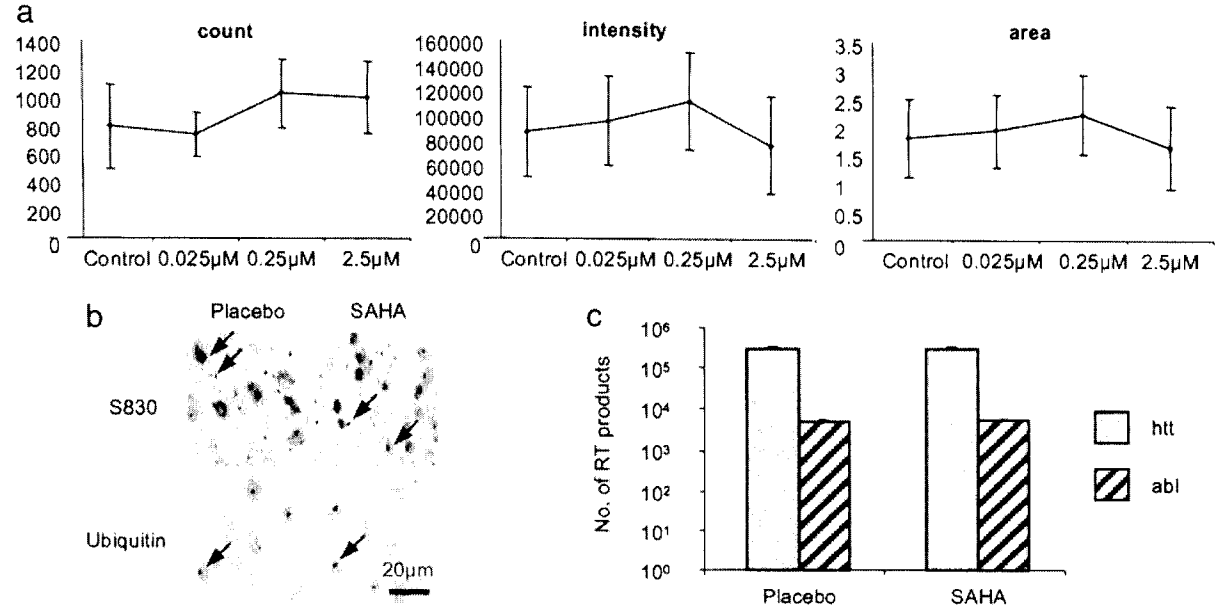

Fig. 5. SAHA does not inhibit polyQ aggregation or decrease transgene protein levels. (*a*) Quantification of aggregate load in hippocampal slice cultures that have been incubated in the presence of SAHA or HOP-β-CD for 4 weeks. SAHA has no effect on aggregate count, aggregate fluorescence intensity, or aggregate area. Error bars = SD. (*b*) Immunodetection of polyQ aggregates (arrow) using antibodies raised against huntingtin (S830) and ubiquitin in postmortem brains from R6/2 mice at 13 weeks of age that had been administered SAHA or placebo for 8 weeks (age 13 weeks). (*c*) Real-time PCR to determine the level of expression of the R6/2 transgene and *c-abl* oncogene. R6/2 mice (10–11 weeks) had been treated with 0.67 g/liter SAHA ($n = 7$) or placebo ($n = 7$) for 17 days.

Concentrations of 25 and 250 μM proved toxic. After 3 and 4 weeks there was no difference in the aggregate load between slices cultured in 0.025, 0.25, or 2.5 μM SAHA as compared with vehicle control (Fig. 5*a*). By a less quantitative immunohistochemical approach, no treatment-related differences in aggregate load were detected by using either antihuntingtin or antiubiquitin antibodies to immunoprobe sections of postmortem brains from R6/2 mice (Fig. 5*b*.).

SAHA Does Not Down-Regulate the R6/2 Transgene. To ensure that SAHA is not acting directly on the transgene promoter to down-regulate the R6/2 transgene, RNA was prepared from the brains of R6/2 mice that had been treated with either 0.67 g/liter SAHA or placebo for 17 days. Experiments were performed in triplicate, and the number of real-time PCR products was determined for the R6/2 transgene by using the *c-abl* oncogene as control (Fig. 5*c*). There is no difference in the level of expression of the R6/2 transgene ($P = 0.92$) or *c-abl* ($P = 0.69$) between SAHA- and placebo-treated mice.

Discussion

HDAC inhibitors have been shown to reduce polyQ toxicity in a *Drosophila* model of HD (11). We now show that the potent HDAC inhibitor, SAHA, dramatically improves Rotarod performance in the R6/2 HD mouse model. R6/2 mice treated with 0.67 g/liter SAHA demonstrated a significant improvement at 8 weeks of age after only 3 weeks of drug administration. At 12 weeks, the R6/2 mice taking SAHA were performing as well as the placebo group did at 8 weeks, indicating a delay by as much as 1 month in the decline in Rotarod performance. These results are yet more impressive given that our mice were housed in environmentally enriched conditions, which alone improved the Rotarod performance of R6/2 mice by ≈40% of the difference between R6/2 and WT (29). Therefore, drugs tested in our preclinical trials must cause significant additional improvement to be registered as effective. Our demonstration that SAHA treatment in part redresses the loss of striatal Nissl staining suggests that this may represent a neuropathological correlate of motor impairment.

SAHA is a small hydrophobic molecule and its relative insolubility in aqueous solution posed considerable difficulties. To combat this, we determined that SAHA is capable of forming a complex with HOP-β-CD with greatly enhanced aqueous solubility. Cyclodextrins are doughnut-shaped molecules consisting of six (α), seven (β), or eight (γ) glucose units linked by α-1,4 glycosidic bonds with their hydrophobic faces innermost. Small hydrophobic molecules can enter the central cavity to form a complex with the cyclodextrin. Because the hydrophilic surfaces of the cyclodextrins face outward, aqueous solubility is imparted on the complexes. Complexation with cyclodextrins can have additional benefits. These include a reduction in drug toxicity and irritation at the site of administration, masking of unpleasant tastes, and alteration of the pharmacokinetic profile of a drug, often increasing the half-life. HOP-β-CD is a nontoxic semisynthetic cyclodextrin, which is widely used *in vitro* and *in vivo* as a drug carrier in both enteral and parenteral formulations (36).

SAHA did not ameliorate the failure of R6/2 mice to gain weight, possibly reflecting its narrow therapeutic window with beneficial effects being masked by its toxicity. When SAHA administration was initiated at 30 days, doses ≥1.33 g/liter were toxic to both WT and R6/2 mice. Adverse effects were also seen in both WT and R6/2 mice at the effective dose of 0.67 g/liter, with mice failing to gain weight at the same rate as placebo-treated mice. However, despite this inherent toxicity, no R6/2 mice or WT mice died before the termination of the experiments at 13 weeks, and maintenance of grip strength in SAHA-treated R6/2 mice may indicate a sparing of muscle atrophy.

This study corroborates the use of HDAC inhibitors as therapeutic compounds for HD. Our demonstration that SAHA administration increases histone acetylation supports the hypothesis that it acts by redressing transcriptional repression. Although our results demonstrate that the identification of potential therapeutic compounds in *Drosophila* models can translate to preclinical mouse trials, we would caution against

proceeding too rapidly to clinical trials. Demonstration of efficacy with SAHA is particularly encouraging as this drug is $\approx 10^3$ fold more potent than the butyrate class of HDAC inhibitors [on a molar basis as an inhibitor of HDAC activity (15)] that are also under consideration. However, novel hydroxamic acid derivatives with enhanced activity as potential HD therapeutics also should be assessed.

We thank Nancy Wexler and the Hereditary Disease Foundation for discussions and inspiration and Caroline Whitehouse and David Grimwade for help with real-time PCR. This work was supported by grants from the Wellcome Trust (Grants 051897, 060360, and 066270), the Hereditary Disease Foundation, the Huntington's Disease Society of America, the Human Frontiers Science Program (Grant RG0132), the Medical Research Council (Grant G9800001), the DeWitt Wallace Fund for Memorial Sloan–Kettering Cancer Center, the National Institutes of Health (Grant CA-0974823), and the Kleberg Foundation. Memorial Sloan–Kettering Cancer Center and Columbia University jointly hold the patents on the hydroxamic hybrid polar compounds, including SAHA, which are exclusively licensed to Aton Pharma, Inc., of which P.A.M. and V.M.R. are founders. Both institutions and the founders have an equity position in Aton Pharma, Inc.

1. Bates, G. P., Harper, P. S. & Jones, A. L., eds. (2002) *Huntington's Disease, Oxford Monographs on Medical Genetics* (Oxford Univ. Press, Oxford).
2. Cha, J. H., Kosinski, C. M., Kerner, J. A., Alsdorf, S. A., Mangiarini, L., Davies, S. W., Penney, J. B., Bates, G. P. & Young, A. B. (1998) *Proc. Natl. Acad. Sci. USA* **95,** 6480–6485.
3. Luthi-Carter, R., Strand, A., Peters, N. L., Solano, S. M., Hollingsworth, Z. R., Menon, A. S., Frey, A. S., Spektor, B. S., Penney, E. B., Schilling, G., *et al.* (2000) *Hum. Mol. Genet.* **9,** 1259–1271.
4. Luthi-Carter, R., Hanson, S. A., Strand, A. D., Bergstrom, D. A., Chun, W., Peters, N. L., Woods, A. M., Chan, E. Y., Kooperberg, C., Krainc, D., *et al.* (2002) *Hum. Mol. Genet.* **11,** 1911–1926.
5. Kazantsev, A., Preisinger, E., Dranovsky, A., Goldgaber, D. & Housman, D. (1999) *Proc. Natl. Acad. Sci. USA* **96,** 11404–11409.
6. Steffan, J. S., Kazantsev, A., Spasic-Boskovic, O., Greenwald, M., Zhu, Y. Z., Gohler, H., Wanker, E. E., Bates, G. P., Housman, D. E. & Thompson, L. M. (2000) *Proc. Natl. Acad. Sci. USA* **97,** 6763–6768.
7. Shimohata, T., Nakajima, T., Yamada, M., Uchida, C., Onodera, O., Naruse, S., Kimura, T., Koide, R., Nozaki, K., Sano, Y., *et al.* (2000) *Nat. Genet.* **26,** 29–36.
8. Nucifora, F. C., Jr., Sasaki, M., Peters, M. F., Huang, H., Cooper, J. K., Yamada, M., Takahashi, H., Tsuji, S., Troncoso, J., Dawson, V. L., *et al.* (2001) *Science* **291,** 2423–2428.
9. McCampbell, A., Taye, A. A., Whitty, L., Penney, E., Steffan, J. S. & Fischbeck, K. H. (2001) *Proc. Natl. Acad. Sci. USA* **98,** 15179–15184.
10. Hughes, R. E., Lo, R. S., Davis, C., Strand, A. D., Neal, C. L., Olson, J. M. & Fields, S. (2001) *Proc. Natl. Acad. Sci. USA* **98,** 13201–13206.
11. Steffan, J. S., Bodai, L., Pallos, J., Poelman, M., McCampbell, A., Apostol, B. L., Kazantsev, A., Schmidt, E., Zhu, Y. Z., Greenwald, M., *et al.* (2001) *Nature* **413,** 739–743.
12. Li, S. H., Cheng, A. L., Zhou, H., Lam, S., Rao, M., Li, H. & Li, X. J. (2002) *Mol. Cell. Biol.* **22,** 1277–1287.
13. Dunah, A. W., Jeong, H., Griffin, A., Kim, Y. M., Standaert, D. G., Hersch, S. M., Mouradian, M. M., Young, A. B., Tanese, N. & Krainc, D. (2002) *Science* **296,** 2238–2243.
14. Marks, P., Rifkind, R. A., Richon, V. M., Breslow, R., Miller, T. & Kelly, W. K. (2001) *Nat. Rev. Cancer* **1,** 194–202.
15. Richon, V. M., Emiliani, S., Verdin, E., Webb, Y., Breslow, R., Rifkind, R. A. & Marks, P. A. (1998) *Proc. Natl. Acad. Sci. USA* **95,** 3003–3007.
16. Richon, V. M., Sandhoff, T. W., Rifkind, R. A. & Marks, P. A. (2000) *Proc. Natl. Acad. Sci. USA* **97,** 10014–10019.
17. Marks, P. A., Richon, V. M. & Rifkind, R. A. (2000) *J. Natl. Cancer Inst.* **92,** 1210–1216.
18. Marks, P. A., Rifkind, R. A., Richon, V. M. & Breslow, R. (2001) *Clin. Cancer Res.* **7,** 759–760.
19. Bates, G. P. & Murphy, K. P. (2002) in *Huntington's Disease, Oxford Monographs on Medical Genetics,* eds. Bates, G. P., Harper, P. S. & Jones, A. L. (Oxford Univ. Press, Oxford), pp. 387–426.
20. Mangiarini, L., Sathasivam, K., Seller, M., Cozens, B., Harper, A., Hetherington, C., Lawton, M., Trottier, Y., Lehrach, H., Davies, S. W. & Bates, G. P. (1996) *Cell* **87,** 493–506.
21. Davies, S. W., Turmaine, M., Cozens, B. A., DiFiglia, M., Sharp, A. H., Ross, C. A., Scherzinger, E., Wanker, E. E., Mangiarini, L. & Bates, G. P. (1997) *Cell* **90,** 537–548.
22. Ferrante, R. J., Andreassen, O. A., Jenkins, B. G., Dedeoglu, A., Kuemmerle, S., Kubilus, J. K., Kaddurah-Daouk, R., Hersch, S. M. & Beal, M. F. (2000) *J. Neurosci.* **20,** 4389–4397.
23. Ferrante, R. J., Andreassen, O. A., Dedeoglu, A., Ferrante, K. L., Jenkins, B. G., Hersch, S. M. & Beal, M. F. (2002) *J. Neurosci.* **22,** 1592–1599.
24. Chen, M., Ona, V. O., Li, M., Ferrante, R. J., Fink, K. B., Zhu, S., Bian, J., Guo, L., Farrell, L. A., Hersch, S. M., *et al.* (2000) *Nat. Med.* **6,** 797–801.
25. Karpuj, M. V., Becher, M. W., Springer, J. E., Chabas, D., Youssef, S., Pedotti, R., Mitchell, D. & Steinman, L. (2002) *Nat. Med.* **8,** 143–149.
26. Mangiarini, L., Sathasivam, K., Mahal, A., Mott, R., Seller, M. & Bates, G. P. (1997) *Nat. Genet.* **15,** 197–200.
27. Smith, D. L., Portier, R., Woodman, B., Hockly, E., Mahal, A., Klunk, W. E., Li, X. J., Wanker, E., Murray, K. D. & Bates, G. P. (2001) *Neurobiol. Dis.* **8,** 1017–1026.
28. Hochberg, Y. & Benjamini, Y. (1990) *Stat. Med.* **9,** 811–818.
29. Hockly, E., Cordery, P. M., Woodman, B., Mahal, A., Van Dellen, A., Blakemore, C., Lewis, C. M., Hannan, A. J. & Bates, G. P. (2002) *Ann. Neurol.* **51,** 235–242.
30. Sathasivam, K., Woodman, B., Mahal, A., Bertaux, F., Wanker, E. E., Shima, D. T. & Bates, G. P. (2001) *Hum. Mol. Genet.* **10,** 2425–2435.
31. Butler, L. M., Agus, D. B., Scher, H. I., Higgins, B., Rose, A., Cordon-Cardo, C., Thaler, H. T., Rifkind, R. A., Marks, P. A. & Richon, V. M. (2000) *Cancer Res.* **60,** 5165–5170.
32. Bancroft, J. D. & Stevens, A. (1990) *Theory and Practice of Histological Techniques* (Churchill Livingstone, New York), 3rd Ed.
33. Grimwade, D., Outram, S. V., Flora, R., Ings, S. J., Pizzey, A. R., Morilla, R., Craddock, C. F., Linch, D. C. & Solomon, E. (2002) *Cancer Res.* **62,** 4730–4735.
34. Cohen, L. A., Amin, S., Marks, P. A., Rifkind, R. A., Desai, D. & Richon, V. M. (1999) *Anticancer Res.* **19,** 4999–5005.
35. Wolfensohn, S. & Lloyd, M. (1998) *Handbook of Laboratory Animal Management and Welfare* (Blackwell, Oxford).
36. Uekama, K., Hirayama, F. & Irie, T. (1998) *Chem. Rev.* **98,** 2045–2076.

Two histone deacetylase inhibitors, trichostatin A and sodium butyrate, suppress differentiation into osteoclasts but not into macrophages

Md. Mizanur Rahman, Akiko Kukita, Toshio Kukita, Takeo Shobuike, Takahiro Nakamura, and Osamu Kohashi

Histone deacetylase (HDAC) inhibitors are emerging as a new class of anticancer therapeutic agents and have been demonstrated to induce differentiation in some myeloid leukemia cell lines. In this study, we show that HDAC inhibitors have a novel action on osteoclast differentiation. The effect of 2 HDAC inhibitors, trichostatin A (TSA) and sodium butyrate (NaB), on osteoclastogenesis was investigated using rat and mouse bone marrow cultures and a murine macrophage cell line RAW264. Both TSA and NaB inhibited the formation of preosteoclast-like cells (POCs) and multinucleated osteoclast-like cells (MNCs) in rat bone marrow culture. By reverse transcription-polymerase chain reaction analysis, TSA reduced osteoclast-specific mRNA expression of cathepsin K and calcitonin receptor (CTR). In contrast, TSA and NaB did not affect the formation of bone marrow macrophages (BMMs) induced by macrophage colony-stimulating factor as examined by nonspecific esterase staining. Fluorescence-activated cell sorting analysis showed that TSA did not affect the surface expression of macrophage markers for CD11b and F4/80 of BMMs. TSA and NaB also inhibited osteoclast formation and osteoclast-specific mRNA expression in RAW264 cells stimulated with receptor activator of nuclear factor-κB (NF-κB) ligand (RANKL). Transient transfection assay revealed that TSA and NaB dose dependently reduced the sRANKL-stimulated or tumor necrosis factor α (TNF-α)–stimulated transactivation of NF-κB–dependent reporter genes. The treatment of RAW264 cells with TSA and NaB inhibited TNF-α–induced nuclear translocation of NF-κB and sRANKL-induced activation of p38 mitogen-activated protein kinase (MAPK) signals. These data suggest that both TSA and NaB exert their inhibitory effects by modulating osteoclast-specific signals and that HDAC activity regulates the process of osteoclastogenesis. (Blood. 2003;101:3451-3459)

Introduction

Histone deacetylase (HDAC) inhibitors are known as agents that modulate the expression of genes by increasing histone acetylation, thereby regulating chromatin structure and transcription.[1,2] However, these inhibitors were not discovered based on their ability to inhibit HDAC activity. HDAC inhibitors include several structurally diverse natural products. Currently, there are several classes of HDAC inhibitors, including butyrate, hydroxamic acid, benzamide, and cyclic peptides. The simplest compound, butyrate, is a short-chain fatty acid derived from bacterial metabolism of dietary fiber in the colon. Butyrate was thought to be important for proper epithelial cell regulation, but was also found to have an antiproliferative and differentiation-inducing activity on various human colon carcinoma cells, normal cells, and neoplastic cells.[3-5] On the other hand, a hydroxamic acid, trichostatin A (TSA), is a more potent HDAC inhibitor that was identified as having potential therapeutic value against cancer in screens for agents that induce differentiation of murine erythroleukemia cells.[6,7] These HDAC inhibitors induce differentiation, inhibit cell proliferation, and induce apoptosis of tumor cells in cultures and animal models[3-7,8] and are emerging as a new class of potential therapeutic agents for the treatment of solid and hematologic malignancies.

The effect of both sodium butyrate (NaB) and TSA on myeloid cell differentiation was well investigated using human promyelocytic leukemia cell lines, HL-60, U937, and a novel myeloid cell line, SN-1.[3,9,10] NaB treatment enhanced the promoter activity of a myeloid marker, the integrin CD11c/CD18 gene, in U937 cells and triggered differentiation of these 3 cell lines toward monocytic lineage.[11,12] TSA alone showed a minimal effect on the expression of other monocyte cell surface markers, CD14 and CD11b, but TSA and 9-*cis*-retinoic acid (RA) synergistically stimulated the expression of CD14 in HL-60 cells.[13] Likewise, the stimulatory effect of HDAC inhibitors on cell differentiation has been well investigated. In contrast, little is known about whether these factors have also an inhibitory effect on the differentiation of cells. Recently, it has been reported that another HDAC inhibitor, suberoylanilide hydroxamic acid (SAHA), represses the expression of cytokines such as tumor necrosis factor α (TNF-α) and interferon γ (IFN-γ) when human peripheral blood mononuclear cells (PBMCs) are stimulated with lipopolysaccharide (LPS).[14] In addition, NaB and TSA have also been found to suppress activation of nuclear factor κB (NF-κB) in colon cells.[5] These results suggest that HDAC inhibitors may exhibit anti-inflammatory properties.[5,15,16] Thus, HDAC inhibitors not only up-regulate but also down-regulate the expression of genes.

Osteoclasts are bone-resorptive multinucleated cells derived from hematopoietic stem cells.[17,18] Differentiation of osteoclasts is regulated by soluble or membrane-bound molecules expressed by osteoblasts and stromal cells in bone microenvironment.[19] One

From the Department of Microbiology, Saga Medical School, Saga, Japan; and Section of Oral Cellular and Molecular Biology, Division of Oral Biological Science, Kyushu University, Kyushu, Japan.

Submitted August 28, 2002; accepted December 18, 2002. Prepublished online as *Blood* First Edition Paper, January 2, 2003; DOI 10.1182/blood-2002-08-2622.

Supported in part by a Grant for Scientific Research from the Japanese Ministry of Education, Science and Culture (project no.13671942).

M.M.R. and A.K. contributed equally to this work.

Reprints: Akiko Kukita, Department of Microbiology, Saga Medical School, Nabeshima 5-1-1, Saga, 849-8501, Japan; e-mail: kukita@post.saga-med.ac.jp.

The publication costs of this article were defrayed in part by page charge payment. Therefore, and solely to indicate this fact, this article is hereby marked "advertisement" in accordance with 18 U.S.C. section 1734.

such factor, receptor activator of NF-κB ligand (RANKL), a membrane-bound member of the TNF family, is essential for osteoclast differentiation. RANKL interacts with its receptor, RANK, on osteoclast progenitor cells and stimulates the signaling pathway for osteoclastogenesis.[20] Recent studies have shown that the ligation of RANK with RANKL recruits TNF receptor–associated factors (TRAFs) such as TRAF6, which activates NF-κB and the mitogen-activated protein kinase (MAPK), c-jun N-terminal kinase (JNK) pathways.[21,22] The role of NF-κB and TRAF6 in osteoclastogenesis has been shown by gene disruption studies.[23-25] Other types of MAPKs, extracellular signal–regulated kinases (ERKs) and p38 MAPK, are also known to be activated by stimulation with RANKL.[26,27] Recently, several investigators have reported that a p38 MAPK–specific inhibitor, SB203580, specifically inhibits osteoclast differentiation, suggesting that the p38 MAPK pathway also plays an important role in osteoclastogenesis.[26,27]

The cell lineage of osteoclasts is very close to that of macrophages, and both macrophages and osteoclasts are considered to be generated from common progenitor cells. Some macrophage cell lines can differentiate into osteoclasts in the presence of RANKL or in coculture with osteoblasts.[28-30] In recent work, we have reported that the formation of mononuclear osteoclast precursor cells (POCs) and multinucleated osteoclasts (MNCs) were modulated by the addition of factors such as interleukin 15 (IL-15), IL-10, RANKL, and TNF-α to rat bone marrow culture systems.[31-33] Because both NaB and TSA are able to induce monocyte differentiation in some hematopoietic cell lines, such agents may influence the differentiation of osteoclasts. In addition, it is not well known whether these agents have any effect on the differentiation of hematopoietic cells in primary bone marrow culture systems. We therefore attempted to examine the effect of TSA or NaB on osteoclast differentiation, using a rat bone marrow culture system. Surprisingly, we found that these HDAC inhibitors specifically suppressed osteoclast differentiation but did not affect macrophage formation. We have also investigated whether TSA or NaB affects NF-κB and MAPK signaling pathways that are stimulated with RANKL. Both TSA and NaB inhibited these signal activations.

Materials and methods

Materials

Male Sprague Dawley rats and ddY mice, aged 5 to 7 weeks, were obtained from Seac Yoshitomi (Fukuoka, Japan). α-Minimum essential medium (α-MEM) was purchased from Gibco (Grand Island, NY). Fetal calf serum (FCS) was purchased from Biowhittaker (Walkersville, MD). 1α,25-Dihydroxy vitamin D_3 (1α,25-$(OH)_2D_3$) was purchased from Bimol (Plymouth Meeting, PA). Recombinant human TNF-α was purchased from Boehringer Mannheim (Mannheim, Germany). Recombinant human soluble RANKL (sRANKL) and human macrophage colony-stimulating factor (hM-CSF) were purchased from Pepro-Tech (London, United Kingdom). The cytochemical staining kits for tartrate-resistant acid phosphatase (TRAP) and nonspecific esterase (NSE) staining were obtained from Sigma (St Louis, MO). TSA and NaB were purchased from Sigma. Rat monoclonal antibody, antimouse F4/80 (CI:A3-1) was purchased from BMA Biomedicals (Rheinstrasse, Switzerland). Fluorescein isothiocyanate (FITC)–conjugated rat monoclonal antibody, antimouse CD11b (Mac-1; M1.70) was purchased from Immunotech (Marseille, France). Rabbit polyclonal antibodies against NF-κB p65 and phosphorylated p38 (Tyr 182)–R and mouse monoclonal antibody against actin (C-2) were purchased from Santa Cruz Biotechnology (Santa Cruz, CA).

Bone marrow cell culture

Cultures of rat bone marrow cells were carried out as described by Kukita et al.[34,35] Briefly, bone marrow cells were isolated from tibias and femurs of rats. For the formation of MNCs, whole bone marrow cells were cultured in 24-well culture plates (Falcon, Lincoln Park, NJ) for 5 days in α-MEM containing 15% FCS in the presence of 10^{-8} M 1α,25$(OH)_2D_3$ and 10% (vol/vol) heat-treated conditioned medium derived from rat osteoblastic cell line ROS17/2.8 (htROSCM), as described by Kukita et al.[34] For the formation of POCs, stroma-free bone marrow cells (2×10^6 cells/mL) were cultured in 96-well culture plates (Falcon) for 4 days in α-MEM containing 15% FCS in the presence of 10^{-8} M 1α,25$(OH)_2D_3$ and 10% (vol/vol) heat-treated conditioned medium and TNF-α (10 ng/mL) as described previously.[33,35] In some cultures, stroma-free bone marrow cells were cultured for 4 days in the presence of M-CSF (1 ng/mL) to induce macrophage cell formation. In the cultures of mouse bone marrow, cells were suspended in α-MEM containing 15% FCS and cultured in 48-well plates (1×10^6 cells/mL). Osteoclast differentiation was induced in the presence of M-CSF (50 ng/mL) and sRANKL (50 ng/mL) for 4 days of culture. For the formation of bone marrow macrophages, cells were cultured in the presence of M-CSF (50 ng/mL) for 3 days. Various concentrations of TSA or NaB were added after 24 hours of culture. At the end of the culture, the cells were fixed and then stained using a commercial kit for TRAP or NSE, marker enzymes for osteoclasts or macrophages, respectively. $TRAP^+$ cells with more than 3 nuclei were counted as MNCs, and $TRAP^+$ mononuclear cells formed in stroma-free rat bone marrow cells were counted as POCs.

Culture of macrophage cell line

RAW-D is a subclone of murine macrophage cell line RAW264 and has high potential to differentiate into osteoclasts (Watanabe T et al, unpublished data, 2003). RAW-D cells were cultured in α-MEM containing 10% FCS. For osteoclast differentiation, cells were cultured at a density of 1.5×10^5 cells/mL in the presence of sRANKL for 3 days. For immunoblotting, RAW-D cells were preincubated with TSA (100 nM) or NaB (1 mM) for 24 hours, then stimulated with TNF-α (100 ng/mL) or sRANKL (100 ng/mL) for 30 minutes.

Flow cytometry

At the end of culture, adherent mouse bone marrow cells or RAW-D cells were harvested with 0.02% EDTA (ethylenediaminetetraacetic acid) in phosphate-buffered saline (PBS). For staining for Mac-1 antigen, cells were stained with FITC-conjugated anti-CD11b (Mac-1) monoclonal antibody. For staining for F4/80 antigen, cells were incubated with rat antimouse F4/80 antibody, followed by incubation with a second antibody, FITC-conjugated antirat IgG. Cells were then analyzed by flow cytometry (FACScan; Becton Dickinson, Erembodegem, Belgium).

RT-PCR analysis

Nonadherent rat bone marrow cells (1.1×10^7) or RAW-D cells (1.5×10^5 cells/mL) were cultured in 60-mm tissue culture dishes (Falcon) in the presence of various factors and TSA or NaB for 4 days or 3 days, respectively. Total RNA was extracted by using a commercial kit (Isogen; Nippon Gene, Toyama, Japan) and subjected to polymerase chain reaction (PCR) using a reverse transcription-PCR (RT-PCR) kit (Takara, Kyoto, Japan). The following primers were used for RT-PCR analysis: mouse calcitonin receptor (CTR; sense, 5′-TTTCAAGAACCTTAGCTGC-CAGAG-3′, antisense, 5′-CAAGGCACGGACAATGTTGAGAAG-3′)[36]; mouse cathepsin K (sense 5′-ATGTGGGGGCTCAAGGTT-3′, antisense, 5′-CCACAAGATTCTGGGGACTC3′); rat CTR (sense 5′-AAGAACAT-GTT(C/T)CT(C/G/T)ACTTA-3′, antisense, 5′-ACAAACTGGA(T/C)(T/G)CCCAGCAGGGGCAC-3′)[37]; rat cathepsin K (sense, 5′-CAGTGTGGT-TCCTGTTGGG-3, antisense, 5′-ACATCTTGGGGAAGCTGGC-3′)[33]; rat (mouse) RANK (sense, 5′-TTAAGCCAGTGCTTCACGGG-3′, antisense, 5′-ACGTAGACCACGATGATGTCGC-3′)[38]; mouse CD11b (sense, 5′-CTTAAAGCTCTTCTGGTCACAGCC-3′, antisense, 5′-GTATTCTCCTTG-CAGTTTTGGTGC-3′)[39]: mouse Emr1 (F4/80) (sense, 5′-GAATCTTGGCCAA-GAAGAGAC-3′, antisense, 5′-GAATTCTCCTTGTATATCATCAGC-3′)[40]; rat

(mouse) glyceraldehyde-3-phosphate dehydrogenase (GAPDH) (sense, 5′-CATGGAGAAGGCTGGGGCTC-3′, antisense, 5′-AACGGATACATTGGGG-TAG-3′).[41] PCR products were separated on a 1.5% agarose gel and stained with ethidium bromide. As an internal control for RNA quantity, the same cDNA was amplified using primers specific for GAPDH mRNA.

Luciferase assays

Renilla luciferase plasmid, pΔTK-RL (provided by Dr Ouchida, Okayama University), which has basal thymidine kinase promoter, was used as an internal control, as described previously.[42] NF-κB–dependent reporter plasmid, p55IgKluci, and the control vector, p55luci, were provided by Dr Fujita (Tokyo Metropolitan Institute of Medical Science).[43] RAW-D cells were cotransfected with p55IgKluci or p55luci and pΔTK-RL by using a commercial transfection reagent, fugene-6 (Roche Diagnostics, Basel, Switzerland). After 24 hours, cells were treated with different concentrations of TSA or NaB and sRANKL or TNF-α. The cells were then harvested 24 hours later in Promega (Madison, WI) lysis buffer. The activity of firefly and Renilla luciferase was measured using a reagent kit (Promega) and normalized to the Renilla luciferase activity of a cotransfected pΔTK-RL vector to correct for variation in transfection efficiency.

Protein isolation and Western blot analysis

Cells were grown in 60-mm plates. Cells treated with sRANKL were lysed in a sodium dodecyl sulfate (SDS) lysis buffer (0.12M Tris [tris(hydroxymethyl)aminomethane]–HCl, pH 6.8, 2% SDS, 10% glycerol). Whole-cell extracts were treated at 90°C for 2 minutes and then sonicated. Nuclear extracts were prepared from cells treated with TNF-α according to the method described previously.[44] Briefly, cells were washed with ice-cold PBS and incubated at 4°C for 8 minutes in 400 μL buffer containing 0.1% Nonidet P-40 (NP-40), 10 mM HEPES (N-2-hydroxyethylpiperazine-N′-2-ethanesulfonic acid)–KOH, pH 7.9, 10 mM KCl, 0.1 mM EDTA, 1 mM dithiothreitol (DTT), 2 mM $MgCl_2$, 5 μM amidinophenyl methanesulfonyl fluoride hydrochloride (APMSF), 0.5 M sucrose, and 2 μg/mL leupeptin. The cells were then scraped into tubes and centrifuged at 14 000 rpm for 10 minutes at 4°C. The pellets were rinsed with the above buffer without NP-40. Nuclear extracts were prepared by resuspending the nuclear pellets with 20 μL of a high-salt buffer (20 mM HEPES-KOH, pH 7.9, 1.5 mM $MgCl_2$, 420 mM NaCl, 0.2 mM EDTA, 1 mM DTT, 5% glycerol, 5 μM APMSF, 2 μg/mL leupeptin), incubating on ice for 40 minutes, and then centrifuging at 14 000 rpm for 10 minutes at 4°C. The nuclear extracts were then mixed with 30 μL of low-salt buffer (20 mM HEPES-KOH, pH 7.9, 50 mM KCl, 0.2 mM EDTA, 1 mM DTT, 20% glycerol, 5 μM APMSF, 2 μg/mL leupeptin). Protein concentrations of the nuclear extracts were determined using a commercial kit (Bio-Rad Laboratories, Hercules, CA). Ten microliters of whole cell extracts or an equal amount of proteins (10 μg) of nuclear extracts was fractionated under reducing conditions in 10% polyacrylamide gels and transferred to nitrocellulose filters (Schleincher and Schuell, Dassel, Germany). The filters were blocked in 5% low-fat milk and dissolved in PBS plus 0.1% Tween-20 (PBST) at room temperature for 2 hours. After extensive washing in PBST, the filters were probed with antiphosphorylated p38 (1:1000 dilution), anti–NF-κB p65 (1:500 dilution), or antiactin (1:1000 dilution) antibodies. The filters were then incubated with horseradish peroxidase (HRP)–conjugated antirabbit immunoglobulin G (IgG) or antimouse IgG and developed using the enhanced chemiluminescence (ECL) detection system (Amersham, Buckinghamshire, United Kingdom). For p38 Western blot analysis, the same sample was analyzed by antimouse actin antibody as a control for protein quantity.

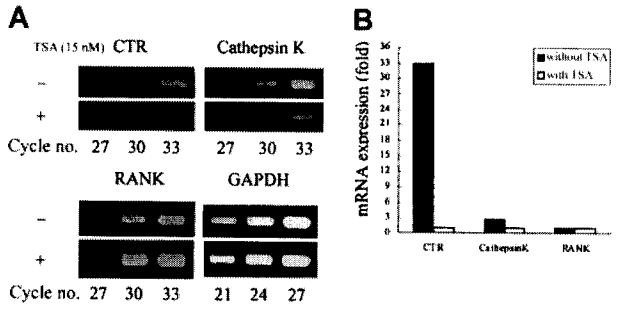

Figure 2. TSA selectively reduces osteoclast-specific mRNA expression. (A) Stroma-free rat bone marrow cells were cultured for 4 days with or without 15 nM TSA for the formation of POCs. Total RNA was prepared and reverse transcribed, and cDNA was amplified for the number of PCR cycles, using specific primers designed for genes of CTR, cathepsin K, RANK, and GAPDH. The PCR products were stained with ethidium bromide. (B) Relative expression of CTR, cathepsin K, and RANK is shown. The intensity of the bands was determined by densitometry and normalized by the level of GAPDH.

Results

TSA or NaB inhibits osteoclast differentiation in bone marrow cultures

We first examined the effect of HDAC inhibitors on osteoclastogenesis using TSA and NaB. The $TRAP^+$ MNCs or POCs are separately formed in 2 types of rat bone marrow culture systems.[34,35] Both TSA and NaB inhibited the formation of $TRAP^+$ MNCs in a dose-dependent manner in whole bone marrow culture (Figure 1A-B). As low as 5 nM TSA or 0.5 mM NaB was sufficient for 78% or 98% reduction of $TRAP^+$ MNCs formation, respectively. Both TSA and NaB dose-dependently inhibited the formation of POCs in stroma-free rat bone marrow culture (Figure 1A-B). These results demonstrate that both TSA and NaB strongly suppress osteoclast differentiation directly by inhibiting the formation of precursor cells of osteoclasts. To determine whether the inhibitory effect of these agents correlates with expression of the

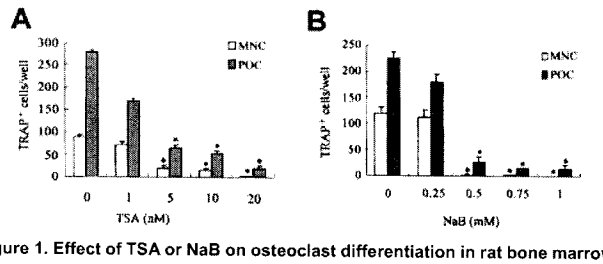

Figure 1. Effect of TSA or NaB on osteoclast differentiation in rat bone marrow culture. Whole rat bone marrow cells or stroma-free rat bone marrow cells for forming MNCs (□) or POCs (▨) were cultured as described in "Materials and methods" in the presence of various concentrations of TSA (A) or NaB (B). TSA or NaB was added after 24 hours of incubation. The cells were stained for TRAP, and the number of $TRAP^+$ MNCs and POCs was counted in each well. Each bar represents the mean ± SEM of quadruplicate cultures. Data were analyzed by Student *t* test. $^*P < .001$ compared with the culture without TSA or NaB.

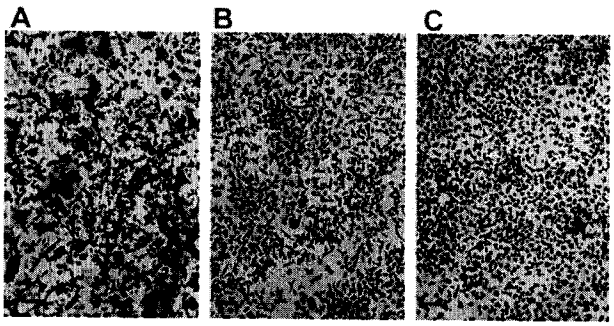

Figure 3. Demonstration of $TRAP^+$ MNCs in the mouse bone marrow culture treated with sRANKL and M-CSF in the presence of TSA or NaB. Mouse bone marrow cells were cultured in the presence of hM-CSF (50 ng/mL) and sRANKL (50 ng/mL) with or without TSA or NaB for 4 days. (A) Without TSA or NaB; (B) with 20 nM TSA; (C) with 1 mM NaB. The cells were then fixed and stained for TRAP. A number of $TRAP^+$ MNCs were observed in the culture without TSA or NaB (A). No $TRAP^+$ MNCs were observed in cultures with TSA or NaB (B-C). Scale bars = 100 μm.

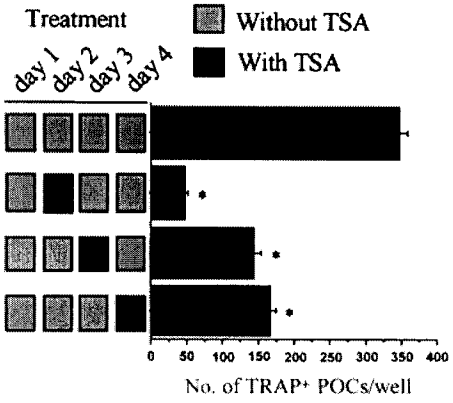

Figure 4. Time course of the effect of TSA on the formation of TRAP⁺ POCs. Stroma-free rat bone marrow cells were cultured under the conditions necessary to form POCs for 4 days with (■) or without (□) 10 nM TSA, following the indicated treatment schedule. Culture was fed every day with fresh medium, hormone, factors, and TSA. Before changing to new medium, the culture was washed 3 times by replacing 80% of the culture medium with fresh medium to eliminate the remaining factors. Factors and TSA were then added for the indicated periods. After 4 days of culture, the cells were fixed and stained for TRAP. The number of TRAP⁺ mononuclear cells was counted in each well. Each value represents the mean ± SEM of quadruplicate cultures. Data were analyzed by Student *t* test. *$P < .001$ compared with the culture without TSA.

osteoclast-specific CTR and cathepsin K mRNA, total RNA was prepared and analyzed by semiquantitative RT-PCR. Figure 2A-B shows RT-PCR analysis of CTR and cathepsin K mRNA expression treated with or without TSA. The level of CTR and cathepsin K mRNA was decreased in the cultures treated with TSA. In contrast, TSA did not have any effect on the level of RANK mRNA.

In cultures of mouse bone marrow cells, TRAP⁺ osteoclast-like cells are formed in the presence of M-CSF and sRANKL.[45-47] We also examined the effect of TSA and NaB on this formation of osteoclast-like cells. TSA or NaB dose-dependently inhibited the formation of TRAP⁺ MNCs in mouse bone marrow cell culture (data not shown). Figure 3 demonstrates the mouse bone marrow cultures treated with or without 20 nM TSA or 1 mM NaB. TSA or NaB dramatically decreased the number of TRAP⁺, osteoclast-like cells. In contrast, the number of cells in the culture did not decrease compared to that of the cells in the culture without TSA or NaB. These data indicate that the effect of TSA or NaB is not toxic, but rather is selectively inhibitory to osteoclastogenesis.

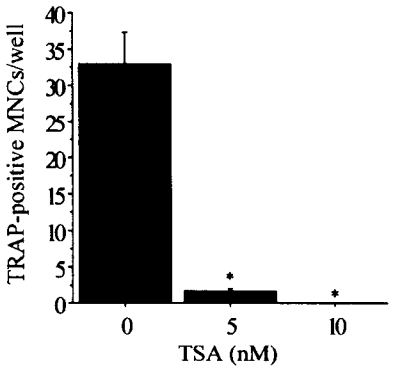

Figure 5. Effect of TSA on fusion of POCs in the presence of sRANKL. Stroma-free rat bone marrow cells were cultured in 96-well culture plates under the condition to form POCs for 4 days. The cells were then washed 3 times with α-MEM containing 15% FCS and further incubated for 2 days in the presence of 30 ng/mL sRANKL with or without TSA. Cells were then fixed and stained for TRAP. The number of TRAP⁺ MNCs was counted in each well. Each value represents the mean ± SEM of quadruplicate cultures. Data were analyzed by Student *t* test. *$P < .001$ compared with the culture without TSA.

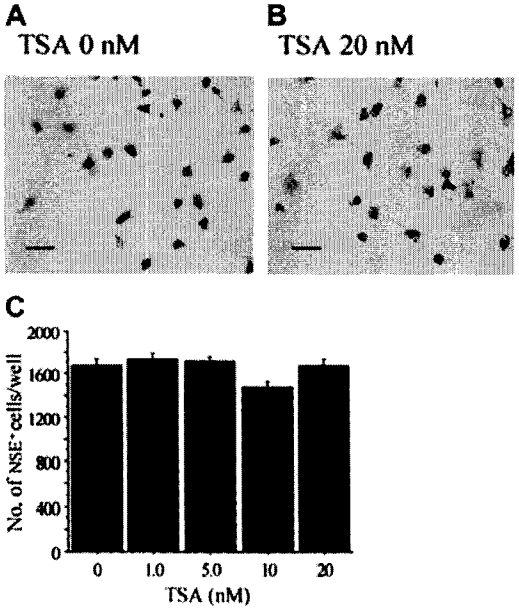

Figure 6. TSA does not affect the formation of M-CSF–induced NSE⁺ cells. Demonstration of NSE⁺ cells in rat bone marrow culture stimulated with M-CSF in the presence (B) or absence (A) of TSA. Scale bars = 100 μm. (C) Dose effect of TSA on the formation of NSE⁺ cells in stroma-free rat bone marrow culture. Stroma-free bone marrow cells were cultured in the presence of hM-CSF (1 ng/mL) for 4 days. Various concentrations of TSA were added after 24 hours of incubation. The cells were then fixed and stained for NSE (A-B), and the number of NSE⁺ cells was counted in each well (C). Each bar represents the mean ± SEM of quadruplicate cultures.

We next examined whether TSA affects the early stage or the late stage of the TRAP⁺ POC formation by performing temporal treatment with TSA. As shown in Figure 4, the effect on the number of TRAP⁺ POCs is more pronounced when TSA is added earlier. We recently showed that sRANKL induces the formation of TRAP⁺ MNCs from preformed POCs in rat bone marrow cell culture.[34] To investigate whether TSA has any effect in the fusion of the preformed POCs in the presence of sRANKL, the preformed POCs were incubated for 3 days with different concentrations of

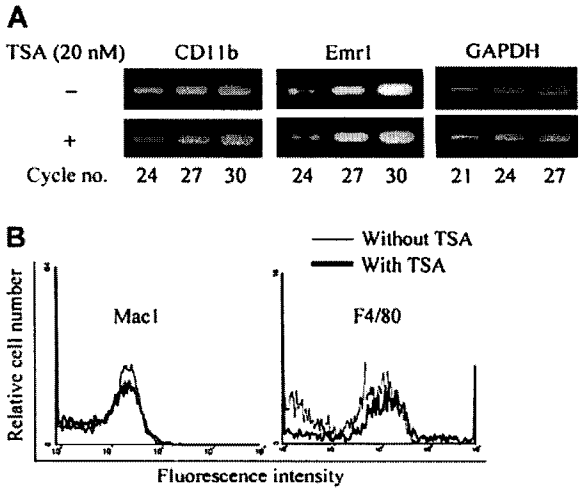

Figure 7. TSA does not affect the expression of macrophage-associated phenotypes in mouse bone marrow culture. (A) RT-PCR analysis of mouse bone marrow macrophage (mBMMs) formed in the presence or absence of TSA. (B) FACS analysis of surface markers Mac-1 and F4/80 of mBMMs formed in the presence or absence of TSA. Mouse whole bone marrow cells were cultured in the presence of hM-CSF (50 ng/mL) with or without TSA (20 nM) for 3 days. Total RNA was prepared and analyzed by RT-PCR (A). Adherent cells were harvested and stained with anti-F4/80 or FITC-conjugated anti–Mac-1 antibody (B).

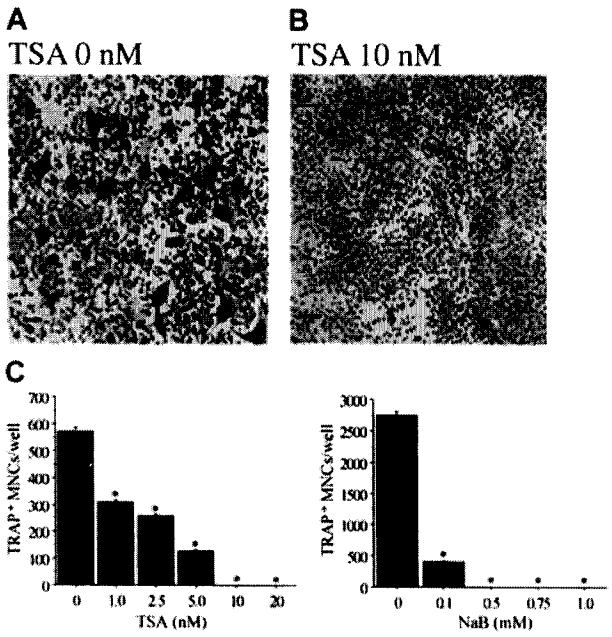

Figure 8. TSA or NaB inhibits osteoclast differentiation of RAW-D cells stimulated with sRANKL. Demonstration of TRAP+ cells in RAW-D cells stimulated with sRANKL in the presence (B) or absence (A) of TSA. (C) Dose-dependent effect of TSA or NaB on the formation of TRAP+ MNCs in RAW-D stimulated with sRANKL. RAW-D cells (1.5×10^5 cells/mL) were cultured for 3 days in the presence of sRANKL (30 ng/mL) with various concentrations of TSA or NaB. TSA or NaB was added after 24 hours of incubation. Cells were then fixed and stained for TRAP. The number of TRAP+ MNCs was counted in each well. Each value represents the mean ± SEM of quadruplicate cultures. Data were analyzed by Student *t* test. *$P < .001$ compared with the culture without TSA. Scale bars = 100 μm.

TSA. TSA dose-dependently inhibited the fusion of POCs (Figure 5). Thus, TSA suppresses not only the formation of preosteoclasts but also the multinucleation of preosteoclasts.

TSA or NaB does not affect Mac-1 or F4/80 expression in M-CSF–induced bone marrow macrophages

The cell lineage of the osteoclasts is considered to be very close to that of macrophages.[48] When M-CSF stimulates bone marrow cells, M-CSF–dependent bone marrow macrophages (BMMs) appear.[49,50] When we treated stroma-free rat bone marrow cells with hM-CSF for 3 days, most of the adherent cells were positive for NSE, which is a marker enzyme for macrophages (Figure 6A). Addition of various concentrations of TSA did not have any effect on the formation of NSE+ cells (Figure 6B-C). We also examined the effect of NaB, which also had no effect on the formation of NSE+ cells (data not shown).

In mouse bone marrow culture, neither TSA nor NaB had any effect on the formation of NSE+ cells (data not shown). We then analyzed by RT-PCR whether the levels of mRNA for macrophage-associated phenotypes such as Mac-1 (CD11b) and F4/80 in mouse BMMs were influenced by the addition of TSA. As shown in Figure 7A, TSA had no effect on the level of mRNA for CD11b and emr1 (encoding F4/80 antigen) induced by M-CSF in BMMs. Finally, we analyzed the surface expression of Mac-1 and F4/80 antigen of mouse BMMs by fluorescent activated cell sorting (FACS). As shown in Figure 7B, TSA had no effect on the expression of either Mac-1 or F4/80. These results together indicate that TSA or NaB does not affect macrophage differentiation in bone marrow culture.

Effect of TSA or NaB on osteoclast differentiation of RAW-D cells stimulated by sRANKL

A macrophage cell line, RAW 264, differentiates into osteoclasts in the presence of sRANKL.[26,51] We investigated the effect of TSA or NaB on the formation of TRAP+ MNCs using a subclone of RAW 264, RAW-D, which efficiently differentiates into osteoclasts. When RAW-D cells were cultured in the presence of sRANKL (30 ng/mL) for 3 days, a large number of TRAP+ cells were formed, as shown in Figure 8A. Addition of various concentrations of TSA or NaB inhibited TRAP+ MNCs formation from RAW-D cells (Figure 8B-C). In this culture system, 1 nM TSA or 0.1 mM NaB was sufficient for 50% or 80% reduction of TRAP+ MNC formation, respectively. The concentrations were 5 times lower than those required for a similar reduction in bone marrow culture. We also examined whether TSA would affect the level of osteoclast-specific CTR and cathepsin K mRNAs. As shown in Figure 9A, when RAW-D cells differentiate into osteoclasts in the presence of sRANKL, the expression of cathepsin K and CTR mRNA is increased. Addition of TSA inhibited this stimulation of osteoclast-specific mRNAs. These results demonstrate that TSA inhibits osteoclast differentiation from macrophages. We also analyzed the mRNA level of RANK, CD11b (Mac-1), and emr1 (F4/80) by RT-PCR analysis. Addition of sRANKL decreased the expression of CD11b and emr1 when RAW-D cells differentiated into osteoclasts in the presence of sRANKL, whereas the expression of CD11b and emr1 was not decreased in the presence of TSA, as shown in Figure 9A. To further characterize the macrophage phenotypes, we performed FACS analysis of RAW-D cells stimulated with sRANKL in the presence or absence of TSA. As shown in Figure 9B, the surface expression of Mac-1 and F4/80 was

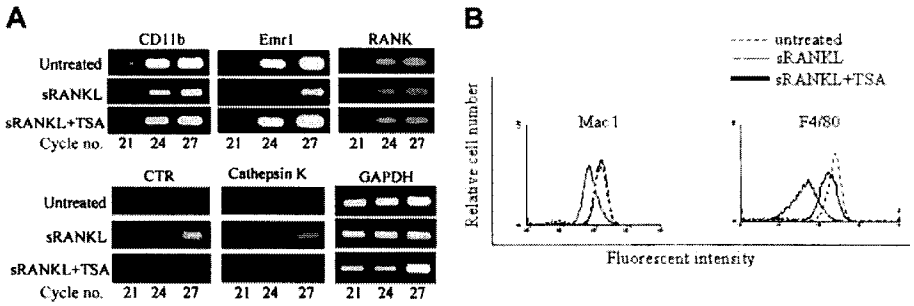

Figure 9. TSA inhibits the expression of CTR and cathepsin K but not CD11b or F4/80 in RAW-D cells stimulated with sRANKL. (A) Effect of TSA on the expression of various mRNAs of RAW-D cells stimulated with sRANKL. RAW-D cells were cultured with sRANKL in the presence or absence of TSA (10 nM), and total RNA was prepared. Semiquantitative RT-PCR was used to assess the changes in the expression of various genes. cDNA was amplified for the number of PCR cycles indicated and visualized on agarose gels with ethidium bromide. GAPDH levels were used for comparison. (B) FACS analysis of RAW-D cells. RAW-D cells were treated with sRANKL for 3 days in the presence or absence of TSA (10 nM). TSA was added after 24 hours of incubation. Cells were then stained with antimouse Mac-1 or F4/80 antibodies and analyzed by FACS.

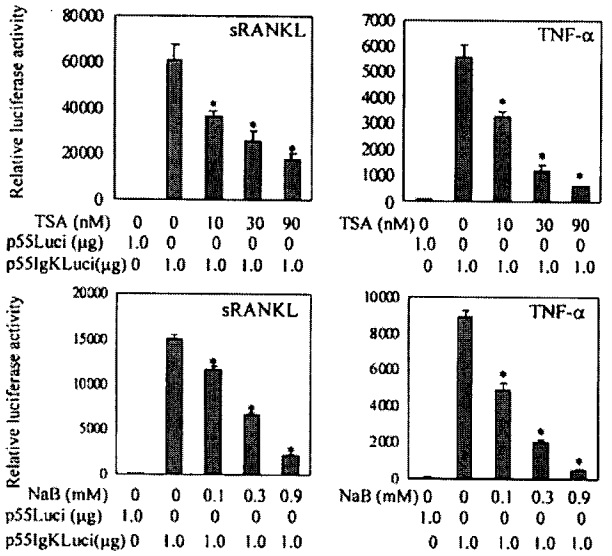

Figure 10. TSA and NaB decrease NF-κB–dependent transactivation in RAW-D cells. RAW-D cells were transiently transfected with 1 μg NF-κB–dependent reporter plasmid p55IgKLuci or control vector p55Luci. Transiently transfected cells were stimulated with TNF-α or sRANKL for 24 hours. Various concentrations of TSA or NaB were added with TNF-α (20 ng/mL) or sRANKL (100 ng/mL). Renilla luciferase expression vector, pΔTK-RL (0.25 μg), was used as internal control for transfection. Bars represent the mean ± SEM of 3 independent transfections. Data were analyzed by Student *t* test. **P* < .001 compared with the culture without TSA or NaB treatment.

decreased when RAW-D cells were stimulated with sRANKL. The treatment of RAW-D cells with TSA prevented the reduction of Mac-1 and F4/80 expression. These results together suggest that RAW-D cells are not able to differentiate into osteoclasts and retain macrophage-associated phenotypes in the presence of TSA, even when the cells are stimulated with sRANKL.

TSA or NaB affects sRANKL/TNF-α–induced activation of NF-κB and MAPK signaling pathways

RANKL-RANK signaling plays an essential role in osteoclast differentiation and function. The activation of NF-κB and MAPKs pathways is thought to be critical in signaling osteoclast differentiation.[26,27,52] We first determined whether TSA- or NaB-mediated suppression of osteoclast differentiation is related to the modulation of NF-κB activation. We transiently transfected the RAW-D cells with NF-κB–dependent reporter plasmid p55IgKLuci and treated them with sRANKL or TNF-α. As shown in Figure 10, sRANKL or TNF-α stimulated NF-κB–dependent transactivation in RAW-D cells. Treatment with TSA or NaB dose-dependently reduced the sRANKL- or TNF-α–stimulated transactivation of NF-κB–dependent reporter genes (Figure 10). The influence of TSA or NaB on NF-κB activation was further examined by Western blotting using RAW-D cells. Nuclear extracts of RAW-D cells stimulated with TNF-α for 30 minutes were analyzed using antibody to NF-κB p65 subunit. Pretreatment of RAW-D cells with TSA or NaB for 24 hours dramatically reduced nuclear translocation of NF-κB p65, as shown in Figure 11A. These results suggest that the treatment with TSA or NaB affects the NF-κB signaling pathway in RAW-D cells.

Recently, it has been shown that the p38 MAPK pathway plays an important role in RANKL-induced osteoclast differentiation in bone marrow–derived osteoclast precursor cells and the RAW 264 macrophage cell line.[26,27] We next investigated the effect of TSA or NaB on the activation of p38 MAPK, using the antibody against phosphorylated-p38 MAPK. Figure 11B shows Western blot analysis of RAW-D cells stimulated with sRANKL in the presence or absence of TSA or NaB. The level of expression of phosphorylated p38 MAPK was increased by treatment of RAW-D cells with sRANKL for 30 minutes. Pretreatment of RAW-D cells with TSA or NaB for 24 hours suppressed the sRANKL-induced activation of p38 MAPK. These results suggest that inhibitory function of TSA or NaB may also include the p38 MAPK pathway.

Discussion

The HDAC inhibitors, TSA and NaB, are strong inhibitors for osteoclastogenesis

NaB has been known to have biologic activity, especially to induce differentiation of cells in several culture systems. The structurally different compound TSA also induces differentiation of leukemia cells. Similar action exhibited by NaB and TSA suggested that the effects of both agents were mediated by their ability to inhibit HDAC. Currently, several HDAC inhibitors are used for therapy. NaB not only induces differentiation of some leukemia cells, but also induces gene expression and differentiation in some primary cells such as epithelial cells, hepatocytes, and liver cells.[53-55] Because NaB is a product generated in intestine by bacterial metabolism, it has been considered that NaB has some effect on epithelial cells. NaB stimulated the expression of phenotypes in human enterocytes and primary liver culture and reduced glucose transporter expression in hepatocytes.[53-55] On the other hand, it is also known that TSA induces differentiation of some leukemia cells.[13,56] However, the effect of these agents on other primary cells, except epithelial cells, is not well known. Because the HDAC inhibitors are used in therapeutic medicine for leukemia and lymphoma,[57,58] it is important to know the effect on the cells in primary bone marrow culture. Iwami et al[59] reported that NaB stimulated osteoblast differentiation but inhibited osteoclast differentiation. They concluded that the inhibitory effect of NaB on osteoclastogenesis was related to the cytotoxicity of NaB on bone marrow cells. They incubated bone marrow cells with NaB for 8 days, but we treated bone marrow cells and RAW-D cells with TSA or NaB for 3 or 2 days and found that the TSA and NaB had an inhibitory effect on osteoclastogenesis. In our culture system, the effect of these agents was not cytotoxic but was specific for the cells of osteoclast lineage.

The inhibitory effect was examined by using different markers in mouse and rat bone marrow cultures and a macrophage cell line,

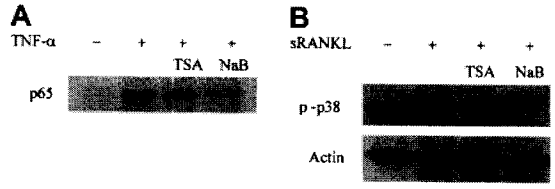

Figure 11. TSA and NaB affect NF-κB and p38 MAPK signaling pathways in RAW-D cells. (A) TSA or NaB suppresses the nuclear translocation of NF-κB p65 in RAW-D cells stimulated with TNF-α. RAW-D cells were treated without or with TSA (100 nM) or NaB (1 mM) for 24 hours, followed by treatment with TNF-α for 30 minutes. Nuclear extracts were prepared and analyzed by Western blotting using NF-κB p65 antibody. (B) TSA or NaB suppresses activation of p38 MAPK in RAW-D cells stimulated with sRANKL. RAW-D cells were preincubated with or without TSA (100 nM) or NaB (1 mM) for 24 hours and stimulated with sRANKL (100 ng/mL) for 30 minutes. Whole-cell lysates were prepared and analyzed by Western blotting using phosphorylated p38 MAPK antibody. The bottom lane indicates equal loading of protein probed for actin antibody.

RAW 264. In both culture systems, both agents exhibited the same activity, which reduced osteoclast differentiation but did not affect the expression of macrophage markers such as CD11b and F4/80. Several reports have shown that the HDAC inhibitors modulate myeloid cell differentiation, but the effect of these agents on the expression of macrophage markers is still not known.[11-13] High doses of TSA slightly induced the expression of CD14 and CD11b, but the addition of both TSA and 9-*cis*-RA resulted in enhancement of CD14 expression.[13] TSA treatment of the cells seems enough to inhibit osteoclastogenesis but not enough to induce macrophage differentiation. Figure 12 summarizes the effect of HDAC inhibitors on the differentiation into osteoclasts and macrophages. Because these agents are known to inhibit cell proliferation,[60] we analyzed whether these agents affect the growth of RAW-D. Treatment of RAW-D cells for 2 days with 10 nM TSA, which completely inhibited osteoclastogenesis, resulted in 25% reduction of the cell numbers (data not shown). Inhibitory activity of TSA and NaB on osteoclast differentiation seems not to be derived from the inhibitory effect of cell proliferation.

NF-κB and MAPK may be involved in the inhibitory effect of TSA and NaB

Differentiation and activation of osteoclasts depend on the signal through RANK stimulated with RANKL. NF-κB knockout mice exhibit osteopetrosis[61] and is one of the important signaling molecules of RANKL.[21] We found that NF-κB–dependent transcriptional activity was dose-dependently repressed by the treatment of these agents. In addition, the protein level of NF-κB in the nucleus after stimulation also decreased. NF-κB is considered to be involved in not only the process of differentiation but also in maturation of osteoclasts.[21] HDAC inhibitors also inhibited both of the osteoclast differentiation processes, preosteoclast formation and fusion. Inhibitory action of these agents on osteoclastogenesis seems to involve the inhibitory effect of these agents on NF-κB activation. Some investigators have reported that NaB can suppress NF-κB activation in different cell types, including colon cancer cell lines and epithelial cells isolated from the colon.[5,16] Recently, Chakravortty et al[62] reported that NaB prevented activation of NF-κB and inhibited nitric oxide production of RAW 264.7 cells stimulated with LPS. These results support our data on the suppression of HDAC inhibitors on NF-κB activation by HDAC inhibitors. On the other hand, other investigators reported that after NF-κB enters the nucleus, the transactivation of NF-κB can be regulated directly by phosphorylating or acetylating of NF-κB itself.[63,64] In their studies, the treatment of the cells with HDAC inhibitors such as TSA augmented the transactivation of NF-κB–dependent reporter gene. These results are opposite to our data, but they used cells that are different from ours. Because NF-κB is ubiquitously expressed in many types of cells, the role of NF-κB in the signals is thought to be different in each signal and cell. Further studies are necessary to elucidate the mechanism of inhibitory activity of HDAC inhibitors on NF-κB activation by RANKL in macrophage cells.

MAPKs transmit signals from extracellular stimuli to induce cell proliferation and differentiation. Among MAPKs, JNK and p38 MAPK have been shown to be involved in osteoclast differentiation.[22,26] In this study, we found that the phosphorylation of a MAPK, p38, decreased after treatment with TSA or NaB, suggesting that the inhibition of the p38 MAPK pathway may also be involved in the inhibitory action of these agents. We also tried to see the effect of these agents on the activation of the JNK pathway, but we could not find any strong activation of JNK signals or any effect of these agents on activation of JNK by Western blot analysis in RAW-D cells (data not shown).

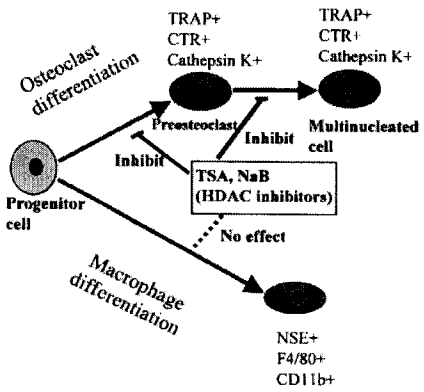

Figure 12. Effect of HDAC inhibitors on the differentiation into osteoclasts and macrophages. HDAC inhibitors suppressed the processes of osteoclast differentiation, POC formation, as well as MNC formation, whereas they did not affect macrophage differentiation.

Likewise, HDAC inhibitors affected both of signaling pathways, NF-κB and MAPK. Treatment with HDAC inhibitors is considered to increase the acetylation level of histone, which precedes the induction of gene expression. However, we have not determined which genes are affected by these HDAC inhibitors. One possibility for inhibition of MAPK may be an activation of protein kinase phosphatase gene. Li et al[65] recently reported that mitogen-activated protein kinase phosphatase 1 (MKP-1) plays a role in the regulation of the MAPK pathway and that phosphorylation and acetylation of histone are associated with transcriptional induction of MKP-1. The treatment with HDAC inhibitors may induce MKP-1 and prevent the p38 MAPK signaling pathway. In addition, rather than histone being the substrate for HDAC, transcriptional regulators could become acetylated. Several transcriptional regulators have been shown to be substrates for HDAC, including NF-κB, GATA-1, and p53.[63,66,67] Acetylation of transcription factors may modulate their activity and influence osteoclastogenesis. Recent reports describe the use of chromatin immunoprecipitation assay to analyze whether promoters of genes are regulated by acetylation of histone or transcription factor itself.[68,69] To determine the genes and transcription factors modulated by TSA or NaB in macrophages stimulated with RANKL, further studies will be required.

Possible efficacy of HDAC inhibitors in therapy for bone disease

In this study, we present the novel action of 2 HDAC inhibitors, TSA and NaB, on osteoclastogenesis. Osteoclasts have a crucial role in physiologic bone remodeling and also function in the pathologic bone loss that occurs associated with inflammatory diseases such as rheumatoid arthritis and periodontal disease.[70,71] They are also involved in postmenopausal osteoporosis.[72] Our findings open up an additional avenue to search out drugs specific for the treatment of these diseases.

Acknowledgements

The authors thank Dr M. Ouchida (Okayama University) for donating reporter plasmid, pΔTK-RL, and Dr T. Fujita (Tokyo Metropolitan Institute of Medical Science) for donating plasmids, p55IgKluci and p55luci.

References

1. Richon VM, O'Brien JP. Histone deacetylase inhibitors: a new class of potential therapeutic agents for cancer treatment. Clin Cancer Res. 2002;8:662-664.
2. Marks P, Rifkind RA, Richon VM, Breslow R, Miller T, Kelly WK. Histone deacetylases and cancer: causes and therapies. Nat Rev Cancer. 2001;1:194-202.
3. Hutt-Taylor SR, Harnish D, Richardson M, Ishizaka T, Denburg JA. Sodium butyrate and a T lymphocyte cell line-derived differentiation factor induce basophilic differentiation of the human promyelocytic leukemia cell line HL-60. Blood. 1988;71:209-215.
4. Souleimani A, Asselin C. Regulation of c-myc expression by sodium butyrate in the colon carcinoma cell line Caco-2. FEBS Lett 1993;326: 45-50.
5. Yin L, Laevsky G, Giardina C. Butyrate suppression of colonocyte NF-kappa B activation and cellular proteasome activity. J Biol Chem. 2001;276: 44641-44646.
6. Yoshida M, Nomura S, Beppu T. Effects of trichostatins on differentiation of murine erythroleukemia cells. Cancer Res. 1987;47:3688-3691.
7. Yoshida M, Kijima M, Akita M, Beppu T. Potent and specific inhibition of mammalian histone deacetylase both in vivo and in vitro by trichostatin A. J Biol Chem. 1990;265:17174-17179.
8. He LZ, Tolentino T, Grayson P, et al. Histone deacetylase inhibitors induce remission in transgenic models of therapy-resistant acute promyelocytic leukemia. J Clin Invest. 2001;108:1321-1330.
9. Rius C, Cabanas C, Aller P. The induction of vimentin gene expression by sodium butyrate in human promonocytic leukemia U937 cells. Exp Cell Res. 1990;188:129-134.
10. Hayashi Y, Honma Y, Niitsu N, et al. SN-1, a novel leukemic cell line with t(11;16)(q23;p13): myeloid characteristics and resistance to retinoids and vitamin D3. Cancer Res. 2000;60:1139-1145.
11. Rubio MA, Lopez-Rodriguez C, Nueda A, et al. Granulocyte-macrophage colony-stimulating factor, phorbol ester, and sodium butyrate induce the CD11c integrin gene promoter activity during myeloid cell differentiation. Blood 1995;86:3715-3724.
12. Corbi AL, Lopez-Rodriguez C. CD11c integrin gene promoter activity during myeloid differentiation. Leuk Lymphoma. 1997;25:415-425.
13. Nagy L, Kao HY, Chakravarti D, et al. Nuclear receptor repression mediated by a complex containing SMRT, mSin3A, and histone deacetylase. Cell. 1997;89:373-380.
14. Leoni F, Zaliani A, Bertolini G, et al. The antitumor histone deacetylase inhibitor suberoylanilide hydroxamic acid exhibits antiinflammatory properties via suppression of cytokines. Proc Natl Acad Sci U S A. 2002;99:2995-3000.
15. Inan MS, Rasoulpour RJ, Yin L, Hubbard AK, Rosenberg DW, Giardina C. The luminal short-chain fatty acid butyrate modulates NF-kappaB activity in a human colonic epithelial cell line. Gastroenterology. 2000;118:724-734.
16. Wu GD, Huang N, Wen X, Keilbaugh SA, Yang H. High-level expression of I kappa B-beta in the surface epithelium of the colon: in vitro evidence for an immunomodulatory role. J Leukoc Biol. 1999;66:1049-1056.
17. Burger EH, Van der Meer JW, van de Gevel JS, et al. In vitro formation of osteoclasts from long-term cultures of bone marrow mononuclear phagocytes. J Exp Med. 1982;156:1604-1614.
18. Kurihara N., Suda T., Miura Y., et al. Generation of osteoclasts from isolated hematopoietic progenitor cells. Blood. 1989;74:1295-1302.
19. Suda T, Takahashi N, Martin TJ. Modulation of osteoclast differentiation. Endocr Rev. 1992;13: 66-80.
20. Suda T, Takahashi N, Udagawa N, Jimi E, Gillespie MT, Martin TJ. Modulation of osteoclast differentiation and function by the new members of the tumor necrosis factor receptor and ligand families. Endocr Rev. 1999;20:345-357.
21. Kobayashi N, Kadono Y, Naito A, et al. Segregation of TRAF6-mediated signaling pathways clarifies its role in osteoclastogenesis. EMBO J. 2001;20:1271-1280.
22. Srivastava S, Toraldo G, Weitzmann MN, Cenci S, Ross FP, Pacifici R. Estrogen decreases osteoclast formation by down-regulating receptor activator of NF-kappa B ligand (RANKL)–induced JNK activation. J Biol Chem. 2001;276:8836-8840.
23. Iotsova V, Caamano J, Loy J, Yang Y, Lewin A, Bravo R. Osteopetrosis in mice lacking NF-kappaB1 and NF-kappaB2. Nat Med. 1997;3:1285-1289.
24. Naito A, Azuma S, Tanaka S, et al. Severe osteopetrosis, defective interleukin-1 signalling and lymph node organogenesis in TRAF6-deficient mice. Genes Cells. 1999;4:353-362.
25. Lomaga MA, Yeh WC, Sarosi I, et al. TRAF6 deficiency results in osteopetrosis and defective interleukin-1, CD40, and LPS signaling. Genes Dev. 1999;13:1015-1024.
26. Matsumoto M, Sudo T, Saito T, Osada H, Tsujimoto M. Involvement of p38 mitogen-activated protein kinase signaling pathway in osteoclastogenesis mediated by receptor activator of NF-kB ligand (RANKL). J Biol Chem. 2000;275:31155-31161.
27. Lee SE, Woo KM, Kim SY, et al. The phosphatidylinositol 3-kinase, p38, and extracellular signal-regulated kinase pathways are involved in osteoclast differentiation. Bone. 2002;30:71-77.
28. Shin JH, Kukita A, Ohki K, Katsuki T, Kohashi O. In vitro differentiation of the murine macrophage cell line BDM-1 into osteoclast-like cells. Endocrinology. 1995;136:4285-4292.
29. Miyamoto A, Kunisada T, Hemmi H, et al. Establishment and characterization of an immortal macrophage-like cell line inducible to differentiate to osteoclasts. Biochem Biophys Res Commun. 1998;242:703-709.
30. Hsu H, Lacey DL, Dunstan CR, et al. Tumor necrosis factor receptor family member RANK mediates osteoclast differentiation and activation induced by osteoprotegerin ligand. Proc Natl Acad Sci U S A. 1999;96:3540-3545.
31. Ogata Y, Kukita A, Kukita T, et al. A novel role of IL-15 in the development of osteoclasts: inability to replace its activity with IL-2. J Immunol. 1999; 162:2754-2760.
32. Xu LX, Kukita T, Kukita A, Otsuka T, Niho Y, Iijima T. Interleukin-10 selectively inhibits osteoclastogenesis by inhibiting differentiation of osteoclast progenitors into preosteoclast-like cells in rat bone marrow culture system. J Cell Physiol. 1995;165:624-629.
33. Komine M, Kukita A, Kukita T, Ogata Y, Hotokebuchi T, Kohashi O. Tumor necrosis factor-α cooperates with receptor activator of nuclear factor kB ligand in generation of osteoclasts in stromal cell-depleted rat bone marrow cell culture. Bone. 2001;28:474-483.
34. Kukita A, Kukita T, Hata K, Kurisu K, Kohashi O. Heat-treated osteoblastic cell (ROS 17/2.8)–conditioned medium induces the formation of osteoclast-like cells. Bone Miner. 1993;23:113-127.
35. Kukita A, Kukita T, Shin JH, Kohashi O. Induction of mononuclear precursor cells with osteoclastic phenotypes in a rat bone marrow culture system depleted of stromal cells. Biochem Biophys Res Commun. 1993;196:1383-1389.
36. Wada S, Udagawa N, Akatsu T, Nagata N, Martin TJ, Findlay DM. Regulation by calcitonin and glucocorticoids of calcitonin receptor gene expression in mouse osteoclasts. Endocrinology. 1997;138:521-529.
37. Ikegame M, Rakopoulos M, Zhou H, et al. Calcitonin receptor isoforms in mouse and rat osteoclasts. J Bone Miner Res. 1995;10:59-65.
38. Nakagawa N, Kinosaki M, Yamaguchi K, et al. RANK is the essential signaling receptor for osteoclast differentiation factor in osteoclastogenesis. Biochem Biophys Res Commun. 1998;253:395-400.
39. Laribee RN, Klemsz MJ. Loss of PU.1 expression following inhibition of histone deacetylases. J Immunol. 2001;167:5160-5166.
40. Matsuo K, Owens JM, Tonko M, Elliott C, Chambers TJ, Wagner EF. Fosl1 is a transcriptional target of c-Fos during osteoclast differentiation. Nat Genet. 2000;24:184-187.
41. van der Pluijn G, Most W, van der Wee-Pals L, de Groot H, Papapoulos S, Löwik C. Two distinct effects of recombinant human tumor necrosis factor-α on osteoclast development and subsequent resorption of mineralized matrix. Endocrinology. 1991;129:1596-1604.
42. Kukita A, Kukita T, Ouchida M, Maeda H, Yatsuki H, Kohashi O. Osteoclast-derived zinc finger (OCZF) protein with POZ domain, a possible transcriptional repressor, is involved in osteoclastogenesis. Blood. 1999;94:1987-1997.
43. Fujita T, Nolan GP, Ghosh S, Baltimore D. Independent modes of transcriptional activation by the p50 and p65 subunits of NF-kappa B. Genes Dev. 1992;6:775-787.
44. Schutze S, Potthoff K, Machleidt T, Berkovic D, Wiegmann K, Kronke M. TNF activates NF-kappa B by phosphatidylcholine-specific phospholipase C-induced "acidic" sphingomyelin breakdown. Cell. 1992;71:765-776.
45. Lacey DL, Timms E, Tan HL, et al. Osteoprotegerin ligand is a cytokine that regulates osteoclast differentiation and activation. Cell. 1998;93:165-176.
46. Tsurukai T, Udagawa N, Matsuzaki K, Takahashi N, Suda T. Roles of macrophage-colony stimulating factor and osteoclast differentiation factor in osteoclastogenesis. J Bone Miner Metab. 2000; 18:177-184.
47. Udagawa N, Takahashi N, Jimi E, et al. Osteoblasts/stromal cells stimulate osteoclast activation through expression of osteoclast differentiation factor/RANKL but not macrophage colony-stimulating factor. Bone. 1999;25:517-523.
48. Udagawa N, Takahashi N, Akatsu T, et al. Origin of osteoclasts: mature monocytes and macrophages are capable of differentiating into osteoclasts under a suitable microenvironment prepared by bone marrow-derived stromal cells. Proc Natl Acad Sci U S A. 1990;87:7260-7266.
49. Takeshita S, Kaji K, Kudo A. Identification and characterization of the new osteoclast progenitor with macrophage phenotypes being able to differentiate into mature osteoclasts. J Bone Miner Res. 2000;15:1477-1488.
50. Kobayashi K, Takahashi N, Jimi E, et al. Tumor necrosis factor alpha stimulates osteoclast differentiation by a mechanism independent of the ODF/RANKL-RANK interaction. J Exp Med. 2000;191:275-286.
51. Shevde NK, Bendixen AC, Dienger KM, Pike JW. Estrogens suppress RANK ligand-induced osteoclast differentiation via a stromal cell independent mechanism involving c-Jun repression. Proc Natl Acad Sci U S A. 2000;97:7829-7834.
52. Matsumoto M, Sudo T, Maruyama M, Osada H, Tsujimoto M. Activation of p38 mitogen-activated protein kinase is crucial in osteoclastogenesis

induced by tumor necrosis factor. FEBS Lett. 2000;486:23-28.

53. Sanderson IR, Ezzell RM, Kedinger M, et al. Human fetal enterocytes in vitro: modulation of the phenotype by extracellular matrix. Proc Natl Acad Sci U S A. 1996;93:7717-7722.
54. Rhoads DB, Takano M, Gattoni-Celli S, Chen CC, Isselbacher KJ. Evidence for expression of the facilitated glucose transporter in rat hepatocytes. Proc Natl Acad Sci U S A. 1988;85:9042-9046.
55. Niki T, Rombouts K, De Bleser P, et al. A histone deacetylase inhibitor, trichostatin A, suppresses myofibroblastic differentiation of rat hepatic stellate cells in primary culture. Hepatology. 1999;29:858-867.
56. Wang J, Saunthararajah Y, Redner RL, Liu JM. Inhibitors of histone deacetylase relieve ETO-mediated repression and induce differentiation of AML1-ETO leukemia cells. Cancer Res. 1999;59:2759-2765.
57. Kosugi H, Towatari M, Hatano S, et al. Histone deacetylase inhibitors are the potent inducer/enhancer of differentiation in acute myeloid leukemia: a new approach to anti-leukemia therapy. Leukemia 1999;13:1316-1324.
58. Piekarz RL, Robey R, Sandor V, et al. Inhibitor of histone deacetylation, depsipeptide (FR901228), in the treatment of peripheral and cutaneous T-cell lymphoma: a case report. Blood. 2001;98:2865-2868.
59. Iwami K, Moriyama T. Effects of short chain fatty acid, sodium butyrate, on osteoblastic cells and osteoclastic cells. Int J Biochem. 1993;25:1631-1635.
60. Siavoshian S, Segain JP, Kornprobst M, et al. Butyrate and trichostatin A effects on the proliferation/differentiation of human intestinal epithelial cells: induction of cyclin D3 and p21 expression. Gut. 2000;46:507-514.
61. Franzoso G, Carlson L, Xing L, et al. Requirement for NF-kappa B in osteoclast and B-cell development. Genes Dev. 1997;11:3482-3496.
62. Chakravortty D, Koide N, Kato Y, et al. The inhibitory action of butyrate on lipopolysaccharide-induced nitric oxide production in RAW 264.7 murine macrophage cells. J Endotoxin Res. 2000;6:243-247.
63. Chen Lf, Fischle W, Verdin E, Greene WC. Duration of nuclear NF-kappaB action regulated by reversible acetylation. Science. 2001;293:1653-1657.
64. Zhong H, May MJ, Jimi E, Ghosh S. The phosphorylation status of nuclear NF-kappa B determines its association with CBP/p300 or HDAC-1. Mol Cell. 2002;9:625-636.
65. Li J, Gorospe M, Hutter D, Barnes J, Keyse SM, Liu Y. Transcriptional induction of MKP-1 in response to stress is associated with histone H3 phosphorylation-acetylation. Mol Cell Biol. 2001;21:8213-8224.
66. Boyes J, Byfield P, Nakatani Y, Ogryzko V. Regulation of activity of the transcription factor GATA-1 by acetylation. Nature. 1998;396:594-598.
67. Gu W, Roeder RG. Activation of p53 sequence-specific DNA binding by acetylation of the p53 C-terminal domain. Cell. 1997;90:595-606.
68. Maehara K, Uekawa N, Isobe K. Effects of histone acetylation on transcriptional regulation of manganese superoxide dismutase gene. Biochem Biophys Res Commun. 2002;295:187-192.
69. Jin C, Li H, Murata T, Sun K, Horikoshi M, Chiu R, Yokoyama KK. JDP2, a repressor of AP-1, recruits a histone deacetylase 3 complex to inhibit the retinoic acid-induced differentiation of F9 cells. Mol Cell Biol. 2002;22:4815-4826.
70. Mills BG. Bone resorbing cells and human clinical conditions. In: Hall BK, ed. The Osteoclast. Bone. Vol 2. Boca Raton, FL: CRC Press; 1991:175-251.
71. Sterrett JD. The osteoclast and periodontitis. J Clin Periontol. 1986;13:258-269.
72. Cooper C, Melton LJ III. In: Marcus R, Feldman D, Kelsey, J eds. Osteoporosis. Academic Press, New York, NY; 1996:419.

nature medicine

Hdac2 regulates the cardiac hypertrophic response by modulating Gsk3β activity

Chinmay M Trivedi[1,2,9], Yang Luo[2,8,9], Zhan Yin[2,8,9], Maozhen Zhang[2,8], Wenting Zhu[1], Tao Wang[2], Thomas Floss[3], Martin Goettlicher[4], Patricia Ruiz Noppinger[5], Wolfgang Wurst[3], Victor A Ferrari[2], Charles S Abrams[6], Peter J Gruber[2,7] & Jonathan A Epstein[1,2]

In the adult heart, a variety of stresses induce re-expression of a fetal gene program in association with myocyte hypertrophy and heart failure. Here we show that histone deacetylase-2 (Hdac2) regulates expression of many fetal cardiac isoforms. Hdac2 deficiency or chemical histone deacetylase (HDAC) inhibition prevented the re-expression of fetal genes and attenuated cardiac hypertrophy in hearts exposed to hypertrophic stimuli. Resistance to hypertrophy was associated with increased expression of the gene encoding inositol polyphosphate-5-phosphatase f *(Inpp5f)* resulting in constitutive activation of glycogen synthase kinase 3β (Gsk3β) via inactivation of thymoma viral proto-oncogene (Akt) and 3-phosphoinositide-dependent protein kinase-1 (Pdk1). In contrast, *Hdac2* transgenic mice had augmented hypertrophy associated with inactivated Gsk3β. Chemical inhibition of activated Gsk3β allowed Hdac2-deficient adults to become sensitive to hypertrophic stimulation. These results suggest that Hdac2 is an important molecular target of HDAC inhibitors in the heart and that Hdac2 and Gsk3β are components of a regulatory pathway providing an attractive therapeutic target for the treatment of cardiac hypertrophy and heart failure.

Heart disease is the leading cause of death in the United States, and congestive heart failure (CHF) represents the final common pathway of many forms of heart disease. Most therapies for CHF primarily modulate hemodynamics, despite the fact that marked alterations in cardiac myocyte gene expression, energy utilization and intracellular signaling are well documented to be part of a vicious cycle that leads to progressive worsening of cardiac function[1–5].

A characteristic feature of CHF is the reactivation of a "fetal gene program"[6], although the regulatory mechanisms that affect this program are poorly understood. This transcriptional switch involves the simultaneous regulation of numerous cardiac genes. High-order regulation of gene transcription is at least partially controlled by a complex array of modifications of core histones, proteins that complex with DNA to form chromatin. Acetylation of histone tails results in relaxation of chromatin structure and enhances gene expression. Acetylation is mediated by histone acetyl transferases (HATs), and the converse reaction, deacetylation, is mediated by histone deacetylases (HDACs) and generally results in repression of transcription[7]. HDACs are composed of a highly conserved family, with homologs in yeast and humans that fall into three subfamilies[8]. Mammalian class I HDACs are related to the *Saccharomyces cerevisiae* proteins Rpd3, Hos1 and Hos2, and include Hdac1, 2, 3 and 8. Mammalian class II HDACs are related to the yeast proteins Hda1 and Hos3, and include Hdac4, 5, 6, 7 and 9. Mammalian class III HDACs (Sirtuins) are related to the yeast Sir2 protein. HDAC inhibitors such as trichostatin A (TSA) and valproic acid inhibit both class I and class II HDACs (ref. 9).

Recently, compelling biochemical and genetic evidence has indicated that class II HDACs can regulate hypertrophic gene expression in the heart[10–13]. Inactivation of *Hdac5* and *Hdac9* each result in a predisposition to cardiac hypertrophy. Nuclear localization of class II HDACs, and thus their ability to repress myocyte enhancer factor-2 (Mef2)-dependent hypertrophic gene expression, is regulated by phosphorylation of critical serine residues that are conserved in class II, but not class I, HDACs. These data indicate that class II HDACs repress cardiac hypertrophy. However, our group and others have provided evidence that treatment of animals or isolated cardiac myocytes with HDAC inhibitors can block the hypertrophic response to a series of pharmacologic and mechanical stresses[14–17]. Hence, we postulated that class I HDACs might normally function in the heart to

[1]Department of Cell and Developmental Biology, 1156 Basic Research Building II, and [2]Cardiovascular Institute, 956 Basic Research Building II, University of Pennsylvania School of Medicine, 421 Curie Boulevard, Philadelphia, Pennsylvania 19104, USA. [3]Institute of Developmental Genetics, GSF National Research Center for Environment and Health, and [4]Technical University Munich and Toxicology Department of the GSF National Research Center for Environment and Health, Ingolstaedter Landstrasse 1, 85764 Neuherberg, Germany. [5]Max-Planck Institute for Molecular Genetics, Department of Vertebrate Genomics, Hessische Str. 3-4, 10115 Berlin, Germany. [6]Hematology-Oncology Division, 912 Basic Research Building II, University of Pennsylvania School of Medicine, and [7]The Cardiac Center, 905 Basic Research Building II, Children's Hospital of Philadelphia, 421 Curie Boulevard, Philadelphia, Pennsylvania 19104, USA. [8]Present addresses: Novartis Institutes of Biomedical Research, 100 Technology Square, Cambridge, Massachusetts 02139, USA (Y.L.), Institute of Hydrobiology, Chinese Academy of Sciences, 7 Donghu South Road, Wuhan 430072, China (Z.Y.) and Department of Cardiology, Xinhua Hospital, Shanghai Jiao Tong University School of Medicine, 1665 Kong Jiang Road, Shanghai 200092, China (M.Z.). [9]These authors contributed equally to the work. Correspondence should be addressed to J.A.E. (epsteinj@mail.med.upenn.edu).

Received 10 October 2006; accepted 17 January 2007; published online 18 February 2007; doi:10.1038/nm1552

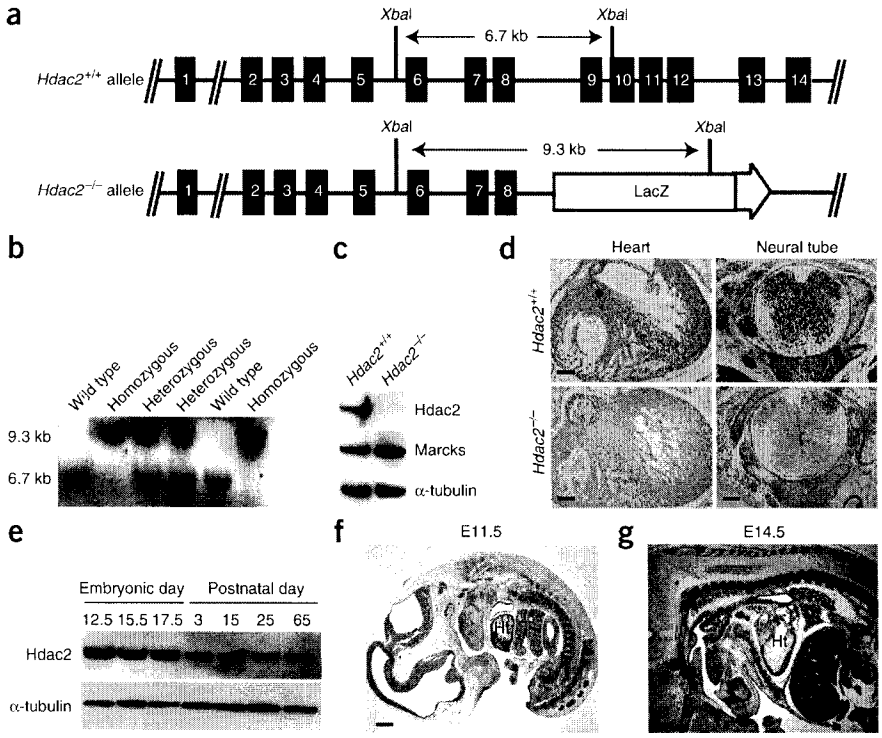

Figure 1 Inactivation of *Hdac2*. (**a**) Schematic representation of wild-type (*Hdac2*$^{+/+}$, top) and gene-trap (*Hdac2*$^{-/-}$, bottom) alleles. Exons are represented by black boxes. The sizes of the expected restriction fragments recognized by the Southern probe (indicated) are shown. (**b**) Southern blot of E15.5 embryos resulting from a cross between *Hdac2*$^{-/-}$ heterozygotes. (**c**) Western blot of total embryonic tissue from wild-type and *Hdac2*$^{-/-}$ embryos shows loss of Hdac2 protein in knockout embryos. The protein Marcks, encoded by the adjacent 3′ gene was expressed normally. (**d**) Hdac2 immunohistochemistry. Expression was present in the heart and neural tube of wild-type E14.5 embryos (brown) but was absent from *Hdac2*$^{-/-}$ littermates. Scale bar, 200 μm. (**e**) Western blot analysis shows Hdac2 protein expression in embryonic and postnatal hearts. (**f**,**g**) Hdac2 immunohistochemistry. Hdac2 protein was strongly expressed in the heart (Ht) at E11.5 (**f**; scale bar, 400 μm) and E14.5 (**g**; scale bar, 200 μm) (red).

repress antihypertrophic pathways, although experimental evidence in direct support of this suggestion is lacking[15,18].

Here we directly examined the role of the class I HDAC gene *Hdac2* during embryonic development and in the adult heart, by transgenic overexpression and by gene inactivation. *Hdac2*-null mice were unable to reactivate the fetal gene program or to exhibit normal hypertrophic responses. Transgenic overexpression of *Hdac2* in the heart reactivated fetal genes and induced cardiac hypertrophy. Biochemical analysis indicated that these responses were mediated by a Gsk3β-dependent pathway.

RESULTS

Inactivation of *Hdac2*

Hdac2-deficient mice were created from a gene-trap embryonic stem cell (ES) line (**Fig. 1a,b** and **Supplementary Table 1** online). Southern blot, PCR and sequence analysis revealed a partial deletion of *Hdac2*, removing exons 9–14, which encode portions of the catalytic domain. The fusion protein expected to result from the gene trap would lack deacetylase activity. We confirmed that the gene-trap insertion resulted in loss of wild-type Hdac2 expression, by western blotting (**Fig. 1c**) and immunohistochemistry (**Fig. 1d**). Notably, protein expression of myristoylated alanine-rich protein kinase C substrate (Marcks), which is encoded by the gene located immediately downstream of *Hdac2*, was not affected by the insertional mutation (**Fig. 1c**).

Hdac2 was expressed throughout gestation and in adult mice (**Fig. 1e**). At embryonic day (E)11.5–14.5, protein expression was robust in myocardial nuclei (**Fig. 1d,f,g**), although expression was also evident in the neural tube (**Fig. 1d**) and elsewhere. Hdac2 protein was not evident in homozygous *Hdac2*$^{-/-}$ embryos (**Fig. 1c,d**).

Hdac2$^{-/-}$ pups were identified at birth and in the first postnatal days, although some intrauterine loss was noted and occasional resorbing fetuses were found at late gestation (**Supplementary Table 1**). However, nearly half of the surviving *Hdac2*$^{-/-}$ pups identified at birth succumbed during the first 25 postnatal days, whereas all wild-type and heterozygous littermates survived (**Fig. 2a**). Substantial postnatal lethality was confined to the first month of age, after which the survival curve paralleled that of wild-type mice. Between postnatal days (P) 0 and 3, we could not distinguish homozygous pups from heterozygous and wild-type littermates on the basis of their appearance (**Fig. 2b**). By P10, homozygous mice were smaller than wild-type mice and appeared lethargic (**Fig. 2b**). A marked difference in body size was apparent through the first month of life (**Fig. 2b**) but thereafter became less evident. By 2 months of age, homozygous mice were generally indistinguishable from wild-type mice (**Fig. 2b**) and had equivalent body weights. Normalization of body size and appearance was not due to a selection bias or loss of affected homozygotes, as individual runted mice were observed to normalize over time. Thus, loss of Hdac2 results in partial perinatal lethality; surviving mice recover and appear grossly normal after 2 months of age.

Perinatal cardiomyocyte defects

In *Hdac2*$^{-/-}$ mice, the most notable abnormalities were seen in the heart. At E14.5, the hearts of *Hdac2*$^{-/-}$ mice appeared normal (**Fig. 2c**). By late gestation and in the newborn period (P1, **Fig. 2c**), *Hdac2*$^{-/-}$ hearts showed a thickened myocardial compact zone with reduced trabeculation, which was evident through P8 (**Fig. 2d**). Although these hearts were smaller than those of wild-type littermates at this age (**Fig. 2d**), the overall size of *Hdac2*$^{-/-}$ mice was also smaller than that of wild-type mice, such that the heart to body weight ratio was increased in *Hdac2*$^{-/-}$ mice (mean ± s.e.m.: 0.865 ± 0.155 versus 0.661 ± 0.094, $n = 6$ in each group, $P < 0.003$). This increase is consistent with the thickened ventricular wall and decreased ventricular cavity size seen in *Hdac2*$^{-/-}$hearts (**Fig. 2d**). Notably, the difference in heart to body weight ratio disappeared after 2 months of age.

Cardiac enlargement can be caused by hypertrophy or hyperplasia of cardiac myocytes. We did not observe any difference in myocyte cell size by routine histology or electron microscopy. However, proliferation rates of cardiac myocytes in *Hdac2*$^{-/-}$ mice were elevated (**Fig. 2c** and **Supplementary Table 2** online), but no difference in the level of apoptosis was noted (data not shown). At E15.5, we noted a slight

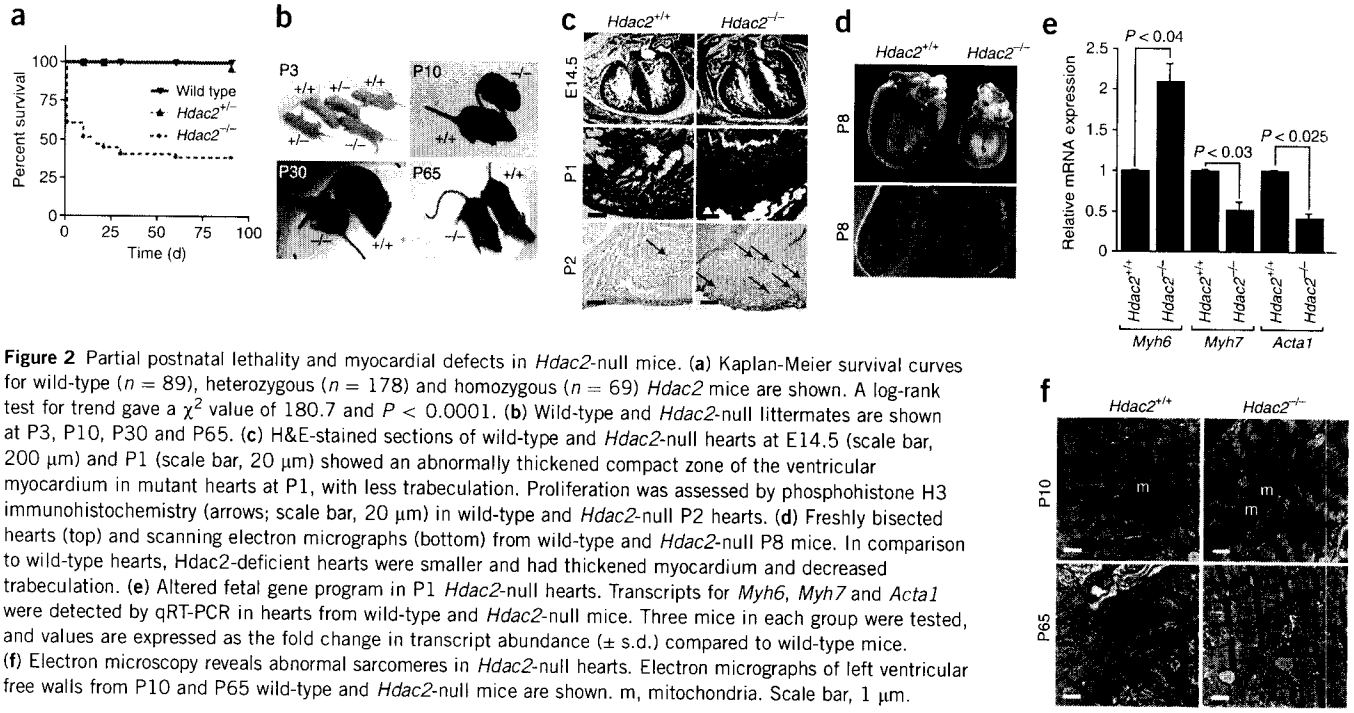

Figure 2 Partial postnatal lethality and myocardial defects in *Hdac2*-null mice. (**a**) Kaplan-Meier survival curves for wild-type ($n = 89$), heterozygous ($n = 178$) and homozygous ($n = 69$) *Hdac2* mice are shown. A log-rank test for trend gave a χ^2 value of 180.7 and $P < 0.0001$. (**b**) Wild-type and *Hdac2*-null littermates are shown at P3, P10, P30 and P65. (**c**) H&E-stained sections of wild-type and *Hdac2*-null hearts at E14.5 (scale bar, 200 μm) and P1 (scale bar, 20 μm) showed an abnormally thickened compact zone of the ventricular myocardium in mutant hearts at P1, with less trabeculation. Proliferation was assessed by phosphohistone H3 immunohistochemistry (arrows; scale bar, 20 μm) in wild-type and *Hdac2*-null P2 hearts. (**d**) Freshly bisected hearts (top) and scanning electron micrographs (bottom) from wild-type and *Hdac2*-null P8 mice. In comparison to wild-type hearts, Hdac2-deficient hearts were smaller and had thickened myocardium and decreased trabeculation. (**e**) Altered fetal gene program in P1 *Hdac2*-null hearts. Transcripts for *Myh6*, *Myh7* and *Acta1* were detected by qRT-PCR in hearts from wild-type and *Hdac2*-null mice. Three mice in each group were tested, and values are expressed as the fold change in transcript abundance (± s.d.) compared to wild-type mice. (**f**) Electron microscopy reveals abnormal sarcomeres in *Hdac2*-null hearts. Electron micrographs of left ventricular free walls from P10 and P65 wild-type and *Hdac2*-null mice are shown. m, mitochondria. Scale bar, 1 μm.

increase in Ki67 staining, which became more apparent by P2 (**Supplementary Table 2**). Increased cell proliferation at P2 was confirmed by phosphohistone H3 immunostaining (**Fig. 2c** and **Supplementary Table 2**). Quantitative real-time PCR (qRT-PCR) analysis of P1 heart tissue revealed alterations in fetal cardiac isoform gene expression (**Fig. 2e**). *Hdac2*$^{-/-}$ hearts showed decreased expression of the mRNAs encoding fetal β-myosin heavy chain (β-MHC, also known as myosin heavy polypeptide 7, Myh7) and α-skeletal actin (α-SA, also known as alpha skeletal actin 1, Acta1), whereas the mRNA encoding α-myosin heavy chain (α-MHC, also known as myosin heavy polypeptide 6, Myh6) was upregulated (**Fig. 2e**).

We also observed abnormalities of myocyte maturation in *Hdac2*$^{-/-}$ hearts. Electron microscopic evaluation at P10 of hearts from these mice revealed increased numbers of mitochondria and abnormal sarcomere structure (**Fig. 2f**). Sarcomere length was reduced compared to hearts from wild-type mice (0.98 ± 0.20 versus 1.43 ± 0.02 μM, $P < 0.01$). Z-bands were broad and fuzzy in appearance (**Fig. 2f**). Microarray analysis showed 7- to 100-fold downregulation of genes encoding structural components of the sarcomere, including cardiac myosin light chain and heavy chain, tropomyosin, troponin and α-actinin (data not shown, see **Supplementary Methods** online). These structural and gene expression changes were largely resolved by P65 (**Fig. 2f** and data not shown). Cardiac function of *Hdac2*$^{-/-}$ mice older than 2 months of age appeared normal, according to electrocardiogram (ECG)-gated magnetic resonance imaging (MRI) (ejection fraction: 86% in wild-type mice versus 82% in *Hdac2*$^{-/-}$ mice, $n = 2$; cardiac output: 15.7 ml/min in wild-type mice versus 15.1 ml/min in *Hdac2*$^{-/-}$ mice, $n = 2$) and echocardiography (ejection fraction by Simpson's method: 73.6%, $n = 5$ in wild-type mice versus 76.8%, $n = 7$ in *Hdac2*$^{-/-}$ mice).

Hdac2 regulates cardiac hypertrophy

Mice that lack the unusual homeobox gene *Hod* (also known as *Hop*) exhibit a cardiac phenotype that overlaps with that described here for *Hdac2* mutants, characterized by abnormalities in the balance between cardiac myocyte differentiation and proliferation[19,20]. Overexpression of *Hod* in the adult heart causes cardiac hypertrophy, which can be prevented by treatment with HDAC inhibitors[15]. Hence we sought to determine if loss of Hdac2 would protect adult mice from developing cardiac hypertrophy induced by Hod overexpression. We crossed *Hdac2*$^{+/-}$, *Hod* transgenic (*Hod*-Tg) mice with *Hdac2*$^{+/-}$ mice and examined the heart to body weight ratios of offspring at P60. At this time point, Hdac2 deficiency alone did not alter this measurement from that in wild-type littermates (**Fig. 3a**). As reported previously, transgenic expression of *Hod* resulted in significant cardiac hypertrophy (**Fig. 3a** and **Supplementary Table 3** online). However, this hypertrophic response was not apparent in *Hod*-Tg, *Hdac2*$^{-/-}$ mice (**Fig. 3a** and **Supplementary Table 3**). Re-expression of the fetal gene program, which normally accompanies Hod-induced cardiac hypertrophy, was not evident in the *Hdac2*-deficient background. Natriuretic peptide precursor type A (*Nppa*, encoding atrial natriuretic factor, ANF) (encoding ANF), *Myh7* (encoding β-MHC) and *Acta1* (encoding α-SA) were all upregulated in *Hod*-Tg hearts, and this upregulation was prevented by the absence of Hdac2 (**Fig. 3b**). Likewise, *Myh6* (encoding α-MHC) was significantly ($P < 0.002$) downregulated in *Hod*-Tg hearts but was slightly increased in *Hod*-Tg, *Hdac2*$^{-/-}$ littermates (**Fig. 3c**).

We sought to determine if adult mice lacking Hdac2 would be resistant to isoproterenol (ISO)-induced and transaortic constriction (TAC)-induced hypertrophy. Wild-type and *Hdac2*$^{-/-}$ littermates at 2 months of age were treated with a constant infusion of saline or ISO for 2 weeks. As predicted, wild-type mice exhibited marked cardiac hypertrophy, as revealed by an increase in the heart to body weight ratio (**Fig. 3a**). Similar effects were apparent for the ratio of heart weight to tibia length, a measure of body size (**Supplementary Table 3**). Transcripts for *Nppa*, *Myh7* and *Acta1* increased in abundance (**Fig. 3b**), and those for *Myh6* decreased (**Fig. 3c**). Hypertrophy of *Hdac2*$^{-/-}$ mice in response to ISO was not apparent (**Fig. 3a**), and reactivation of the fetal gene program was not observed

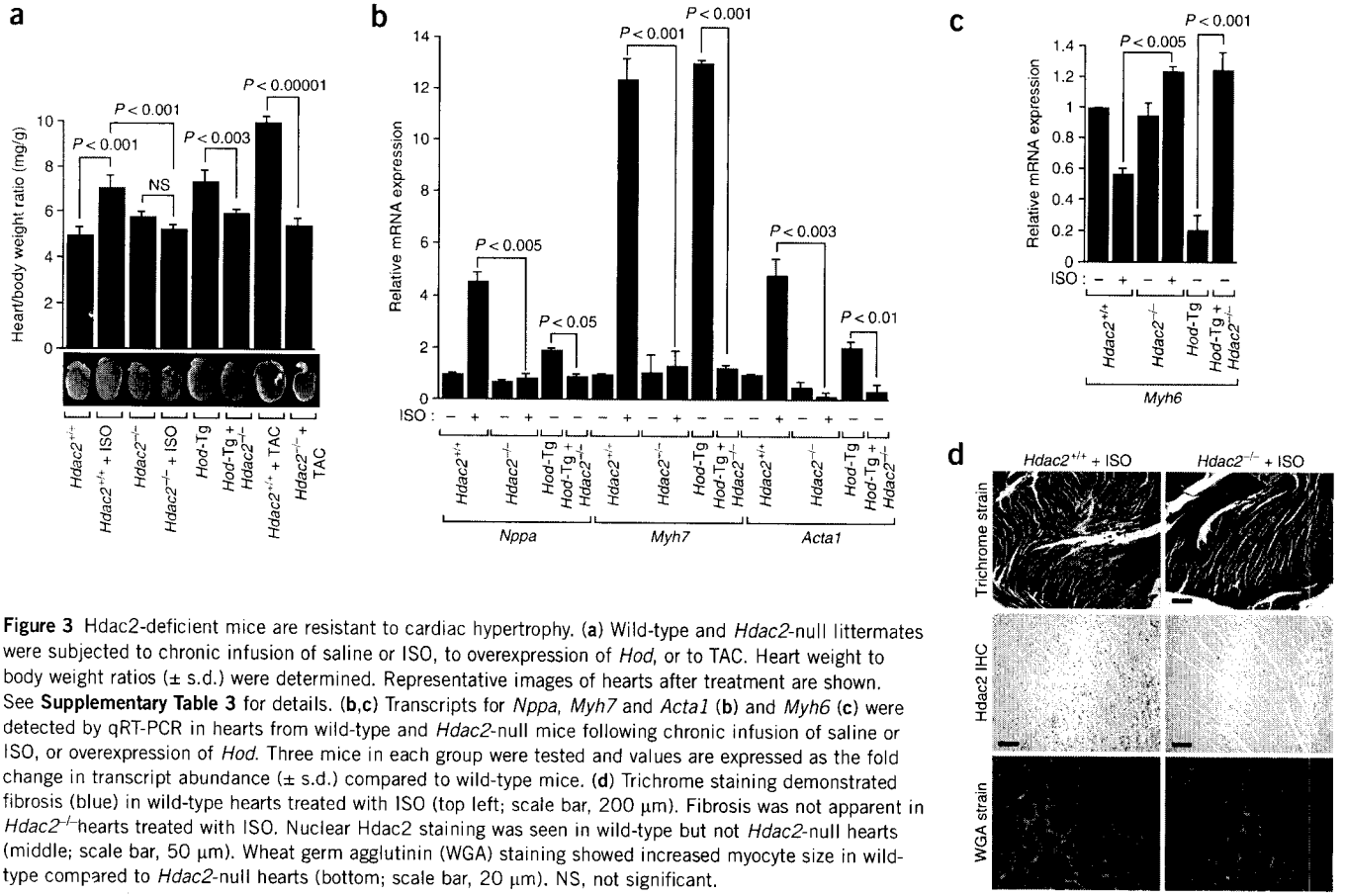

Figure 3 Hdac2-deficient mice are resistant to cardiac hypertrophy. (**a**) Wild-type and *Hdac2*-null littermates were subjected to chronic infusion of saline or ISO, to overexpression of *Hod*, or to TAC. Heart weight to body weight ratios (± s.d.) were determined. Representative images of hearts after treatment are shown. See **Supplementary Table 3** for details. (**b**,**c**) Transcripts for *Nppa*, *Myh7* and *Acta1* (**b**) and *Myh6* (**c**) were detected by qRT-PCR in hearts from wild-type and *Hdac2*-null mice following chronic infusion of saline or ISO, or overexpression of *Hod*. Three mice in each group were tested and values are expressed as the fold change in transcript abundance (± s.d.) compared to wild-type mice. (**d**) Trichrome staining demonstrated fibrosis (blue) in wild-type hearts treated with ISO (top left; scale bar, 200 μm). Fibrosis was not apparent in *Hdac2*$^{-/-}$hearts treated with ISO. Nuclear Hdac2 staining was seen in wild-type but not *Hdac2*-null hearts (middle; scale bar, 50 μm). Wheat germ agglutinin (WGA) staining showed increased myocyte size in wild-type compared to *Hdac2*-null hearts (bottom; scale bar, 20 μm). NS, not significant.

(**Fig. 3b**,**c**). Patchy areas of fibrosis apparent in the ventricles of wild-type hearts treated with ISO were not evident in ISO-treated *Hdac2*$^{-/-}$ hearts (**Fig. 3d**), and cellular hypertrophy, as demonstrated by wheat germ agglutinin staining (WGA), was not evident (**Fig. 3d**). (ImageJ quantification of myocyte cross sectional area was 106.9 μm^2 for *Hdac2*$^{-/-}$ mice, $n = 196$, two hearts; 232.8 μm^2 for wild type mice, $n = 203$, two hearts.) Wild-type mice that underwent TAC surgery exhibited marked cardiac hypertrophy after 14 d, whereas there was no hypertrophy in *Hdac2*$^{-/-}$ mice (**Fig. 3a** and **Supplementary Table 3**).

We used the *Myh6* (encoding α-MHC) promoter to overexpress *Hdac2* in the adult heart, in order to determine whether Hdac2 is not only necessary for hypertrophic responsiveness but also sufficient. We confirmed overexpression by western blotting in two independent transgenic lines. In both cases, heart to body weight ratios were increased in transgenic mice by 4 weeks of age and increasing cardiac hypertrophy was documented at 8 weeks (**Fig. 4a**). Reactivation of the fetal gene program was also evident (**Fig. 4b**). Overexpression of *Hdac2* augmented the cardiac hypertrophy induced by overexpression of *Hod*, such that compound transgenic mice (carrying one copy of each transgene) had enormous hearts with significantly greater hypertrophy ($P < 0.000003$) than either transgenic line alone (**Fig. 4c**). Thus, both loss- and gain-of-function experiments support a critical role for Hdac2 in the regulation of cardiac hypertrophy.

Hdac2 regulates *Inpp5f* and Gsk3β

Although alternative mechanisms of action have been described[21,22], HDACs commonly function as transcriptional corepressors. Therefore, we examined the genes upregulated in *Hdac2*-deficient hearts that could be implicated in growth control. Among other upregulated genes identified by microarray analysis (data not shown), we detected a previously described, though poorly characterized, gene encoding phosphatidylinositol-4,5-bisphosphate (PIP2) and phosphatidyl inositol-3,4,5-trisphosphate (PIP3) phosphatase, named *Inpp5f* (refs. 23,24). PIP3 levels are critical for regulation of the phosphatidylinositol-3-kinase (PI3K)-Akt pathway, which is important for growth control in many systems including the heart, where it has been previously implicated in hypertrophic signaling[25]. The *Inpp5f* transcript was upregulated 2.2-fold (assessed by qRT-PCR) in *Hdac2*$^{-/-}$hearts (**Fig. 5a**), whereas it was significantly ($P < 0.0001$) downregulated in *Hdac2*-Tg hearts (**Fig. 5a**). Downregulation of *Inpp5f* was not seen in transgenic mice overexpressing *Hdac1* or *Hdac3* in the heart, and these mice did not develop cardiac hypertrophy (**Supplementary Fig. 1** online). In cultured H9c2 rat ventricular myocytes, treatment with the HDAC inhibitor TSA resulted in upregulation of *Inpp5f*, whereas overexpression of *Hdac2* caused *Inpp5f* to be downregulated (**Supplementary Fig. 2** online). Inpp5f removes the 5′-phosphate from PIP3 (ref. 24) and can affect the Akt pathway: indeed, transfection of *Inpp5f* resulted in downregulation of phospho-Akt and phospho-Gsk3β in H9c2 cells (**Fig. 5b**) and in COS-7 cells (data not shown). This effect was readily apparent despite an estimated transfection efficiency of 50%. Transfection of an alternatively spliced isoform that is expressed in a tissue-specific fashion[23] but is predicted to lack phosphatase activity had no effect on Akt and Gsk3β phosphorylation (data not shown). Furthermore, the decrease in Akt and Gsk3β phosphorylation induced by *Inpp5f* overexpression was reversed by co-transfection with a

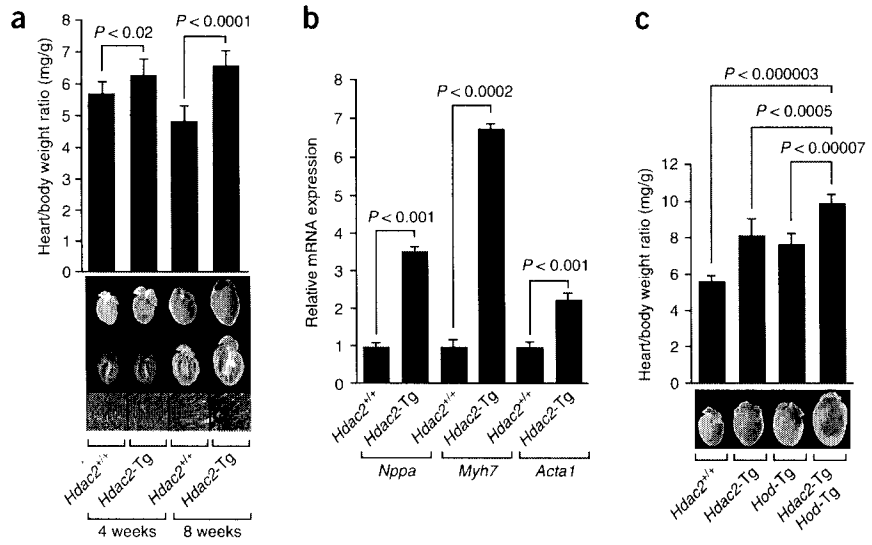

Figure 4 Transgenic overexpression of *Hdac2* causes cardiac hypertrophy. (**a**) Heart to body weight ratios of *Hdac2*-Tg mice at the ages of 4 weeks ($n = 9$) and 8 weeks ($n = 8$) are shown. Representative images of the hearts are shown in the middle panel, and high magnification views of ventricular cardiac myocytes are shown in the bottom panel. (**b**) Fetal gene transcript levels were detected in wild-type ($n = 3$) and *Hdac2*-Tg mice ($n = 3$) at 2 months of age by qRT-PCR. (**c**) *Hod* overexpression enhanced Hdac2-dependent cardiac hypertrophy. Heart to body weight ratios of wild-type ($n = 7$), *Hdac2*-Tg ($n = 8$), *Hod*-Tg ($n = 7$) and doubly transgenic *Hdac2*-Tg *Hod*-Tg mice ($n = 7$) are shown, with representative images of explanted hearts.

constitutively activated *Akt* (ca*Akt*) (**Fig. 5b**), suggesting that Akt is functioning downstream of Inpp5f and is capable of regulating Gsk3β. Knockdown of *Inpp5f* in H9c2 cells with siRNA resulted in enhanced Akt phosphorylation (**Fig. 5c**). Thus, *Inpp5f* is upregulated in the absence of Hdac2 and is downregulated when Hdac2 is overexpressed, and Inpp5f is capable of modulating the Akt-Gsk3β pathway.

Numerous hypertrophic stimuli, including β-adrenergic agonists, result in phosphorylation of Akt and Gsk3β, with resultant inactivation of Gsk3β (refs. 25–29). The ability of Hdac2 to regulate *Inpp5f* suggests that signaling downstream of PI3K might be attenuated in the hearts of Hdac2-deficient mice subjected to hypertrophic stimulation. Under basal conditions, $Hdac2^{-/-}$ hearts showed decreased Akt and Gsk3β phosphorylation, although total levels of these kinases were unchanged (**Fig. 5d**). Levels of phospho-mammalian target of rapamycin (mTOR), forkhead box O3A (FoxO3A) and forkhead box O1 (FoxO1) were also reduced, consistent with downregulation of the Akt pathway, whereas levels of phospho-protein kinase A (Pka), protein kinase C (Pkc) and integrin-linked kinase (Ilk) were unchanged (**Fig. 5d** and **Supplementary Fig. 3** online). We also found a notable difference in the response to ISO between wild-type and $Hdac2^{-/-}$ littermates: $Hdac2^{-/-}$ hearts contained far less of the phosphorylated forms of Akt and Pdk1 (**Fig. 5e**). Phosphorylation of the downstream kinase Gsk3β was also significantly reduced, despite no change in the total levels of these proteins **Fig. 5e**). PI3K is an upstream activator of the Akt-Pdk1-Gsk3β pathway and the phosphatase and tensin homolog (Pten) opposes PI3K-mediated activation of the pathway. However, no

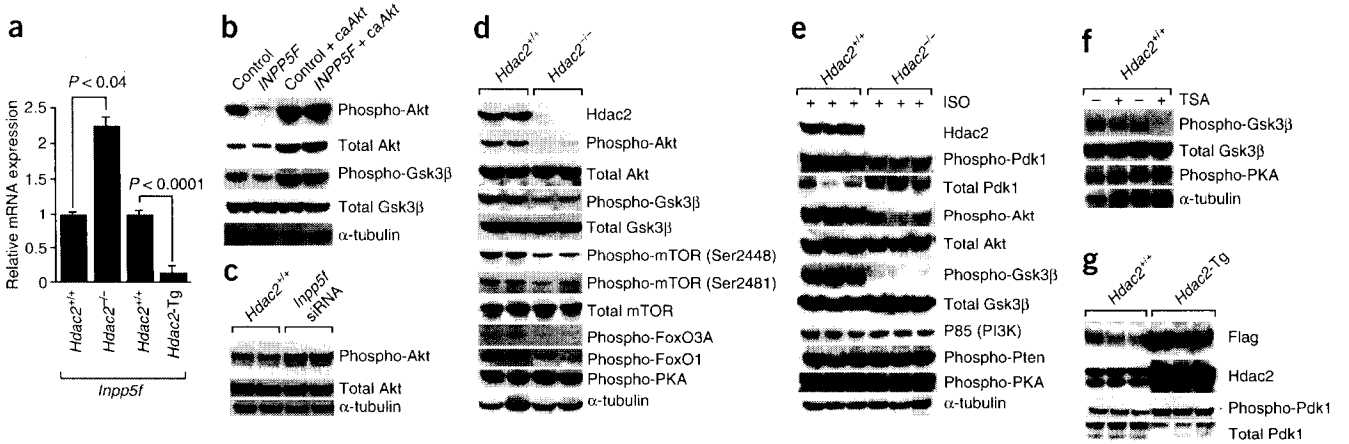

Figure 5 Hdac2 regulates a Pdk-Akt-Gsk3β pathway in the heart. (**a**) Transcripts for *Inpp5f* were detected by qRT-PCR in hearts from 2-month-old wild-type, *Hdac2*-null and *Hdac2*-Tg mice. Three mice in each group were tested and values are expressed as the fold change in abundance (± s.d.) compared to that in wild-type littermates. (**b**) Overexpression of *INPP5F* in H9c2 cells resulted in decreased phosphorylation of Gsk3β and Akt. Phosphorylated and total Gsk3β and Akt were measured by western blot with or without transfection of *INPP5F* and ca*Akt* expression vectors. (**c**) H9c2 cells were treated with siRNA to knockdown expression of *Inpp5f*, and total and phosphorylated Akt levels were measured by western blotting. (**d**) Western blots of myocardium from 2-month-old wild-type and *Hdac2*-null mice; α-tubulin is shown as a loading control. (**e**) Western blots of myocardium from 2-month-old wild-type and *Hdac2*-null mice subjected to the infusion of saline or ISO for 14 d. Phospho-PKA is shown as a control for phosphorylated proteins, and α-tubulin is shown as a loading control. (**f**) Western blots of myocardium from 2-month-old mice treated for 14 d with TSA (0.6 mg/kg/day; +) or with vehicle alone (–). (**g**) Western blot analysis of myocardium from 2-month-old wild-type and *Hdac2*-Tg mice. Transgenically expressed *Hdac2* was epitope-tagged and was detected using a Flag antibody. Both endogenous and transgenically expressed Hdac2 were detected by the Hdac2 antibody. (Note that the western blots for phosphorylated species were considerably underexposed as compared to those in **Figure 5d,e** in order to demonstrate increased abundance of these species in transgenic samples.) All western blots were performed at least twice with similar results.

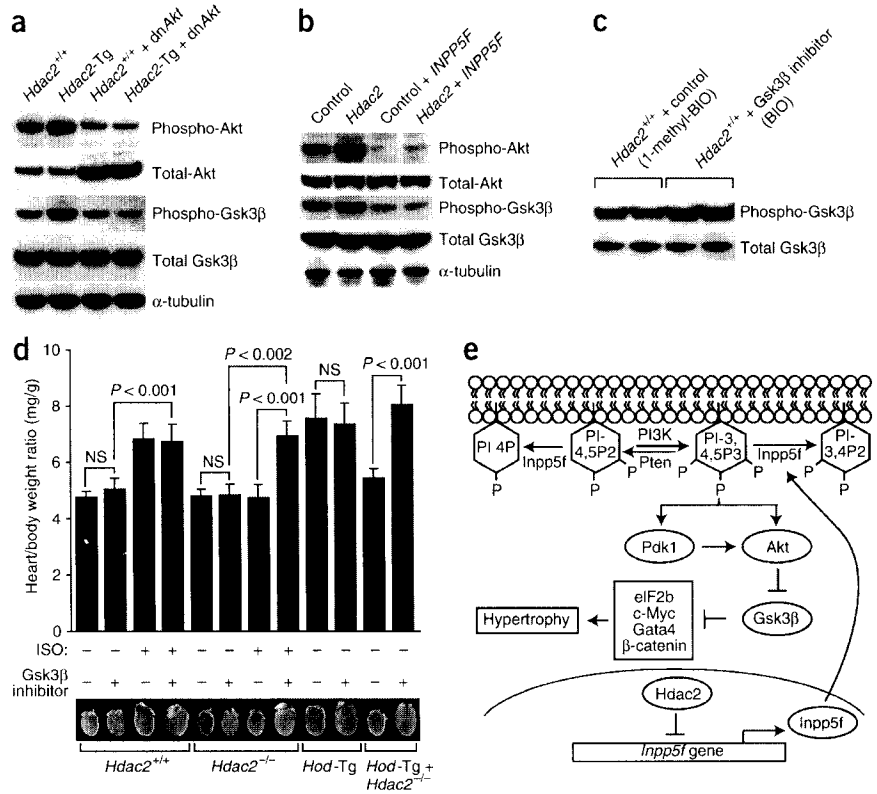

Figure 6 Gsk3β inhibition rescues resistance to cardiac hypertrophy in *Hdac2*-null mice. (**a**) Western blot analysis of cardiac myocytes isolated from wild-type and *Hdac2*-Tg mice, either infected or not with dn*Akt*. (**b**) Western blot analysis of H9c2 cells with or without transfection of *Hdac2* and *INPP5F* expression vectors. (**c**) Mice treated with a Gsk3β inhibitor or a kinase-inactive control compound were assayed for cardiac Gsk3β phosphorylation. (**d**) Mice of the indicated genotypes were subjected to saline or ISO infusion and were treated with Gsk3β inhibitor (+) or kinase-inactive control (–) for 14 d. Heart to body weight ratios (± s.d.) were determined. Representative images of explanted hearts are shown. See **Supplementary Table 3** for details. (**e**) Model of Hdac2 function in hypertrophic signaling. PI3K phosphorylates the membrane PIP2 at the 3′ position of the inositol ring, thus producing PIP3. This reaction is reversed by Pten. Accumulation of PIP3 leads to recruitment of the protein kinase Akt and its activator Pdk1 to the cell membrane. Activated Akt and Pdk1 inactivate Gsk3β by causing its phosphorylation. This relieves inhibition of several hypertrophic signaling pathways leading to cardiac hypertrophy. Hdac2 suppresses *Inpp5f* expression. As Inpp5f can remove the 5′ phosphate from PIP2 and PIP3, Hdac2 deficiency would deplete PIP3, resulting in decreased Akt signaling, increased Gsk3β activity and resistance to hypertrophic stimulation. NS, not significant. All western blots were performed at least twice with similar results.

change was seen in the phosphorylation status of the p85 subunit of PI3K (**Fig. 5e**) or in PI3K activity (data not shown), or in Pten activation (**Fig. 5e**). Hence, loss of Hdac2 regulates this pathway downstream of PI3K but upstream of Akt-Pdk1-Gsk3β, consistent with our finding of upregulated *Inpp5f* expression.

Chemical HDAC inhibitors, like the genetic ablation of *Hdac2*, promote resistance to hypertrophic stimuli[15–17]. We sought to determine if the HDAC inhibitor TSA might function in the heart by causing activation of Gsk3β. We noted a substantial decrease in Gsk3β phosphorylation in hearts of mice treated for 2 weeks with daily intraperitoneal injections of TSA at doses sufficient to impair hypertrophic responsiveness (**Fig. 5f**). Taken together, these results suggest that *Hdac2* inactivation and TSA treatment each result in activation of Gsk3β, which may be sufficient to account for the observed resistance to cardiac hypertrophy in these models given the established role of Gsk3β in hypertrophic signaling[26–29].

Biochemical changes observed in *Hdac2*-Tg hearts were precisely opposite those seen in *Hdac2*$^{-/-}$ hearts. We noted a marked increase in levels of phosphorylated Akt, phospho-Pdk1 and phospho-Gsk3β (**Fig. 5g**), associated with decreased *Inpp5f* levels. Hence, Hdac2 is both necessary and sufficient to modulate Akt and Gsk3β activity and cardiac hypertrophy. Further support for the hypothesis that Akt regulates Gsk3β in this tissue derives from experiments in which we isolated cardiac myocytes from *Hdac2*-Tg mice. After primary culture, these cells continued to show increased phosphorylation of Akt and Gsk3β (**Fig. 6a**). However, infection of these cells with an adenovirus encoding a dominant-negative *Akt* (dn*Akt*) reduced both phospho-Akt and phospho-Gsk3β levels (**Fig. 6a**). In H9c2 myocytes, overexpression of *Hdac2* increased Akt and Gsk3β phosphorylation (**Fig. 6b**), presumably via downregulation of *Inpp5f* expression (**Fig. 5a** and **Supplementary Fig. 2**). Consistent with this model, co-transfection with *Inpp5f* prevented Hdac2-mediated upregulation of Akt and Gsk3β phosphorylation (**Fig. 6b**).

To determine if constitutive activation of Gsk3β is the primary cause of resistance to hypertrophy in *Hdac2*$^{-/-}$ mice, we tested the ability of a chemical Gsk3β inhibitor to restore hypertrophic responsiveness to *Hdac2*$^{-/-}$ mice. We treated 2-month-old mice with daily intraperitoneal injections of (2′Z,3′E)-6-bromoindirubin-3′-oxime (BIO), a Gsk3β-specific inhibitor, for 2 weeks, or with the kinase-inactive control compound 1-methyl-BIO. We documented that treatment with BIO effectively inhibited Gsk3β *in vivo*, by examining the ratio of phospho-Gsk3β to total Gsk3β in heart extracts, as Gsk3β is known to undergo N-terminal autophosphorylation upon catalytic inhibition[30]. Treatment with BIO resulted in a significant increase of Gsk3β phosphorylation as compared to treatment with the control compound (~73% increase in phosphorylated Gsk3β, **Fig. 6c**). Treatment with either compound did not result in substantial changes in heart to body weight ratio in wild-type or *Hod*-Tg mice (**Fig. 6d** and **Supplementary Table 3**). Notably, BIO treatment of ISO-treated *Hdac2*$^{-/-}$ mice restored their ability to undergo hypertrophy (**Fig. 6d**). Likewise, *Hod*-Tg mice on an *Hdac2*$^{-/-}$ background, which did not show hypertrophy under baseline conditions (**Fig. 3a**), showed significantly increased heart to body weight ratios when exposed to Gsk3β inhibition (**Fig. 6d**). Taken together, these results indicate that inhibition of Gsk3β is sufficient to abolish the antihypertrophic effects of Hdac2 deficiency, thus demonstrating the functional significance of Akt-Pdk1-Gsk3β signaling in Hdac2-deficient hearts.

DISCUSSION

The role of the HDAC family in cardiac myocyte homeostasis is complex[10,12]. The available data suggest that class I and class II HDACs play opposing roles in the regulation of hypertrophic pathways.

Class II HDACs function to repress hypertrophy[11,13], whereas Hdac2, a class I HDAC, is required for at least some hypertrophic responses. Pharmacologic inhibitors that block catalytic activity of both class I and class II HDACs prevent hypertrophic responses in both isolated myocytes and intact mice[14,15], suggesting that the predominant targets of these chemical inhibitors are class I HDACs. Our data suggest that Hdac2 is likely to be a major molecular target of HDAC inhibitors in the heart, although we cannot rule out partially redundant functions of other class I HDACs. These observations have clinical significance because HDAC inhibitors are in phase 1 and phase 2 clinical trials for the treatment of cancer, and cardiac side effects may emerge[9,31,32]. These results also suggest that Hdac2 inhibition may be useful for the treatment of cardiac hypertrophy and heart failure.

The phenotype of Hdac2-deficient mice partially overlaps with that of Hod-deficient mice[19,20]. Inactivation of either gene leads to partially penetrant embryonic lethality, with abnormalities of myocyte proliferation and differentiation apparent during late gestation. Both genes play a role in the hypertrophic response of the adult myocardium, and overexpression of either induces hypertrophy. These observations are consistent with the proposal that Hod and Hdac2 are components of a transcriptional repression complex[15]. Thus cardiac hypertrophy induced by overexpression of *Hod* is rescued by inactivation of *Hdac2*. However, significant differences in the knockout phenotypes exist, and both Hod and Hdac2 are likely to have functions that are unrelated to their roles within a shared complex.

We observed that Hdac2 modulates an intracellular signaling cascade downstream of PI3K. As HDACs normally function as repressors of transcription, the activation of this kinase cascade suggests that Hdac2 may repress expression of a phosphatase, and our discovery of Hdac2 regulation of *Inpp5f* is consistent with this hypothesis. Thus our data support a model in which Hdac2 regulation of *Inpp5f* modulates PIP3 levels in the heart and thereby affects the degree to which hypertrophic signals are transmitted via the PI3K-Akt-Gsk3β pathway (**Fig. 6e**). Like Pten, Inpp5f degrades PIP3: whereas Pten removes the 3′ phosphate of PIP3, Inpp5f removes the 5′ phosphate. This functional similarity to Pten implicates *Inpp5f* as a candidate tumor suppressor gene. Notably, *Inpp5f* maps to a previously identified tumor suppressor locus[33,34]. Thus, the ability of Hdac2 to regulate *Inpp5f* may be relevant to the mechanism of action of HDAC inhibitors as therapeutic agents in cancer[35]. It is worth noting that a recent report indicates that HDAC inhibition in cancer cells results in activation of Gsk3β (ref. 36).

Alternative functions of Hdac2, unrelated to chromatin remodeling and transcriptional repression, remain as possible causes of Gsk3β activation. Substrates for deacetylation, in addition to histones, have been well described[37], and functions unrelated to catalytic activity may also exist. Thus it will be critical in future experiments to determine whether the catalytic activity of Hdac2 is required for its normal function in the heart and to identify the relevant substrates. In this regard, it remains possible that the fusion protein produced by the gene-trap insertion in our *Hdac2*-mutant mice retains an unrecognized functional activity despite loss of the catalytic domain, resulting in a hypomorphic allele, although an independent function of the residual N-terminal domain has not been previously described.

Reactivation of the fetal gene program is a clinically and experimentally useful hallmark of cardiac hypertrophy. Our results, demonstrating altered expression of fetal sarcomere isoforms in Hdac2-deficient embryos and a failure to reactivate fetal gene expression under hypertrophic stress, suggest that the genetic programs that regulate the balance between fetal myocyte proliferation and differentiation may be closely related to the programs that regulate cardiac myocyte size in the postmitotic adult myocardium. The finding that Hdac2 regulates this program without affecting basal adult cardiac function implicates Hdac2 as an attractive therapeutic target for interventions to prevent pathologic responses without altering basal cardiac activity.

METHODS

***Hdac2*$^{-/-}$ knockout mice.** The *Hdac2* gene-trap clone was obtained from the German Genetrap Consortium (ES clone no. W035F03). The *Hdac2* genomic locus is interrupted by insertion of the pT1-βgeo vector, which integrated into intron 8. Chimeric mice were produced by blastocyst injection according to standard protocols. Mice were genotyped by Southern blotting and PCR. *Hdac2*$^{+/+}$ and *Hdac2*$^{-/-}$ mice were genotyped by PCR using 5′-TGCTG CAGTGTGGCGCAGACTCC-3′, 5′-GCGCTGACATGGCAACAAACTACTCA TGG-3′, 5′-CTGGAGAAGGCCCGACCATCC-3′ and 5′-CATGCGCTGCCAC ATGCAACTTTGC-3′ primers. The loss of Hdac2 expression was confirmed with immunostaining using a rabbit polyclonal antibody targeted to the C terminus of Hdac2 (Zymed, 51-5100). Histological sections were stained with wheat germ agglutinin (Sigma). *Hod*-Tg have been described[15].

***Hdac2*-transgenic mice.** A cDNA encoding mouse Flag-tagged *Hdac2* was cloned into an expression plasmid containing the *Myh6* (encoding α-MHC) promoter, and transgenic mice were generated by standard techniques. Genotyping was performed by PCR analysis of genomic DNA, and cardiac specific expression of Hdac2 was revealed by qRT-PCR, immunohistochemistry or western blot analysis using antibodies to Flag tag (Sigma), GFP (Cell Signaling) or Hdac2 (Zymed). *Hdac1* and *Hdac3*-Tg mice were generated in a similar fashion.

Treatment with isoproterenol, trichostatin A and a Gsk3β inhibitor. Isoproterenol (Sigma, I5627) was delivered to 8- to 10-week-old mice by implanting a micro-osmotic pump (Alzet, Durect; model 1002) subcutaneously under pentobarbital anesthesia. ISO (30 mg/kg/d) or vehicle (Dulbecco's phosphate buffered saline, Gibco) was infused subcutaneously for 14 d. Mice were given the Gsk3β inhibitor (2′*Z*, 3′*E*)-6-bromoindirubin-3′-oxime (BIO, Calbiochem, 361550, 300 μl of a 50 μM solution prepared in DMSO:PBS 2:1 per day) or a control compound (1-methyl-BIO, Calbiochem, 361556) at an equivalent dose by daily intraperitoneal injection for 14 d. This dose of active compound was chosen by performing a dose response test and selecting the minimal dose necessary to induce maximal Gsk3β phosphorylation. TSA (0.6 mg/kg/d) was administered as described[15], daily for 14 d.

Transverse aortic constriction (TAC). Mice were anaesthetized with a mixture of ketamine (100 mg/kg) and xylazine (2.5 mg/kg). Visualization of the aortic arch was gained by left anterior thoracotomy. TAC was created using a 7–0 suture tied around the aorta and a 27-gauge needle in the region of the arch located between right and left carotid arteries. The needle was then gently retracted, yielding a 60–80% constriction with an outer aortic diameter of approximately 0.3 mm (ref. 38). The sham procedure was identical except that the aorta was not ligated. Simultaneous catheterization and direct pressure recordings (using ADInstruments 1.4 F pressure catheter model # SPR-671) of both the right carotid artery and abdominal aorta in control mice ($n = 5$) indicated a pressure gradient of 59 ± 11 mm Hg (mean ± s.d.) using this technique. Mice were allowed to recover and were killed 14 d after surgery. All procedures involving mice were approved by the University of Pennsylvania Institutional Animal Care and Use Committee.

Magnetic resonance imaging and echocardiography. EKG-gated MRI of live intubated and sedated (1% isoflurane) mice was performed using a 4.7-Tesla, horizontal-bore spectrometer with an elliptical surface coil as described[39]. For echocardiography, chest hair was removed and mice were anaesthetized using an integrated isoflurane-based system. In brief, mice were first allowed to inhale 2% isoflurane in a glass chamber, then intubated via nose cone with 1–1.5% isoflurane to maintain anesthesia. The mice were kept warm on a heated platform, and temperature and ECG were continuously monitored. Images were obtained using a Vevo 770 VisualSonic scanner equipped with a 30-MHz probe.

Western blotting and transfections. We used antibodies to Hdac2 (1: 200 dilution, Zymed), α-tubulin, (1:5,000 dilution, Sigma, T6199), α-actinin (1:1,000 dilution, Sigma, A7811), MARCK (1:1,000 dilution, Chemicon, AB5427), cyclophillin-A (1:1,000 dilution, Ambion, 7375), phospho-Gsk3β (Ser 9), total Gsk3β, phospho-Akt (Ser 473), total Akt, phospho-Pdk1 (Ser 241), total Pdk1, phospho-mTOR, total mTOR, phospho-FoxO3A (1:1,000 dilution, Cell Signaling) and phospho-FoxO1 (Upstate). Primary antibody binding was visualized by using the Westernbreeze Kit (Invitrogen) according to the manufacturer's instructions. The *INPP5F* human cDNA clone was obtained from Invitrogen (97002RG). dn*Akt* and ca*Akt* adenovirus constructs have been described[40,41]. Cells were infected with *dnAkt* or *caAkt* adenovirus (50 particles/cell) for 12 h. H9c2 (ATCC # CRL-1446) and COS-7 cells were transiently transfected with or without *INPP5F* and harvested 24 h after transfection for western blot analysis. *Inpp5f* siRNA (L-059393-00) was obtained from Dharmacon and transfected into H9c2 cells using RNAiMax (Invitrogen) according to the manufacturer's protocol. Efficient (74.5% ± 6.7%, $n = 6$) knockdown of *Inpp5f* with *Inpp5f* siRNA was verified by real-time quantitative PCR. Mock-transfected cells served as the negative control.

Statistics. Comparison of survival rates was performed by Kaplan-Meier analysis with PRISM software (GraphPad). All measurement data are expressed as mean ± s.d. The statistical significance of differences between groups was analyzed by Student's *t*-test. Differences were considered significant at a *P*-value < 0.05.

Database accession numbers. Genbank: NM_008229 (Hdac2); U71441 (α-MHC promoter).

Note: Supplementary information is available on the Nature Medicine website.

ACKNOWLEDGMENTS

We thank J. Tobias for his help with microarray data analysis; A. Granger and M. Levin for assistance with cardiac myocyte isolation; K.J. Duffy for his help with analysis of echocardiography data; R. Zhou for assistance with magnetic resonance imaging; and T. Force (Thomas Jefferson University) for dn*Akt* and ca*Akt* adenovirus and constructs, and for advice with the manuscript. This work was supported by the US National Institutes of Health (RO1 HL071546 to J.A.E.). J.A.E. holds the W.W. Smith Endowed Chair for Cardiovascular Research at the University of Pennsylvania. C.M.T. is supported by an American Heart Association postdoctoral fellowship.

AUTHOR CONTRIBUTIONS

C.M.T. contributed significantly to the writing of the manuscript. M.Z. performed histological sectioning of embryo and heart tissue. W.Z. assisted with siRNA experiments. T.W. performed TAC surgery. T.F., M.G., P.R.N. and W.W. created the *Hdac2* gene-trap ES line. V.A.F. carried out echocardiography and MRI studies. C.S.A. helped with PI3K activity experiments and provided advice related to PI3K signaling. P.J.G. was instrumental during early stages of the project and initiated Hdac2 expression studies. J.A.E. conceived, designed and directed the study, supervised C.M.T., Y.L., Z.Y., M.Z., T.W. and W.Z., and wrote the manuscript.

COMPETING INTERESTS STATEMENT

The authors declare competing financial interests (see the *Nature Medicine* website for details).

Published online at http://www.nature.com/naturemedicine
Reprints and permissions information is available online at http://npg.nature.com/reprintsandpermissions

1. Jessup, M. & Brozena, S. Heart failure. *N. Engl. J. Med.* **348**, 2007–2018 (2003).
2. Schrier, R.W. & Abraham, W.T. Hormones and hemodynamics in heart failure. *N. Engl. J. Med.* **341**, 577–585 (1999).
3. Huss, J.M. & Kelly, D.P. Mitochondrial energy metabolism in heart failure: a question of balance. *J. Clin. Invest.* **115**, 547–555 (2005).
4. Hoshijima, M. & Chien, K.R. Mixed signals in heart failure: cancer rules. *J. Clin. Invest.* **109**, 849–855 (2002).
5. Heineke, J. & Molkentin, J.D. Regulation of cardiac hypertrophy by intracellular signalling pathways. *Nat. Rev. Mol. Cell Biol.* **7**, 589–600 (2006).
6. Izumo, S., Nadal-Ginard, B. & Mahdavi, V. Protooncogene induction and reprogramming of cardiac gene expression produced by pressure overload. *Proc. Natl. Acad. Sci. USA* **85**, 339–343 (1988).
7. Wolffe, A.P. Histone deacetylase: a regulator of transcription. *Science* **272**, 371–372 (1996).
8. Ekwall, K. Genome-wide analysis of HDAC function. *Trends Genet.* **21**, 608–615 (2005).
9. Thiagalingam, S. *et al.* Histone deacetylases: unique players in shaping the epigenetic histone code. *Ann. NY Acad. Sci.* **983**, 84–100 (2003).
10. McKinsey, T.A. & Olson, E.N. Cardiac histone acetylation–therapeutic opportunities abound. *Trends Genet.* **20**, 206–213 (2004).
11. Zhang, C.L. *et al.* Class II histone deacetylases act as signal-responsive repressors of cardiac hypertrophy. *Cell* **110**, 479–488 (2002).
12. McKinsey, T.A. & Olson, E.N. Toward transcriptional therapies for the failing heart: chemical screens to modulate genes. *J. Clin. Invest.* **115**, 538–546 (2005).
13. Chang, S. *et al.* Histone deacetylases 5 and 9 govern responsiveness of the heart to a subset of stress signals and play redundant roles in heart development. *Mol. Cell. Biol.* **24**, 8467–8476 (2004).
14. Antos, C.L. *et al.* Dose-dependent blockade to cardiomyocyte hypertrophy by histone deacetylase inhibitors. *J. Biol. Chem.* **278**, 28930–28937 (2003).
15. Kook, H. *et al.* Cardiac hypertrophy and histone deacetylase-dependent transcriptional repression mediated by the atypical homeodomain protein Hop. *J. Clin. Invest.* **112**, 863–871 (2003).
16. Kee, H.J. *et al.* Inhibition of histone deacetylation blocks cardiac hypertrophy induced by angiotensin II infusion and aortic banding. *Circulation* **113**, 51–59 (2006).
17. Kong, Y. *et al.* Suppression of class I and II histone deacetylases blunts pressure-overload cardiac hypertrophy. *Circulation* **113**, 2579–2588 (2006).
18. Kook, H. & Epstein, J.A. Hopping to the beat. Hop regulation of cardiac gene expression. *Trends Cardiovasc. Med.* **13**, 261–264 (2003).
19. Chen, F. *et al.* Hop is an unusual homeobox gene that modulates cardiac development. *Cell* **110**, 713–723 (2002).
20. Shin, C.H. *et al.* Modulation of cardiac growth and development by HOP, an unusual homeodomain protein. *Cell* **110**, 725–735 (2002).
21. Chen, C.S., Weng, S.C., Tseng, P.H., Lin, H.P. & Chen, C.S. Histone acetylation-independent effect of histone deacetylase inhibitors on Akt through the reshuffling of protein phosphatase 1 complexes. *J. Biol. Chem.* **280**, 38879–38887 (2005).
22. Yuan, Z.L., Guan, Y.J., Chatterjee, D. & Chin, Y.E. Stat3 dimerization regulated by reversible acetylation of a single lysine residue. *Science* **307**, 269–273 (2005).
23. Choi, J.D. *et al.* A novel variant of Inpp5f is imprinted in brain, and its expression is correlated with differential methylation of an internal CpG island. *Mol. Cell. Biol.* **25**, 5514–5522 (2005).
24. Minagawa, T., Ijuin, T., Mochizuki, Y. & Takenawa, T. Identification and characterization of a sac domain-containing phosphoinositide 5-phosphatase. *J. Biol. Chem.* **276**, 22011–22015 (2001).
25. Dorn, G.W. II & Force, T. Protein kinase cascades in the regulation of cardiac hypertrophy. *J. Clin. Invest.* **115**, 527–537 (2005).
26. Haq, S. *et al.* Glycogen synthase kinase-3beta is a negative regulator of cardiomyocyte hypertrophy. *J. Cell Biol.* **151**, 117–130 (2000).
27. Antos, C.L. *et al.* Activated glycogen synthase-3 beta suppresses cardiac hypertrophy *in vivo*. *Proc. Natl. Acad. Sci. USA* **99**, 907–912 (2002).
28. Morisco, C. *et al.* The Akt-glycogen synthase kinase 3beta pathway regulates transcription of atrial natriuretic factor induced by beta-adrenergic receptor stimulation in cardiac myocytes. *J. Biol. Chem.* **275**, 14466–14475 (2000).
29. Hardt, S.E. & Sadoshima, J. Glycogen synthase kinase-3beta: a novel regulator of cardiac hypertrophy and development. *Circ. Res.* **90**, 1055–1063 (2002).
30. Zhang, F., Phiel, C.J., Spece, L., Gurvich, N. & Klein, P.S. Inhibitory phosphorylation of glycogen synthase kinase-3 (GSK-3) in response to lithium. Evidence for autoregulation of GSK-3. *J. Biol. Chem.* **278**, 33067–33077 (2003).
31. Bolden, J.E., Peart, M.J. & Johnstone, R.W. Anticancer activities of histone deacetylase inhibitors. *Nat. Rev. Drug. Discov.* **9**, 769–784 (2006).
32. Marks, P.A., Richon, V.M., Breslow, R. & Rifkind, R.A. Histone deacetylase inhibitors as new cancer drugs. *Curr. Opin. Oncol.* **13**, 477–483 (2001).
33. Baldinu, P. *et al.* Identification of a novel candidate gene, CASC2, in a region of common allelic loss at chromosome 10q26 in human endometrial cancer. *Hum. Mutat.* **23**, 318–326 (2004).
34. Peiffer-Schneider, S. *et al.* Mapping an endometrial cancer tumor suppressor gene at 10q25 and development of a bacterial clone contig for the consensus deletion interval. *Genomics* **52**, 9–16 (1998).
35. Marks, P.A. & Dokmanovic, M. Histone deacetylase inhibitors: discovery and development as anticancer agents. *Expert Opin. Investig. Drugs* **14**, 1497–1511 (2005).
36. Skov, S. *et al.* Cancer cells become susceptible to natural killer cell killing after exposure to histone deacetylase inhibitors due to glycogen synthase kinase-3-dependent expression of MHC class I-related chain a and B. *Cancer Res.* **65**, 11136–11145 (2005).
37. Johnson, C.A. & Turner, B.M. Histone deacetylases: complex transducers of nuclear signals. *Semin. Cell Dev. Biol.* **10**, 179–188 (1999).
38. Rockman, H.A. *et al.* Segregation of atrial-specific and inducible expression of an atrial natriuretic factor transgene in an in vivo murine model of cardiac hypertrophy. *Proc. Natl. Acad. Sci. USA* **88**, 8277–8281 (1991).
39. Zhou, R., Pickup, S., Glickson, J.D., Scott, C.H. & Ferrari, V.A. Assessment of global and regional myocardial function in the mouse using cine and tagged MRI. *Magn. Reson. Med.* **49**, 760–764 (2003).
40. Matsui, T. *et al.* Adenoviral gene transfer of activated phosphatidylinositol 3′-kinase and Akt inhibits apoptosis of hypoxic cardiomyocytes *in vitro*. *Circulation* **100**, 2373–2379 (1999).
41. Wang, Q. *et al.* Protein kinase B/Akt participates in GLUT4 translocation by insulin in L6 myoblasts. *Mol. Cell. Biol.* **19**, 4008–4018 (1999).

WILEY InterScience® DISCOVER SOMETHING GREAT

American Journal of Hematology 81:981–983 (2006)

Histone Deacetylase Inhibitor FK228 is a Potent Inducer of Human Fetal Hemoglobin

Hua Cao* and George Stamatoyannopoulos

Division of Medical Genetics, University of Washington, Seattle, WA

We investigated the induction of the human fetal globin gene using five potent histone deacetylase (HDAC) inhibitors: FK-228, HC-Toxin, Trichostatin, MS-275, and Apicidin, using in vitro assays and cultures of primary human erythroblasts. The results showed that FK228 is the most potent inducer of fetal hemoglobin and exhibits its effects in picomolar concentrations. FK228 should be considered as a potential therapeutic for induction of fetal hemoglobin in patients with β chain hemoglobinopathies. Am. J. Hematol. 81:981–983, 2006. © 2006 Wiley-Liss, Inc.

Key words: fetal hemoglobin; sickle cell disease; thalassemia; histone deacetylase inhibitors

INTRODUCTION

Several pharmacological agents have been used for the induction of fetal hemoglobin in animal models and in humans [1,2]. Since the discovery of the induction of Hb F by butyrate in patients with sickle cell disease and thalassemia [3,4], several histone deacetylase inhibitors have been shown to be γ globin gene inducers in vitro and in human erythroid cell cultures. Except for butyrate, none of these HDAC inhibitors has been used in patients with the common β chain hemoglobinopathies, thalassemia, and sickle cell disease.

The cyclic depsipeptide FK228 is a highly potent histone deacetylase inhibitor extensively studied in animal models and currently used in clinical trials of patients with various malignancies [5–8]. Because of its current use in humans, we tested whether FK228 is an inducer of fetal hemoglobin and compared it to four other known HDAC inhibitors [9].

MATERIALS AND METHODS

Effects on the γ globin gene and on fetal hemoglobin were assessed using two systems:

1. Dual luciferase assays consisting of cultures of GM979 erythroleukemia cells stably transfected with a $\mu LCR\beta_{pr}R_{luc}{}^{A}\gamma_{pr}F_{luc}$ plasmid [10], which is composed of a 3.1 kb μLCR cassette linked to a renilla luciferase gene driven by a 315 bp β gene promoter (β-luciferase) and a firefly luciferase gene driven by a 1.4 kb $^{A}\gamma$ gene promoter (γ-luciferase) [10]. The activity of γ and β gene promoters was quantitated by determining the ratio of the activity of γ firefly luciferase over the total luciferase $[\gamma^{F}/(\gamma^{F} + 2\beta^{R})]$, as previously described [10].
2. Measurements of fetal hemoglobin positive (F-positive) erythroblasts and γ/γ+β globin mRNA ratios in BFUe colonies produced from peripheral blood mononuclear cells of normal individuals. Colonies were plucked from methylcellulose plates on culture day 14 for staining with anti-Hb F antibody and on day 12 for isolation of RNA and analysis of human γ and β globin mRNAs by RNAse protection.

RESULTS AND DISCUSSION

Results obtained using the dual luciferase assay are plotted in Fig. 1A. Notice the induction of γ promoter activity by all the HDAC inhibitors. Importantly, FK228 induced the γ gene promoter in a con-

*Correspondence to: Hua Cao, Medical Genetics, University of Washington Seattle, WA 98195, USA.
E-mail: huacao@u.washington.edu

Contract grant sponsor: NIH; Contract grant numbers: HL20899 and DK45365.

Received for publication 1 March 2006; Accepted 22 April 2006

Published online 3 August 2006 in Wiley InterScience (www.interscience.wiley.com).
DOI: 10.1002/ajh.20676

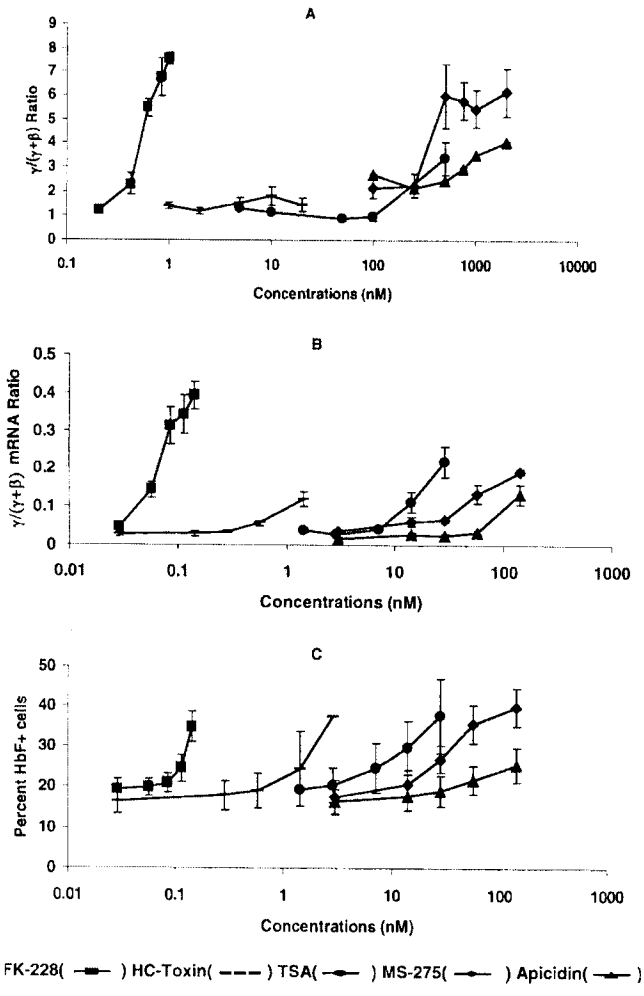

Fig. 1. A. Induction of human γ gene promoter activity by HDAC inhibitors. Results from the dual luciferase assay. Cells were treated with increasing concentration of FK-228 (■), HC-Toxin (---), TSA (●), MS-275 (◆), and Apicidin (▲). Vertical bars indicate SEM. Note that FK228 induces γ promoter activity in concentrations that are about 1000-fold lower compared with the other four compounds. B. Induction of γ globin mRNA in BFUe cultures derived erythroblasts. Note the increase of γ/γ+β ratio by picomolar concentrations of FK228. C. Induction of Hb F-positive erythroblasts. Note the consistent increase of Hb F-positive erythroblasts as the concentration of the compounds increases in culture. Also note that FK228 induces the production of F erythroblasts in concentrations which are about 100-fold lower compared with the other compounds.

centration about 1000-fold lower than those of the other compounds. Notice that FK228 induced the γ gene promoter by 7.81-fold when only 1 nM of the compound was present in the culture.

The effect of FK228 on mRNA production by the endogenous human globin genes are shown in Fig. 1B. Notice that the induction of γ/γ+β ratio by FK228 took place in concentrations which were about 500-fold lower compared with those of the other compounds.

Staining of the cultured primary erythroid cells with anti-fetal hemoglobin antibodies and measurement of the frequency of F-positive erythroblasts are required to verify that fetal hemoglobin is indeed induced by potential Hb F inducers. Such results are shown in Fig. 1C. In the BFUe colonies cultured in the presence of FK228, F-erythroblasts increased from 13.3% to 34.9% when 100 pM of FK228 was present in the culture. In contrast, similar frequencies of F erythroblasts were observed in the cultures of the other compounds when they were present in 5–200 nM concentrations.

The development of new therapeutics for clinical use is a prolonged process driven by financial considerations. Such considerations are inhibitory for the development of compounds for treatment of β chain hemoglobinopathies, i.e. diseases of limited financial appeal to the pharmaceutical industry. Over the last 25 years many compounds have been shown to induce fetal hemoglobin [1,2], but only hydroxyurea has reached clinical application. Hydroxyurea was approved by FDA for the treatment of polycythemia vera before its effect on induction of fetal hemoglobin was discovered. The use of hydroxyurea for treatment of patients with sickle cell disease was facilitated and accelerated because only the investigation of a new indication rather than the de novo preclinical and clinical studies necessary for FDA approval of a new therapeutic was required. The example of hydroxyurea suggests that a fruitful approach for the discovery of new inducers of fetal hemoglobin is the search among compounds already used in humans for other indications.

FK228 is currently used in clinical trials of patients with cancer [5–8]. Studies of fetal hemoglobin in such patients may show whether FK228 induces fetal hemoglobin in humans in nontoxic concentrations. Demonstration of induction of fetal hemoglobin in such patients is likely to stimulate testing of the effects of this compound in patients with β chain hemoglobinopathies.

ACKNOWLEDGMENTS

The authors thank Dr. Masaaki Tomoi at Research Information Management Division, Fujisawa Pharmaceutical Co. for kindly providing FK228 for this research.

REFERENCES

1. Stamatoyannopoulos G. Control of globin gene expression during development and erythroid differentiation. Exp Hematol 2005;33:259–271.
2. Stamatoyannopoulos G, Grosveld F. Hemoglobin switching. In: Stamatoyannopoulos G, Majerus P, Perlmutter R, Varmus H, editors. The Molecular Basis of Blood Disease, 3th ed. Philadelphia: WB Saunders, 2001. pp 135–182.

3. Perrine SP, Ginder GD, Faller DV, et al. A short-term trial of butyrate to stimulate fetal-globin-gene expression in the beta-globin disorders. N Engl J Med 1993;328:81–86.
4. Atweh GF, Sutton M, Nassif I, et al. Sustained induction of fetal hemoglobin by pulse butyrate therapy in sickle cell disease. Blood 1999;93:1790–1797.
5. Piekarz RL, Robey R, Sandor V, et al. Inhibitor of histone deacetylation, depsipeptide (FR901228), in the treatment of peripheral and cutaneous T-cell lymphoma: A case report. Blood 2001;98: 2865–2868.
6. Marshall JL, Rizvi N, Kauh J, et al. A phase I trial of depsipeptide (FR901228) in patients with advanced cancer. J Exp Ther Oncol 2002;2:325–332.
7. Sandor V, Bakke S, Robey RW, et al. Phase I trial of the histone deacetylase inhibitor, depsipeptide (FR901228, NSC 630176), in patients with refractory neoplasms. Clin Cancer Res 2002;8:718–728.
8. Byrd JC, Marcucci G, Parthun MR, et al. A phase I and pharmacodynamic study of depsipeptide (FK228) in chronic lymphocytic leukemia and acute myeloid leukemia. Blood 2005;105:959–967.
9. McCaffrey PG, Newsome DA, Fibach E, Yoshida M, Su MS. Induction of gamma-globin by histone deacetylase inhibitors. Blood 1997;90:2075–2083.
10. Skarpidi E, Vassilopoulos G, Li Q, Stamatoyannopoulos G. Novel in vitro assay for the detection of pharmacologic inducers of fetal hemoglobin. Blood 2000;96:321–326.

0026-895X/07/7205-1111–1123$20.00
MOLECULAR PHARMACOLOGY
Copyright © 2007 The American Society for Pharmacology and Experimental Therapeutics
Mol Pharmacol 72:1111–1123, 2007

Vol. 72, No. 5
36772/3262309
Printed in U.S.A.

Identification of Two New Synthetic Histone Deacetylase Inhibitors That Modulate Globin Gene Expression in Erythroid Cells from Healthy Donors and Patients with Thalassemia[S]

Antonello Mai, Katija Jelicic, Dante Rotili, Antonella Di Noia, Elena Alfani, Sergio Valente, Lucia Altucci, Angela Nebbioso, Silvio Massa, Renzo Galanello, Gerald Brosch, Anna Rita Migliaccio,[1] and Giovanni Migliaccio

Istituto Pasteur–Fondazione Cenci Bolognetti, Dipartimento di Studi Farmaceutici, Università degli Studi di Roma "La Sapienza", Roma, Italy (A.M., D.R., S.V.); Dipartimento di Biologia Cellulare e Neuroscienze (K.J., A.D.N., E.A., G.M.) e Dipartimento di Ematologia, Oncologia e Medicina Molecolare (A.R.M.), Istituto Superiore di Sanità, Roma, Italy; Dipartimento Farmaco Chimico Tecnologico, Università degli Studi di Siena, Siena, Italy (S.M.); Dipartimento di Patologia Generale, Seconda Università degli Studi di Napoli, Napoli, Italy (L.A., A.N.); Dipartimento di Scienze Biomediche e Biotecnologie, Università degli Studi di Cagliari, Cagliari, Italy (R.G.); Division of Molecular Biology, Biocenter, Innsbruck Medical University, Innsbruck, Austria (G.B.); and Department of Medicine and Myeloproliferative Disorders Research Consortium (MPD-RC), University of Illinois at Chicago, Chicago, Illinois (A.R.M.)

Received April 4, 2007; accepted July 25, 2007

ABSTRACT

We have identified two new histone deacetylase (HDAC) inhibitors (9 and 24) capable of inducing the expression of γ-globin and/or β-globin promoter-driven reporter genes in a synthetic model of Hb switch. Both compounds also increased, with different mechanisms, the γ/(γ+β) ratio expressed in vitro by normal human erythroblasts. Compound 9 increased the levels of γ-globin mRNA and the γ/(γ+β) ratio (both by 2-fold). Compound 24 increased by 3-fold the level of γ-globin and decreased by 2-fold that of β-globin mRNA, increasing the γ/(γ+β) ratio by 6-fold, and raising (by 50%) the cell HbF content. Both compounds raised the acetylation state of histone H4 in primary cells, an indication that their activity was mediated through HDAC inhibition. Compounds 9 and 24 were also tested as γ/(γ+β) mRNA inducers in erythroblasts obtained from patients with β^0 thalassemia. Progenitor cells from patients with β^0 thalassemia generated in vitro morphologically normal proerythroblasts that, unlike normal cells, failed to mature in the presence of EPO and expressed low β-globin levels but 10 times higher-than-normal levels of the α hemoglobin-stabilizing protein (AHSP) mRNA. Both compounds ameliorated the impaired in vitro maturation in β^0 thalassemic erythroblasts, decreasing AHSP expression to normal levels. In the case of two patients (of five analyzed), the improved erythroblast maturation was associated with detectable increases in the γ/(γ+β) mRNA ratio. The low toxicity exerted by compounds 9 and 24 in all of the assays investigated suggests that these new HDAC inhibitors should be considered for personalized therapy of selected patients with β^0 thalassemia.

This work was partially supported by grants from AIRC 2006 (to A.M.), PRIN 2006038137_005 (to A.M.), PRIN 2006052835_003 (to L.A.); Ministero per l'Università e la Ricerca Scientifica e Tecnologica grants RBNE0189JJ 006, RBNE01sp72 003 (to A.R.M.) and MM06103241 (to G.M.); National Cancer Institute grant P01-CA108671-01A2 (to the Myeloproliferative Disorders Research Consortium); and European Union grant LSHC-CT2005-518417) (to L.A.).

[1] Current affiliation: Mount Sinai School of Medicine, New York, New York.

This work was partially presented as a poster at the annual meeting of the American Society of Hematology in 2004 [Mai A, Massa S, Di Noia A, Jelicic K, Alfani E, Di Rico MC, Di Baldassarre A, Migliaccio AR, and Migliaccio G (2004) *Blood* **104:**1216] and as an oral presentation at the annual meeting of the European Hematology Association in 2005 [Di Noia A, Jelicic K, Mai A, Massa S, Di Rico MC, Di Baldassarre A, Alfani E, Migliaccio AR, and Migliaccio G (2005)].

Article, publication date, and citation information can be found at http://molpharm.aspetjournals.org.

doi:10.1124/mol.107.036772.

[S] The online version of this article (available at http://molpharm.aspetjournals.org) contains supplemental material.

In mammals, the development of erythroid cells is characterized by sequential ontogenetic hemoglobin (Hb) switches. In man, the first embryonic-to-fetal Hb (HbF) switch occurs after 2 months of gestation and is followed by a switch from HbF to adult Hb, which begins at mid-gestation and is completed 6 months after birth. HbF expression is retained by a minority (1–3%) of normal adult red cells (Stamatoyannopoulos and Grosveld, 2001).

β Thalassemia and sickle-cell anemia are inherited genetic disorders, both arising from mutations in one of the genes, β-globin, that encode adult Hb. Sickle-cell anemia is due to a missense mutation leading to glutamate-valine substitution at position 6 of the β-globin chain. β Thalassemia may be traced to numerous genetic mutations resulting either in loss

ABBREVIATIONS: Hb, hemoglobin; HbF, fetal hemoglobin; EPO, erythropoietin; AHSP, α hemoglobin-stabilizing protein; HAT, histone acetyltransferase; HDAC, histone deacetylase; HDACI, histone deacetylase inhibitor; SAHA, suberoylanilide hydroxamic acid; MS-275, pyridin-3-ylmethyl *N*-[[4-[(2-aminophenyl)carbamoyl]phenyl]methyl]carbamate; APHA, aroyl pyrrolyl hydroxyamide; UBHA, uracil-based hydroxyamide; μLCR, micro locus control region; R, *Renilla reniformi*; F, firefly; DMSO, dimethyl sulfoxide; AFU, arbitrary fluorescence units; HBSS, Hanks' balanced salt solution; PCR, polymerase chain reaction; IP, immunoprecipitation; HEMA, human erythroblast massive amplification.

(more precisely defined β^0-) or reduced β-globin expression (Olivieri, 1999). Patients with β thalassemia or sickle-cell anemia are healthy until birth, when their red cells contain HbF. Furthermore, patients with β thalassemia or sickle-cell disease that coinherit genetic mutations allowing the retention of HbF production postnatally (hereditary persistence of fetal hemoglobin syndrome), have no or mild clinical phenotype (Olivieri, 1999). These observations, and additional clinical studies, have allowed us to calculate that pharmacological re-activation of γ-globin production up to ~10 to 20% of β-globin levels in adult red cells would be sufficient to ameliorate the symptoms of sickle-cell disease and β thalassemia (Noguchi et al., 1988).

Numerous studies have been undertaken to identify HbF inducers for the cure of hemoglobinopathies. In primates, HbF has been induced by cell cycle-specific cytotoxic drugs [cytosine arabinoside (Papayannopoulou et al., 1984) and hydroxyurea (Letvin et al., 1984)]. Both drugs also induced HbF in phase I-II clinical trials in patients with sickle-cell disease and β thalassemia (Platt et al., 1984; Veith et al., 1985). These trials have indicated hydroxyurea as the treatment of choice for sickle-cell anemia (Bradai et al., 2003). This drug, however, is not devoid of counter-indications, is not effective in all patients with sickle-cell disease and has modest effects in the patients with β thalassemia. The search for additional and less toxic agents, therefore, continues (Atweh and Schechter, 2001).

Two enzyme superfamilies, histone acetyltransferases (HATs) and histone deacetylases (HDACs), exert antagonistic epigenetic controls on gene expression through chromatin re-modeling (Hassig and Schreiber, 1997). HATs induce histone acetylation, favoring chromatin relaxation and exposing gene regulatory regions to the transcription machinery. HDAC catalyze histone deacetylation, resulting in the formation of tightly supercoiled, transcriptionally silent, "heterochromatin" regions (Felsenfeld and Groundine, 2003). Specific histone acetylation patterns have recently been shown to play a role in the murine β-globin switch, suggesting that HDACs might participate in the silencing complex that represses γ-globin expression (Forsberg et al., 2000). Hence, the hypothesis that HDAC inhibitors (HDACIs) might represent pharmacological reactivators of HbF (Cao, 2004).

The proof of concept for the use of HDACI as pharmacologic HbF inducers was provided by the observation that sheep fetuses continuously infused with sodium butyrate, a well known albeit weak (millimolar range) HDACI, displayed delayed HbF-to-adult-Hb switch (Perrine et al., 1988). Subsequent studies showed that butyrate, its analogs phenylbutyrate and valproic acid, additional short chain fatty acids, and their hydroxyamide derivatives induce HbF synthesis in human erythroid cultures (Perrine et al., 1989), in adult baboons (Constantoulakis et al., 1989), in some patients with β thalassemia (Perrine et al., 1993; Sher et al., 1995), and in the majority of patients with sickle-cell disease (Atweh et al., 1999). The rapid metabolism, inconvenient mode of application, and weak HbF-inducing activity of these compounds, however, prompted the search for alternative HbF-inducing HDACIs. A variety of HDACIs, mostly with unrelated chemical structures [trichostatin A, trapoxin, suberoylanilide hydroxamic acid (SAHA), MS-275, apicidin, scriptaid, and analogs], have been shown to be capable of inducing HbF in vitro and/or in vivo (Cao, 2004; Cao et al., 2004). Their potential use for the cure of hemoglobinopathies remains unclear because of their modest effects as HbF inducers and their high cell toxicity.

The aim of this study was to identify new, possibly less toxic, HDACI capable of inducing HbF, using a two step screening strategy. First, HDACI were screened for their potential to increase expression of a $^A\gamma$-driven reporter in GM979 cells stably transfected with a dual luciferase reporter construct (Skarpidi et al., 2000). Second, selective compounds were evaluated for their capability to increase the $\gamma/(\gamma+\beta)$ ratio expressed in vitro by normal adult erythroblasts (Migliaccio et al., 2002). The two most potent compounds identified with this second screening were, finally, tested for their ability to restore the impaired maturation of erythroblasts obtained in vitro from patients with β^0 thalassemia.

Materials and Methods

Construction of the HDACI Library. The synthetic schemes, experimental preparation procedures, physical and chemical data, and registry number for the new compounds 2, 3, 13 to 19, and 23 to 25 are reported in the Supplemental Data. Compounds 1, 4 to 12, and 20 to 22 were synthesized as described previously (see references in Supplemental Data). SAHA (Vorinostat) was purchased from Sigma Aldrich Chemical Co. (St. Louis, MO). The HDACI belong to the chemical classes of aroyl pyrrolyl hydroxyamides (APHAs; compounds 1–6), aryloxopropenylpyrrolyl hydroxyamides (compounds 7–19), and uracil-based hydroxyamides (UBHAs; compounds 20–25) and were tested against the maize deacetylases HD2, HD1-B (class I HDAC), and HD1-A (class II HDAC). Inhibitory assays were performed according to established procedures (Brosch et al., 1996b; Kölle et al., 1998) based on the ability of a compound to inhibit the maximal amount of tritiated acetic acid, as quantified by scintillation counting, liberated from radioactively labeled chicken core histones by each purified enzyme. In brief, maize HDACs (50 μl) were first preincubated with increasing concentrations of compounds for 15 min on ice and then incubated for 30 min at 30°C with total [^{3}H]acetate-prelabeled chicken reticulocyte histones (10 μl of a 2 mg/ml solution). The reaction was stopped by adding 36 μl of 1 M HCl/0.4 M acetate and 800 μl of ethyl acetate. After centrifugation (10,000*g*, 5 min), the radioactivity present in the supernatant (600 μl) was counted in a scintillation counter (LS 6500; Beckman Coulter, Fullerton, CA). SAHA was included in the assay as reference, and blank solvents were used as negative controls. Maize HDACs were purified as described previously (Brosch et al., 1996a; Kölle et al., 1998). IC_{50} values were calculated with Microsoft Excel software (Microsoft Corp, Redmond, WA) and expressed as mean (± S.D.) of triplicate determinations as summarized in Supplemental Table 3. All of the compounds inhibited maize HDACs, albeit with a wide range of efficiency (IC_{50} between 0.004 and 39 μM). Four of them (compounds 8, 9, 11, and 12), were selectively active on class II enzymes (selectivity ratio >10). None of them was selective for the class I enzyme. As expected on the basis of previous results (see references in Supplemental Data), the six compounds of the UBHA family expressed IC_{50} values lower than those of SAHA. In particular, compound 24 was 2- to 30-fold more potent than SAHA in inhibiting the maize HD1-B and HD1-A.

Activation of $^A\gamma$-Driven Reporter Expression. The μLCRβprRluc$^A\gamma$prFlucGM979 cell line was obtained by stably transfecting the murine erythroleukemia GM979 cell line with a dual-luciferase reporter containing a 3.1-kilobase pair μLCR cassette including the DNase I hypersensitive core of the 5′ hypersensitive sites HS1, HS2, HS3, and HS4, linked to 315 base pairs of the human β-globin promoter and 1.4-kb of the $^A\gamma$-globin promoter driving the *Renilla reniformis* (R) and the firefly (F) luciferase genes, respectively (Skarpidi et al., 2000). μLCRβprRluc$^A\gamma$prFlucGM979 cells,

indicated from now on as GM979 for brevity, were frozen within 1 month from transfection and thawed when requested for the assay. As such, they may not be representative of the cells established by Skarpidi et al. (2000). GM979 cells were maintained in RPMI 1640 medium containing 10% (v/v) fetal calf serum (EuroClone, Milan, Italy), 100 units/ml penicillin, 100 mg/ml streptomycin, 2 mM glutamine, and 400 μg/ml G418 as described previously (Migliaccio et al., 2005). The effect of HDACI on the expression of the $^{A}\gamma$-driven reporter was evaluated by incubating the cells with increasing concentrations of each compound solubilized in DMSO [final concentration, 0.1% (v/v)]. Negative controls were represented by cells incubated with DMSO alone. After 4 days of incubation, cells were harvested and $^{A}\gamma$-F and β-R luciferase activities determined in triplicate using the Dual Luciferase Reporter Assay System (Promega, Madison, WI). as described by the manufacturer. Luminescence was measured with the Lumat LB9507 Luminometer (Berthold Technologies, Bad Wildbad, Germany) and expressed in arbitrary fluorescence units (AFU). Results are expressed as mean (± S.D.) of triplicate assays and are presented both as absolute values and as activity ratios ($^{A}\gamma$-F AFU/$^{A}\gamma$-F AFU + 2β-R AFU).

Human Subjects. Buffy coats from the peripheral blood of at least 15 to 20 different healthy donors were obtained from the Italian Red Cross Blood Bank (Rome, Italy). Blood from five patients with β^0 thalassemia was collected before routine transfusion at the Center for Studies on Thalassemia, University of Cagliari, Italy. All the patients were homozygous for the nonsense β^0 39 mutation (Trecartin et al., 1981). This mutation reduces β-globin mRNA expression through a nonsense-mediated mRNA decay mechanism (Zhang et al., 1998) and should have no consequence on the conformation of the β-globin locus. Human blood was collected according to guidelines established by the local ethical committee for human subject studies.

Cell Processing. Mononuclear blood cells were separated by centrifugation at 400*g* for 30 min over Ficoll-Hypaque (GE Healthcare, Chalfont St. Giles, Buckinghamshire, UK). Light-density cells were collected, washed with Hanks' balanced salt solution (HBSS) supplemented with 1% (w/v) bovine serum albumin and either cultured directly or cryopreserved in 10% dimethyl sulfoxide (Sigma).

Activation of the Endogenous γ-Globin Gene in Primary Human Erythroblasts. Human proerythroblasts were obtained by culturing light-density blood cells (10^6 cells/ml) in Iscove's modified Dulbecco's medium (Mascia Brunelli, Milan, Italy) containing fetal bovine serum [20% (v/v); Hyclone, Logan, UT], stem cell factor (10 ng/ml; Amgen, Thousand Oaks, CA), erythropoietin (EPO; 1 U/ml) (Epoetina alfa, Dompè Biotec, Milan, Italy), interleukin-3 (1 ng/ml) (Bouty, Milan, Italy), dexamethasone (10^{-6} M) (Sigma), and estradiol (10^{-6} M) (Sigma), as described previously (Migliaccio et al., 2002). The homogeneous population of proerythroblasts generated after 8 to 12 days in these cultures mature in 4 days up to the stage of orthochromatic erythroblasts once transferred in cultures supplemented with fresh medium and EPO (1 U/ml) alone (Calbiochem, Darmstadt, Germany). The effect of HDACI on the expression of the endogenous globin genes was determined by adding each of them at increasing concentrations at the beginning of the maturation culture. Cells were then harvested 4 days later for further analyses.

Phenotypic Analysis. Cell morphology was analyzed according to standard criteria on cytocentrifuged (Shandon, Astmoor, England) smears stained with May-Grünwald-Giemsa (Sigma).

RNA Isolation and Quantitation of Globin Gene Expression by Real-Time PCR. Total RNA was isolated from 10^6 cells using TRIzol (Invitrogen, Carlsbad, CA). Total RNA (1 μg) was reverse-transcribed with 250 ng of random primers, 1 μl of dNTP (10 mM), and 1 μl of RNase OUT (recombinant RNase inhibitor, 40 U/μl) (Invitrogen), as described by the manufacturer. Quantitative real-time PCR was carried out in a Prism 7700 Sequence Detection System (Applied Biosystems, Foster City, CA), using the TaqMan Master Mix containing AmpliTaq Gold DNA polymerase with 5′-3′ nuclease activity, which hydrolyzes a dual fluorescently labeled, target-specific oligonucleotide (TaqMan probe). The sequence of the amplification primers and of the probes used for γ- and β-globin were described previously (Di Baldassarre et al., 2007). Primers and probes for α-globin were represented by: forward, 5′-CTCTTCTG-GTCCCCACAGACT-3′; reverse, 5′-GGCCTTGACGTTGGTCTTG-3′; probe, 5′- 5-carboxyfluorescein-ACCATGGTGCTGTCTCCTGCCG-5-carboxytetramethylrhodamine-3′ (Applied Biosystems, Warrington, Cheshire, UK). α Hemoglobin stabilizing protein (AHSP) mRNA was evaluated with an assay on demand (TaqManGene expression assays; Applied Biosystems). For multiplex PCR in real-time relative quantization, target and endogenous reference control were amplified in the same tube with the TaqMan hGAPDH, which contained the selected primer/probe set (20× solution; Applied Biosystems) according to the manufacturer's instructions. Each determination was performed in triplicate. The level of a specific mRNA (X) was expressed in arbitrary units, using hGPDH as calibrator, according to the following algorithm: ΔC_t = [C_tX − C_tGPDH], where C_t is the X threshold cycle, and presented as $2^{-\Delta C_t}$. γ/(γ+β) and α/non-α expression ratios were calculated as $2^{-\Delta C_t}\gamma/2^{-\Delta C_t}\gamma+2^{-\Delta C_t}\beta$ and $2^{-\Delta C_t}\alpha/2^{-\Delta C_t}\gamma+2^{-\Delta C_t}\beta$, respectively.

Determination of Cell HbF Content. Cells were washed twice in HBSS and lysed in 50 mM Tris-HCl, pH 7.4, 150 mM NaCl, 1 mM EGTA, 1% Nonidet P-40, 0.25% sodium deoxycholate, 1 mM NaF, 0.5 mM phenylmethylsulfonyl fluoride, 1 μg/ml aprotinin, 1 μg/ml leupeptin, and 1 mM sodium orthovanadate. Lysates were centrifuged for 10 min at 12,000*g*, and supernatants were used for HbF determination with a specific enzyme-linked immunosorbent assay kit (Bethyl Lab Inc., Montgomery, TX), using the HbF standard provided by the kit, as calibrator. The amount of the immunoreaction was assessed by densitometry at 450 nm with a Victor^3 Multilabel Counter 1420 (PerkinElmer Life and Analytical Sciences–Wallac Oy, Turku, Finland).

Determination of H4 Acetylation by Flow Cytometry. Levels of H4 acetylation were measured as described by Ronzoni et al. (2005). In brief, 1 × 10^6 cells were fixed for 15 min in 1% formaldehyde in HBSS on ice and permeabilized with 200 μl of 0.1% Triton X-100 in HBSS for 10 min at room temperature. Cells were first incubated with an anti-acetyl-Histone H4 (1:50 dilution; Upstate, Charlottesville, VA) for 1 h at room temperature and then with the R-phycoerythrin–conjugated AffiniPure F(ab′)2 Fragment Donkey Anti-Rabbit IgG (H+L) (1:100 dilution; Jackson ImmunoResearch Laboratories Inc., West Grove, PA) for 1 h at room temperature in the dark. Cell fluorescence was analyzed with an Epics Elite ESP (Beckman Coulter). Nonspecific fluorescence signals were gated on cells incubated with R-phycoerythrin–conjugated AffiniPure F(ab′)2 Fragment Donkey Anti-Rabbit IgG (H+L) alone.

Human Cell Lines. The human nonerythroid U937 cell line and the human breast cancer ZR75.1 cell line were cultured in RPMI 1640 medium with 10% fetal calf serum, 100 U/ml penicillin, 100 μg/ml streptomycin, 250 ng/ml amphotericin B, 10 mM HEPES, and 2 mM glutamine.

In Vitro HDAC Inhibition Assay against Human HDAC1 and HDAC4. The functional complexes containing human HDAC1 and HDAC4 were purified by immunoprecipitation (IP) from U937 and ZR75.1 cells, respectively. Cells were lysed in IP buffer (50 mM Tris-HCl, pH 7.0, 180 mM NaCl, 0.15% Nonidet P-40, 10% glycerol, 1.5 mM $MgCl_2$, 1 mM $NaMO_4$, and 0.5 mM NaF) with a protease inhibitor cocktail (Sigma), for 10 min on ice and centrifuged at 14,700*g* for 30 min. Extracts (1000 μg/ml of protein) were precleared by incubating with 20 μl of A/G plus Agarose (Santa Cruz Biotechnology, Santa Cruz, CA) for up to 1 h on a rocking table at 4°C. Supernatants were then transferred into a new tube and incubated again either with an anti-HDAC1 (Abcam, Cambridge, MA) or anti-HDAC4 (Sigma) antibody (3 μg) or with an irrelevant IgG (Santa Cruz Biotechnology), as negative control, overnight at 4°C on a rocking table. The following day, 20 μl of A/G plus Agarose (Santa Cruz) was added to each IP and incubation continued for 2 h. The beads were washed twice in PBS and re-suspended in 20 μl of sterile PBS. The HDAC assay was carried out using a labeled [^{3}H]histone

H4 peptide linked to streptavidin agarose beads, according to the supplier instructions (Upstate), as described by Mai et al. (2006).

Determination of H3 and α-Tubulin Acetylation. The effects of compounds 9 and 24 on histone H3 and α-tubulin acetylation were determined by Western blot analysis of protein extracts prepared from U937 cells that had been exposed to increasing compound concentrations for 16 h. For determination of α-tubulin acetylation, 25 μg of total protein extracts were separated on a 10% polyacrylamide gel, blotted, and probed by Western blot with antibodies specific for acetylated α-tubulin (dilution 1:500; Sigma) and total extracellular signal-regulated kinases (dilution, 1:1000; Santa Cruz Biotechnology), as loading control. For quantification of histone H3 acetylation, 100 μg of total protein extracts were separated on a 15% polyacrylamide gel, blotted, and analyzed by Western blot with antibodies specific either for the acetylated (dilution, 1:1000; Upstate) or total form (Abcam, loading control) of histone H3.

Statistical Analysis. Statistical analysis was obtained with the Origin 5.0 software for Windows (OriginLab Corp., Northampton, MA).

Results

Screening of HDACI as Inducer of Reporter Genes under the Control of Synthetic $^{A}\gamma$- and β-Globin Promoters. Increasing concentrations (0.02–20 μM) of the compounds described in Fig. 1 were tested for their ability to affect the luciferase activity driven by either the $^{A}\gamma$- or β-globin promoter expressed by GM979 cells incubated with each compound for at least 4 days. Under the conditions of the assay, GM979 cells have a doubling time of 48 h; therefore, this experimental design allowed the cells to proliferate at least twice in the presence of the HDACI, maximizing the likelihood that a compound would affect chromatin configuration. The results obtained are summarized in Table 1 as follows: 1) maximal induction, or repression, on the activity of the $^{A}\gamma$- and β-driven reporters; 2) maximal alteration in $^{A}\gamma$-F/($^{A}\gamma$-F + 2β-R)-reporter activity ratio; and 3) lower con-

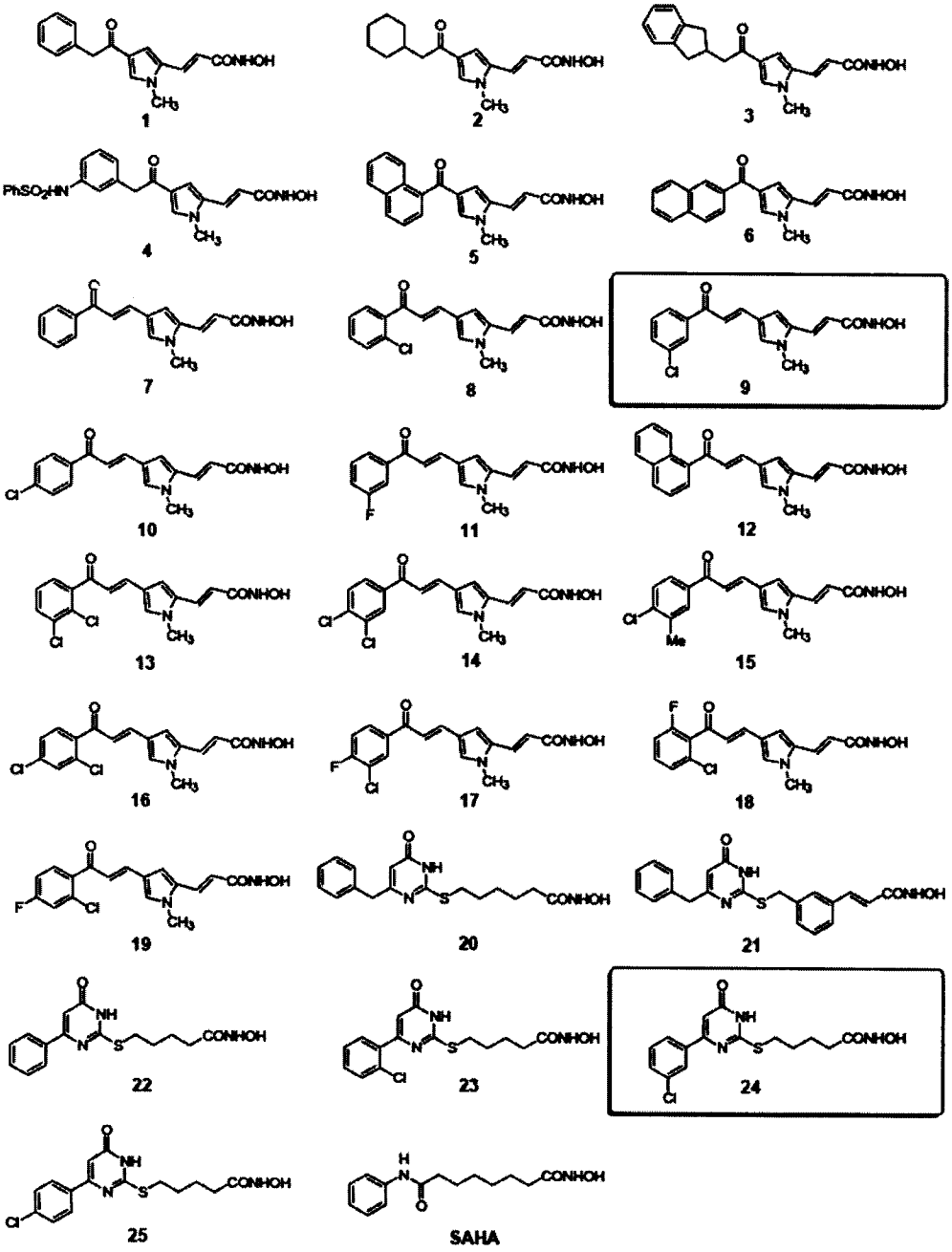

Fig. 1. Chemical structures of the HDACIs included in the library and analyzed in this study. The library contains previously reported and newly synthesized HDACIs identified using the maize HDACs inhibitory assay (see Supplemental Data). These compounds belong to three different chemical classes: aroyl pyrrolyl hydroxyamides (APHAs) (1–6), aryloxopropenylpyrrolyl hydroxyamides (7–19), and uracil-based hydroxyamides (UBHAs) (20–25). The rectangles highlight the two compounds (9 and 24) most extensively analyzed in this study. The chemical structure of SAHA (vorinostat) is included for comparison.

centration of the compound, which induced the maximal alteration. The number of cells present in the culture by the end of the assay was also recorded and expressed as number of cell duplications, as a measure of toxicity. GM979 cells were incubated in parallel cultures with SAHA and with the vehicle (DMSO) as positive and negative controls, respectively.

As in the studies summarized earlier (Cao et al., 2004), no relationship was observed between chemical structure of a compound and its effect on the activity of the $^{A}\gamma$- and β-driven reporters. For example, among the three isomers 8, 9, and 10, two, 8 and 9, induced the $^{A}\gamma$-driven reporter, whereas the third, compound 10, did not. Among all of the HDACIs tested, compounds 7, 8, 9, 11, 22, and 23 were all more effective than SAHA in inducing expression of the $^{A}\gamma$-driven reporter, with maximal activity between 0.2 and 2 μM (Table 1). Some of them (7, 8, 11, 22, and 23) also induced the β-driven reporter activity. As a consequence, they had little or no effect on the $^{A}\gamma$-F/($^{A}\gamma$-F + 2β-R) reporter activity ratio. It is noteworthy that compound 9 preferentially induced the activity of the $^{A}\gamma$-driven reporter and increased the $^{A}\gamma$-F/($^{A}\gamma$-F + 2β-R)-reporter activity ratio 2-fold more efficiently than SAHA (Table 1). Among all the HDACIs investigated, compound 24 had the "unique" ability to selectively increase the β-driven reporter activity.

As sign of toxicity, the number of cells present by the end of the assay in the presence of the different compounds was measured and the number of cell duplications that had occurred during the assay calculated and presented in Table 1. Because this number is an exponent, 0 means that the number of cells remained constant (i.e., the number of cells that died was equal to that of cells that proliferated), a negative number means that the number of cells that died was higher than that of cells that proliferated (toxicity), and a positive number means that the number of cells that proliferated was higher than that of cells that died. The interpretation that differences in positive numbers are indication of toxicity is debatable. In fact, it may be related to differences in cell cycle length as a result of increased time spent to reprogram the cell expression profile in response to the HDACI. With the exception of compounds 11 and 23, none of the HDACIs included in this study, including SAHA, decreased the number of GM979 cells alive by the end of the assay below input values (Table 1), an indication of their low toxicity in this cell system.

Activity of HDACI on the Expression of the Endogenous Globin Genes in Primary Erythroblasts Obtained in Vitro from Healthy Donors. Human erythroblasts obtained in human erythroblast massive amplification (HEMA) cultures express maximal and ontogenetically correct level of γ- and β-globin mRNA after 3 to 4 days of EPO-induced maturation (Di Baldassarre et al., 2007). Therefore, to evaluate the effects of HDACI on the expression of the endogenous globin genes, proerythroblasts were generated in vitro from healthy donors and allowed to mature in the presence of selected compounds for 4 days. By the end of the 4 days, erythroblasts were harvested and counted (as indication of toxicity), and mRNA and protein were extracted for quantitative RT-PCR and HbF determination, respectively. The compounds included in the assay were represented by compounds 9 and 24, for their respective selectivity as $^{A}\gamma$- and β-promoter inducers in GM979 cells. At least another member of each class (compounds 11, 23, and 25), with comparable IC_{50} values in the HDAC inhibition screening, as control of specificity, and SAHA, for comparison, were also analyzed. Compound 24 was included in the analyses because its selec-

TABLE 1

Reporter-inducer activity of compounds 1–25 on GM979 cells

Standard deviations are within 10% and are not reported for clarity. The number of cell duplications was calculated according to the formula: number of duplications at day x = $\log_2$ (cell number at day x/cell number at day 0).

Compound	Concentration	γ-F	β-R	$\gamma/(\gamma+2\beta)$	Number of Cell Duplications
	μM		*% of control*		
1	2	423.3	210.2	198.7	0.64 ± 0.17
2	0.6	499.5	279.6	177.1	0.69 ± 0.17
3	2	514.4	529	99	0.19 ± 0.17
4	6	25.6	134.6	19.4	2.36 ± 0.17
5	20	167.6	242.3	68.5	2.34 ± 0.17
6	6	179.5	178	100.3	0.96 ± 0.17
7	2	937.7	544.4	173.8	0.34 ± 0.17
8	2	266.5	350.8	77.5	2.42 ± 0.17
9	2	897.9	338.5	264.8	1.07 ± 0.17
10	0.2	78.6	94.8	83.7	1.9
11	2	255.7	207.6	122.9	−0.11 ± 0.17
12	Toxic	N.D.	N.D.	N.D.	N.D.
13	0.02	95.5	83.0	114.0	2.0
14	0.2	100.2	98.5	102.4	2.2
15	0.2	125.0	113.3	112.0	2.1
16	0.2	167.7	115.6	142.8	2.0
17	0.2	107.2	120.1	90.0	1.0
18	0.2	114.8	112.0	102.0	1.4
19	0.2	99.5	98.1	100.0	1.2
20	2	85.8	131.8	65.3	1.79
21	0.2	181.3	178.9	101.3	0.20
22	2	261.8	272.5	96.1	0.29
23	2	268.6	253.7	101.3	−0.70
24	2	117.7	234.8	50.3	0
25	0.2	173.0	267.8	64.7	1.94
SAHA	0.2	189.1	153.1	123.2	1.29
DMSO	1% (v/v)	100	100	100	2.4 ± 0.17

N.D., not determined.

tivity as a β-promoter inducer suggested to us that it would represent a negative control. Each HDACI was used at the minimal concentration that was maximally effective (either 0.2 or 2 μM) on GM979 cells.

As expected (Cao, 2004), SAHA (0.2–2 μM) increased by 10-fold (from 0.05 to 0.20–0.39) the γ/(γ+β) ratio expressed by normal erythroblasts (Fig. 2A). Among the tested compounds, 9 and 25 all significantly increased the γ/(γ+β) expression ratio above background, with efficiency either comparable (compound 9) or 30% lower (compound 25) than SAHA. In contradiction to results obtained in GM979 cells, compound 24 also increased the γ/(γ+β) ratios. Furthermore, this compound significantly, although modestly (by 50%), increased the amount of HbF contained in normal erythroblasts by the end of the culture (Fig. 2B).

To detail the mechanism that mediated the increase in γ/(γ+β) expression ratio in normal cells exposed to these compounds, a second set of experiments determined their concentration/response curve on the expression levels of γ- and β-globin mRNA. The effects of compounds 11, 23, and 24 on γ- and β-globin expression remained modest up to concentrations of 3 μM (results not shown). In contrast, both compounds 9 and 24 transiently affected (induced or suppressed, respectively), expression of the endogenous β-globin at 0.02 μM and significantly increased, by 2-fold, the expression of γ-globin, with maximal effects at concentrations of 2 μM (compound 9) and 0.2 μM (compound 24), respectively. As a result, they also increased the γ/(γ+β) expression ratio (Fig. 3). However, the increase was clearly due to different mechanisms. In the case of the compound 9, the increase in expression ratio was due to the different magnitude of the increments of γ-globin and β-globin mRNA. In the case of compound 24, it was due to a combination of γ-globin mRNA increase and β-globin mRNA decrease. As a result, although the two compounds induced similar increases in the level of γ-globin mRNA (≈ from 2.0 to 3.5 $2^{-\Delta C_t}$), compound 24 was 3 times more active than compound 9 in increasing the γ/(γ+β) ratio (from ≈ 0.05 to 0.30 and 0.10, respectively) (Fig. 3). It is noteworthy that compound 24 is the one that increased the HbF content per cell up to detectable levels (Fig. 2B). Neither compound 9 nor compound 24 consistently affected the levels of α-globin and AHSP, included in the analysis as control of specificity, expressed by normal erythroblasts (results not shown).

Inhibition of Human Class I (HDAC1) and Class IIa (HDAC4) HDACs and Deacetylation of Histone H3 and α-Tubulin in U937 Cells and of Histone H4 in Primary Proerythroblasts. HDACI library was based on the assumption that the maize HD2, although structurally different from mammalian HDACs, was considered a predictor model for mammalian class I HDACs (Brosch et al., 1996b), whereas HD1-B (Lechner et al., 2000) and HD1-A (Brosch et al., 1996a) were considered homologous to mammalian class I and II HDACs, respectively. More recent data call into question the validity for human enzymes of class selectivity identified with the maize HDAC isoforms (Mai et al., 2006). Mammalian HDACs, in fact, are organized within the cells in complexes with other HDACs and DNA-binding proteins. In these complexes, one of the HDAC isoforms (usually of class I) exerts the catalytic function, whereas the other (usually of class IIa or b) acts as regulator of the catalytic enzyme (Verdin et al., 2003; Minucci and Pelicci, 2006). Therefore, to clarify the class selectivity of compounds 9 and 24 for human HDACs, we performed inhibitory assays against the enzymatic activity of HDAC complexes purified by immunoprecipitation with antibodies specific for human HDAC1 (class I) and HDAC4 (class IIa) (Table 2). SAHA was used as control. Compound 24, which was potent but not selective in maize, inhibited at least as efficiently as SAHA both class I and class IIa human HDACs (IC_{50} = 0.2 μM in both cases). On the other hand, compound 9 was weak (10-fold less efficient than SAHA) but class IIa-selective. Therefore, in both cases, there was a good correlation between inhibition of maize and human HDAC class isoforms.

To clarify whether the HDAC inhibitory activity exerted by the compounds in vitro did correspond to increased histone acetylation in vivo, we measured the levels of acetylation of histone H3 and α-tubulin in U937 cells incubated with increasing concentration of compounds (Fig. 4). Again, SAHA was included as a control. The acetylation levels of α-tubulin were analyzed as indicator of functional inhibition of HDAC6, a class IIb HDAC isoform (Haggarty et al., 2003). In

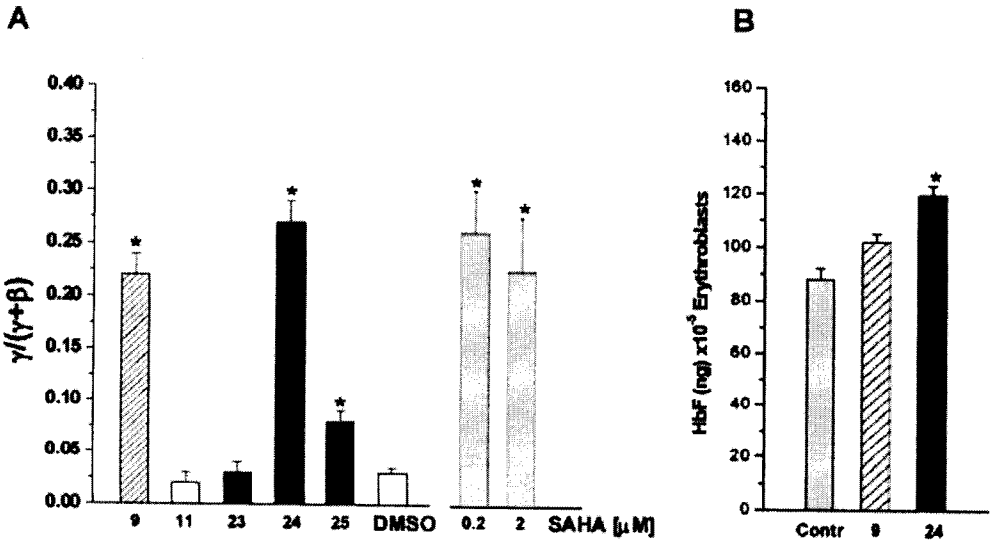

Fig. 2. Effects of selected HDACIs on the γ/(γ+β) mRNA ratio (A) and on the HbF content (B) expressed by primary erythroblasts obtained from healthy donors. Proerythroblasts were obtained in HEMA and were induced to mature for 4 days with EPO in the presence or in the absence of the indicated HDACI. HDACIs were used at the minimal concentration that was effective on GM979 cells and presented in Table 1. These concentrations are either 0.2 μM (compounds 9 and 25) or 2 μM (compounds 11, 23, and 24). Results obtained in parallel cultures incubated with SAHA (0.2–2 μM) are presented for comparison. Data are presented as mean (± S.D.) of five to six separate assays, each with a different donor, performed in triplicate. The γ/(γ+β) mRNA ratios observed in cultures with or without DMSO are 0.03 ± 0.005 and 0.023 ± 0.004, respectively. Values statistically different from untreated controls are indicated by * ($p < 0.5$) and ** ($p < 0.01$).

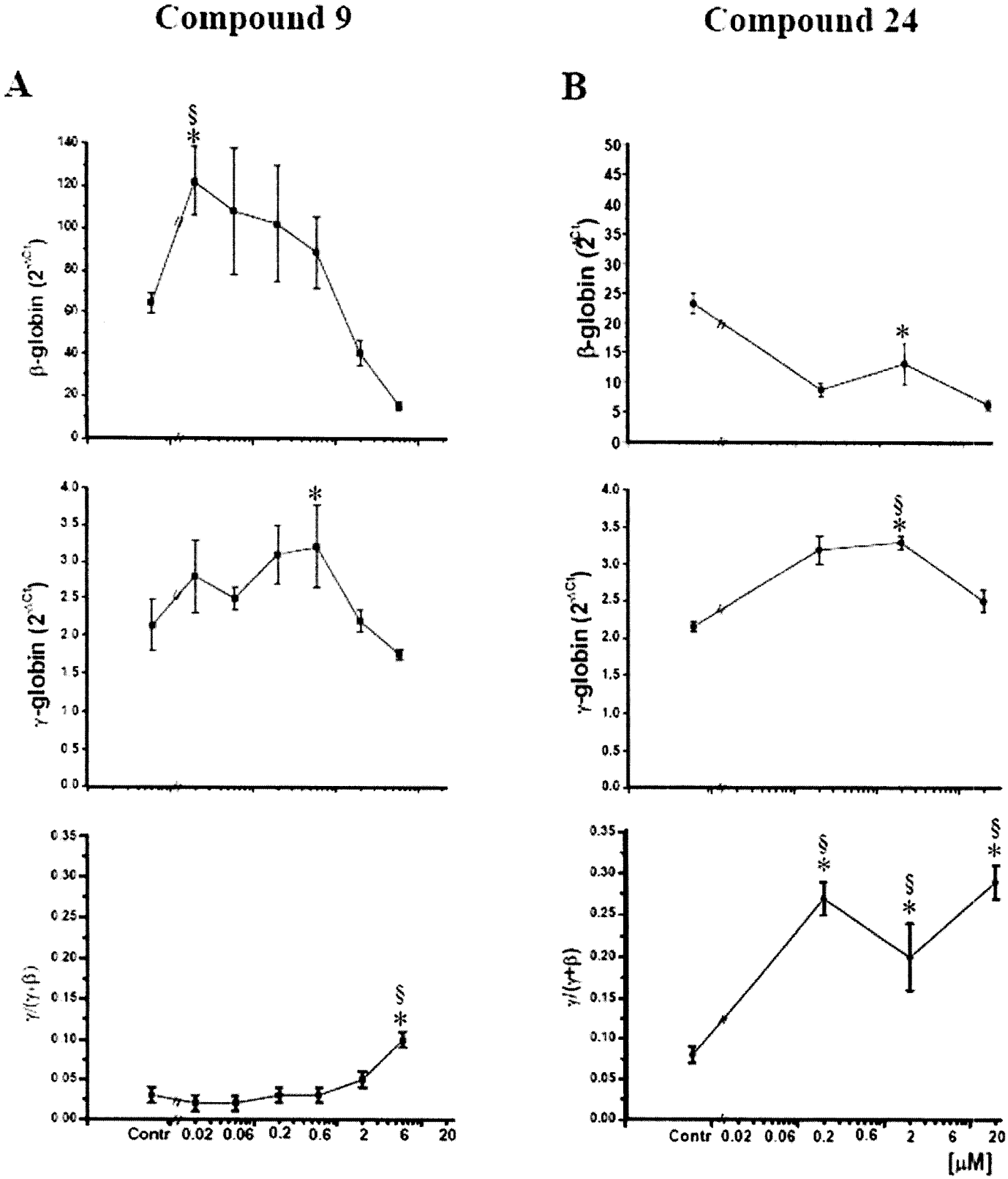

Fig. 3. Concentration/response curve for compounds 9 (A) and 24 (B) on the levels of β- and γ-globin mRNA and on the γ/(γ+β) ratio, expressed by normal human erythroblasts. Cells incubated with DMSO were used as negative control (Contr). Results are presented as mean (± S.D.) of a single experiment performed in triplicate and are representative of those observed in at least five to six experiments, each with a different donor. § and * indicate values statistically different ($p < 0.05$) from control by paired t test and analysis of variance, respectively. See the legend to Fig. 2 for further details. In the experiment presented in B, untreated cells expressed levels of β and γ globin mRNA of 23.3 ± 1.8 versus 2.2 ± 0.1, respectively. The values expressed by untreated cells in the experiment presented in A were not measured.

these experiments, compounds 9 and 24 induced similar levels of α-tubulin acetylation, levels that were slightly lower than those induced by SAHA. Therefore, compounds 9 and 24, which had a clear different activity on class IIa HDAC (Table 2), exerted similar levels of inhibition on the class IIb isoform (Fig. 4). Differential inhibition on class IIb and IIa enzymes has been already reported for other molecules with HDACI activity (Mai et al., 2006) and is consistent with the distinctive chemical structure of the two classes of HDAC isoforms (Minucci and Pelicci, 2006). In addition, compound 9 was less efficient than SAHA, and compound 24 was as efficient as SAHA in inducing histone H3 acetylation. The differences observed between compounds 9 and 24 in histone H3 acetylation inducing activity in vivo are consistent with their potency as inhibitors of class IIa HDAC in vitro (see Table 2). It is also possible, however, that the difference between compounds 9 and 24 in histone acetylation was because the compounds had been used at equimolar rather than equitoxic concentrations.

As an indication that the induction of HbF synthesis exerted by the compounds in primary erythroblasts was mediated by increased levels of histone acetylation, we compared by flow cytometry the acetylation state of histone H4 in normal erythroblasts that had matured in the absence or in the presence of compounds 9 and 24 (Fig. 5). The acetylation state of histone H3 was not analyzed because of low abundance of this protein in primary cells does not allow its evaluation by flow cytometry. A clear increase above background (AFU = 523 versus 170) in the acetylation state of histone H4 was observed in cells incubated with compound 9. A small, but detectable, increase in acetylation levels of histone H4 was also observed in cells incubated with compound 24 (256 versus 170).

The fact that HDACI had increased the levels of H4 acetylation in primary erythroblasts is proof that they had inhibited HDAC activity in these cells. Two recent publications have demonstrated that increases in the levels of hystone H4 acetylation, obtained either through HDAC inhibition (Fathallah et al., 2007) or through activation of the p38 MAPK signaling (Aerbajinai et al., 2007), are responsible for the increased γ-globin expression induced in adult erythroblasts by butyrate and thalidomide, respectively. It is conceivable, therefore, that the increased levels of H4 acetylation were directly responsible for the effects of compounds 9 and 24 on γ-globin expression observed in this study.

TABLE 2

Comparison of the inhibitory activity of compounds 9 and 24 and SAHA on human class I (HDAC1) and II (HDAC4) HDAC isoforms purified from human cell lines

Enzymatic activities are expressed as percentage of the control activity exerted by the enzyme alone.

Compound	Class I (HDAC1)	Class IIa (HDAC4)
	%	%
SAHA		
0.2 μM	52.2 ± 1.4	66.6 ± 1.6
2.0 μM	15.5 ± 1.4	33.8 ± 1.1
9		
0.2 μM	108.2 ± 7.1	94.3 ± 0.6
0.6 μM	116.0 ± 2.8	98.1 ± 0.3
2.0 μM	113.3 ± 4.3	89.8 ± 0.7
6.0 μM	107.5 ± 3.9	78.0 ± 0.2
20 μM	102.8 ± 2.1	41.8 ± 0.8
24		
0.2 μM	55.1 ± 0.7	70.3 ± 0.7
0.6 μM	29.8 ± 1.6	43.5 ± 0.01
2.0 μM	14.2 ± 0.9	30.8 ± 0.6
6.0 μM	9.8 ± 0.07	18.4 ± 0.8
20 μM	8.5 ± 0.05	17.0 ± 0.6

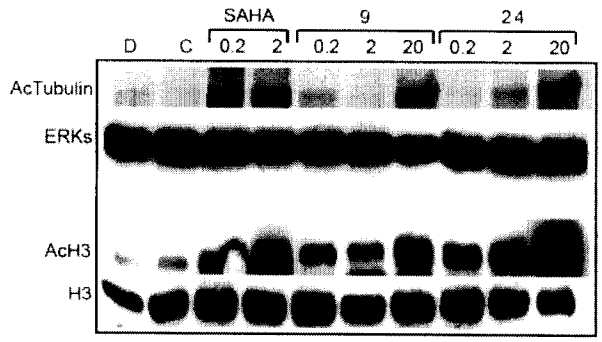

Fig. 4. Effects of compounds 9 and 24 on the levels of H3 and α-tubulin acetylation in U937 cells. U937 cells were incubated either with increasing concentration of SAHA (positive control) and of compounds 9 and 24 (0.2–20 μM in all the cases), as indicated. Untreated cells (C) and cells incubated with DMSO alone (D) were analyzed as negative controls.

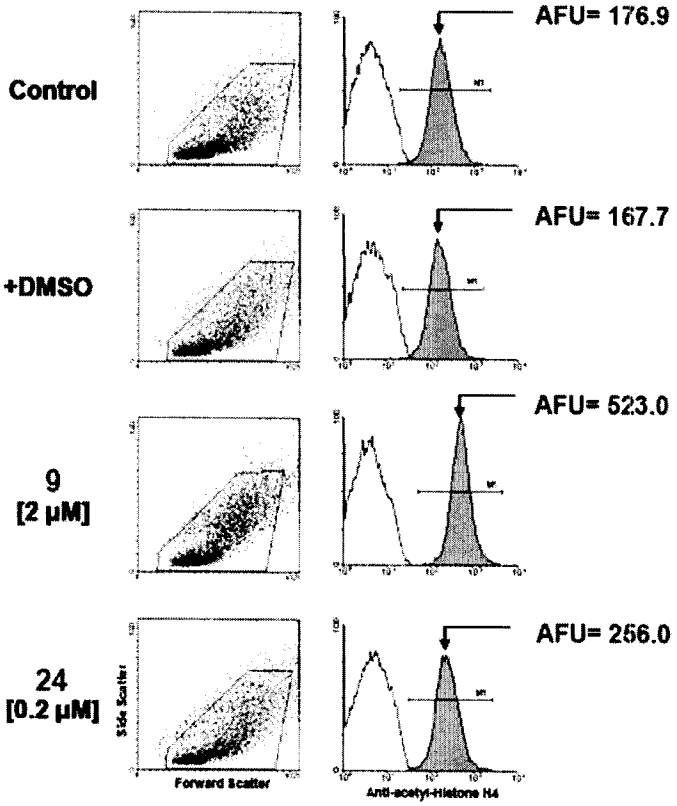

Fig. 5. Effects of compounds 9 and 24 on the level of histone H4 acetylation in primary erythroblasts obtained from healthy donors. Proerythroblasts obtained in HEMA were cultured with EPO alone (control, top panel) or with EPO plus DMSO (vehicle, negative control), or compound 9 or 24, as indicated. After 4 days, the cells were harvested and the levels of H4 acetylation measured by flow cytometry. The forward and side scatter plots present the gate used for the fluorescence analyses presented in the histograms on the right. The white and gray area correspond to the fluorescence intensity expressed by cells labeled with an irrelevant antibody or with the anti-acetyl-histone H4, respectively. The average fluorescence intensity (AFU, in arbitrary units) expressed by cells incubated with the anti-acetyl-histone H4 is reported on the right, and is proportional to the acetylation state of histone H4 in the cell population analyzed (Ronzoni et al., 2005).

Comparison of in Vitro Differentiation of Normal and β^0 Thalassemic Erythroblasts. It has been reported already that progenitor cells present in the blood from healthy donors, as well as those present in the blood from patients with β^0 thalassemia, generate high numbers of erythroblasts in ex vivo expansion cultures (Fibach et al., 1989; Migliaccio et al., 2002). However, the differences between the in vitro maturation of normal and β^0 thalassemic erythroblasts are still poorly defined. For this reason, a pilot study compared number, morphology, and level of globin gene expression of erythroblasts obtained in vitro from healthy and β^0 thalassemic donors.

Under HEMA conditions, mononuclear blood cells from patients with β^0 thalassemia generated, in 10 to 12 days, a proerythroblast population that, although slightly lower in number (-fold increase with respect to day 0 = 0.52 ± 0.22 versus 1.71 ± 0.84 in β^0 thalassemic and normal cultures, respectively, $p < 0.01$), was equivalent in morphology to that generated by the corresponding normal cells (Fig. 6). However, whereas normal pro-erythroblasts transferred in cultures containing only EPO matured in 4 days up to the stage of orthochromatic erythroblasts (Fig. 6A), those obtained from patients with β^0 thalassemia matured poorly, remaining large in size, with large nuclei and poorly condensed chromatin (Fig. 6B). Such retarded maturation was reflected by increased proliferation. In fact, normal proerythroblasts have limited proliferative capacity and proliferate only one to three times before initiating terminal maturation. Some of them will undergo apoptosis. As a result of the balance between the two processes, the number of cells after 4 days of maturation culture remain similar to input (-fold increase = 0.85 ± 0.28). In contrast, in the corresponding maturation cultures seeded with β^0 thalassemic proerythroblasts, the number of cells increased by ~2-fold (-fold increase = 1.99 ± 0.93) by day 4. Although the difference from the 2-fold increase is not statistically significant, this result indicates that β^0 thalassemic proerythroblasts proliferate more and/or die less than normal cells when exposed to EPO alone.

Differences were also observed in the levels of globin gene expressed by normal and β^0 thalassemic erythroblasts after 4 days of maturation culture in EPO alone. AHSP was included in this analyses because of its abundant expression in erythroid cells (Kihm et al., 2002) and because of the function of its product to bind free α-chains, stabilizing their structure and limiting their ability to participate in chemical reactions that generate reactive oxygen species (Feng et al., 2004). Normal orthochromatic erythroblasts expressed high levels of α- and β-globin ($2^{-\Delta C_t}$ in the 10–100 range for both) and relatively low levels of γ-globin and AHSP ($2^{-\Delta C_t}$ in the 1–10 range) (Fig. 6). The levels of α- and β-globin expressed by normal cells obtained from different donors were very similar. In contrast, the donor variability in γ-globin and AHSP expression was as high as 10-fold (see the corresponding SD in Fig. 6A). As expected, β^0 thalassemic erythroblasts expressed levels of α- and γ-globin not statistically different from those expressed by the corresponding cells obtained from healthy donors, but significantly less β-globin than normal cells ($2^{-\Delta C_t}$ in the order of magnitude of 1–10). We were surprised to find, however, that β^0 thalassemic cells expressed significantly more AHSP (by 1 log) than normal cells (Fig. 6). With the exception of AHSP, the subject-to-subject variability in globin genes expression in β^0 thalassemic erythroblasts was much wider than that observed with the corresponding cells from healthy donors (Fig. 6B). More specifically, the difference in β-globin expression among erythroblasts obtained from different patients was so wide that, in the case of two patients, it was only 10-fold lower than normal.

Compounds 9 and 24 Restore the Impaired in Vitro Maturation of β^0 Thalassemic Erythroblasts. In a last set of experiments, compounds 9 and 24 were tested for their ability to restore the impaired maturation expressed in vitro by erythroblasts obtained from patients with β^0 thalassemia.

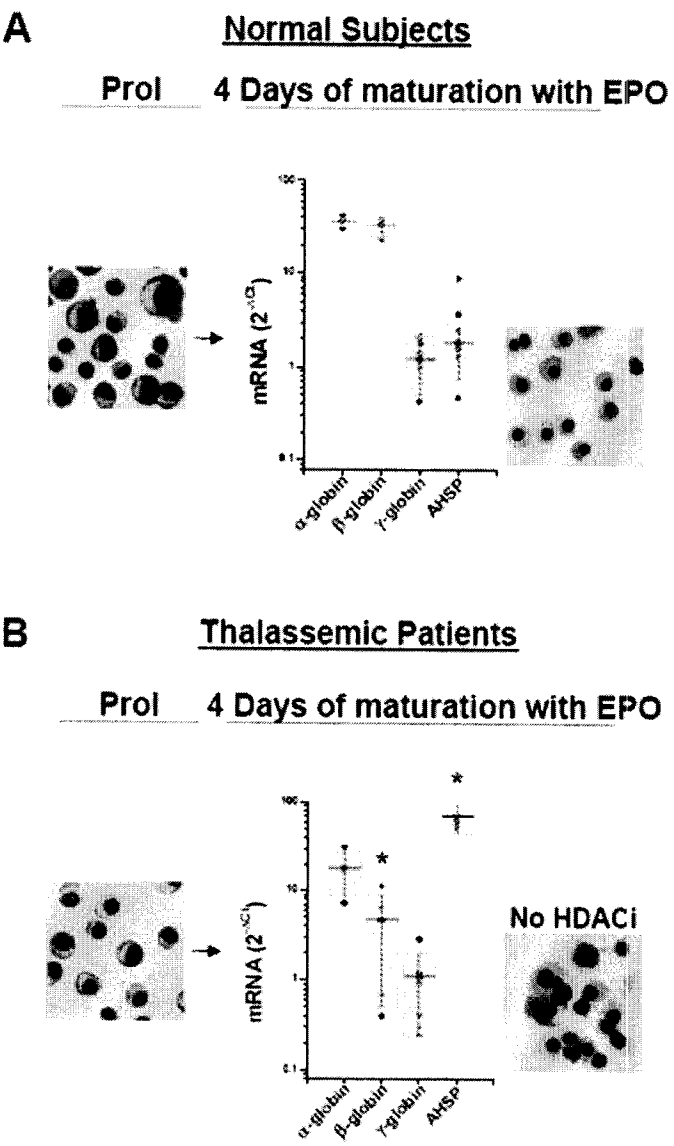

Fig. 6. Comparison of the in vitro maturation of primary pro-erythroblasts obtained from healthy donors (A) or from patients with β^0 thalassemia (B), as indicated. Pro-erythroblasts were obtained in the proliferative phase of HEMA (prol) and induced to mature for 4 days with EPO. Cell morphology before (Prol) and after maturation was analyzed by May-Grunwald staining (original magnification, 40×). Expression levels of α-, β- and γ-globin, and AHSP, in cells at the end of the maturation culture were analyzed by quantitative RT-PCR and expressed as $2^{-\Delta C_t}$. Data obtained with a total of three to seven healthy donors and five patients with thalassemia (each donor is represented by a different symbol) are presented. The straight line and the shaded area indicate the mean (± S.D.) obtained in all the experiments. Expression levels in β^0 thalassemic erythroblasts statistically different ($p < 0.01$) from those of normal cells are indicated by *.

By morphological criteria, both compounds 9 and 24 restored the in vitro maturation of β^0 thalassemic erythroblasts as orthochromatic cells became readily detectable in the cultures (Fig. 7). By expression analysis, β^0 thalassemic erythroblasts that matured in the presence of these compounds expressed significantly lower levels of β-globin (by 10-fold) and of AHSP (by 2- to 10-fold). In particular, the levels of AHSP expressed by β^0 thalassemic cells exposed to compound 9 became no longer statistically different from those expressed by normal erythroblasts obtained from healthy donors (Fig. 6 and 7).

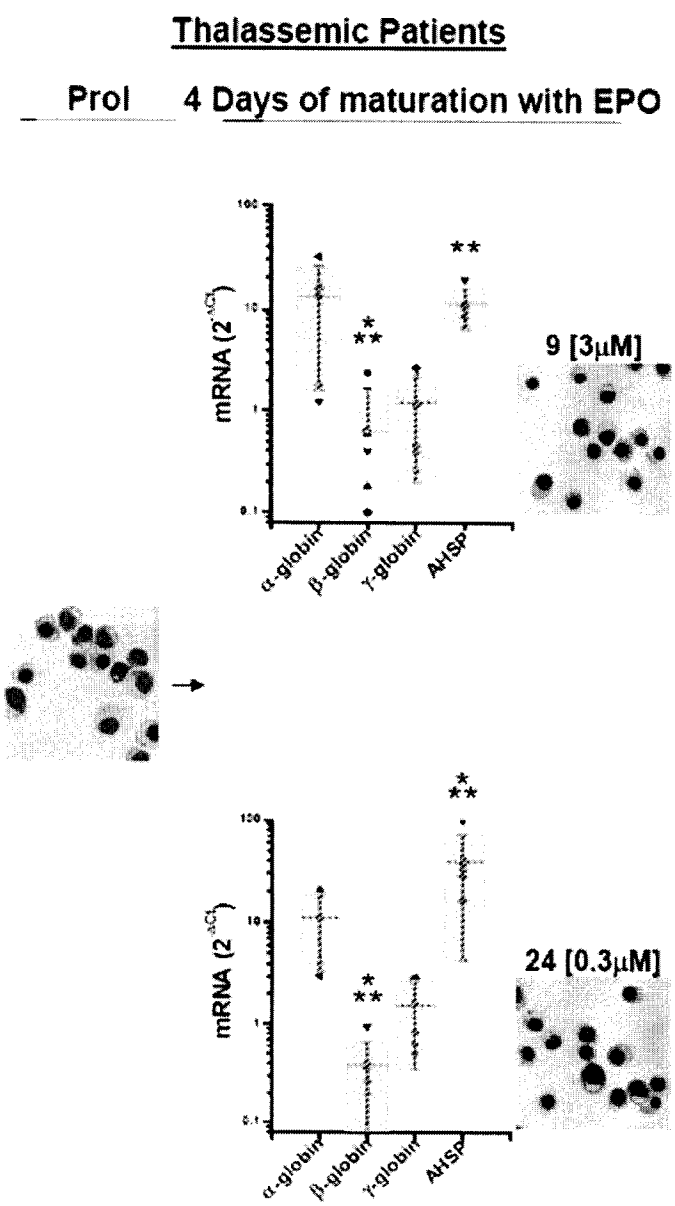

Fig. 7. Compounds 9 (top) and 24 (bottom) both restore the impaired in vitro maturation of proerythroblasts from patients with β^0 thalassemia. The morphology of the cells before (Prol) and after the 4 days of maturation in the presence of EPO plus each compound was analyzed by May-Grunwald staining (original magnification, 40×). Expression levels of α-, β-, and γ-globin, and AHSP, in cells cultured for 4 days in the presence of the compounds were analyzed by quantitative RT-PCR and expressed as $2^{-\Delta Ct}$. Data obtained with a total of five patients with β^0 thalassemia (each donor is represented by a different symbol, the same as in Fig. 6B) are presented. The levels of mRNA expressed by cells treated with DMSO alone are presented as control and ranged from 91% (γ-globin) to 107% (α-globin) of those expressed by untreated cells and presented in Fig. 6. The straight line and the shaded area indicate the mean (± S.D.) obtained in all the experiments. Values statistically different from those expressed by untreated normal and β^0 thalassemic erythroblasts, and presented in Fig. 6, are indicated by * and by **, respectively.

On average, neither compound 9 nor compound 24 affected the $\gamma/(\gamma+\beta)$ expression ratio in the β^0 thalassemic erythroblasts (Fig. 7 and results not shown). However, as shown by the detailed concentration/response curves on gene expression presented in Fig. 8, in the case of two patients with β^0 thalassemia, those whose cells expressed the highest baseline levels of β-globin, both compounds increased the $\gamma/(\gamma+\beta)$ ratio by 4- to 6-fold. Compound 9 did not significantly affect γ-globin expression but decreased that of β-globin (by 4-fold) in both patients. Compound 24 decreased β-globin expression (by 4-fold) and significantly increased γ-globin expression (by 2-fold) in both patients. In contrast with the results on normal cells, compound 9 decreased α-globin (by 4-fold) in one patient (Fig. 8A). As a result, the α/non-α expression ratio was not affected by the compound in one patient and was increased (by 20-fold) in the other one. Compound 24 had opposite effects on α-globin expression in the two patients: it increased it in one patient (the same who responded to compound 9) and decreased it in the other (Fig. 8B). Consequently, the α/non-α expression ratio was significantly increased (by 4-fold) in one patient and was not affected in the other one.

Toxicity Exerted by Compounds 9 and 24 in Cultures of Normal and β^0 Thalassemic Human Erythroblasts. Last but not least, Fig. 9 compares the toxicity exerted by compounds 9 and 24 in maturation cultures of normal and β^0 thalassemic erythroblasts. In cultures of normal cells, both compounds 9 and 24 decreased the number of cells alive by the end of the maturation culture less than SAHA, almost at all the concentrations tested. Therefore, both HDACI were at least no more toxic than SAHA at the concentrations (0.2 and 2 μM) found to be active as γ-globin inducer in normal erythroblasts. On the other hand, both compounds 9 and 24 were far less toxic in cultures of β^0 thalassemic erythroblasts than they were in those of normal cells. Compound 24 had no effect on the cell number over the wide range of concentrations tested, whereas compound 9 exerted a 50% inhibitory activity at the concentration (3 μM) that was effective as $\gamma/(\gamma+\beta)$ inducer in these cells.

Discussion

We have identified new synthetic HDACI capable to affect expression of γ-driven and/or of β-driven reporter activity in GM979 cells. Three compounds (8, 9, and 11) increased expression of both $^A\gamma$- and β-driven reporter activities. The effects exerted on the two promoters were of different magnitude and occurred at different concentrations (Table 1). This allowed us to define a concentration window at which a compound was more potent as $^A\gamma$- than as β-driven reporter inducer (Table 1). Compound 9, in particular, was 2-fold more potent than SAHA as inducer of $\gamma/(\gamma+\beta)$ expression ratio. On the other hand, compound 24, exclusively affected expression of the β-driven reporter in this synthetic model of Hb switch (Table 1).

Selected compounds were then tested for their ability to modify expression of the γ- and β-globin genes in normal erythroblasts. Two of them, compounds 9 and 24, altered

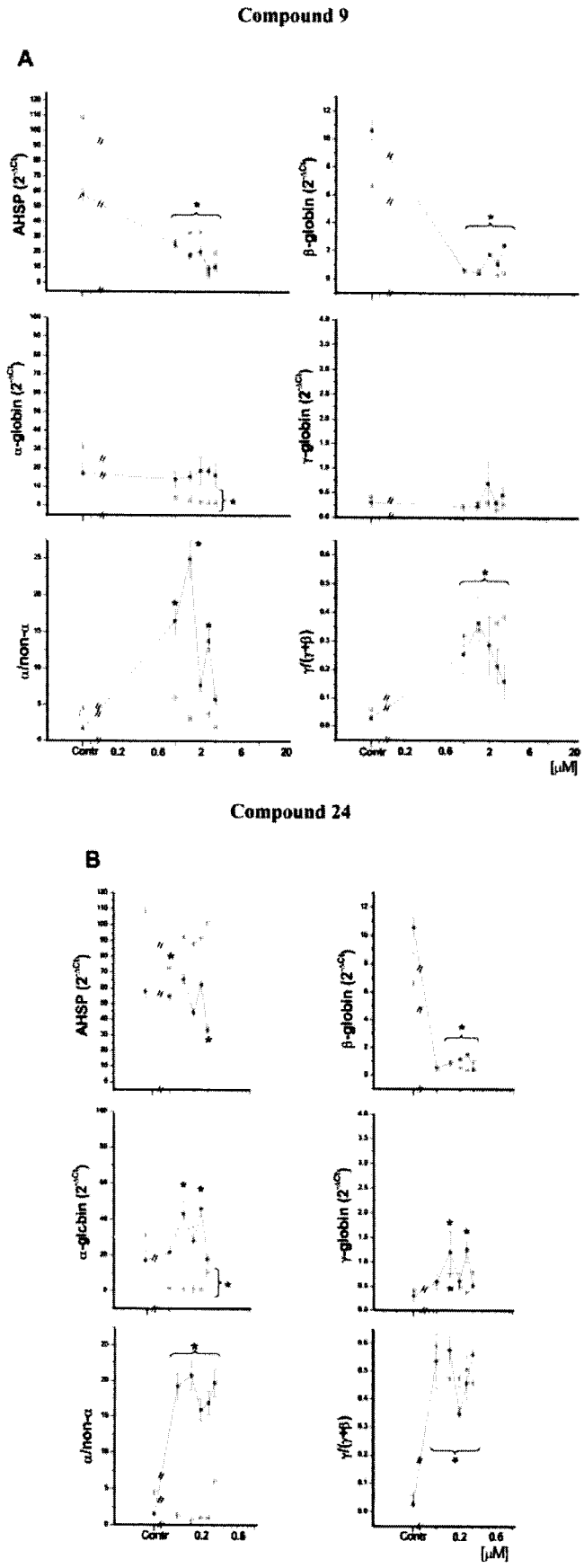

Fig. 8. Concentration/response curves of compounds 9 (A) and 24 (B) on the levels of α-, β-, and γ-globin, as well as AHSP, mRNA expressed by primary erythroblasts obtained from two separate patients with β^0 thalassemia (each color represents a different donor). The corresponding α/non-α and $\gamma/\gamma+\beta$ ratios are reported on the bottom (see legend to Fig. 7 for more information). Results are presented as mean (± S.D.) of single experiments performed in triplicate. * indicate values statistically different ($p < 0.05$) from controls.

expression of the endogenous globin genes, with no or minimal effects on that of α-globin and AHSP (Fig. 2, 3 and results not shown). Because maximal effects on γ- and β-globin expression were induced at different concentrations (Fig. 3) also, in this case, it was possible to identify a concentration window at which $\gamma/(\gamma+\beta)$ was significantly increased (3–8-fold). It is noteworthy that the concentrations (0.2–3 μM) that mostly increased the $\gamma/(\gamma+\beta)$ ratio in primary and in GM979 cells were the same. The synthetic double-reporter assay used in our laboratory only partially predicted the activity of a compound on the endogenous promoters in primary cells. In fact, two of the compounds (8 and 11) active on GM979 cells failed to induce the endogenous genes, whereas one compound (9) induced the β-driven reporter while suppressing expression of the endogenous β-globin gene. This might be because the GM979 cells, while thawed in our laboratory, had partially drifted from those established by Skarpidi et al. (2000).

There was no apparent relationship between class-selective inhibition of maize and human HDACs exerted by a compound (Supplemental Tables 2 and 3) and its efficacy as $\gamma/(\gamma+\beta)$ inducer (Figs. 2 and 3). In fact, compound 11, which was the most class-II selective HDACI (selectivity ratio, 176), was inactive in the γ-globin gene inducing assay, whereas the related but less class II-selective (selectivity ratio, 71) compound 9 was a good $\gamma/(\gamma+\beta)$ inducer (Figs. 2 and 3). On the other hand, compound 24 lacked class selectivity and was more potent than compound 9 as a $\gamma/(\gamma+\beta)$ inducer. Compounds 9 and 24, however, exerted their effects through at least partially different mechanisms (preferential activation of γ- versus β-globin expression versus activation of γ- and inhibition of β-globin expression). The discovery that mammalian HDAC are assembled within the cells as multicomplexes of more than one isoenzyme, each one exerting a specific function, with many other DNA-binding proteins (Minucci and Pelicci, 2006) is rendering obsolete both the concept of class selectivity and the use of the maize enzyme assay as a screening method to predict pharmacologically relevant HDACI. Furthermore, it is likely that a specific HDAC complex regulates the globin gene locus. In this regard, it has been recently reported that the effect of butyrate on γ-globin expression is mediated by the class I HDAC3 (Mankidy et al., 2006), an enzyme part of the complex that include HDAC4 (Verdin et al., 2003). It is conceivable, then, that the identification of the specific HDAC complexes involved in the regulation of the globin locus, which may include but may not be limited to the HDAC3-HDAC4 complex, will finally allow the prediction of the chemical structure of the HDACI most effective as HbF inducer.

Orthochromatic erythroblasts obtained from healthy donors expressed high levels of AHSP and of globin genes (Fig. 6). We were surprised to find that the levels of AHSP expressed by erythroblasts obtained from different donors were different by 1-log (Fig. 6). Three-fold variability in AHSP expression has been recently described in reticulocytes obtained from different healthy subjects. This variability has

been ascribed to a T-homopolymer polymorphism in the putative gene promoter (T18 versus T15) (Lai et al., 2006). The higher (10-fold) variability observed here might be due to the fact that the T18 polymorphism affects most prominently AHSP expression at early than at late stages of maturation or to the existence, in the AHSP locus, of additional regulatory polymorphisms, still to be identified. Further studies will clarify this point.

Erythroblasts obtained from patients with β^0 thalassemia had a clearly abnormal maturation profile in response to EPO. β^0 thalassemic erythroblasts matured poorly, as documented by their morphology, and expressed levels of β-globin 1- to 5-log lower than normal (Fig. 7). We were surprised to find that β^0 thalassemic erythroblasts expressed levels of AHSP 10 times higher than normal. The reason for such high expression is unknown. Because expression of AHSP increases with erythroblast maturation (dos Santos et al., 2004), it is unlikely that such high levels are a reflection of retarded cell maturation. Instead, the significant ($p < 0.05$) linear correlation between the amount of AHSP and that of α-globin mRNA present in erythroblasts obtained from different patients (data not shown) suggests that it might result from an auto-regulatory loop, triggered by the concentration of uncoupled α-chains in the cytoplasm of these cells.

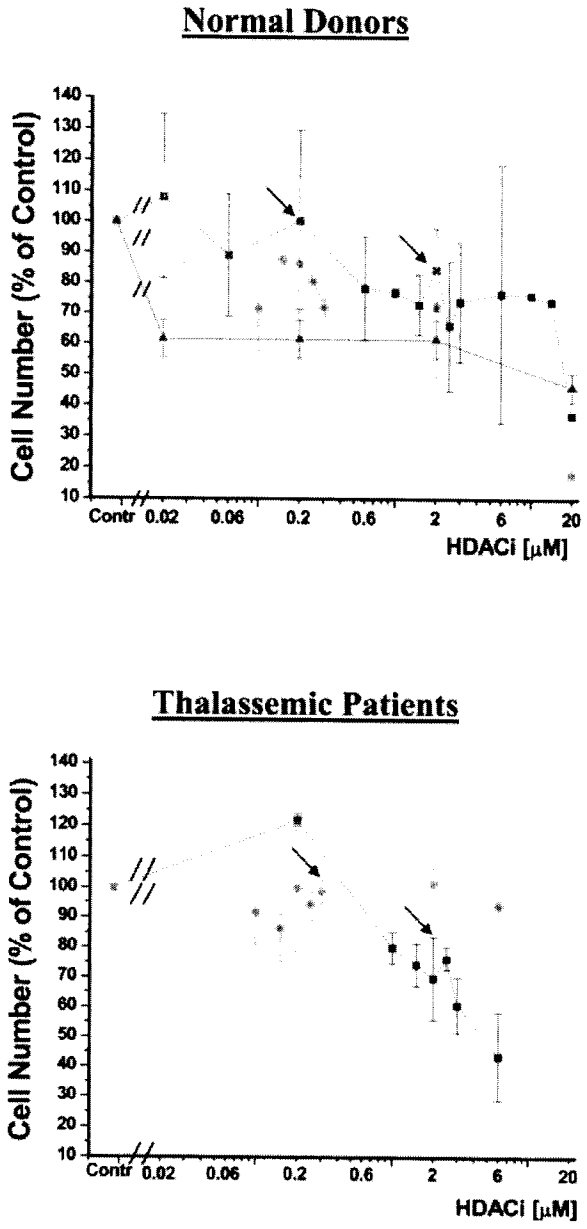

Fig. 9. Toxicity exerted by compounds 9 (squares) and 24 (circles) in cultures of normal (top) and β^0 thalassemic (bottom) erythroblasts, as indicated. Toxicity was evaluated based on the number of cells observed by the end (4 days) of the maturation culture. The number of cells observed in the presence of SAHA (triangles) and of DMSO (the vehicle, shaded area) is also reported, for comparison. Results are expressed as percentage of untreated control cells (100% = 0.85 ± 0.28 versus 1.99 ± 0.93 × 10^6 cells in cultures from healthy and β^0 thalassemic donors, respectively) and are presented as mean (± S.D.) of five to six separate assays. The arrows indicate the concentrations used in Figs. 2 and 7, respectively.

Compounds 9 and 24 both restored the morphological maturation of β^0 thalassemic erythroblasts (Fig. 7). The molecular mechanism used by each compound is not obvious. In fact, in only two patients of five analyzed was it possible to demonstrate that the improved maturation was associated with increased $\gamma/(\gamma+\beta)$ ratios (Fig. 8 and Supplemental Fig. 1). The alterations induced in these two patients were consistent with those induced in normal cells: compound 9 decreased β-globin expression, whereas compound 24 increased γ-globin expression and reduced β-globin expression. It is possible that similar modifications were induced by these compounds in erythroblasts from all the patients included in this study but went undetected because of the time point (4 days of culture) chosen for analysis. Heterogeneity of in vivo response of patients with β^0 thalassemia or sickle-cell anemia to treatment with the HDACI butyrate has been described previously (Perrine et al., 1993; Sher et al., 1995). It has been reported that such heterogeneity is retained by cells obtained from the same patients in vitro (Fathallah et al., 2007). Therefore, a comparison of the response to compounds 9 and 24 of erythroblasts obtained in vitro from patients who do or do not respond to butyrate might provide indications whether these compounds could be used for personalized therapies. These experiments will be performed in the near future.

A difference between the response to compounds 9 and 24 of normal and β^0 thalassemic erythroblasts was represented by the fact that in normal cells, compounds 9 and 24 did not affect α-globin and AHSP expression, whereas both of them reduced the expression of these genes in β^0 thalassemic erythroblasts: the reduction of α-globin expression was modest (by 5-fold) and donor-dependent; the reduction of AHSP expression was of greater magnitude (in the case of compound 9, it was reduced down to the levels observed in normal cells) and was donor-independent (Figs. 7 and 8 and Supplemental Fig. 1). It is tempting to interpret this last result as an indication that the level of AHSP expression was normalized because the concentration of free α-chains in the cytoplasm of the cells had been reduced. However, it is also possible that the effects of HDACI on AHSP expression are independent of their action on the β-globin locus. For example, in β^0 thalassemic erythroblasts, HDACI might interfere with the homeostatic regulatory loop, involving α-globin and AHSP, activated by the cells to compensate for the presence of defective β-chains. In other words, the effects of HDACI on AHSP regulation might function as modifier of the β thalassemic trait, at least in vitro. The hypothesis that AHSP might represent a gene modifier that, as the hereditary per-

sistence of fetal hemoglobin mutation, might ameliorate the phenotype of thalassemic patients was originally suggested by the observation that double AHSP^{null} β thalassemic mice have an exacerbated phenotype (Kong et al., 2004). Although not supported by clinical evidence so far (Viprakasit et al., 2004; Lai et al., 2006), this hypothesis is worthy of further investigation because it might lead to the identification of additional targets for the therapy of sickle-cell anemia and/or β thalassemia.

In conclusion, using a new assay based on primary erythroblasts, we have identified two new HDACIs, compounds 9 and 24, that specifically altered the levels of γ- and β-globin expressed by these cells increasing the γ/(γ+β) ratio with limited donor-to-donor variability. One of the compounds (24) also increased the HbF content of normal cells. Both compounds restored the defective morphological maturation and increased the γ/(γ+β) ratio expressed by β^0 thalassemic erythroblasts in vitro. Because of their low toxicity in all of the assays investigated, we suggest that compounds 9 and 24 might represent new candidates for pharmacological reactivation of HbF for the treatment of patients with β^0 thalassemia.

Acknowledgments

Recombinant human stem cell factor was provided by Amgen (Thousand Oaks, CA). Mitchell Weiss and George Atweh are gratefully acknowledged for support and encouragement. The collaboration of Fabrizio Martelli for graphic assistance, of Mariacristina Di Rico for the initial luciferase assays, and of Valerie Smith for editorial assistance is also greatly appreciated.

References

Aerbajinai W, Zhu J, Gao Z, Chin K, Rodgers GP (2007) Thalidomide induces γ-globin gene expression tghorugh increased reactive oxygen species-mediated p38 MAPK signalling and histone H4 acetylation in adult erythropoiesis. *Blood*, in press.

Atweh GF, Sutton M, and Nassif I (1999) Sustained induction of fetal hemoglobin by pulse butyrate therapy in sickle cell disease. *Blood* **93:**1790–1797.

Atweh GF and Schechter AN (2001) Pharmacologic induction of fetal hemoglobin: raising the therapeutic bar in sickle cell disease. *Curr Opin Hematol* **8:**123–130.

Bradai M, Abad MT, Pissard S, Lamraoui F, Skopinski L, and De Montalembert M (2003) Hydroxyurea can eliminate transfusion requirements in children with severe β-thalassemia. *Blood* **102:**1529–1530.

Brosch G, Goralik-Schramel M, and Loidl P (1996a) Purification of histone deacetylase HD1-A of germinating maize embryos. *FEBS Lett* **393:**287–291.

Brosch G, Lusser A, Goralik-Schramel M, and Loidl P (1996b) Purification and characterization of a high molecular weight histone deacetylase complex (HD2) of maize embryos. *Biochemistry* **35:**15907–15914.

Cao H (2004) Pharmacological induction of fetal hemoglobin synthesis using histone deacetylase inhibitors. *Hematology* **9:**223–233.

Cao H, Stamatoyannopoulos G, and Jung M (2004) Induction of human γ globin gene expression by histone deacetylase inhibitors. *Blood* **103:**701–709.

Constantoulakis P, Knitter G, and Stamatoyannopoulos G (1989) On the induction of fetal hemoglobin by butyrates: in vivo and in vitro studies with sodium butyrate and comparison of combination treatments with 5-AzaC and AraC. *Blood* **74:**1963–1971.

Di Baldassarre A, Di Rico M, Di Noia A, Confini T, Iacone A, Marchisio M, Miscia S, Alfani E, Migliaccio AR, Stamatoyannopoulos G, et al. (2007) Protein kinase Calpha is differentially activated during neonatal and adult erythropoiesis and favors of a reporter gene under the control of the ^{A}γ globin-promoter in cellular models of hemoglobin switching. *J Cell Biochem* **101:**411–424.

dos Santos CO, Duarte AS, Saad ST, and Costa FF (2004) Expression of alpha-hemoglobin stabilizing protein gene during human erythropoiesis. *Exp Hematol* **32:**157–162.

Fathallah H, Weinberg RS, Galperin Y, Sutton M, Atweh GF (2007) Role of epigenetic modifications in normal globin gene regulation and butyrate-mediated induction of fetal hemoglobin. *Blood*, in press.

Felsenfeld G and Groundine M (2003) Controlling the double helix. *Nature* **421:**448–453.

Feng L, Gell DA, Zhou S, Gu L, Kong Y, Li J, Hu M, Yan N, Lee C, Rich AM, et al. (2004) Molecular mechanism of AHSP-mediated stabilization of alpha-hemoglobin. *Cell* **119:**629–640.

Fibach E, Manor D, Oppenheim A, and Rachmilewitz EA (1989) Proliferation and maturation of human erythroid progenitors in liquid culture. *Blood* **73:**100–103.

Forsberg EC, Downs KM, Christensen HM, Im H, Nuzzi PA, and Bresnick EH (2000) Developmentally dynamic histone acetylation pattern of a tissue specific chromatin domain. *Proc Natl Acad Sci U S A* **97:**14494–14499.

Haggarty SJ, Koeller KM, Wong JC, Grozinger CM, Schreiber SL (2003) Domain-selective small-molecule inhibitor of histone deacetylase 6 (HDAC6)-mediated tubulin deacetylation. *Proc Natl Acad Sci U S A* **100:**4389–4394.

Hassig CA and Schreiber SL (1997) Nuclear histone acetylases and deacetylases and transcriptional regulation: HATs off to HDACs. *Curr Opin Chem Biol* **1:**300–308.

Kihm AJ, Kong Y, Hong W, Russell JE, Rouda S, Adachi K, Simon MC, Bobel GA, and Weiss MJ (2002) An abundant erythroid protein that stabilizes free alpha-hemoglobin. *Nature* **417:**758–763.

Kölle D, Brosch G, Lechner T, Lusser A, and Loidl P (1998) Biochemical methods for analysis of histone deacetylases. *Methods* **15:**323–331.

Kong Y, Zhou S, Kihm AJ, Katein AM, Yu X, Gell DA, Mackay JP, Adachi K, Foster-Brown L, Louden CS, et al. (2004) Loss of alpha-hemoglobin-stabilizing protein impairs erythropoiesis and exacerbates beta-thalassemia. *J Clin Invest* **114:**1457–1466.

Lai MI, Jiang J, Silver N, Best S, Menzel S, Mijovic A, Colella S, Ragoussis J, Garner C, Weiss MJ, et al. (2006) Alpha-hemoglobin stabilizing protein is a quantitative trait gene that modifies the phenotype of beta-thalassaemia. *Br J Haematol* **133:**675–682.

Lechner T, Lusser A, Pipal A, Brosch G, Loidl A, Goralik-Schramel M, Sendra R, Wegener S, Walton JD, and Loidl P (2000) RPD3-Type histone deacetylases in maize embryos. *Biochemistry* **39:**1683–1692.

Letvin NL, Linch DC, Beardsley GP, Mc Intyre KW, and Nathan DG (1984) Augmentation of fetal-hemoglobin production in anemic monkeys by hydroxyurea. *N Engl J Med* **310:**869–873.

Mai A, Massa S, Rotili D, Simeoni S, Ragno R, Botta G, Nebbioso A, Miceli M, Altucci L, and Brosch G (2006) Design, synthesis, and biological properties of novel uracil-containing histone deacetylase inhibitors. *J Med Chem* **49:**6046–6056.

Mankidy R, Faller DV, Mabaera R, Lowrey CH, Boosalis MS, White GL, Castaneda SA, Perrine SP (2006) Short-chain fatty acids induce γ-globin gene expression by displacement of a HDAC3-NCoR repressor complex. *Blood* **108:**3179–3186.

Migliaccio G, Di Baldassarre A, Di Rico C, Di Noia A, Nakamoto B, Cao H, Skarpidi E, and Migliaccio AR (2005) Spontaneus switch from ^{A}γ- to β-globin promoter activity in a stable transfected dual reporter vector. *Blood Cells Mol Dis* **34:**174–180.

Migliaccio G, Di Pietro R, Di Giacomo V, Di Baldassarre A, Migliaccio AR, Maccioni L, Galanello R, and Papayannopoulou T (2002) In vitro mass cell production of human erythroid cells from the blood of normal donors and β^0-thalassemic patients. *Blood Cells Mol Dis* **28:**169–180.

Minucci S and Pelicci PG (2006) Histone deacetylase inhibitors and the promise of epigenetic (and more) treatments for cancer. *Nat Rev Cancer* **6:**38–51.

Noguchi CT, Rodgers GP, Serjeant G, and Schechter AN (1988) Levels of fetal haemoglobin necessary for the treatment of sickle cell disease. *N Engl J Med* **318:**96–99.

Olivieri NF (1999) The beta-thalassemias. *N Engl J Med* **341:**99–109.

Papayannopoulou T, Torrealba de Ron A, Veith R, Knitter G, and Stamatoyannopoulos G (1984) Arabinosylcytosine induces fetal hemoglobin in baboons by perturbing erythroid cell differentiation kinetics. *Science* **224:**617–619.

Perrine SP, Rudolph A, and Faller DV (1988) Butyrate infusions in the ovine fetus delay the biologic clock for globin gene switching. *Proc Natl Acad Sci U S A* **85:**8540–8542.

Perrine SP, Miller BA, and Faller DV (1989) Sodium butyrate enhances fetal globin gene expression in erythroid progenitors of patients with Hb SS and β-thalassemia. *Blood* **74:**454–459.

Perrine SP, Ginder GD, Faller DV, Dover GH, Ikuta T, Witkowska HE, Cai SP, Vichinsky EP, and Olivieri NF (1993) A short-term trial of butyrate to stimulate fetal-globin-gene expression in the β-globin disorders. *N Engl J Med* **328:**81–86.

Platt OS, Orkin SH, Dover G, Beardsley GP, Miller B, and Nathan DG (1984) Hydroxyurea enhances fetal hemoglobin production in sickle cell anemia. *J Clin Invest* **74:**652–656.

Ronzoni S, Faretta M, Ballarini M, Pelicci PG, and Minucci S (2005) New methods to detect histone acetylation levels by flow cytometry. *Cytometry A* **66:**52–61.

Sher GD, Ginder GD, Little J, Yang S, Dover GJ, and Olivieri NF (1995) Extended therapy with intravenous arginine butyrate in patients with β-hemoglobinopathies. *N Engl J Med* **332:**1606–1610.

Skarpidi E, Vassilopoulos G, Li Q, and Stamatoyannopoulos G (2000) Novel in vitro assay for the detection of pharmacologic inducers of fetal hemoglobin. *Blood* **96:**321–326.

Stamatoyannopoulos G and Grosveld F (2001) Hemoglobin switching, in *The Molecular Basis of Blood Diseases*, 3rd ed. (Stamatoyannopoulos G, Majerus PW, Perlmutter RM, Varmus H, eds) pp 135–182, W.B. Saunders Publishing Co., Philadelphia.

Trecartin RF, Liebhaber SA, Chang JC, Lee YW, and Kan YW (1981) β^0-thalassemia in Sardinia is caused by a nonsense mutation. *J Clin Invest* **68:**1012–1017.

Veith R, Galanello R, Papayannopoulou T, and Stamatoyannopoulos G (1985) Stimulation of F-cell production in patients with sickle-cell anemia treated with cytarabine or hydroxyurea. *N Engl J Med* **313:**1571–1575.

Verdin E, Dequiedt F, Kasler HG (2003) Class II histone deacetylases: versatile regulators. *Trends Genet* **19:**286–293.

Viprakasit V, Tanphaichitr VS, Chinchang W, Sangkla P, Weiss MJ, and Higgs DR (2004) Evaluation of alpha hemoglobin stabilizing protein (AHSP) as a genetic modifier in patients with beta thalassemia. *Blood* **103:**3296–3299.

Zhang J, Sun X, Qian Y, and Maquat LE (1998) Intron function in the nonsense-mediated decay of beta-globin mRNA: indications that pre-mRNA splicing in the nucleus can influence mRNA translation in the cytoplasm. *RNA* **4:**801–815.

Address correspondence to: Anna Rita Migliaccio, Dipartimento di Ematologia, Oncologia e Medicina Molecolare, Istituto Superiore di Sanità, viale Regina Elena 299, 00161 Roma, Italy. E-mail: migliar@iss.it

Histone deacetylase inhibitors: new drugs for the treatment of inflammatory diseases?

Frédéric Blanchard and Céline Chipoy

Histone deacetylase (HDAC) inhibitors induce cell cycle arrest and differentiation in cancer cells and have been in Phase I–II clinical trials for the treatment of various solid or haematological malignancies. In recent years, HDAC inhibitors have emerged as potent contenders for anti-inflammatory drugs, offering new lines of therapeutic intervention for rheumatoid arthritis or lupus erythematosus. The molecular mode of action of HDAC inhibitors is still controversial but seems to rely on reduced inflammatory mediator production, such as nitric oxide or cytokines, which implies inhibition of the transcription factor NF-κB. These anti-inflammatory effects will hopefully lead us to appreciate the complex anti-tumour effects of HDAC inhibitors.

The major symptoms of inflammation, namely pain, redness, swelling and elevated body temperature, result from the deregulation of a subset of genes; the so-called pro-inflammatory genes that maintain physiological homeostasis. Within this set of inflammatory molecules, soluble mediators such as nitric oxide (NO), prostaglandins (PGs) and cytokines have been studied extensively because of their importance in controlling blood pressure, vascular permeability, platelet aggregation, leukocyte infiltration, organ failure and/or regeneration, body temperature and production of acute phase protein in the liver. Interestingly, the major anti-inflammatory drugs, salicylates (aspirin) and glucocorticoids (dexamethasone), are known to inhibit activation of transcription factors such as NF-κB that are crucial for the production of inflammatory mediators [1]. Novel anti-inflammatory therapies include other NF-κB inhibitors (peptides, peptidomimetic and natural compounds) [1] or anti-cytokine antibodies [i.e. anti-tumour necrosis factor (TNF)-α] [2].

The packaging of DNA sequences in nucleosomes and higher-order chromatin structures has been implicated in the regulation of transcription and, until recently, it has been widely accepted that the presence of nucleosomes blocks the accessibility of specific transcription factors to their cognate binding sequences [3,4]. Recent advances in the study of gene expression have disclosed numerous posttranslational modifications to histone N-termini. Acetylation, in particular, is regulated by the opposing actions of histone acetyl transferase (HAT) enzymes and histone deacetylase (HDAC) enzymes, and the patterns of acetylated histone residues contribute to the histone code hypothesis for epigenetic regulation of gene expression [5]. Although exceptions do exist depending on the nature of the gene [6], a common view has emerged that associates the recruitment of HAT activity with transcriptional activation, and HDAC activity with transcriptional repression. Thus, HDAC inhibitors induce the expression of numerous genes, inhibit cell proliferation and induce differentiation and/or apoptosis of tumour cells *in vitro* and *in vivo* [7,8]. Therefore, they are considered as a new class of therapeutic agents for the treatment of solid and haematological malignancies [9]. For example, HDAC inhibition induces gelsolin, which in turn is implicated in actin filament reorganization and change in cell shape [10], whereas drug-dependent inhibition of DNA synthesis and growth arrest in

Frédéric Blanchard
Univ Nantes,
EA 3822,
Laboratory of Pathophysiology of Bone Resorption and Therapy of Primitive Bone Tumours,
1 rue Gaston Veil,
44035 Nantes cedex 1,
France
e-mail: frederic.blanchard@sante.univ-nantes.fr
Céline Chipoy
INSERM,
ERI7,
44035 Nantes cedex 1,
France

1359-6446/04/$ – see front matter PII: S1359-6446(04)03309-4

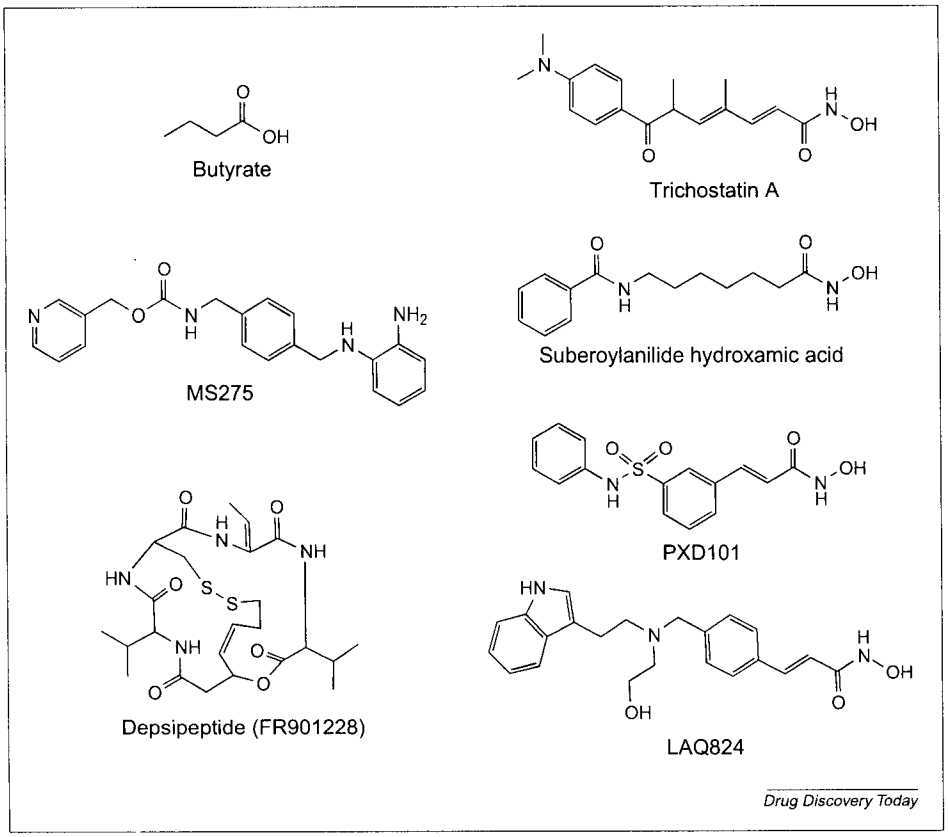

FIGURE 1
Small molecules that inhibit histone deacetylase *in vitro* and *in vivo*.

early G1 phase partly depends on the cyclin-dependent kinase inhibitor $p21^{WAF1}$ [11]. In addition, growth arrest could be related to enhanced acetylation of non-histone targets, such as p53 [7,12].

However, epigenetic modifications of chromatin structure are known to accompany every major cell function, such as embryonic development, cell growth, differentiation, apoptosis, DNA repair and cell interactions [8,13], suggesting that HDAC inhibitors could be therapeutic candidates not only for malignancies but also many other non-malignant diseases. For instance, butyrate, the simplest HDAC inhibitor, has been found to be important for proper epithelial cell regulation, especially in the colon [14]. Butyrate and trichostatin A (TSA), although structurally unrelated compounds, both reduce interleukin (IL)-8 production and induce cell differentiation in colonic epithelial cells [15]. TSA also induces histone hyperacetylation, thus these observations soon led to the hypothesis that HDAC inhibitors could be used to treat ulcerative colitis or other inflammatory diseases via inhibition of cell proliferation and reduction of inflammatory cytokine production. A global analysis of gene expression estimated that between 2% and 9% of the genome might be regulated by HDAC inhibitors, with equal numbers of tested genes activated or repressed [8,16]. This review summarizes recent, sometimes conflicting, results indicating that HDAC inhibitors are able to repress transcription, possess anti-inflammatory properties and, therefore, could be used to improve the treatment of ulcerative colitis, rheumatoid arthritis, lupus erythematosus, endotoxemia and hepatic injury.

HDAC inhibitors

Mammalian HDACs have been classified into three classes [7,17,18]. Class I HDACs (HDACs 1, 2, 3 and 8) are homologues of yeast RPD3 and are found exclusively in the nucleus. Class II HDACs (HDACs 4, 5, 6, 7, 9 and 10), homologues of yeast Hda1, are found in both the nucleus and the cytoplasm. HDAC11 has properties of both class I and class II HDACs. Class III HDACs (Sirt1–Sirt7) are homologues of yeast Sir2 and form a structurally distinct class of NAD-dependent enzymes [7,17,18]. Northern blot and serial analysis of gene expression indicated that both class I and II HDACs have tissue-specific expression profiles [7,19]. HDAC1, 2 and 3 are ubiquitously expressed in the various immune tissues [19] and their expression in human peripheral blood mononuclear cells (PBMC) is increased by polyclonal activators (phorbol ester and α-CD3 antibodies) and HDAC inhibitors, but not by lipopolysaccharide (LPS) [19].

Currently, there are several HDAC inhibitors including butyrate, hydroxamic acid, benzamide and cyclic peptides (Figure 1) [7,8,12]. The simplest compound, butyrate, is a short-chain fatty acid derived from bacterial metabolism of dietary fibres in the colon. Butyrate inhibits all class I and II HDACs (IC_{50} in the mM range) except HDAC6 and 10 [7,18]. By contrast, TSA is a hydroxamic acid identified as having a potential therapeutic value against cancer in screens for agents that induce differentiation of erythroleukemia cells [20]. TSA inhibits all class I and II HDACs (IC_{50} = 1–10 nM) [7,17,18,21]. More recently, suberoylanilide hydroxamic acid (SAHA) was designed as a hydroxamate-containing small-molecule inhibitor of class I and II HDACs (IC_{50} = 10–300 nM; Figure 1), which binds directly to the zinc-containing pocket of HDACs [21,22]. Numerous other hydroxamate-containing compounds against HDAC, such as PXD101 and LAQ824, have been developed and tested in Phase I–II clinical trials (Figure 1) [12]. Another promising HDAC inhibitor (IC_{50} = 1 nM) is the depsipeptide FR901228 (or FK228), a natural product isolated from *Chromobacterium violaceum* [8,23]. This cyclic peptide is currently in Phase II clinical trials for cutaneous T-cell lymphoma and refractory solid tumours [24]. An example of a benzamide analogue that acts as a HDAC inhibitor is MS275 (Figure 1), which is suitable for both *in vitro* and *in vivo* applications [7,25]. Interestingly, MS275 preferentially inhibits HDAC1

TABLE 1

Inflammatory models sensitive to HDAC inhibitors

Inflammatory disease	*In vitro*	*In vivo*	Inflammation
Ulcerative colitis	Colonic epithelial cells	Dextran sulfate sodium-induced colitis	Inhibition
Rheumatoid arthritis	Synoviocytes	Adjuvant arthritis	Inhibition
Lupus erythematosus (nephritis)	Splenocyte and mesangial cells	MRL-*lpr/lpr* mice	Inhibition
Endotoxemia	PBMC and macrophages	LPS injections	Inhibition
Hepatitis	Hepatocytes	Con A-induced hepatic injury	Inhibition
Asthma	Lung epithelial cells	Bronchial biopsies from subjects with asthma	Activation
Neurodegenerative diseases, stroke and traumatic brain injuries	Microglial cells	None	Activation

Abbreviation: Con A, concanavalin A.

(IC_{50} = 300 nM) versus HDAC3 (IC_{50} = 8 μM) and has no inhibitory activity towards HDAC8 (IC_{50} >100 μM) [17].

HDAC inhibitors, cytokine and NO expression and inflammatory diseases

Recent results have indicated that HDAC inhibitors can reduce the cytokine and NO production that contribute to various inflammatory diseases [15,26–28]. Thus, the observation that butyrate and TSA inhibit IL-8 expression in colonic epithelial cells suggested that HDAC inhibitors can be used for the effective treatment of ulcerative colitis through increased histone acetylation and reduced production of pro-inflammatory cytokines by the intestinal epithelium (Table 1) [14,15,26]. Additionally, butyrate inhibited dendritic cell maturation and IL-12 production [27], and reduced IL-2 transcription in T-cells [28]. These results suggested that bacteria could escape the host defence in the gastrointestinal tract by producing high amounts of the HDAC inhibitor, butyrate. Indeed, daily oral treatment of mice with 50 mg kg^{-1} SAHA reduced the clinical and cytokine abnormalities in dextran sulfate sodium-induced colitis significantly [29]. Furthermore, numerous human clinical trials indicated that butyrate enemas (around 100 mM) resulted in marked improvement or remission in ulcerative colitis [30,31]. The usefulness of local butyrate administration was also observed in ulcerative colitis that is refractory to conventional salicylate treatment [31]. However, at present, there is little clinical data indicating that other HDAC inhibitors can be used as effective anti-inflammatory drugs and appropriate human clinical trials are urgently required.

In the simple animal model of mice injected with LPS, a single oral administration of SAHA reduced circulating level of TNF-α, IL-1β, IL-6 and interferon (IFN)-γ in a dose-dependent manner (0.1–50.0 mg kg^{-1}) (Table 1) [29]. Interestingly, SAHA also inhibited secretion of these cytokines in LPS-stimulated PBMC (Table 1). The specificity of SAHA was also demonstrated by the fact that this HDAC inhibitor reduced NO production by thioglycolate-elicited mouse peritoneal macrophages, IL-12 secretion by monocytes without any modification of T-cell-receptor-stimulated IFN-γ production in PBMC [29]. Butyrate also reduced IL-12 production by human blood monocytes [32], and inhibited NO production in RAW macrophage cells [33]. Altogether, these results highlighted the anti-inflammatory properties of HDAC inhibitors during endotoxemia, an effect that could be related to the reduction of pro-inflammatory cytokines and NO production by monocytes and/or macrophages rather than by T-cells.

Systemic lupus erythematosus (SLE) is one of the autoimmune diseases characterized by heightened levels of cytokines produced by T-cells, polyclonal B-cell activation, dysregulated autoantibody production and renal inflammation. Interestingly, TSA and SAHA inhibited IL-6, IL-10, IL-12 and IFN-γ production by splenocytes of MRL-*lpr/lpr* mice, a model of SLE (Table 1) [34], as well as by human lupus T-cells [35]. In splenocytes, HDAC inhibitors induced histone H3 and H4 acetylation but did not alter cell viability [34]. Moreover, in glomerular mesangial cells stimulated with LPS and cytokines, TSA inhibited the production of TNF-α, IL-6, IL-12 and NO in a dose-dependent manner [34,36]. Finally, in MRL-*lpr/lpr* mice, subcutaneous injections of TSA (0.5 mg kg^{-1}) significantly reduced proteinuria, glomerulonephritis and splenomegaly, as well as the renal pathology index, without changing the circulating level of autoantibodies, immune complex deposition and/or complement fixation in the glomerulus [34]. Thus HDAC inhibitors could have therapeutic benefit in the treatment of SLE, to inhibit nephritis independent of autoantibody production (Table 1).

In a mouse model of concanavalin A-induced hepatic injury, a model that is TNF-α- and IL-18-dependent, SAHA (50 mg kg^{-1} administered orally) prevented the elevation of alanine amino transaminase by 50%, suggesting an attenuation of hepatic injury (Table 1) [29].

HDAC inhibitors and transcription factors

Several results have demonstrated inhibition of NF-κB transcriptional activity after treatment with HDAC inhibitors. As initially reported, this transcription factor is crucial for the expression of numerous pro-inflammatory mediators, such as inducible NO synthase (iNOS), IL-6, IL-8, IL-10 and IL-12 [29,34,36]. Moreover, other anti-inflammatory drugs, such as salicylates and glucocorticoids, are also known to inhibit NF-κB [1]. However, and as discussed in a subsequent section, activation of NF-κB by HDAC inhibitors has also been described in the literature.

At the level of the iNOS gene, it has been demonstrated that overexpression of HDAC2, 4, 5 or 6 in mesangial cells augmented iNOS promoter activity, and TSA inhibited it [36]. Therefore, HDACs were not only transcriptional

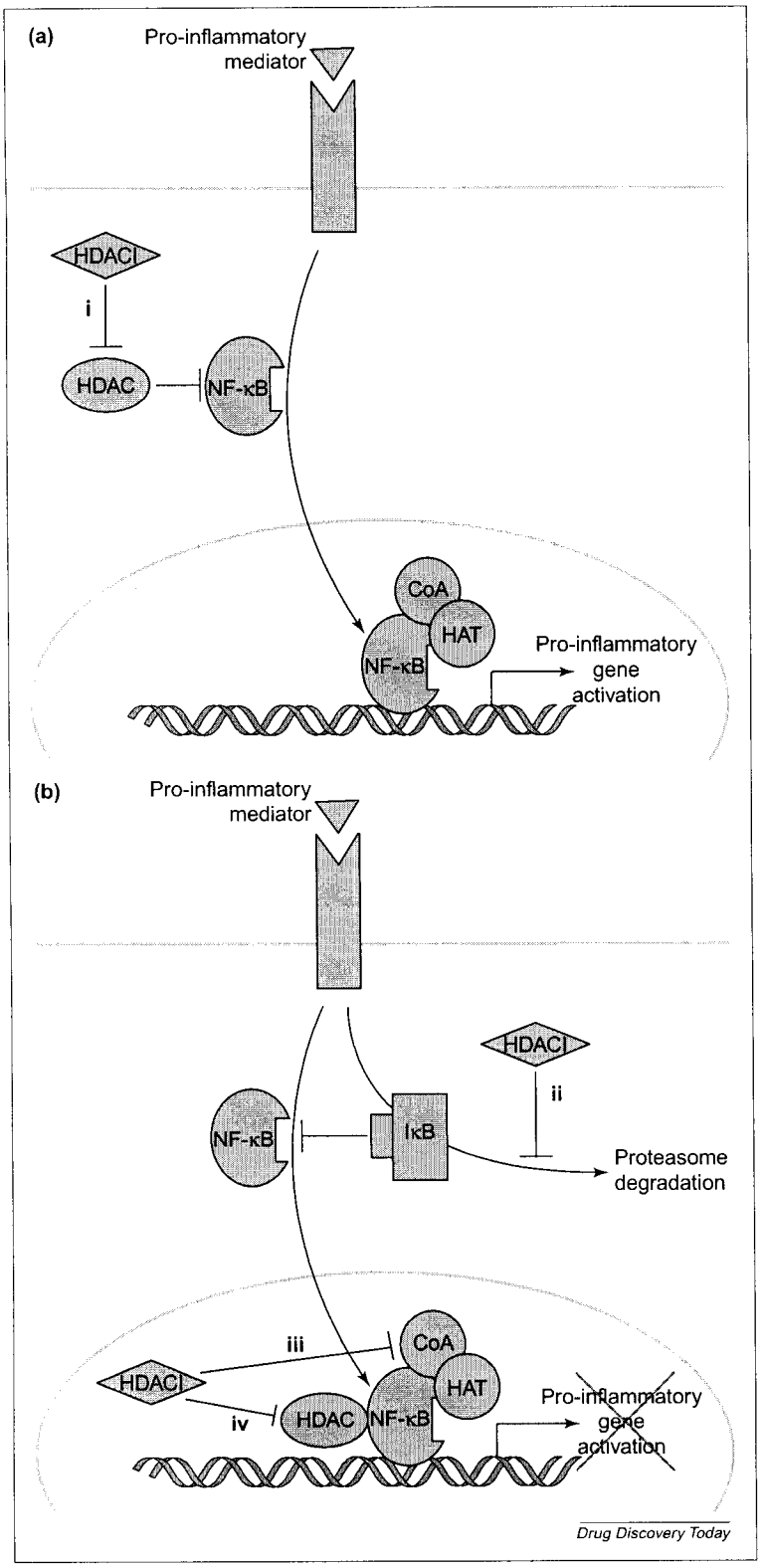

FIGURE 2

HDAC inhibitors regulate NF-κB. Histone deacetylase inhibitors (HDACI) can be either activators of pro-inflammatory gene (A, activation labelled i) or inhibitors (B, inhibitions labelled ii, iii and iv) based on their molecular target, the pro-inflammatory mediator used or the cell type. Abbreviations: CoA, transcriptional co-activator.

repressors but also transcriptional activators for particular genes concerned with NO production. Transcriptional activation by HDAC in mesangial cells required NF-κB for three reasons: (i) HDAC2 increased the activity of an artificial NF-κB responsive promoter; (ii) TSA inhibited this activity without altering NF-κB nuclear translocation or DNA binding; and (iii) HDAC2 interacted directly with NF-κB (Figure 2b, inhibition labelled iv) [36]. In fact, studies with different gene promoters indicated that HDAC inhibition, at levels that induce global histone acetylation, might leave specific regulatory regions relatively unaffected. These treatments lead to transcriptional inhibition by mechanisms that reduced expression, recruitment or activation of various transcriptional cofactors such as NcoA1 or the acetyltransferase CBP/p300 (Figure 2b, inhibition labelled iii) [37,38].

The mechanisms leading to NF-κB inhibition by HDAC inhibitors appeared different in other cell lineages. In a monocyte and/or macrophage cell line, butyrate and TSA prevented the nuclear translocation of NF-κB, as well as NF-κB-dependent promoter activity [39]. In the same cells stimulated with LPS, butyrate reduced NO production by stabilization of IκB, an inhibitor of NF-κB, and downregulation of iNOS expression [33]. In a colon cell line, butyrate and TSA inhibited the proteosome-dependent degradation of IκB, nuclear translocation and DNA binding of NF-κB, as well as NF-κB-regulated gene expression (Figure 2b, inhibition labelled ii) [14].

The signal transducers and activators of transcription (STAT) factors are major signalling molecules downstream of numerous cytokine receptors, such as IFN, IL-2 or IL-6 receptors. Recently, it has been shown that STAT1 and 2 associated with HDAC1 (but not with HDAC4 and 5), leading to enhanced gene expression after IFN-α treatment [40]. Thus, TSA inhibited the expression of IFN-α-induced genes [40]. The IFN-γ-STAT1 system also required HDAC1, 2 and 3 activities and the STAT3-dependent transcription was inhibited by TSA in certain cell systems [41]. Together with the inhibitory role of TSA on IL-2 responses and HDAC1 recruitment to STAT5 target genes [42,43], these results lead to hypothesize that the recruitment of class I HDACs might be required generally for STAT-dependent transcriptional regulation and propagation of the inflammatory reaction.

HDAC inhibitors, inflammation and cancer: an example of osteo-articular diseases

Here, osteo-articular tissue will be used as an example to discuss how inhibition of inflammation and bone resorption by HDAC inhibitors could help explain their anti-tumour activities. However, this hypothesis, which could be extended to other tissues and malignancies, needs additional evaluation in animal models and human clinical trials.

Primary or metastatic bone tumours favour inflammation and osteoclast-mediated bone resorption. The candidates for osteolytic mediators are vitamins (VitD3), hormones (*para*-thyroid hormone and *para*-thyroid hormone-related peptide) and cytokines [receptor activator of NF-kB ligand (RANKL), IL-1, TNF-α, IL-6 type cytokines]

[46–49]. These cytokines are produced by osteoblastic or tumour cells, by infiltrating macrophages or lymphocytes. Subsequently, peri-tumour osteolysis activates the release of matrix-associated cytokines, such as transforming growth factor-β (TGF-β) and bone morphogenetic proteins (BMPs) (Figure 3), which increase tumour proliferation. Thus, a vicious cycle is established between tumour growth and associated inflammation and/or bone resorption (Figure 3) [46,47]. Therefore, recent trials were performed to evaluate the therapeutic potential of anti-resorption agents such as bisphosphonates in the treatment of osteosarcoma, chondrosarcoma, myeloma and metastatic bone tumours [48].

In an osteosarcoma xenograft model in nude mice, FR901228 reduced the tumour volume to 30% [44]. Thus, HDAC inhibitors, by inducing tumour regression, are promising anti-tumour agents against paediatric bone tumours [25,44]. FR901228 directly induced apoptosis in osteosarcoma cells via induction of Fas ligand and/or Fas signalling and subsequent activation of caspases (Figure 3) [44]. Another action of HDAC inhibitors on tumour growth might be indirect through inhibition of tumour-associated inflammation and bone resorption. Thus, butyrate and TSA suppressed osteoclast differentiation induced by RANKL on bone marrow cultures or the macrophage cell line RAW264 (Figure 3), but did not modify the formation of mature macrophages induced by macrophage colony-stimulating factor [39]. In RAW264 cells treated with RANKL, butyrate and TSA decreased NF-κB-dependent gene transactivation by preventing NF-κB nuclear translocation (Figure 3) [39]. *In vivo*, the inhibitory effects of HDAC inhibitors on bone resorption were observed in a mouse model of rheumatoid arthritis [45]. In this model, 10% butyrate cream or 1% TSA ointment reduced joint swelling, cell infiltration, synovial hyperplasia, pannus formation and cartilage and bone destruction. These effects correlated with (i) inhibition of synovial cell proliferation via induced expression of the cell cycle inhibitors $p16^{INK4}$ and $p21^{WAF1}$, and (ii) reduced production of TNF-α in the synovium of arthritic mice [45].

Contraindications in inflammatory diseases

In contrast to these anti-inflammatory effects, TSA and SAHA have been shown to strongly potentiate microglial inflammation. These HDAC inhibitors enhanced the LPS-induced expression of IL-6, TNF-α, macrophage inflammatory protein-2 and NO in primary microglial cells as well as in neural co-cultures (Table 1) [50]. Therefore, histone acetylation could participate in the inflammatory response associated with a variety of neurodegenerative diseases, stroke and traumatic brain injuries. Whether the inducing effect of HDAC inhibitors on microglial inflammation rely on expression of different HDAC isoforms or other tissue-specific variations remains to be determined. In this context, the use of new type-selective HDAC inhibitors could be particularly interesting, as discussed in a subsequent section.

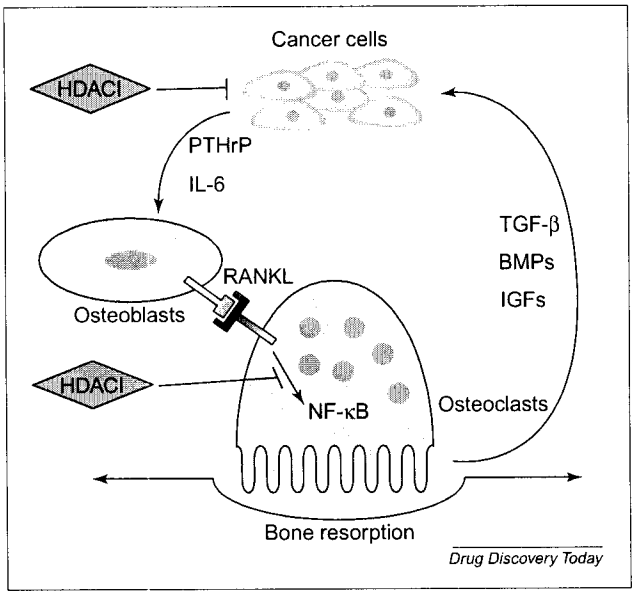

FIGURE 3

HDAC inhibitors, bone tumours and inflammation/bone resorption. Histone deacetylase inhibitors (HDACI) inhibit tumour proliferation and/or survival and associated inflammation/bone resorption via neutralization of NF-κB in osteoclasts. This dual effect of HDACI could lead to reduced levels of pro-inflammatory cytokines and growth factors in the tumour microenvironment and thus participate in tumour regression. Abbreviations: IGFs, insulin-like growth factors; PTHrP, *para*-thyroid hormone-related peptide.

TSA also enhanced IL-8 production by SV-40-transformed lung epithelial cells treated with LPS, suggesting an inducing role of TSA on airway inflammation (Table 1) [51]. Other experiments indicated that bronchial biopsies from patients with asthma have reduced HDAC activities and induced HAT activities [52]. The increased expression of pro-inflammatory genes in asthma could therefore be related to histone hyperacetylation, precluding the use of HDAC inhibitors for the treatment of this disease [53,54].

Similarly, increased histone hyperacetylation was found within the TNF-α promoter in monocytes from patients with diabetes [55]. THP1 monocytic cells treated with high glucose or TSA have induced TNF-α mRNA levels, in correlation with increased HAT and decreased HDAC1 binding to the TNF-α promoter, suggesting that histone hyperacetylation is also implicated in diabetes-induced inflammatory disease [55].

In microglial cells, a NF-κB inhibitor prevented induction of NO and cytokine production by TSA [50]. Similarly, HDAC inhibitors enhanced NF-κB activation in the lungs [51–54] and in THP1 monocytic cells [55]. In line with these results, other groups demonstrated that the interaction of NF-κB with HDAC1 represses transcription in resting cells, whereas the interaction with CBP/p300 activates transcription in stimulated cells [56]. NF-κB is acetylated at multiple lysine residues by CBP/p300 acetyltransferase, impairing IκB assembly and increasing NF-κB transcriptional activation [57,58]. Inversely, acetylated NF-κB is subject to deacetylation by HDAC3, promoting

IκB binding, nuclear export and termination of the NF-κB signal. In this scheme, HDAC inhibitors such as TSA induced an NF-κB-dependent reporter-gene (Figure 2a, activation labelled i) [55–58]. Most presumably, inhibitory or inducing effects of HDAC inhibitors on NF-κB rely on the cell type and expression of a different set of HDAC isoforms, as well as the source of cell stimulation (e.g. LPS, cytokines and high glucose levels).

New HDAC inhibitors

Based on their various sub-cellular localization, intra-tissue variation and non-redundant activity, the different HDACs are certainly implicated in various specific cellular processes, such as proliferation, metabolism and differentiation. For example, class I HDACs are mainly nuclear enzymes, whereas class II HDACs localize either to the cell nucleus or to the cytoplasm, depending on their phosphorylation and subsequent binding of 14–3-3 proteins.

Moreover, class II HDACs display a tissue-specific expression, whereas class I HDACs are ubiquitously expressed [7,17–19,59]. Thus, it is speculated that the ideal anti-inflammatory HDAC inhibitor will target the specific HDAC isoform primarily expressed in inflamed tissues and implicated in inflammatory mediator production. Numerous published data suggest that class I HDACs, most presumably HDAC1, 2 and 3, could have inflammatory properties [7,19,36,40,41,43]. Interestingly, butyrate and MS275 show a somewhat preferential inhibitory effect against particular class I HDACs [17,18]. However, butyrate has an IC_{50} in the mM range and a short half-life that limits its effectiveness as a therapeutic agent. Therefore, synthesis of new short fatty acid or benzamide structural homologues could help in the design of true isoform-selective, highly active inhibitors within class I HDACs. Already, chemical manipulation of hydroxamate compounds has led to the discovery of selective class II HDAC inhibitors [59] that should now be studied as modulators of inflammation. Of course, the development of new cost effective assays for the screening of specific HDAC inhibitors will help delineate more effective, less toxic and clinically relevant anti-inflammatory reagents [17,21]. Ideally, new *in vitro* and cell-based assays should be used that closely model the situation in cytokine and NO producing cells.

Peptide therapy could also provide an interesting outlook for the design of specific HDAC inhibitors. Small membrane-penetrating peptides have the potential to block the signalling pathways selectively, especially in NF-κB-dependent pathways [1]. Therefore, peptides designed to prevent interaction between a particular HDAC and NF-κB or other transcription factors could represent promising anti-inflammatory reagents.

Conclusions and perspectives

Butyrate improves the efficacy of conventional anti-inflammatory treatments in refractory ulcerative colitis [31], therefore, future trials will certainly analyse association of salicylates, glucocorticoids and/or anti-cytokine immunotherapy with low dose HDAC inhibitors for the treatment for other inflammatory diseases. Whether the administration of HDAC inhibitors should be local or systemic will certainly depend on the nature of the inflammatory disease, on the extent of inflammation and its aggressiveness. *In vitro* and *in vivo* anti-inflammatory effects of HDAC inhibitors seem to rely on three factors: (i) inhibition of cytokine and NO production; (ii) inhibition of key transcription factors (NF-κB and STAT); and (iii) inhibition of proliferation or induction of differentiation of normal cells during inflammation (synoviocytes and colonic epithelial cells). Abnormal cytokine release contributes to pathogenesis and the spreading of numerous inflammatory diseases, as confirmed by knockout animal models and anti-cytokine therapies [2]. Thus, downregulation of cytokine production by HDAC inhibitors could explain their striking anti-inflammatory activities. However, *in vivo* studies that directly demonstrate an effect of HDAC inhibitors on inflammation through modulation of NF-κB and cytokine production have not yet been published.

The major transduction pathways studied in this field of inflammatory mediators are NF-κB and STAT transcription factors that could directly interact with various HDACs for gene induction [36–38,40,41,43]. Future research will focus on whether important steps rely on modifications of histone or on original mechanisms targeting transcription factors acetylation, sub-cellular localization or transcriptional activity through recruitment of transcriptional co-activators. Discoveries in these fields will enable the production of new arrays to screen for more specific HDAC inhibitors and new anti-inflammatory drugs or their combinations. A better understanding of HDAC mode-of-action will also permit the design of inhibitory peptides that should be specific for HDAC isoforms, or even for specific interactions between one particular HDAC and one given transcription factor.

The effect of HDAC inhibitors on normal cell proliferation and differentiation during inflammation could be related to their anti-neoplastic effects because both are associated with induction of the cell cycle inhibitor $p21^{WAF1}$ [45]. Moreover, there is an interesting new avenue of therapeutic use of HDAC inhibitors for the treatment of malignancies associated with inflammation, such as primary or metastatic bone tumours [44–48]. The growth of malignant cells is highly regulated by the local environment, and pro-inflammatory mediators can enhance tumour proliferation. Therefore, by reducing cytokine production, HDAC inhibitors could limit tumour growth. Additionally, HDAC inhibitors could suppress tumour expansion, at least in part, by the inhibition of neovascularization [60,61]. Altogether, it appears that these drugs act as anti-tumour reagents at multiple steps: tumour proliferation and apoptosis; angiogenesis and tumour

dissemination; and pro-inflammatory reactions associated with tumour development.

HDAC inhibitors are thus emerging as a new class of drugs that could be used for the treatment of solid or haematological malignant tumours, as well as numerous inflammatory diseases. However, human clinical trials are urgently needed to confirm that HDAC inhibitors can be used as effective anti-inflammatory drugs. Moreover, HDAC inhibitors might also enhance lung and microglial inflammation as well as high glucose-induced inflammation [50–55]. Thus, studies in the field of hyperglycaemia, airway and neural inflammation are particular hotspots to understand more precisely the cell-specific molecular mode-of-action of HDAC inhibitors and to describe more clearly their contraindications. Non-exhaustively, these include diabetes, asthma, neurodegenerative diseases, stroke and traumatic brain injuries.

Acknowledgements

We thank Kanji Mori for critical comments on this manuscript and acknowledge support from the Région des Pays de Loire, the Association de Recherche sur le Cancer (ARC), INSERM (Contrat de Recherche Stratégique n°4CR06F), the Ministère de la Recherche (ACI n°TS/0220044) and the Comité des Pays de Loire de la Ligue Contre le Cancer, France.

References

1 D'Acquisto, F. *et al.* (2002) Inhibition of nuclear factor kappa B (NF-kB): an emerging theme in anti-inflammatory therapies. *Mol. Interv.* 2, 22–35
2 Zagury, D. and Gallo, R.C. (2004) Anti-cytokine Ab immune therapy: present status and perspectives. *Drug Discov. Today* 9, 72–81
3 Zlatanova, J. *et al.* (1999) Chromatin structure revisited. *Crit. Rev. Eukaryot. Gene Expr.* 9, 245–255
4 Archer, T.K. *et al.* (1992) Transcription factor loading on the MMTV promoter: a bimodal mechanism for promoter activation. *Science* 255, 1573–1576
5 Cheung, P. *et al.* (2000) Signaling to chromatin through histone modifications. *Cell* 103, 263–271
6 Glaser, K.B. *et al.* (2003) Gene expression profiling of multiple histone deacetylase (HDAC) inhibitors: defining a common gene set produced by HDAC inhibition in T24 and MDA carcinoma cell lines. *Mol. Cancer Ther.* 2, 151–163
7 de Ruijter, A.J. *et al.* (2003) Histone deacetylases (HDACs): characterization of the classical HDAC family. *Biochem. J.* 370, 737–749
8 Weidle, U.H. and Grossmann, A. (2000) Inhibition of histone deacetylases: a new strategy to target epigenetic modifications for anticancer treatment. *Anticancer Res.* 20, 1471–1485
9 Kelly, W.K. *et al.* (2003) Phase I clinical trial of histone deacetylase inhibitor: suberoylanilide hydroxamic acid administered intravenously. *Clin. Cancer Res.* 9, 3578–3588
10 Mielnicki, L.M. *et al.* (1999) Epigenetic regulation of gelsolin expression in human breast cancer cells. *Exp. Cell Res.* 249, 161–176
11 Archer, S.Y. *et al.* (1998) p21(WAF1) is required for butyrate-mediated growth inhibition of human colon cancer cells. *Proc. Natl. Acad. Sci. U. S. A.* 95, 6791–6796
12 McLaughlin, F. *et al.* (2003) The cell cycle, chromatin and cancer: mechanism-based therapeutics come of age. *Drug Discov. Today* 8, 793–802
13 Jaenisch, R. and Bird, A. (2003) Epigenetic regulation of gene expression: how the genome integrates intrinsic and environmental signals. *Nat. Genet.* 33, 245–254
14 Yin, L. *et al.* (2001) Butyrate suppression of colonocyte NF-kappa B activation and cellular proteasome activity. *J. Biol. Chem.* 276, 44641–44646
15 Huang, N. *et al.* (1997) Inhibition of IL-8 gene expression in Caco-2 cells by compounds which induce histone hyperacetylation. *Cytokine* 9, 27–36
16 Chambers, A.E. *et al.* (2003) Histone acetylation-mediated regulation of genes in leukaemic cells. *Eur. J. Cancer* 39, 1165–1175
17 Hu, E. *et al.* (2003) Identification of novel isoform-selective inhibitors within class I histone deacetylases. *J. Pharmacol. Exp. Ther.* 307, 720–728
18 Guardiola, A.R. and Yao, T.P. (2002) Molecular cloning and characterization of a novel histone deacetylase HDAC10. *J. Biol. Chem.* 277, 3350–3356
19 Dangond, F. and Gullans, S.R. (1998) Differential expression of human histone deacetylase mRNAs in response to immune cell apoptosis induction by trichostatin A and butyrate. *Biochem. Biophys. Res. Commun.* 247, 833–837
20 Yoshida, M. *et al.* (1987) Effects of trichostatins on differentiation of murine erythroleukemia cells. *Cancer Res.* 47, 3688–3691
21 Wegener, D. *et al.* (2003) Recent progress in the development of assays suited for histone deacetylase inhibitor screening. *Mol. Genet. Metab.* 80, 138–147
22 Marks, P.A. *et al.* (2004) Histone deacetylase inhibitors: development as cancer therapy. *Novartis Found. Symp.* 259, 269–281
23 Nakajima, H. *et al.* (1998) FR901228, a potent antitumor antibiotic, is a novel histone deacetylase inhibitor. *Exp. Cell Res.* 241, 126–133
24 Sandor, V. *et al.* (2002) Phase I trial of the histone deacetylase inhibitor, depsipeptide (FR901228, NSC 630176), in patients with refractory neoplasms. *Clin. Cancer Res.* 8, 718–728
25 Jaboin, J. *et al.* (2002) MS-27-275, an inhibitor of histone deacetylase, has marked *in vitro* and *in vivo* antitumor activity against pediatric solid tumors. *Cancer Res.* 62, 6108–6115
26 Gibson, P.R. *et al.* (1999) Colonic epithelial cell activation and the paradoxical effects of butyrate. *Carcinogenesis* 20, 539–544
27 Saemann, M.D. *et al.* (2002) Bacterial metabolite interference with maturation of human monocyte-derived dendritic cells. *J. Leukoc. Biol.* 71, 238–246
28 Diakos, C. *et al.* (2002) Novel mode of interference with nuclear factor of activated T-cells regulation in T-cells by the bacterial metabolite n-butyrate. *J. Biol. Chem.* 277, 24243–24251
29 Leoni, F. *et al.* (2002) The antitumor histone deacetylase inhibitor suberoylanilide hydroxamic acid exhibits anti-inflammatory properties via suppression of cytokines. *Proc. Natl. Acad. Sci. U. S. A.* 99, 2995–3000
30 Luhrs, H. *et al.* (2002) Butyrate inhibits NF-kappaB activation in lamina propria macrophages of patients with ulcerative colitis. *Scand. J. Gastroenterol.* 37, 458–466
31 Vernia, P. *et al.* (2003) Topical butyrate improves efficacy of 5-ASA in refractory distal ulcerative colitis: results of a multicentre trial. *Eur. J. Clin. Invest.* 33, 244–248
32 Saemann, M.D. *et al.* (2000) Anti-inflammatory effects of sodium butyrate on human monocytes: potent inhibition of IL-12 and up-regulation of IL-10 production. *FASEB J.* 14, 2380–2382
33 Chakravortty, D. *et al.* (2000) The inhibitory action of butyrate on lipopolysaccharide-induced nitric oxide production in RAW 264.7 murine macrophage cells. *J. Endotoxin Res.* 6, 243–247
34 Mishra, N. *et al.* (2003) Histone deacetylase inhibitors modulate renal disease in the MRL-lpr/lpr mouse. *J. Clin. Invest.* 111, 539–552
35 Mishra, N. *et al.* (2001) Trichostatin A reverses skewed expression of CD154, interleukin-10, and interferon-gamma gene and protein expression in lupus T cells. *Proc. Natl. Acad. Sci. U. S. A.* 98, 2628–2633
36 Yu, Z. *et al.* (2002) Histone deacetylases augment cytokine induction of the iNOS gene. *J. Am. Soc. Nephrol.* 13, 2009–2017
37 Wilson, M.A. *et al.* (2002) The histone deacetylase inhibitor trichostatin A blocks progesterone receptor-mediated transactivation of the mouse mammary tumor virus promoter *in vivo*. *J. Biol. Chem.* 277, 15171–15181
38 Montecino, M. *et al.* (1999) Chromatin hyperacetylation abrogates vitamin D-mediated transcriptional upregulation of the tissue-specific osteocalcin gene *in vivo*. *Biochemistry* 38, 1338–1345
39 Rahman, M.M. *et al.* (2003) Two histone deacetylase inhibitors, trichostatin A and sodium butyrate, suppress differentiation into osteoclasts but not into macrophages. *Blood* 101, 3451–3459
40 Nusinzon, I. and Horvath, C.M. (2003) Interferon-stimulated transcription and innate antiviral immunity require deacetylase activity and histone deacetylase 1. *Proc. Natl. Acad. Sci. U. S. A.* 100, 14742–14747

41 Klampfer, L. *et al.* Requirement of histone deacetylase activity for signaling by STAT1. *J. Biol. Chem.* (in press)
42 Koyama, Y. *et al.* (2000) Histone deacetylase inhibitors suppress IL-2-mediated gene expression prior to induction of apoptosis. *Blood* 96, 1490–1495
43 Xu, M. *et al.* (2003) STAT5-induced Id-1 transcription involves recruitment of HDAC1 and deacetylation of C/EBPbeta. *EMBO J.* 22, 893–904
44 Imai, T. *et al.* (2003) FR901228 induces tumor regression associated with induction of Fas ligand and activation of Fas signaling in human osteosarcoma cells. *Oncogene* 22, 9231–9242
45 Chung, Y.L. *et al.* (2003) A therapeutic strategy uses histone deacetylase inhibitors to modulate the expression of genes involved in the pathogenesis of rheumatoid arthritis. *Mol. Ther.* 8, 707–717
46 Hofbauer, L.C. *et al.* (2001) Receptor activator of nuclear factor-kappaB ligand and osteoprotegerin: potential implications for the pathogenesis and treatment of malignant bone diseases. *Cancer* 92, 460–470
47 Grimaud, E. *et al.* (2002) Bone remodelling and tumour grade modifications induced by interactions between bone and swarm rat chondrosarcoma. *Histol. Histopathol.* 17, 1103–1111
48 Green, J.R. (2003) Antitumor effects of bisphosphonates. *Cancer* 97, 840–847
49 Chambers, T.J. (2000) Regulation of the differentiation and function of osteoclasts. *J. Pathol.* 192, 4–13
50 Suuronen, T. *et al.* (2003) Regulation of microglial inflammatory response by histone deacetylase inhibitors. *J. Neurochem.* 87, 407–416
51 Iwata, K. *et al.* (2002) Trichostatin A, a histone deacetylase inhibitor, down-regulates interleukin-12 transcription in SV-40-transformed lung epithelial cells. *Cell. Immunol.* 218, 26–33
52 Ito, K. *et al.* (2002) Expression and activity of histone deacetylases in human asthmatic airways. *Am. J. Respir. Crit. Care Med.* 166, 392–396
53 Ito, K. *et al.* (2002) A molecular mechanism of action of theophylline: Induction of histone deacetylase activity to decrease inflammatory gene expression. *Proc. Natl. Acad. Sci. U. S. A.* 99, 8921–8926
54 Rahman, I. (2002) Oxidative stress, transcription factors and chromatin remodelling in lung inflammation. *Biochem. Pharmacol.* 64, 935–942
55 Miao, F. *et al.* (2004) *In vivo* chromatin remodeling events leading to inflammatory gene transcription under diabetic conditions. *J. Biol. Chem.* 279, 18091–18097
56 Zhong, H. *et al.* (2002) The phosphorylation status of nuclear NF-kappa B determines its association with CBP/p300 or HDAC-1. *Mol. Cell* 9, 625–636
57 Chen, L.F. *et al.* (2002) Acetylation of RelA at discrete sites regulates distinct nuclear functions of NF-kappaB. *EMBO J.* 21, 6539–6548
58 Chen, L.F. and Greene, W.C. (2003) Regulation of distinct biological activities of the NF-kappaB transcription factor complex by acetylation. *J. Mol. Med.* 81, 549–557
59 Mai, A. *et al.* (2003) Discovery of (aryloxopropenyl)pyrrolyl hydroxyamides as selective inhibitors of class IIa histone deacetylase homologue HD1-A. *J. Med. Chem.* 46, 4826–4829
60 Kwon, H.J. *et al.* (2002) Histone deacetylase inhibitor FK228 inhibits tumor angiogenesis. *Int. J. Cancer* 97, 290–296
61 Sasakawa, Y. *et al.* (2003) Antitumor efficacy of FK228, a novel histone deacetylase inhibitor, depends on the effect on expression of angiogenesis factors. *Biochem. Pharmacol.* 66, 897–906

Related articles in other Elsevier journals

Histone deacetylases: silencers for hire
Ng, H.H. and Bird, A. (2000) *Trends Biochem. Sci.* 25, 121–126

Histone deacetylase inhibitors in cancer therapy: is transcription the primary target?
Johnstone, R.W. and Licht, J.D. (2003) *Cancer Cell.* 4, 13–18

The cell cycle, chromatin and cancer: mechanism-based therapeutics come of age
McLaughlin, F. *et al.* (2003) *Drug Discov. Today* 8, 793–802

Altered acetylation in polyglutamine disease: an opportunity for therapeutic intervention?
Taylor, J.P. and Fischbeck, K.H. (2002) *Trends Mol. Med.* 8, 195–197

Osteoarthritis and Cartilage (2008) ■■, ■■■–■■■

doi:10.1016/j.joca.2007.10.014

Osteoarthritis and Cartilage

International Cartilage Repair Society

OARSI OSTEOARTHRITIS RESEARCH SOCIETY INTERNATIONAL

Trichostatin A, a histone deacetylase inhibitor, suppresses synovial inflammation and subsequent cartilage destruction in a collagen antibody-induced arthritis mouse model[1]

Y. Nasu M.D.†, K. Nishida M.D., Ph.D., Associate Professor†‡*, S. Miyazawa M.D., Ph.D.†, T. Komiyama M.D.†, Y. Kadota M.D.†, N. Abe M.D., Ph.D.†, A. Yoshida†, S. Hirohata M.D., Ph.D.§, A. Ohtsuka M.D., Ph.D.‡ and T. Ozaki M.D., Ph.D.†

† *Department of Orthopaedic Surgery, Okayama University Graduate School of Medicine, Dentistry and Pharmaceutical Sciences, 2-5-1 Shikata-cho, Okayama City, Okayama 700-8558, Japan*

‡ *Department of Human Morphology, Okayama University Graduate School of Medicine, Dentistry and Pharmaceutical Sciences, 2-5-1 Shikata-cho, Okayama City, Okayama 700-8558, Japan*

§ *Department of Molecular Biology and Biochemistry, Okayama University Graduate School of Medicine, Dentistry and Pharmaceutical Sciences, 2-5-1 Shikata-cho, Okayama City, Okayama 700-8558, Japan*

Summary

Objective: To investigate the effect of the histone deacetylase (HDAC) inhibitor, trichostatin A (TSA), on joint inflammation and cartilage degeneration in a collagen antibody-induced arthritis (CAIA) mouse model.

Methods: CAIA mice were given daily subcutaneous injections of various concentrations of TSA (0, 0.5, 1.0, and 2.0 mg/kg) and various parameters were monitored for 14 days. On Day 15, the hind paws were examined histologically. To investigate the effects of TSA on the expressions of matrix metalloproteinase (MMP)-3, MMP-13, tissue inhibitor of MMP-1 (TIMP-1), and acetyl-H4 by chondrocytes, another group of mice was sacrificed on Day 6. *In vitro* direct effect of TSA was examined by real-time PCR for mRNA of type II collagen, aggrecan, MMP-3, and MMP-13 in murine chondrogenic ATDC5 cells after pro-inflammatory cytokine stimulation.

Results: In the TSA-treated group, clinical arthritis was significantly ameliorated in a dose-dependent manner. The severity of synovial inflammation and the cartilage destruction score were significantly lower in the TSA 2.0 mg/kg group compared to the other TSA-treated groups. On immunohistochemistry, the number of MMP-3 and MMP-13-positive chondrocytes was significantly lower in the TSA 2.0 mg/kg group than in the control group. In contrast, the number of TIMP-1-positive cells and acetyl-histone H4-positive cells was significantly higher in the TSA 2.0 mg/kg group than in the control group. TSA suppressed interleukin 1-β and tumor necrosis factor-α-stimulated up-regulation of MMP-3, but not MMP-13 mRNA expression by ATDC5.

Conclusion: The systemic administration of TSA ameliorated synovial inflammation in CAIA mice. Subsequently cartilage destruction was also suppressed by TSA, at least in part, by modulating chondrocyte gene expression.

Key words: Histone deacetylase inhibitor, Trichostatin A, Collagen antibody-induced arthritis, Rheumatoid arthritis, Cartilage destruction, Matrix metalloproteinase, Tissue inhibitor of matrix metalloproteinase.

Introduction

Rheumatoid arthritis (RA) is a systemic disease, characterized by multiple joint inflammation associated with synovial hyperplasia, as well as concomitant bone and cartilage destruction. The high levels of pro-inflammatory cytokines and proteases that are released from synovial tissue cause changes in chondrocyte metabolism and matrix degradation, which lead to cartilage destruction[1,2].There is an increasing evidence that prompt anti-tumor necrosis factor (TNF)-α therapy effectively decreases not only synovial inflammation, but also bone and cartilage destruction; however, these inhibitory effects are limited to certain patient populations[3–5].

Recent reports suggest that the epigenetic regulation of gene expression may be a novel therapeutic approach for arthritis[6]. It has been previously shown in an animal arthritis model that modification of histone acetylation by histone deacetylase (HDAC) inhibitors, such as trichostatin A (TSA) or depsipeptide (FK228), can successfully ameliorate the synovial inflammation *via* the up-regulation in synovial fibroblasts of cell cycle regulators, such as $p16^{INK4a}$ and $p21^{Cip1/WAF1}$[7,8]. More recently, Jungel *et al.* demonstrated that TSA sensitizes synovial fibroblasts to tumor necrosis factor-related apoptosis inducing ligand (TRAIL)-induced apoptosis, which provides another mechanism for understanding the effect that HDAC inhibitors have in the regulation of cell proliferation[9]. It has also been shown in mice that

[1]This work was supported by a Grant from the Japan Orthopaedics and Traumatology Foundation, Inc, No. 148.

*Address correspondence and reprint requests to: Dr Keiichiro Nishida, Department of Human Morphology, Science of Functional Recovery and Reconstruction, Okayama University Graduate School of Medicine, Dentistry and Pharmaceutical Sciences, 2-5-1 Shikata-cho, Okayama 700-8558, Japan. Tel: 81-86-235-7273; Fax: 81-86-229-2797.; E-mail: knishida@md.okayama-u.ac.jp

Received 6 March 2007; revision accepted 15 October 2007.

HDAC inhibitors may contribute to the inhibition of bone destruction *via* the suppression of osteoclastogenesis by inducing INF-β[10]. However, there is not enough evidence to determine whether HDAC inhibitors alter the gene expression of chondrocytes by modifying the chromatin structure.

Cartilage destruction in arthritis is mainly mediated by the breakdown of cartilage extracellular matrix (ECM) by two distinct proteases: the matrix metalloproteinases (MMPs) and the aggrecanases[11]. Young *et al.* examined the effect of HDAC inhibitors on chondrocyte expression of MMP or aggrecanases *in vitro* and in an explant assay. They demonstrated that HDAC inhibitors exhibit a chondro-protective property by blocking the expression of pro-inflammatory cytokine-induced MMP-1, MMP-13, and a disintegrin and metalloproteinase with thrombospondin motifs (ADAMTS) aggrecanases at the mRNA and protein levels[12]. However, it is unclear whether the inhibitory effects that HDAC inhibitors have on chondrocyte protease expression correlate *in vivo* with pathogenesis. Thus, in this study, the effect of various amounts of TSA on cartilage destruction was examined in a collagen antibody-induced arthritis (CAIA) mouse model. The effects of TSA on chondrocyte protease expression were examined by immunohistochemistry. To address whether TSA affects chondrocyte function directly, murine ATDC5 chondrogenic cells were stimulated by pro-inflammatory cytokines, and the effect of TSA on chondrocyte gene expressions was examined by real-time polymerase chain reaction (PCR). The results of the current study might provide further evidence that HDAC inhibitors, by inhibiting the pathogenic process of cartilage degradation, can have a role in the treatment of arthritis.

Methods

ANIMALS, ARTHRITIS INDUCTION, AND TSA TREATMENT

Twenty-four, 6–7-week-old, male DBA/1 mice (Charles River Japan, Yokohama, Japan) were used to evaluate the disease modifying activity of TSA *in vivo*. All animal research was conducted in accordance with the requirements of the Okayama University Animal Research Committee. The mice were housed at the Laboratory Animal Center for Biochemical Research, Okayama University Graduate School of Medicine and Dentistry, under standard diurnal conditions, fed a standard commercial diet, and given tap water *ad libitum*. Arthritis was induced by an arthritogenic cocktail of four monoclonal antibodies (mAbs) to type II collagen (Chondrex, Redmond, WA, USA) combined with lipopolysaccharide (LPS) simulation according to Terato's method[13,14]. The mice were injected intraperitoneally with 2 mg of mAb on Day 0 and Day 1 (4 mg total), followed by intraperitoneal (i.p.) injection of 50 μg of LPS on Day 2. After the onset of clinically detectable arthritis, the treatment group ($n = 18$) was given daily hypodermic injections of TSA (Sigma–Aldrich, Oakville, Ontario, Canada) (0.5, 1.0, or 2.0 mg/kg of body weight in the TSA 0.5, TSA 1.0, TSA 2.0 groups, respectively) until the end of the experiment (Day 14). The TSA was dissolved in dimethyl sulfoxide (DMSO) and then diluted with phosphate buffer saline (PBS) to the final concentration. Control mice ($n = 6$) were injected with 0.1% DMSO. In addition to these groups, five CAIA mice treated with 2.0 mg/kg of TSA and five control mice were sacrificed on Day 6 for immunohistochemical analysis of articular cartilage [Fig. 1(A)].

CLINICAL EVALUATION OF ARTHRITIS

The mice were monitored for the development of arthritis every day after the first mAb injection. According to the method of Terato *et al.*[13], each limb was graded individually on a scale of 0–4, where 0 = normal, 1 = mild but definite redness and swelling of the ankle or wrist or redness and swelling of any degree in any single digit, 2 = moderate to severe redness and swelling of the ankle or wrist, 3 = redness and swelling of the entire foot including the digits, and 4 = maximally inflamed limb, with involvement of multiple joints. The maximum cumulative clinical arthritis score for each mouse was 16.

HISTOLOGIC ANALYSIS OF HIND PAWS

On Day 15, the mice were euthanized by the systemic perfusion of 4% paraformaldehyde in 0.1 M PBS under general anesthesia. The limbs were dissected and fixed in the same solution for 24 h. The samples were decalcified in 0.3 M ethylenediaminetetraacetic acid (EDTA) (pH 7.5) for 7–10 days, divided into two blocks along the sagittal plane, dehydrated in a graded ethanol series, and embedded in paraffin. Standard sagittal sections measuring 4.5 μm were prepared and stained with hematoxylin and eosin. Histologic examinations for synovial inflammation, as well as bone and cartilage damage, were performed independently by two of the authors (KN and YN). The sections were graded according to the system described by Sancho *et al.*[15], where grade 0 = no inflammation, grade 1 = slight thickening of the synovial cell layer and/or some inflammatory cells in the sublining, grade 2 = thickening of the synovial lining, infiltration of the sublining, and localized cartilage

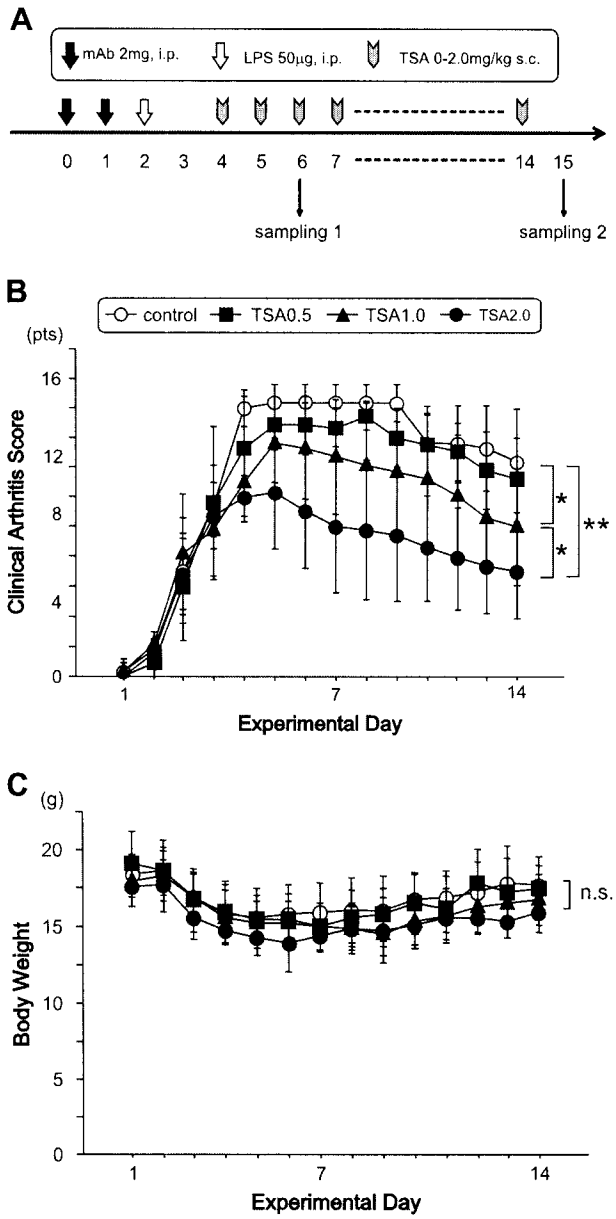

Fig. 1. Arthritis induction in mice and the effects of TSA. (A) The arthritis induction and TSA treatment protocol. Sampling 1: sections for immunohistochemistry. Sampling 2: histological evaluation of arthritis and cartilage destruction. (B) Severity of the clinical signs in untreated (CAIA) and TSA-treated mice (see Methods for scoring system). TSA treatment had a dose-dependent inhibitory effect against CAIA. (C) Body weight changes by group. After the onset of clinical arthritis, all mice lost a small amount of weight. No significant differences were observed among the groups. Data are expressed as the means (symbols) ± S.E.M. (error bars) (*$P < 0.05$ and **$P < 0.001$ by Bonferroni/Dunn analysis).

erosions, and grade 3 = infiltration in the synovial space, pannus formation, cartilage destruction, and bone erosion. Cartilage destruction was graded according to the system described by Kamekura *et al.*[16], where grade 0 = no apparent changes, grade 1 = loss of superficial zone in articular cartilage, grade 2 = defects limited above the tidemark, grade 3 = defects extending to the calcified cartilage, and grade 4 = exposure of the subchondral bone.

IMMUNOHISTOCHEMISTRY OF ARTICULAR CARTILAGE

Immunohistochemistry was performed as previously described using the paraffin sections of paw joint tissues obtained from control and TSA 2.0 group mice ($n = 5$ each) on Day 6[14]. Immunostaining for MMP-3, MMP-13, tissue inhibitor of MMP-1 (TIMP-1), and acetyl-histone H4 was performed on sections obtained from the hind paw joints of the mice on Day 6. For MMP-3, MMP-13, and TIMP-1 immunohistochemistry, deparaffinized and dehydrated sections were pretreated by boiling in 10 mmol/l of citrate buffer (pH 6) for 10 min, and then allowed to slowly cool to room temperature. To detect acetyl-histone H4, the slides were treated with 1 mg/ml of hyaluronidase (*Streptomyces Hyaluroliticus*, Seikagaku Co., Tokyo, Japan) for 2 h at room temperature. Endogenous peroxidase was blocked by immersing the specimens in 0.3% H_2O_2 in PBS; the specimens were then treated with 10% normal goat serum. Rabbit polyclonal anti-MMP-3 antibody (10 μg/ml; Sigma–Aldrich), anti-MMP-13 antibody (20 μg/ml; Sigma–Aldrich), anti-TIMP-1 antibody (30 μg/ml; Sigma–Aldrich), and anti-acetyl-histone H4 antibody (30 mg/ml; Cell Signaling Technology, Beverly, MA, USA) were used as the primary antibodies; they were incubated with the specimens at room temperature over night and then washed with PBS. Then, they were incubated with biotinylated goat anti-rabbit antibody (Vector Laboratories, Burlingame, CA, USA) (7.5 μg/ml) at room temperature for 30 min (for MMP-3, MMP-13, and TIMP-1) or for 1 h (for acetyl-histone H4). Tissue sections were visualized by diaminobenzidine (DAB) and counterstained by methyl green or eosin. Stained sections incubated with normal rabbit non-immune serum or those incubated without primary antibodies were used as negative controls. The immunopositive cells were counted individually in three different areas under a light microscope (magnification: 400×); the number of cells was then averaged. The percentage of immunopositive chondrocytes was determined by dividing the number of positive chondrocytes by the total number of chondrocytes in all cartilage layers within the field.

CELL CULTURE

Murine ATDC5 chondrogenic cells were obtained from the Riken Cell Bank (Tsukuba, Japan). Cells were grown in a standard medium of Dulbecco's modified Eagle's medium (DMEM)/F-12 containing 5% fetal bovine serum (FBS) at 37°C under 5% CO_2. The medium was replaced every other day.

CONVENTIONAL REVERSE TRANSCRIPTION POLYMERASE CHAIN REACTION (RT-PCR) AND REAL-TIME PCR FOR DETECTION OF mRNA OF ECM PROTEINS AND MMPs

ATDC5 cells were seeded at a density of 10^6 cells/well into 6-well dishes, starved in serum-free medium for 24 h, stimulated with both TNF-α (1 ng/ml) and interleukin (IL)-1β (10 ng/ml) and incubated with or without 2 μM of TSA under an atmosphere of 5% CO_2 for 6 h. Total RNA was isolated from cultured cells with Isogen reagent (Nippon Gene, Toyama, Japan), and reverse-transcribed to cDNA using Rever Tra Ace (Toyobo, Tokyo, Japan).

Conventional RT-PCR was performed to confirm the alteration of type II collagen (Col2a1) and aggrecan expression at the mRNA level. The cDNAs underwent PCR amplification in the presence of 10 pmol of each specific primer, 200 μM deoxyribonucleotide triphosphates, and 0.5 U Taq DNA polymerase (Qiagen K.K., Tokyo, Japan). PCR comprised 20 cycles for β-actin, 35 cycles for Col2a1, and 40 cycles for aggrecan, with denaturing at 94°C for 30 s, annealing at 60°C for 30 s, and extension at 72°C for 40 s in each cycle using an automated thermal cycler (Perkin–Elmer Applied Biosystems, Foster, CA, USA). PCR products were analyzed by agarose gel electrophoresis and visualized with ethidium bromide under UV light.

For quantitative analysis of MMP-3 and MMP-13 expression, real-time PCR reactions were performed on a LightCycler instrument (Roche Diagnostics, Mannheim, Germany) using a LightCycler FastStart DNA Master SYBR Green I kit (Roche Molecular Biochemicals, Mannheim, Germany) as recommended by the manufacturer. The final expression value was calculated by dividing the level of target mRNA expression by the level of β-actin mRNA expression, and expressed as fold change over unstimulated control in figures.

The primer sequences of the Col2a1, aggrecan, MMP-3, -13 (Greiner bio-one, Tokyo, Japan) and β-actin (Sigma–Aldrich) used were as follows: for Col2a1, 5′-ACGAAGCGGCTGGCAACCTCA-3′ (forward) and 5′-CCCTCG GCCCTCATCTCTACATCA-3′ (reverse); for aggrecan, 5′-GTGAGGACCT GGTAGTGCGAGTGA-3′ (forward) and 5′-GAGCCTGGGCGATAGTGGAA TATA-3′ (reverse): for MMP-3, 5′-ATGAAAATGAAGGGTCTTCCGG-3′ (forward) and 5′-GCAGAAGCTCCATACCAGCA-3′ (reverse); for MMP-13, 5′-ATGCATTCAGCTATCCTGGCCA-3′ (forward) and 5′-AAGATTGCATTT CTCGGAGCCTG-3′ (reverse) and for β-actin, 5′-GGGGTGTTGAAGGTC TCAAA-3′ (forward) and 5′-GATCTGGCACCACACCTTCT-3′ (reverse).

STATISTICAL ANALYSIS

The statistical significance of the differences between the groups was analyzed using the Bonferroni/Dunn test for the analysis of clinical scores and the non-parametric Mann–Whitney *U* test for the histological, immunohistochemical and *in vitro* analysis. Differences were considered statistically significant when the *P* value was equal to or less than 0.05.

Results

AMELIORATION OF JOINT PATHOLOGY AFTER TSA TREATMENT IN CAIA MICE

Clinically apparent arthritis developed at Day 4 in all CAIA mice, with marked swelling or redness of the joints of the limbs. The arthritis in the control mice with CAIA ($n = 6$) progressed rapidly and markedly. The clinical active arthritis score peaked on Day 6, with scores (mean ± SD [standard deviation]) of 15.0 ± 1.1 in the control group and 13.8 ± 1.4 in the TSA 0.5 group. In contrast, the arthritis score was significantly less in the mice treated with daily subcutaneous (s.c.) injections of TSA 1.0 mg/kg/day (12.8 ± 2.1) and TSA 2.0 mg/kg/day (10.0 ± 3.1) ($P < 0.001$). The clinical arthritis scores were significantly lower in these mice, and continued to decrease until the end of observation. On Day 14, the clinical arthritis scores were 11.7 ± 2.9, 10.8 ± 2.3, 8.1 ± 3.2, and 5.7 ± 2.7 in the control, TSA 0.5, TSA 1.0, and the TSA 2.0 groups, respectively. Statistical analysis showed that TSA decreased the clinical arthritis in a dose-dependent manner [Fig. 1(B)].

The *in vivo* toxicity of TSA was assessed by daily monitoring of body weight, food intake, and behavior of the mice in the treatment and control groups. All mice survived the treatment period. On Day 14, there were no significant differences in the body weights among the four groups of mice [Fig. 1(C)].

HISTOLOGIC ASSESSMENT OF THE SEVERITY OF JOINT INFLAMMATION AND CARTILAGE DESTRUCTION

Sections of paw joint tissues obtained from the control group showed marked pathologic changes, including synovial hyperplasia, with a large number of infiltrating inflammatory cells, extensive pannus formation at the cartilage–bone junction, and severe cartilage destruction. The pathology of paw joint sections obtained from the treatment groups was less severe with no to mild inflammation. The mean synovial inflammation score (grades ± SD) were 3.0 ± 0.3, 2.8 ± 0.6, 2.2 ± 0.8, and 1.4 ± 0.9 in the control, TSA 0.5, TSA 1.0, and TSA 2.0 groups, respectively. Synovial inflammation was significantly less severe in the TSA 1.0 and TSA 2.0 groups than in the other groups ($P < 0.05$) (Fig. 2).

The cartilage destruction score developed by Kamekura *et al.* was used to evaluate the extent of cartilage destruction in each mouse. The cartilage destruction scores (mean ± SD) were 3.6 ± 0.5, 3.1 ± 0.7, 2.6 ± 0.7, and 1.5 ± 0.5 in the control, TSA 0.5, TSA 1.0 and TSA 2.0 groups, respectively (Fig. 3).

IMMUNOHISTOCHEMISTRY

To evaluate the *in vivo* effects of TSA on the expression of proteolytic enzymes in articular cartilage, immunohistochemical analysis was performed using the hind paw joint

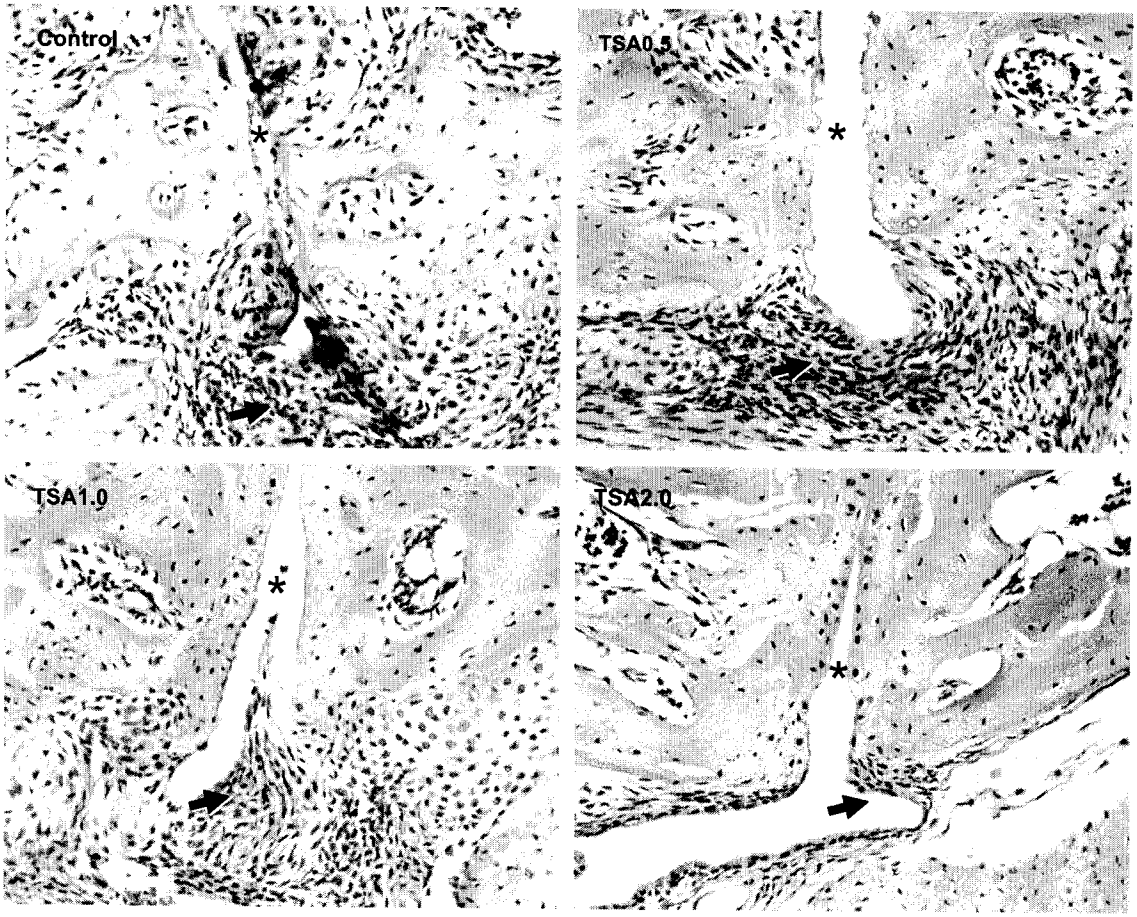

Fig. 2. Histological evaluation of arthritis. The severity of synovial inflammation was evaluated histologically in the specimens obtained on Day 15. Representative results showing the histological appearance of the hind paws are seen in the upper panel. The control group specimens showed synovial hyperplasia, inflammatory cells proliferation, pannus formation, and bone destruction. Joint pathology was less severe in TSA-treated mice. Arrows: synovial hyperplasia, asterisk: joint space. Original magnification: 100×. The mean synovial inflammation score was significantly lower in the TSA 1.0 mg/kg and TSA 2.0 mg/kg groups than in the control group ($n = 6$). Error bars express ±S.E.M. ($^*P < 0.01$ and $^{**}P < 0.001$ by Bonferroni/Dunn analysis).

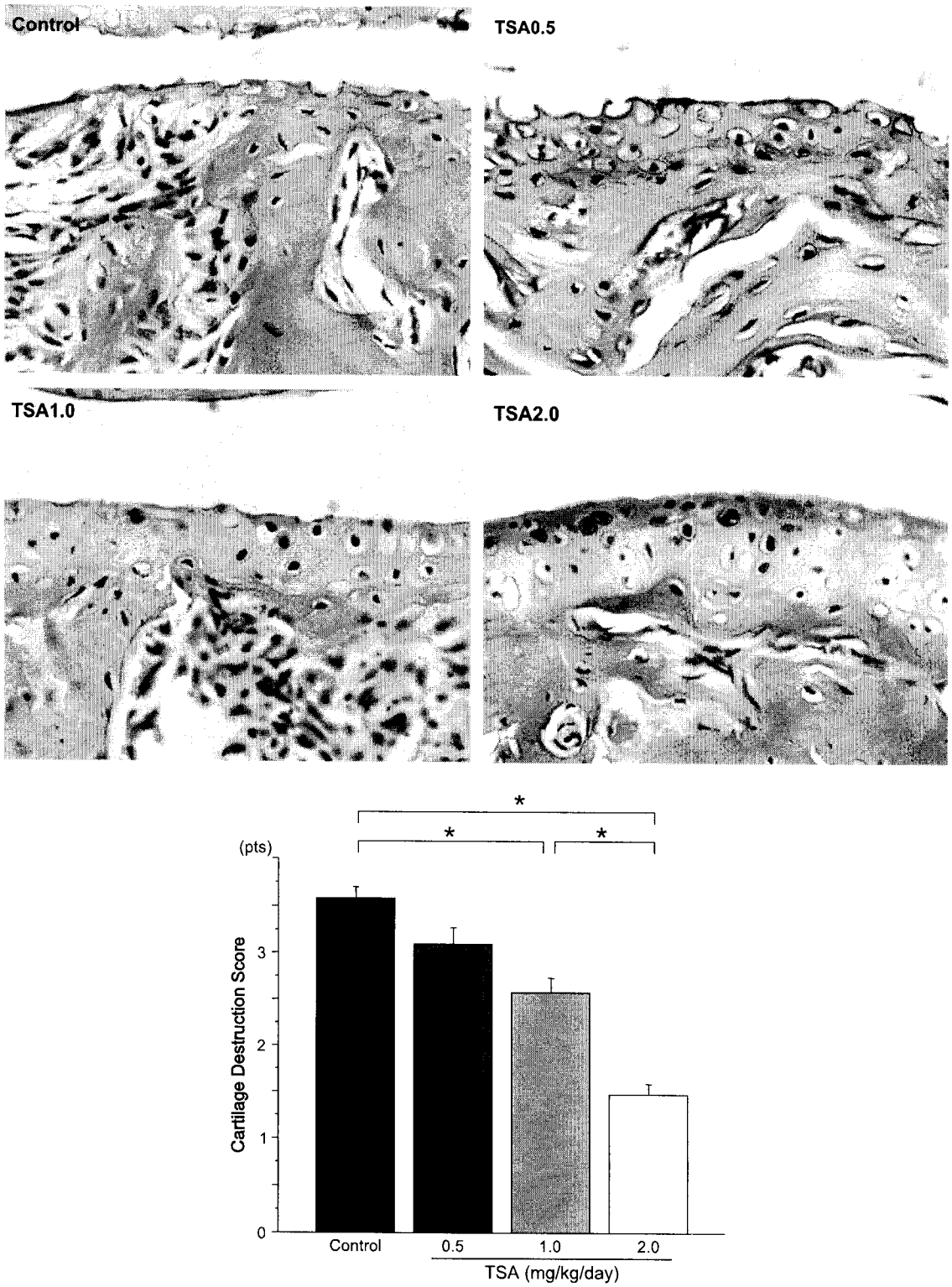

Fig. 3. Inhibition of cartilage destruction by TSA treatment. Representative photographs of each grade of cartilage destruction, grade 4 in the control group, grade 3 in the TSA 0.5 mg/kg group, grade 2 in the TSA 1.0 mg/kg group, and grade 1 in the TSA 2.0 mg/kg group. Original magnification: 400×. The total cartilage destruction score was significantly lower in the TSA 1.0 mg/kg and TSA 2.0 mg/kg groups than in the control group ($n = 6$ each). Error bars express ±S.E.M. (*$P < 0.001$ by Bonferroni/Dunn analysis).

specimens obtained on Day 6 from the control and TSA 2.0 group mice. The Day 6 samples from both untreated and treated mice showed synovial hyperplasia and inflammatory cell infiltration, but the articular cartilage structure was preserved.

Next, the endogenous MMP-3, MMP-13 and TIMP-1 levels in the articular cartilage chondrocytes were examined. Chondrocytes in inflammatory articular cartilage were strongly stained for both MMP-3 and MMP-13. The population of MMP-3-positive cells was significantly lower in the TSA-treated group than in the control group. There were significant differences in the population of MMP-13-positive chondrocytes between the TSA 2.0 and control groups. As well, the number of TIMP-1-positive chondrocytes was significantly higher in the TSA 2.0 group than in the control group (Fig. 4).

Chondrocyte acetylation was examined using immunohistochemical staining for acetylated histone H4. Intensely positive staining for acetyl-histone H4 was observed in the chondrocytes of the cartilage obtained from the TSA 2.0 group. The population of acetyl-histone H4-positive chondrocytes in the cartilage obtained from the TSA 2.0 group was significantly higher than from the control group (Fig. 5).

RT-PCR AND QUANTITATIVE REAL-TIME PCR

The pro-inflammatory cytokine stimulation with IL-1β (10 ng/ml) and TNF-α (1 ng/ml) and TSA treatment did not affect the cell count and cell morphology of ATDC5 during 6 h of experimental period [Fig. 6(A)]. At the present experimental period, treatment by TSA did not show significant catabolic effect on type II collagen and aggrecan [Fig. 6(B)]. In contrast, MMPs were much more influenced by cytokine stimulation than type II collagen and aggrecan. Cytokine stimulation of the cells induced MMP-3 (31-fold) and MMP-13 (7.4-fold) expression at 6 h, and co-incubation with TSA (2 μM) significantly down-regulated MMP-3 mRNA expression ($P < 0.05$) and showed the tendency to down-regulate the MMP-13 expression (not significant) [Fig. 6(C)]. The experiments were done at least three times and generated similar results.

Discussion

MMPs play a central role in cartilage breakdown by degrading type II collagen and aggrecans, which are major components of the ECM of articular cartilage[17]. Chondrocytes are also involved in cartilage breakdown by secreting high amounts of MMPs in conditions of arthritis[18]. Although several strategies have been designed to develop effective inhibitors that prevent the expression and activation of MMP within the joints, no effective clinical agents have yet been reported. In the current study, the *in vivo* effect of HDAC inhibitors on chondrocyte expression of MMPs in CAIA mice was examined. It was demonstrated that TSA ameliorated the clinical arthritis score and the degree of joint inflammation, as well as the amount of cartilage destruction, in a dose-dependent manner. Chondrocyte expression of MMP-3 and MMP-13, which may play a prominent role in cartilage destruction, was significantly affected by TSA treatment, as shown by the immunohistochemistry and *in vitro* analysis. These findings suggest that modification of the chromatin structure of the key genes involved in the pathogenesis of arthritis might play a beneficial role in the regulation of synovial inflammation and subsequent cartilage destruction in arthritis. The control of catabolic gene expression by TSA may be, at least in part, a direct effect of TSA on chondrocytes, as suggested by the up-regulation of histone H4 acetylation after TSA treatment.

The precise mechanism that underlies the suppression of MMP by HDAC inhibitors is still unknown. The expression and production of MMPs are regulated by a variety of extracellular signals *via* the transcriptional activation of cytokines, growth factors, or matrix molecules[2,11]. Among the pro-inflammatory cytokines, IL-1 plays a central role in the induction of MMP-1, -3, -8, -13, and -14[17]. Our previous study showed that FK228 inhibited IL-1β and TNF-α expression in the synovium of CAIA[7]. A similar effect on cytokine expression was observed in human RA synovial fibroblasts (RASFs) treated with TSA *in vitro* (unpublished data). Thus, it is reasonable to suggest that HDAC inhibitors indirectly contribute to the suppression of cartilage destruction through inhibition of the production and release of pro-inflammatory cytokines from synovial tissue.

The activation of MMPs depends on signal transduction pathways, mainly in the mitogen-activated protein (MAP) kinase and I-κB pathway; this is followed by activation of various transcriptional factors, such as nuclear factor of activated T-cells (NFAT), signal transducer and activator of transcription (STAT), nuclear factor kappaB (NF-κB), and activator protein-1 (AP-1)[11]. These transcriptional factors offer multiple therapeutic targets that should be investigated with respect to their ability to protect cartilage from enzymatic degradation[19]. Klampfer *et al.* demonstrated that STAT-dependent transcription of interferon-gamma (IFN-γ) was inhibited by HDAC inhibitors, such as TSA butyrate and suberoylanilide hydroxamic acid (SAHA), in colorectal carcinoma cell lines[20]. The inhibition of NF-κB activity by HDAC inhibitors was also recently reported in several cell systems[21,22]. Moreover, the AP-1 binding site is present in the promoter region of all MMPs, except for MMP-2, which suggests *jun/fos* transcription factor binding plays a central role[17]. HDAC inhibitors reportedly block the induction of *c-jun* transcription by inhibiting the recruitment of the pre-initiation complex (RNA polymerase II and transcription factor IIB (TFIIB)) to the *c-jun* promoter[23]. These facts suggest that HDAC activity might be involved in multiple steps within the MMP activation pathways, and that its inhibition by HDAC inhibitors may reduce chondrocyte MMP expression in CAIA mice.

Importantly, the biological activity of MMP is balanced *via* the inhibition of active enzymes by TIMP, which form a stable and irreversible equimolar complex[24]. In arthritis model mice, TIMP-1, showing a similar expression profile to that of MMP-3, was highly expressed during the acute phases of arthritis[25]. However, the amount of TIMPs that was present was insufficient to suppress MMPs' activity under the conditions of arthritis[26,27]. Pelletier *et al.* demonstrated that IL-1 significantly decreased TIMP-1 synthesis in OA and RA culture cartilage explants, whereas the synthesis of MMPs was increased[28]. Yoshihara *et al.* reported that MMPs/TIMPs ratios were higher in RA than OA, and that they were correlated to degrading activity. They concluded that the local imbalance of MMPs to TIMPs may contribute to cartilage destruction[29]. In this regard, it has been suggested that the delivery of functional TIMPs' genes may result in the inhibition of cartilage degradation. A recent report showed that TIMP-1-transduced cartilage resists the catabolic effects of IL-1, and has reduced MMP activity, as well as decreased loss of type II collagen[30]. In the current study, we did not examine whether the amount that TIMP-1 was up-regulated by TSA treatment was sufficient to block cartilage MMPs activity. However, the down-regulation of MMPs

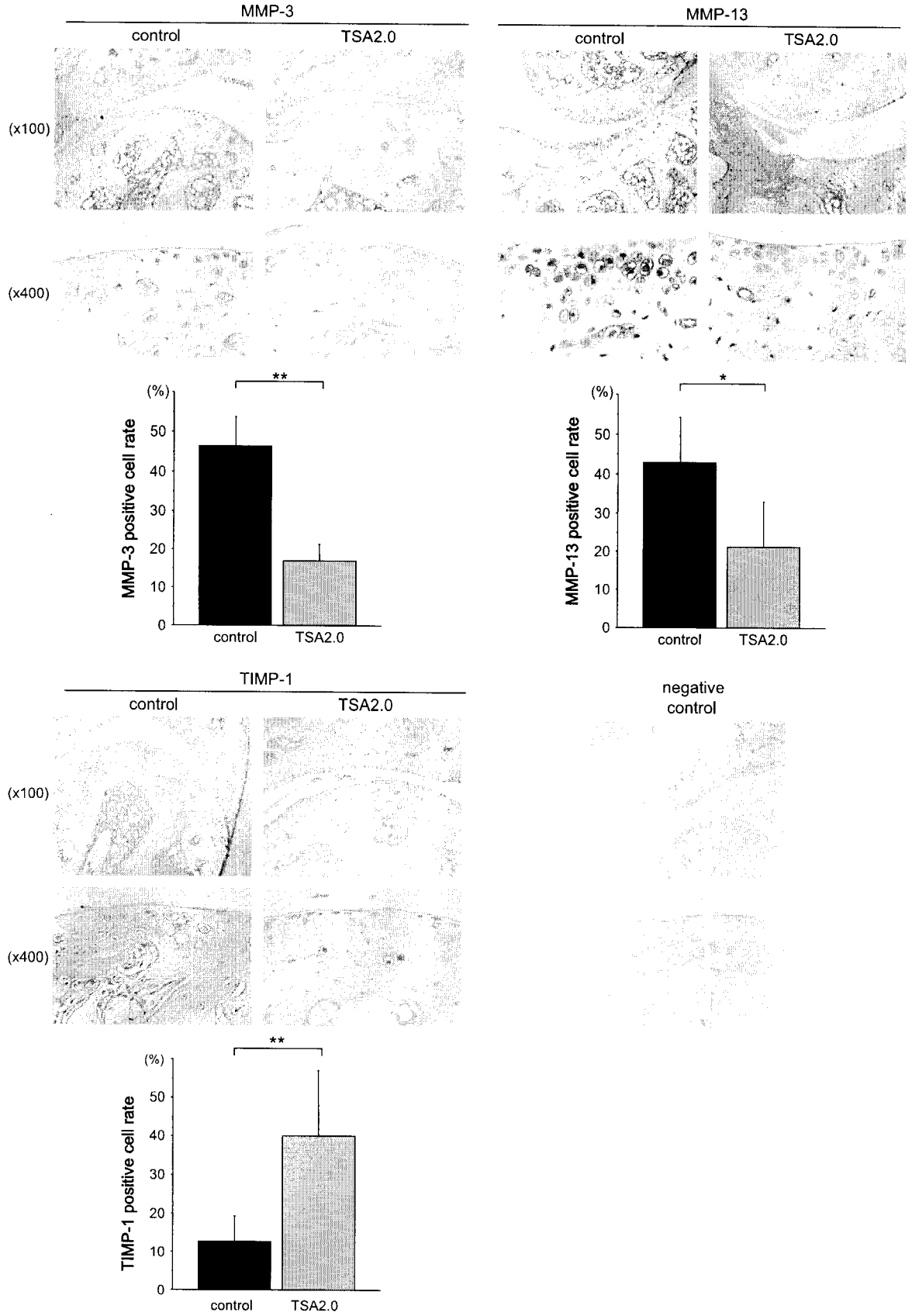

Fig. 4. Immunohistochemical staining of MMP-3, MMP-13, and TIMP-1 in joint cartilage. The number of MMP-3 and MMP-13-positive chondrocytes was significantly lower in the TSA 2.0 mg/kg group ($n = 5$) than in the control group ($n = 5$). In contrast, TIMP-1 was strongly expressed in the joint cartilage obtained from the TSA 2.0 mg/kg group. The population of TIMP-1-positive chondrocytes was significantly higher in the TSA 2.0 mg/kg group than in the control group. Representative immunohistochemistry results are shown in the upper panels. Error bars express ±SD (*$P < 0.01$, **$P < 0.001$ by Mann–Whitney U test).

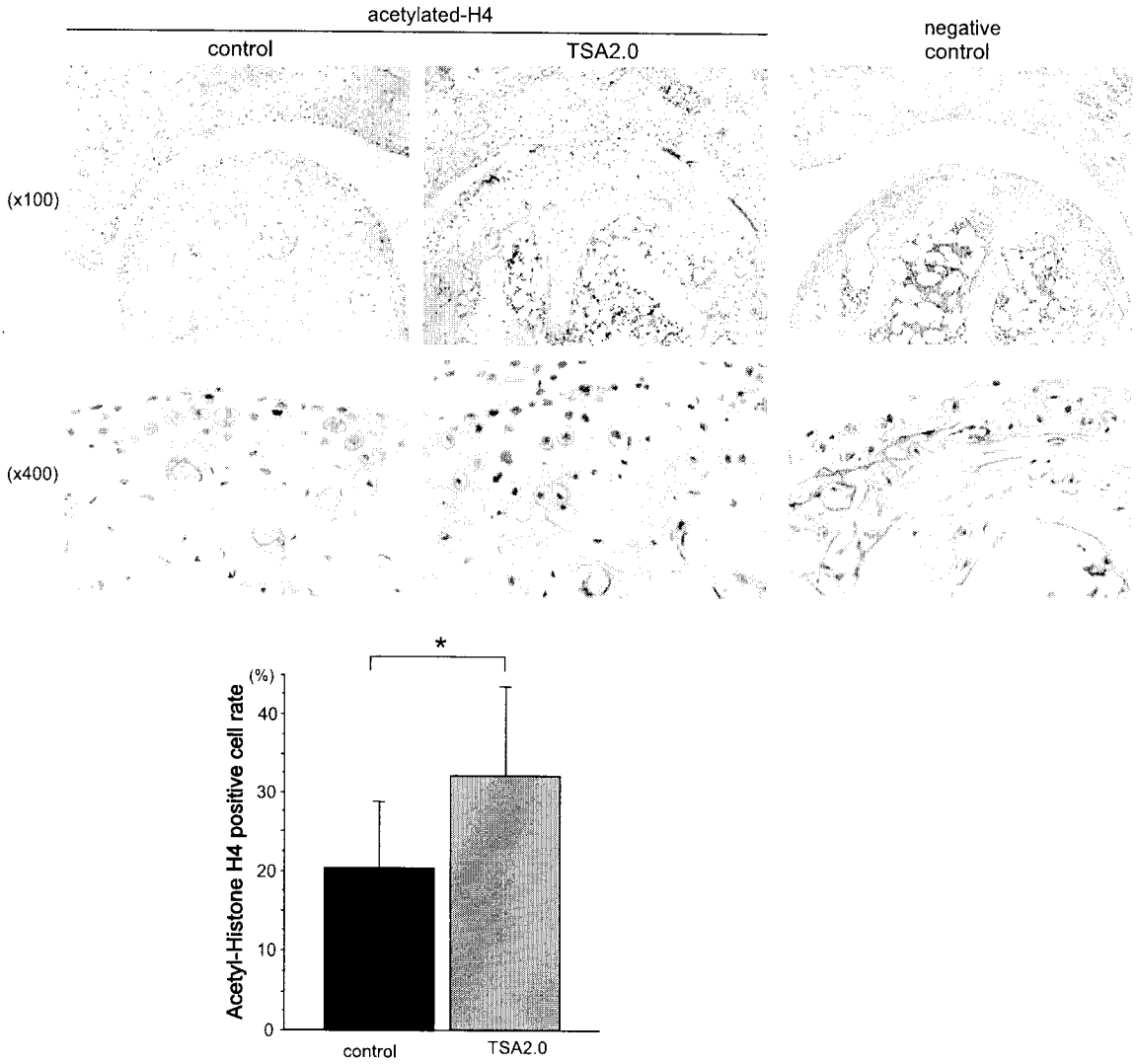

Fig. 5. Immunohistochemical staining for acetyl-histone H4. Cartilage specimens obtained from the control and TSA 2.0 mg/kg groups ($n = 5$ each) were positive for acetyl-histone H4 (left panels). The number of acetyl-histone H4-positive cells was higher in the TSA 2.0 mg/kg group than in the control group. Error bars express ±SD (*$P < 0.05$ by Mann–Whitney U test).

expression and the up-regulation of TIMPs expression were noted in the chondrocytes of TSA-treated CAIA; this indicates that the inhibition of HDAC activity might lead to a modification of chondrocyte gene expression, which results in the correction of the imbalance between MMPs and TIMPs.

The direct effect of HDAC inhibitors on cytokine-induced chondrocyte gene expression was first demonstrated by Young *et al.*[12]. They reported that the IL-1α/oncostatin M (OSM)-induced expression of MMP-1, -13, ADAMTS-4, -5, and -9 was suppressed by TSA in human chondrosarcoma cell line and human articular chondrocytes. Thus, we considered that the control of catabolic gene expression by TSA seen in the present study may be, at least in part, a direct effect TSA on chondrocytes. As the change in histone H4 acetylation in chondrocytes from TSA-treated animals seen in the present study was only moderate (from 20 to 30% positive chondrocytes), and could not account for the observed TSA-induced chondro-protective effect of TSA, we performed the *in vitro* assay using ATDC5 to examine whether TSA directly affects the chondrocyte gene expression. In our *in vitro* experimental protocol, the treatment by TSA did not show the significant suppressive effect on type II collagen and aggrecan mRNA expression. In contrast, it was demonstrated that pro-inflammatory cytokine-induced MMP-3 mRNA expression was significantly down-regulated by TSA treatment in murine chondrogenic ATDC5 cells. On the other hand, the expression of pro-inflammatory cytokine-induced MMP-13 was likely to be reduced by TSA treatment, but not significantly. This discrepancy with the results of previous study[12] might be due to the difference of stimulation, incubation time with TSA, and cell type used. However, these results cumulatively suggest that TSA might exert the chondro-protective effect not only by suppression of synovitis, but also by directly modulating the gene expressions of chondrocytes.

Finally, in this study, it was found that daily administration of TSA successfully ameliorated the clinical arthritis seen in the mouse CAIA model in a dose-dependent manner. The TSA-treated groups had significantly less histological joint inflammation and cartilage destruction. Immunohistochemical study showed that, compared to controls, there was a significant down-regulation of MMPs expression,

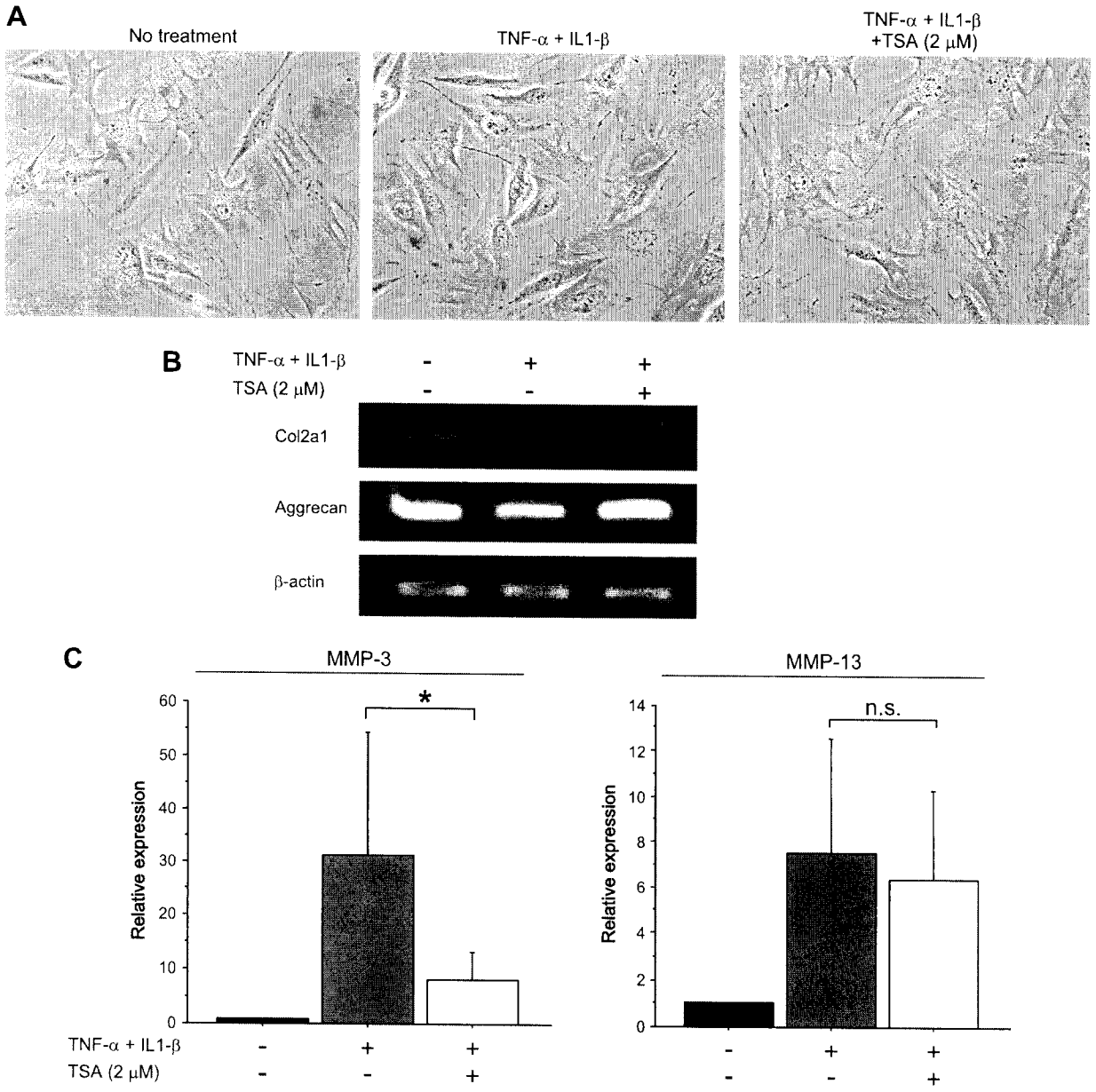

Fig. 6. Effect of pro-inflammatory cytokine and TSA on the morphology and gene expression of murine ATDC5 chondrogenic cells. (A) Morphologic features of ATDC5 cells examined by phase-contrast microscopy. No differences were observed in the TSA-treated cells compared with non-stimulated or cytokine-stimulated cells. Original magnification: 200×. (B) The effect of cytokine stimulation and TSA treatment on the expression of type II collagen (Col2a1), aggrecan examined by RT-PCR. TSA did not show the significant catabolic effect on type II collagen and aggrecan expression. (C) The effect of cytokine stimulation and TSA treatment on the expression of MMP-3 and -13 mRNA by ATDC5 examined by real-time PCR. Cytokine-induced expression of MMP-3, but not MMP-13 was significantly suppressed by TSA treatment. All values are averages in triplicated tests. Error bars express ±SD (*$P < 0.05$ by Mann–Whitney U test, n.s.: not significant).

up-regulation of TIMP-1 expression, and hyperacetylation in the joint cartilage chondrocytes of the TSA-treated groups. *In vitro* examination demonstrated that TSA down-regulated the pro inflammatory cytokine-induced MMP-3 mRNA expression in chondrocytes without showing the suppressive effect of type II collagen and aggrecan gene expressions. The precise mechanism that underlies the regulation of chondrocyte gene expression by HDAC inhibitors remains unknown. However, our results suggest that HDAC inhibitors may have a direct inhibitory effect on cartilage destruction in inflammatory arthritis.

Conflict of interest

The authors have no conflict of interest.

Acknowledgments

The authors would like to thank Ms M. Hachioji, Department of Orthopaedic Surgery, Science of Functional Recovery and Reconstruction, Okayama University Graduate School of Medicine, Dentistry and Pharmaceutical Sciences, for her expert technical assistance.

References

1. Huber LC, Distler O, Tarner I, Gay RE, Gay S, Pap T. Synovial fibroblasts: key players in rheumatoid arthritis. Rheumatology (Oxford) 2006;45:669–75.
2. Yasuda T. Cartilage destruction by matrix degradation products. Mod Rheumatol 2006;16:197–205.
3. Bathon JM, Martin RW, Fleischmann RM, Tesser JR, Schiff MH, Keystone EC, *et al.* A comparison of etanercept and methotrexate in patients with early rheumatoid arthritis. N Engl J Med 2000;343: 1586–93.
4. Klareskog L, van der Heijde D, de Jager JP, Gough A, Kalden J, Malaise M, *et al.* Therapeutic effect of the combination of etanercept and methotrexate compared with each treatment alone in patients with rheumatoid arthritis: double-blind randomised controlled trial. Lancet 2004;363:675–81.
5. Smolen JS, Van Der Heijde DM, St Clair EW, Emery P, Bathon JM, Keystone E, *et al.* Predictors of joint damage in patients with early rheumatoid arthritis treated with high-dose methotrexate with or without concomitant infliximab: results from the ASPIRE trial. Arthritis Rheum 2006;54:702–10.
6. Blanchard F, Chipoy C. Histone deacetylase inhibitors: new drugs for the treatment of inflammatory diseases? Drug Discov Today 2005; 10:197–204.
7. Nishida K, Komiyama T, Miyazawa S, Shen ZN, Furumatsu T, Doi H, *et al.* Histone deacetylase inhibitor suppression of autoantibody-mediated arthritis in mice *via* regulation of p16INK4a and p21(WAF1/Cip1) expression. Arthritis Rheum 2004;50:3365–76.
8. Chung YL, Lee MY, Wang AJ, Yao LF. A therapeutic strategy uses histone deacetylase inhibitors to modulate the expression of genes involved in the pathogenesis of rheumatoid arthritis. Mol Ther 2003; 8:707–17.
9. Jungel A, Baresova V, Ospelt C, Simmen BR, Michel BA, Gay RE, *et al.* Trichostatin A sensitises rheumatoid arthritis synovial fibroblasts for TRAIL-induced apoptosis. Ann Rheum Dis 2006;65:910–2.
10. Nakamura T, Kukita T, Shobuike T, Nagata K, Wu Z, Ogawa K, *et al.* Inhibition of histone deacetylase suppresses osteoclastogenesis and bone destruction by inducing IFN-beta production. J Immunol 2005;175:5809–16.
11. Rannou F, Francois M, Corvol MT, Berenbaum F. Cartilage breakdown in rheumatoid arthritis. Joint Bone Spine 2006;73:29–36.
12. Young DA, Lakey RL, Pennington CJ, Jones D, Kevorkian L, Edwards DR, *et al.* Histone deacetylase inhibitors modulate metalloproteinase gene expression in chondrocytes and block cartilage resorption. Arthritis Res Ther 2005;7:R503–12.
13. Terato K, Hasty KA, Reife RA, Cremer MA, Kang AH, Stuart JM. Induction of arthritis with monoclonal antibodies to collagen. J Immunol 1992;148:2103–8.
14. Kato H, Nishida K, Yoshida A, Takada I, McCown C, Matsuo M, *et al.* Effect of NOS2 gene deficiency on the development of autoantibody mediated arthritis and subsequent articular cartilage degeneration. J Rheumatol 2003;30:247–55.
15. Sancho D, Gomez M, Viedma F, Esplugues E, Gordon-Alonso M, Garcia-Lopez MA, *et al.* CD69 downregulates autoimmune reactivity through active transforming growth factor-beta production in collagen-induced arthritis. J Clin Invest 2003;112:872–82.
16. Kamekura S, Hoshi K, Shimoaka T, Chung U, Chikuda H, Yamada T, *et al.* Osteoarthritis development in novel experimental mouse models induced by knee joint instability. Osteoarthritis Cartilage 2005;13: 632–41.
17. Pap T, Gay S, Schett G. Matrix metalloproteinases. In: Smolen SJ, Lipsky EP, Eds. Targeted Therapies in Rheumatology. London: Martin Dunitz 2003:483–501.
18. Berenbaum F. 'Rheumatoid chondritis' or the place of cartilage in rheumatoid inflammation. Br J Rheumatol 1998;37:4–6.
19. Huang L. Targeting histone deacetylases for the treatment of cancer and inflammatory diseases. J Cell Physiol 2006;209:611–6.
20. Klampfer L, Huang J, Swaby LA, Augenlicht L. Requirement of histone deacetylase activity for signaling by STAT1. J Biol Chem 2004;279: 30358–68.
21. Miao F, Gonzalo IG, Lanting L, Natarajan R. *In vivo* chromatin remodeling events leading to inflammatory gene transcription under diabetic conditions. J Biol Chem 2004;279:18091–7.
22. Zhong H, May MJ, Jimi E, Ghosh S. The phosphorylation status of nuclear NF-kappa B determines its association with CBP/p300 or HDAC-1. Mol Cell 2002;9:625–36.
23. Yamaguchi K, Lantowski A, Dannenberg AJ, Subbaramaiah K. Histone deacetylase inhibitors suppress the induction of c-Jun and its target genes including COX-2. J Biol Chem 2005;280:32569–77.
24. Bode W, Fernandez-Catalan C, Grams F, Gomis-Ruth FX, Nagase H, Tschesche H, *et al.* Insights into MMP–TIMP interactions. Ann N Y Acad Sci 1999;878:73–91.
25. Schurigt U, Stopfel N, Huckel M, Pfirschke C, Wiederanders B, Brauer R. Local expression of matrix metalloproteinases, cathepsins, and their inhibitors during the development of murine antigen-induced arthritis. Arthritis Res Ther 2005;7:R174–88.
26. Hegemann N, Wondimu A, Ullrich K, Schmidt MF. Synovial MMP-3 and TIMP-1 levels and their correlation with cytokine expression in canine rheumatoid arthritis. Vet Immunol Immunopathol 2003;91:199–204.
27. Dean DD, Martel-Pelletier J, Pelletier JP, Howell DS, Woessner JF Jr. Evidence for metalloproteinase and metalloproteinase inhibitor imbalance in human osteoarthritic cartilage. J Clin Invest 1989;84:678–85.
28. Martel-Pelletier J, McCollum R, Fujimoto N, Obata K, Cloutier JM, Pelletier JP. Excess of metalloproteases over tissue inhibitor of metalloprotease may contribute to cartilage degradation in osteoarthritis and rheumatoid arthritis. Lab Invest 1994;70:807–15.
29. Yoshihara Y, Nakamura H, Obata K, Yamada H, Hayakawa T, Fujikawa K, *et al.* Matrix metalloproteinases and tissue inhibitors of metalloproteinases in synovial fluids from patients with rheumatoid arthritis or osteoarthritis. Ann Rheum Dis 2000;59:455–61.
30. Kafienah W, Al-Fayez F, Hollander AP, Barker MD. Inhibition of cartilage degradation: a combined tissue engineering and gene therapy approach. Arthritis Rheum 2003;48:709–18.

Please cite this article in press as: Nasu Y et al., Trichostatin A, a histone deacetylase inhibitor, suppresses synovial inflammation and sub-

[Epigenetics 1:2, 67-75; April/May/June 2006]; ©2006 Landes Bioscience

Review

Rationale for the Use of Histone Deacetylase Inhibitors as a Dual Therapeutic Modality in Multiple Sclerosis

Steven G. Gray[1,2,*]

Fernando Dangond[2,3,*]

[1]Departments of Clinical Medicine & Oncology; Institute of Molecular Medicine; Trinity Sciences Health Centre; St James's Hospital; Dublin, Ireland

[2]Laboratory of Transcriptional and Immune Regulation; Brigham and Women's Hospital Laboratories; Cambridge, Massachusetts USA

[3]Berlex Laboratories; Wayne, New Jersey USA

*Correspondence to: Steven G. Gray; Departments of Clinical Medicine & Oncology; Institute of Molecular Medicine; Trinity Sciences Health Centre Rm 2.09; St James's Hospital; Dublin 8, Ireland; Tel.: +00353.1.6083620; Email: sgray@stjames.ie/ Fernando Dangond; Berlex Laboratories; 6 West Belt; Wayne, New Jersey 07470-6806 USA; Tel.: 973.317.5549; Fax: 973.305.3527; Email: Fernando_Dangond @berlex.com

Received 01/25/06; Accepted 03/05/06

Previously published online as an *Epigenetics* E-publication: http://www.landesbioscience.com/journals/epigenetics/abstract.php?id=2678

KEY WORDS

multiple sclerosis, therapy, histone deacetylase, inhibitors, epigenetics

ACKNOWLEDGEMENTS

This work was supported by NIH KO8CA80084 (F.D.). The authors would like to acknowledge those authors whose work could not be cited through reference limitations.

ABSTRACT

Major recent advances in the field of chromatin remodeling have dramatically changed our understanding of the ways in which genes are regulated. Epigenetic regulators such as histone deacetylases (HDACs) and histone acetyltransferases (HATs) are increasingly being implicated as direct or indirect components in the regulation of expression of neuronal, immune and other tissue specific genes. HDACs and HATs have been shown to play important roles in cell growth, cell cycle control, development, differentiation and survival. Mutations in genes that encode HDAC-binding proteins cause neurological disorders, such as MeCP2 mutations in Rett's syndrome. Mutations of CBP, a gene with HAT function, cause the mental retardation-associated Rubinstein-Taybi syndrome. Recently, HDAC inhibitors have been found to ameliorate progression of the spinal muscular atrophy (SMA) motor neuron disease and the Huntington disease mouse models. The neuroprotective role of HDAC inhibitors seems to extend to other diseases that share mechanisms of oxidative stress, inflammation and neuronal cell apoptosis. HDAC inhibitors also have widespread modulatory effects on gene expression within the immune system and have been used successfully in the lupus and rheumatoid arthritis autoimmune disease models. Recently, we demonstrated the efficacy of the HDAC inhibitor Trichostatin A in ameliorating disease in the multiple sclerosis (MS) animal model, experimental autoimmune encephalomyelitis (EAE). In this review we describe the current literature surrounding these inhibitors and propose a rationale for harnessing both their neuroprotective and anti-inflammatory effects to treat MS, an autoimmune, demyelinating and degenerative disease of the human central nervous system (CNS).

INTRODUCTION

Multiple Sclerosis (MS) is a demyelinating disease characterized by chronic inflammation of the central nervous system (CNS) white matter. First noted by Charcot in 1868,[1] axonal degeneration is a prominent feature in MS[2] and is recognized as a primary cause of permanent disability in this disease. The drastic decline in quality of life and loss of productivity caused by MS exert a significant human and societal cost. Recent estimates from Europe place the annual cost of caring for MS patients in the range of 15,000–60,000 depending upon the severity of the disease.[3]

While a large body of work within the last decade has enhanced our understanding of the fundamental nature of MS, basic research into its etiology, pathophysiology and treatment faces enormous challenges, and this may in part be due to the great variability in the clinical presentation and course of MS. The clinical classification of MS includes several types: relapsing remitting MS (RRMS), primary progressive (PPMS), relapsing progressive (RPMS) and a secondary progressive form (SPMS) of the disease. Of these, the RRMS form is the most prevalent.

Within the past two decades, work on the animal model of MS, experimental autoimmune encephalomyelitis (EAE), has strengthened the hypothesis that MS immunopathology is largely due to the cytotoxic action on the CNS of myelin-specific pro-inflammatory T cells.[4] However, there is evidence that humoral immune responses (antibodies produced by plasma cells) also play distinctive roles in the pathogenesis of this complex disorder.[5] Thus, MS is an inflammatory and demyelinating disease in which many factors (genetic and environmental) may act in concert to influence disease susceptibility and progression. MS is also now considered a neurodegenerative disease, since neuronal loss, brain atrophy and cognitive decline may occur even in the absence of overt inflammation.

Factors that have prevented our understanding of this complex disease include the heterogeneity observed in both its histopathology and its clinical course. In one particular study, four histopathological patterns could be discerned in MS lesions. Two of these seemed to indicate autoimmune or T-cell directed myelin degeneration while the other two suggested a pattern commonly seen in viral or toxin induced demyelination.[6] These histopathological patterns, however, do not address the intrinsic heterogeneity seen in disease progression, which may be influenced by the number and severity of exacerbations (also referred to as "attacks") or the speed in accumulation of clinical disability.

For over more than a decade, immunomodulatory drugs are being introduced to treat MS. These drugs, which include β-interferons (Avonex, Betaseron and Rebif) and an immune modulator termed Copaxone, reduce the number of clinical attacks and the number of lesions detected by magnetic resonance imaging (MRI), but they are only used by injection, and may cause toxicity in some patients.[7] More recently, the chemotherapeutic agent Novantrone (mitoxantrone) was added to the MS drug armamentarium. The heterogeneity of the disease may also be reflected in the variable response of patients to these immunomodulatory treatments.

In this review we shall briefly describe the histone deacetylase (HDAC) superfamily, the various inhibitors available for these enzymes and will discuss their potential use as a dual (i.e., anti-inflammatory and neuroprotective) therapeutic modality in the treatment of MS. We shall discuss the current literature on HDACs with regard to neurological conditions and available reports on the effects of HDAC inhibitors on molecular mechanisms associated with MS.

THE NUCLEOSOME

The nucleosome is the fundamental unit of chromatin. It is composed of a histone octamer (H2A and H2B dimers and a H3/H4 tetramer) surrounded by 146 bp of DNA. Gene expression regulation occurs at several levels, one of which is the dynamic variability of nucleosomal architecture. This is primarily achieved via condensation or relaxation of the nuclesome. These events are in part regulated by nuclear enzymes that modify the state of acetylation of lysines in the amino terminal tail of histones. These enzymes are known as histone deacetylases (HDACs) which lead to histone deacetylation and nucleosomal condensation, and histone acetyltransferases (HATs) which lead to histone hyperacetylation and nucleosomal relaxation. The latter generally correlates with enhanced gene transcription, since the physical separation of the DNA from the histone octamer permits the contact of activating transcription factors and the transcriptional machinery with the target DNA promoters.

HDACs and HATs

With the isolation and biochemical characterization of the first HDACs and HATs new paradigms in the regulation of gene expression have been exposed. These regulatory enzymes not only alter the acetylation status of histones, but also, via protein-protein interactions, play critical roles in many cellular processes including transcription, cell cycle progression, differentiation and apoptosis.[8,9] We cloned HDAC3 in human and mouse,[10,11] and with the aid of HDAC inhibitors, showed that HDACs play roles in cell activation, differentiation, hormonal gene expression and survival.[10-15]

HATs can be loosely grouped together on the basis of sequence similarity to yeast proteins into the GNAT (GCN5-related N-acetyltransferase) superfamily of proteins.[16] HDACs can be grouped either into a superfamily of proteins including bacterial members[17] or into three classes based on their similarity to three yeast genes.[8,9] Class I HDACs (HDACs 1, 2, 3 and 8) share homology with the yeast RPD3 gene. Class II HDACs (HDACs 4–7 and 9–11) share similarity with HDA1 genes. Class III HDACs (SIRTs 1-7) share homology with the NAD-dependent silent information regulator 2 (Sir2 or Sirtuin) gene family. Recently a fourth class of HDAC was suggested based on the distinctive structure of HDAC11.[17] The complexity of HDAC gene regulation in response to various stimuli is exemplified by the ability of members of this family to undergo alternative splicing.[18]

SPECIFIC INHIBITORS FOR HDACS AND HATS

Generally, HDAC inhibitors can be separated into three categories: short chain fatty acids, naturally occurring compounds and synthetic derivatives. Historically, sodium butyrate, a short chain fatty acid, was one of the first compounds shown to cause an increase in histone acetylation.[19] However, sodium butyrate effects are not exclusive to histones, as it causes additional pleiotropic effects including the hypermethylation of DNA.[20] Several other butyrate or short chain fatty acid derivatives have since been shown to have a similar HDAC inhibitory activity.[21] In the second, natural compound category, the first specific HDAC inhibitor described was the hydroxamate trichostatin A (TSA), originally isolated as a fungistatic antibiotic from the *Streptomyces platensis* strain.[22] Other naturally occurring compounds which have HDAC inhibitory effects, among a rapidly growing list, include apicidin, HC toxin, depudecin and FR901228. Because of the interest in these inhibitors for their therapeutic potential several synthetic compounds have also been generated including hybrid polar compounds such as suberoylanilide hydroxamic acid (SAHA), cyclic tetrapeptides, benzamides and others.[23]

Small molecule inhibitor screening is increasingly being used to identify and target for the most part HDACs, but some inhibitors for HATs have also been identified[18] Many of the small molecule HDAC inhibitors have an aliphatic chain that occupies a tubular pocket in the target HDAC enzyme, and coordinate a Zn^{2+} molecule at the bottom of this pocket, as demonstrated with crystallographic methods,[23] resulting in inactivation of this catalytic site. This mechanism, however, may not be operative in the case of sodium butyrate, as competitive inhibition studies have suggested that it may not be competitive, thus not associating directly with this site.[24]

Several histone deacetylase inhibitors have now undergone Phase I/Phase II clinical trials as anticancer agents. Several of these trials have reached publication and as such there is an emerging understanding of the potential side effects and dose-limiting toxicities of these drugs. For the most part these first generation inhibitors have shown well tolerated safety profiles.[23,25,26]

MOLECULAR MECHANISMS OF HDACs AND HATs IN NEURODEGENERATION

Neuronal traits are modulated by HDAC/REST complexes. The first indication that histone acetylation may be important in neuronal settings came from a study of neuronal fractions in 1975.[27] Subsequently, important roles for HDACs and HATs in the regulation of neuron specific genes have been demonstrated. One of the best-established mechanisms elucidated concerns genes that are controlled

by a silencer element (repressor element-1 (RE1)/neuronal restrictive silencer element (NRSE). A specific repressor protein known as repressor element 1 silencing transcription factor (REST) binds to this element and prevents the expression of neuronal genes in nonneuronal cells.[28] REST is a critical protein in development as it is required for viability in knockout mice, and transient expression of a dominant negative form of this protein causes precocious neuronal differentiation.[29] Downregulation of REST gene expression is thus essential for proper neuronal differentiation.[29] Accordingly, links between dysregulated REST activity and the selective loss of neurons has been shown in a study of Down's syndrome.[30]

REST contains two distinct repressor domains, one located at the N-terminus and the other at the C-terminus of the protein.[31] Two distinct neuronal repressor complexes have now been isolated containing both REST and HDACs. The first of these complexes involves direct interactions with mSin3A/B at the N-terminus which then recruits HDACs to repress gene expression.[29,32,33] The C-terminal repression domain associates with a novel protein called CoREST.[29] This protein also interacts with HDACs through its SANT domain and has been shown to be essential for repression.[34] Recent research has shown that the REST/CoREST complex is essential for actively repressing genes essential for the neuronal phenotype.[29] The ATP-dependent remodeling complex SWI/SNF also plays a role in REST mediated neuronal gene regulation as it has recently emerged that CoREST recruits several SWI/SNF members, indicating that active chromatin remodeling is an element in REST-mediated repression.[29]

Other HDAC-related mechanisms have been implicated in neuronal gene transcription or neuronal integrity. For instance, the myelin transcription factor 1 (Myt1) gene family has recently been shown to regulate neural transcription by the recruitment of a Sin3B histone deacetylase containing complex.[35] Recently it has also been shown that the intracellular trafficking of histone deacetylase HDAC4 from its normal location within the cytoplasm to the nucleus is a critical component of low-potassium or excitotoxic glutamate induced neuronal cell death.[36]

It has also recently been demonstrated that the Class II and Class III histone deacetylases play pivotal roles in the survival and differentiation of neurons.[37,38] For instance, inactivation of an MEF2D/ HDAC5 complex by depolarization-mediated calcium influx promotes cerebellar granule neuron survival.[39]

Motor neuron genes modulated by HDACs. In addition to RE1/NSRE-directed repression of specific genes, motor neurons have been shown to express unique combinations of LIM-type homeodomain factors to define motor column identity by regulating particular gene expression profiles.[40] LIM homeodomain transcription factors have been shown to be regulated through a complex containing HDACs,[41] and as such motor neuron pathfinding may be guided through an HDAC-directed process.

E2f transcription factor and HDACs: a link to neuronal survival mechanisms. An essential feature for neuronal survival has also been linked to constitutive repression of E2F1 transcriptional activity through HDAC proteins.[42] Elevated levels of E2f1 leads to neuronal apoptosis[43] and enhanced immune cell proliferation,[44] factors that could be deleterious in MS. It has since been shown that p130 is the predominant Rb family member associated with E2F in neurons, and that its major partner for repression of pro-apoptotic genes is through a p130-E2F4 complex which recruits the chromatin modifiers HDAC1 and Suv39H1 to promote gene silencing and neuron survival.[45] We have also found that HDAC inhibitors reduce levels of E2f class I proteins in vivo,[46] as demonstrated by others in vitro.[47] These observations may help explain why HDAC inhibitors, which induce histone hyperacetylation, block immune cell proliferation[10] and enhance neuronal survival.[48] An example is Valproic acid (VPA), a commonly used mood stabilizer and anti-epileptic drug, also identified as an HDAC inhibitor.[26] Treatment of cultured rat neurons with VPA prevents spontaneous apoptosis, suggesting a role for HDAC inhibition in mediating the neuroprotective action of this drug.[49] In subsequent sections we will discuss this protective role of HDAC inhibitors in more detail.

Role of histone hyperacetylation and neuronal differentiation in other species. The histone acetyltransferase Querkopf has been shown to be critical for the development of the murine cerebral cortex.[50] Further evidence for the importance of histone acetylation in neurogenesis comes from studies in *Drosophila* and *Xenopus*. Mutation of the putative *Drosophila* HAT *enoki mushroom*, gives rise to reduced axonal structures in particular brain regions associated with olfactory learning and memory.[51] In *Xenopus* embryo development, XNGN-1, a member of the neurogenin family and critical regulator of neuronal differentiation recruits two HATs in order to promote neuronal differentiation.[52]

HDAC inhibitors lead to acetylation of the Sp1 transcription factor. Promotion of acetylation of the transcription factor Sp1 by the HDAC inhibitor TSA has been well documented.[9] Acetylated Sp1 is also seen in response to oxidative stress in neuronal cortical cell cultures.[48] Interestingly, HDAC inhibitors not only enhance Sp1 acetylation but also protect neuronal cortical cells from oxidative stress-induced cell death, suggesting that primary Sp1 acetylation in response to oxidative stress is a compensatory, albeit insufficient, anti-oxidant response. Other transcription factors with potential roles in neurodegeneration, whose stability or DNA-binding activity may depend on their acetylation state include E2F,[53] p53[54] and the cAMP response element binding protein (CREB).[55] Activated CREB binds to the promoter regions of a number of genes implicated in neuroprotection,[56] and expression of these genes is enhanced upon recruitment, by CREB, of CBP and P300 proteins that have HAT activity.[57]

HUMAN NEUROLOGIC DISEASES ASSOCIATED WITH HDAC/HAT IMBALANCE

Huntington disease. Huntington disease is an autosomal dominant, late-onset neurodegenerative disease characterized by cognitive dysfunction, psychiatric symptoms and movement disorders.[58] The disease is caused by an expansion of a polyglutamine repeat within the amino terminus of the predominantly cytosolic protein huntingtin (htt). The expanded repeat region results in nuclear translocation and aggregation of the mutant htt, and has been implicated as the causative event in the pathogenesis of this disease.[59] Several studies have since shown that the repeat-containing htt interacts directly with the HATs CBP and P/CAF.[59] This aberrant complex has been shown to associate with p53 and to repress transcription of the Sp1 target gene $p21^{WAF1/CIP1}$.[60] One of the most important features of this association is that the nuclear localization of CBP is altered such that it aggregates into intranuclear inclusions in neuronal cells.[60,61] Thus a depletion of this HAT from its normal localization seems to result in aberrant transcriptional control. However, cell-free assays have shown that the mutant htt protein has the ability to inhibit the activity of three HATs, CBP, p300 and P/CAF,[62] and thus a direct interference mechanism may also be involved. In addition, a cell line

model of neuronal death caused by polyglutamine-expanded htt was associated with degradation of CBP indicating that the mutant htt may function to actively eliminate CBP from the affected neurons.[63] The negative effect on $p21^{WAF1/CIP1}$ transcription by the htt-containing complex may also play a crucial role in neurodegeneration, since $p21^{WAF1/CIP1}$ inhibits cyclin dependent kinases, prevents caspase activation, and enhances neuronal sprouting or survival (reviewed in ref. 64). Recently, another potential neuroprotective mechanism mediated by wild type htt was described, in which htt sequesters REST transcription factor in the neuronal cytoplasm, preventing its nuclear repressive action on neuronal growth and differentiation genes.[65] Overexpression of wild type htt leads, for instance, to induction of a REST target gene, brain-derived neurotrophic factor (BDNF).[66]

Rubinstein-taybi syndrome (RTS). RTS is a developmental, autosomal dominant syndrome characterized by dysmorphic features, mental retardation and an increased risk of cancer.[67] Mutations in CBP have since been shown to be causative for this syndrome,[68] and heterozygous CBP-deficient mouse strains exhibit partial similarities.[69-71] In one mutation analysis a missense mutation was identified which abolished the HAT activity of CBP indicating that the loss of this activity may be the cause of RTS due to unopposed gene repression by HDACs, and the authors suggest that treating patients with HDAC inhibitors may therefore have beneficial effects in these patients.[72] A second mutational screen identified mutations within the PHD domain of CBP resulting in loss of its HAT activity.[73]

Spinocerebellar ataxia 1 (SCA1). This disease, which is caused by expansion of abnormal CAG repeats in the ataxin-1 gene encoding an abnormally elongated polyglutamine tract, is associated with unsteady gait due to spinocerebellar pathway degeneration. Recently, it has been shown that ataxin-1 binds to HDAC3[74] and to the HDAC-binding proteins 14-3-3[75] and SMRT.[74] Perturbation of HDAC corepressor complexes by ataxin-1 may mediate abnormal gene expression that culminates in SCA1 neurodegeneration.

Dentatorubral-pallidoluysian atrophy (DRPLA). DRPLA, is a neurodegenerative condition caused by polyglutamine expansion within the Atrophin-1 protein. Recent studies demonstrated hypoacetylation of histone H3 in brain tissues of a mouse model for this condition.[76]

Amyotrophic lateral sclerosis. Amyotrophic lateral sclerosis (ALS), also known as Lou Gehrig's disease, is a motor neuron disease characterized by progressive degeneration of upper and lower motor neurons. Evidence that histone acetylation may be playing a role in this disease came from studies in mouse models.

In one study, reactive astrocytes from a transgenic mouse model of ALS but not from control mice were found to be immunopositive for CBP.[77] In a different setting, caspase-6 mediated downregulation of CBP was found to occur in amyotrophic lateral sclerosis model mice.[78]

USE OF HDAC INHIBITORS TO TREAT NEURODEGENERATIVE DISEASE OR CEREBRAL ISCHEMIA MODELS

In vivo treatment of Huntington disease models. In a cell culture model treatment of cells with sodium butyrate caused the redistribution of Huntingtin-positive nuclear bodies.[79] Treatment of a *Drosophila* Huntington disease model with an HDAC inhibitor was shown to arrest neurodegeneration and indicates that the use of these compounds in neurodegenerative disorders could prove to be a viable therapeutic option.[62] Similar results were also observed for the yeast model of expanded polyglutamine, where treatments with the inhibitor TSA mitigated the effects on affected gene promoters.[80] More recently, it has been demonstrated that the HDAC inhibitors SAHA and sodium butyrate can ameliorate Huntington motor deficits and characteristic neuropathology and extend survival in mouse models.[81-83]

One issue concerning the use of HDAC inhibitors to treat this disease has been whether mutant Htt protein affects the HDAC activity in declining neurons, but a recent study has shown that levels and activity of HDAC are unaffected in such cells.[84]

An initial Phase I clinical study on the therapeutic potential of sodium phenylbutyrate in the treatment of huntingtons have been initiated, and a 12 gene biomarker showed a small but statistically significant decrease in the expression of this marker set in 10 of 12 patients after four weeks of treatment. When the marker genes were scored individually, 8 of 12 genes showed significant decreases in expression in response to four weeks of treatment with phenylbutyrate,[85] indicating that this drug may have a therapeutic benefit in the treatment of this disease.

In vivo treatment of motor neuron disease (SMA, SBMA and ALS) models. Spinal muscular atrophy (SMA) is an autosomal recessive condition in which degeneration of the anterior horn cells of the spinal cord occurs, which leads eventually to muscular paralysis and atrophy. At present, there is no effective treatment for this condition. SMA is typically associated with loss of expression of the survival motor neuron (SMN) gene. Treatment of a mouse model of this disease with sodium butyrate ameliorated the SMA symptoms raising the possibility that treating affected individuals with HDAC inhibitors may be an effective therapeutic modality.[86] It has subsequently been shown that SMN associates with the corepressor mSin3A and consequently with HDACs.[87] In a mouse model of SMA, overexpression of the heat shock protein 70 chaperone ameliorates the SMA phenotype.[88] HDACs complexed with this protein have been shown to have increased catalytic activity.[89] We have shown that treating cells with HDAC inhibitors upregulates the expression of Hsp70,[14] indicating that this may be an additional mechanism by which HDAC inhibitors ameliorate this disorder.

Phenylbutyrate is currently an FDA approved drug for the treatment of cyclic urea disorders but has also been shown to inhibit histone deacetylases.[90] When taken orally, the most common toxicities observed for Phenybutyrate were dyspepsia and fatigue.[91] Phase I studies using intravenous fusion of drug found that dose limiting toxicities included reversible neurocortical toxicity characterized by somnolence and confusion.[92-94] Recently pilot trials for Phenylbutyrate have been carried out for SMA. The results of this study found that the major toxicity observed was temporary stomach ache.[95,96] Oral administration of Phenylbutyrate (triButyrate®) significantly increased SMN expression in the leukocytes of SMA patients.[96]

Another murine motor neuron disease model, spinal and bulbar muscular atrophy (SBMA), has been shown recently to respond favorably to oral treatment with the HDAC inhibitor sodium butyrate.[97] SBMA is caused by an expanded polyglutamine repeat in the androgen receptor and is characterized by motor neuron loss in the brainstem and spinal cord. Dorsal root sensory neurons are also affected. The histopathological features are ameliorated by treatment with sodium butyrate in this model, which correlates with tissue histone hyperacetylation.[97]

Rouaux et al. demonstrated that apoptotic neurons from an amyotrophic lateral sclerosis (ALS) mouse model indeed have reduced histone acetylation, indicating that HDAC inhibitors could

potentially target this abnormality in ALS as well.[78] Preliminary experiments using cultured cells indicated that histone deacetylase inhibitors could prove to have therapeutic benefit.[98] We have shown in the ALS G93A SOD1 model that phenylbutyrate prolongs the survival and improves disability in this transgenic model .[99] An additional study has shown the benefit of a combination therapy containing phenylbutyrate and the antioxidant (AEOL 10150) to achieve an increased overall survival of 19%.[100]

Dentatorubral-pallidoluysian atrophy (DRPLA). Sodium butyrate treatment for a mouse model of DRPLA ameliorated the neurodegenerative phenotype and relieved the histone hypoacetylation observed in this model.[76]

In vivo treatment of cerebral ischemia models. Animal models of focal cerebral ischemia and reperfusion, induced by occlusion of the middle cerebral artery, have also responded favorably to treatment with the HDAC inhibitors vaproic acid and TSA, by a reduction in infarct volume.[101,102] In the ischemic cortex and striatum of vehicle treated rats, there was a decrease in histone H3 acetylation, which was reversed by treatment with valproic acid and correlated with elevated tissue levels of the neuroprotective chaperone HSP70 101.

POTENTIAL FOR THE USE OF HDAC INHIBITORS AS A THERAPEUTIC MODALITY IN MS

Immune system effects of HDAC inhibitors that have relevance to MS. The functional classification of T cells is based upon the cytokine profiles each particular group generates upon their activation.[103] Pro-inflammatory (IFN-γ-mediated Th1 phenotype) $CD4^+$ T cells have been shown to be pathogenic in the EAE animal model of MS.[104] The production of IFN-γ induces antigen presenting cells to secrete IL-12, a cytokine that potently stimulates differentiation of naive (Th0) cells into Th1 cells.[105] Mice deficient for the IL-12p40 gene are resistant to EAE and neutralizing antibodies to IL-12 inhibit the in vivo development of EAE.[105] Several recent studies have shown the potential for the use of HDAC inhibitor therapy to limit IL-12 effects in vitro. In particular, sodium butyrate has been shown to inhibit T cell proliferation and the expression of both IL-12 and IFN-γ in human immune cells.[10,13,106]

Other pro-inflammatory stimuli, such as lipopolysaccharide (LPS) and TNF-α activate several key genes through the nuclear transcription factor NF-κB, which plays pivotal roles in the regulation of immune reactivity, processes in which HDACs are also known to be involved. Several key pro-inflammatory genes, such as TNF-α and iNOS, are dependent on NF-κB transcription. NF-κB has been shown to associate with HDACs to repress gene expression,[25] or with HATs to activate gene expression.[25] In addition to associating with HATs NF-κB has also been shown to be reversibly acetylated. Deacetylation by HDACs is crucial to regulate the duration of its transcriptional activity.[107] Treatment of cells with HDAC inhibitors was shown to induce the expression of various genes including IL-6 and IL-8.[108,109] Other studies have shown that butyrate can suppress NF-κB activation and its related responses.[110] It appears that butyrate suppresses the secretion of IL-8 in normal cells but enhances its expression in cancer cells.[111] However, another study has shown that treating cancer cells with HDAC inhibitors downregulates IL-8 expression.[112] Thus, HDAC inhibitors may therefore be able to inhibit NF-κB-mediated inflammatory responses by a variety of mechanisms in normal cells. Some evidence for this is provided by a study in Crohn's disease which demonstrated that butyrate was capable of inhibiting NF-κB-mediated inflammation and reducing pro-inflammatory cytokine mRNA expression.[113] Butyrate may inhibit this response by interfering with the process of degradation of I-κB, an inhibitory protein that blocks NF-κB translocation to the nucleus. Thus, sequestration of NF-κB in the cytoplasm may be a mechanism by which sodium butyrate also acts to exert anti-inflammatory effects in a manner similar to proteasome inhibitors.[110, 113, 114] The result is a decrease in the pro-demyelinating TNF-α and the pro-oxidant iNOS by HDAC inhibitors,[115] an outcome of potential benefit for MS.

Th1 cells also secrete the proinflammatory cytokine IL-2. HDAC inhibitors inhibit the expression of IL-2[116] and IL-2 mediated gene expression.[117] IL-2 itself seems to modulate HDAC1 gene expression in the mouse.[118] However, human studies have not shown a direct regulatory role for this cytokine in the regulation of HDAC1.[119] We have shown downregulation of the IL-2 receptor mRNA in mouse CNS tissues by TSA,[46] as demonstrated for cells in vitro[120] indicating that HDAC inhibitors inhibit the IL-2 pathway at several levels. Additional evidence for the potential use of HDAC inhibitors in blocking CD4+ T cells comes from early experiments which showed that n-butyrate could induce antigen-specific unresponsiveness in CD4+ T cells in vivo. Previous stimulation by antigen was found to be necessary for this effect as cells treated with n-butyrate alone were unaffected.[121] A follow-up study using butyric acid derivatives to induce antigen specific T cell inactivation confirmed these early results and demonstrated that these derivatives sequestered activated Th1 cells into the G_1 phase of the cell cycle. This suggests that such compounds have the potential to induce energy in activated $CD4^+$ T cells.[122]

A different type of $CD4^+$ T helper cell has been shown to have an anti-inflammatory, pro-humoral and protective role in EAE. These cells are termed Th2 cells, and produce IL-4, IL5, IL-10 or IL-13. Treating cells with HDAC inhibitors has been shown to increase the expression of IL-10.[106] However, in systemic lupus erythematosus (SLE) cells, treatment with HDAC inhibitors actually downregulated expression of IL-10 and other cytokines, suggesting that these compounds may have disease-specific effects.[123] The anti-inflammatory role of HDAC inhibitors has been further demonstrated by the ability of these agents to decrease glomerulonephritis in the MRL-lpr/lpr mouse model of lupus.[123]

A third type of Th cell (Th3) has been associated with EAE. These are cells which produce TGF-β1 and serve a protective role in this model.[124] T cell clones isolated from MS patients presenting with acute attacks were predominantly Th1-like, secreted no TGF-β1 and those isolated following remission belonged to a mixture of Th0, Th1 and Th2.[125] TGF-β1 signaling has been shown to be intimately tied with HATs and HDACs.[9] We and others have shown that treatments of cells with HDAC inhibitors induces TGF-β1 expression and signaling,[9,126] which by virtue of its immunosuppressive role may help ameliorate MS.

MS is a polygenic disease and its complex nature is reflected in its clinical heterogeneity. The strongest genetic association observed for MS lies in the 6p21 chromosomal region harboring the MHC class II genes. These heterodimeric cell surface glycoproteins are comprised of heavy and light chains, bind and display peptide antigens in a complex that is recognized by $CD4^+$ T lymphocytes and leads to the generation of an immune reaction. To date T cells reactive to the major constituents of myelin have been identified in EAE, have high antigenic affinity to MHC-presented myelin fragments, and appear to drive the disease process.[4]

The regulation of expression of the MHC-II genes has recently been shown to be intimately linked to both HATs and HDACs. The transactivator CIITA controls MHC-II gene expression and is recruited to these gene promoters as part of an enhanceosome complex that includes the HATs p300 and CBP.[127] In addition to associating with HATs, CIITA was recently shown to have intrinsic HAT activity,[127] and is itself acetylated.[127] Thus activation of MHC-II genes appear to be governed in part through the action of HATs. Repression of MHC-II genes also involves HDACs. The transcriptional repressor Blimp-1 (PRDI-BF1) has been shown to directly regulate the expression of CIITA.[128] This protein has been shown to associate with HDACs both indirectly through the recruitment of the Groucho family of corepressors,[129] and directly by recruiting HDAC1 or HDAC2.[130] The expression of the Class II HLA-DR genes has been shown to be repressed through the action of HDAC1.[131] Accordingly, HDAC inhibitors upregulate the expression of MHC-II genes.[127] Thus, HDAC inhibitors would appear to enhance the risk of disease progression in MS as they may enhance this aspect (i.e., antigen presentation by MHC to the T cell receptor) of T cell activation rather than abrogate it.

However, besides the first stimulatory event provided by MHC presentation of antigen, other (i.e., costimulatory) signals are required for T cell activation. The binding of costimulatory molecules on the antigen presenting cell (APC) with their ligands on the T cell surface are required for T cells to undergo signals that culminate in activation, clonal expansion and cytotoxicity. One such pathway consists of the binding of CD28 on T cells with B7.1 or B7.2 costimulatory molecules on the APC. In MS patients it has been shown that the upregulation of costimulatory molecules may be important for the pathogenesis of this disease. In one study when MS plaques were compared against inflammatory stroke lesions from the same brain it was found that while B7.2 expression was observed in both, expression of B7.1 was restricted to just the MS plaques.[132] Similar studies found enhanced expression of B7.1 on B cells isolated from the peripheral blood and spinal fluid of MS patients compared to controls, while B7.2 levels were similar.[133] A reduction in the expression of B7.1 might help ameliorate the pathogenesis of MS. HDAC inhibitors prevent IFN-γ-induced upregulation of B7.1 expression and enhance constitutive as well as cytokine induced expression of B7.2,[134] which may have beneficial effects in MS, as B7-2 may have a pro-Th2 function.

One of the hallmarks of MS involves perivascular infiltration of inflammatory cells into the CNS, requiring both the adhesion and transmigration of these cells through the blood brain barrier (BBB). It is likely that matrix metalloproteinases (MMPs), which are expressed by activated T cells, monocytes, astrocytes and microglial cells, may be involved in this perivascular transmigration process, allowing the inflammatory cells access to the CNS. In MS patients the majority of macrophages found in active and necrotic lesions stain positive for MMP-1, -2, -3 and -9, and a small number of astrocytes were also found to be MMP-2, -3 and -9 positive in acute and chronic MS lesions.[135]

Various studies have investigated the effects of HDAC inhibitors on MMP expression. One early report indicated that treating epithelial cells with sodium butyrate led to a slight induction of MMP-9.[136] However a recent study using the HDAC inhibitor apicidin in breast epithelial cells found no effect on MMP-9 expression, but that MMP-2 was specifically downregulated by this inhibitor.[137] In addition, a key negative regulator of matrix metalloproteinases (RECK), was found to be upregulated following treatment with trichostatin A, which resulted in inhibited MMP2 activation in the cell line used.[138] In rat colon cancer cells, downregulation of both MMP-2 and MMP-9 were observed following treatments with sodium butyrate.[139] As a caveat, butyrate has been shown to enhance the expression of stromelysin-1 (MMP-3) in mesenchymal cells, but only after the expression of this MMP had been induced by cytokines. By itself, butyrate was unable to stimulate stromelysin expression.[140]

The regulation of MMPs is tightly linked to the expression of tissue inhibitors of metalloproteinases or TIMPs. Recent studies have shown that invasion of human colon cancer cells can be inhibited by butyrate. The mechanism involves upregulating the activity of TIMP-1 and TIMP-2.[141] Treating MS patients with HDAC inhibitors may therefore prevent the breakdown of the BBB and thus effectively block entry of inflammatory cells.

Finally, HDAC inhibitors have been shown to enhance expression in vitro of IFN-α and β,[142] both known to have beneficial effects in MS patients. Thus, the anti-inflammatory effects of HDAC inhibitors are broad and reflect a combined action on transcriptional mechanisms that converge at the interface of cell survival, differentiation or activation.

HDAC inhibitors ameliorate myelin oligodendrocyte glycoprotein (MOG)-induced EAE via anti-inflammatory and neuroprotective mechanisms. We recently completed a study demonstrating that the HDAC inhibitor TSA ameliorates EAE disability and spinal cord inflammation, demyelination and axonal loss, and used microarrays and QRT-PCR to assess spinal cord gene regulation in vivo by this inhibitor.[46] Multiple genes are upregulated by TSA in spinal cords of EAE mice, including anti-oxidant, neuroprotective and neuronal differentiation genes. Not surprisingly, several neuronal trait genes known to be repressed by REST-HDAC complexes, such as sodium channel Nav1.2 and dopamine beta hydroxylase, are upregulated by TSA in the CNS of these mice. Genes known to harbor Sp1-binding sites, such as the anti-oxidant glutathione peroxidase, were also upregulated, and a number of E2f1 target genes were downregulated in EAE spinal cords. The latter observation may be of particular relevance to MS, as we recently reported activation of the E2f pathway in peripheral blood of MS patients.[143] Pro-inflammatory genes such as IL-12p35, IL-2 receptor and the costimulatory molecule CD28, all previously shown to be downregulated in cells in vitro,[106] were downregulated by TSA in the spleen of these EAE animals. Strikingly, TSA treatment led to histone hyperacetylation and inhibition of caspases 3 and 9 in spinal cords, which correlated with preservation of neuronal counts and spinal cord volume, as compared to spinal cords from the vehicle treated mice.

Neuronal apoptosis has recently been shown to occur concomitantly with reduced histone acetylation[144] or elevated E2F1 transcription factor activity.[43] E2F1-induced apoptosis is executed via caspase 3 activation.[43] Caspase 3 is activated in EAE CNS tissues,[145] and correlates with optic neuritis-related disability.[14] In EAE mice treated with TSA, we showed that the drug resulted in decreased spinal cord caspase 3 activation.[46]

CONCLUSIONS

The previous sections have described a potential role for HDAC/HAT imbalance in inflammation and neurodegeneration, which could influence MS mechanisms. We had previously shown that HDAC mRNAs were elevated in activated immune cells,[10] suggesting their potential roles as activation markers or treatment targets. In the EAE model, we showed that TSA activates a transcriptional program that culminates in decreased caspase 3 activation.[46] The dual goal of

transcriptional therapy with HDAC inhibitors is therefore to a) suppress the overactive immune system and b) derepress HDAC-dependent anti-oxidant and neuroprotective (e.g., pro-neuronal differentiation and anti-caspase) genetic programs that help attenuate the ongoing CNS insult. HDAC inhibitors affect many of the inflammatory and pro-apoptotic pathways proposed to be involved in the disease process in EAE.

Because of their ability to upregulate developmentally-silenced fetal globin genes, HDAC inhibitors have been used effectively in patients with hemoglobinopathies, such as sickle cell anemia and thalassemia,[147] and this treatment has been proven safe. Also safe has been the treatment of children with ornithine transcarbamylase deficiency, an urea cycle disorder, with the HDAC inhibitor sodium phenylbutyrate,[148] which acts in this disorder by activating new pathways of waste-nitrogen excretion. Several HDAC inhibitors are thus tolerable by the oral route at doses sufficient to achieve biological activity,[149] and some are undergoing phase II trials in human cancer.[23] Although side effects have been reported, such as dyspepsia, fatigue, nausea and hypocalcemia, these are reversible upon dose adjustment. This reversibility of action upon drug withdrawal makes this class of drugs advantageous in comparison to other chemotherapeutic interventions that irreversibly affect DNA. It therefore seems justified to initiate testing of these drugs in pilot clinical trials for their applicability in MS.

References

1. Kornek B, Lassmann H. Axonal pathology in multiple sclerosis. A historical note. Brain Pathol 1999; 9:651-6.
2. Trapp BD, Ransohoff R, Rudick R. Axonal pathology in multiple sclerosis: Relationship to neurologic disability. Curr Opin Neurol 1999; 12:295-302.
3. Rieckmann P. Improving MS patient care. J Neurol 2004; 251:v69-v73.
4. Sercarz EE. Driver clones and determinant spreading. J Autoimmun 2000; 14:275-7.
5. Burgoon MP, Gilden DH, Owens GP. B cells in multiple sclerosis. Front Biosci 2004; 9:786-96.
6. Lucchinetti C, Bruck W, Parisi J, Scheithauer B, Rodriguez M, Lassmann H. Heterogeneity of multiple sclerosis lesions: Implications for the pathogenesis of demyelination. Ann Neurol 2000; 47:707-17.
7. Rolak LA. Multiple sclerosis treatment 2001. Neurol Clin 2001; 19:107-18.
8. Gray SG, Ekström TJ. The human histone deacetylase family. Exp Cell Res 2001; 262:75-83.
9. Gray SG, Teh BT. Histone acetylation/deacetylation and cancer: An "open" and "shut" case? Curr Mol Med 2001; 1:401-29.
10. Dangond F, Hafler DA, Tong JK, Randall J, Kojima R, Utku N, Gullans SR. Differential display cloning of a novel human histone deacetylase (HDAC3) cDNA from PHA-activated immune cells. Biochem Biophys Res Commun 1998; 242:648-52.
11. Dangond F, Foerzner D, Weremowicz S, Morton CC, Beier DR, Gullans SR. Cloning and expression of a murine histone deacetylase 3 (mHdac3) cDNA and mapping to a region of conserved synteny between murine chromosome 18 and human chromosome 5. Mol Cell Biol Res Commun 1999; 2:91-6.
12. Dangond F, Henriksson M, Zardo G, Caiafa P, Ekström TJ, Gray SG. Differential expression of class I HDACs: Roles of cell density and cell cycle. Int J Oncol 2001; 19:773-7.
13. Dangond F, Gullans SR. Differential expression of human histone deacetylase mRNAs in response to immune cell apoptosis induction by trichostatin A and butyrate. Biochem Biophys Res Commun 1998; 247:833-7.
14. Gray SG, Iglesias AH, Teh BT, Dangond F. Modulation of splicing events in histone deacetylase 3 by various extracellular and signal transduction pathways. Gene Expr 2003; 11:13-21.
15. Lizcano F, Koibuchi N, Fukuda H, Dangond F, Chin WW. Cell type-specific roles of histone deacetylase in TR ligand- independent transcriptional repression. Mol Cell Endocrinol 2001; 172:13-20.
16. Yang XJ. The diverse superfamily of lysine acetyltransferases and their roles in leukemia and other diseases. Nucleic Acids Res 2004; 32:959-76.
17. Gregoretti I, Lee YM, Goodson HV. Molecular evolution of the histone deacetylase family: Functional implications of phylogenetic analysis. J Mol Biol 2004; 338:17-31.
18. Gray SG. Histone acetyltransferases and histone deacetylases in gene regulation and as drug targets. In: Devita Jr VT, Hellman S, Rosenberg SA, eds. Progress in Oncology 2004. Sudbury Jones and Bartlett, 2004:99-128.
19. Boffa LC, Vidali G, Mann RS, Allfrey VG. Suppression of histone deacetylation in vivo and in vitro by sodium butyrate. J Biol Chem 1978; 253:3364-6.
20. Boffa LC, Mariani MR, Parker MI. Selective hypermethylation of transcribed nucleosomal DNA by sodium butyrate. Exp Cell Res 1994; 211:420-3.
21. Lea MA, Randolph VM. Induction of reporter gene expression by inhibitors of histone deacetylase. Anticancer Res 1998; 18:2717-22.
22. Yoshida M, Kijima M, Akita M, Beppu T. Potent and specific inhibition of mammalian histone deacetylase both in vivo and in vitro by trichostatin A. J Biol Chem 1990; 265:17174-9.
23. Minucci S, Pelicci PG. Histone deacetylase inhibitors and the promise of epigenetic (and more) treatments for cancer. Nat Rev Cancer 2006; 6:38-51.
24. Cousens LS, Gallwitz D, Alberts BM. Different accessibilities in chromatin to histone acetylase. J Biol Chem 1979; 254:1716-23.
25. Gray SG, De Meyts P. Role of histone and transcription factor acetylation in diabetes pathogenesis. Diabetes Metab Res Rev 2005; 21:416-33.
26. Yoo CB, Jones PA. Epigenetic therapy of cancer: Past, present and future. Nat Rev Drug Discov 2006; 5:37-50.
27. Sarkander HI, Fleischer-Lambropoulos H, Brade WP. A comparative study of histone acetylation in neuronal and glial nuclei enriched rat brain fractions. FEBS Lett 1975; 52:40-3.
28. Belyaev ND, Wood IC, Bruce AW, Street M, Trinh JB, Buckley NJ. Distinct RE1 silencing transcription factor-containing complexes interact with different target genes. J Biol Chem 2004; 279:556-61.
29. Ballas N, Grunseich C, Lu DD, Speh JC, Mandel G. REST and its corepressors mediate plasticity of neuronal gene chromatin throughout neurogenesis. Cell 2005; 121:645-57.
30. Bahn S, Mimmack M, Ryan M, Caldwell MA, Jauniaux E, Starkey M, Svendsen CN, Emson P. Neuronal target genes of the neuron-restrictive silencer factor in neurospheres derived from fetuses with Down's syndrome: A gene expression study. Lancet 2002; 359:310-5.
31. Thiel G, Lietz M, Cramer M. Biological activity and modular structure of RE1-silencing transcription factor (*REST*), a repressor of neuronal genes. J Biol Chem 1998; 273:26891-9.
32. Huang YF, Myers SJ, Dingledine R. Transcriptional repression by REST: Recruitment of *Sin3A* and *histone* deacetylase to neuronal genes. Nat Neurosci 1999; 2:867-72.
33. Roopra A, Sharling L, Wood IC, Briggs T, Bachfischer U, Paquette AJ, Buckley NJ. Transcriptional repression by neuron-restrictive silencer factor is mediated via the SIN3-histone deacetylase complex. Mol Cell Biol 2000; 20:2147-57.
34. You A, Tong JK, Grozinger CM, Schreiber SL. CoREST is an integral component of the CoREST- human histone deacetylase complex. Proc Natl Acad Sci USA 2001; 98:1454-8.
35. Romm E, Nielsen JA, Kim JG, Hudson LD. Myt1 family recruits histone deacetylase to regulate neural transcription. J Neurochem 2005; 93:1444-53.
36. Bolger TA, Yao TP. Intracellular trafficking of histone deacetylase 4 regulates neuronal cell death. J Neurosci 2005; 25:9544-53.
37. Anekonda TS, Reddy PH. Neuronal protection by sirtuins in Alzheimer's disease. J Neurochem 2006; 96:305-13.
38. Ajamian F, Suuronen T, Salminen A, Reeben M. Upregulation of class II histone deacetylases mRNA during neural differentiation of cultured rat hippocampal progenitor cells. Neurosci Lett 2003; 346:57-60.
39. Linseman DA, Bartley CM, Le SS, Laessig TA, Bouchard RJ, Meintzer MK, Li M, Heidenreich KA. Inactivation of the myocyte enhancer factor-2 repressor histone deacetylase-5 by endogenous Ca2+) //calmodulin-dependent kinase II promotes depolarization-mediated cerebellar granule neuron survival. J Biol Chem 2003; 278:41472-81.
40. Sharma K, Sheng HZ, Lettieri K, Li H, Karavanov A, Potter S, Westphal H, Pfaff SL. LIM homeodomain factors Lhx3 and Lhx4 assign subtype identities for motor neurons. Cell 1998; 95:817-28.
41. Bach I, Rodriguez-Esteban C, Carriere C, Bhushan A, Krones A, Rose DW, Glass CK, Andersen B, Izpisua Belmonte JC, Rosenfeld MG. RLIM inhibits functional activity of LIM homeodomain transcription factors via recruitment of the histone deacetylase complex. Nat Genet 1999; 22:394-9.
42. Boutillier AL, Trinh E, Loeffler JP. Constitutive repression of E2F1 transcriptional activity through HDAC proteins is essential for neuronal survival. Ann NY Acad Sci 2002; 973:438-42.
43. Hou ST, Callaghan D, Fournier MC, Hill I, Kang L, Massie B, Morley P, Murray C, Rasquinha I, Slack R, MacManus JP. The transcription factor E2F1 modulates apoptosis of neurons. J Neurochem 2000; 75:91-100.
44. Wu L, Timmers C, Maiti B, Saavedra HI, Sang L, Chong GT, Nuckolls F, Giangrande P, Wright FA, Field SJ, Greenberg ME, Orkin S, Nevins JR, Robinson ML, Leone G. The E2F1-3 transcription factors are essential for cellular proliferation. Nature 2001; 414:457-62.
45. Liu DX, Nath N, Chellappan SP, Greene LA. Regulation of neuron survival and death by *p130* and associated chromatin modifiers. Genes Dev 2005; 19:719-32.
46. Camelo S, Iglesias AH, Hwang D, Due B, Ryu H, Smith K, Gray SG, Imitola J, Duran G, Assaf B, Langley B, Khoury SJ, Stephanopoulos G, De Girolami U, Ratan RR, Ferrante RJ, Dangond F. Transcriptional therapy with the histone deacetylase inhibitor trichostatin A ameliorates experimental autoimmune encephalomyelitis. J Neuroimmunol 2005; 164:10-21.
47. Suzuki T, Yokozaki H, Kuniyasu H, Hayashi K, Naka K, Ono S, Ishikawa T, Tahara E, Yasui W. Effect of trichostatin A on cell growth and expression of cell cycle- and apoptosis-related molecules in human gastric and oral carcinoma cell lines. Int J Cancer 2000; 88:992-7.

48. Ryu H, Lee J, Olofsson BA, Mwidau A, Deodoglu A, Escudero M, Flemington E, Azizkhan-Clifford J, Ferrante RJ, Ratan RR. Histone deacetylase inhibitors prevent oxidative neuronal death independent of expanded polyglutamine repeats via an Sp1-dependent pathway. Proc Natl Acad Sci USA 2003; 100:4281-6.
49. Jeong MR, Hashimoto R, Senatorov VV, Fujimaki K, Ren M, Lee MS, Chuang DM. Valproic acid, a mood stabilizer and anticonvulsant, protects rat cerebral cortical neurons from spontaneous cell death: A role of histone deacetylase inhibition. FEBS Lett 2003; 542:74-8.
50. Thomas T, Voss AK, Chowdhury K, Gruss P. Querkopf, a MYST family histone acetyltransferase, is required for normal cerebral cortex development. Development 2000; 127:2537-48.
51. Scott EK, Lee T, Luo L. enok encodes a *Drosophila* putative histone acetyltransferase required for mushroom body neuroblast proliferation. Curr Biol 2001; 11:99-104.
52. Koyano-Nakagawa N, Wettstein D, Kintner C. Activation of *Xenopus* genes required for lateral inhibition and neuronal differentiation during primary neurogenesis. Mol Cell Neurosci 1999; 14:327-39.
53. Martinez-Balbas MA, Bauer UM, Nielsen SJ, Brehm A, Kouzarides T. Regulation of E2F1 activity by acetylation. Embo J 2000; 19:662-71.
54. Gu W, Roeder RG. Activation of p53 sequence-specific DNA binding by acetylation of the p53 C-terminal domain. Cell 1997; 90:595-606.
55. Lu Q, Hutchins AE, Doyle CM, Lundblad JR, Kwok RP. Acetylation of cAMP-responsive element-binding protein (CREB) by CREB-binding protein enhances CREB-dependent transcription. J Biol Chem 2003; 278:15727-34.
56. Wilson BE, Mochon E, Boxer LM. Induction of bcl-2 expression by phosphorylated CREB proteins during B-cell activation and rescue from apoptosis. Mol Cell Biol 1996; 16:5546-56.
57. Michael LF, Asahara H, Shulman AI, Kraus WL, Montminy M. The phosphorylation status of a cyclic AMP-responsive activator is modulated via a chromatin-dependent mechanism. Mol Cell Biol 2000; 20:1596-603.
58. Davies S, Ramsden DB. Huntington's disease. Mol Pathol 2001; 54:409-13.
59. Di Prospero NA, Fischbeck KH. Therapeutics development for triplet repeat expansion diseases. Nat Rev Genet 2005; 6:756-65.
60. Steffan JS, Kazantsev A, Spasic-Boskovic O, Greenwald M, Zhu YZ, Gohler H, Wanker EE, Bates GP, Housman DE, Thompson LM. The Huntington's disease protein interacts with p53 and CREB-binding protein and represses transcription. Proc Natl Acad Sci USA 2000; 97:6763-8.
61. Nucifora Jr FC, Sasaki M, Peters MF, Huang H, Cooper JK, Yamada M, Takahashi H, Tsuji S, Troncoso J, Dawson VL, Dawson TM, Ross CA. Interference by huntingtin and atrophin-1 with cbp-mediated transcription leading to cellular toxicity. Science 2001; 291:2423-8.
62. Steffan JS, Bodai L, Pallos J, Poelman M, McCampbell A, Apostol BL, Kazantsev A, Schmidt E, Zhu YZ, Greenwald M, Kurokawa R, Housman DE, Jackson GR, Marsh JL, Thompson LM. Histone deacetylase inhibitors arrest polyglutamine-dependent neurodegeneration in *Drosophila*. Nature 2001; 413:739-43.
63. Jiang H, Nucifora Jr FC, Ross CA, DeFranco DB. Cell death triggered by polyglutamine-expanded huntingtin in a neuronal cell line is associated with degradation of CREB-binding protein. Hum Mol Genet 2003; 12:1-12.
64. Langley B, Gensert JM, Beal MF, Ratan RR. Remodeling chromatin and stress resistance in the central nervous system: Histone deacetylase inhibitors as novel and broadly effective neuroprotective agents. Curr Drug Targets CNS Neurol Disord 2005; 4:41-50.
65. Zuccato C, Tartari M, Crotti A, Goffredo D, Valenza M, Conti L, Cataudella T, Leavitt BR, Hayden MR, Timmusk T, Rigamonti D, Cattaneo E. Huntingtin interacts with *REST/NRSF* to modulate the transcription of *NRSE*-controlled neuronal genes. Nat Genet 2003; 35:76-83.
66. Zuccato C, Ciammola A, Rigamonti D, Leavitt BR, Goffredo D, Conti L, MacDonald ME, Friedlander RM, Silani V, Hayden MR, Timmusk T, Sipione S, Cattaneo E. Loss of huntingtin-mediated *BDNF* gene transcription in Huntington's disease. Science 2001; 293:493-8.
67. Rubinstein JH, Taybi H. Broad Thumbs and toes and facial abnormalities. Am J Dis Child 1963; 105:588-608.
68. Bartsch O, Schmidt S, Richter M, Morlot S, Seemanová E, Wiebe G, Rasi S. DNA sequencing of *CREBBP* demonstrates mutations in 56% of patients with Rubinstein-Taybi syndrome (RSTS) and in another patient with incomplete RSTS. Hum Genet 2005; 117:485-93.
69. Oike Y, Hata A, Mamiya T, Kaname T, Noda Y, Suzuki M, Yasue H, Nabeshima T, Araki K, Yamamura K. Truncated CBP protein leads to classical *Rubinstein-Taybi* syndrome phenotypes in mice: Implications for a dominant-negative mechanism. Hum Mol Genet 1999; 8:387-96.
70. Tanaka Y, Naruse I, Maekawa T, Masuya H, Shiroishi T, Ishii S. Abnormal skeletal patterning in embryos lacking a single Cbp allele: A partial similarity with Rubinstein-Taybi syndrome. Proc Natl Acad Sci USA 1997; 94:10215-20.
71. Tanaka Y, Naruse I, Hongo T, Xu M, Nakahata T, Maekawa T, Ishii S. Extensive brain hemorrhage and embryonic lethality in a mouse null mutant of *CREB*-binding protein. Mech Dev 2000; 95:133-45.
72. Murata T, Kurokawa R, Krones A, Tatsumi K, Ishii M, Taki T, Masuno M, Ohashi H, Yanagisawa M, Rosenfeld MG, Glass CK, Hayashi Y. Defect of histone acetyltransferase activity of the nuclear transcriptional coactivator CBP in *Rubinstein-Taybi syndrome*. Hum Mol Genet 2001; 10:1071-6.
73. Kalkhoven E, Roelfsema JH, Teunissen H, den Boer A, Ariyurek Y, Zantema A, Breuning MH, Hennekam RCM, Peters DJM. Loss of CBP acetyltransferase activity by *PHD* finger mutations in *Rubinstein-Taybi* syndrome. Hum Mol Genet 2003; 12:441-50.
74. Tsai CC, Kao HY, Mitzutani A, Banayo E, Rajan H, McKeown M, Evans RM. Ataxin 1, a SCA1 neurodegenerative disorder protein, is functionally linked to the silencing mediator of retinoid and thyroid hormone receptors. Proc Natl Acad Sci USA 2004; 101:4047-52.
75. Chen HK, Fernandez-Funez P, Acevedo SF, Lam YC, Kaytor MD, Fernandez MH, Aitken A, Skoulakis EM, Orr HT, Botas J, Zoghbi HY. Interaction of akt-phosphorylated ataxin-1 with 14-3-3 mediates neurodegeneration in spinocerebellar ataxia type 1. Cell 2003; 113:457-68.
76. Ying M, Xu R, Wu X, Zhu H, Zhuang Y, Han M, Xu T. Sodium butyrate ameliorates histone hypoacetylation and neurodegenerative phenotypes in a mouse model for *DRPLA*. J Biol Chem 2005.
77. Chung YH, Joo KM, Lee YJ, Kim MJ, Cha CI. Reactive astrocytes express cAMP-response-element-binding protein (CREB) binding protein (*CBP*) in the central nervous system of transgenic mice expressing a human *Cu/Zn* superoxide dismutase mutation. Neurosci Lett 2003; 343:159-62.
78. Rouaux C, Jokic N, Mbebi C, Boutillier S, Loeffler JP, Boutillier AL. Critical loss of CBP/p300 histone acetylase activity by caspase-6 during neurodegeneration. EMBO J 2003; 22:6537-49.
79. Kegel KB, Meloni AR, Yi Y, Kim YJ, Doyle E, Cuiffo BG, Sapp E, Wang Y, Qin ZH, Chen JD, Nevins JR, Aronin N, DiFiglia M. Huntingtin is present in the nucleus, interacts with the transcriptional corepressor C-terminal binding protein, and represses transcription. J Biol Chem 2002; 277:7466-76.
80. Hughes RE, Lo RS, Davis C, Strand AD, Neal CL, Olson JM, Fields S. Altered transcription in yeast expressing expanded polyglutamine. Proc Natl Acad Sci USA 2001; 98:13201-6.
81. Ferrante RJ, Kubilus JK, Lee J, Ryu H, Beesen A, Zucker B, Smith K, Kowall NW, Ratan RR, Luthi-Carter R, Hersch SM. Histone deacetylase inhibition by sodium butyrate chemotherapy ameliorates the neurodegenerative phenotype in *Huntington's* disease mice. J Neurosci 2003; 23:9418-27.
82. Hockly E, Richon VM, Woodman B, Smith DL, Zhou X, Rosa E, Sathasivam K, Ghazi-Noori S, Mahal A, Lowden PA, Steffan JS, Marsh JL, Thompson LM, Lewis CM, Marks PA, Bates GP. Suberoylanilide hydroxamic acid, a histone deacetylase inhibitor, ameliorates motor deficits in a mouse model of Huntington's disease. Proc Natl Acad Sci USA 2003; 100:2041-6.
83. Gardian G, Browne SE, Choi DK, Klivenyi P, Gregorio J, Kubilus JK, Ryu H, Langley B, Ratan RR, Ferrante RJ, Beal MF. Neuroprotective effects of phenylbutyrate in the *N171-82Q* transgenic mouse model of Huntington's disease. J Biol Chem 2005; 280:556-63.
84. Hoshino M, Tagawa K, Okuda T, Murata M, Oyanagi K, Arai N, Mizutani T, Kanazawa I, Wanker EE, Okazawa H. Histone deacetylase activity is retained in primary neurons expressing mutant huntingtin protein. J Neurochem 2003; 87:257-67.
85. Borovecki F, Lovrecic L, Zhou J, Jeong H, Then F, Rosas HD, Hersch SM, Hogarth P, Bouzou B, Jensen RV, Krainc D. Genome-wide expression profiling of human blood reveals biomarkers for Huntington's disease. Proc Natl Acad Sci USA 2005; 102:11023-8.
86. Chang JG, Hsieh-Li HM, Jong YJ, Wang NM, Tsai CH, Li H. Treatment of spinal muscular atrophy by sodium butyrate. Proc Natl Acad Sci USA 2001; 98:9808-13.
87. Zou J, Barahmand-pour F, Blackburn ML, Matsui Y, Chansky HA, Yang L. Survival motor neuron (SMN) protein interacts with transcription corepressor mSin3A. J Biol Chem 2004; 279:14922-8.
88. Adachi H, Katsuno M, Minamiyama M, Sang C, Pagoulatos G, Angelidis C, Kusakabe M, Yoshiki A, Kobayashi Y, Doyu M, Sobue G. Heat shock protein 70 chaperone overexpression ameliorates phenotypes of the spinal and bulbar muscular atrophy transgenic mouse model by reducing *nuclear-localized* mutant *Androgen* receptor protein. J Neurosci 2003; 23:2203-11.
89. Johnson CA, White DA, Lavender JS, O'Neill LP, Turner BM. Human class I histone deacetylase complexes show enhanced catalytic activity in the presence of ATP and Coimmunoprecipitate with the ATP-dependent chaperone protein Hsp70. J Biol Chem 2002; 277:9590-7.
90. Svechnikova I, Gray SG, Kundrotiene J, Ponthan F, Kogner P, Ekström TJ. Apoptosis and tumor remission in liver tumor xenografts by *4-phenylbutyrate*. Int J Oncol 2003; 22:579-88.
91. Gilbert J, Baker SD, Bowling MK, Grochow L, Figg WD, Zabelina Y, Donehower RC, Carducci MA. A phase I dose escalation and bioavailability study of oral sodium phenylbutyrate in patients with refractory solid tumor malignancies. Clin Cancer Res 2001; 7:2292-300.
92. Gore SD, Weng LJ, Zhai S, Figg WD, Donehower RC, Dover GJ, Grever M, Griffin CA, Grochow LB, Rowinsky EK, Zabalena Y, Hawkins AL, Burks K, Miller CB. Impact of the putative differentiating agent sodium phenylbutyrate on myelodysplastic syndromes and acute myeloid leukemia. Clin Cancer Res 2001; 7:2330-9.
93. Gore SD, Weng LJ, Figg WD, Zhai S, Donehower RC, Dover G, Grever MR, Griffin C, Grochow LB, Hawkins A, Burks K, Zabelena Y, Miller CB. Impact of prolonged infusions of the putative differentiating agent sodium phenylbutyrate on myelodysplastic syndromes and acute myeloid leukemia. Clin Cancer Res 2002; 8:963-70.
94. Carducci MA, Gilbert J, Bowling MK, Noe D, Eisenberger MA, Sinibaldi V, Zabelina Y, Chen TL, Grochow LB, Donehower RC. A Phase I clinical and pharmacological evaluation of sodium phenylbutyrate on an 120-h infusion schedule. Clin Cancer Res 2001; 7:3047-55.

95. Mercuri E, Bertini E, Messina S, Pelliccioni M, D'Amico A, Colitto F, Mirabella M, Tiziano FD, Vitali T, Angelozzi C, Kinali M, Main M, Brahe C. Pilot trial of phenylbutyrate in spinal muscular atrophy. Neuromuscul Disord 2004; 14:130-5.
96. Brahe C, Vitali T, Tiziano FD, Angelozzi C, Pinto AM, Borgo F, Moscato U, Bertini E, Mercuri E, Neri G. Phenylbutyrate increases *SMN* gene expression in spinal muscular atrophy patients. Eur J Hum Genet 2005; 13:256-9.
97. Minamiyama M, Katsuno M, Adachi H, Waza M, Sang C, Kobayashi Y, Tanaka F, Doyu M, Inukai A, Sobue G. Sodium butyrate ameliorates phenotypic expression in a transgenic mouse model of spinal and bulbar muscular atrophy. Hum Mol Genet 2004; 13:1183-92.
98. Corcoran LJ, Mitchison TJ, Liu Q. A novel action of histone deacetylase inhibitors in a protein aggresome disease model. Curr Biol 2004; 14:488-92.
99. Ryu H, Smith K, Camelo SI, Carreras I, Lee J, Iglesias AH, Dangond F, Cormier KA, Cudkowicz ME, H Brown R, Ferrante RJ. Sodium phenylbutyrate prolongs survival and regulates expression of anti-apoptotic genes in transgenic amyotrophic lateral sclerosis mice. J Neurochem 2005; 93:1087-98.
100. Petri S, Kiaei M, Kipiani K, Chen J, Calingasan NY, Crow JP, Beal MF. Additive neuroprotective effects of a histone deacetylase inhibitor and a catalytic antioxidant in a transgenic mouse model of amyotrophic lateral sclerosis. Neurobiol Dis 2005.
101. Ren M, Leng Y, Jeong M, Leeds PR, Chuang DM. Valproic acid reduces brain damage induced by transient focal cerebral ischemia in rats: Potential roles of histone deacetylase inhibition and heat shock protein induction. J Neurochem 2004; 89:1358-67.
102. Qi X, Hosoi T, Okuma Y, Kaneko M, Nomura Y. Sodium 4-phenylbutyrate protects against cerebral ischemic injury. Mol Pharmacol 2004; 66:899-908.
103. Abbas AK, Murphy KM, Sher A. Functional diversity of helper T lymphocytes. Nature 1996; 383:787-93.
104. Kuchroo VK, Das MP, Brown JA, Ranger AM, Zamvil SS, Sobel RA, Weiner HL, Nabavi N, Glimcher LH. B7-1 and B7-2 costimulatory molecules activate differentially the Th1/Th2 developmental pathways: Application to autoimmune disease therapy. Cell 1995; 80:707-18.
105. Bright JJ, Musuro BF, Du C, Sriram S. Expression of IL-12 in CNS and lymphoid organs of mice with experimental allergic encephalitis. J Neuroimmunol 1998; 82:22-30.
106. Saemann MD, Bohmig GA, Osterreicher CH, Burtscher H, Parolini O, Diakos C, Stockl J, Horl WH, Zlabinger GJ. Anti-inflammatory effects of sodium butyrate on human monocytes: Potent inhibition of IL-12 and up-regulation of IL-10 production. Faseb J 2000; 14:2380-2.
107. Chen L, Fischle W, Verdin E, Greene WC. Duration of nuclear NF-kappaB action regulated by reversible acetylation. Science 2001; 293:1653-7.
108. Ashburner BP, Westerheide SD, Baldwin Jr AS. The p65 (RelA) subunit of NF-kappaB interacts with the histone deacetylase (HDAC) corepressors *HDAC1* and *HDAC2* to negatively regulate gene expression. Mol Cell Biol 2001; 21:7065-77.
109. Vanden Berghe W, De Bosscher K, Boone E, Plaisance S, Haegeman G. The nuclear *factor-kappa B* engages *CBP/p300* and *histone* acetyltransferase activity for transcriptional activation of the *interleukin-6* gene promoter. J Biol Chem 1999; 274:32091-8.
110. Luhrs H, Gerke T, Boxberger F, Backhaus K, Melcher R, Scheppach W, Menzel T. Butyrate inhibits interleukin-1-mediated nuclear factor-kappa B activation in human epithelial cells. Dig Dis Sci 2001; 46:1968-73.
111. Gibson PR, Rosella O, Wilson AJ, Mariadason JM, Rickard K, Byron K, Barkla DH. Colonic epithelial cell activation and the paradoxical effects of butyrate. Carcinogenesis 1999; 20:539-44.
112. Huang N, Katz JP, Martin DR, Wu GD. Inhibition of *IL-8* gene expression in Caco2 cells by compounds which induce histone hyperacetylation. Cytokine 1997; 9:27-36.
113. Segain JP, Raingeard de la Bletiere D, Bourreille A, Leray V, Gervois N, Rosales C, Ferrier L, Bonnet C, Blottiere HM, Galmiche JP. Butyrate inhibits inflammatory responses through NFkappaB inhibition: Implications for Crohn's disease. Gut 2000; 47:397-403.
114. Yin L, Laevsky G, Giardina C. Butyrate suppression of colonocyte NF-kappa B activation and cellular proteasome activity. J Biol Chem 2001; 276:44641-6.
115. Huuskonen J, Suuronen T, Nuutinen T, Kyrylenko S, Salminen A. Regulation of microglial inflammatory response by sodium butyrate and short-chain fatty acids. Br J Pharmacol 2004; 141:874-80.
116. Takahashi I, Miyaji H, Yoshida T, Sato S, Mizukami T. Selective inhibition of *IL-2* gene expression by trichostatin A, a potent inhibitor of mammalian histone deacetylase. J Antibiotics 1996; 49:453-7.
117. Koyama Y, Adachi M, Sekiya M, Takekawa M, Imai K. Histone deacetylase inhibitors suppress *IL-2*-mediated gene expression prior to induction of apoptosis. Blood 2000; 96:1490-5.
118. Bartl S, Taplick J, Lagger G, Khier H, Kuchler K, Seiser C. Identification of mouse histone deacetylase 1 as a growth factor-inducible gene. Mol Cell Biol 1997; 17:5033-43.
119. Gray SG, Svechnikova I, Hartmann W, O'Connor L, Aguilar-Santelises M, Ekström TJ. IGF-II and IL-2 act synergistically to alter *HDAC1* expression following treatments with trichostatin A. Cytokine 2000; 12:1104-9.
120. Moreira JM, Scheipers P, Sorensen P. The histone deacetylase inhibitor Trichostatin A modulates CD4+ T cell responses. BMC Cancer 2003; 3:30.
121. Gilbert KM, Weigle WO. Th1 cell anergy and blockade in G_1 a phase of the cell cycle. J Immunol 1993; 151:1245-54.
122. Gilbert KM, Wahid R, Fecher NP, Freeman JP, Fifer EK. Potential clinical use of butyric acid derivatives to induce antigen- specific T cell inactivation. J Pharmacol Exp Ther 2000; 294:1146-53.
123. Mishra N, Reilly CM, Brown DR, Ruiz P, Gilkeson GS. Histone deacetylase inhibitors modulate renal disease in the *MRL-lpr/lpr* mouse. J Clin Invest 2003; 111:539-52.
124. Khoury SJ, Hancock WW, Weiner HL. Oral tolerance to myelin basic protein and natural recovery from experimental autoimmune encephalomyelitis are associated with downregulation of inflammatory cytokines and differential upregulation of transforming growth factor beta, interleukin 4, and prostaglandin E expression in the brain. J Exp Med 1992; 176:1355-64.
125. Correale J, Gilmore W, McMillan M, Li S, McCarthy K, Le T, Weiner LP. Patterns of cytokine secretion by autoreactive proteolipid protein- specific T cell clones during the course of multiple sclerosis. J Immunol 1995; 154:2959-68.
126. Gray SG, Yakovleva T, Hartmann W, Tally M, Bakalin G, Ekström TJ. IGF-II enhances trichostatin A-induced *TGFβ1* and *p21^{Waf1,Cip1,Sdi1}* expression in Hep3B cells. Exp Cell Res 1999; 253:618-28.
127. Zika E, Ting JPY. Epigenetic control of MHC-II: Interplay between CIITA and histone-modifying enzymes. Curr Opin Immunol 2005; 17:58-64.
128. Piskurich JF, Lin KI, Lin Y, Wang Y, Ting JP, Calame K. BLIMP-I mediates extinction of major histocompatibility class II transactivator expression in plasma cells. Nat Immunol 2000; 1:526-32.
129. Ren B, Chee KJ, Kim TH, Maniatis T. PRDI-BF1/Blimp-1 repression is mediated by corepressors of the Groucho family of proteins. Genes Dev 1999; 13:125-37.
130. Yu J, Angelin-Duclos C, Greenwood J, Liao J, Calame K. Transcriptional repression by blimp-1 (PRDI-BF1) involves recruitment of histone deacetylase. Mol Cell Biol 2000; 20:2592-603.
131. Osborne A, Zhang H, Yang WM, Seto E, Blanck G. Histone deacetylase activity represses gamma interferon-inducible *HLA-DR* gene expression following the establishment of a DNase I- hypersensitive chromatin conformation. Mol Cell Biol 2001; 21:6495-506.
132. Windhagen A, Newcombe J, Dangond F, Strand C, Woodroofe MN, Cuzner ML, Hafler DA. Expression of costimulatory molecules B7-1 (CD80), B7-2 (CD86, and interleukin 12 cytokine in multiple sclerosis lesions. J Exp Med 1995; 182:1985-96.
133. Genc K, Dona DL, Reder AT. Increased CD80(+) B cells in active multiple sclerosis and reversal by interferon beta-1b therapy. J Clin Invest 1997; 99:2664-71.
134. Bohmig GA, Krieger PM, Saemann MD, Wenhardt C, Pohanka E, Zlabinger GJ. n-butyrate downregulates the stimulatory function of peripheral blood- derived antigen-presenting cells: A potential mechanism for modulating T-cell responses by short-chain fatty acids. Immunology 1997; 92:234-43.
135. Maeda A, Sobel RA. Matrix metalloproteinases in the normal human central nervous system, microglial nodules, and multiple sclerosis lesions. J Neuropathol Exp Neurol 1996; 55:300-9.
136. Fiorino AS, Zvibel I. Disruption of cell-cell adhesion in the presence of sodium butyrate activates expression of the 92 kDa type IV collagenase in MDCK cells. Cell Biol Int 1996; 20:489-99.
137. Kim MS, Son MW, Kim WB, In Park Y, Moon A. Apicidin, an inhibitor of histone deacetylase, prevents H-ras-induced invasive phenotype. Cancer Lett 2000; 157:23-30.
138. Liu LT, Chang HC, Chiang LC, Hung WC. Histone deacetylase inhibitor up-regulates RECK to inhibit MMP-2 activation and cancer cell invasion. Cancer Res 2003; 63:3069-72.
139. Aparicio T, Kermorgant S, Lewin MJ, Lehy T. Effects of HGF on the production of matrix metalloproteinases by colonic cancer cells DHD/K12. C R Seances Soc Biol Fil 1998; 192:311-5.
140. Pender SL, Quinn JJ, Sanderson IR, MacDonald TT. Butyrate upregulates stromelysin-1 production by intestinal mesenchymal cells. Am J Physiol Gastrointest Liver Physiol 2000; 279:G918-24.
141. Emenaker NJ, Calaf GM, Cox D, Basson MD, Qureshi N. Short-chain fatty acids inhibit invasive human colon cancer by modulating uPA, TIMP-1, TIMP-2, mutant *p53, Bcl-2, Bax, p21* and *PCNA* protein expression in an in vitro cell culture model. J Nutr 2001; 131:3041S-6S.
142. Shuttleworth J, Morser J, Burke DC. Expression of *interferon-alpha* and *interferon-beta* genes in human lymphoblastoid (Nawalma) cells. Eur J Biochem 1983; 133:399-404.
143. Iglesias AH, Camelo S, Hwang D, Villanueva R, Stephanopoulos G, Dangond F. Microarray detection of E2F pathway activation and other targets in multiple sclerosis peripheral blood mononuclear cells. J Neuroimmunol 2004; 150:163-77.
144. Rouaux C, Jokic N, Mbebi C, Boutillier S, Loeffler JP, Boutillier AL. Critical loss of CBP/P300 histone acetylase activity by caspase-6 during neurodegeneration. EMBO J 2003; 22:6537-49.
145. Ahmed Z, Doward AI, Pryce G, Taylor DL, Pocock JM, Leonard JP, Baker D, Cuzner ML. A role for caspase-1 and -3 in the pathology of experimental allergic encephalomyelitis: Inflammation versus degeneration. Am J Pathol 2002; 161:1577-86.
146. Meyer R, Weissert R, Diem R, Storch MK, de Graaf KL, Kramer B, Bahr M. Acute neuronal apoptosis in a rat model of multiple sclerosis. J Neurosci 2001; 21:6214-20.
147. Faller DV, Perrine SP. Butyrate in the treatment of sickle cell disease and beta-thalassemia. Curr Opin Hematol 1995; 2:109-17.
148. Maestri NE, Brusilow SW, Clissold DB, Bassett SS. Long-term treatment of girls with ornithine transcarbamylase deficiency. N Engl J Med 1996; 335:855-9.
149. Gore SD, Carducci MA. Modifying histone to tame cancer: Clinical development of sodium phenylbutyrate and other histone deacetylase inhibitors. Expert Opin Investig Drugs 2000; 9:2923-34.

Neurobiology of Disease

Histone Deacetylase 6 Inhibition Compensates for the Transport Deficit in Huntington's Disease by Increasing Tubulin Acetylation

Jim P. Dompierre,[1,2]* Juliette D. Godin,[1,2]* Bénédicte C. Charrin,[1,2] Fabrice P. Cordelières,[1,2,3] Stephen J. King,[4] Sandrine Humbert,[1,2] and Frédéric Saudou[1,2,3]

[1]Institut Curie, [2]Centre National de la Recherche Scientifique Unité Mixte de Recherche 146, and [3]Plate-forme Imagerie Cellulaire et Tissulaire, F-91405 Orsay, France, and [4]Division of Molecular Biology and Biochemistry, School of Biological Sciences, University of Missouri-Kansas City, Kansas City, Missouri 64110

A defect in microtubule (MT)-based transport contributes to the neuronal toxicity observed in Huntington's disease (HD). Histone deacetyiase (HDAC) inhibitors show neuroprotective effects in this devastating neurodegenerative disorder. We report here that HDAC inhibitors, including trichostatin A (TSA), increase vesicular transport of brain-derived neurotrophic factor (BDNF) by inhibiting HDAC6, thereby increasing acetylation at lysine 40 of α-tubulin. MT acetylation *in vitro* and in cells causes the recruitment of the molecular motors dynein and kinesin-1 to MTs. In neurons, acetylation at lysine 40 of α-tubulin increases the flux of vesicles and the subsequent release of BDNF. We show that tubulin acetylation is reduced in HD brains and that TSA compensates for the transport- and release-defect phenotypes that are observed in disease. Our findings reveal that HDAC6 inhibition and acetylation at lysine 40 of α-tubulin may be therapeutic targets of interest in disorders such as HD in which intracellular transport is altered.

Key words: Huntington's disease; polyglutamine; transport; microtubules; BDNF; neuroprotection

Introduction

Huntington's disease (HD), a devastating neurodegenerative disorder characterized by cognitive and motor deficits, is caused by an abnormal polyglutamine (polyQ) expansion in the N-terminal part of the huntingtin protein (htt) (MacDonald et al., 2003). Recent studies have identified an altered microtubule (MT)-dependent transport of organelles in HD (Gunawardena et al., 2003; Szebenyi et al., 2003; Gauthier et al., 2004; Lee et al., 2004; Trushina et al., 2004). Using fast three-dimensional (3D) videomicroscopy and biochemical approaches, we previously demonstrated that htt associates with molecular motors and activates the MT-dependent transport of vesicles containing brain-derived neurotrophic factor (BDNF) (Gauthier et al., 2004). Wild-type (WT) htt enhances the velocity of the vesicles and reduces the amount of time they spend not moving (pausing time). In HD, in which the htt contains the polyQ expansion, the intracellular transport of BDNF-containing vesicles is altered, resulting in reduced trophic support of neurons and their death. We reasoned that it should be possible to use fast 3D videomicroscopy to screen for compounds able to restore intracellular transport.

Currently, there is no treatment available for HD patients, although several studies in yeast, *Drosophila*, mammalian cells, and mice have identified compounds of therapeutic interest. Among these compounds are histone deacetylase (HDAC) inhibitors such as suberoylanilide hydroxamic acid (SAHA) and trichostatin A (TSA), which have shown neuroprotective effects by inhibiting the HDAC1 enzyme (Butler and Bates, 2006). These drugs are not specific for a given HDAC and act on other HDACs, such as HDAC6 (Haggarty et al., 2003). Unlike other HDACs, HDAC6 is a cytoplasmic enzyme that interacts with and deacetylates MTs *in vitro* and *in vivo* (Hubbert et al., 2002; Matsuyama et al., 2002; Zhang et al., 2003). Acetylation is associated with stable MTs, although this relationship is not clear-cut. Some studies have shown that acetylation enhances MT stability (Hubbert et al., 2002; Matsuyama et al., 2002), whereas others have suggested that acetylation occurs only on stable and not dynamic MTs, but the acetylation itself does not stabilize MTs (Haggarty et al., 2003).

Received Jan. 5, 2007; revised Feb. 19, 2007; accepted Feb. 22, 2007.

This work was supported by grants from Agence Nationale de la Recherche (MRAR-018-01 to F.S.), Association Française contre les Myopathies (F.S.), Association pour la Recherche sur le Cancer (ARC; 3665 to S.H.), Fondation pour la Recherche Médicale and Fondation BNP Paribas (F.S.), Fédération pour la recherche sur le cerveau (F.S.), HighQ Foundation (F.S., S.H.), Provital P. Chevalier (F.S., S.H.), and National Institutes of Health (NS 48501 to S.J.K.). J.P.D. was supported by the HighQ foundation and currently by Trophos. J.D.G. was supported by a Région Ile de France doctoral fellowship, and B.C.C. was supported by an ARC doctoral fellowship. S.H. is an Institut National de la Santé et de la Recherche Médicale (INSERM) investigator. F.S. is a recipient of a European Molecular Biology Organization Young Investigator award and an INSERM/Assistante Publique-Hôpitaux de Paris investigator. We gratefully acknowledge J. C. Wong, R. Mazitschek, and S. L. Schreiber, who were supported by the Initiative for Chemical Genetics-National Cancer Institute; B. Gilquin, S. Khochbin, V. Lessmann, N. Galjart, M. E. MacDonald, R. Y. Tsien, and M. A. Knossow for reagents and/or discussions; Harvard Brain Tissue Resource Center (Belmont, MA), which is supported in part by PHS Grant MH/NS 31862, for providing human brain tissue; and members of the Saudou/Humbert laboratory for help and comments.

*J.P.D. and J.D.G. contributed equally to this work.

Correspondence should be addressed to either of the following: Sandrine Humbert, Institut Curie, Unité Mixte de Recherche (UMR) 146, F-91405 Orsay, France, E-mail: Sandrine.Humbert@curie.u-psud.fr; or Frederic Saudou, Institut Curie, UMR 146, F-91405 Orsay, France, E-mail: Frederic.Saudou@curie.u-psud.fr.

DOI:10.1523/JNEUROSCI.0037-07.2007

 0270-6474/07/273571-13$15.00/0

Interestingly, a recent report indicates that α-tubulin acetylation at lysine 40 of *Tetrahymena thermophila* enhances the recruitment of the molecular motor kinesin-1 to MTs and promotes anterograde transport of the kinesin-1 cargo JNK (c-Jun N-terminal kinase)-interacting protein (JIP1) in differentiated neuronal cells (Reed et al., 2006), suggesting a possible link between HDAC6 inhibition and the stimulation of MT-dependent trafficking of vesicles. Given that MT-dependent vesicular transport is altered in HD and that HDAC inhibitors show a neuroprotective effect, we tested whether MT acetylation could regulate vesicular transport and compensate for the observed transport deficit in HD. We report that HDAC inhibitors that selectively enhance tubulin but not histone acetylation lead to the stimulation of MT-dependent transport of BDNF and prevent the alteration observed in HD mutant cells. We show that this effect is specific to HDAC6 inhibition and to the acetylation of α-tubulin at lysine 40. We demonstrate *in vitro* that purified cytoplasmic dynein and recombinant kinesin-1 bind more effectively to acetylated MTs. Enhancing MT acetylation leads to the recruitment of molecular motors kinesin-1 and cytoplasmic dynein to MTs thereby stimulating anterograde and retrograde transport. We show that this increased transport leads to the enhancement of the anterograde flux of vesicles and the subsequent release of BDNF in the normal and pathological conditions. Our data provide strong evidence for a functional role of MT acetylation on vesicular transport. Furthermore, we identify drugs that could restore the transport deficit in HD.

Materials and Methods

Statistical analyses. Statview 4.5 software (SAS Institute, Cary, NC) was used for statistical analyses. All data herein described were performed in duplicate or triplicate. Data are expressed as means ± SEM. Statistical analyses may be found in the supplemental material (available at www.jneurosci.org).

DNA constructs. Constructs encoding BDNF, BDNF-enhanced green fluorescent protein (eGFP), end-binding protein 3 (EB3)-eGFP, HDAC6, inactive HDAC6 (HDAC6m1m2), mCherry-α-tubulin, htt-480–17Q, and htt-480–68Q, were described previously (Haubensak et al., 1998; Saudou et al., 1998; Seigneurin-Berny et al., 2001; Stepanova et al., 2003; Shaner et al., 2004). The mCherry-α-tubulin lysine 40 to alanine mutation (K40A) construct with the mutation at the acetylation site was generated by QuikChange site-directed mutagenesis (Stratagene, La Jolla, CA) using the WT mCherry-α-tubulin plasmid as a nonmutated parental template and complementary oligonucleotides containing the desired mutation (5′-GATGCCAAGTGACGCGACAATTGGGGGAGGAG-3′).

Antibodies. The polyclonal antibodies used were the following: anti-detyrosinated tubulin (AB3201; Millipore, Bedford, MA), anti-tyrosinated tubulin (Amersham Biosciences, Piscataway, NJ), anti-GFP (Millipore), anti-HDAC6 (Seigneurin-Berny et al., 2001), anti-histone H3, and anti-acetylated histone H3 (Cell Signaling, Boston, MA). The monoclonal antibodies used were the following: anti-htt (2166), anti-kinesin heavy chain (KHC; clone H2), and anti-dynein intermediate chain (DIC; clone 74.1; Millipore); anti-α-tubulin (clone DM1A), anti-α-tubulin (clone DM1A)-FITC conjugated antibodies, anti-acetylated tubulin, anti-β-tubulin cyanine 3 (Cy3)-conjugated antibodies (Sigma, St. Louis, MO); anti-p150^{Glued}, anti-EB1, anti-KIF3A (BD Bioscience, San Jose, CA); and anti-KHC (SUK4; Covance Research Products, Berkeley, CA) (Ingold et al., 1988). The monoclonal antibody anti-acetylated α-tubulin (Zymed, San Francisco, CA) was conjugated to Alexa Fluor 488 using the Alexa Fluor monoclonal antibody labeling kit (Invitrogen, Eugene, OR). Anti-mouse and anti-rabbit secondary antibodies conjugated to Alexa Fluor 488, Alexa Fluor 555, and Alexa Fluor 647 were purchased from Invitrogen. Anti-mouse and anti-rabbit secondary antibodies conjugated to HRP were purchased from Jackson ImmunoResearch (West Grove, PA).

Cytoplasmic dynein purification. Cytoplasmic dynein from bovine brain tissue was purified and isolated from dynactin as described previously (Bingham et al., 1998), except that the homogenization buffer included 45 nM okadaic acid. The purified dynein was diluted in 45% glycerol and stored at −20°C. Absence of any significant contamination from dynactin was established through SDS-PAGE and Western blotting.

Cell culture, transfection, and drug treatments. Mouse striatal cells derived from WT htt (WT striatal cells, +/+) mice and from *Hdh*^{Q109} knock-in (109Q/109Q) mice, HEK293 cells, Cos7 cells, and primary cortical neurons were prepared and cultured as described previously (Xia et al., 1996; Trettel et al., 2000; Humbert et al., 2002; Gauthier et al., 2004). HEK293 cells were transfected by the calcium phosphate technique. Primary cortical neurons were transfected as described previously (Xia et al., 1996) or electroporated with the rat neuron Nucleofector kit according to the supplier's manual (Amaxa Biosystems, Cologne, Germany). Forskolin (10 μM; Sigma) and IBMX (100 μM; Sigma) were added to the culture 5 h after transfection. Neuronal cells were transfected for 4 h with small interfering RNA (siRNA) htt or the corresponding scrambled RNA (19 nucleotides of RNA plus TT) 1 d before BDNF-eGFP transfection. The siRNA sequence targeting mouse htt (siRNA-htt) corresponds to the coding regions 185–206 (GenBank accession number XM 132009). The siRNA sequence targeting mouse or rat KIF5B (kinesin-1) corresponds to the coding region 1215–1233 (GenBank accession number XM 341638). The siRNA sequence targeting human KIF3A (kinesin-2) corresponds to the coding region 1633–1651 (accession number XM 007054). The scrambled RNA htt have the same nucleotide composition as the siRNA-htt but lack a significant sequence homology to any other gene (Gauthier et al., 2004). Transfected or untransfected cells were treated with various HDAC inhibitors: TSA (100 nM, 1 μM, or 5 μM for cell biology and biochemistry, respectively; Sigma), SAHA (2 μM; Coger, Paris, France), MS-275 (HDAC1 inhibitor; 3 μM; Alexis Biochemicals, Lausen, Switzerland), or tubacin (6 μM) (Haggarty et al., 2003) for 4 h; sodium phenylbutyrate (NaPB; 10 mM; Alexis Biochemicals) for 4 or 16 h; and taxol (100 nM; Sigma) for 1 h. Treatment with DMSO (Sigma) was used as a control.

Cell extracts, immunoblotting experiments, and MT preparation. Cells were lysed 1–4 h after drug treatment with 1% Triton lysis buffer (160 mM NaCl, 50 mM HEPES, 2.5 mM $MgCl_2$, 1.5 mM $CaCl_2$, 2.5 mM KCl, and 1% Triton X-100, pH 7.4, containing 1 mM PMSF, 2 μg/ml aprotinin, 2 μg/ml leupeptin, 2 μg/ml pepstatin). The extracts were sonicated and centrifuged at 11,000 × *g* (15 min; 4°C). Proteins (1–20 μg) were loaded onto SDS-PAGE and subjected to Western blot analysis.

MTs were depolymerized on ice for 15 min, and the reaction was centrifuged at 10,000 × *g* for 15 min at 4°C as described previously (Goldstein et al., 1986). MTs in the supernatant (S) were polymerized at 33°C for 30 min by addition of GTP (1 mM final) and taxol (20 μM final; Sigma). Polymerized MTs were pelleted by centrifugation at 10,000 × *g* for 45 min. After centrifugation, 1 μl of 2% SDS buffer was added to the S, and the pellet (P) was resuspended in 1% SDS buffer, heated 5 min at 100°C, and sonicated before loading. The same volume of each fraction was analyzed by Western blot.

Brain tissues. Tissues (striatum) were obtained from the Harvard Brain Tissue Resource Center (HBTRC; Belmont, MA): three controls (samples 1–3), one HD grade 3 (HD3; sample 4) patient, and one HD grade 4 (HD4; sample 5) patient. Striatal postmortem samples correspond, respectively, to brain numbers 4741, 4744, 4751, 4797, 4640 as numbered by the HBTRC. Samples were homogenized in NP-40 lysis buffer and cleared by centrifugation at 6000 × *g* (15 min; 4°C). Western blot analysis was performed on 30 ng (acetylated α-tubulin) or 1 μg (total tubulin) of total extracts.

BDNF immunoenzyme assays. BDNF assays were performed on cortical neurons 48 h after electroporation with BDNF and WT or polyQ-htt constructs. To measure transport-dependent release, cells were depolarized (treatment for 20 min with DMEM containing high K^+ (30 mM $CaCl_2$, 30 mM NaCl, 28 mM KCl), treated 30 min with DMEM, washed, and depolarized again (second depolarization, K2). For TSA treatment, cells were maintained in TSA (1 μM) during all of the steps. The amount of BDNF was measured in S fractions and cell lysates using the BDNF

Emax Immunoassay System (Promega, Charbonnieres, France) as described previously (Gauthier et al., 2004).

MT binding assays. Three micrograms of purified tubulin (Cytoskeleton, Denver, CO) were polymerized in PEM buffer (100 mM PIPES, pH 6.7, 1 mM EGTA, 1 mM $MgCl_2$) in the presence of 200 μM taxol (Sigma) and 1 mM GTP (Sigma) for 30 min at 37°C. MTs were pelleted at 20,000 × *g* for 30 min, resuspended in PEM buffer containing 20 μM taxol, 1 mM GTP, and 50 mM NaCl, and then sheared with a 25 ga needle (Ligon et al., 2006). MTs were acetylated *in vitro* by addition of 1% anhydride acetic acid (AA) for 10 min at 37°C (Piperno and Fuller, 1985). Acetylated and unacetylated MTs were then incubated with either 50 ng of recombinant kinesin (Cytoskeleton) or 30 ng dynein for 10 min at 37°C in the presence of 50 μM AMP-PNP (5′-adenyly-limidodiphosphate). MTs were finally pelleted onto a 12 mm coverslip precoated with poly-D-lysine (BD Bioscience) at 27,000 × *g* for 15 min (Evans et al., 1985), fixed, and visualized by immunofluorescence.

MTs containing the WT mCherry-α-tubulin or K40A construct were purified by two successive rounds of depolymerization/repolymerization from transfected and TSA-treated (1 μM) HEK293 cells as described for MT preparation, except that all of the procedures were performed in the presence of 5 μM TSA to maintain MT acetylation and 10 mM ATP to remove endogenous motors. MTs were resuspended in PEM buffer, polymerized, incubated with recombinant motors, and pelleted as described above. mCherry-α-tubulin was visualized using the anti-GFP antibody. Absence of binding of endogenous kinesin-1 and cytoplasmic dynein on polymerized MTs was verified by immunostaining.

Immunofluorescence experiments. Neurons and cells were grown on glass coverslips, transfected with various constructs of HDAC6 or of mCherry-α-tubulin, and fixed in anhydrous methanol at −20°C for 5 min and incubated with anti-tubulin, anti-acetylated-tubulin, anti-HDAC6, or anti-acetylated histone H3 antibodies. To visualize molecular motors along MTs, the cell fixation protocol was adapted from Vaughan et al. (1999). Briefly, cells were incubated for 1 min in PBS at room temperature and fixed in anhydrous methanol at −20°C for 5 min and incubated with anti-DIC, anti-KHC, and anti-p150^{Glued} antibodies. In the case of double labeling with two mouse monoclonal antibodies, cells were first fixed and incubated with the primary antibodies anti-kinesin, anti-DIC, or anti-p150^{Glued} antibodies, then cells were washed with 0.1% PBS/BSA and incubated with the anti-mouse secondary antibodies conjugated with Alexa Fluor 488 and 555. Cells then underwent a second fixation (anhydrous methanol at −20°C for 5 min) and were incubated with FITC-conjugated anti-α-tubulin or Cy3-conjugated anti-β-tubulin antibodies. For *in vitro* experiments, pelleted MTs were fixed with either 4% paraformaldehyde in PHEM buffer for 20 min or anhydrous −20°C methanol for 5 min and incubated, respectively, with anti-KHC or anti-DIC antibodies. Pictures were captured with a 3D deconvolution imaging system as described previously (Gauthier et al., 2004).

Videomicroscopy experiments. Videomicroscopy experiments were done 2–3 d after transfection. The cells were cotransfected with BDNF-eGFP and various constructs of HDAC6, mCherry-α-tubulin, or the corresponding empty vectors with a DNA ratio of 1:4 and treated as described above. Live videomicroscopy was performed using an imaging system detailed previously (Gauthier et al., 2004). Cells were grown on a glass coverslip that was mounted in a Ludin chamber. The microscope and the chamber were kept at 33°C for striatal cells and 37°C for neurons and Cos7 cells. Stacks of 11 images with a Z step of 0.3 μm were acquired with a 100× PlanApo numerical aperture 1.4 oil immersion objective coupled to a piezo device. Images were collected in stream mode using a CoolSnap HQ camera (Roper Scientific, Trenton, NJ) set at 2 × 2 binning with an exposure time of 50–150 ms (frequency of 2 s). All stacks were treated by automatic batch deconvolution using the point spread function of the optical system. All dynamic parameters of intracellular transport are from data that were typically obtained for each condition from two to three independent transfections with a total of ~2000–8000 measures in 11–40 independent cells.

Image processing and data analyses. For videomicroscopy experiments, projections, animations, and analyses (tracking and colocalizations) were generated using ImageJ software (written by W. Rasband at the National Institutes of Health and available at http://rsb.info.nih.gov/ij/). Dynamics were characterized by tracking positions of eGFP vesicles in cells as a function of time with an especially developed plug-in (http://rsb.info.nih.gov/ij/plugins/track/track.html). During tracking, the Cartesian coordinates of the centers of vesicles were used to calculate dynamic parameters (velocity, pausing time, directionality). The threshold for null displacement corresponds to one pixel over the time interval (i.e., 129 nm/2 s = 4 μm/min). For two-color videomicroscopy, an additional midplane on the *z*-axis was captured in the red channel for every stack completed in the GFP channel. Time projections were generated as follows. After binarization and erosion of the deconvolved images, a composite-projected merge of the 31 frames of the experiment was next generated by continuously substracting the previous frame, thus displaying only the differences between adjacent frames. This time projection allows one to visualize the paths followed by vesicles over the recording time (1 min) (Toomre et al., 1999).

The flux in one direction Φ_{dir} was calculated by expressing, for each neuron, the summed individual-traveled distances in this direction d_i, multiplied by the mean of velocity in the same direction v_{dir}, divided by the number of vesicles moving in this direction n_{dir}, according to the following:

$$\Phi_{dir} = \frac{\Sigma_i d_i \times \bar{v}_{dir}}{n_{dir}}$$

The quantification of the portion of MT-associated proteins (MAPs) signal associated to MTs, was achieved by creating a binary mask from the MT image. First, a Gaussian filter with a five-pixel radius was used to smooth the original image. To get rid of the uneven background, a 3D top-hat filter was then applied, using a 5 × 5 × 2 pixel kernel. The MT image was further binarized using the overall minimum gray level value of the full stack as a threshold. MT gray level value was set to one, whereas the surrounding background pixels were set to zero to obtain the mask image. Finally, the mask was dilated by 5 × 5 pixels to ensure the retrieval of all of the dots of the MAPs associated to MTs in the remainder of the process. The image of MAP signal on MTs was obtained by multiplying the latter and the MAP image. The resultant image was then subtracted to the original MAP image to retrieve the image of the MAP signal excluded from the MTs. Quantifications were expressed as the quotient of the overall MAP signal associated to the MTs and the overall MAP signal. All processes were automated using macros written for ImageJ extended by a homemade plug-in for 3D top-hat filtering (all homemade ImageJ plug-ins are available on request at fabrice.cordelieres@curie.u-psud.fr).

Linescan analyses. MT intensity profiles were obtained using MT profiler, a homemade plug-in to the open-source software ImageJ. A defined rectangular region of interest was placed around the MT, one of the shortest-bound touching the MT plus tip. The connected maximum intensity path was retrieved in 3D, starting from the tip. Fluorescence signal was then quantified along this path. For quantification of motor recruitment on MT and *in vitro* experiments, results were expressed as the density of fluorescence (sum of motor intensity along the path divided by the length of MT) and were normalized to control. Ten single MTs per cell (10 cells) were chosen randomly for quantification.

Results

TSA and SAHA increase BDNF intracellular transport and compensate for the trafficking deficit in HD

To test the hypothesis that HDAC inhibitors may regulate vesicular transport, we analyzed the dynamics of BDNF-containing vesicles using fast 3D videomicroscopy followed by deconvolution (Gauthier et al., 2004). Indeed, the control of intracellular dynamics of BDNF-containing vesicles is of particular importance in HD. BDNF is actively transported in corticostriatal-projecting neurons and released in the striatum (Altar et al., 1997) where it acts as a prosurvival factor for the striatal neurons that are particularly vulnerable in HD (Saudou et al., 1998; Baquet et al., 2004). The cellular localization, processing, and secretion of mature BDNF-eGFP are indistinguishable from those of

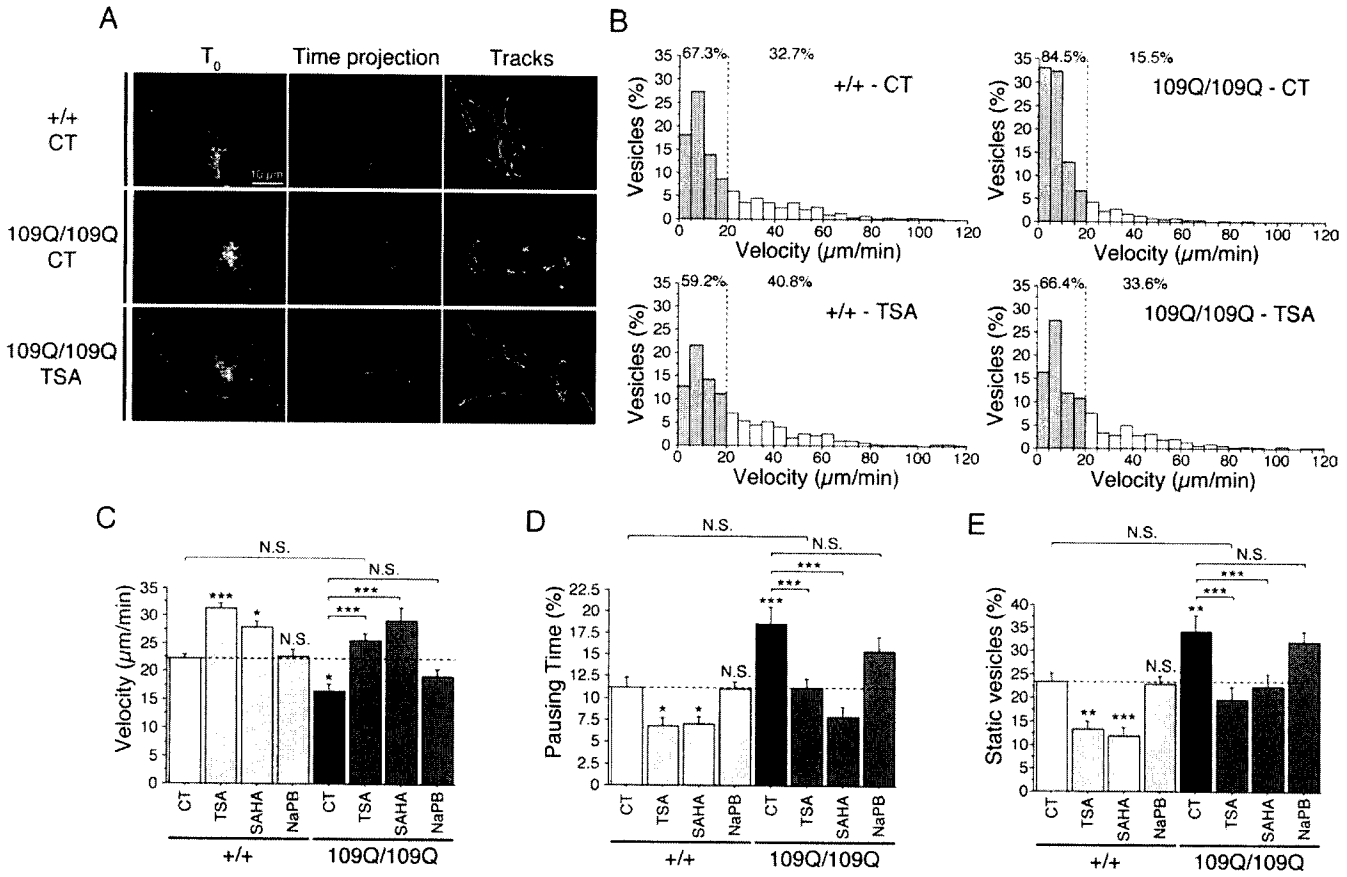

Figure 1. TSA and SAHA stimulate vesicular transport of BDNF and rescue transport defect in HD Cells. ***A***, ***B***, WT (+/+) and 109Q/109Q cells transfected with BDNF-eGFP were treated for 4 h with DMSO (0.1%, CT), TSA (1 μM), or SAHA (2 μM) and analyzed by videomicroscopy. ***A***, The displacement of BDNF vesicles is reduced in 109Q/109Q compared with +/+ cells as shown by 3D reconstruction of the first time point (T_0), time projection of moving structures over the 1 min experiment, and visualization of 10 paths followed by individual vesicles (Tracks). The altered BDNF transport in 109Q/109Q cells (CT) is restored by treating cells with TSA. ***B***, Analysis of the distribution of vesicular velocities shows a marked increase in the number of vesicles that have a low velocity in 109Q/109Q cells compared with +/+ cells. The distribution of velocities in TSA-treated 109Q/109Q cells is similar to the distribution in +/+ cells. Filled bars correspond to nonmoving and low-moving vesicles, and open bars correspond to high-speed moving vesicles. ***C–E***, WT (+/+) and 109Q/109Q cells transfected with BDNF-eGFP were treated for 4 h with DMSO (0.1%, control, CT), TSA (1 μM), SAHA (2 μM), or NaPB (10 mM) and analyzed by videomicroscopy. Dynamics were quantified by the use of three parameters: the mean velocity of vesicles (***C***), their pausing time (***D***), and the percentage of static vesicles (***E***). Dashed lines correspond to the control values. N.S., Not significant. $^*p < 0.05$; $^{**}p < 0.01$; $^{***}p < 0.001$.

endogenous BDNF (Haubensak et al., 1998; Hartmann et al., 2001; Kohara et al., 2001).

We investigated the effect of HDAC inhibition in the normal and the HD pathological situations by using cell lines derived from striatal precursor cells of knock-in mice in which a CAG expansion was inserted into the endogenous mouse htt gene (Trettel et al., 2000). These cell lines carry either two copies of WT htt (WT striatal cells, +/+) or two copies of mutant htt (homozygous HD mutant cells, 109Q/109Q). We transfected WT and HD mutant cells with BDNF-eGFP and monitored the movement of BDNF-containing vesicles by acquiring 3D time-series images (Fig. 1*A*). Individual vesicles were then tracked by measuring the *x*, *y*, and *z* coordinates of the vesicles over time. Visualization of the paths of 10 individual vesicles randomly selected in WT and 109Q/109Q cells revealed a significant reduction in the displacement of BDNF vesicles in the HD situation (Fig. 1*A*). As reported previously (Gauthier et al., 2004), analysis of velocity distribution demonstrated a significant loss of rapidly moving vesicles in HD mutant cells compared with WT cells [32.7% for control (CT) +/+ vs 15.5% for CT 109Q/109Q] (Fig. 1*B*). We next treated cells with TSA and found that TSA treatment increased the percentage of high-velocity vesicles in the WT cells and restored the distribution of velocities in 109Q/109Q cells (40.8% for TSA +/+ vs 32.7% for CT +/+ and 33.6% for TSA 109Q/109Q vs 15.5% for CT 109Q/109Q) (Fig. 1*A*,*B*) (supplemental videos 1–3, available at www.jneurosci.org as supplemental material) back to that of the WT situation, indicating that TSA rescues the alteration of transport in HD cells. We next determined the mean vesicle velocity of moving vesicles between two pauses and the percentage of pausing time of vesicles (time spent by the vesicles without moving). These two parameters are particularly relevant to reflect changes in transport efficiency. In 109Q/109Q cells, the velocity and the pausing time of BDNF vesicles were significantly different than those of +/+ cells (Fig. 1*C*,*D*). TSA treatment rescued vesicular transport by significantly increasing the velocity and decreasing the pausing time of BDNF-containing vesicles. We also analyzed the movement of all of the vesicles that are present in cells by calculating the mean percentage of colocalization of vesicles between two successive time points (Manders et al., 1992). A high level of colocalization indicates that vesicles are not moving (static vesicles). The percentage of static vesicles was significantly reduced by TSA treatment both in +/+ and 109Q/109Q cells (Fig. 1*E*). Finally, TSA treatment did not obviously modify the distribution of BDNF relative to intracellular markers of the secretory pathway, excluding the possibility that BDNF could be transferred to other types of organelles having different dynamics (data not shown). Together, these results demonstrate

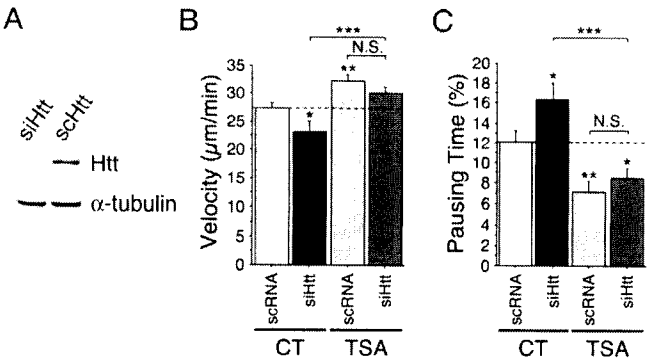

Figure 2. TSA stimulates vesicular transport of BDNF through an htt-independent mechanism. WT (+/+) cells were transfected with BDNF-eGFP and siRNA directed against mouse htt (siHtt) or scramble RNA (scRNA) 1 d before BDNF-eGFP transfection. ***A***, Total extracts were analyzed by Western blot for htt and α-tubulin levels. ***B***, ***C***, Cells were treated for 4 h with DMSO (0.1%, CT) or TSA (1 μM) and analyzed by videomicroscopy. Dynamics were quantified by the use of the mean velocity of vesicles per cell (***B***) and their pausing time (***C***). Dashed lines correspond to the control values. N.S., Not significant. $*p < 0.05$; $**p < 0.01$; $***p < 0.001$.

that TSA stimulates transport of BDNF and rescues the intracellular transport defect in HD mutant cells.

We next analyzed the effects of other HDAC inhibitors, such as SAHA and NaPB, on BDNF vesicular dynamics (Fig. 1*C–E*). Whereas TSA and SAHA significantly increased BDNF transport in +/+ and 109Q/109Q cells, NaPB had no significant effect. Statistical analyses revealed that TSA and SAHA stimulated transport of BDNF and rescued the intracellular transport defect in HD mutant cells to a similar extent (supplemental material, available at www.jneurosci.org).

The stimulatory effect of SAHA and TSA on transport is independent of htt

It has been demonstrated previously by us and other groups that WT htt directly regulates transport. Indeed, increasing htt levels through its overexpression increases transport efficiency, whereas reducing the levels through RNA interference (RNAi) reduces transport efficiency (Gunawardena et al., 2003; Gauthier et al., 2004). To analyze whether TSA and SAHA could act directly on htt to promote vesicular trafficking, we studied the effect of these drugs in cells containing low levels of htt (Fig. 2). Striatal +/+ cells were transfected with BDNF-eGFP and either siRNA directed against htt or the corresponding scrambled RNA. As expected, cells with reduced htt levels (Fig. 2*A*) showed reduced BDNF vesicle velocity and increased pausing time compared with cells transfected with control RNA (Fig. 2*B*, *C*). However, TSA (and SAHA; data not shown) increased BDNF vesicular transport to similar extents in both conditions, showing that the enhanced BDNF transport induced by these drugs does not depend on htt (Fig. 2*B*,*C*). Thus, TSA and SAHA stimulate BDNF trafficking through an htt-independent mechanism.

SAHA and TSA increase tubulin acetylation

Although HDACs have been widely described to control the acetylation state of histones acting as transcription activators or repressors (Taddei et al., 2005), they also deacetylate cytoplasmic proteins including tubulin (Hubbert et al., 2002; Matsuyama et al., 2002; Zhang et al., 2003). Because BDNF transport is MT dependent (Gauthier et al., 2004), we assessed the acetylation state of α-tubulin in our assay. We treated striatal +/+ cells with TSA, SAHA, and NaPB and used immunofluorescence to analyze the acetylation state of α-tubulin (Fig. 3*A*). We used histone H3 as a control. The three HDAC inhibitors increased the levels of acetylation of histone H3. However, only TSA and SAHA affected tubulin acetylation. We obtained the same results from immunoblotting extracts of treated WT cells: SAHA and TSA increased histone H3 and tubulin acetylation, whereas even after 16 h of treatment, NaPB increased only the acetylation of histone H3, not the acetylation of α-tubulin (Fig. 3*B*). In conclusion, these results indicate that only those HDAC inhibitors that increase tubulin acetylation also increase BDNF transport, suggesting that tubulin acetylation may play a role in the regulation of intracellular transport.

TSA increases BDNF intracellular transport and tubulin acetylation through an HDAC6-dependent mechanism

HDACs are divided into three subfamilies: class I, II, and III (Drummond et al., 2005). TSA and SAHA inhibit class I and II HDACs, whereas NaPB only inhibits class I HDACs. Therefore, TSA and SAHA may affect transport through a class II protein. Of the class II HDACs, HDAC6 is unique, being located only in the cytoplasm and having a tubulin deacetylase activity (Hubbert et al., 2002; Matsuyama et al., 2002; Zhang et al., 2003). TSA may thus affect transport specifically through HDAC6 inhibition. Therefore, we analyzed by immunofluorescence (Fig. 3*C*) and immunoblotting (Fig. 3*D*) the effects on WT cells of two HDAC inhibitors, tubacin and MS-275, which specifically inhibit HDAC6 and HDAC1, respectively (Haggarty et al., 2003; Hu et al., 2003). Tubacin and MS-275 had opposite effects: tubacin increased the acetylation of tubulin but not of histone H3, whereas MS-275 increased the acetylation of histone H3 but not of tubulin. These results in striatal cells are consistent with previous studies in NIH 3T3 cells (Haggarty et al., 2003), demonstrating that HDAC6 preferentially deacetylates tubulin over histone H3. We next analyzed the effect of tubacin and MS-275 on BDNF transport. We found that tubacin increased the velocity of BDNF vesicles (Fig. 3*E*) and reduced their pausing time (Fig. 3*F*), whereas MS-275 had no effect. We conclude that tubacin, which is a specific inhibitor of HDAC6, preferentially increases tubulin acetylation and stimulates intracellular transport.

To further demonstrate the involvement of HDAC6 in the TSA-mediated effect on transport, we overexpressed WT HDAC6 (HDAC6WT) or HDAC6m1m2, an HDAC6 mutant having no deacetylase activity (Seigneurin-Berny et al., 2001), in striatal cells. We next treated the cells with TSA and analyzed by immunofluorescence the level of acetylation of α-tubulin in transfected and untransfected cells. A threshold concentration of 100 nM of TSA was sufficient to enhance significantly the acetylation of α-tubulin (Fig. 3*G*) and to stimulate vesicular transport (Fig. 3*H*,*I*). As described previously (Matsuyama et al., 2002), overexpression of HDAC6WT, but not of HDAC6m1m2, inhibited the acetylation of MTs that is induced by TSA. This also demonstrates that tubulin acetylation induced by TSA is because of the inhibition of the deacetylase activity of HDAC6. In agreement, only high concentrations of TSA are able to overcome the effect of increased HDAC6 activity to induce tubulin acetylation in the HDAC6WT-overexpressing cells (data not shown; Matsuyama et al., 2002). We then compared the dynamics of BDNF vesicles between HDAC6WT and HDAC6m1m2 transfected cells. Strikingly, we found that the stimulatory effect of TSA on BDNF transport was lost in cells expressing HDAC6WT (Fig. 3*H*,*I*). However, in cells overexpressing the nonactive HDAC6m1m2 mutant, the TSA-induced increase in BDNF vesicle velocity and decrease in pausing time were not affected compared with untransfected cells. Together, these results show that

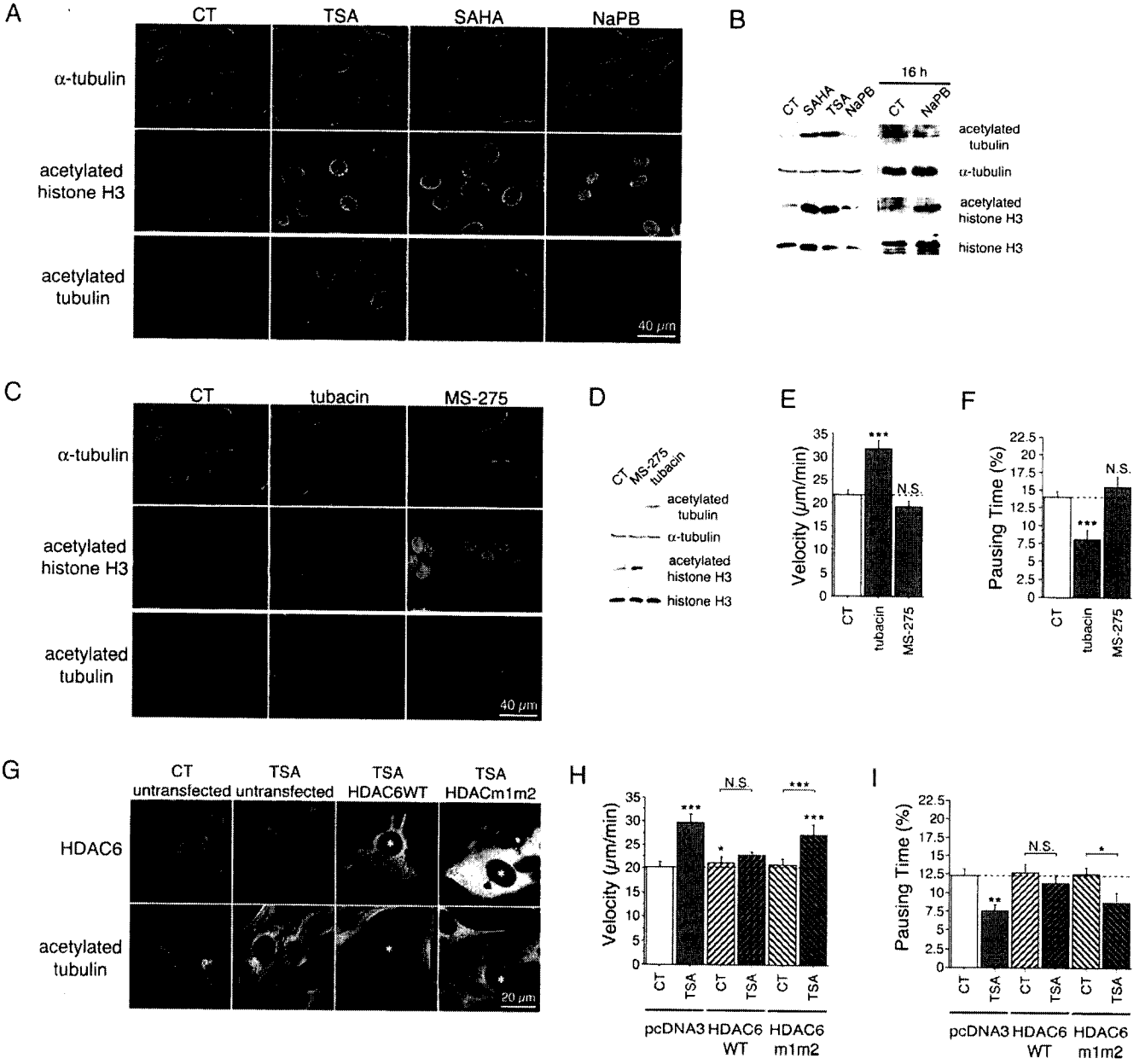

Figure 3. TSA and SAHA acetylate MTs and stimulate vesicular transport of BDNF through an HDAC6-dependent mechanism. ***A***, ***B***, WT (+/+) cells were treated for 4 h with DMSO (0.1%, control, CT), TSA (1 μM), SAHA (2 μM), and NaPB [10 mM (***A***, ***B***, left) or for 16 h (***B***, right)] and analyzed by immunofluorescence (***A***) or Western blot (***B***) for the presence of acetylated tubulin, α-tubulin, acetylated histone H3, and histone H3. ***C***, WT (+/+) cells were treated for 4 h with DMSO (0.1%, CT), tubacin (6 μM), and MS-275 (3 μM) and stained for α-tubulin, acetylated histone H3, and acetylated tubulin. ***D***, Extracts from WT cells treated for 4 h with DMSO (0.1%, CT), MS-275 (3 μM), or tubacin (6 μM) were processed by Western blot and analyzed for acetylated tubulin, α-tubulin, acetylated histone H3, and histone H3. ***E***, ***F***, WT (+/+) cells transfected with BDNF-eGFP were treated as in ***D*** and analyzed by videomicroscopy. ***G***, Untransfected cells and cells transfected with HDAC6WT or HDAC6m1m2 were treated with DMSO (0.1%, CT) and TSA (100 nM) for 4 h and immunostained with anti-HDAC6 and anti-acetylated tubulin antibodies. HDAC6WT or HDAC6m1m2 transfected cells are labeled with an asterisk. ***H***, ***I***, Striatal cells were cotransfected with BDNF-eGFP and with HDAC6WT, HDAC6m1m2, or the corresponding empty vector (pcDNA3), treated with DMSO (0.1%, CT) and TSA (100 nM) for 4 h, and analyzed by videomicroscopy. Dashed lines correspond to the control values. N.S., Not significant. $^*p < 0.05$; $^{**}p < 0.01$; $^{***}p < 0.001$.

TSA-induced activation of BDNF transport is mediated, at least in part, through the inhibition of HDAC6 deacetylase activity.

Tubulin acetylation correlates with enhanced transport but not with MT stability

We next considered how TSA, HDAC6 inhibition, and the subsequent increased acetylation of tubulin could contribute to increased intracellular transport. Acetylation has been associated with stable MTs. Therefore, we first analyzed the effect of TSA and tubacin on MT growth in striatal cells using MT EB3 coupled to eGFP. EB3 is a neuron-specific "plus-end" binding protein of the EB1 family, whose dynamics reflect the plus-end MT polymerization rate (Stepanova et al., 2003). As a positive control, we used taxol, a potent stimulator of MT stabilization. Low concentrations of taxol reduced the MT polymerization rate (supplemental Fig. 1*A*, available at www.jneurosci.org as supplemental material). However, neither TSA nor tubacin significantly affected the MT polymerization rate, suggesting that acetylation has no detectable effect on polymerization. Also, TSA had no effect on the localization of endogenous EB1 (supplemental Fig. 2*A*, available at www.jneurosci.org as supplemental material). Because these approaches give only an indirect value of MT po-

Table 1. Effect of HDAC inhibition on microtubule dynamics and stability

		Polymerization rate (μm/min)	Depolymerization rate (μm/min)	Catastrophe frequency (min^{-1})	Rescue frequency (min^{-1})
WT	CT ($n = 71$)	13.536 ± 0.776	13.448 ± 0.811	2.77 ± 0.134	2.726 ± 0.136
	TSA ($n = 48$)	12.108 ± 0.862	11.776 ± 0.86	2.935 ± 0.138	2.898 ± 0.138
K40A	CT ($n = 106$)	12.224 ± 0.522	14.819 ± 1.027	2.937 ± 0.115	2.779 ± 0.12

MT dynamics are not affected by acetylation. MT dynamic parameters in Cos7 cells transfected with WT mCherry-α-tubulin or mCherry-α-tubulin K40A and treated or not with TSA (1 μM) were determined by tracking the MT tips.

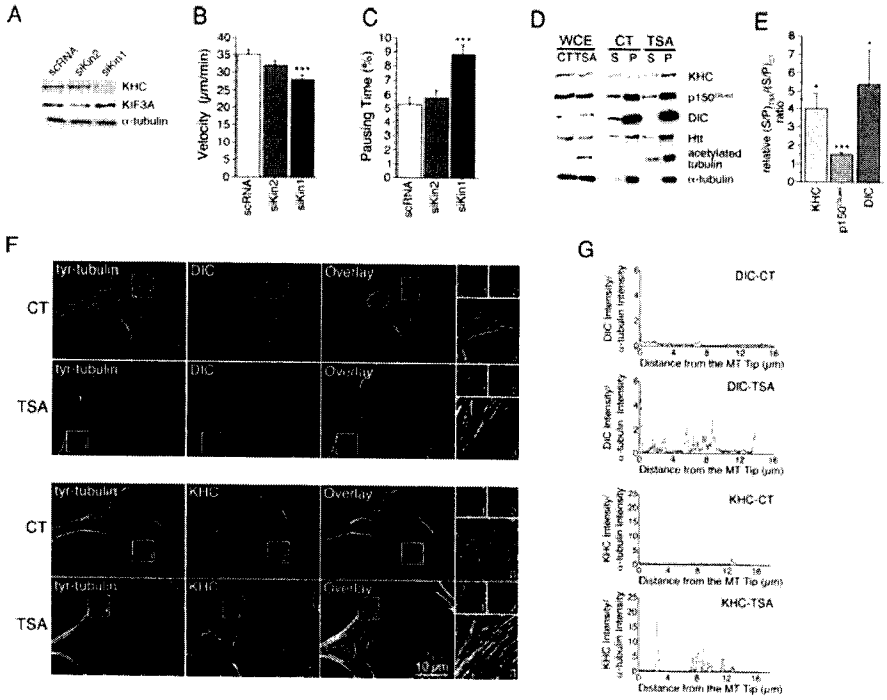

Figure 4. Inhibition of tubulin deacetylation increases the recruitment of motor complex proteins on MTs. ***A–C***, WT (+/+) cells were transfected with BDNF-eGFP and siRNA directed against scramble RNA (scRNA), kinesin 2 (siKin2), or kinesin 1 (siKin1) 1 d before BDNF-eGFP transfection. ***A***, Total extracts were analyzed by Western blot for kinesin-1 (KHC), kinesin-2 (KIF3A), and α-tubulin. ***B***, ***C***, Cells were analyzed by videomicroscopy. Dynamics were quantified by the use of the mean velocity of vesicles per cell (***B***) and their pausing time (***C***). ***D***, MT polymerization experiments were performed from WT cells treated for 4 h with DMSO (0.5%, control, CT) or TSA (5 μM), and analyzed for the presence of kinesin (KHC), dynactin (p150^{Glued}), dynein (DIC), htt, acetylated tubulin, and α-tubulin in S and P fractions using whole-cell extract (WCE). ***E***, Quantitative assessment of the optical density of kinesin (KHC), dynactin (p150^{Glued}), dynein (DIC) expressed as $(S/MT\ P)_{TSA}/(S/MT\ P)_{CT}$ ratios. Results were normalized to 1. $^*p < 0.05$; $^{***}p < 0.001$. ***F***, WT (+/+) cells were treated for 4 h with DMSO (0.1%, CT) or TSA (1 μM), fixed, and stained for tyrosinated tubulin (green) and dynein (DIC; red) or kinesin (KHC; red). Insets correspond, respectively, to a 1.5× and 3× enlargement of the black and white and color images. ***G***, Representative linescan analyses of the distributions of dynein (DIC) and kinesin (KHC) from the MT tips in CT (blue) and after TSA (1 μM; red) treatment.

lymerization, we aimed to analyze the effect of increased tubulin acetylation on other MT dynamic parameters. We used Cos7 cells because these cells contain all of the machinery required for tubulin acetylation and, in contrast to neuronal cells, have a large and flattened cytoplasm as well as a low density of MTs. These cells were transfected with mCherry-α-tubulin (Shaner et al., 2004) and treated or not with TSA. Monitoring the dynamics of mCherry-α-tubulin in transfected cells allowed the analysis of the polymerization and depolymerization of MTs at a single MT level as well as the determination of rescue and catastrophe frequencies. These parameters are defined as the transitions between depolymerization and repolymerization phases (rescue) and between repolymerization and depolymerization phases (catastrophe). We tracked MT tips and found that the rates of MT polymerization and depolymerization were not affected by the presence of TSA (Table 1). Also, we observed no significant differences in the rescue and catastrophe frequencies after TSA treatment, suggesting that MT acetylation has little or no effect on MT dynamics.

Finally, we also assessed by immunofluorescence and immunoblotting analyses the levels of tubulin detyrosination. Detyrosination occurs after MT assembly and is considered a marker of MT stability (Westermann and Weber, 2003). We found that unlike taxol, TSA and tubacin did not affect tubulin detyrosination (supplemental Fig. 1*B*,*C*, available at www.jneurosci.org as supplemental material). Because we did not find any clear association between MT acetylation and stability, we next analyzed the influence of MT stabilization on intracellular transport. We examined this by treating striatal WT cells with TSA or taxol and comparing the dynamics of BDNF vesicles. TSA increased intracellular transport of BDNF, whereas taxol had no significant effect on vesicle velocity and pausing time (supplemental Fig. 1*D*,*E*, available at www.jneurosci.org as supplemental material). Together, these results indicate that tubulin acetylation increases transport but has no effect on MT stability and, conversely, that stabilizing MTs has no impact on BDNF intracellular transport.

Inhibition of tubulin deacetylation in cells increases recruitment of dynein/dynactin and kinesin-1 motor complexes to MTs

We have shown previously that BDNF transport is under the control of the retrograde dynein/dynactin complex (Gauthier et al., 2004). However, the molecular motor leading to anterograde transport of BDNF vesicles is unknown. Recent studies have suggested an association between kinesin-1 and HAP1 (Huntingtin-associated protein 1) (McGuire et al., 2006). Using an RNAi approach, we tested the effect of lowering the levels of kinesin-1 and -2 on BDNF trafficking. We found that BDNF transport was reduced in cells treated with siRNA directed against kinesin-1 but not in cells treated with siRNA directed against kinesin-2 (Fig. 4*A–C*). This suggests that the BDNF vesicular transport depends on the anterograde motor kinesin-1 but not on kinesin-2. Our findings are in agreement with the involvement of conventional kinesin-1 in the anterograde transport of the BDNF receptor TrkB (Yano and Chao, 2004) and with the recent study showing the importance of kinesin-1 in the *in vivo* transport of BDNF in retinal cells (Butowt and von Bartheld, 2007).

Given that acetylation of MTs, and not their stabilization, correlates with increased transport and the observation that the MT-based transport of BDNF involves the dynein/dynactin (Gauthier et al., 2004) and kinesin-1 motor complexes, led us to hypothesize that MT acetylation could regulate the binding of these motor complexes to MTs. Therefore, we analyzed the association of dynein/dynactin and kinesin-1 to MTs under TSA

treatment using biochemical approaches. MTs from striatal +/+ cells treated or not with TSA were depolymerized and centrifuged to isolate the soluble fraction containing free tubulin and soluble proteins (Fig. 4*D*). This fraction was subjected to a subsequent polymerization and sedimentation. We obtained two fractions: the soluble proteins in the S and the polymerized MTs and MAPs in the P. Under TSA treatment, we observed a statistically significant increase in the association of KHC, p150^{Glued} dynactin subunit, and DIC to MTs (Fig. 4*D*,*E*).

We next analyzed by immunofluorescence the distribution of DIC and KHC on tyrosinated MTs in the absence or presence of TSA (Fig. 4*F*). As expected, we observed that KHC was associated with punctate structures along the MTs and that the levels of DIC were higher at the plus ends of polymerizing MTs. When WT cells were treated with TSA, the recruitment of these proteins to MTs was clearly increased (Fig. 4*F*, insets). Notably, we observed an increased association of these motor proteins along the entire length of the MTs. In support, we also observed an increased recruitment of the p150^{Glued} subunit of dynactin (supplemental Fig. 2*A*, available at www.jneurosci.org as supplemental material). In contrast, the localization and intensity of EB1, an MT polymerizing plus-end tracking protein, was not affected by TSA treatment. We quantified the recruitment of the motor proteins to MTs by creating a binary mask from the MT image. Analysis of >30 cells (three independent experiments) per condition revealed a statistically significant increase in the association of DIC, KHC, and p150^{Glued} but not EB1 to the MTs (DIC: 122.0% with respect to CT, unpaired *t* test, $t_{(77)} = -2.757$, $p = 0.008$; KHC: 131.6% with respect to CT, unpaired *t* test, $t_{(75)} = -3.311$, $p = 0.0014$) (supplemental Fig. 2*A*, available at www.jneurosci.org as supplemental material).

As an anti-tyrosinated tubulin antibody stains dynamic MTs, we further confirmed the increased binding of DIC, KHC, and p150^{Glued} to the total pool of MTs using an anti-α-tubulin antibody. We quantified the recruitment of the proteins to the MTs by performing 3D linescan analyses on individual MTs. Single MTs were identified using α-tubulin staining, and a line following the MT structure was generated automatically using an ImageJ plug-in (Fig. 4*G*). The level of recruitment was expressed as the pixel intensity over the MT length and normalized to control. Again, data from two independent experiments revealed a statistically significant increase in the recruitment of DIC, kinesin, and p150^{Glued} but not EB1 (DIC: 153.2% with respect to CT, unpaired *t* test, $t_{(154)} = -3.226$, $p = 0.0015$; KHC: 231.0% with respect to CT, unpaired *t* test, $t_{(164)} = -4.022$, $p < 0.0001$) (supplemental Fig. 2*B*, available at www.jneurosci.org as supplemental material). Interestingly, analysis of individual linescans reveals an increase in binding along the entire length of the MTs (Fig. 4*G*). Altogether, our results show that increasing tubulin acetylation leads to the recruitment of DIC, kinesin, and p150^{Glued} to MTs.

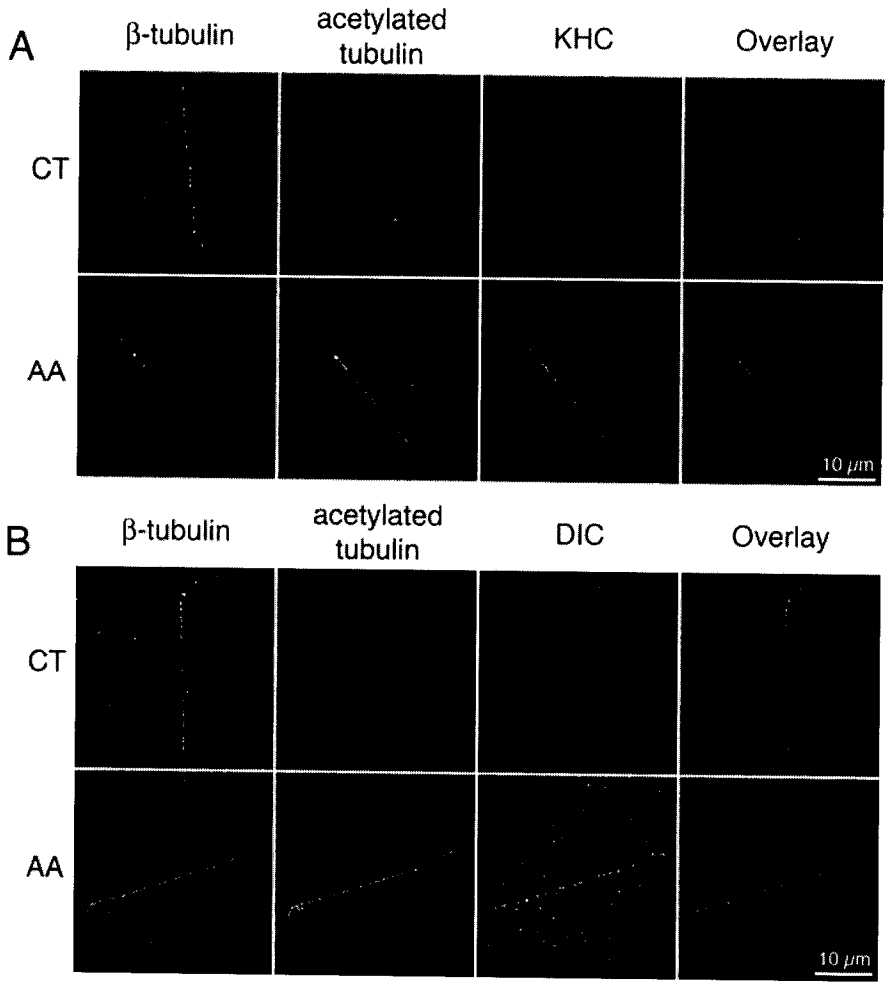

Figure 5. *In vitro* binding of molecular motors to MTs is enhanced by acetylation. ***A***, ***B***, Recombinant MTs were polymerized and incubated or not with 1% AA for 10 min, incubated with recombinant kinesin (***A***) or with purified dynein (***B***), pelleted onto coverslips, fixed, and stained for β-tubulin, acetylated tubulin, and kinesin (KHC) (***A***) or dynein (DIC) (***B***).

In vitro binding of molecular motors to MTs is enhanced by acetylation

To investigate whether the increased recruitment of cytoplasmic dynein and kinesin-1 depends directly on the acetylation of MTs, we tested the *in vitro* binding of purified motor components directly on polymerized MTs. Purified tubulin was polymerized into MTs that were next chemically acetylated using AA as described previously (Piperno and Fuller, 1985). Acetylated MTs were pelleted onto coverslips and analyzed by immunostaining. We found that AA treatment induced acetylation at lysine 40 of α-tubulin and had no obvious effect on the length of the MTs or on the level of their detyrosination (supplemental Fig. 3, available at www.jneurosci.org as supplemental material).

Having created a system for the acetylation of MTs *in vitro*, we assessed the binding of kinesin-1 and cytoplasmic dynein to these acetylated MTs, using methods described previously (Ligon et al., 2006). For kinesin-1, we used a recombinant protein that corresponds to the human KHC motor domain and binds effectively to MTs (Wada et al., 2000). To assess the binding of dynein to MTs, we purified cytoplasmic dynein from bovine brain tissue (Bingham et al., 1998). Absence of any significant contamination from dynactin was established through SDS-PAGE and Western

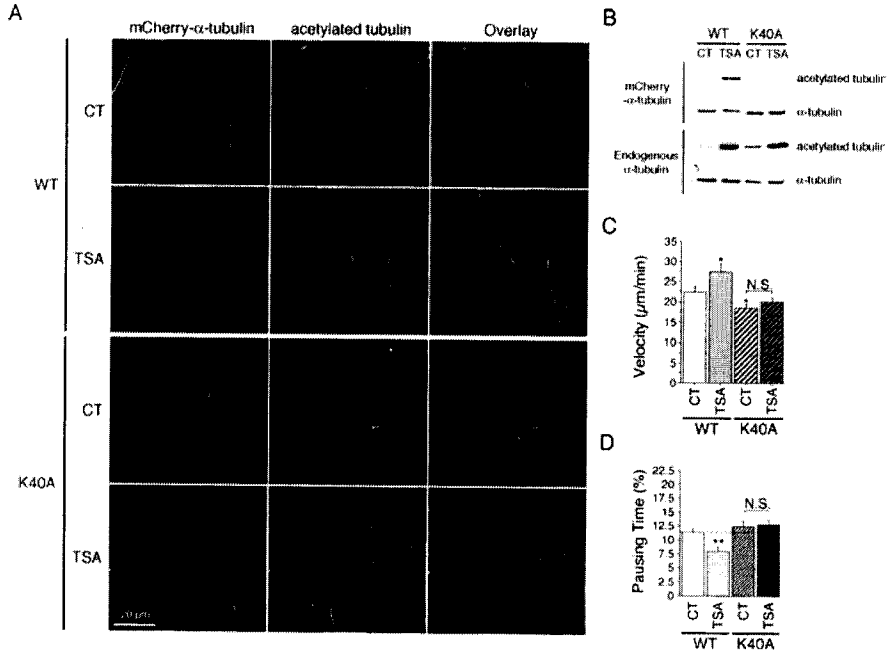

Figure 6. Tubulin acetylation at lysine 40 regulates intracellular transport. ***A***, WT (+/+) cells transfected with WT mCherry-α-tubulin or with mCherry-α-tubulin K40A were treated with DMSO (0.1%, control, CT) or TSA (1 μM) for 4 h, fixed, and immunostained for acetylated tubulin. ***B***, HEK 293 cells were transfected and treated as in ***A*** and analyzed by immunoblotting for acetylated- and total-α-tubulin. ***C***, ***D***, WT (+/+) cells were cotransfected with BDNF-eGFP and with WT mCherry-α-tubulin or with mCherry-α-tubulin K40A, treated with DMSO (0.1%, CT) or TSA (1 μM) for 4 h, and analyzed by videomicroscopy. Dashed lines correspond to the control values. N.S., Not significant. $*p < 0.05$; $**p < 0.01$.

blotting (data not shown). Polymerized MTs were chemically acetylated and incubated with either recombinant KHC or purified dynein and pelleted onto coverslips. Consistent with previous studies (Wada et al., 2000; Mallik et al., 2005), we observed in the control condition a binding of KHC and dynein (Fig. 5). We next determined the binding of both KHC and cytoplasmic dynein after tubulin acetylation and observed a marked increase in the recruitment of motors to the acetylated MTs. We quantified the fluorescence intensity of molecular motors along MTs by performing linescan analyses on 60–150 individual MTs. The increase in the binding of KHC and dynein to acetylated MTs was statistically significant (data from two independent experiments; KHC: 262.5% with respect to CT, unpaired *t* test, $t_{(134)} = -3.394$, $p = 0.0009$; DIC: 358.8% with respect to CT, unpaired *t* test, $t_{(67)} = -3.923$, $p = 0.0002$). We conclude that tubulin acetylation leads to the direct recruitment of the molecular motors cytoplasmic dynein and kinesin-1 on MTs.

Mutation of the acetylation site in tubulin inhibits acetylation and reduces recruitment of motor complex proteins and BDNF transport

To unequivocally establish that MT acetylation promotes the attachment of motor complex proteins to MTs and subsequently the efficiency of transport, we generated a K40A mutant in mCherry-α-tubulin because mutation of this lysine of α-tubulin in *T. thermophila* and in *Chlamydomonas reinhardtii* results in decreased acetylation of tubulin (Kozminski et al., 1993; Gaertig et al., 1995). This mCherry-α-tubulin K40A mutant was correctly incorporated into the MTs as shown by immunofluorescence (Fig. 6*A*), and videomicroscopy experiments did not reveal any differences in the MT dynamics parameters compared with the WT mCherry-α-tubulin (Table 1). However, the ability of this mutant to be acetylated after TSA treatment was lost compared with the WT mCherry-α-tubulin as demonstrated by immunofluorescence (Fig. 6*A*) and Western blotting analyses (Fig. 6*B*). We next analyzed the consequences of the K40A mutation on the dynamics of BDNF vesicles by performing two-color 3D videomicroscopy on striatal cells transfected with BDNF-eGFP and with the WT or the K40A form of mCherry-α-tubulin (Fig. 6*C*,*D*) (supplemental videos 4–7, available at www.jneurosci.org as supplemental material). In control conditions in which cells show a low level of acetylation, we observed a small reduction of BDNF transport in cells expressing the mCherry-α-tubulin K40A construct. However, whereas TSA significantly increased BDNF transport in WT mCherry-α-tubulin-expressing cells, the ability of TSA to increase BDNF transport was lost in mCherry-α-tubulin K40A-expressing cells showing that the stimulatory effect of TSA requires acetylation of tubulin at lysine 40 (supplemental videos 4–7, available at www.jneurosci.org as supplemental material).

Because TSA treatment increases the association of dynein/dynactin and kinesin-1 to MTs, we determined *in vitro* the recruitment of motors to MTs that contain either an intact lysine 40 or a lysine mutated into an alanine. We transfected HEK293 cells with WT mCherry-α-tubulin or K40A constructs, treated the cells with TSA (1 μM), and then purified the MTs by two successive rounds of depolymerization/polymerization in the presence of TSA and high ATP concentration. These conditions led to the removal of most, if not all, motors from the MTs (data not shown). The purified MT fraction was next repolymerized, incubated with either recombinant KHC or purified dynein, and analyzed as above except that quantifications were expressed as a kinesin (or dynein) intensity/mCherry-α-tubulin intensity/MT length ratio. Quantification of motors on MTs revealed a statistically significant reduction in the binding of both KHC and dynein when lysine 40 was mutated (data from two independent experiments; KHC: 35.8% with respect to wild type, unpaired *t* test, $t_{(161)} = 5.214$, $p < 0.0001$; dynein: 33.7% with respect to wild type, unpaired *t* test, $t_{(171)} = 5.416$, $p < 0.0001$). Altogether, our *in vitro* experiments demonstrate that MT acetylation on lysine 40 increases motor recruitment to MTs.

MT acetylation is altered in HD patients and is enhanced by TSA in neurons

To assess the physiological relevance of our findings to HD, we determined the level of tubulin acetylation in postmortem striatal samples from grade 3 and 4 HD patients. Strikingly, we found a dramatic decrease in the level of acetylated-α-tubulin in HD patients compared with control individuals (Fig. 7*A*). The total levels of α-tubulin were not changed, further demonstrating a specific decrease of tubulin acetylation in HD.

We next tested whether HDAC inhibitors are able to increase acetylation levels in cortical neurons. Indeed, postmitotic differentiated neurons have stable MTs and a high level of acetylation. However, TSA treatment still led to a significant increase in the

acetylation of MTs as confirmed both by immunostaining approaches and by immunoblotting analyses (Fig. 7*B*,*C*). TSA had a similar capacity to induce MT acetylation in neurons as in other cell types such as Cos7 cells and WT or mutant striatal cells (supplemental Fig. 4*A*, available at www.jneurosci.org as supplemental material). We also analyzed the effect of TSA on the distribution of BDNF-eGFP vesicles in cortical neurons and found, as for striatal cells, no significant changes in the localization of BDNF vesicles (supplemental Fig. 4*B*, available at www.jneurosci.org as supplemental material).

Acetylation at Lys40 of tubulin enhances bidirectional transport in cortical neurons

We next investigated the effect of lysine 40 mutation on both MT acetylation and transport in neurons. Whereas TSA treatment led to a significant increase of tubulin acetylation when neurons express the WT mCherry-α-tubulin, TSA was unable to induce acetylation in neurons that express mCherry-α-tubulin K40A (Fig. 7*D*). We then analyzed anterograde and retrograde transport of BDNF-eGFP in neurites of cortical neurons, because we observed that TSA induced the recruitment to MTs of both anterograde and retrograde motors *in vitro* and in cells. TSA treatment significantly increased intracellular transport of vesicles in both directions to the same extent (Fig. 7*E*,*F*). Additional analyses revealed that none of the transport values were significantly affected by the overexpression of WT mCherry-α-tubulin (data not shown). Strikingly, we found that the capacity of TSA to increase transport in either direction was lost when α-tubulin cannot be acetylated at lysine 40 (Fig. 7*E*,*F*).

We next determined the net flux of BDNF vesicles in both anterograde and retrograde directions. We found that MT acetylation at lysine 40 induced a significant increase in the net flux in both directions. This effect was abolished when α-tubuiin cannot be acetylated at lysine 40 (Fig. 7*G*). Together, we conclude that TSA mediates its stimulatory effect on BDNF transport in neurons through the acetylation of α-tubulin at lysine 40.

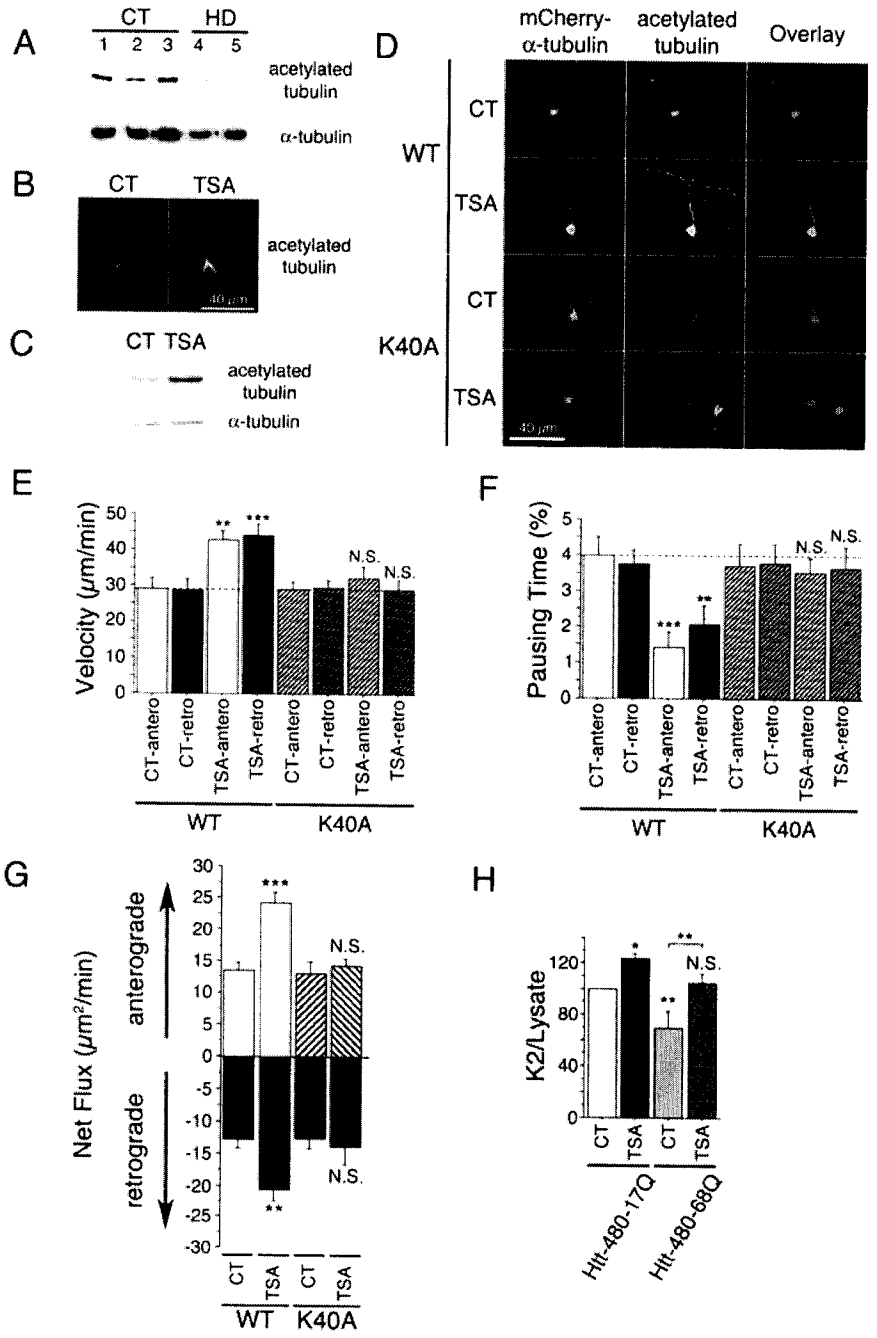

Figure 7. Tubulin acetylation at lysine 40 stimulates bidirectional transport and rescues BDNF release in HD. ***A***, Acetylated tubulin levels are decreased in the brain of HD patients. Protein extracts are prepared from whole striatum of CT (samples 1–3) and HD individuals (HD grade 3, sample 4; HD grade 4, sample 5) and analyzed by immunoblotting for acetylated and total α-tubulin. ***B***, ***C***, Cortical neurons were treated with DMSO (0.1%, CT) or TSA (1 μM) for 4 h and analyzed by immunofluorescence (***B***) and immunoblotting (***C***) for the presence of acetylated tubulin. ***D***, Cortical neurons were transfected with WT mCherry-α-tubulin or mCherry-α-tubulin K40A, treated for 4 h with DMSO (0.1%, CT) or TSA (1 μM), and analyzed by immunofluorescence for the presence of mCherry-α-tubulin (red) and acetylated tubulin (green). ***E***, ***F***, Cortical neurons were cotransfected with BDNF-eGFP and either WT mCherry-α-tubulin or mCherry-α-tubulin K40A, treated for 4 h with DMSO (0.1%, CT) or TSA (1 μM), and anterograde and retrograde vesicular movements in neurites were analyzed by videomicroscopy. Dotted lines correspond to the control values. ***G***, TSA treatment increases anterograde and retrograde flux in a lysine 40-dependent manner. ***H***, Cortical neurons were electroporated with BDNF and either htt-480–17Q or htt-480–68Q and treated for 4 h with DMSO (0.1%, CT) or TSA (1 μM). Transport-dependent BDNF release after a second KCl-induced depolarization is expressed as a K2/lysate ratio. N.S., Not significant. $^{*}p < 0.05$; $^{**}p < 0.01$; $^{***}p < 0.001$.

MT acetylation in neurons promotes release of BDNF in HD

To analyze the physiological consequences of an increased transport in primary neurons, we electroporated primary cultures of cortical neurons with constructs encoding BDNF and N-terminal fragments of htt that contain the first 480 amino acids with 17Q or 68Q and determined the capacity of neurons to release BDNF when treated with TSA. The 480 N-terminal fragment of htt is as efficient as the full-length htt in promoting intracellular transport (data not shown). We first depolarized neurons to release the pool of vesicles present at the

membrane and performed a K2 30 min after the first one to release the vesicles that had been transported to the plasma membrane (Gauthier et al., 2004). The quantity of BDNF released during the K2 normalized to the BDNF content in neuronal lysates reflects transport-dependent release of BDNF. This value was decreased when MTs are depolymerized (Gauthier et al., 2004). As described previously (Gauthier et al., 2004), htt that contains the polyQ expansion released a lower amount of BDNF compared with WT htt (Fig. 7*H*). However, TSA induced a statistically significant increase in the release of BDNF in neurons expressing either WT or polyQ htt. Our results show that by acetylating MTs at lysine 40, TSA promotes axonal transport and the release of BDNF from neurons. Furthermore, TSA is efficient at restoring the disrupted BDNF transport and release in disease, making it of therapeutic interest in HD.

Discussion

We demonstrate here that HDAC inhibitors increase MT-dependent transport by the inhibition of HDAC6. This inhibition leads to increased acetylation of lysine 40 of α-tubulin and the subsequent recruitment of kinesin-1 and dynein/dynactin to the more acetylated MTs. Our results are in agreement with a recent study by Verhey et al. (Reed et al., 2006) that demonstrated a role for the acetylation at Lys40 of α-tubulin in *T. thermophila* in the regulation of kinesin-1 binding to MTs. α-Tubulin acetylation at Lys40 was found to enhance kinesin-1 motility along MTs *in vitro*. In cells, MT acetylation induced an increase in the transport of JIP1. In particular, pharmacological inhibition of HDAC6 in neurons led to the redirection of kinesin-1 transport of JIP1 to the tips of the neurites. Our study shows that, in addition to the recruitment of kinesin-1, MT acetylation also leads to the recruitment of the retrograde motor dynein. Analysis of the dynamic properties of BDNF-containing vesicles revealed that MT acetylation stimulates not only anterograde but also retrograde transport, suggesting a general role for MT acetylation in the stimulation of intracellular dynamics through the recruitment of both anterograde and retrograde motors. A general role for MT acetylation is also supported by the observations that not only transport of cargo proteins such as JIP1 but also of BDNF-containing vesicles is enhanced when MTs are acetylated. In support, we also found that stimulation of vesicular transport was not restricted to BDNF-containing vesicles as intracellular dynamics of lysosomes and of VSV-G, a glycoprotein from the vesicular stomatitis virus, which can be used to follow vesicular transport in the secretory pathway, were also enhanced by TSA treatment (data not shown).

How does acetylated tubulin recruit molecular motors? According to cryoelectron microscopy and 3D reconstruction of intact MTs, lysine 40 is located in the lumen of the MT (Nogales et al., 1998). The increased binding *in vitro* of dynein and kinesin-1 to acetylated MTs (present study and Reed et al., 2006) suggests that motors are directly recruited to acetylated MTs. Therefore, one possible explanation for how acetylation could lead to an increased binding of motor proteins is that acetylation could change the conformation of MTs to a form with higher affinity for motors. In agreement, several studies focusing on the binding of kinesin-1 to MTs have demonstrated a change in the conformations between plain MTs and MT-kinesin complexes, suggesting that MTs might regulate intracellular transport through modulations of their core structure (Krebs et al., 2004; Skiniotis et al., 2004). A similar mechanism could occur for the dynein/dynactin complex. In support, dynein and kinesin-1 share an overlapping binding site on MTs (Mizuno et al., 2004).

We show that HDAC inhibitors that enhance tubulin acetylation compensate for the transport deficit in striatal cells that contain a pathological polyQ expansion in the htt protein. In particular, using various parameters to assess intracellular transport (mean velocity, pausing time, percentage of static vesicles, and processivity), we show that treatment of HD cells with TSA and SAHA almost completely restore BDNF transport values to the control situation. Although the transport of mitochondria is not altered in HD striatal cells (Gauthier et al., 2004), we observed defects in the transport of small vesicles, such as lysosomes, suggesting an impairment in the transport of other organelles than BDNF in HD (data not shown). Interestingly, the beneficial effect of HDAC6 inhibition is also not restricted to BDNF-containing vesicles because TSA treatment enhances transport of lysosomes and of secretory vesicles such as VSV-G-labeled organelles. Therefore, HDAC6 inhibition, by acting on a wide population of organelles whose transport is altered in disease, could have a larger and more efficient therapeutic effect.

As shown in this study and by Verhey et al. (Reed et al., 2006), this mechanism is relevant in neurons because HDAC6 inhibition in primary cultures of neurons results in an effective MT acetylation and stimulates axonal transport. Indeed, tubacin treatment of hippocampal neurons enhances anterograde transport of JIP1 to the tips of neurites (Reed et al., 2006). We show here that MT acetylation stimulates both anterograde and retrograde transport of BDNF-containing vesicles in the neurites of cortical neurons. Finally, we found that TSA treatment leads to BDNF release in cortical neurons expressing polyQ htt. Together with our previous observations demonstrating an impairment in the axonal transport and subsequent release of BDNF vesicles in cortical neurons expressing polyQ htt, this adds to the rationale that HDAC6 inhibition could be an effective therapeutic strategy in HD.

HDAC6 was reported previously to participate in the clearance of misfolded ubiquitinated proteins in cells by promoting dynein/retrograde dependent transport of such proteins to the centrosome (Kawaguchi et al., 2003). PolyQ-containing proteins, such as htt, also accumulate into aggregates of misfolded proteins that are actively transported to the centrosome to be degraded by the ubiquitin-proteasome system (UPS) or through autophagic degradation when the UPS is impaired (Ravikumar et al., 2002; Ciechanover and Brundin, 2003; Qin et al., 2003; Iwata et al., 2005). Interestingly, efficient autophagic degradation of polyQ-containing peptides is dependent on HDAC6, dynein, and MT-dependent transport (Webb et al., 2004; Iwata et al., 2005; Ravikumar et al., 2005). Here, we dissected the mechanism by which tubulin acetylation enhances intracellular transport along MTs. We believe this HDAC6-dependent mechanism to be distinct from those involved in the clearance of misfolded aggregates for several reasons. First, whereas this transport is a dynein/retrograde-dependent transport to the centrosome, TSA stimulates anterograde and retrograde transport. Second, we show that HDAC6 inhibition increases transport both in WT cells and in primary cultures of neurons. These experiments were performed independently of the pathological context. Third, in experiments using mutant cells that recapitulate the genetic situation observed in HD patients, no microscopically visible aggregates could be detected (data not shown). Finally, we show that HDAC6 inhibition rescues intracellular transport in the pathological situation. These experiments are close to the physiological conditions because full length WT and mutant htt are present in striatal cells at endogenous levels and do not involve the overexpression of short polyQ-htt fragments that are highly susceptible to aggregate formation.

Inhibition of tubulin deacetylases other than HDAC6 could also be of interest in an HD context. In particular, the NAD+-dependent sirtuin 2 (SIRT2) HDAC shows some substrate preference for tubulin peptides compared with histone peptides, and SIRT2 knockdown through siRNA results in tubulin hyperacetylation (North et al., 2003). It will be interesting, when available, to test whether selective SIRT2 inhibitors are able to stimulate intracellular transport.

HDAC inhibitors, such as SAHA, TSA, and NaPB, exhibit neuroprotective effects by inhibiting the HDAC1 enzyme (Butler and Bates, 2006). Here we show that some of these drugs could also protect neurons in HD by promoting the intracellular transport of BDNF through the inhibition of HDAC6 and subsequent tubulin acetylation. Our results support the strategy of combining drugs that allow an effective inhibition of the enzymes of both HDAC1 and HDAC6 families.

Our results validate the use of 3D fast videomicroscopy to screen for compounds able to restore intracellular transport in HD neurons. We show here that the increased acetylation of MTs induced by HDAC6 inhibitors can act as a general mechanism to regulate MT-based transport. Therefore, our finding may also have implications for other neurodegenerative disorders, such as Alzheimer's disease (AD), in which intracellular transport is altered (Kamal et al., 2001; Pigino et al., 2003; Stokin et al., 2005). Indeed, the analysis of postmortem brain samples from AD patients revealed reduced α-tubulin acetylation in neurons with neurofibrillary forms of tau (Hempen and Brion, 1996; Saragoni et al., 2000).

References

Altar CA, Cai N, Bliven T, Juhasz M, Conner JM, Acheson AL, Lindsay RM, Wiegand SJ (1997) Anterograde transport of brain-derived neurotrophic factor and its role in the brain. Nature 389:856–860.

Baquet ZC, Gorski JA, Jones KR (2004) Early striatal dendrite deficits followed by neuron loss with advanced age in the absence of anterograde cortical brain-derived neurotrophic factor. J Neurosci 24:4250–4258.

Bingham JB, King SJ, Schroer TA (1998) Purification of dynactin and dynein from brain tissue. Methods Enzymol 298:171–184.

Butler R, Bates GP (2006) Histone deacetylase inhibitors as therapeutics for polyglutamine disorders. Nat Rev Neurosci 7:784–796.

Butowt R, von Bartheld CS (2007) Conventional kinesin-I motors participate in the anterograde axonal transport of neurotrophins in the visual system. J Neurosci Res, in press.

Ciechanover A, Brundin P (2003) The ubiquitin proteasome system in neurodegenerative diseases: sometimes the chicken, sometimes the egg. Neuron 40:427–446.

Drummond DC, Noble CO, Kirpotin DB, Guo Z, Scott GK, Benz CC (2005) Clinical development of histone deacetylase inhibitors as anticancer agents. Annu Rev Pharmacol Toxicol 45:495–528.

Evans L, Mitchison T, Kirschner M (1985) Influence of the centrosome on the structure of nucleated microtubules. J Cell Biol 100:1185–1191.

Gaertig J, Cruz MA, Bowen J, Gu L, Pennock DG, Gorovsky MA (1995) Acetylation of lysine 40 in alpha-tubulin is not essential in *Tetrahymena thermophila*. J Cell Biol 129:1301–1310.

Gauthier LR, Charrin BC, Borrell-Pages M, Dompierre JP, Rangone H, Cordelieres FP, De Mey J, MacDonald ME, Lessmann V, Humbert S, Saudou F (2004) Huntingtin controls neurotrophic support and survival of neurons by enhancing BDNF vesicular transport along microtubules. Cell 118:127–138.

Goldstein LS, Laymon RA, McIntosh JR (1986) A microtubule-associated protein in *Drosophila melanogaster*: identification, characterization, and isolation of coding sequences. J Cell Biol 102:2076–2087.

Gunawardena S, Her LS, Brusch RG, Laymon RA, Niesman IR, Gordesky-Gold B, Sintasath L, Bonini NM, Goldstein LS (2003) Disruption of axonal transport by loss of huntingtin or expression of pathogenic polyQ proteins in *Drosophila*. Neuron 40:25–40.

Haggarty SJ, Koeller KM, Wong JC, Grozinger CM, Schreiber SL (2003) Domain-selective small-molecule inhibitor of histone deacetylase 6 (HDAC6)-mediated tubulin deacetylation. Proc Natl Acad Sci USA 100:4389–4394.

Hartmann M, Heumann R, Lessmann V (2001) Synaptic secretion of BDNF after high-frequency stimulation of glutamatergic synapses. EMBO J 20:5887–5897.

Haubensak W, Narz F, Heumann R, Lessmann V (1998) BDNF-GFP containing secretory granules are localized in the vicinity of synaptic junctions of cultured cortical neurons. J Cell Sci 111:1483–1493.

Hempen B, Brion JP (1996) Reduction of acetylated alpha-tubulin immunoreactivity in neurofibrillary tangle-bearing neurons in Alzheimer's disease. J Neuropathol Exp Neurol 55:964–972.

Hu E, Dul E, Sung CM, Chen Z, Kirkpatrick R, Zhang GF, Johanson K, Liu R, Lago A, Hofmann G, Macarron R, de los Frailes M, Perez P, Krawiec J, Winkler J, Jaye M (2003) Identification of novel isoform-selective inhibitors within class I histone deacetylases. J Pharmacol Exp Ther 307:720–728.

Hubbert C, Guardiola A, Shao R, Kawaguchi Y, Ito A, Nixon A, Yoshida M, Wang XF, Yao TP (2002) HDAC6 is a microtubule-associated deacetylase. Nature 417:455–458.

Humbert S, Bryson EA, Cordelieres FP, Connors NC, Datta SR, Finkbeiner S, Greenberg ME, Saudou F (2002) The IGF-1/Akt pathway is neuroprotective in Huntington's disease and involves Huntingtin phosphorylation by Akt. Dev Cell 2:831–837.

Ingold AL, Cohn SA, Scholey JM (1988) Inhibition of kinesin-driven microtubule motility by monoclonal antibodies to kinesin heavy chains. J Cell Biol 107:2657–2667.

Iwata A, Riley BE, Johnston JA, Kopito RR (2005) HDAC6 and microtubules are required for autophagic degradation of aggregated huntingtin. J Biol Chem 280:40282–40292.

Kamal A, Almenar-Queralt A, LeBlanc JF, Roberts EA, Goldstein LS (2001) Kinesin-mediated axonal transport of a membrane compartment containing beta-secretase and presenilin-1 requires APP. Nature 414:643–648.

Kawaguchi Y, Kovacs JJ, McLaurin A, Vance JM, Ito A, Yao TP (2003) The deacetylase HDAC6 regulates aggresome formation and cell viability in response to misfolded protein stress. Cell 115:727–738.

Kohara K, Kitamura A, Morishima M, Tsumoto T (2001) Activity-dependent transfer of brain-derived neurotrophic factor to postsynaptic neurons. Science 291:2419–2423.

Kozminski KG, Diener DR, Rosenbaum JL (1993) High level expression of nonacetylatable alpha-tubulin in *Chlamydomonas reinhardtii*. Cell Motil Cytoskeleton 25:158–170.

Krebs A, Goldie KN, Hoenger A (2004) Complex formation with kinesin motor domains affects the structure of microtubules. J Mol Biol 335:139–153.

Lee WC, Yoshihara M, Littleton JT (2004) Cytoplasmic aggregates trap polyglutamine-containing proteins and block axonal transport in a *Drosophila* model of Huntington's disease. Proc Natl Acad Sci USA 101:3224–3229.

Ligon LA, Shelly SS, Tokito MK, Holzbaur EL (2006) Microtubule binding proteins CLIP-170, EB1, and p150^{Glued} form distinct plus-end complexes. FEBS Lett 580:1327–1332.

MacDonald ME, Gines S, Gusella JF, Wheeler VC (2003) Huntington's Disease. Neuromolecular Med 4:7–20.

Mallik R, Petrov D, Lex SA, King SJ, Gross SP (2005) Building complexity: an in vitro study of cytoplasmic dynein with in vivo implications. Curr Biol 15:2075–2085.

Manders EM, Stap J, Brakenhoff GJ, van Driel R, Aten JA (1992) Dynamics of three-dimensional replication patterns during the S-phase, analysed by double labelling of DNA and confocal microscopy. J Cell Sci 103:857–862.

Matsuyama A, Shimazu T, Sumida Y, Saito A, Yoshimatsu Y, Seigneurin-Berny D, Osada H, Komatsu Y, Nishino N, Khochbin S, Horinouchi S, Yoshida M (2002) In vivo destabilization of dynamic microtubules by HDAC6-mediated deacetylation. EMBO J 21:6820–6831.

McGuire JR, Rong J, Li SH, Li XJ (2006) Interaction of Huntingtin-associated protein-1 with kinesin light chain: implications in intracellular trafficking in neurons. J Biol Chem 281:3552–3559.

Mizuno N, Toba S, Edamatsu M, Watai-Nishii J, Hirokawa N, Toyoshima YY, Kikkawa M (2004) Dynein and kinesin share an overlapping microtubule-binding site. EMBO J 23:2459–2467.

Nogales E, Wolf SG, Downing KH (1998) Structure of the alpha beta tubulin dimer by electron crystallography. Nature 391:199–203.

North BJ, Marshall BL, Borra MT, Denu JM, Verdin E (2003) The human Sir2 ortholog, SIRT2, is an NAD+-dependent tubulin deacetylase. Mol Cell 11:437–444.

Pigino G, Morfini G, Pelsman A, Mattson MP, Brady ST, Busciglio J (2003) Alzheimer's presenilin 1 mutations impair kinesin-based axonal transport. J Neurosci 23:4499–4508.

Piperno G, Fuller MT (1985) Monoclonal antibodies specific for an acetylated form of alpha-tubulin recognize the antigen in cilia and flagella from a variety of organisms. J Cell Biol 101:2085–2094.

Qin ZH, Wang Y, Kegel KB, Kazantsev A, Apostol BL, Thompson LM, Yoder J, Aronin N, DiFiglia M (2003) Autophagy regulates the processing of amino terminal huntingtin fragments. Hum Mol Genet 12:3231–3244.

Ravikumar B, Duden R, Rubinsztein DC (2002) Aggregate-prone proteins with polyglutamine and polyalanine expansions are degraded by autophagy. Hum Mol Genet 11:1107–1117.

Ravikumar B, Acevedo-Arozena A, Imarisio S, Berger Z, Vacher C, O'Kane CJ, Brown SD, Rubinsztein DC (2005) Dynein mutations impair autophagic clearance of aggregate-prone proteins. Nat Genet 37:771–776.

Reed NA, Cai D, Blasius TL, Jih GT, Meyhofer E, Gaertig J, Verhey KJ (2006) Microtubule acetylation promotes kinesin-1 binding and transport. Curr Biol 16:2166–2172.

Saragoni L, Hernandez P, Maccioni RB (2000) Differential association of tau with subsets of microtubules containing posttranslationally-modified tubulin variants in neuroblastoma cells. Neurochem Res 25:59–70.

Saudou F, Finkbeiner S, Devys D, Greenberg ME (1998) Huntingtin acts in the nucleus to induce apoptosis but death does not correlate with the formation of intranuclear inclusions. Cell 95:55–66.

Seigneurin-Berny D, Verdel A, Curtet S, Lemercier C, Garin J, Rousseaux S, Khochbin S (2001) Identification of components of the murine histone deacetylase 6 complex: link between acetylation and ubiquitination signaling pathways. Mol Cell Biol 21:8035–8044.

Shaner NC, Campbell RE, Steinbach PA, Giepmans BN, Palmer AE, Tsien RY (2004) Improved monomeric red, orange and yellow fluorescent proteins derived from *Discosoma* sp. red fluorescent protein. Nat Biotechnol 22:1567–1572.

Skiniotis G, Cochran JC, Muller J, Mandelkow E, Gilbert SP, Hoenger A (2004) Modulation of kinesin binding by the C-termini of tubulin. EMBO J 23:989–999.

Stepanova T, Slemmer J, Hoogenraad CC, Lansbergen G, Dortland B, De Zeeuw CI, Grosveld F, van Cappellen G, Akhmanova A, Galjart N (2003) Visualization of microtubule growth in cultured neurons via the use of EB3-GFP (end-binding protein 3-green fluorescent protein). J Neurosci 23:2655–2664.

Stokin GB, Lillo C, Falzone TL, Brusch RG, Rockenstein E, Mount SL, Raman R, Davies P, Masliah E, Williams DS, Goldstein LS (2005) Axonopathy and transport deficits early in the pathogenesis of Alzheimer's disease. Science 307:1282–1288.

Szebenyi G, Morfini GA, Babcock A, Gould M, Selkoe K, Stenoien DL, Young M, Faber PW, MacDonald ME, McPhaul MJ, Brady ST (2003) Neuropathogenic forms of huntingtin and androgen receptor inhibit fast axonal transport. Neuron 40:41–52.

Taddei A, Roche D, Bickmore WA, Almouzni G (2005) The effects of histone deacetylase inhibitors on heterochromatin: implications for anticancer therapy? EMBO Rep 6:520–524.

Toomre D, Keller P, White J, Olivo JC, Simons K (1999) Dual-color visualization of trans-Golgi network to plasma membrane traffic along microtubules in living cells. J Cell Sci 112:21–33.

Trettel F, Rigamonti D, Hilditch-Maguire P, Wheeler VC, Sharp AH, Persichetti F, Cattaneo E, MacDonald ME (2000) Dominant phenotypes produced by the HD mutation in STHdh(Q111) striatal cells. Hum Mol Genet 9:2799–2809.

Trushina E, Dyer RB, Badger II JD, Ure D, Eide L, Tran DD, Vrieze BT, Legendre-Guillemin V, McPherson PS, Mandavilli BS, Van Houten B, Zeitlin S, McNiven M, Aebersold R, Hayden M, Parisi JE, Seeberg E, Dragatsis I, Doyle K, Bender A, et al. (2004) Mutant huntingtin impairs axonal trafficking in mammalian neurons in vivo and in vitro. Mol Cell Biol 24:8195–8209.

Vaughan KT, Tynan SH, Faulkner NE, Echeverri CJ, Vallee RB (1999) Colocalization of cytoplasmic dynein with dynactin and CLIP-170 at microtubule distal ends. J Cell Sci 112:1437–1447.

Wada Y, Hamasaki T, Satir P (2000) Evidence for a novel affinity mechanism of motor-assisted transport along microtubules. Mol Biol Cell 11:161–169.

Webb JL, Ravikumar B, Rubinsztein DC (2004) Microtubule disruption inhibits autophagosome-lysosome fusion: implications for studying the roles of aggresomes in polyglutamine diseases. Int J Biochem Cell Biol 36:2541–2550.

Westermann S, Weber K (2003) Post-translational modifications regulate microtubule function. Nat Rev Mol Cell Biol 4:938–947.

Xia Z, Dudek H, Miranti CK, Greenberg ME (1996) Calcium influx via the NMDA receptor induces immediate early gene transcription by a MAP kinase/ERK-dependent mechanism. J Neurosci 16:5425–5436.

Yano H, Chao MV (2004) Mechanisms of neurotrophin receptor vesicular transport. J Neurobiol 58:244–257.

Zhang Y, Li N, Caron C, Matthias G, Hess D, Khochbin S, Matthias P (2003) HDAC-6 interacts with and deacetylates tubulin and microtubules in vivo. EMBO J 22:1168–1179.

PHOTO / DONNA COVENEY

Fujimoto

New visualization methods could improve early diagnosis of disease

Elizabeth Thomson
News Office

In work that could improve diagnoses of many eye diseases, MIT researchers have developed a new type of laser for taking high-resolution, 3-D images of the retina, the part of the eye that converts light to electrical signals that travel to the brain.

The research will be presented at the Conference on Lasers and Electro-Optics and the Quantum Electronics and Laser Science Conference in Baltimore on May 10.

The new imaging system is based on Optical Coherence Tomography (OCT), which uses light to obtain high-resolution, cross-sectional images of the eye to visualize subtle changes that occur in retinal disease. OCT was developed in the early 1990s by MIT Professor James Fujimoto, Eric Swanson at MIT Lincoln Laboratory and collaborators; Fujimoto is an author of the report to be presented in May.

"Within the last few years optical coherence tomography has become a standard diagnostic for ophthalmology. New techniques are now enabling dramatic increases in image acquisition speeds. These advances promise to enable new an dimensional visualization could improve early dia and treatment monitorin who holds appointments ment of Electrical Enginee er Science and the Resea Electronics.

Conventional OCT i yields a series of two-di sectional images of the re combined to form a 3-D in

See **EYE IMA**
Page 4

r team reverses ner's-like ms in mice

ies may prove accessible

Deborah Halber
lews Office Correspondent

ains had atrophied like those of Alzheim- ts regained long-term memories and the ter living in an enriched environment, IT's Picower Institute for Learning and n the April 29 online edition of Nature. also were achieved with a new experi- igs.

Picower Professor of Neuroscience in f Brain and Cognitive Sciences, and col- it environmental enrichment—for labo- g exposed to stimuli that enhance their chological well-being—induced the ani- start to sprout new connections.

g because our results show that learning roved and 'lost' long-term memories can n after a significant number of neurons lost in the brain," said Tsai, who is also

See **ALZHEIMER'S**
Page 2

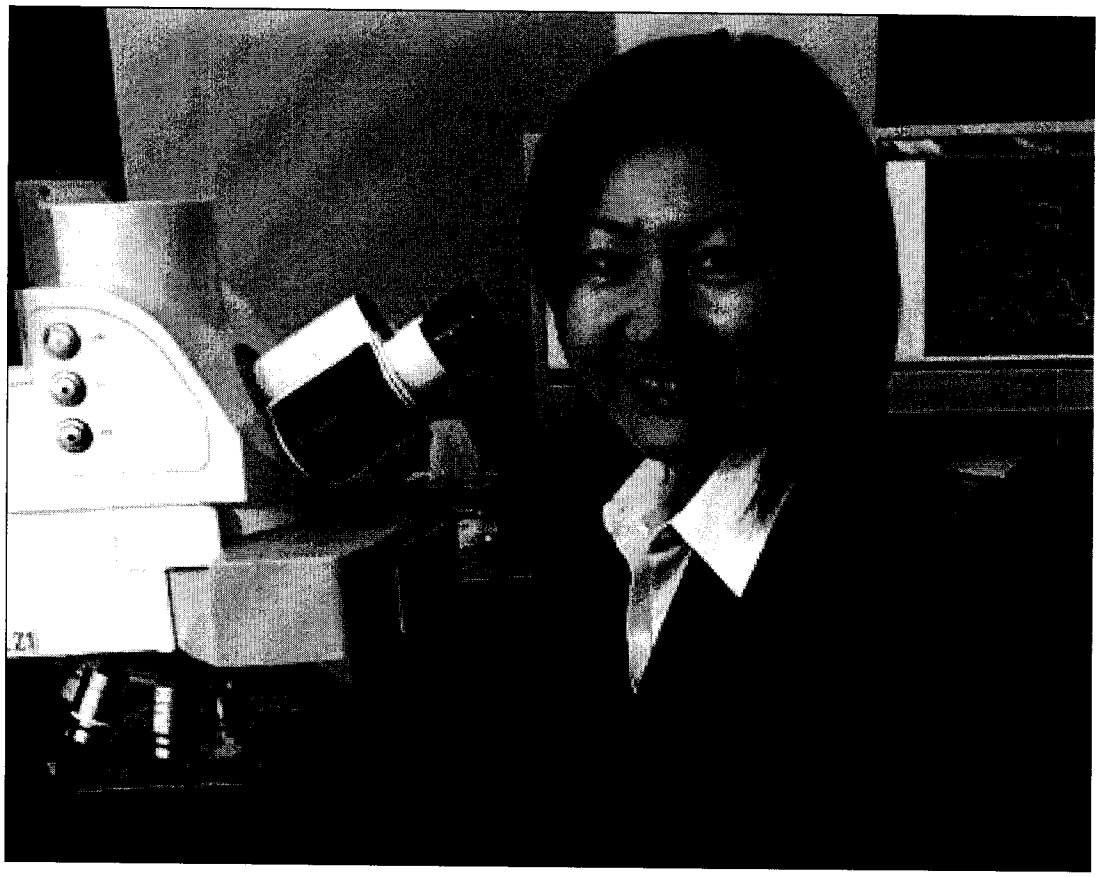

PH

Li-Huei Tsai, Picower Professor of Neuroscience in the Department of Brain and Cognitive Sciences, an found that exposing lab mice to certain environmental stimuli induced the animals' brain cells to make r

urges support for basic science

rah Halber
ce Correspondent

rt Horvitz started study- molecular processes in ne had no idea whether ever be relevant to any- obscure little organism

with a Nobel prize under ow knows his pioneering med cell death has pro- for possible new inter- S, cancer, autoimmune y others.

avid H. Koch Professor y and Howard Hughes

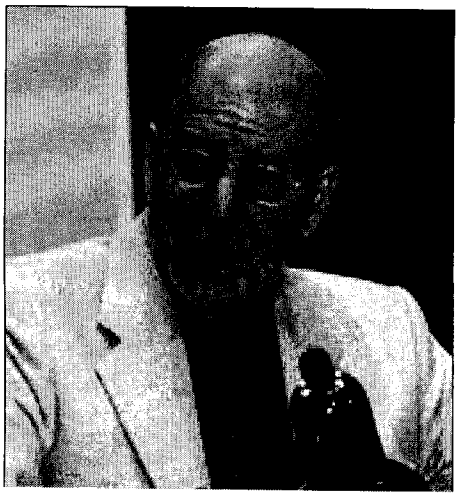

Systems biology, in search of a me tries out language of machines, in

Robin H. Ray
News Office Correspondent

Sociology professor Joan Fujimura, visiting MIT from the University of Wisconsin at Madison, discussed her recent work at a Program in Science, Technology and Society (STS) colloquium on April 23. Formerly a specialist in anthropology at Stanford, Fujimura has since focused her attention on the sociology of science, particularly notions of nature/culture and science/society in the fields of genetics, bioinformatics and systems biology in the United States, Europe and Japan.

my research," and she f biology mirrors a lot o oretical and methodol that we have in STS." A problem"—in STS as m biology—"is how to re ity and still say somethi coherent."

Systems biology is a field, one that even its p define to mutual satisf explicit about their onto Fujimura said. Some s term "systems biology" to projects exploring in networks. Others see it

PHOTO / **DONNA COVENEY**

ector of arts communication
the Arts, joins in the African
ide of Stata as part of MIT's
ities.

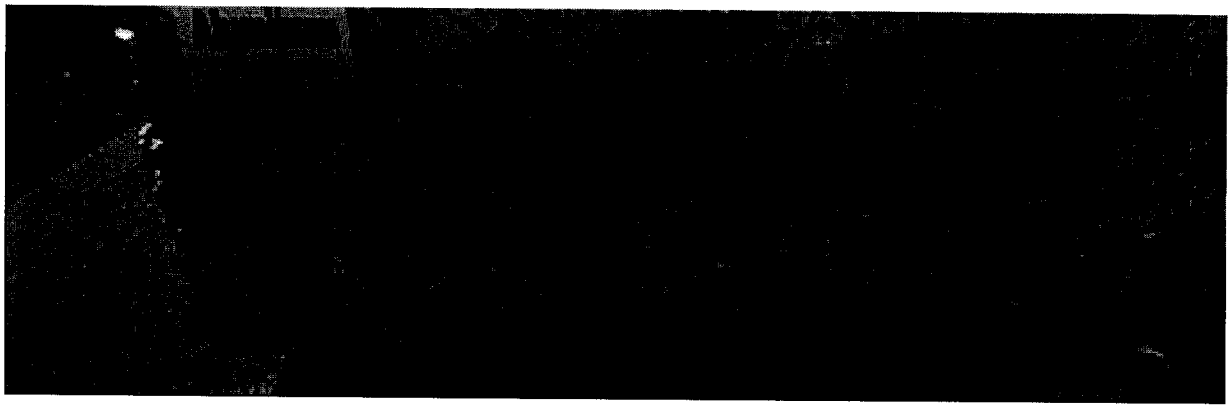

PHOTO

Earth day

This bale of aluminum soda cans and other containers was outside Stata to remind people to recycle.

es Ferguson

Broad Institute will screen 'No End in Sight'

"No End in Sight: The American Occupation of Iraq," a film directed by Charles Ferguson, visiting scholar at MIT's Center for International Studies, will be screened for the public in the auditorium of the Broad Institute of MIT and Harvard on Wednesday, May 2, at 6 p.m.

"No End in Sight" won a special jury prize at the 2007 Sundance Film Festival, held in Park City, Utah. The screening, to be followed by a discussion with the director, is sponsored by the MIT Center for International Studies' Starr Forum.

"No End in Sight" analyzes Iraq's descent into guerilla war, warlord rule, criminality and anarchy.

Based on more than 200 hours of footage, the film retells the events following the fall of Baghdad in 2003 through interviews of such high-ranking officials as former Deputy Secretary of State Richard Armitage, Ambassador Barbara Bodine (who was in charge of Baghdad during the spring of 2003), Lawrence Wilkerson, former chief of staff to Colin Powell, and General Jay Garner (who was in charge of the occupation of Iraq through May 2003), as well as Iraqi civilians, American soldiers and prominent analysts.

Ferguson received his B.A. in mathematics from Berkeley and his Ph.D. in political science from MIT. The author of three books, he has been a senior fellow at the Brookings Institution and a visiting scholar at MIT and Berkeley, and he is a life member of the Council on Foreign Relations.

The Broad Institute is at 7 Cambridge Center (corner of Main and Ames streets). Please R.S.V.P. to nhuch@mit.edu.

EIMER'S

ı Page 1

s Medical Institute inves-
ts at the possibility that
ı can be improved even
s of dementia."
the researchers' results
even severely afflicted
ionally lucid.

ırs

ıs also able to mimic the
an enriched environment
lzheimer's-like mice with
ase (HDAC) inhibitors.
nily of 11 enzymes that
aster regulators of gene
s that inhibit HDACs are
stages and are not avail-
ion for use for Alzheim-

l histones act as spools
)NA winds, forming a
cell nucleus known as
ıes are modified in vari-
ling through a process

deacetylation with HDAC inhibitors leads to increased acetylation.)

Certain HDAC inhibitors open up chromatin. This allows transcription and expression of genes in chromatin structures that had been too tightly packed to allow certain genes to be transcribed.

There has been exponential growth in HDAC research over the past decade. HDAC inhibitors are currently being tested in preclinical studies to treat Huntington's disease patients. Some HDAC inhibitors are on the market to treat certain forms of cancer. They may help chemotherapy drugs better reach their targets by opening up chromatin and exposing DNA. "To our knowledge, HDACs have not been used to treat Alzheimer's disease or dementia," Tsai said. "Future research should address whether HDAC inhibitors will be effective for treating neurodegenerative diseases."

A better model

Brain atrophy occurs during normal aging and is an early feature of neurodegenerative diseases. However, there are few effective animal models for these diseases, limiting researchers' ability to explore strategies for recovering learning and memory after substantial brain damage had already taken place.

Tsai's laboratory developed a transgenic mouse in which expression of p25, a protein implicated in various neurodegenerative diseases, can be switched on or off with a change in diet. Mice that expressed the p25 protein had significant loss of brain cells and acted as though they did not remember tasks they had previously learned.

"It's not clear if memories were simply lost or became inaccessible due to synaptic and neuronal loss," wrote Tsai. "In the latter case, it might be possible to reestablish the access to such memories if sufficient refinement of the neuronal network can be achieved by the remaining neurons."

In 2003, a man who was barely conscious for nearly 20 years regained speech and movement at a Mountain View, Ark., rehabilitation center. Last year, doctors

See ALZHEIMER'S

AWARDS AN

Professor Ian Waitz
the first Hunsaker Pr
nautics in the Departn
tics and Astronautics.
enables the professor t
tinue to make, contribu
front of important fiel
sciences."

The chair is named
saker, the pioneering
who founded the depar
aerodynamics and airc
program in the United
tinues Hunsaker's pio
spirit with his work in
mechanics, thermodyı
flows, aeroacoustics ar
aspects of these discipli
environmental issues as
craft design and operatic

Waitz is the director
for AiR Transportation
sions Reduction, an M
aviation cooperative rese
sponsored by the Federa
istration, NASA and Trai

Submit awar
commencem

Tech Talk will publisl
issue in print and onlin
annual special section li
winners of annual award
along with photographs

Names of award win
mitted to Tech Talk by
day, May 10, in order to
awards issue. Please no
Infinite Mile Awards or
side organizations.

All submissions to
should be made online
newsoffice/awards.html.

All photographs mu
shwright@mit.edu. Plea
the subjects and include
photographer.

To see the 2006 Aw

e (Cell/B.E.), the micro-
owers the new PlaySta-
ntertainment system.
our-week Independent
course in January, stu-
earned about the new
hey designed and imple-
to run directly on Play-
s. The student team with
a 3-D version of the clas-
later presented its work
experience at the Game
ence in March.
which focused around
lel programming to stu-
by Saman Amarasinghe,
T's Department of Elec-
and Computer Science,
h of IBM.
students—with no back-
el programming or the
ngine—were able to get
ne from scratch in just
1 largely goes to show
d determination of our
with the availability of
1 for Cell development,"

the course, students
with the Cell/B.E. and
ioices compare to other
ectures. Students also
oject teams and partici-
-long project to develop
1 on the Cell Broadband
IBM Cell SDK available
erWorks.
dband Engine is going to
architecture that has the
cluded in a wide range
cations and solutions in
abbah. "This course was
n the details of a highly
ocessor and challenge
where the performance,
lity could be applied out-
ased on the feedback we
e students, it was a tre-
"

osted by the Computer
ip at MIT posts informa-
e, including lectures and
t has been visited more
s since the completion of

Department of Electrical
Computer Science, with
1 Sony, plan to jointly
gain in 2008. More infor-
ind at cag.csail.mit.edu/

rrently hosting a first-of-
ming contest—the Cell
ige—for college and uni-
n 25 different countries,
zes and awards for the
applications of the Cell
e. All information on eli-
requirements, and entry
e found at www-304.ibm.
niversity/students/con-
tml.

a creative spark that inspires young people and others interested in invention to believe they, too, can contribute to society," said Merton Flemings, director of the Lemelson-MIT Program.

Ioannis (Yannis) Miaoulis, president and director of the Museum of Science, echoed Flemings' enthusiasm for this first-ever event.

"We are very pleased to collaborate with the Lemelson-MIT Program. The hands-on engineering activities, combined with special guest presentations, are a perfect complement to the museum's programs," Miaoulis said.

One highlight event of EurekaFest is "The Windy 500," an engineering design challenge created to "drive" interest and enthusiasm among more than 100 Massachusetts high school students and their teachers.

Student teams will collaborate on a surprise project with science and engineering mentors in a race against time and each other. Tom and Ray Magliozzi, aka Click and Clack, the hosts of "Car Talk" from National Public Radio, will be on hand to declare one team the victor of "The Windy 500." They will also present several other awards, including "The Most Inventive Use of Duct Tape" award and the "Oh No, I Can't Believe It!" award.

Timothy Swager

an from the University of Illinois at Urbana-Champaign—will join a panel discussion, "Inventors Who Shape Our World," at the Museum of Science on Thursday, May 3 at 3 p.m.

Also speaking in "Inventors Who Shape Our World," beginning at 4 p.m., are MacArthur Professor of Chemistry Timothy Swager, the 2007 winner of the $500,000 Lemelson-MIT Prize, and Dartmouth College engineering professor Lee Lynd, the 2007 winner of the $100,000 Lemelson-MIT Award for Sustainability. Among Swager's inventions is an amplified chemical sensor that can detect vapors of common explosives, such as TNT. Lynd's work focuses on the cost-effective conversion of cellulosic biomass into ethanol for fuel.

Both sessions are open to the public and included with the Museum of Science exhibit halls admission.

Two other accomplished inventors, Iqbal Quadir and H. Harish Hande, will lead a day-long workshop at MIT titled "Invention to Venture: Affordable Technology" on Saturday, May 5, from 9:30 a.m. to 3:30 p.m. Quadir founded Grameenphone, the largest and fastest-growing mobile phone company in Bangladesh, and Hande co-founded Solar Energy Light Company,

For a full list of event
tions, visit web.mit.edu/i
html.

Admission to the ever
of Science is free for MI
valid ID.

PHOTO COURTESY / LEI

MIT graduate student I
invented a device for ra
heights, is this year's win
Lemelson-MIT Student F

PHOTO

Puppet principles

Joe Zane, who taught Introduction to the Visual Arts this semester, poses with puppets made during his course. The self-portrait made of upholstery foam with ping pong balls, fake fur and felt. These and other puppets were featurec N52-390 to entice potential puppeteers to the CAVS artist's presentation "Let's Put on a Puppet Show!" offered to r MIT community and the public on Friday, April 6.

Century
uction will

ALZHEIMER'S

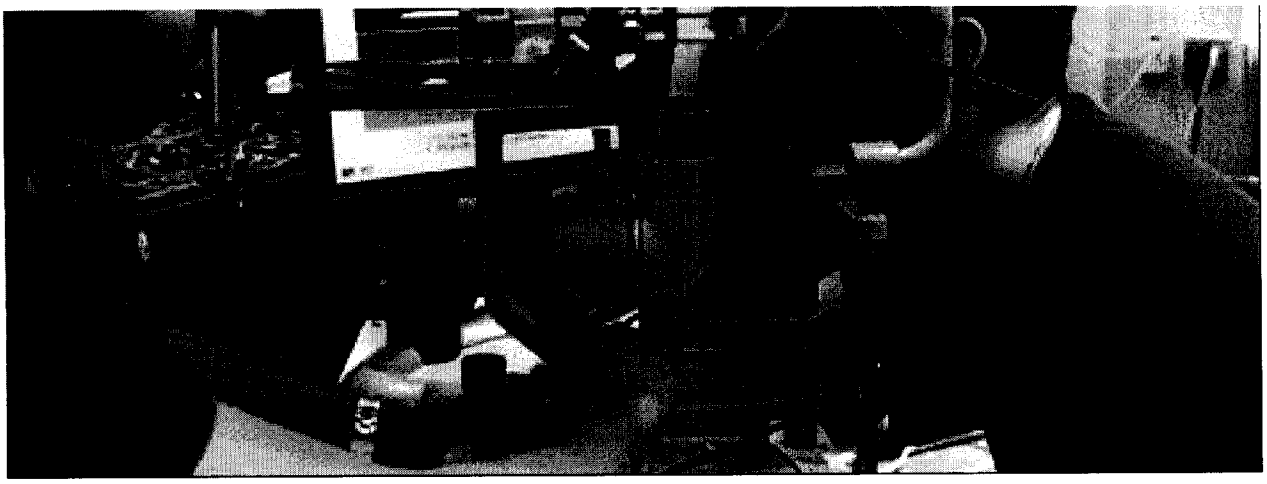

PHOTO / DONNA COVENEY

Fujimoto, center, with students using the eye-imaging technique he began developing in the early 1990s. With his head s Desmond C. Adler, graduate student in materials science. At left, taking measurements, is Vivek Srinivasan, graduate al engineering and computer science.

MAGING

1 Page 1

s by scanning light back the eye, measuring the of reflected light along lines that, row by row, lution images.
CT systems scan the eye rom several hundred to lines per second. But a 1 only keep the eye still ond, limiting the amount onal data that can be acquired.

Now, using the new laser, researchers in Fujimoto's group report retinal scans at record speeds of up to 236,000 lines per second, a factor of 10 improvement over current OCT technology.

Future clinical studies, as well as further development, may someday enable ophthalmologists to routinely obtain three-dimensional "OCT snapshots" of the eye, containing comprehensive volumetric information about the microstructure of the retina. Such snapshots could potentially improve diagnoses of retinal diseases such as diabetic retinopathy, glaucoma and age-related macular degeneration.

Fujimoto's colleagues on the work are Robert Huber, a visiting scientist at MIT now at the Ludwig-Maximilians University in Germany, Desmond C. Adler and Vivek Srinivasan. Adler and Srinivasan are both graduate students in EECS.

The current research was sponsored by the National Science Foundation, the National Institutes of Health and the Air Force Office of Scientific Research.

ell portrays MIT campus design process

orah Halber
ce Correspondent

ons of what would even-
e Ray and Maria Stata
rumpled pieces of paper,
od and plexiglass blocks
sembling a mass of dis-

ot designs, exactly, but
ipts by architect Frank
diverse group of MIT
iture inhabitants of the
o think about what they
react, directly and emo-
opositions on the table

ehind the conceptual-
nd construction of the
four other major build-
ne's Zesiger Sports and
Steven Holl's Simmons
ea's Brain and Cognitive
x and Fumihiko Maki's
he Media Laboratory—
William J. Mitchell's new
MIT: Designing a Cam-
y-First Century."
ner dean of the MIT
cture, is the Alexander
sor of Architecture and

ings came to be. "The behind-the-scenes story about how architecture gets done—a rarely told story, a hard-to-tell story—needed to be written," Mitchell said.

Architecture is not "sitting down in a room and dreaming things up," he said. "There's money involved, and politics, and incredibly complex social forces and endless negotiation, and you have to try to make great buildings out of all that."

Mitchell, by including pictures of

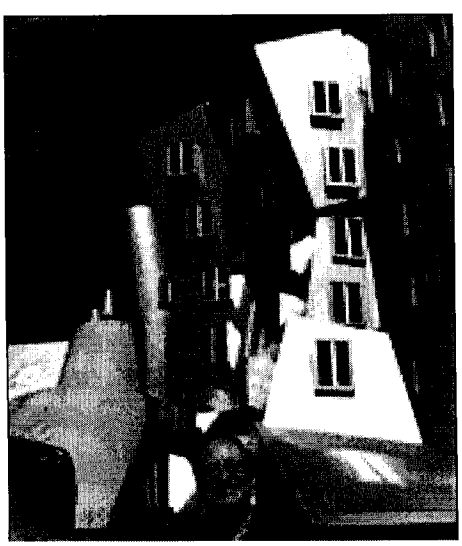

for practical reasons." The result is a book that appeals to an audience that includes the general public as well as urban designers and architects.

Stata was a particularly challenging project because Frank Gehry's extraordinary Guggenheim Museum in Bilbao, Spain, had projected him into "rock star fame," Mitchell wrote. Everyone had an opinion about him. Mitchell, meanwhile, was very aware of Gehry's professionalism: his attention to detail, his responsiveness to his client's day-to-day needs, his ability to keep costs in check. "Some people thought because he did radical things that he must be a crazy man," Mitchell said. "But he's a highly experienced, extremely skilled architect. And I knew the match to MIT would be fantastic." It was Mitchell who managed to keep Gehry's name in play for the project and helped mediate the ongoing, sometimes contentious discussions.

The process did generate more than a few infuriated e-mails when Gehry at one point suggested that the interior space mimic an "orangutan village." But in the end, the ensuing discussion led to a pivotal organization scheme for research groups within the building. And the Stata Center did not, Mitchell attested, come in absurdly over budget. "On a dollars-per-square-

ing fundamental challe
economy, environment,
and way of life in the 2
said in an April 26 staten
of the National Academ
(NAE).

"As an independent
nearly 2,000 of the nati
plished engineers cha
the federal governmen
informed advice on tech
the NAE can and will p
role in securing our nat
wrote.

Vest will deliver the
ment address at MIT be
new NAE leadership role

The NAE is part of t
emies, which also incl
Academy of Sciences, I
cine and National Re
These independent, nor
serve as advisers to go
public on issues related
neering and medicine. N
consists of the nation's p
who are elected by the
distinguished achieveme

The NAE presiden
employee of the organiz
quarters in Washingtor
serves as the vice chai
Research Council, the p
arm of the National Acad

Vest served as MIT
1990 through 2004. Dur
worked to strengthen
industry relations and
ber of initiatives to brii
research issues to broa
tion," according to the N

Selected as a membe
Commission on the Inte
ties of the United States
ons of Mass Destruction
its report in 2005, Vest
science and engineerin
the analysis. He led a U
Energy task force on the
programs in 2002-2003 a
idential advisory commi
sign of the Internationa
1992-1994. Vest was vice
cil on Competitiveness f
former chair of the Ass
can Universities, and se
Secretary of Education'
the Future of Higher Edu

Vest was elected to
"for technical and edu
tions to holographic in
leadership as an educa
rently serves on the NAI

Vest earned a B.S. d
cal engineering from W
versity in 1963. He rece
Ph.D. degrees in 1964
tively, from the Univer
where he later held the
of engineering, provost
for academic affairs. He
10 honorary doctoral de

velop inexpensive, porta-
ices and might also offer
into how cells change as
division.
ional methods, the MIT
cells to remain in fluid
eing measured, opening
of possible applications,
lis, senior author of a
rk that appeared in the
ature.
weighing cells, the tech-
sed to "weigh nanopar-
olayers of biomolecules
in solution that is six
ıde more sensitive than
s sensor methods. One
ursuing is mass-based
way to weigh and count
id Manalis, an associate
"s Departments of Bio-
ıg and Mechanical Engi-

-measurement methods
on down to a zeptogram

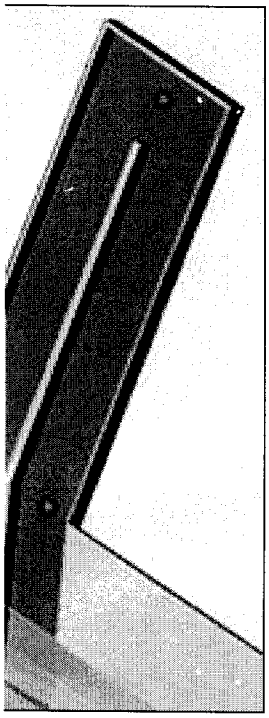

GE COURTESY / **SCOTT MANALIS**

have developed a tiny
used to weigh single
As particles flow through
equency of vibration of
een) is slightly altered,
s of the particles to be

frequency at which the material naturally tends to vibrate) inside a vacuum. When a molecule sits on the slab, the frequency changes slightly, and the mass of the molecule can be calculated by measuring that change.

This measurement must be performed in a vacuum to prevent air (or fluid) from interfering with the frequency of oscillation. However, cells cannot survive in a vacuum, so they must be measured in fluid, which diminishes the accuracy of the measurement.

The researchers solved this dilemma by placing the fluid containing the sample inside the silicon slab, which still oscillates within a vacuum surrounding it. The biological sample is pumped through a microchannel that runs across the slab, without impairing its ability to vibrate.

"The resonator is sealed in a tiny vacuum cavity inside the chip, so there is virtually no resistance to the vibration," said co-lead author Thomas Burg, a research associate in biological engineering. "This

IMAGE COURTESY / **THOMAS BURG**

This illustration shows an artistic depiction of the concept that enables measuring the mass of a single bacterium and single nanoparticles in fluid with a very high resolution. A hollow resonator, represented by a hollow, fluid-filled guitar string, vibrates while small particles, represented here by a red bacterium, flow through it. As the particles flow through the resonator, they change the frequency (tone) of the vibration.

few years. Every step along the way will open up new possibilities," he said.

The researchers can also measure the mass density of particles or cells "by varying the density of the surrounding solution," said Michel Godin, co-lead author and postdoctoral associate in biological engineering.

The research team is already looking into several applications for the new technique.

One area of great promise is creating a device that would mimic the cell-counting capabilities of flow cytometers, which are often used to monitor CD4 cell numbers in AIDS patients. By counting CD4 cells, a

a cheap and robust a
mercially available flow
typically cost more than
said.

"Since the device is b
conventional semicond
techniques, it could pote
a disposable format," he

William Rodriguez, ar
at Massachusetts Gener
familiar with Manalis' r
new technology could h
impact on AIDS testing

See **CEL**
Page 6

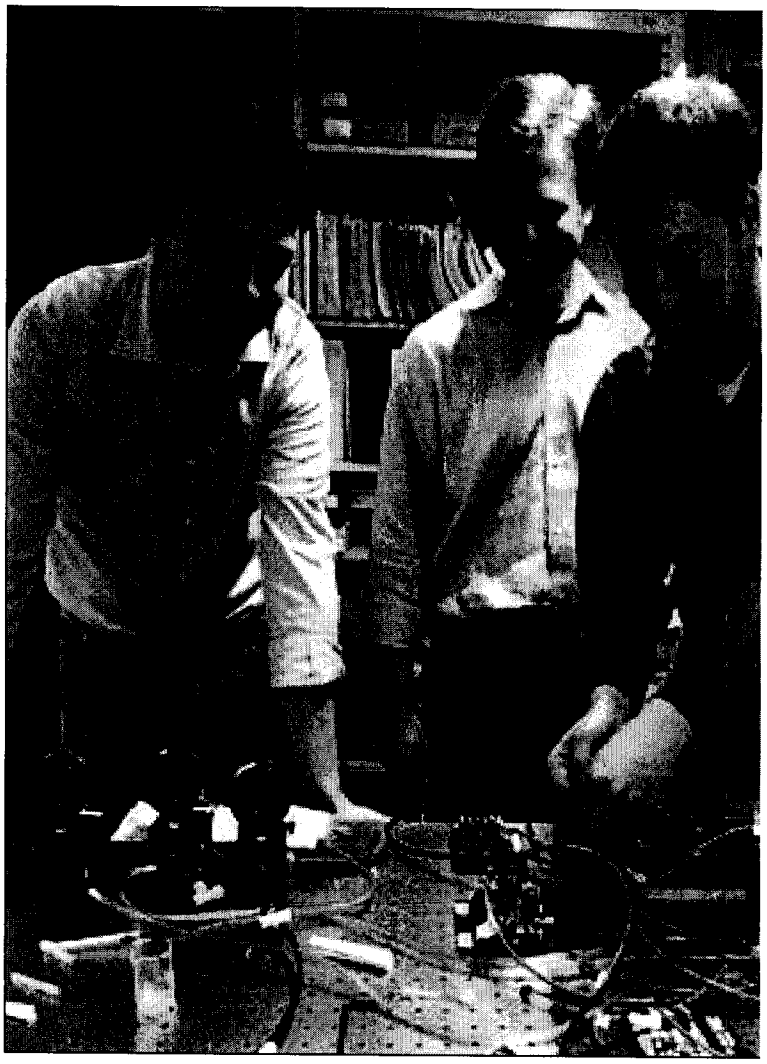

PH

Postdoctoral associate Michel Godin, left, Associate Professor Scott Ma
engineering and postdoctoral associate Thomas Burg are part of an M
developed a technique to measure the mass of single cells.

rofessor teaches 'excitement' of solving math–and life–probl

ɔrah Halber
ɔe Correspondent

outhern Ethiopian town
ra grew up, mathematics
ooks were scarce. High
/ho were as inspired by
he was borrowed their

ıs been named a Martin

ematics at Grand Valley State University in Allendale, Mich., specialized in the branch of mathematics called combinatorics, which studies collections of objects that meet certain criteria. An example of a combinatorial problem is: What is the number of possible ways to order a deck of 52 playing cards? The answer involves multiplying 51 digits and arriving at a number 68 digits long.

Besides solving problems, combinator-

rithmic checking proced
in the summer of 2005,
study a special class of
tion algorithms. Using
cleverly, the student was
lenging and new probl
combinatorial identities,"

Tefera is energized
undergraduates. "I bel
undergraduate research
factor for cultivating and

David J. Goldston, cur-
-in-residence with the
School of Public and
airs at Princeton, will
guished Public Service

for investment in high-
development (R&D) has
J.S. competitiveness and
y to our nation's innova-
EEE-USA President John

S. engineers thrive in an

array of initiatives for Lieberman, including the Clean Air Act (1990); the Technology Talent Act (2001); the Homeland Security Department Authorization (2002); the National Nanotechnology R&D Act (2003); and the National Innovation Act (2005), among others.

IEEE-USA award recipients are recognized for their professionalism and technical achievements, as well as literary contributions to public awareness and understanding of the engineering profession in the United States.

PHOTO / **DONNA COVENEY**

William B. Bonvillian

the field at the end of t
became clear that the
Project was not going t
medical problems, an
systems were massively
than the older "one gen
had foreseen. One res
proliferation of "omics"-
metabolomics, glycomi
of the genome splinter
subspecialties.

Are biosystems engine

Biologists looking f
ing about the complexity
have reached, in Fujimu
very different repositorie
is largely mechanistic, a
drawn from control theor
using terms like "circuit
"redundancy" and "rol
are also used to describe
traffic, robots and airpla
one prominent systems
Kitano, used a schematic
hydraulic control system
ical systems. This reduc
begun to look less usef
increasingly aware of the
ing organisms.

Or are they intestines'

The other line of thir
by British scientist Je
looks to natural ecosys
His work, said Fujimura,
rized as "diverse, dynam
exploring the multitude
that inhabit and indeed
the human body. Again,
tems biology as a mirr
Fujimura noted, "I would
now witnessing the reint
place, interaction, multip
environment, dynamics
what previously had be
unsituated and unidire
reductionist molecular g

Fujimura has had a
MIT, interacting with
area while teaching two
the development of sys
another that examines h
population is conceptu
tionalized in human gen
a recent e-mail, she ren
was concerned about th
here for just one seme
glad that I did!"

S

Page 5

ere.
a cheap, simple CD4
that can be used by a
h worker...would be a
vance in global health,"
iguez.
o planning a collabora-
sociate professor of biol-
on, who is interested in
mass density of a single
goes through cell divi-
w method, scientists can
single cell and observe
iod of time. Changes in
ate to production of pro-
ew way to study what the
ivision, Manalis said.
ation of the new technol-
small particles, or beads.
now the size of particles
g-delivery devices, coat-
mposite materials, said
ed that the new technol-
the "gold standard" way
particles one by one.
on the Nature paper are
IT postdoctoral associate
neering; Wenjiang Shen,
John S. Foster of Inno-
nology in Santa Barbara,
Babcock of Innovative
and Affinity Biosensors

was funded by the
of Health Cell Decision
ie Institute for Collabora-
ies from the U.S. Army
the Air Force Office of
ch, the National Science
ie Natural Sciences and
arch Council of Canada.

HORVITZ

Continued from Page 1

Medical Institute investigator, delivered the 35th annual Killian Award lecture April 24. Winner of the 2006-2007 James R. Killian Jr. Faculty Achievement Award, Horvitz spoke on "Worms, Life and Death: Cell Suicide in Development and Disease."

Horvitz is concerned that because of declining government support, today's young researchers will not have the same freedom he did to pursue basic research. "Basic research may lead not only to intellectually stimulating findings, but also to major insights of a practical nature," he said. "Basic research must be supported outside the private sector by governments and foundations because only such organizations can act on a basis that will benefit humanity but cannot possibly constitute a business plan."

The current downward trajectory of government funding "is positively frightening," Horvitz said. It underestimates the rate of inflation in the cost of doing biomedical research. Six to 8 percent annual increases are needed simply to maintain the current level, he said, while 10 to 12 percent increases are needed to "propel biomedical research to take advantage of current knowledge." The average 1 percent increases over the past few years have led to "an unprecedented low success rate for new projects," Horvitz said.

"Without the NIH (National Institutes of Health—the major government supporter of biomedical research), I have deep concern for the future of government-funded basic science," he said.

Horvitz has identified many genes involved in pathways of key processes that correlate directly to human development and disease. In the roundworm, there are 131 cells generated during development that are not found in the adult because they die through normal programmed cell death. Biologists used to think that only old or damaged cells died off, but researchers now know that cell death is "an active process, governed by specific genes," he said.

Cells die in many scenarios—tadpoles lose their tails as they turn into frogs, and webbing between the fingers of humans in utero is sculpted out by programmed cell death, while ducks retain their webbed feet because those cells are not killed off.

Because the process can go right, it can also go wrong. Many disorders stem from a disruption in the perfect equilibrium between cell division and programmed cell death. Some, like cancer, involve too little cell death. Some, like neurodegenerative diseases, involve too much.

The Horvitz laboratory has identified genes and proteins involved in the four-step genetic pathway of cell division and death. The human counterparts of the roundworm genes are potential therapeutic targets in a broad range of diseases. "If we could inhibit a killer gene, we could prevent the pathological process of programmed cell death and cause dying cells to survive," he said. "For diseases involving too little cell death, such as cancer, if we could activate the cell death pathway, we should be able to cause cells to die that have otherwise escaped death."

Potential therapeutics developed by a biotechnology company Horvitz founded are now in clinical trials.

Established in 1971 as a tribute to MIT's 10th president, the Killian Award recognizes extraordinary professional accomplishment by an MIT faculty member. The winner delivers a lecture in the spring term.

s that as a member of
ence and Artificial Intel-
L), she has grown accus-
3.5 million surroundings
r. She can always count
city, clean running water
ded by the latest technol-
ent trip to Laare, Kenya,
gs she depended on.
ommunity Technology
is located at the Laare
nity Church compound
of the amenities Walcott
omed to. The small class-
; when the electricity is
t reveals a thin layer of
plastic chairs and hand-
bles that serve as office
ining manual is used to
10 to 15 students.
s the differences posed
enges, but she was more
omise of the small com-
n by any of its shortcom-
; how much gets done in
Walcott marvels. "There
for potential growth and
still be done."
was founded in 2005
rts of Eric Mibuari, an
ginally from Laare, and
ervice Center. It was one
s taken on by the CSAIL
rogram. It was founded
al computer awareness
are residents by provid-
l inexpensive training on
ers.
ter began to operate in
120 students have been
) computers, helping a
er of them find better
achers, clerks and tech-
titutions and businesses.
it easier for some of the
ito more advanced com-
other technical colleges

project is still in what
as its initial stages. Wal-
ie was going to an area
l very little exposure to
ie was not prepared for
ence the teachers sent
nary schools had with

ott and her colleague,
also an MIT graduate
e schools to send teach-
ne experience working
With this in mind, Wal-
rriculum geared toward
eachers to the Edubun-
ducational software and
ys to incorporate it into

st lesson with the teach-
parent that none of the
prior experience with
he class would not be
rriculum that she had
, she adapted her curric-
to include topics ranging
of the computers to basic
ardware.
eling frustrated by this

Hashmi, a graduate student in system design and management (SDM), had spent five and a half years in the United States earning her undergraduate and master's degrees in computer science and math and finding a great job in her field. But on her return to Saudi Arabia, she found "technology is just catching up. And women always get left behind."

She also noted that since people who are educated often leave, the "area gets drained. The reason I went back is because I wanted to give back."

In 2005, Hashmi moved home to work for the College of Business Administration, a private college established seven years ago in the city of Jeddah, the second-largest city in Saudi Arabia. Due to gender segregation policies, the 500 women enrolled are separated from the 1,400 male students.

In 2006, Hashmi coordinated a partnership for the women's campus with Women in Technology (WIT), which is funded by the Middle East Partnership Initiative of the U.S. Department of State and managed by the Institute of International Education, to teach Saudi women basic computing skills. WIT's goal is to empower women by teaching them basic computing and IT skills at a low cost. WIT receives support from Microsoft Unlimited Potential curric-

local women affordable computer training. The students named the enterprise Student Women Initiative For Technology, or

PHOTO COURTESY / **MIT SLOAN**

Nada Hashmi

An outside trainer en
to become Microsoft
women then taught the
Office suite, as well as
Internet and e-commerc
women.

Hashmi said one of
parts of the project was
provided the 50 student
a sense of working in
"They had to go throug
and manage funds, and
with a president and a
she said.

The project won th
prize in the Jeddah Eco
legiate Business Venture

Hashmi was in the Ur
SDM program and was
toring students. When
most satisfying about the
"working with the stude
them change and grow."

Hashmi has a B.A. in
and math from Washin
an M.S. in computer scie
versity of Maryland. Ha
to Saudi Arabia, Hashr
tinuing to help her socie
projects. "Education is
With education, you ca
self," Hashmi said.

'WACK!' weighs the impact of feminist

Elizabeth Knox
News Office Correspondent

"WACK! Art and the Feminist Revolution," published by MIT Press to accompany an exhibition of the same name, inspires challenging questions. The exhibition, originating in Los Angeles, is a collection of art produced by women during the height of the feminist movement, primarily the late 1960s through the 1970s. One of the purposes of the exhibition and its catalogue is to rouse discussion about both the impact of the feminist art movement and the need to re-examine this art today. The book and the exhibition are ambitious, confrontational and far-ranging in scope.

The WACK! exhibition, based in Los Angeles' Museum of Contemporary Art, was proposed and curated by Cornelia Butler. It is the largest-ever exhibition of work entirely by women artists; its level of ambition, commitment and organization is suggested by a glance at the page listing lenders to the exhibition—184 strong, many the artists themselves.

The catalogue includes not only full-color, high-quality plates, but also short biographies of each artist or collective and essays by respected art history scholars. The attention to design is evident from the arresting wraparound cover image depicting Martha Rosler's "Body Beautiful, or Beauty Knows No Pain: Hot House, or Harem," a tangle of women's bod-

The arrangement allows the reader to first examine the work on its own, then to learn more about the artists, and finally to read in depth about the movement. The format also encourages flipping backwards and forwards through the pages to reference plates or bios.

The scope of the works—from harrowing performances such as that of Marina Abramovic and Gina Pane to paintings by Joan Semmel and Judith F. Baca—and the amount of information included permit even the uninformed reader to form well-grounded opinions and make connections among artists and artworks. Readers not as familiar with feminist art will encounter artists not well known in the United States.

The organizers were
ing an international sp
and succeeded in bring
work of artists from 21
artists' contributions enc
ty of ideas and cultural ir
be outside many Western

Ironically, considering
flavor of the show, the
included are overwhelr
black American wom
individually, compared t
American women. The
work from Spiderwor
Native-American collec
1975 and still active toda
At (an African-An
active between 197
not seem like eno
the rich output fr
Valerie Smith's ess
dence: Black Wor
1960s and 70s," pr
stance, if not more

Why "WACK!"
says in her introdu
of feminist art ha
theorized and acce
and museum institu
have added "the g
that list. Though r
ists are already w
both the art world
public—Cindy Sh
Neel, for example
to shock.

One could arg
popularity of telev

PHOTO

Water power

T Sea Grant designed an autonomous vehicle called the 'Katrina' boat, which can collect samples from waters that may be unsafe to drink or travel or
on the Charles River on Monday, April 23, as part of the Cambridge Science Festival.

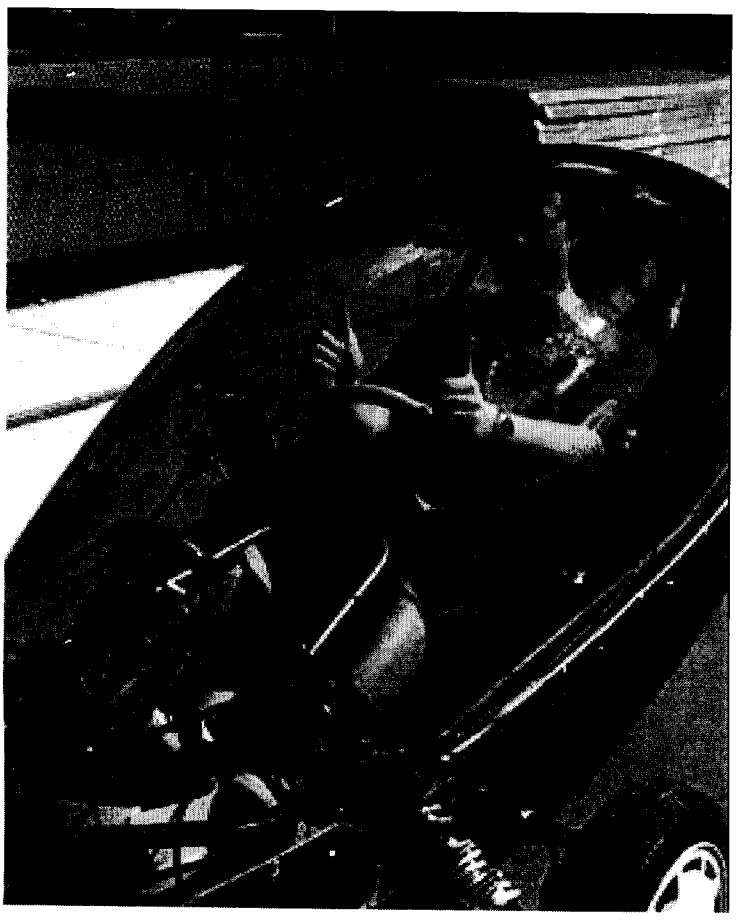

Broad Institute presents World Music V

Two of MIT's world music ensembles, Gamelan Galak Tika and Rambax, will present a World Music Weekend at the Broad Institute on Saturday and Sunday, May 5 and May 6.

Gamelan Galak Tika, MIT's resident Balinese music ensemble of 30 musicians playing a shimmering orchestra of metallophones, gongs and drums, will perform traditional and modern music from Bali on Saturday, May 5, at 8 p.m. General admission is $12; $8 for students, senior citizens and MIT and Harvard community members; and free for MIT and Harvard students and children under the age of 12.

Gamelan Galak Tika will perform the world premiere of "Wariga," the newest composition by Dewa Ketut Alit, one of Bali's most innovative young composers. "Wariga," loosely translated, means "calendrical convergence," and the piece is inspired by the auspicious and inauspicious days found in the cycles of the Balinese calendar. The ensemble, led by MIT Professor Evan Ziporyn, will also perform "Taruna Jaya," or "Dance of the Victorious Youth," an e composition, featuring Laksawana; "Gringsing"; dro," a groundbreaking the group, features two together. For more infor galaktika.org.

Rambax MIT, an en: to learning the art of sab and dance tradition of of Senegal, West Afric free concert on Sunday, Titled "Cosaan" ("tradit language), the event c lese drumming, song an features the traditional dance known as simb. ists include Senegalese and dancers Paa Seck, Ngom, Cheikh Ngom a Co-directed by artist-in- Touré and Associate I Tang, Rambax MIT cor dents and other member munity. For more infor mit.edu/rambax.

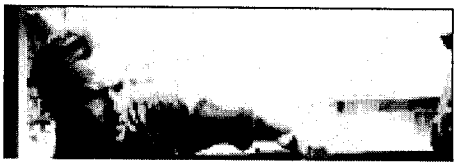

1: Biochem J. 2007 Dec 15;408(3):317-26. Links

The epigenetic signature of CFTR expression is co-ordinated via chromatin acetylation through a complex intronic element.

Paul T, **Li S**, **Khurana S**, **Leleiko NS**, **Walsh MJ**.

Department of Pediatrics, Mount Sinai School of Medicine, One Gustave L. Levy Place, New York, NY 10029, USA.

The CFTR (cystic fibrosis transmembrane conductance regulator) gene is a tightly regulated and differentially expressed transcript in many mucosal epithelial cell types. It appears that DNA sequence variations alone do not explain CFTR-related gastrointestinal disease patterns and that epigenetic modifiers influence CFTR expression. Our aim was to characterize the native chromatin environment in cultured cells for intestinal CFTR expression by determining the relationship between histone acetylation and occupation of CFTR by multiple transcription factors, through a common regulatory element. We used HDAC (histone deacetylase) inhibition and ChIP (chromatin immunoprecipitation) analyses to define regions associated with acute acetylation of histone at the CFTR locus. We identified a region within the first intron associated with acute acetylation of histone H4 as an epigenetic signature corresponding to an intestine-specific enhancer element for CFTR. DHS (DNase I-hypersensitivity) assays and ChIP were used to specify control elements and occupation by regulatory factors. Quantitative ChIP procedures indicate that HNF1alpha (hepatic nuclear factor 1alpha) and Cdx2 (caudal homeobox protein 2) occupy and regulate through a novel intronic enhancer element of CFTR and that Tcf4 (T-cell factor 4) overlaps the same DNA element. RNAi (RNA interference) of Tcf4 and HNF1alpha decreased intestinal cell CFTR expression, identifying these as positive regulatory factors and CFTR as a target for Wnt signalling. We have linked the acetylation signature of nucleosomal histones to active intestinal CFTR expression and occupation by transcription factors HNF1alpha, Cdx2 and Tcf4 which converge to modify chromatin architecture. These studies suggest the therapeutic potential of histone modification strategies, such as inhibition of HDAC activity, to treat CFTR-associated disease by selectively enhancing CFTR expression

Regulation of peroxisome proliferator-activated receptor γ coactivator 1α (PGC-1α) and mitochondrial function by MEF2 and HDAC5

Michael P. Czubryt*, John McAnally*, Glenn I. Fishman†, and Eric N. Olson*‡

*Department of Molecular Biology, University of Texas Southwestern Medical Center, 6000 Harry Hines Boulevard, Dallas, TX 75390-9148; and †Division of Cardiology, New York University School of Medicine, 550 First Avenue, OBV-A615, New York, NY 10016

Contributed by Eric N. Olson, December 13, 2002

The myocyte enhancer factor-2 (MEF2) transcription factor regulates muscle development and calcium-dependent gene expression. MEF2 activity is repressed by class II histone deacetylases (HDACs), which dissociate from MEF2 when phosphorylated on two serine residues in response to calcium signaling. To explore the potential importance of MEF2/HDAC interactions in the heart, we generated transgenic mice expressing a signal-resistant form of HDAC5 under cardiac-specific and doxycycline-inducible regulation. Transgene expression resulted in sudden death in male mice accompanied by loss and morphologic changes of cardiac mitochondria and down-regulation of mitochondrial enzymes. The transcriptional coactivator PGC-1α, a master regulator of mitochondrial biogenesis and fatty acid oxidation, was also down-regulated in response to HDAC5 expression. Examination of the *PGC-1α* promoter revealed two MEF2-binding sites that mediate transcriptional activation by MEF2 and repression by HDAC5. These findings identify *PGC-1α* as a key target of the MEF2/HDAC regulatory pathway and demonstrate this pathway's importance in maintenance of cardiac mitochondrial function.

Acetylation of nucleosomal histones represents a central mechanism for regulation of gene expression. Histone acetylation relaxes chromatin, allowing access of the transcriptional machinery to specific regions of DNA. Control of this process is tightly regulated and can affect individual genes in a specific and directed fashion (1). Acetylation of histones by histone acetyltransferases is associated with activation of gene expression. Conversely, gene repression is achieved by histone deacetylases (HDACs) (2).

HDACs in mammalian cells comprise three distinct classes on the basis of protein structure and homology to yeast HDACs. Class I and III HDACs are ubiquitously expressed, whereas class II HDACs are highly enriched in striated muscles and brain (2). Class II HDACs (HDAC4, 5, 7, and 9) repress transcriptional activity of myocyte enhancer factor-2 (MEF2) transcription factors, which are also highly expressed in muscle and brain (3). This repression is relieved by phosphorylation of HDACs on two conserved serine residues, creating docking sites for the 14–3-3 chaperone protein, which mediates translocation of class II HDACs out of the nucleus (4). Mutation of these serine residues to alanines in HDAC5 prevents 14–3-3 binding and export to the cytosol (4–6). This signal-resistant HDAC mutant, which we refer to here as HDAC5S/A, acts as a dominant negative regulator of MEF2 signaling, because it binds and represses MEF2 factors but cannot be exported from the nucleus. Because histone acetyltransferases (HATs) and HDACs compete for the same binding site on MEF2, class II HDACs may also inhibit binding of HATs to MEF2 and subsequent histone acetylation (7). Expression of HDAC5S/A in neonatal rat cardiomyocytes prevents agonist-induced hypertrophy and activation of the fetal cardiac gene program (8). The notion that class II HDACs may counteract hypertrophic signals is supported by the recent demonstration that *HDAC9* mutant mice show an exaggerated response to hypertrophic stimuli (8).

To further investigate the importance of HDAC5 in cardiac function, we generated transgenic mice harboring a doxycycline (DOX)-inducible cardiac-specific transgene encoding the HDAC5S/A signal-resistant mutant. Because this mutant is able to efficiently inhibit MEF2 transactivation (4), we hypothesized that it would allow us to more clearly identify MEF2/HDAC targets free from complications of unknown kinases and phosphatases that may alter the activity of endogenous HDAC5. Expression of HDAC5S/A in the adult heart resulted in sudden death of male mice accompanied by gross aberrations in mitochondrial architecture and down-regulation of mitochondrial enzymes and the transcriptional coactivator peroxisome proliferator-activated receptor (PPAR) γ coactivator 1α (PGC-1α). PGC-1α coactivates numerous transcription factors involved in metabolism, including MEF2, and cardiac-specific overexpression of PGC-1α is sufficient to induce mitochondrial biogenesis (9–11). We show that two MEF2-binding sites in the *PGC-1α* upstream region mediate transcriptional responsiveness to MEF2 and repression by HDAC5, identifying the MEF2/HDAC pathway as a key regulator of the *PGC-1α* gene and mitochondrial biogenesis in the heart.

Methods

Generation of Transgenic Animals. We cloned the cDNA for human HDAC5 containing serine-to-alanine mutations at amino acids 259 and 498 into the tetracycline (tet)-responsive pUHG-10 vector to generate the tetHDAC5S/A vector (4). This vector was injected into B6C3F1 mouse oocytes and implanted into surrogate female ICR mice. Transgenic offspring were bred to α-myosin heavy chain (MHC)-tet transactivator transgenic mice while receiving 200 μg/ml DOX in water (12). Animals were maintained on DOX as needed. All animal protocols were approved by the Institutional Animal Care and Use Committee of the University of Texas Southwestern Medical Center.

Histology and Microscopy. For light microscopy, hearts were fixed overnight in 10% formalin, then embedded in paraffin, sectioned at 5 μm, and stained with hematoxylin/eosin. Alternatively, sections were immunostained with anti-FLAG primary antibody (20 μg/ml; Sigma–Aldrich) and goat anti-mouse fluorescein isothiocyanate conjugated secondary antibody (1:1,000; Vector Laboratories, Burlingame, CA). For transmission electron microscopy, hearts were fixed overnight in 3% glutaraldehyde in PBS at 4°C, then postfixed in 1% OsO_4 and dehydrated in an ethanol series. Samples were then embedded in Spurr resin (Ted Pella, Redding, CA), stained with uranyl acetate and lead citrate, and sectioned at 80 nm.

Abbreviations: HDAC, histone deacetylase; MEF2, myocyte enhancer factor-2; HDAC5S/A, HDAC5 double serine-to-alanine mutant; PPAR, peroxisome proliferator-activated receptor; PGC-1α, PPARγ coactivator 1α; DOX, doxycycline, ChIP, chromatin immunoprecipitation; MHC, myosin heavy chain; tet, tetracycline.

‡To whom correspondence should be addressed. E-mail: Eric.Olson@utsouthwestern.edu.

CELL BIOLOGY

Western Blot Analysis. Protein was isolated from hearts by homogenization in lysis buffer (PBS, 0.1% Triton X-100/1 mM EDTA, pH 7.4) containing Complete protease inhibitors (Roche Diagnostics). After electrophoresis and blotting onto Sequi-blot poly(vinylidene difluoride) membranes (Bio-Rad), blots were probed with anti-FLAG antibodies and horseradish peroxidase-conjugated secondary antibodies (Amersham Pharmacia Biosciences). Signal was detected with Western blotting Luminol Reagent (Santa Cruz Biotechnology), followed by exposure of blots to BioMax film (Kodak).

Cell Culture and Luciferase Assays. COS cells were maintained in 10% FBS in DMEM. Fugene 6 (Roche Diagnostics) was used for all transfections. The first 3.1 kb of genomic sequence upstream of the ATG translational start codon for mouse *PGC-1α* was amplified from BAC RPCI23–260A10 (CHORI-BacPac, Oakland, CA; www.chori.org) by high-fidelity PCR and TA cloned into the pCRII-TOPO vector (upstream primer: 5′-GGGGTACCCCATTTGGGAATCCTCTATACAAAGTTG-3′; downstream primer: 5′-GAAGATCTTCCCAGCTCCCGAATGACG-3′), then subcloned into the pGL3 basic luciferase reporter vector (Promega). A QuikChange kit (Stratagene) was used for site-directed mutagenesis of this reporter with primers to introduce several A/T to C/G mutations in the two putative MEF2-binding sites (MEF2 site 1-distal: 5′-AAGACAGAGAGAAAATTAACCATGGAAACTGCCTGGGGAG-3′; MEF2 site 2-proximal: 5′-ATGGTGCTTTATAAATTAGGTCTAGATGCATAGGGACTTT-3′; mutations are underlined). Luciferase assays were performed on COS cell lysates by using a kit (Promega). Cardiomyocytes were isolated from neonatal rat pups as described (8). After isolation, cells were grown overnight and then infected in serum-free medium with adenoviruses encoding either cytomegalovirus (CMV)-GFP or CMV-HDAC5S/A at a multiplicity of infection of 50/cell or were left uninfected (8). After infection, cells were incubated in serum-free medium for 24 h then harvested for RNA isolation.

Electrophoretic Gel Mobility-Shift Assay. Double-stranded oligomers were labeled with [^{32}P]dCTP by using Klenow DNA polymerase. Labeled oligomers were incubated with extracts from COS cells transfected with either GFP or MEF2C expression plasmids, and gel mobility-shift assays were performed as described (13). DNA–protein complexes were resolved on 6% acrylamide gels and exposed to BioMax film.

RNA Analysis. Total cardiac RNA was isolated from mice by using Trizol (Invitrogen). A 20-μg aliquot representative of three animals per sample group was then analyzed on Affymetrix U74Av2 microarrays. A subset of differentially expressed RNAs was further characterized by semiquantitative RT-PCR. Briefly, 2 μg of RNA from each sample was used to generate cDNA by using a SuperScript First-Strand Synthesis kit (Invitrogen). PCR was carried out by using primers specific to each gene of interest, with product labeling by [^{32}P]dCTP. Cycling parameters were determined for each product to ensure linearity of response, and reactions lacking reverse transcriptase were carried out as negative controls. PCR products were resolved on 6% acrylamide native gels and exposed to BioMax film. A similar protocol was followed for semiquantitative RT-PCR of rat neonatal cardiomyocytes, and for DNA isolated by chromatin immunoprecipitation (ChIP).

ChIP. After adenoviral infection, neonatal rat cardiomyocytes were prepared for ChIP assays by using a commercial kit and antiacetyl-histone H3 antibodies (Upstate Biotechnology, Lake Placid, NY). After ChIP, DNA was purified by phenol/chloroform extraction and PCR carried out as described above.

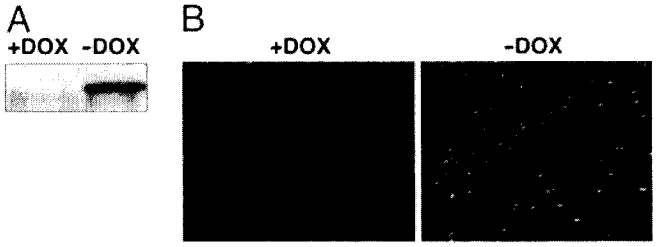

Fig. 1. Characterization of HDAC5S/A expression in DOX-inducible HDAC5S/A mice. (*A*) Western blotting of equal amounts of total cardiac protein of α-MHC-tTA/tetHDAC5S/A double transgenic mice before or after DOX withdrawal. (*B*) Immunohistochemical staining for FLAG-HDAC5S/A of cardiac sections from double transgenic mice before or after DOX withdrawal.

Results

Generation of Transgenic HDAC5S/A Mice. Our initial goal was to express the signal-resistant HDAC5 protein, HDAC5S/A, in the heart and to determine the consequences on cardiac gene expression. Attempts to generate mice transgenic for HDAC5S/A under control of the α-MHC promoter were unsuccessful, suggesting that constitutive high-level expression of this HDAC5 mutant caused lethality (T. A. McKinsey and E.N.O., unpublished results). We therefore incorporated a tet-off inducible system in which transgene expression is inhibited in the presence of the tet analog, DOX, but is induced upon withdrawal of the drug (12). FLAG-tagged HDAC5S/A was cloned into a tet-responsive expression vector to generate a tetHDAC5 mouse line. This line was crossed with transgenic mice harboring a tet transactivator (*tTA*) gene under control of the α-MHC promoter (α-MHC-tTA mice) to provide cardiac-specific expression (12).

We confirmed expression of HDAC5S/A by Western blot analysis of total protein from cardiac extracts in the presence or absence of DOX. No transgene expression was detected in the presence of DOX (Fig. 1*A*) or in noncardiac tissues such as liver (data not shown). Maximal transgene expression was attained within 5 days after DOX withdrawal. Immunohistochemistry of cardiac sections using anti-FLAG antibody revealed intense staining of cardiac nuclei after withdrawal of DOX (Fig. 1*B*). Microarray analysis of total RNA from mice after DOX withdrawal revealed a 3.5-fold increase in HDAC5 expression, but no changes in expression levels of HDAC1, 2, 3, or 6 (see below).

Cardiac Sudden Death and Mitochondrial Defects in HDAC5S/A Mice. Mice harboring both the α-MHC-tTA and tetHDAC5S/A transgenes were normal when maintained on DOX. However, withdrawal of DOX resulted in death of 100% of male mice within 7–10 days (Fig. 2*A*). In contrast, female transgenic mice survived ≈30 days after DOX withdrawal, indicating gender specificity in response to HDAC5S/A. This sexual dichotomy is particularly interesting in light of the phenotype of PPARα-deficient mice. Inhibition of mitochondrial fatty acid import by treatment of $PPAR\alpha^{-/-}$ mice with etomoxir resulted in the death of 100% of male mice, compared with 25% of females, but estrogen treatment of males normalized mortality to that of the females (14). The mechanism underlying increased longevity in the females in our study is currently under investigation. Two days before death, male mice become extremely lethargic, ceasing to groom themselves or respond to handling. Heart rate declined to ≈230 beats per minute in unanesthetized animals, compared with >600 in normal littermates as measured by ECG recording. There was no change in heart-to-body weight ratio at the time of death of male transgenic mice removed from DOX.

Histological examination of cardiac tissue sections revealed signs of cellular necrosis and inflammation in the hearts of male

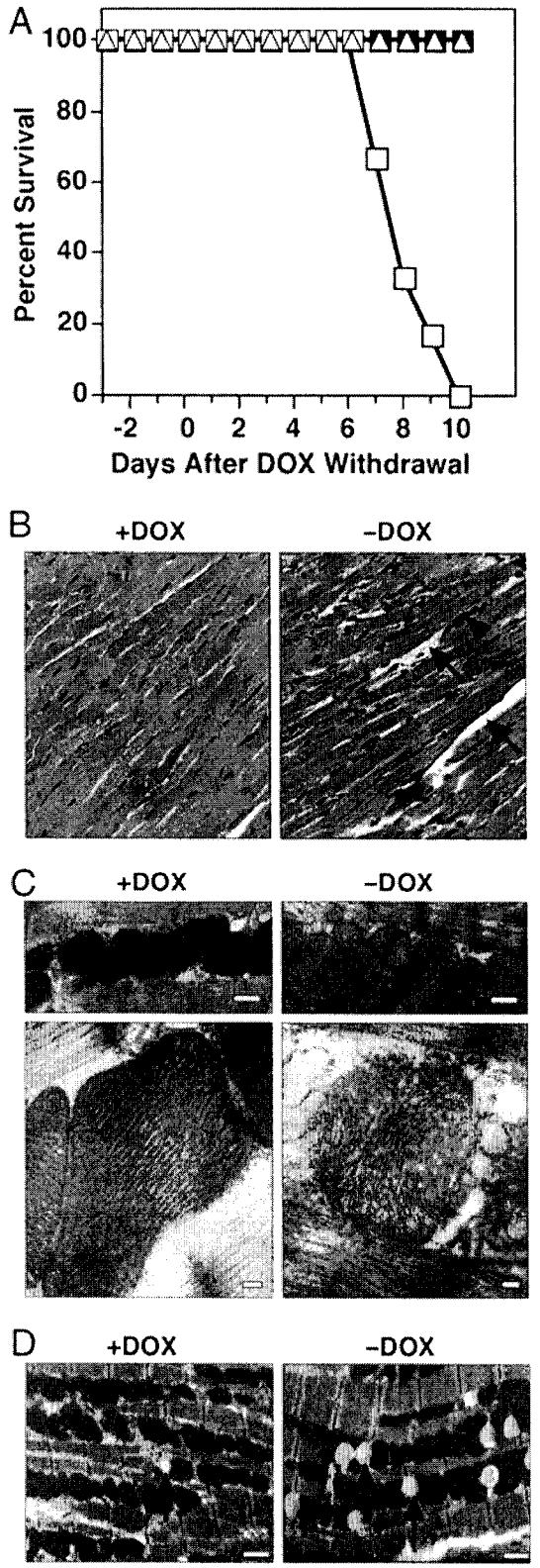

Fig. 2. Cardiac and mitochondrial abnormalities in HDAC5S/A mice. (*A*) Survival curve for male and female HDAC5S/A mice before and after withdrawal of DOX on day 0. Transgene activation results in death of 100% of male mice expressing HDAC5S/A within 10 days ($n = 6$ males or females per group). Squares, males; triangles, females; filled symbols, +DOX; open symbols, −DOX. (*B*) Hematoxylin/eosin-stained cardiac sections from double-transgenic mice before or after DOX withdrawal. Arrows denote areas of cardiomyocyte death or dropout. The arrowhead indicates inflammatory cell infiltration. Magnification is ×40. (*C*) Transmission electron micrographs of mitochondria in double transgenic mice before and after DOX withdrawal. (Bar = 500 nm in *Upper* and 100 nm in *Lower*.) (*D*) Transmission electron micrographs of cardiac sections from control mice (*Left*) or from transgenic mice after 5 days of DOX withdrawal. (Bar = 1 μm.) Arrows denote lipid bodies.

mice after removal of DOX (Fig. 2*B*). Hearts of female mice at the time of death showed high levels of collagen deposition and exhibited dilated cardiomyopathy (data not shown), suggesting a different process of pathogenesis from that in the males.

Further examination of cardiac tissue sections from male mice by transmission electron microscopy revealed dramatic changes in mitochondrial morphology (Fig. 2*C*). The mitochondrial cristae were highly disturbed, and large areas of blebbing could be seen in mice 8 days after DOX withdrawal. These changes led to a loss of electron-dense staining of the mitochondria that was easily visible at lower magnifications (Fig. 2*C*). Mitochondria from these mice appeared swollen and were >60% larger than controls (average mitochondrial area: 0.76 ± 0.42 μm^2 versus 0.47 ± 0.24 μm^2, respectively, $P < 0.0001$; $n = 680–820$). Hearts from animals without DOX also contained significantly fewer mitochondria (86 ± 24 mitochondria per field versus 137 ± 26 in controls, $P < 0.01$; field size = 264 μm^2; $n = 6$ fields).

Transmission electron micrographs also revealed an unusual pattern of lipid body formation in hearts of transgenic mice after DOX withdrawal. Relatively few lipid bodies were seen in hearts from control animals, but numbers increased dramatically at 5 days after DOX withdrawal (Fig. 2*D*). At this stage, mitochondrial morphology appeared normal. The increase in lipid bodies was reversed by 8 days after DOX withdrawal (2.8 ± 1.5 lipid bodies per field in controls versus 10.7 ± 4.5 at 5 days, $P < 0.05$, versus 1.7 ± 1.0 at 8 days; field size = 264 μm^2; $n = 6–12$ fields).

Abnormalities in Cardiac Gene Expression in HDAC5S/A Mice. The mitochondrial abnormalities and behavior of mice removed from DOX were consistent with a loss of cardiac energy reserves and heart failure as the likely cause of death. To further investigate the basis for this phenotype, we isolated total cardiac RNA from mice removed from DOX for 8 days and from mice receiving DOX and analyzed gene expression levels using an Affymetrix U74Av2 microarray (Fig. 3). Expression of a subset of genes was also examined by semiquantitative RT-PCR. Of particular interest were changes in the expression levels of numerous genes involved in the mitochondrial fatty acid oxidation pathway.

PGC-1α, a critical regulator of mitochondrial biogenesis and function, was dramatically down-regulated in mice after withdrawal of DOX, consistent with the mitochondrial pathology observed. We also examined expression of PPARα and PPARγ, nuclear receptors that regulate expression of enzymes involved in fatty acid oxidation and adipogenesis, respectively. Expression of PPARα was unchanged, but expression of PPARγ, which is usually expressed in the heart at very low levels, was up-regulated on DOX withdrawal. This may result from excessive levels of unoxidized fatty acids present in the heart due to inhibition of the fatty acid oxidation pathway (see below), because increases in fatty acid levels may up-regulate PPARγ expression (15–17). The up-regulation of PPARγ may be responsible for the loss of lipid bodies observed between 5 and 8 days of transgene induction (Fig. 2*D*), because the PPARγ agonist troglitazone caused a similar loss of lipid bodies in a rat steatosis model, although the mechanism of this process is unclear (18).

The carnitine palmitoyltransferases M-CPT-I and CPT-II are responsible for mitochondrial import of fatty acids and represent critical rate-limiting steps in the mitochondrial fatty acid oxidation pathway (9). Transcripts encoding both enzymes were down-regulated in mice removed from DOX (Fig. 3). Other key enzymes of this pathway were also dramatically down-regulated

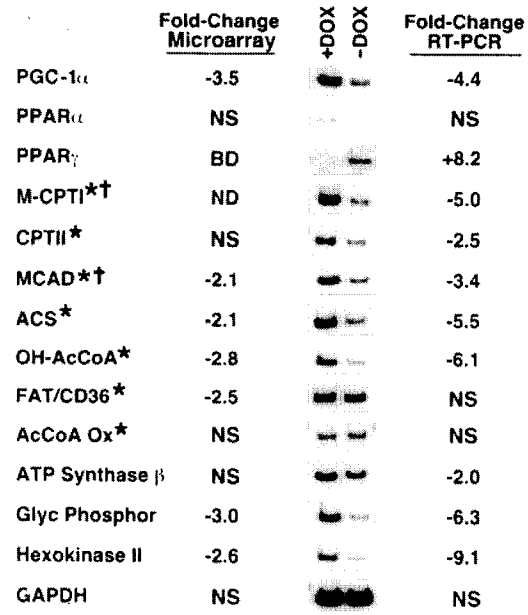

Fig. 3. Inhibition of expression of PGC-1α and metabolic enzymes after DOX withdrawal. Total RNA from hearts of HDAC5S/A mice was analyzed by microarray or by semiquantitative RT-PCR. The fold changes in gene expression for a panel of enzymes involved in cardiac energy metabolism pathways are presented in the chart (+DOX mice vs. −DOX), as well as images of bands obtained for each transcript by RT-PCR. NS, no significant change; BD, below detection limit; ND, not determined; M-CPTI, muscle-type carnitine palmitoyltransferase I; CPTII, carnitine palmitoyltransferase II; MCAD, medium chain acyl-CoA dehydrogenase; ACS, acyl-CoA synthetase; OH-AcCoA, OH-long-chain acyl-CoA dehydrogenase; FAT/CD36, fatty acid translocase; AcCoA Ox, acyl-CoA oxidase; Glyc Phosphor, glycogen phosphorylase. Asterisks denote direct targets of PPARα regulation; crosses denote genes regulated by PGC-1α.

including medium chain acyl-CoA dehydrogenase (MCAD), acyl-CoA synthetase, and OH-long-chain acyl-CoA dehydrogenase. The capacity for fatty acid oxidation is therefore likely to be highly reduced in these animals, which may contribute to the accumulation of lipid bodies observed after 5 days of gene induction (Fig. 2*D*). Expression of these fatty acid oxidation genes is regulated by PPARα (9). Because expression levels of PPARα did not change in these animals, however, the down-regulation of these genes may be due to impaired coactivation by PGC-1α. In fact, expression of M-CPT-I and MCAD is coactivated by PGC-1α (19). Although we cannot rule out the possibility of posttranslational modifications of PPARα being responsible for this effect, some transcriptional targets of PPARα, including the fatty acid translocase/CD36 and acyl-CoA oxidase genes, showed no changes in expression level, suggesting that the down-regulation is not due to changes in PPARα activity directly (Fig. 3).

Various other metabolic enzymes involved in energy generation were down-regulated upon DOX withdrawal, including ATP synthase-β, which is involved directly in ATP synthesis in the mitochondria, glycogen phosphorylase, the rate-limiting enzyme comprising the first step of the glycogenolysis pathway, and hexokinase II, one of the first enzymes in the glycolytic pathway (20). Microarray analysis also revealed down-regulation of the MEF2 transcriptional targets creatine kinase (3.5-fold) and GLUT4 (3-fold), the primary glucose transporter in the myocardium and a target of PGC-1α coactivation (11, 21). Together, these findings indicate that overexpression of a mutant HDAC, which represses MEF2 activity, negatively impacts the major pathways of cardiac energy production. Because PGC-1α acts as a master regulator of mitochondrial biogenesis and gene expression, it was a logical target for the effects of HDAC5S/A on the heart.

Regulation of PGC-1α Expression by MEF2. Class II HDACs repress the activity of MEF2 transcription factors. We therefore examined the 5′ flanking region of the mouse *PGC-1α* gene and identified two putative MEF2-binding sites with conformity to the consensus MEF2 site [CTA(A/T)$_4$TAG/A] (Fig. 4*A*).

Gel-shift analysis of these sites using extracts from MEF2C-transfected COS cells revealed that they bound MEF2C (Fig. 4*B*). Mutated MEF2 sites with A/T to C/G conversions showed no complex formation, demonstrating the specificity of binding.

We then examined whether MEF2 factors were able to activate the *PGC-1α* promoter using a luciferase reporter fused to the 3.1-kb *PGC-1α* promoter region. All three MEF2 factors tested (MEF2C, -A, and -D) significantly activated the *PGC-1α* promoter (Fig. 4*C*). Mutation of either of the two MEF2 sites significantly reduced transactivation by MEF2C (Fig. 4*D*), and mutation of both sites had no further inhibitory effect. Together, these findings demonstrate that both of the MEF2-binding sites are necessary, but neither is sufficient, for transactivation of the *PGC-1α* promoter.

Repression of PGC-1α Expression by HDAC5S/A. On the basis of the ability of MEF2 to activate the *PGC-1α* promoter, we speculated that HDAC5 would repress this promoter, since HDAC5 is recruited by MEF2. Indeed, *PGC-1α* promoter activation could be completely attenuated by expression of HDAC5S/A, but not by the class I HDAC, HDAC3 (Fig. 4*C*), demonstrating a specific effect of HDAC5. HDAC5S/A also suppressed expression of the *PGC-1α* reporter in the absence of exogenous MEF2, possibly due to inhibition of endogenous MEF2 factors present in COS cells. Reporter assays using the homologous human *PGC-1α* promoter region show similar activation and inhibition of the promoter by MEF2 and HDAC5S/A, respectively (data not shown).

To determine whether HDAC5S/A was capable of inhibiting expression of the endogenous *PGC-1α* gene, we infected neonatal rat cardiomyocytes *in vitro* with an adenovirus encoding HDAC5S/A (AdHDAC5S/A) and examined expression of PGC-1α by semiquantitative RT-PCR (8). Infection with AdHDAC5S/A significantly inhibited PGC-1α expression, whereas infection with a control adenovirus expressing GFP (AdCMV-GFP) had no effect (Fig. 4*E*). We conclude that endogenous *PGC-1α* gene expression is modulated by HDAC5.

Histone Deacetylation at an Essential MEF2 Site Correlates with Repression of *PGC-1α*. We examined whether the inhibition of *PGC-1α* gene expression by HDAC5 was due to deacetylation of histones in the region of the essential MEF2-binding sites within the *PGC-1α* promoter by performing ChIP analysis. Acetylation of histones at the distal MEF2-binding site (−2901) was dramatically decreased in cardiomyocytes infected with AdHDAC5S/A compared with noninfected or AdCMV-GFP-infected cardiomyocytes (Fig. 4*F*). No changes were observed in acetylation of histones at the other *PGC-1α* MEF2 site or at the *GAPDH* promoter. Nonimmunoprecipitated input DNA was used as a control.

It might be expected that because the proximal MEF2 site at −1539 was required for transactivation of the luciferase reporter gene (Fig. 4*D*), deacetylation of histones in this region would be observed. One possible explanation for the lack of deacetylation may be that the proximal site is required for assembly of a transcriptional complex, but HDACs themselves are not recruited to this region. Alternatively, dominant-acting histone acetyltransferases may be recruited to the second site but not the more distal site at −2901.

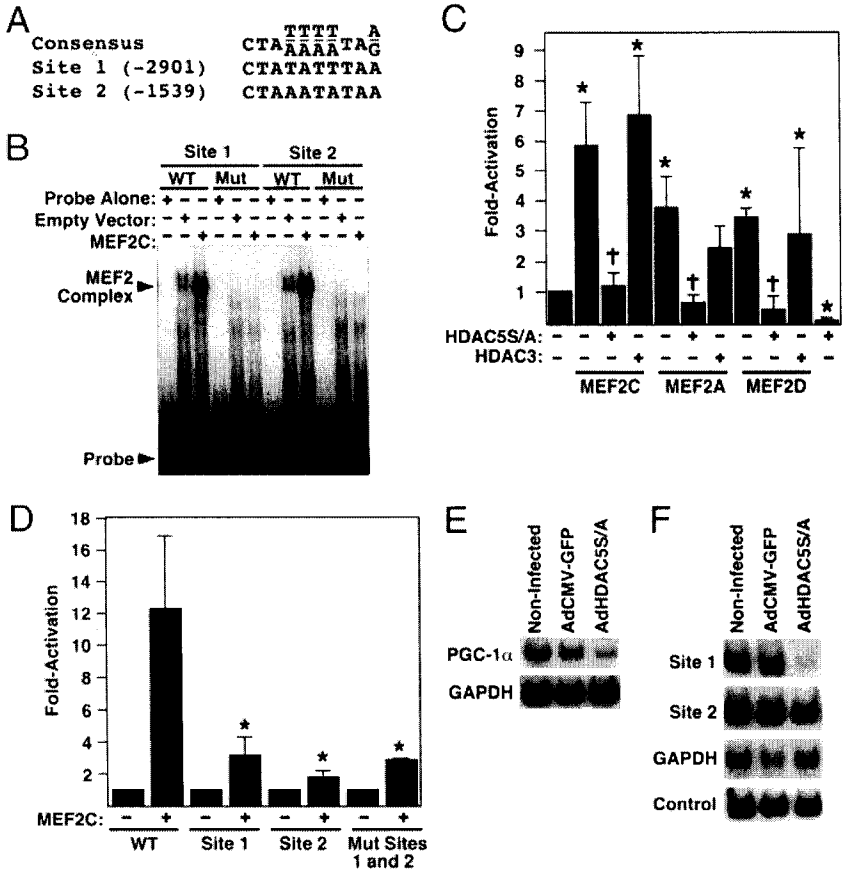

Fig. 4. Regulation of the *PGC-1α* promoter by MEF2 and HDAC5. (*A*) Sequence of putative MEF2 transcription factor-binding sites in the 3.1-kb proximal promoter of the mouse *PGC-1α* gene, compared with the consensus-binding sequence. Numbers in brackets refer to location in base pairs relative to the ATG start codon for *PGC-1α*. (*B*) Electrophoretic mobility-shift assay for binding of MEF2C to the putative MEF2 sites of the 3.1-kb proximal *PGC-1α* promoter. WT, wild-type oligomer; Mut, mutant oligomer with A/T to C/G conversion. (*C*) Activation of *PGC-1α*-promoter–luciferase reporter by MEF2 factors and attenuation by HDAC5S/A in COS cells. Asterisks denote $P < 0.05$ vs. reporter alone; crosses denote $P < 0.05$ vs. same sample in absence of HDAC5S/A. Error bars represent standard deviation of the mean for three experiments. (*D*) Effects of MEF2-binding site mutations in the *PGC-1α* promoter on transcriptional activation by MEF2C. Asterisks denote $P < 0.01$ vs. wild-type reporter plus MEF2C. Error bars represent standard deviation of the mean for three experiments. (*E*) Semiquantitative RT-PCR of PGC-1α expression in noninfected neonatal rat cardiomyocytes compared with cells infected with AdCMV-GFP or AdCMV-HDAC5S/A. (*F*) Immunoprecipitation of acetylated histone H3/DNA complexes from noninfected neonatal rat cardiomyocytes or cells infected with AdCMV-GFP or AdCMV-HDAC5S/A. Immunoprecipitated DNA was subjected to ^{32}P-PCR under nonsaturating conditions using primers for *PGC-1α* promoter MEF2-binding sites or GAPDH. An aliquot of nonimmunoprecipitated DNA was used as an input control.

Discussion

The results of this study suggest a model of high-level control of mitochondrial energy production by MEF2 and HDAC regulation of PGC-1α expression (Fig. 5). This model provides a means of fine-tuning PGC-1α levels in response to changing energy demands and predicts a role for MEF2 in matching increased energy demand during myocyte hypertrophy to increased energy production in the mitochondria.

Previous studies showed that the calcineurin and calcium/calmoduiin-dependent protein kinase (CaMK)-signaling pathways induce the transformation of fast glycolytic skeletal muscle fibers to slow oxidative fibers, accompanied by the up-regulation of PGC-1α (22, 23). Overexpression of PGC-1α in skeletal muscle also results in increased slow fiber number and expression of slow fiber metabolic and contractile genes, which are MEF2-dependent (24). Given that calcineurin and CaMK signaling stimulate MEF2 activity, the present study suggests that MEF2 links these signaling pathways to PGC-1α transcription, providing a potential mechanism for the increase in mitochondrial number and PGC-1α expression observed in response to CaMK signaling in skeletal muscle (23). CaMK stimulates phosphorylation of class II HDACs, leading to their export from the nucleus (4). Our data suggest that inactivation of HDACs by CaMK or related kinases would derepress PGC-1α expression, resulting in increased mitochondrial biogenesis.

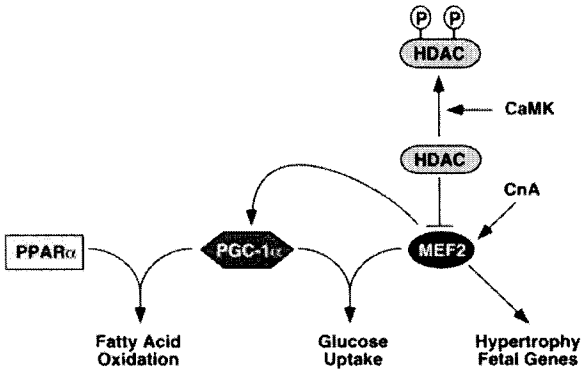

Fig. 5. Model for interactions between MEF2/HDAC5 and PGC-1α. PGC-1α and PPARα cooperate to activate genes encoding enzymes involved in cardiac fatty oxidation. PGC-1α and MEF2C have been demonstrated to regulate glucose uptake in muscle by controlling expression of the GLUT4 glucose transporter, the main glucose uptake mechanism in muscle. MEF2 also regulates fetal gene programs during muscle hypertrophy. CnA, calcineurin.

Overexpression of PGC-1α in the heart enhances mitochondrial biogenesis (10). Conversely, as shown here, down-regulation of PGC-1α expression results in a loss of cardiac mitochondria. We interpret the severe cardiac abnormalities in HDAC5S/A transgenic mice to reflect the extreme potency of this mutant HDAC in suppressing MEF2 activity. Although our initial interest was to determine whether the signal-resistant mutant of HDAC5 could block cardiac hypertrophy *in vivo* as it does *in vitro* (8), the cardiac abnormalities evoked by overexpression of HDAC5S/A suggest that there is likely to be an essential level of MEF2 activity required for cardiac homeostasis, such that suppression of this activity results in cardiac demise. Consistent with this notion, mice lacking *MEF2A* exhibit a deficiency of mitochondria and high postnatal mortality (25). It is tempting to speculate that the phenotype of HDAC5S/A mice reflects the combined loss of function of all MEF2 factors in the adult heart, although we cannot rule out the possible involvement of other transcription factors.

It is possible that the mitochondrial changes observed in the HDAC5S/A over-expressing animals are not directly due to repression of PGC-1α expression, because MEF2 has numerous target genes. Indeed, transcripts encoding a variety of MEF2 target genes were down-regulated by microarray analysis after DOX withdrawal, including β-enolase, phosphoglycerate mutase, and contractile proteins such as skeletal α-actin and α-MHC (results not shown). However, the *in vitro* reporter and ChIP assays, combined with the rapid repression (within 24 h) of PGC-1α expression in isolated cardiomyocytes after AdHDAC5S/A infection, strongly suggest a direct effect of HDAC5S/A on PGC-1α expression.

It remains to be seen whether HDAC repression of PGC-1α expression plays a role in cardiac decompensation and failure in human disease progression. Heart failure is often marked by mitochondrial dysfunction, and children with genetic mitochondrial diseases commonly present with cardiovascular deficiencies, indicating that precise balance is required between mitochondrial energy production and cardiac energy demand (26, 27). The rapid progression of heart failure in HDAC5S/A mice suggests that depletion of mitochondrial energy stores may play a critical role in this process. A potential model may involve activation of MEF2 factors during adaptive hypertrophy, resulting in activation of fetal gene programs, activation of PGC-1α-dependent fatty acid metabolism and mitochondrial growth, and an increase in work capacity. However, if this activation is prolonged, or if other stresses act on the heart, other mechanisms may activate HDACs, repressing MEF2 activation of PGC-1α expression and negatively impacting fatty acid metabolism and cardiac energy production. This would help explain the observations of a shift from fatty acid oxidation toward glucose utilization in heart failure and fatty acid oxidation enzyme down-regulation in failing human hearts (28, 29). Should HDACs prove to play a role in these pathways, HDAC inhibitors may be efficacious in treatment of cardiac failure by derepressing PGC-1α expression, thereby increasing fatty acid oxidation and energy production.

We thank A. Tizenor for graphics; T. McKinsey and C. Zhang for vectors and valuable discussion; J. Shelton and D. Bellotto for histology; and B. Conklin (University of California, San Francisco) and H. Bujard (University of Heidelberg) for the pUHG-10 vector. We also thank R. Bassel-Duby, O. Nakagawa, and D. Garry for critical reading of the manuscript. E.N.O. was supported by grants from the National Institutes of Health, the Donald W. Reynolds Foundation, and the Texas Advanced Technology Program. M.P.C. was the recipient of a postdoctoral fellowship from the Canadian Institutes for Health Research.

1. Eberharter, A. & Becker, P. B. (2002) *EMBO Rep.* **3,** 224–229.
2. McKinsey, T. A., Zhang, C. L. & Olson, E. N. (2001) *Curr. Opin. Genet. Dev.* **11,** 497–504.
3. Black, B. L. & Olson, E. N. (1998) *Annu. Rev. Cell Dev. Biol.* **14,** 167–196.
4. McKinsey, T. A., Zhang, C. L., Lu, J. & Olson, E. N. (2000) *Nature* **408,** 106–111.
5. Grozinger, C. M. & Schreiber, S. L. (2000) *Proc. Natl. Acad. Sci. USA* **97,** 7835–7840.
6. McKinsey, T. A., Zhang, C. L. & Olson, E. N. (2001) *Mol. Cell. Biol.* **21,** 6312–6321.
7. McKinsey, T. A., Zhang, C. L. & Olson, E. N. (2002) *Trends Biochem. Sci.* **27,** 40–47.
8. Zhang, C. L., McKinsey, T. A., Chang, S., Antos, C. L., Hill, J. A. & Olson, E. N. (2002) *Cell* **110,** 479–488.
9. Lehman, J. J. & Kelly, D. P. (2002) *Clin. Exp. Pharmacol. Physiol.* **29,** 339–345.
10. Lehman, J. J., Barger, P. M., Kovacs, A., Saffitz, J. E., Medeiros, D. M. & Kelly, D. P. (2000) *J. Clin. Invest.* **106,** 847–856.
11. Michael, L. F., Wu, Z., Cheatham, R. B., Puigserver, P., Adelmant, G., Lehman, J. J., Kelly, D. P. & Spiegelman, B. M. (2001) *Proc. Natl. Acad. Sci. USA* **98,** 3820–3825.
12. Yu, Z., Redfern, C. S. & Fishman, G. I. (1996) *Circ. Res.* **79,** 691–697.
13. McFadden, D. G., Charite, J., Richardson, J. A., Srivastava, D., Firulli, A. B. & Olson, E. N. (2000) *Development (Cambridge, U.K.)* **127,** 5331–5341.
14. Djouadi, F., Weinheimer, C. J., Saffitz, J. E., Pitchford, C., Bastin, J., Gonzalez, F. J. & Kelly, D. P. (1998) *J. Clin. Invest.* **102,** 1083–1091.
15. Patane, G., Anello, M., Piro, S., Vigneri, R., Purrello, F. & Rabuazzo, A. M. (2002) *Diabetes* **51,** 2749–2756.
16. Meadus, W. J., MacInnis, R. & Dugan, M. E. (2002) *J. Mol. Endocrinol.* **28,** 79–86.
17. Fabris, R., Nisoli, E., Lombardi, A. M., Tonello, C., Serra, R., Granzotto, M., Cusin, I., Rohner-Jeanrenaud, F., Federspil, G., Carruba, M. O., *et al.* (2001) *Diabetes* **50,** 601–608.
18. Zhou, Y. T., Grayburn, P., Karim, A., Shimabukuro, M., Higa, M., Baetens, D., Orci, L. & Unger, R. H. (2000) *Proc. Natl. Acad. Sci. USA* **97,** 1784–1789.
19. Vega, R. B., Huss, J. M. & Kelly, D. P. (2000) *Mol. Cell. Biol.* **20,** 1868–1876.
20. Depre, C., Rider, M. H. & Hue, L. (1998) *Eur. J. Biochem.* **258,** 277–290.
21. Mora, S. & Pessin, J. E. (2000) *J. Biol. Chem.* **275,** 16323–16328.
22. Chin, E. R., Olson, E. N., Richardson, J. A., Yang, Q., Humphries, C., Shelton, J. M., Wu, H., Zhu, W., Bassel-Duby, R. & Williams, R. S. (1998) *Genes Dev.* **12,** 2499–2509.
23. Wu, H., Kanatous, S. B., Thurmond, F. A., Gallardo, T., Isotani, E., Bassel-Duby, R. & Williams, R. S. (2002) *Science* **296,** 349–352.
24. Lin, J., Wu, H., Tarr, P. T., Zhang, C. Y., Wu, Z., Boss, O., Michael, L. F., Puigserver, P., Isotani, E., Olson, E. N., *et al.* (2002) *Nature* **418,** 797–801.
25. Naya, F. J., Black, B. L., Wu, H., Bassel-Duby, R., Richardson, J. A., Hill, J. A. & Olson, E. N. (2002) *Nat. Med.* **8,** 1303–1309.
26. Guertl, B., Noehammer, C. & Hoefler, G. (2000) *Int. J. Exp. Pathol.* **81,** 349–372.
27. Stanley, W. C. & Chandler, M. P. (2002) *Heart Fail. Rev.* **7,** 115–130.
28. Recchia, F. A., McConnell, P. I., Bernstein, R. D., Vogel, T. R., Xu, X. & Hintze, T. H. (1998) *Circ. Res.* **83,** 969–979.
29. Sack, M. N., Rader, T. A., Park, S., Bastin, J., McCune, S. A. & Kelly, D. P. (1996) *Circulation (Cambridge, U.K.)* **94,** 2837–2842.

THE JOURNAL OF BIOLOGICAL CHEMISTRY

Vol. 280, No. 17, Issue of April 29, pp. 16934–16941, 2005
Printed in U.S.A.

Cyclin D1 Inhibits Peroxisome Proliferator-activated Receptor γ-mediated Adipogenesis through Histone Deacetylase Recruitment*

Received for publication, January 12, 2005, and in revised form, February 14, 2005
Published, JBC Papers in Press, February 14, 2005, DOI 10.1074/jbc.M500403200

Maofu Fu‡, Mahadev Rao‡, Toula Bouras, Chenguang Wang‡, Kongming Wu‡, Xueping Zhang‡, Zhiping Li‡, Tso-Pang Yao§, and Richard G. Pestell‡¶

From the ‡Lombardi Comprehensive Cancer Center, Department of Oncology, Georgetown University, Washington, D. C. 20057 and the §Department of Pharmacology and Cancer Biology, Duke University, Durham, North Carolina 27710

The *cyclin D1* gene encodes the labile serum-inducible regulatory subunit of a holoenzyme that phosphorylates and inactivates the retinoblastoma protein. Overexpression of cyclin D1 promotes cellular proliferation and normal physiological levels of cyclin D1 function to inhibit adipocyte differentiation *in vivo*. We have previously shown that cyclin D1 inhibits peroxisome proliferator-activated receptor (PPAR)γ-dependent activity through a cyclin-dependent kinase- and retinoblastoma protein-binding-independent mechanism. In this study, we determined the molecular mechanism by which cyclin D1 regulated PPARγ function. Herein, murine embryonic fibroblast (MEF) differentiation by PPARγ ligand was associated with a reduction in histone deacetylase (HDAC1) activity. *Cyclin D1*$^{-/-}$ MEFs showed an increased propensity to undergo differentiation into adipocytes. Genetic deletion of *cyclin D1* reduced HDAC1 activity. Reconstitution of cyclin D1 into the *cyclin D1*$^{-/-}$ MEFs increased HDAC1 activity and blocked PPARγ-mediated adipogenesis. PPARγ activity was enhanced in *cyclin D1*$^{-/-}$ cells. Reintroduction of cyclin D1 inhibited basal and ligand-induced PPARγ activity and enhanced HDAC repression of PPARγ activity. Cyclin D1 bound HDAC *in vivo* and preferentially physically associated with HDAC1, HDAC2, HDAC3, and HDAC5. Chromatin immunoprecipitation assay demonstrated that cyclin D1 enhanced recruitment of HDAC1 and HDAC3 and histone methyltransferase SUV39H1 to the PPAR response element of the lipoprotein lipase promoter and decreased acetylation of total histone H3 and histone H3 lysine 9. Collectively, these studies suggest an important role of cyclin D1 in regulation of PPARγ-mediated adipocyte differentiation through recruitment of HDACs to regulate PPAR response element local chromatin structure and PPARγ function.

The *cyclin D1* gene was cloned as a breakpoint rearrangement in parathyroid adenoma (1) and as a macrophage colony-stimulating factor-1-responsive gene in the mouse (2). Cyclin D1 encodes a labile growth factor-inducible regulatory subunit of the holoenzyme that phosphorylates and inactivates the retinoblastoma protein (Rb).[1] Cyclin D1 overexpression promotes G_1 phase progression in cultured cells and immunoneutralizing experiments have shown a requirement for cyclin D1 in fibroblast, mammary, and epithelial cell proliferation (3, 4). Furthermore, cyclin D1 overexpression was shown to induce mammary tumorigenesis and to collaborate with the c-*myc* oncogene to induce lymphomagenesis (6). Deletion of the *cyclin D1* gene in mice has demonstrated a key role for cyclin D1 in several distinct processes, including retinal and mammary gland development (7), cellular migration (8), cellular proliferation and survival (9), angiogenesis (10), and adipocyte differentiation (5). *Cyclin D1*$^{-/-}$ MEFs have enhanced adipocyte differentiation in response to PPARγ ligands, which is reversed by cyclin D1 reintroduction (5).

In addition to promoting DNA synthesis and cellular proliferation, cyclin D1 has been shown to inhibit the activity of several transcription factors (V-Myb, MyoD) and nuclear receptors (androgen receptor, PPARγ) (5, 11). Cyclin D1 repression of PPARγ activity is known to have important physiological consequences. Although the mechanisms remain to be determined, several lines of evidence imply a role for histone acetyltransferase activity in cyclin D1 regulation of nuclear receptor function. For example, repression of AR activity by cyclin D1 occurs independently of the cyclin D1 Cdk-binding domain (11, 12) and is reversed by co-expression of either P/CAF or p300 (11). P/CAF physically associates with cyclin D1 (11, 13) through the Ada 2 region (11). Cyclin D1 also binds the histone acetyltransferase p300 (14, 15), a co-activator for PPARγ.

HDAC1, a class 1 histone deacetylase, has been implicated in regulation of adipocyte differentiation. Treatment with histone deacetylase inhibitors promote preadipocyte differentiation (16). HDAC1/mSin3A has been shown to be recruited to the CCAAT/enhancer-binding protein promoter with CCAAT/enhancer-binding protein-β and promoted the deacetylation of histone H4. HDAC3, another member of the HDAC family, associates with PPARγ and Rb to form a PPARγ·Rb·HDAC3 repressor complex and attenuated PPARγ-mediated adipocyte differentiation (17).

Herein, studies were conducted to examine the mechanisms underlying the role of cyclin D1 as an inhibitor of PPARγ function and adipocyte differentiation. As HDAC inhibitors induce adipocyte differentiation of MEFs (16, 17), we assessed

* This work was supported in part by awards from the Susan G. Komen Breast Cancer Foundation, R01CA70896, R01CA75503, R01CA86072, R01CA93596, and R01CA107382 (to R. G. P.) and NIDDK, National Institutes of Health Grant 1 R21DK065220-02 (to M. F.). The costs of publication of this article were defrayed in part by the payment of page charges. This article must therefore be hereby marked "*advertisement*" in accordance with 18 U.S.C. Section 1734 solely to indicate this fact.

¶ To whom correspondence should be addressed: Lombardi Comprehensive Cancer Center, Dept. of Oncology, Georgetown University, Research Bldg. Rm. E501, 3970 Reservoir Rd. NW, Box 571468, Washington, D. C. 20057-1468. Tel.: 202-687-2110; Fax: 202-687-6402; E-mail: pestell@georgetown.edu.

[1] The abbreviations used are: Rb, retinoblastoma protein; MEF, murine embryonic fibroblast; Cdk, cyclin-dependent kinase; PPAR, peroxisome proliferator-activated receptor; PPARE, PPARγ response element; GFP, green fluorescent protein; ChIP, chromatin immunoprecipitation; LPL, lipoprotein lipase; MSCV, murine stem cell virus; IRES, internal ribosome entry segment.

the potential role of cyclin D1 in regulating HDAC activity and adipocyte differentiation. Detailed analyses demonstrated that cyclin D1 induces HDAC activity and blocks adipocyte differentiation. Cyclin D1 physically associates with HDACs and inhibits basal and ligand-induced PPARγ activity through recruitment of HDACs and histone methyltransferase to the PPARγ response element (PPARE) of the lipoprotein lipase (LPL) promoter.

EXPERIMENTAL PROCEDURES

Reagents, Reporter Genes, Expression Vectors, DNA Transfection, and Luciferase Assays—The acyl-coenzyme A oxidase triple PPARE luciferase $(AOX)_3$LUC reporter gene, pCMX-PPARγ, and the HDAC expression vectors (19) were described previously (5, 20). *Cyclin D1*$^{+/+}$ and *cyclin D1*$^{-/-}$ MEFs and 3T3 cells (*cyclin D1*$^{-/-}$ and *cyclin D1*$^{-/+}$) were described previously (5, 21). Cells were transfected by Superfect Transfection reagent (Qiagen, Valencia, CA) as described elsewhere (22). The medium was changed after 5 h, cells were treated with ligand or vehicle as indicated in the figure legends, and luciferase activity was determined after 24 h. Luciferase activity was normalized for transfection efficiency with β-galactosidase or *Renilla* reporters as an internal control. Luciferase assays were performed at room temperature with an Autolumat LB 953 (EG&G Berthold) (20). The -fold effect was determined by comparison to the empty expression vector cassette, and statistical analyses were performed using the Mann Whitney U test. The PPARγ ligand troglitazone was purchased from Calbiochem.

Retroviral Production and Infection—Retroviral production was described elsewhere (8). The coding region of the murine cyclin D1 cDNA (GenBank™ S78355) was inserted into the MSCV-IRESGFP vector at the EcoRI site upstream of the IRES driving expression of GFP. MSCV retroviruses were prepared by transient co-transfection with helper virus into 293T cells, using calcium phosphate precipitation. The retroviral supernatants were harvested 48 h after transfection (23) and filtered through a 0.45-μm filter. *Cyclin D1*$^{+/+}$ and *cyclin D1*$^{-/-}$ MEFs were incubated with fresh retroviral supernatants in the presence of 4 μg/ml Polybrene for 24 h, cultured for 6 days, and subjected to fluorescence-activated cell sorting (FACSVantage SE, BD Biosciences) for GFP-positive cells.

HDAC Assays—HDAC assays were performed using [^{3}H]acetate-incorporated histones isolated from HeLa cells treated with sodium butyrate exactly as described previously (24). Hepatic extracts (600 μg) were immunoprecipitated with saturating amounts of anti-HDAC1 antibodies (10 μg, Santa Cruz) and then incubated with 1 ml of [^{3}H]acetate-labeled HeLa histones (10,000 dpm) for 2 h at 37 °C, and acetylase activity was determined as described previously (24). Alternatively, HDAC1 assay was performed using the HDAC assay kit (Fluorometric Detection, Upstate, NY, catalog number 17-356) according to the manufacturer's instructions. Briefly, hepatic extracts (600 μg dissolved in 600 μl of cell lysate buffer) from *cyclin D1*$^{+/+}$, and *cyclin D1*$^{-/-}$ mice were immunoprecipitated with saturating amounts of anti-HDAC1 antibodies (10 μg) mixed with 30 μl of protein A beads (50% slurry) at 4 °C for 3–6 h. The immunoprecipitate and the protein A beads were collected by centrifugation (30 s in a microfuge at 8,000 × *g*) and washed twice with 500 μl of ice-cold Tris-buffered saline and once with 200 μl of ice cold HDAC assay buffer (25 mM Tris, pH 8.0, 137 mM NaCl, 2.7 mM KCl, 1 mM $MgCl_2$). The beads were resuspended with 60 μl of HDAC assay buffer containing 100 μM HDAC assay substrate and then incubated at 30 °C for 30–60 min. After brief centrifugation, 40 μl of the supernatant was transferred to 96-well plate and incubated with 20 μl of the diluted activator solution at room temperature for 10–15 min. The immunoprecipitated HDAC1 activity was measured in a fluorescence plate reader (excitation = 350 nm, emission = 460 nm) within 60 min.

Induction of Adipocyte Differentiation of MEFs—Induction of adipocyte differentiation of MEFs was performed as previously described (5). Primary MEFs were isolated from 14-day-postcoitus mouse embryos and were maintained at confluence for 1 day before being switched to basal differentiation medium (Dulbecco's modified Eagle's medium supplemented with 10% charcoal-stripped serum and 10 mg of insulin/liter). Differentiation was induced by serum supplemented with 0.2 mM methylisobutylxanthine (Sigma), 5 μM dexamethasone (Sigma), and 10 μg/ml insulin (Sigma) for 3 days. Subsequently, cells were maintained in basal differentiation medium supplemented with troglitazone (5 μM) (Calbiochem) or vehicle as indicated. Retroviral infection was conducted as described previously (5). For Oil Red-O staining, cells were fixed in 10% paraformaldehyde in phosphate-buffered saline for 15 min and rinsed briefly with water and ethanol. Cells were then stained with freshly prepared Oil Red-O solution (6 parts saturated Oil Red-O dye in isopropanol plus 4 parts water) at 37 °C for 15 min, washed with 70% ethanol, and then rinsed with phosphate-buffered saline. Cells were inspected by microscopy.

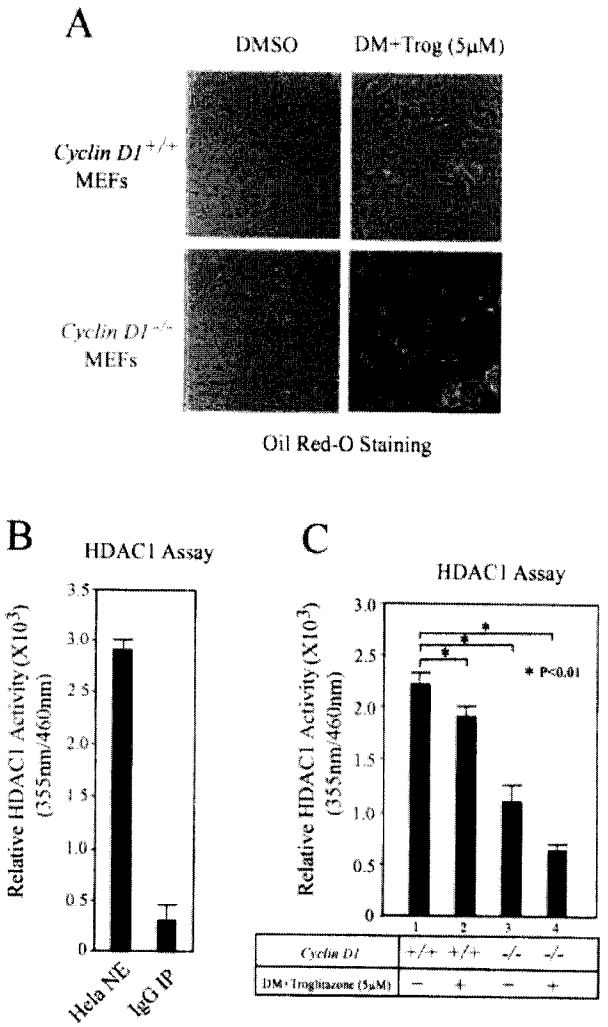

FIG. 1. **Cyclin D1 increases HDAC activity *in vivo* and blocks adipocyte differentiation.** *A*, MEFs derived from either *cyclin D1*$^{+/+}$ or *cyclin D1*$^{-/-}$ were treated with either Me_2SO (*DMSO*) or differentiation medium plus troglitazone (*DM + Trog*) (5 μM) for 10 days. Cells were then stained for Oil Red-O. Adipocytes differentiated from *cyclin D1*$^{-/-}$ MEFs are also shown as an *enlarged inset*. *B* and *C*, HDAC1 activity was assayed using equal amounts of HDAC1 immunoprecipitated from either *cyclin D1*$^{+/+}$ or *cyclin D1*$^{-/-}$ MEFs treated with either control Me_2SO or differentiation medium plus troglitazone. Nuclear extracts (*NE*) from HeLa cells served as a positive control and IgG was applied as a negative control for immunoprecipitation (*IP*).

Immunoprecipitation and Western Blot—293T cells were transfected with an expression vector for cyclin D1. Thirty hours after transfection, the cells lysates were prepared in 600 μl of cell lysis buffer (10 mM HEPES, pH 7.5, 100 mM KCl, 0.4 mM EDTA, 10 mM sodium fluoride, 0.2% Nonidet P-40, 1 mM dithiothreitol, 0.1 mM phenylmethylsulfonyl fluoride with proteinase inhibitors (Roche Diagnostics GmbH, catalog number 1836145). 600 μg of cellular lysate was subjected to immunoprecipitation with 10 μl of anti-HDAC1 antibody (Upstate Biotechnology) and 30 μl of protein A-agarose beads at 4 °C overnight. Normal rabbit IgG was used as a negative control. The beads were washed with 800 μl of cell lysis buffer five times, resuspended in 30 μl of cell lysis buffer plus 6 μl of SDS-PAGE loading buffer, and denatured by heating at 95 °C for 5 min. Proteins were dissolved in 10% SDS-PAGE. The membrane was blotted with either anti-HDAC1 or anti-cyclin D1 antibody (Ab-3, Neomarker) at room temperature for 1 h, then washed three times with 0.05% Tween 20 phosphate-buffered saline. The membrane was then incubated with horseradish peroxidase-conjugated anti-rabbit antibody. The immunoreactive proteins were visualized by an enhanced

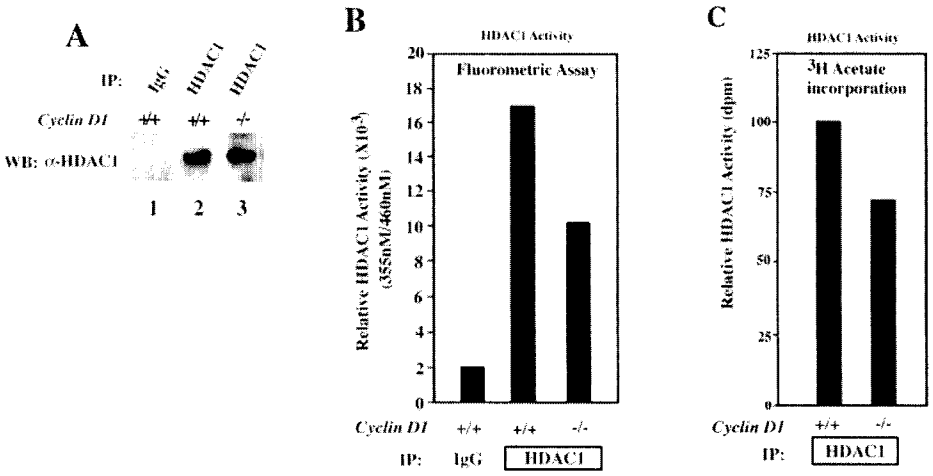

FIG. 2. **Cyclin D1 augments HDAC activity.** HDAC1 activity was assayed upon HDAC1 immunoprecipitation (*IP*) from murine liver lysates. *A*, Western blotting (*WB*) of HDAC1 demonstrating similar amounts of HDAC1 by Western blotting. IgG was applied as a negative control for immunoprecipitation. *B* and *C*, relative HDAC1 activity assayed by HDAC1 immunoprecipitation using hepatocellular extracts from *cyclin D1*$^{+/+}$ or littermate *cyclin D1*$^{-/-}$ mice and incubated with fluorometric-labeled HDAC substrates (*B*) or ^{3}H-labeled histone mix (*C*). Relative HDAC1 activity is shown.

chemiluminescence system (Amersham Biosciences). For immunoprecipitation of cyclin D1 with HDAC1–HDAC5, the expression vectors for cyclin D1 and HDAC1–HDAC5 were transfected into 293T cells. The cell lysates were then immunoprecipitated with the antibody (M2, Sigma), and Western blotting was conducted with an anti-cyclin D1 antibody (Ab-3).

Chromatin Immunoprecipitation (ChIP) assay—ChIP analysis was performed as previously described (25). 2×10^7 3T3 *cyclin D1*$^{-/+}$ or *cyclin D1*$^{-/-}$ cells were grown in Dulbecco's modified Eagle's medium with 10% charcoal-dextran stripped serum for 3 days. Upon treatment, the cells were cross-linked by adding 1.0% formaldehyde buffer containing 100 mM sodium chloride, 1 mM EDTA-Na, pH 8.0, 0.5 mM EGTA-Na, Tris-HCl, pH 8.0, directly to culture medium for 10 min at 37 °C. The medium was aspirated, and the cells washed twice using ice-cold phosphate-buffered saline containing 10 mM dithiothreitol and protease inhibitors. The cells were then lysed with 1% SDS lysis buffer and incubated for 10 min on ice. The cell lysates were sonicated to shear DNA to lengths between 200 and 500 bp, and the samples were diluted 10-fold in ChIP dilution buffer (0.01% SDS, 1.1% Triton X-100, 1.2 mM EDTA, 16.7 mM Tris, pH 8.1, 167 mM NaCl). To reduce nonspecific background, the cell pellet suspension was precleared with 60 μl of salmon sperm DNA/protein-A-agarose-50% slurry (Upstate Biotechnology) for 2 h at 4 °C with agitation. Chromatin solutions were precipitated overnight at 4 °C with rotation using 4 μg of antibodies to either cyclin D1 (HD-11, Santa Cruz), PPARγ (H-100, Santa Cruz), FLAG (Sigma), acetyl histone H3, acetyl histone H3 (lysine 9), methyl histone H3 (lysine 4), HDAC1 (2E10) (Upstate Biotechnology), SUV39H1, or HP1α (Upstate Technology). For a negative control, rabbit or mouse IgG was incubated with the supernatant fraction for 1 h at 4 °C with rotation. 60 μl of salmon sperm DNA/protein A-agarose slurry was added for 2 h at 4 °C with rotation to collect the antibody/histone complex and washed extensively following the manufacturer's protocol. Input and immunoprecipitated chromatin were incubated at 65 °C overnight to reverse cross-linking. After proteinase K digestion for 1 h, DNA was extracted using a Qiagen spin column kit. Precipitated DNAs were analyzed by PCR of 30 cycles. The following oligonucleotides were used for PCR to identify the PPARE in the mouse LPL promoter 5′-AAACCCCTCCTCTCTGCCTC-3′ and 5′-CCTCGGAGGAGGAGTAGGAG-3′ or human LPL promoter, 5′-GGGCCCCCGGGTAGAGTGG-3′ and 5′-CACGCCAAGGCTGCTTATGTGACT-3′. The oligonucleotides to identify the PPARE in the mouse adipocyte fatty acid binding protein (aP2) promoter are 5′-CAAGCCATGCGACAAAGGCA-3′ and 5′-TAGAAGTCGCTCAGGCCACA-3′ (26).

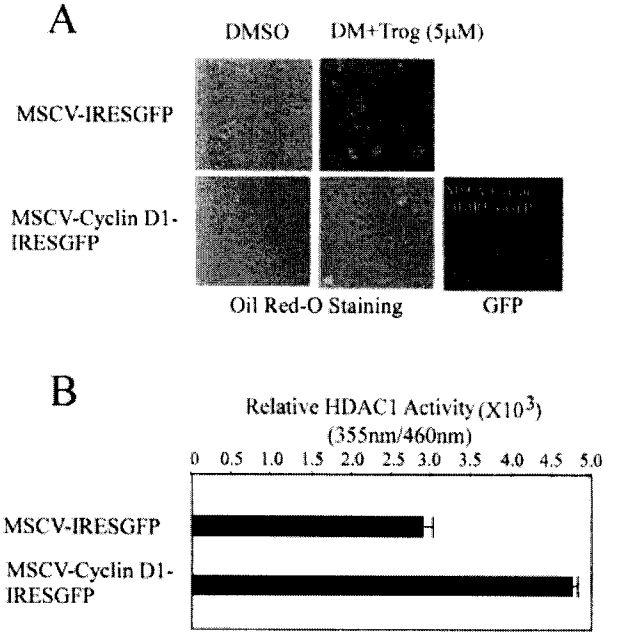

FIG. 3. **Reintroduction of cyclin D1 into *cyclin D1*$^{-/-}$ MEFs increases HDAC activity and blocks adipocyte differentiation.** *A*, *cyclin D1*$^{-/-}$ MEFs were infected with MSCV-cyclin D1-IRESGFP or MSCV-IRESGFP control virus and sorted by fluorescence-activated cell sorting for GFP-positive cells as indicated by GFP fluorescence (*right panel*). The cells were then treated with differentiation media with Me_2SO (*DMSO*) or PPARγ ligand troglitazone (*DM + Trog*) to induce adipocyte differentiation. Oil Red-O staining for the *cyclin D1*$^{-/-}$ MEFs infected either with control vector or MSCV-cyclin D1-IRESGFP virus are shown. Reintroduction of cyclin D1 into *cyclin D1*$^{-/-}$ MEFs blocked adipocyte differentiation. *B*, HDAC1 activity was assayed from equal amounts of cell extracts derived from *cyclin D1*$^{-/-}$ MEFs infected with either control viral vector or MSCV-cyclin D1-IRESGFP. Transduction of cells with cyclin D1 increased HDAC1 activity.

RESULTS

Cyclin D1 Inhibits Adipocyte Differentiation of MEFs and Regulates HDAC1 Activity—In our previous studies, *cyclin D1*$^{-/-}$ MEFs exhibited enhanced differentiation in response to PPARγ ligands (5) indicating that cyclin D1 repression of PPARγ is an important physiological function of cyclin D1 *in vivo*. Several distinct HDAC inhibitors induce differentiation of MEFs into Oil Red-O-positive adipocytes (16, 17). We therefore assessed the role of cyclin D1 in regulating cellular HDAC activity during adipocyte differentiation of MEFs. MEFs derived from either *cyclin D1* wild type or *cyclin D1*$^{-/-}$ mice were treated with differentiation medium and troglitazone, a PPARγ agonist, as described previously (5). The differentiation medium increased the abundance of Oil Red-O-positive lipid droplets in the *cyclin D1*$^{-/-}$ MEFs compared with wild type cells (Fig. 1*A*). This result is consistent with previous observations demonstrating that there is enhanced induction of adipogenesis in *cyclin D1*$^{-/-}$ MEFs with differentiation medium and PPARγ ligand (5). HDAC1 activity assays of these cellular extracts were conducted (Fig. 1*C*). HeLa cell nuclear extracts were used as a positive control (Fig. 1*B*). HDAC1 activity decreased during differentiation. *Cyclin D1*-deficient cells showed reduced HDAC activity, compared with cyclin D1 wild type cells (Fig. 1*C*, *lane 1 versus 3*), with a further reduction upon

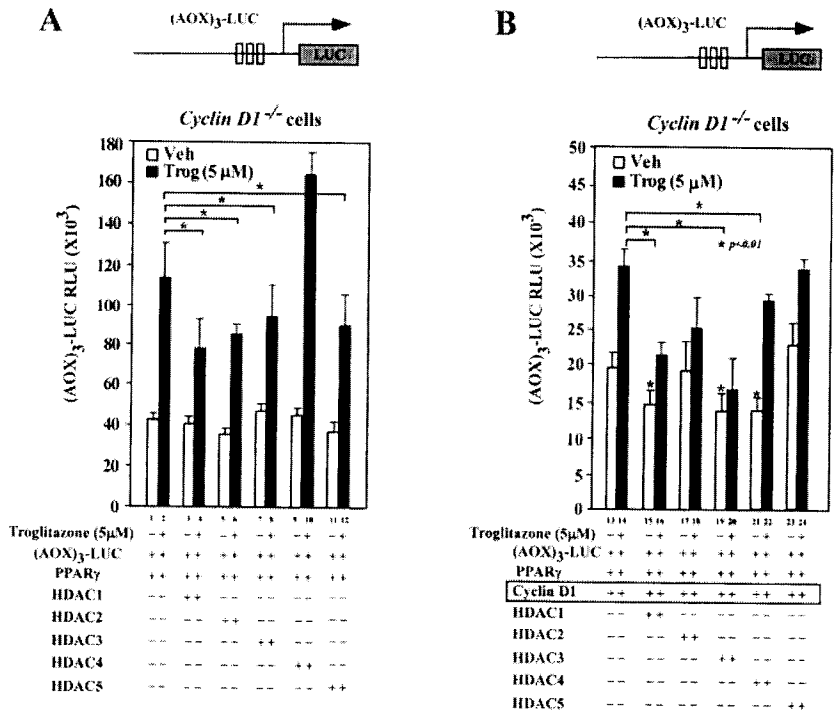

FIG. 4. **Cyclin D1 enhances HDAC repression of PPARγ transactivity.** *Cyclin D1*$^{-/-}$ cells were transfected with expression vector for PPARγ and $(AOX)_3$-LUC reporter along with expression vector for FLAG-HDAC1–HDAC5 with or without cyclin D1 as indicated. Luciferase activity was determined 24 h after treatment with 5 μM troglitazone (*Trog*) or vehicle control (*Veh*) (n = 6).

differentiation (Fig. 1*C*, *lane 2 versus 4*).

Next, we examined whether cyclin D1 regulated HDAC activity. HDAC1 assays of *cyclin D1*$^{-/-}$ and littermate *cyclin D1*$^{+/+}$ mice hepatocellular extracts were conducted. Equal amounts of HDAC1 were confirmed by Western blotting (Fig. 2*A*). The relative HDAC1 activity, assessed either by fluorometric assay (Fig. 2*B*) or by [^{3}H]acetate incorporation (Fig. 2*C*), demonstrated a reduction in HDAC1 activity in *cyclin D1*$^{-/-}$ cells, suggesting that the abundance of cyclin D1 regulates endogenous HDAC1 enzyme activity.

Reconstitution of Cyclin D1 into cyclin D1$^{-/-}$ *MEFs Increases HDAC Activity and Blocks Adipocyte Differentiation*—As reduced cyclin D1 levels correlated with reduced HDAC1 enzyme activities, further experiments were conducted to determine whether reintroduction of cyclin D1 in turn was capable of increasing HDAC1 activity in *cyclin D1*$^{-/-}$ MEFs. *Cyclin D1*$^{-/-}$ MEFs were infected with either an expression vector for cyclin D1 (MSCV-cyclin D1-IRESGFP) or equal amounts of empty expression vector cassette (MSCV-IRESGFP). GFP-positive cells were selected through GFP fluorescence-activated cell sorting as described previously (8) (Fig. 3*A*, *right panel*). MEFs infected with the cyclin D1 expression vector showed increased relative HDAC1 activity compared with vector control (Fig. 3*B*). In addition, reintroduction of cyclin D1 into *cyclin D1*$^{-/-}$ MEFs blocked adipocyte differentiation induced by differentiation medium and PPARγ ligand (Fig. 3*A*). Together, these studies suggest cyclin D1 contributes to cellular HDAC1 activity and regulation of HDAC activity by cyclin D1 plays a role in adipocyte differentiation.

Cyclin D1 Augments HDAC1 Repression—We next examined whether cyclin D1 was capable of augmenting HDAC-dependent transcriptional repression of PPARγ. To this end, gene reporter assays were conducted in *cyclin D1-deficient* cells. A synthetic PPARγ-responsive reporter gene $(AOX)_3$LUC was used, as cyclin D1 is known to inhibit both basal and ligand-induced PPARγ reporter activity. Co-transfection of the expression vectors for FLAG-HDAC1–HDAC5 with PPARγ in *cyclin D1*$^{-/-}$ 3T3 cells demonstrated that HDAC1, -2, -3 and -5 repressed PPARγ-liganded transactivity (Fig. 4*A*). Co-transfection of cyclin D1 inhibited ligand-induced reporter activity by 63% (Fig. 4, *A versus B*, *lane 14 versus 2*). HDAC1–HDAC3 co-transfection with cyclin D1 repressed ligand-induced PPARγ activity even further (Fig. 4*B*, *lanes 16*, *18*, and *20 versus lane 14*). The repressive effect of cyclin D1 was most pronounced with HDAC1 and HDAC3 (Fig. 4*B*, *lanes 16* and *20 versus lane 14*). HDAC1 and HDAC3 co-transfection repressed both basal and liganded PPARE gene activity.

Cyclin D1 Associates with HDACs in Vivo—We have previously shown that PPARγ transactivation induced by ligand was inhibited by cyclin D1 through a Rb- and Cdk-independent mechanism, requiring a region predicted to form a helix-loop-helix structure (5). As HDAC1 is a known inhibitor for adipocyte differentiation, we hypothesized that cyclin D1 might confer repression of PPARγ through association with HDACs. Cyclin D1 may regulate HDAC activity either indirectly or through co-association with HDACs. To determine whether cyclin D1 co-associated with HDACs, immunoprecipitation/Western blotting was conducted. A cyclin D1 expression plasmid was transfected into 293T cells. Immunoprecipitation with an HDAC1 antibody co-precipitated human cyclin D1 with endogenous HDAC1 (Fig. 5*A*, *lane 2*). In contrast, control IgG did not co-precipitate cyclin D1 or HDAC1 (Fig. 5*A*, *lane 1*). To examine whether cyclin D1 associated with HDAC1 *in vivo*, mouse liver lysate was subjected to immunoprecipitation with an anti-HDAC1 antibody. The immunoprecipitate was then resolved in a 7% SDS-PAGE and blotted with anti-cyclin D1 antibody. Immunoprecipitation with the HDAC1 antibody co-precipitated murine cyclin D1 from mouse liver lysate (Fig. 5*B*, *lane 2 versus 1*), indicating that cyclin D1 and HDAC1 are associated *in vivo*.

Several trichostatin A-dependent histone deacetylases were next assessed to examine the possibility that cyclin D1 may co-precipitate with other members of the HDAC family. Immunoprecipitation and Western blotting were conducted with human embryonic kidney 293 cells transfected with expression vectors for either cyclin D1 or FLAG-tagged HDAC1–HDAC5 (Fig. 5*C*). Immunoprecipitation with anti-FLAG antibody for FLAG-HDAC1–HDAC5 and sequential Western blotting of cyclin D1 showed that HDAC1, -2, -3 and -5 co-precipitated cyclin D1. It was also noted that the relative abundance of HDAC1

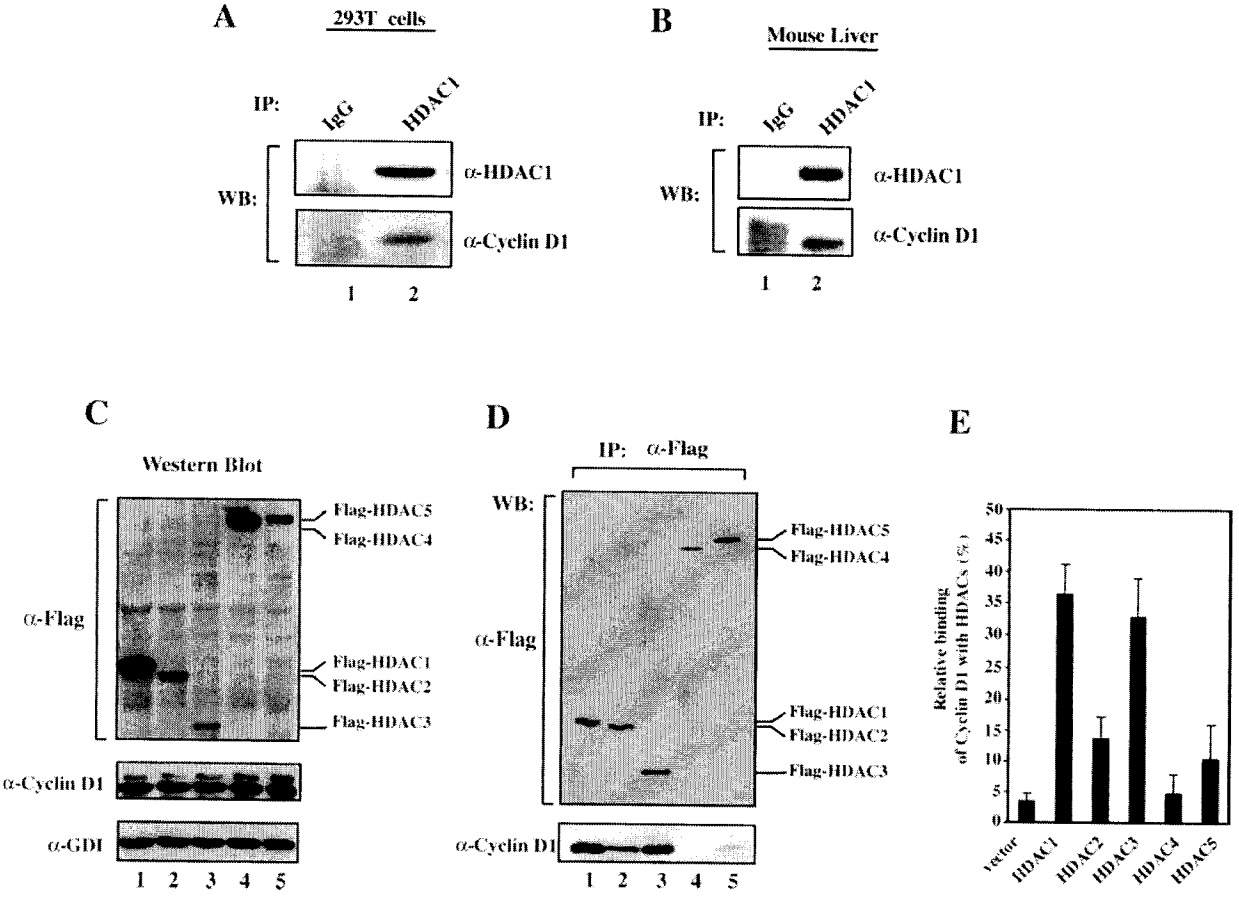

FIG. 5. **Cyclin D1 binds HDACs *in vitro* and *in vivo*.** *A*, immunoprecipitation (*IP*) Western blot (*WB*) analysis of 293T cells transfected with FLAG-tagged cyclin D1. Control IgG or antibody to endogenous HDAC1 were used for immunoprecipitation. Western blot analysis for HDAC1 and cyclin D1 is shown. *B*, HDAC1 immunoprecipitation Western blotting of murine hepatocellular extracts. IgG serves as a negative control for immunoprecipitation. Western blot analysis for HDAC1 and cyclin D1 is shown. *C* and *D*, relative binding affinity of cyclin D1 with HDAC1–HDAC5. *C*, Western blot analysis of 293T cells transfected with expression vectors for FLAG-tagged HDAC1–HDAC5 using antibodies to cyclin D1 (Ab-3) or anti-FLAG antibody. Guanine nucleotide dissociation inhibitor serves as a loading control for total protein. *D*, immunoprecipitation and Western blotting of the cell extracts for endogenous cyclin D1 and FLAG-tagged HDAC1–HDAC5. The cellular lysates were subjected to immunoprecipitation with anti-FLAG antibody for HDAC1–HDAC5, and Western blot was performed for endogenous cyclin D1. *E*, relative affinity of cyclin D1 with HDAC1–5.

and HDAC3 bound to cyclin D1 was greater than HDAC2 and HDAC5 (Fig. 5, *D* and *E*).

Cyclin D1 Enhances Recruitment of HDAC1 and HDAC3 to the PPARE of LPL Promoter—As cyclin D1 inhibited basal and ligand-induced activity of the synthetic PPARE, we examined the protein complexes recruited to the PPARE of the endogenous murine LPL promoter using ChIP assays. A comparison was made between *cyclin D1*$^{+/-}$ and *cyclin D1*$^{-/-}$ MEFs treated with differentiation medium and troglitazone (5 μM) or equal amounts of control vehicle (Fig. 6*A*). The relative abundance of PPARγ at the PPARE was enhanced in the *cyclin D1*$^{-/-}$ MEFs compared with *cyclin D1*$^{+/+}$ MEFs (Fig. 6*A*, *lanes 1 versus 2* and *3 versus 4*). The relative abundance of HDAC1 at the PPARE in *cyclin D1*$^{+/+}$ MEFs was increased 50% compared with the *cyclin D1*$^{-/-}$ cells in the differentiated state (Fig. 6*A*, *lane 3 versus 4*). HDAC3 recruitment at the PPARE was 4-fold greater in the *cyclin D1*$^{+/+}$ compared with *cyclin D1*$^{-/-}$ cells in the differentiated state (Fig. 6*A*, *lane 3 versus 4*), consistent with a model in which cyclin D1 enhances recruitment of HDAC1 and HDAC3 to the PPARE. To determine whether cyclin D1 was sufficient for the enhanced recruitment of HDAC1 to the PPARE, cyclin D1 was reintroduced into *cyclin D1*$^{-/-}$ MEFs by transfecting with either the MSCV-cyclin D1-IRESGFP or MSCV-IRESGFP control virus. The cells were then treated with either differentiation medium and troglitazone or vehicle control. Reintroduction of cyclin D1, which is identified through the FLAG epitope, into *cyclin D1*$^{-/-}$ cells reduced PPARγ recruitment in the presence of differentiation medium (Fig. 6*B*, *lane 3 versus 4*). The relative abundance of HDAC1 at the PPARE was increased in cells expressing cyclin D1 (Fig. 6*B*, *lanes 1 versus 2*, and *3 versus 4*). Together these studies suggest that cyclin D1 enhances recruitment of HDAC1 and HDAC3 to a PPARE *in vivo*.

Cyclin D1 Deficiency Enhances Histone H3 Acetylation—To further confirm the effects of cyclin D1 abundance on the recruitment of HDAC to a PPARE, the relative amount of HDAC1 at a PPARE in the *cyclin D1*$^{-/-}$ and *cyclin D1*$^{+/+}$ cells was determined by ChIP assay of the murine LPL promoter (Fig. 7*A*) or aP2 promoter (Fig. 7*B*) in randomly cycling 3T3 cells. The relative abundance of HDAC1 at the PPARE of either the LPL (Fig. 7*A*, *lane 1 versus 2*) or the aP2 promoter (Fig. 7*B*, *lane 1 versus 2*) was increased in *cyclin D1*$^{+/+}$ cells compared with those of *cyclin D1*$^{-/-}$ cells. PPARγ recruitment to the PPARE of the LPL (Fig. 7*A*, *lane 1 versus 2*) or aP2 promoter (Fig. 7*B*, *lane 1 versus 2*) was reduced in cyclin D1-expressing cells. These data are consistent with a model in which cyclin D1 enhances HDAC1 recruitment to PPAREs.

To examine the functional consequences of the association of cyclin D1 with HDACs, we assessed histone acetylation at the local chromatin structure of the PPARE of the LPL promoter. A comparison was made between *cyclin D1*$^{+/+}$ and *cyclin D1*$^{-/-}$ 3T3 cells. The cells were serum-starved for 48 h and then

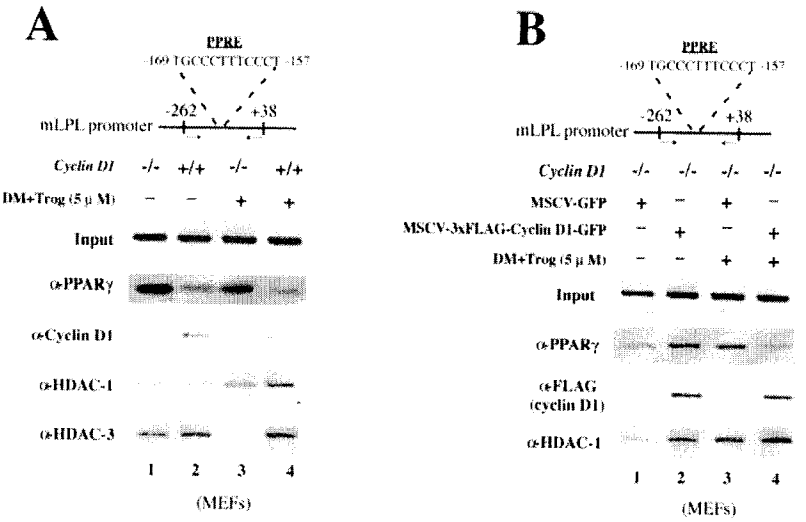

FIG. 6. **Cyclin D1 recruits HDAC1 to the PPARE of the LPL promoter.** *A*, ChIP assay analysis of the PPARγ response element of the murine LPL promoter of *cyclin D1*$^{+/+}$ or *cyclin D1*$^{-/-}$ MEF cells treated with differentiation medium (*DM*) plus either Me_2SO or troglitazone (*Trog*). Immunoprecipitation was conducted with antibodies to PPARγ, cyclin D1, HDAC1, or HDAC3, as indicated. *B*, ChIP analysis of the murine LPL promoter using *cyclin D1*$^{-/-}$ MEFs, infected with either MSCV-IRESGFP control virus or with MSCV-Cyclin D1-IRES-GFP and treated with differentiation medium plus Me_2SO or troglitazone. ChIP assays were conducted with the antibodies as indicated.

treated with 10% serum for 16 h. Endogenous cyclin D1 was detected at the PPARE by ChIP analysis in *cyclin D1*$^{+/+}$ cells (Fig. 7*C*, *lane 2*). PPARγ levels were reduced and the abundance of both HDAC1 and HDAC3 were increased in the *cyclin D1*$^{+/+}$ cells (Fig. 7*C*, *lane 1 versus 2*). Increased HDAC recruitment in *cyclin D1*$^{+/+}$ cells was associated with decreased histone H3 (acetylated Lys-9) (Fig. 7*C*), consistent with the findings that histone H3-Lys-9 deacetylation associates with inactive promoters (27). In keeping with previous studies (28), a reduction in acetylated histone H3 lysine 9 was associated with increased H3 dimethyl lysine 9 and reduced H3 dimethyl Lys-4 (Fig. 7*C*). As the methylation of histone H3 lysine 9 provides binding sites for HP1 proteins (29), we examined the components of the methylase complex known to methylate histone H3 lysine 9. Compared with the *cyclin D1*$^{-/-}$ cells, increased abundance of SUV39H1 and HP1α were identified in the *cyclin D1*$^{+/-}$ cells (Fig. 7*C*), suggesting that cyclin D1 abundance regulated the recruitment of both histone deacetylases and histone methyltransferase to the local chromatin of the LPL promoter.

To determine whether a physiological change in cyclin D1 abundance was capable of altering HDAC recruitment to a PPARE, 3T3 cells were serum-starved for 48 h to reduce cyclin D1 levels in the *cyclin D1*$^{+/+}$ 3T3 cells to barely detectable levels by Western blotting. Under these conditions, the recruitment of PPARγ was only modestly increased in the *cyclin D1*$^{+/+}$ cells, and HDAC1 and HDAC3 recruitment was similar at the PPARE between *cyclin D1*$^{-/-}$ and *cyclin D1*$^{+/+}$ cells (Fig. 7*D*).

To determine whether the observed changes in HDAC recruitment to a PPARE was observed in epithelial cells, MCF7 cells transfected with an expression vector for FLAG-tagged PPARγ were treated with either trichostatin A or troglitazone, and the human LPL promoter was assessed with ChIP assays. Trichostatin A and troglitazone reduced endogenous HDAC3 recruitment to the PPARE of the human LPL promoter associated with increased acetylation of histone H3 and H4. Troglitazone enhanced PPARγ recruitment as evidenced by the anti-FLAG antibody chromatin immunoprecipitation of the PPARE (Fig. 7*E*).

DISCUSSION

Cyclin D1 has been increasingly linked to Cdk-independent transcriptional repression (30, 31). As prior analysis of tissues and cells from *cyclin D1*$^{-/-}$ mice demonstrated an important physiological role for cyclin D1 as an inhibitor of adipocyte differentiation through repression of PPARγ function (5), herein we investigated the mechanisms by which cyclin D1 repressed PPARγ function. HDAC inhibitors are also known to enhance the differentiation of MEFs into adipocytes (16, 17). Thus, both cyclin D1 and histone deacetylases inhibit PPARγ activity and adipogenesis. Cyclin D1-deficient cells exhibited reduced HDAC1 activity, which was increased by the introduction of cyclin D1. Consistent with the finding that cyclin D1 bound HDACs, cyclin D1-deficient cells exhibited increased acetylation of histone H3 Lys-9, a marker of open chromatin configuration found at transcriptionally active promoters (32, 33). Increased cyclin D1 expression, either through viral transduction of a cyclin D1 expression vector or through serum induction, increased HDAC recruitment to a PPARE commensurate with increased deacetylation of histone H3 (Lys-9). The recruitment of HDAC by cyclin D1 may contribute to the Cdk-independent repression of a subset of transcriptional factors including nuclear receptors such as AR and PPARγ by cyclin D1.

In the current studies cyclin D1 co-precipitated HDAC1 *in vivo*. Cyclin D1 preferentially bound HDAC1 and HDAC3. Several lines of evidence demonstrate that cyclin D1 association with HDACs is functionally relevant. Firstly, the target of HDAC function, acetylation of histone H3 lysine 9, was regulated by cyclin D1 abundance in the context of the local chromatin of an endogenous PPARγ-responsive promoter. Secondly, cyclin D1 facilitated the recruitment of HDAC1 to a PPARγ-responsive element in ChIP assays. The acetylation of histone H3 Lys-9, which marks the open chromatin configuration of transcriptionally active promoters, was increased in *cyclin D1*-deficient cells, consistent with the finding that cyclin D1 recruited HDACs. Thirdly, adipocyte differentiation of MEFs decreased HDAC1 activity, and the reintroduction of cyclin D1 into *cyclin D1*$^{-/-}$ cells increased HDAC1 activity and inhibited adipocyte differentiation.

Previous studies have demonstrated that the recruitment of co-repressors, with associated histone deacetylase activity, are involved in the regulation of nuclear receptor function, either in the basal or ligand-activated state. The repression of ligand-induced receptor activation was previously reported for co-repressor complexes coordinated by the SMRT/HDAC1-associated repressor protein (SHARP) (34), the transcription intermediary factor TIF1 (35), and the metastases-associated protein 1 co-repressor MTA (36). The binding of cyclin D1 to HDAC1 and the inhibition of PPARγ-mediated differentiation by cyclin D1 is also consistent with previous studies on the role of HDAC1 in regulation of nuclear receptor function (30).

Adipogenesis involves two distinct phases, the first involving clonal expansion and a second phase involving cell cycle exit

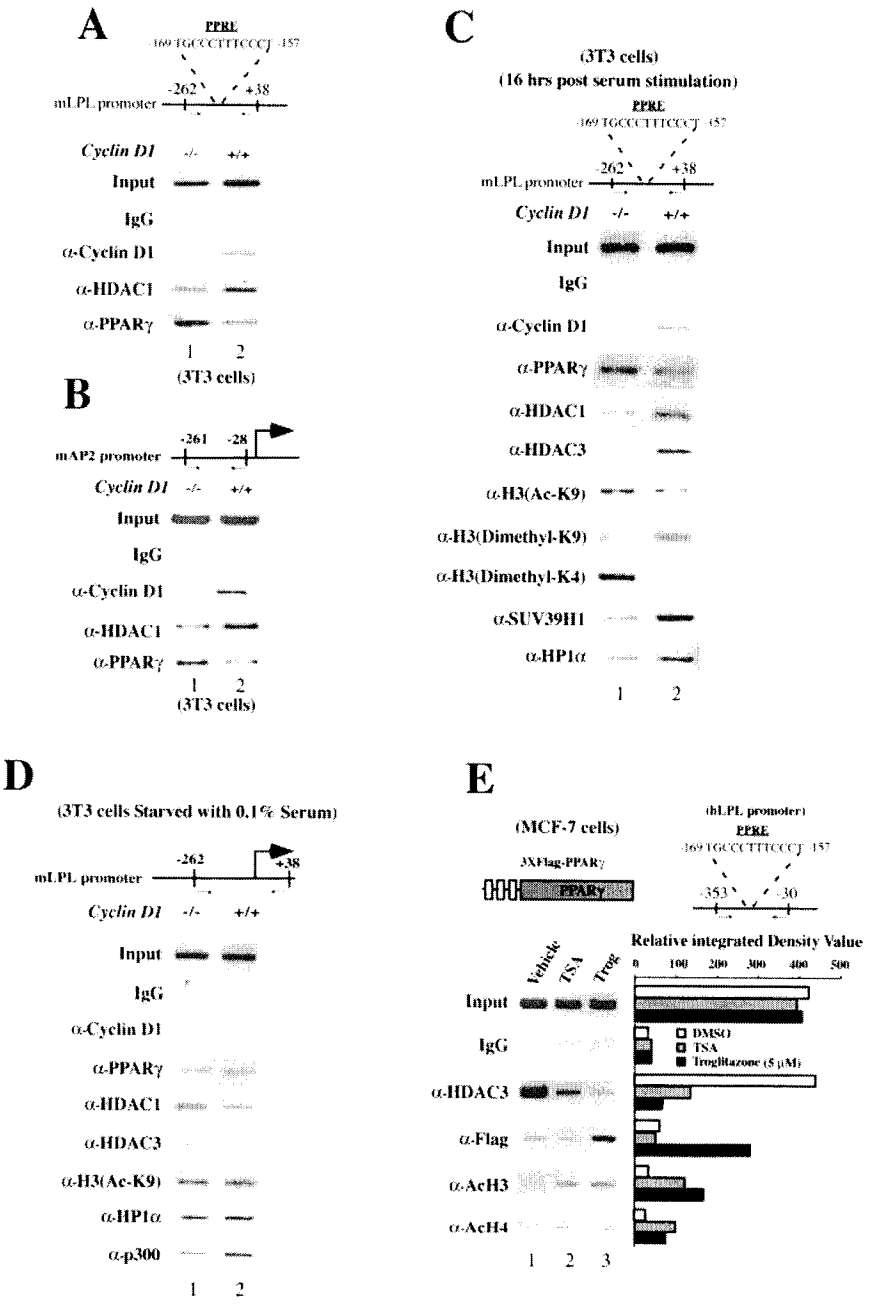

FIG. 7. **Cyclin D1 regulates acetylation of histone H3 at the LPL promoter region.** ChIP assay of HDAC1 recruitment to the PPARE of the murine LPL promoter (*A*) or the aP2 promoter (*B*) in randomly cycling *cyclin D1*$^{+/+}$ or *cyclin D1*$^{-/-}$ 3T3 cells. IgG serves as an antibody negative control. *C*, *cyclin D1*$^{+/+}$ or *cyclin D1*$^{-/-}$ 3T3 cells were serum-starved for 48 h and subjected to 10% serum treatment for 16 h. ChIP analysis of the murine LPL promoter PPARE are shown using the indicated antibodies. *D*, ChIP analysis of the murine LPL promoter in serum-starved *cyclin D1*$^{+/+}$ or *cyclin D1*$^{-/-}$ 3T3 cells are shown. Antibodies used for immunoprecipitation are indicated. *E*, ChIP analysis of the human LPL promoter in MCF7 cells transfected with the FLAG-tagged PPARγ expression vector. Cells were treated with either vehicle (*Veh*), trichostatin A (*TSA*), or troglitazone as indicated in *lanes 1, 2* and *3*. *DMSO*, Me_2SO.

and differentiation (37–39). Cyclin D1 expression inhibits cellular differentiation, the second phase of adipogenesis. This function is consistent with several previous studies in which cyclin D1 inhibited cellular differentiation of other cell types including myocytes (40–42). Our findings are consistent with the previous studies of cell cycle proteins in adipogenesis. Rb inactivation by SV40 large T antigen inhibits adipogenesis (43), and Rb-deficient fibroblasts fail to differentiate into adipocytes when properly stimulated (44). In addition, the cyclin-dependent kinase inhibitors p18 and p21 are up-regulated during adipogenesis, consistent with their role in promoting cell cycle exit (45). Furthermore, studies suggest PPARγ up-regulates the Cdk inhibitors (45), which promote differentiation, consistent with our finding that cyclin D1 inhibits PPARγ.

It is important to distinguish studies of adipocyte differentiation conducted with primary murine embryonic fibroblast (primary MEFs) from those conducted with clonal derivatives of MEFs or immortalized cell lines. It has been shown that 3T3L1 cells and CHO cells undergo differentiation in response to PPARγ ligands and differentiation medium. However, the differentiation medium that induced 3T3-L1 adipogenesis was not sufficient to induce differentiation in wild type MEFs (46), consistent with our findings that *cyclin D1* wild type MEFs are relatively resistant to induction of adipocyte differentiation (5). When primary MEFs (Fig. 6, *A* and *B*) were treated with differentiation medium and PPARγ ligand, the relative amount of HDAC1 and HDAC3 recruited to the PPARE of the LPL promoter in *cyclin D1*-deficient cells was significantly reduced upon differentiation compared with those seen in *cyclin D1* wild type cells (Fig. 6, *A* and *B*). Collectively, these results support the notion that the relative amount of HDAC recruited to the endogenous LPL promoter during adipocyte differentiation is regulated by cyclin D1.

Rb has been shown to recruit HDAC3 to PPARγ target genes and attenuate PPARγ-mediated adipocyte differentiation. Disruption of the PPARγ·Rb·HDAC3 complex by phosphorylation of Rb or inhibition of HDAC activity stimulates adipocyte differentiation (17). In contrast, other groups have suggested a

role of Rb in facilitating the differentiation of preadipocytes and MEFs into adipocytes (43, 44, 47). There are also controversial reports on the role of HDACs during adipogenesis (16–18). Our results demonstrate a role of cyclin D1 in repression of the function of PPARγ through recruitment of HDAC1 and HDAC3. In our previous studies, PPARγ transactivation induced by the ligand BRL49653 was inhibited by cyclin D1 through a Rb- and Cdk-independent mechanism, requiring a region predicted to form a helix-loop-helix structure (5). It is likely that cyclin D1 plays a dual role by promoting cell proliferation and inhibiting cellular differentiation. On one hand, cyclin D1 is up-regulated by mitogenic signaling pathways, as seen in most cancer cells, resulting in phosphorylation of Rb and G_1-S progression through association with and activation of Cdk4/6. On the other hand, cyclin D1 can regulate a subset of transcription factors, including nuclear receptors, through interacting with histone deacetylase activity independent of its Cdk-activation function (31). Further studies are necessary to elucidate the molecular mechanism by which cyclin D1 coordinates its Cdk-dependent and Cdk-independent functions.

Acknowledgements—We thank Dr. Ron Evans, Dr. Wafik El Deiry, and Dr. Chris Glass for plasmids and Leonora Mia Caparas for assistance in preparing the manuscript. Work conducted at the Lombardi Comprehensive Cancer Center was supported by the National Institutes of Health Comprehensive Cancer Center Core Grant CA51008-13 (to R. G. P.).

REFERENCES

1. Motokura, T., Bloom, T., Kim, H. G., Jüppner, H., Ruderman, J. V., Kronenberg, H. M., and Arnold, A. (1991) *Nature* **350,** 512–515
2. Matsushime, H., Roussel, M. F., Ashmun, R. A., and Sherr, C. J. (1991) *Cell* **65,** 701–713
3. Zwijsen, R. M., Klompmaker, R., Wientjens, E. B., Kristel, P. M., van der Burg, B., and Michalides, R. J. (1996) *Mol. Cell. Biol.* **16,** 2554–2560
4. Pagano, M., Theodorus, A. M., Tam, S. W., and Draetta, G. F. (1994) *Genes Dev.* **8,** 1627–1639
5. Wang, C., Pattabiraman, N., Zhou, J. N., Fu, M., Sakamaki, T., Albanese, C., Li, Z., Wu, K., Hulit, J., Neumeister, P., Novikoff, P. M., Brownlee, M., Scherer, P. E., Jones, J. G., Whitney, K. D., Donehower, L. A., Harris, E. L., Rohan, T., Johns, D. C., and Pestell, R. G. (2003) *Mol. Cell. Biol.* **23,** 6159–6173
6. Bodrug, S. E., Warner, B. J., Bath, M. L., Lindeman, G. J., Harris, A. W., and Adams, J. M. (1994) *EMBO J.* **13,** 2124–2130
7. Sicinski, P., Donaher, J. L., Parker, S. B., Li, T., Fazeli, A., Gardner, H., Haslam, S. Z., Bronson, R. T., Elledge, S. J., and Weinberg, R. A. (1995) *Cell* **82,** 621–630
8. Neumeister, P., Pixley, F. J., Xiong, Y., Xie, H., Wu, K., Ashton, A., Cammer, M., Chan, A., Symons, M., Stanley, E. R., and Pestell, R. G. (2003) *Mol. Biol. Cell* **14,** 2005–2015
9. Albanese, C., D'Amico, M., Reutens, A. T., Fu, M., Watanabe, G., Lee, R. J., Kitsis, R. N., Henglein, B., Avantaggiati, M., Somasundaram, K., Thimmapaya, B., and Pestell, R. G. (1999) *J. Biol. Chem.* **274,** 34186–34195
10. Holnthoner, W., Pillinger, M., Groger, M., Wolff, K., Ashton, A. W., Albanese, C., Neumeister, P., Pestell, R. G., and Petzelbauer, P. (2002) *J. Biol. Chem.* **277,** 45847–45853
11. Reutens, A. T., Fu, M., Watanabe, G., Albanese, C., McPhaul, M. J., Balk, S. P., Janne, O. A., Palvimo, J. J., and Pestell, R. G. (2001) *Mol. Endocrinol.* **15,** 797–811
12. Knudsen, K. E., Cavenee, W. K., and Arden, K. C. (1999) *Cancer Res.* **59,** 2297–2301
13. McMahon, C., Suthiphongchai, T., DiRenzo, J., and Ewen, M. E. (1999) *Proc. Natl. Acad. Sci. U. S. A.* **96,** 5382–5387
14. Zwijsen, R. M. L., Buckle, R. S., Hijmans, E. M., Loomans, C. J. M., and Bernards, R. (1998) *Genes Dev.* **12,** 3488–3498
15. Ratineau, C., Petry, M. W., Mutoh, H., and Leiter, A. B. (2002) *J. Biol. Chem.* **277,** 8847–8853
16. Wiper-Bergeron, N., Wu, D., Pope, L., Schild-Poulter, C., and Hache, R. J. (2003) *EMBO J.* **22,** 2135–2145
17. Fajas, L., Egler, V., Reiter, R., Hansen, J., Kristiansen, K., Debril, M. B., Miard, S., and Auwerx, J. (2002) *Dev. Cell* **3,** 903–910
18. Lagace, D. C., and Nachtigal, M. W. (2004) *J. Biol. Chem.* **279,** 18851–18860
19. Ito, A., Kawaguchi, Y., Lai, C.-H., Kovacs, J. J., Higashimoto, Y., Appella, E., and Yao, T.-P. (2002) *EMBO J.* **21,** 6236–6245
20. Watanabe, G., Howe, A., Lee, R. J., Albanese, C., Shu, I. W., Karnezis, A. N., Zon, L., Kyriakis, J., Rundell, K., and Pestell, R. G. (1996) *Proc. Natl. Acad. Sci. U. S. A.* **93,** 12861–12866
21. Albanese, C., Wu, K., D'Amico, M., Jarrett, C., Joyce, D., Hughes, J., Hulit, J., Sakamaki, T., Fu, M., Ben-Ze'ev, A., Bromberg, J. F., Lamberti, C., Verma, U., Gaynor, R. B., Byers, S. W., and Pestell, R. G. (2003) *Mol. Biol. Cell* **14,** 585–599
22. Fu, M., Wang, C., Reutens, A. T., Angeletti, R., Siconolfi-Baez, L., Ogryzko, V., Avantaggiati, M. L., and Pestell, R. G. (2000) *J. Biol. Chem.* **275,** 20853–20860
23. Muller, A. J., Young, J. C., Pendergast, A. M., Pondel, M., Landau, N. R., Littman, D. R., and Witte, O. N. (1991) *Mol. Cell. Biol.* **11,** 1785–1792
24. Bouzahzah, B., Fu, M., Iaavarone, A., Factor, V. M., Thorgeirsson, S. S., and Pestell, R. G. (2000) *Cancer Res.* **60,** 4531–4537
25. Hulit, J., Wang, C., Li, Z., Albanese, C., Rao, M., Di Vizio, D., Shah, S., Byers, S. W., Mahmood, R., Augenlicht, L. H., Russell, R., and Pestell, R. G. (2004) *Mol. Cell. Biol.* **24,** 7598–7611
26. Tang, Q. Q., Zhang, J. W., and Lane, M. D. (2004) *Biochem. Biophys. Res. Commun.* **319,** 235–239
27. Nicolas, E., Roumillac, C., and Trouche, D. (2003) *Mol. Cell. Biol.* **23,** 1614–1622
28. Nakayama, J., Rice, J. C., Strahl, B. D., Allis, C. D., and Grewal, S. I. (2001) *Science* **292,** 110–113
29. Lachner, M., O'Carroll, D., Rea, S., Mechtler, K., and Jenuwein, T. (2001) *Nature* **410,** 116–120
30. Fu, M., Wang, C., Wang, J., Zafonte, B., Lisanti, M. P., and Pestell, R. G. (2002) *Cytokine Growth Factor Rev.* **13,** 259–276
31. Fu, M., Wang, C., Li, Z., Sakamaki, T., and Pestell, R. G. (2004) *Endocrinology* **145,** 5439–5447
32. Felsenfeld, G., and Groudine, M. (2003) *Nature* **421,** 448–453
33. Turner, B. M. (2000) *BioEssays* **22,** 836–845
34. Shih, H. H., Xiu, M., Berasi, S. P., Sampson, E. M., Leiter, A., Paulson, K. E., and Yee, A. S. (2001) *Mol. Cell. Biol.* **21,** 5723–5732
35. Beckstead, R., Ortiz, J. A., Sanchez, C., Prokopenko, S. N., Chambon, P., Losson, R., and Bellen, H. J. (2001) *Mol. Cell* **7,** 753–765
36. Mazumdar, A., Wang, R. A., Mishra, S. K., Adam, L., Bagheri-Yarmand, R., Mandal, M., Vadlamudi, R. K., and Kumar, R. (2001) *Nat. Cell Biol.* **3,** 30–37
37. Gregoire, F. M., Smas, C. M., and Sul, H. S. (1998) *Physiol. Rev.* **78,** 783–809
38. Koutnikova, H., and Auwerx, J. (2001) *Ann. Med.* **33,** 556–561
39. Lane, M. D., Tang, Q. Q., and Jiang, M. S. (1999) *Biochem. Biophys. Res. Commun.* **266,** 677–683
40. Lazaro, J. B., Bailey, P. J., and Lassar, A. B. (2002) *Genes Dev.* **16,** 1792–1805
41. Wei, Q., and Paterson, B. M. (2001) *FEBS Lett.* **490,** 171–178
42. Guo, K., and Walsh, K. (1997) *J. Biol. Chem.* **272,** 791–797
43. Higgins, C., Chatterjee, S., and Cherington, V. (1996) *J. Virol.* **70,** 745–752
44. Chen, P., Riley, D. J., Chen, Y., and Lee, W. (1996) *Genes Dev.* **10,** 2794–2804
45. Morrison, R. F., and Farmer, S. R. (1999) *J. Biol. Chem.* **274,** 17088–17097
46. Alexander, D. L., Ganem, L. G., Fernandez-Salguero, P., Gonzalez, F., and Jefcoate, C. R. (1998) *J. Cell Sci.* **111,** 3311–3322
47. Classon, M., Kennedy, B. K., Mulloy, R., and Harlow, E. (2000) *Proc. Natl. Acad. Sci. U. S. A.* **97,** 10826–10831

Phenylbutyrate up-regulates the *adrenoleukodystrophy-related* gene as a nonclassical peroxisome proliferator

Catherine Gondcaille,[1] Marianne Depreter,[2] Stéphane Fourcade,[1] Maria Rita Lecca,[1] Sabrina Leclercq,[1] Pascal G.P. Martin,[3] Thierry Pineau,[3] Françoise Cadepond,[4] Martine ElEtr,[4] Nathalie Bertrand,[5] Alain Beley,[5] Sandrine Duclos,[1] Dirk De Craemer,[2] Frank Roels,[2] Stéphane Savary,[1] and Maurice Bugaut[1]

[1]Laboratoire de Biologie Moléculaire et Cellulaire, Faculté des Sciences Gabriel, 21000 Dijon, France
[2]Department of Human Anatomy, Embryology, Histology and Medical Physics, Ghent University, 9000 Gent, Belgium
[3]Laboratoire de Pharmacologie et Toxicologie, Institut National de la Recherche Agronomique, 31931 Toulouse, France
[4]Institut National de la Santé et de la Recherche Médicale U488, 94276 Le Kremlin-Bicêtre, France
[5]Laboratoire de Pharmacodynamie, Faculté de Pharmacie, 21000 Dijon, France

X-linked adrenoleukodystrophy (X-ALD) is a demyelinating disease due to mutations in the *ABCD1* (*ALD*) gene, encoding a peroxisomal ATP-binding cassette transporter (ALDP). Overexpression of adrenoleukodystrophy-related protein, an ALDP homologue encoded by the *ABCD2* (*adrenoleukodystrophy-related*) gene, can compensate for ALDP deficiency. 4-Phenylbutyrate (PBA) has been shown to induce both *ABCD2* expression and peroxisome proliferation in human fibroblasts. We show that peroxisome proliferation with unusual shapes and clusters occurred in liver of PBA-treated rodents in a PPARα-independent way. PBA activated *Abcd2* in cultured glial cells, making PBA a candidate drug for therapy of X-ALD. The *Abcd2* induction observed was partially PPARα independent in hepatocytes and totally independent in fibroblasts. We demonstrate that a GC box and a CCAAT box of the *Abcd2* promoter are the key elements of the PBA-dependent *Abcd2* induction, histone deacetylase (HDAC)1 being recruited by the GC box. Thus, PBA is a nonclassical peroxisome proliferator inducing pleiotropic effects, including effects at the peroxisomal level mainly through HDAC inhibition.

Introduction

X-linked adrenoleukodystrophy (X-ALD; OMIM 300100) is an inherited disorder characterized by progressive demyelination of the central nervous system and adrenal insufficiency (Moser et al., 2001). X-ALD is associated with an accumulation of very long-chain fatty acids (VLCFA) in plasma and tissues. The disease is due to mutations in the *ABCD1* (ALD) gene located in Xq28 (Mosser et al., 1993). *ABCD1* encodes the protein ALDP, a peroxisomal member of the ATP-binding cassette family, which is thought to participate in the entry of VLCFA into the peroxisome where VLCFA are β-oxidized. ALDP is a half-transporter, which is supposed to function as a homodimer or a heterodimer, in association with one of the three other peroxisomal ATP-binding cassette half-transporters, ALDRP (adrenoleukodystrophy-related protein), which is the closest homologue of ALDP (Lombard-Platet et al., 1996), PMP70 (70-kD peroxisomal membrane protein; Kamijo et al., 1990), and PMP69 (Holzinger et al., 1997). These transporters are encoded by the *ABCD2* (*Adrenoleukodystrophy-related*), *ABCD3*, and *ABCD4* genes, respectively, and their function is still unclear. Overexpression of ALDRP has been demonstrated to compensate for ALDP deficiency in *Abcd1* −/− mice, thus preventing VLCFA accumulation and the onset of a neurological phenotype (Pujol et al., 2004). Furthermore, restoration of VLCFA β-oxidation could be obtained in X-ALD human fibroblasts transfected with *Abcd2* cDNA (Braiterman et al., 1998; Kemp et al., 1998; Flavigny et al., 1999; Netik et al., 1999; Fourcade et al., 2001). Therefore, pharmacological induction of this partially redundant gene could be a therapeutic strategy for X-ALD. We have shown that fibrates up-regulate *Abcd2*

Dr. Bugaut died on 16 September 2004.

Correspondence to Stéphane Savary: stsavary@u-bourgogne.fr

M. Depreter's present address is Institute for Stem Cell Research, University of Edinburgh, Edinburgh EH9 3JQ, UK.

Abbreviations used in this paper: AOX, acyl-CoA oxidase; DAPA, DNA affinity precipitation assay; EMSA, electrophoretic mobility shift assay; HAT, histone acetyl transferase; HDAC, histone deacetylase; LM, light microscopy; PBA, 4-phenylbutyrate; PP, peroxisome proliferator; TSA, trichostatin A; VLCFA, very long-chain fatty acids; X-ALD, X-linked adrenoleukodystrophy.

The Journal of Cell Biology, Vol. 169, No. 1, April 11, 2005 93–104
http://www.jcb.org/cgi/doi/10.1083/jcb.200501036

expression (Albet et al., 1997, 2001; Berger et al., 1999; Fourcade et al., 2001) in the liver of rodents. Fibrates can restore β-oxidation of VLCFA in the liver of *Abcd1* −/− mice (Netik et al., 1999) but not in brain, possibly due to obstacle of the blood–brain barrier (Waddell et al., 1989; Berger et al., 1999). Fibrates, commonly used as hypolipidemic drugs in human medicine, are peroxisome proliferators (PPs) in rodents. PPs are ligands of a member of the steroid nuclear receptor family named PPARα (PP-activated receptor α). PPARα up-regulates expression of target genes involved in lipid metabolism by binding to a DNA sequence called PPRE (PP response element). However, such a functional PPRE has not been found in the *Abcd2* promoter (Gartner et al., 1998; Fourcade et al., 2001).

4-Phenylbutyrate (PBA) treatment can restore β-oxidation of VLCFA and increase *ABCD2* expression in fibroblasts from X-ALD patients and *Abcd1* −/− mice (Kemp et al., 1998). Furthermore, dietary PBA was shown to be efficient in vivo to reduce the VLCFA levels in the brain of *Abcd1* −/− mice, but *Abcd2* expression has not been analyzed (Kemp et al., 1998). Interestingly, the authors observed a 2.4-fold increase in the number of peroxisomes in 5 mM PBA-treated control or X-ALD human fibroblasts, which was not accompanied by induction of the *PPARα* and peroxisomal *Acyl-CoA Oxidase* (*AOX*) genes but could be linked to the observed induction of the *PEX11α* gene. This hypothesis was strengthened by the demonstration that PBA-mediated hepatic peroxisome proliferation is absent in *Pex11α* −/− mice (Li et al., 2002). Classical PPs do not cause peroxisome proliferation in humans, and fibroblasts are not known to be the target cells for PPs. Moreover, both peroxisome proliferation and *PPARα* and *Aox* induction occur in PP-treated rodents. Kemp et al. (1998) reported induction of *PPARα*, but not of *Aox*, in PBA-treated mice fibroblasts. By contrast, activation of a reporter plasmid containing the rat *Aox* PPRE has been obtained in PBA-treated mouse hepatoma cells (Pineau et al., 1996) and the binding of PBA to PPARα has been demonstrated using C6 rat glioma cells (Liu et al., 2002). It should also be noticed that an increased expression of PPARα has been observed in PBA-treated human glioma cells (Pineau et al., 1996). Together, the data indicate that PBA, a compound structurally related to fibrates, is a PP that acts partially through noncanonical mechanisms.

Sodium butyrate induces a variety of alterations at the molecular and cellular levels. Transcriptional activation, as a result of the inhibition of histone deacetylase (HDAC) activity could represent the main mechanism of action of butyrate (Davie, 2003). PBA, a butyrate analogue, displays also similar pleiotropic effects in vitro and in vivo. It has been reported that PBA induces hyperacetylation of histones (Lea and Randolph, 1998; Warrell et al., 1998). Deacetylase inhibition may account for *ABCD2* induction observed in PBA-treated fibroblasts and probably for *PEX11α* induction, which might be responsible for the PPARα-independent peroxisome proliferation.

Our main objective was to compare the effects of PBA, butyrate, and fibrate on the expression of *Abcd2* and *Aox* and peroxisome proliferation in vivo in the liver and brain of rats and in vitro in hepatic and glial cells. The molecular mechanism of the PBA regulation of *Abcd2* expression was also studied.

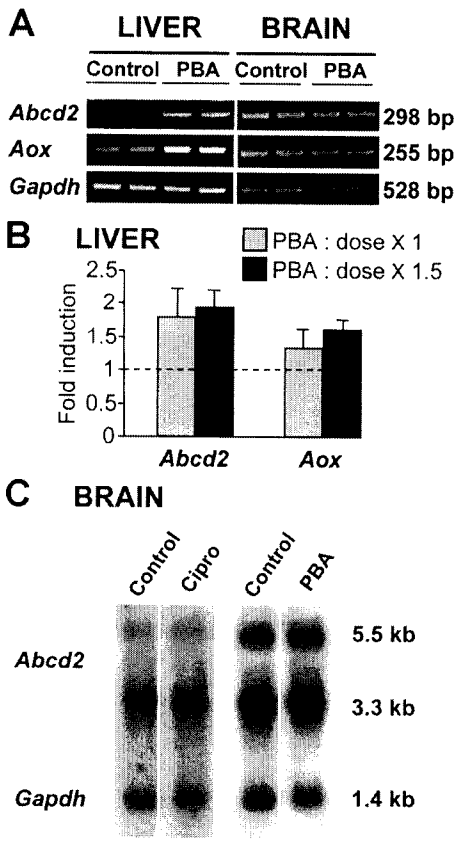

Figure 1. **Expression of the *Abcd2* and *Aox* genes is up-regulated by PBA in liver.** (A) RNA samples from liver and brain of a control rat and from a rat treated per os with PBA (dose ×1.5) for 9 wk were analyzed by RT-PCR in duplicates. (B) RNA was extracted from liver of control rats (n = 10) and rats treated with PBA (dose ×1) for 6–7 wk (n = 6) or PBA (dose ×1.5) for 6–9 wk (n = 4). Samples were individually analyzed twice by RT-PCR. The intensities for *Abcd2* and *Aox* mRNA were quantified by digital imaging and normalized using *glyceraldehyde-phosphate dehydrogenase* (*Gapdh*) intensities. Data (means ± SD) are presented as fold induction in relation to the values for control rats (taken equal to 1 and not depicted in the figure). (C) 2 mg sodium ciprofibrate (Cipro) or 20 mg PBA in 100 μl of water was injected into the cerebral fourth ventricle (100 μl/h). Control rats received equiosmolar amounts of NaCl. RNA was extracted from the whole brain and analyzed individually by Northern blotting (n = 4 for each group of rats).

Results

PBA up-regulates expression of the *Abcd2* and *Aox* genes in liver but not in brain

Because the liver is the main target tissue for PPs and demyelination occurs in the brain of X-ALD patients, we evaluated the impact of PBA on peroxisomal gene expression in these tissues. Rats were treated per os with PBA as described by Kemp et al. (1998) (dose ×1) and also with a higher dose (dose ×1.5) during 6–9 wk. Expression of the *Abcd2* and *Aox* genes was increased in the liver (Fig. 1 A), with marked interindividual variations as it was already seen for PPARα (Lemberger et al., 1996). No significant difference could thus be obtained between the two doses (Fig. 1 B). Considering the 10 treated animals, the average induction was 1.9- and 1.5-fold for the *Abcd2* and *Aox* genes, respectively. Gene induction was observed neither in the brain (Fig. 1 A) nor in the spleen, kidney, and testis (unpublished data).

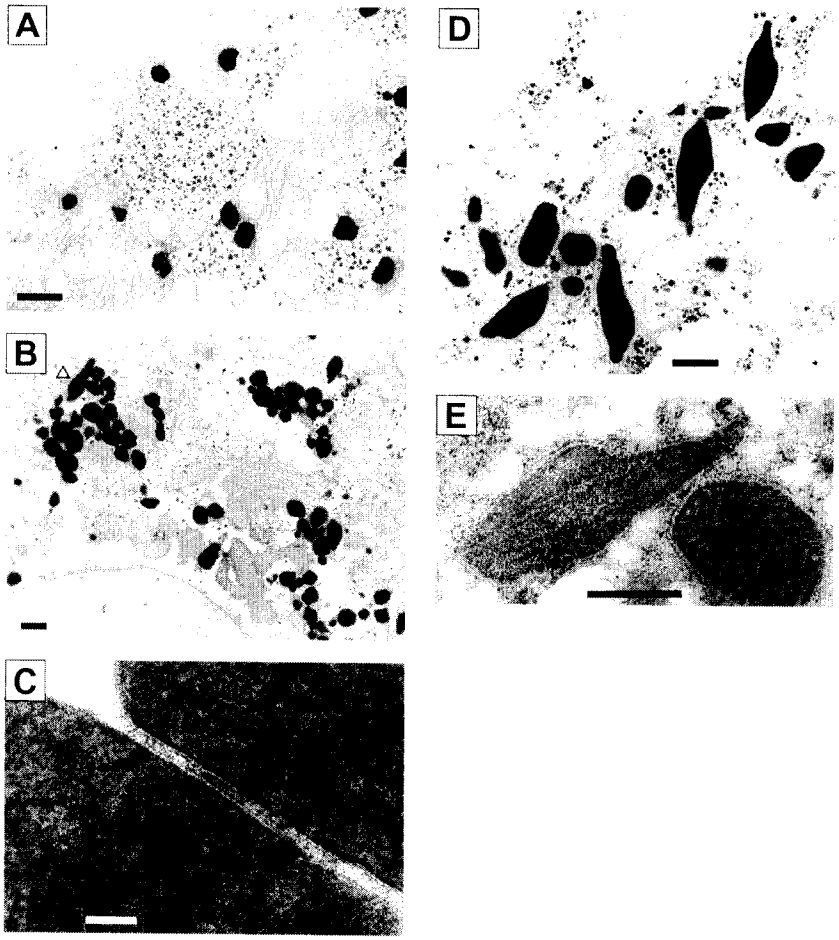

Figure 2. **PBA induces peroxisome proliferation in liver.** (A–D) Peroxisomes were stained for catalase activity. Liver of a control rat (A) and a rat treated per os with PBA (dose ×1.5) for 6 wk (B). Note peroxisome clusters and a phi-shaped peroxisome (arrowhead) in B. (C) Nearly touching peroxisomes suggesting a fission or budding process (Roels, 1991) in liver of a rat treated with PBA (dose ×1) for 6 wk. (D) Four phi-shaped peroxisomes in liver of a rat treated as in C. Unstained nucleoids are clearly visible in several peroxisomes. (E) Immunogold localization of AOX in a phi-shaped peroxisome, adjacent to an unlabeled mitochondrion, in liver of a rat treated as in C. Bars: (A, B, D, and E) 1 μm; (C) 100 nm.

Induction of peroxisomal genes by PPs usually starts several hours after the beginning of a treatment (Motojima, 1997). Because a unique IP injection of PBA (400 mg/kg) was sufficient to weakly induce (1.5-fold) the expression of a PP-sensitive gene (*CYP4A1*; Pineau et al., 1996), we injected 720 mg of PBAper kilogram per day i.p. for 3 d and analyzed mRNA from liver, brain, intestine, muscle, spleen, kidney, and lung. No induction of the *Abcd2* and *Aox* genes was obtained in the seven examined tissues (unpublished data).

The absence of gene induction in the brain after long- and short-term treatments, which could result from a rapid catabolism (the half-life of PBA is ~1–2 h), prompted us to perfuse PBA directly in the fourth ventricle. No induction of the two peroxisomal genes was found in the brain examined as a whole (Fig. 1 C). In the same way, no change in the gene expression was obtained when ciprofibrate was perfused under the same experimental conditions.

PBA treatment induces peroxisome proliferation in liver along with appearance of peroxisomal phi-bodies and clusters

Peroxisomes were observed in the liver of each control and of each per os PBA-treated rat by light microscopy (LM) and EM. When comparing the pooled data from all the treated rats (n = 10) with the pooled data from all the control rats (n = 10), peroxisome proliferation was clearly demonstrated. LM examination showed that the number of peroxisomes per cellular area was higher in the treated animals than in the control animals (×1.4; $P < 0.05$). By EM morphometric analysis, significantly higher numerical density (×2.3; $P < 0.001$), volume density (×2.3; $P < 0.01$), and surface density (×2.2; $P < 0.01$) versus controls were found in the treated rats, giving evidence of peroxisome proliferation (Fig. 2, A and B). Although the average size of peroxisomes was not significantly different in the control and treated rats, a small percentage of peroxisomes in 8 out of 10 treated animals had very large size (D-circle 2.7-fold that of control peroxisomes) and showed peculiar shapes (phi-bodies; Fig. 2 D). These phi-bodies were present in multiple fragments of the same liver and mostly located in the periportal areas. Phi-bodies were never seen in control livers. Furthermore, clusters of up to 10 peroxisomes were present in the rats treated with dose ×1.5 (Fig. 2 B), whereas in the control rats as well as in the rats treated with dose ×1, only clusters of two to three peroxisomes were seen (peroxisomes are considered to belong to a cluster when the distance between neighboring organelles is smaller than twofold of the mean diameter of the peroxisomes of the cluster). The clusters often showed nearly touching peroxisomes (Fig. 2 C). Finally, heterogeneity in the reaction product of catalase activity was detected in proliferated peroxisomes, which was not observed in control rats. AOX was located in peroxisomes by EM immunodetection (Fig. 2 E). The mean label-

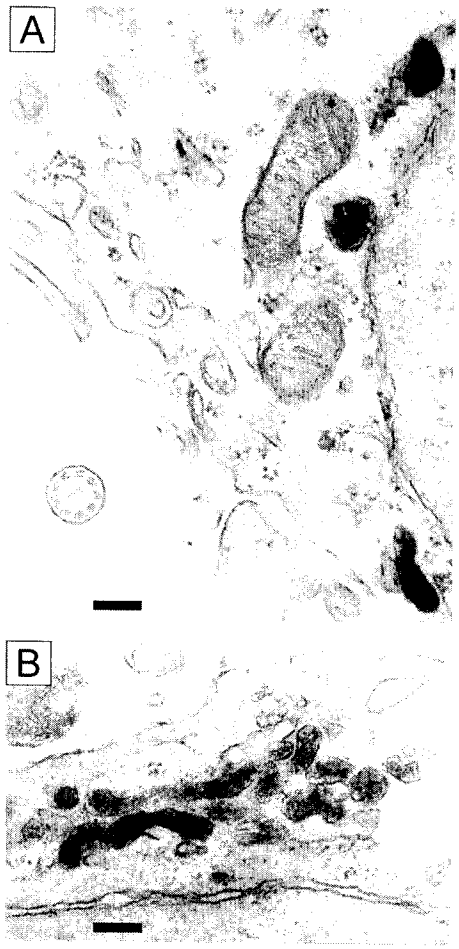

Figure 3. **PBA modifies peroxisome distribution in ependymal cells of the fourth ventricle.** Peroxisomes were stained for catalase activity. Peroxisomes in cells of a control rat (A) or a rat treated per os with dose ×1 of PBA for 6 wk (B). Peroxisomes are small and few when compared with liver (Fig. 2). Peroxisome clusters as shown in B were more frequently observed in treated animals. Cilium is seen in A. Bars, 200 nm.

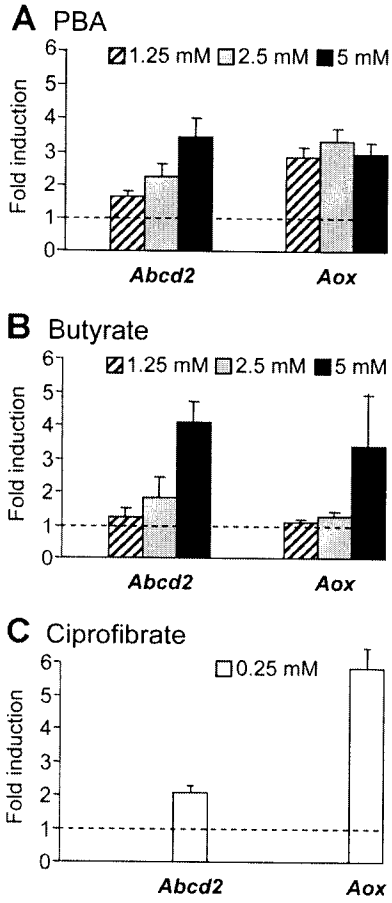

Figure 4. **Peroxisomal genes are inducible by PBA and butyrate in hepatocytes.** Rat primary hepatocytes were cultured in the presence of different concentrations of PBA, butyrate, and ciprofibrate for 72 h. Total RNA was analyzed by RT-PCR for *Abcd2* and *Aox* expression. Results are presented as fold induction in relation to the control values for cells cultured in the absence of drug. Control data, taken equal to 1, are not reported in the figure. Data represent means ± SD of two independent experiments.

ing density for AOX was increased by a factor of 1.3 in PBA-treated rats (n = 3) in comparison with control rats (n = 3). In addition, when the volume density of the peroxisomes was taken into account, the total labeling differed by a factor 2.5 between the control and treated rats. Although not significant, these differences are in agreement with RT-PCR data (Fig. 1, A and B).

A weak but significant dose effect was observed in the liver of the PBA-fed rats. The number of peroxisomes per cellular area measured by LM increased by 1.4-fold with dose ×1 and 1.7-fold with dose ×1.5. Furthermore, the EM morphometry values were always higher in the liver of rats (n = 4) treated with dose ×1.5 (numerical density: ×2.7, volume density: ×3.1, and surface density: ×2.9) than in the rats (n = 6) treated with dose ×1 (×2.1, ×1.9, and ×1.8, respectively). A peroxisome proliferation index was calculated for each treated animal (n = 10) versus the mean value of 10 control animals considering successively the number of peroxisomes per cellular area measured by LM and each of the three EM morphometry values. When the four proliferation factors of each treated animal were ranked (n = 40), the dose effect was significant ($P < 0.001$). In fact, the different animals did not respond to the PBA treatment to the same extent with regard to the number of peroxisomes, as it was observed already for the induction of peroxisomal genes (Fig. 1 B). In some animals, a clear proliferative effect co-occurred with a higher induction of peroxisomal genes.

The number of peroxisomes per cellular area was studied by LM in the kidney (tubulus contortus I cells) and the intestinal epithelium, two PP-sensitive tissues, and showed no significant differences between the control rats (n = 3) and the per os treated rats (n = 3) with dose ×1 of PBA.

In the rats i.p. injected with PBA during 3 d, LM examination revealed no peroxisome proliferation in the liver, in agreement with the absence of induction of peroxisomal genes as mentioned in the previous paragraph.

PBA treatment modifies the peroxisome distribution in ependymal cells of the fourth ventricle

Peroxisomes were also studied by EM in ependymal cells lining the fourth ventricle of control rats (n = 7) and per os PBA-treated rats with doses ×1 (n = 3) or ×1.5 (n = 3). A 1.4-fold ($P = 0.05$) increase in the number of peroxisomes per cytoplas-

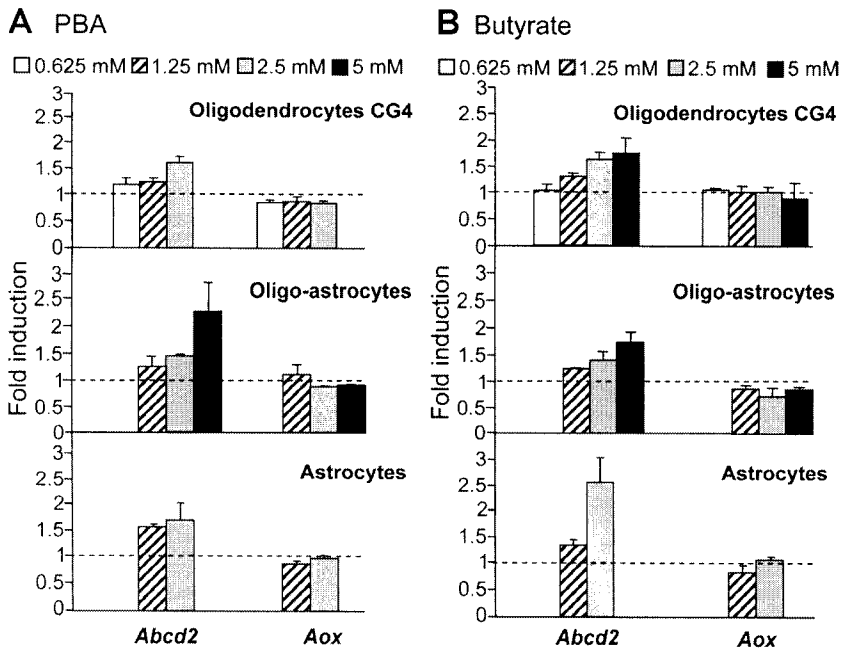

Figure 5. ***Abcd2* is inducible by PBA and butyrate in glial cells.** Differentiated CG-4 oligodendrocytes, pure primary astrocytes, and mixed primary cultures of oligodendrocytes and astrocytes were treated with different concentrations of PBA (A) and butyrate (B) for 72 h. Gene expression was analyzed by RT-PCR. Results are means ± SD of three independent experiments and presented as in Fig. 4.

mic area occurred together with more frequent clusters (×2.0; $P < 0.05$) (Fig. 3). However, EM revealed no difference in ependymal cells of the choroid plexus or lining the lateral wall of the lateral ventricle and in stem cells of the subventricular zone. These stem cells contained only very few and small catalase particles.

When PBA was infused directly into the fourth ventricle, no effect on peroxisomes was observed by EM in ependymal cells, whereas infusion of ciprofibrate caused a decrease (×0.67; $P < 0.05$) in the number of peroxisomes per cell profile.

PBA and butyrate induce expression of peroxisomal genes and proliferation of peroxisomes in primary cultures of hepatocytes

Considering the short half-life of butyrate in living animals (~6 min), primary cultures of rat hepatocytes were treated with butyrate, PBA, and ciprofibrate for 72 h to gain insight into the mechanisms involved in the regulation of gene expression and peroxisome biogenesis. PBA and butyrate displayed a similar dose-dependent activation of *Abcd2* expression (Fig. 4). However, the increase in *Aox* mRNA levels was lower after butyrate treatment than after PBA treatment (Fig. 4). Furthermore, the *Abcd2* expression level relative to *Aox* level was higher with PBA and butyrate than with ciprofibrate (Fig. 4). Therefore, the effects on peroxisomal gene expression in primary hepatocytes appeared to be different for the three compounds.

Catalase-stained peroxisomes were visualized in hepatocytes by LM. The number of peroxisomes per cellular area was increased 1.4-fold ($P < 0.01$) in PBA-treated cells versus controls for dose 1.25 mM and 1.8-fold ($P < 0.001$) for dose 2.5 mM. An increase was also seen when cells were treated with butyrate: 1.3-fold ($P < 0.05$) for dose 1.25 mM and 1.4-fold ($P < 0.01$) for dose 2.5 mM. A similar increase (×1.7; $P < 0.001$) was obtained after 0.25 mM ciprofibrate treatment.

PBA and butyrate, but not ciprofibrate, induce *Abcd2* expression and peroxisome proliferation in cultured glial cells

In the prospect of a possible pharmacological therapy of X-ALD, it is relevant to try to induce *Abcd2* expression in glial cells. In differentiated CG4 cells, pure primary astrocytes, and mixed primary cultures of glial cells, we observed a dose-dependent induction of *Abcd2* expression after PBA or butyrate treatment but no effect on *Aox* expression (Fig. 5, A and B). When the glial cells were treated with 0.25 and 0.5 mM ciprofibrate, we observed no change in the *Abcd2* and *Aox* expression in the three types of cell culture (unpublished data).

We also examined the peroxisomes by LM after immunolocalization of catalase in C6 rat glioma cells treated with 5 mM PBA or 0.5 mM ciprofibrate. The number of peroxisomes per cellular area was significantly higher in PBA-treated cells than in controls (×2.0; $P < 0.01$) but remained unchanged in ciprofibrate-treated cells. The PBA treatment generated a change in cell morphology, characterized by a fibroblastic aspect, which was much less marked when cultures were treated with ciprofibrate (unpublished data).

PBA induction of the *Abcd2* gene and peroxisome proliferation does not require PPARα

We have previously shown that fenofibrate induction of *Abcd2* and *Aox* in the liver of rodents requires the presence of PPARα (Fourcade et al., 2001). To test whether or not PBA induction of the peroxisomal genes is dependent on PPARα, fibroblasts from control and *PPARα* −/− mice were treated with PBA or fenofibrate and mRNA was analyzed. In contrast to hepatocytes (Fig. 4), the peroxisomal genes in control fibroblasts were not induced by fenofibrate (Fig. 6 A), as observed in glial cells (unpublished data). PBA elicited the same dose-dependent induction of *Abcd2* in both *PPARα* +/+ and *PPARα* −/−

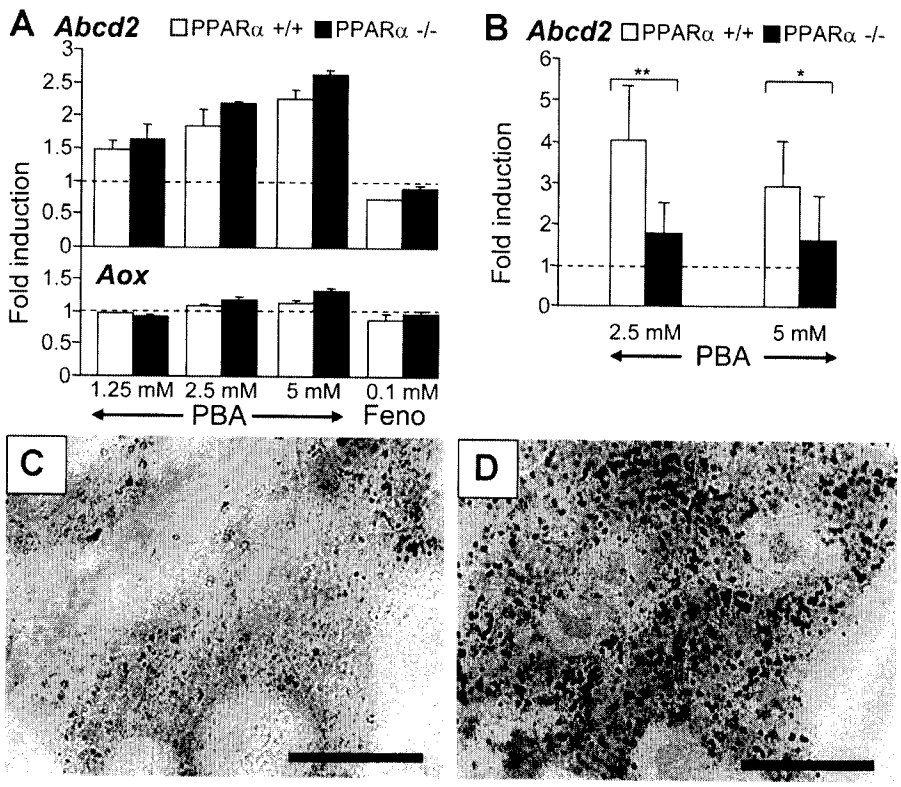

Figure 6. **PBA causes *Abcd2* induction and peroxisome proliferation in PPARα −/− cells.** Fibroblasts (A) and hepatocytes (B) were prepared from fetal and adult liver, respectively, of *PPARα* +/+ and *PPARα* −/− mice and exposed to PBA or fenofibrate (Feno) for 72 h. Gene expression was analyzed by RT-PCR. Data are means ± SD of two to five independent experiments and presented as in Fig. 4. Untreated (C) or 2.5 mM PBA-treated (D) hepatocytes from *PPARα* −/− mice were examined for the number of peroxisomes by LM after anti-catalase protein A–gold immunolabeling with silver enhancement. Bars, 20 μm.

fibroblasts, indicating that it does not require PPARα to activate *Abcd2* (Fig. 6 A). The changes in expression of *Aox* in the PBA-treated fibroblasts were too weak (as already observed in PBA-treated normal fibroblasts by Kemp et al. [1998]) to conclude whether or not their induction by PBA is PPARα dependent (Fig. 6 A). Similar results were obtained using hepatocytes, except that PBA induction of *Abcd2* was significantly higher in *PPARα* +/+ cells than in *PPARα* −/− cells (Fig. 6 B), indicating that the extra induction of *Abcd2* in normal hepatocytes is PPARα dependent. Furthermore, the peroxisome proliferation induced by PBA in control hepatocytes (see the section PBA and butyrate induce expression of peroxisomal genes and proliferation of peroxisomes in primary cultures of hepatocytes) was maintained in *PPARα* −/− hepatocytes (Fig. 6, C and D) as the peroxisome number measured by LM was increased in cells treated with 2.5 (×1.7; $P < 0.05$) and 5.0 mM PBA (×1.4; $P < 0.05$). This result was confirmed using EM (×2.7 in 5.0 mM PBA-treated cells).

Trichostatin A (TSA), a potent HDAC inhibitor, increases *Abcd2* expression in hepatocytes only at high doses

From these results, we hypothesized that in hepatocytes only part of PBA induction of *Abcd2* can be ascribed to HDAC inhibition, and the other part to PPARα activation. To test this hypothesis, we treated rat primary hepatocytes with TSA, a specific inhibitor of HDAC at nanomolar concentrations, using different doses (0.03–3 μM) and times (24, 48, and 72 h). Expression of *Abcd2* was enhanced only at high doses (1–3 μM) of TSA, and the response was limited (×1.6 on average; Fig. 7).

Dose-dependent induction of the *Abcd2* promoter by PBA or butyrate requires only the basic promoter

The rat *Abcd2* promoter contains a CCAAT box (−53) surrounded by two putative GC boxes respectively located at −65 (GC2: CCGCCC) and −35 (GC1: GGGTGG), the three motifs being very well conserved in mouse and human (Fourcade et al., 2001). To identify the molecular mechanism of induction by PBA, COS-7 cells were transiently transfected with a plasmid construct (p277) containing the first 83 bp of the promoter (Fourcade et al., 2001) upstream from the luciferase reporter gene. Transfected cells were then exposed to different doses of PBA or butyrate for 36 h and analyzed for their luciferase activity. Under fibrate treatment, the construct was unable to mediate any induction in similar experiments (Fourcade et al., 2001). In the presence of PBA or butyrate, we observed a strong dose-dependent induction (Fig. 8 A). Similar results were obtained with the p2206 construct containing 2 kb of the

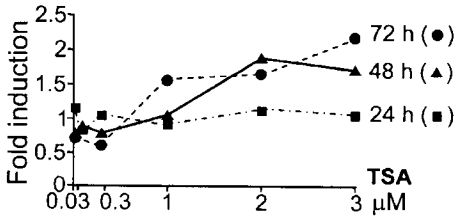

Figure 7. **TSA, a potent HDAC inhibitor, induces *Abcd2* expression.** Rat primary hepatocytes were treated with different doses of TSA and for different times. *Abcd2* expression was analyzed by RT-PCR. Results from three independent experiments are presented as fold induction of the control values (equal to 1) for untreated cells.

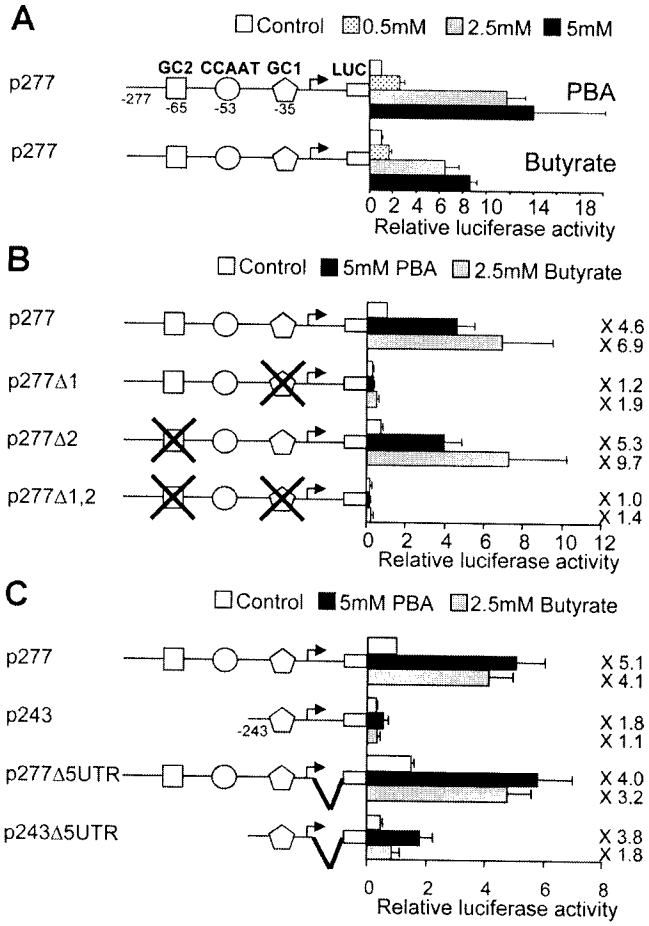

Figure 8. **The GC and CCAAT boxes control basal expression and allow full induction of the basic *Abcd2* promoter by PBA and butyrate.** COS-7 cells were cotransfected with constructs containing normal or mutated *Abcd2* promoter upstream of the luciferase reporter gene and pCMV-βGal to allow normalization of the luciferase activity. Mutations of the GC and CCAAT boxes and deletions are indicated in the schematic diagram. The cells were cultured with or without different doses of PBA or butyrate. (A) Analysis of the dose-dependent effect of PBA and butyrate. (B) Analysis of the role of the GC boxes. (C) Analysis of the role of the CCAAT box and of 5′UTR sequence. In each experiment, results are presented in relation to the luciferase activity of untreated p277-transfected cells taken equal to 1. Fold induction showing the effect of the treatment for each construct is indicated. Data are shown as means ± SD of three to six independent experiments performed in triplicate wells.

promoter (p2206) (unpublished data), indicating that the basic promoter (83 bp) is sufficient to mediate full induction of the *Abcd2* gene by PBA.

PBA-response and basal activity of the *Abcd2* promoter depends on a GC box and a CCAAT box

It has been reported that mutation or deletion of a GC box can abolish the response to butyrate (Lu and Lotan, 1999) and that HDAC1 can repress transcription by direct interaction with Sp1 and Sp3 (Doetzlhofer et al., 1999; Davie, 2003). The CCAAT box has also been demonstrated to play an important role in gene activation by HDAC inhibitors through the CCAAT-binding protein NF-Y (a trimeric association of NF-YA, NF-YB, and NF-YC) and recruitment of histone acetyl transferase (HAT) activity (McCaffrey et al., 1997; Jin and Scotto, 1998). Therefore, we further analyzed the role of the GC and CCAAT boxes in the basal activity of the *Abcd2* promoter and in the context of PBA induction.

We first compared in independent experiments the activity of p277 with the activities of p277Δ1, p277Δ2, and p277Δ1,2 (where one or both GC boxes is mutated; Fig. 8 B) or with the activities of p243 (construct devoid of 34 bp of the 5′ region containing the GC2 and CCATT boxes), p277Δ5UTR, and p243Δ5UTR (constructs devoid of 52 bp of the 5′ untranslated region) (Fig. 8 C). Mutation of the GC1 box markedly decreased the basal activity of the reporter gene (3.6- and 5.6-fold reduction for p277Δ1 and p277Δ1,2, respectively), underlining the functional importance of this GC box for basal *Abcd2* expression (Fig. 8 B). By contrast, mutation of the GC2 box caused a minor decrease in basal activity (Fig. 8 B). Deletion of the 34 bp containing the GC2 and CCATT boxes displayed a 3.2-fold decrease in the basal activity, which is more pronounced than the one observed with p277Δ2 (1.3-fold; Fig. 8 C). This observation suggests a functional role for the CCAAT box in the basal activity of the promoter. Moreover, basal activity of p277Δ5UTR was 1.5-fold higher, suggesting that some repression was mediated through the deleted 5′-UTR sequence. However, deletion of the 5′-UTR sequence in the p243 construct did not show any difference (Fig. 8 C).

Interestingly, the effect of PBA and butyrate treatment was abolished by the mutation of the GC1 box, indicating that the GC1 box is not only essential for basal activity but is also the key element of the activation by PBA or butyrate (Fig. 8 B). This capability of induction was also decreased in the p243 construct (1.8-fold induction) showing that the presence of the GC1 box is sufficient to mediate PBA induction but suggesting that the presence of the CCAAT box (which is not sufficient alone; see p277Δ1,2) is necessary to mediate full induction by PBA (Fig. 8 C). Deletion of the 5′-UTR sequences did not alter significantly the levels of induction by PBA or butyrate (Fig. 8 C).

The GC1 and CCAAT boxes bind their cognate factors, and HDAC-1 is recruited through the GC1 box

To explore the capability of the GC1 and CCAAT boxes of the *Abcd2* promoter to bind in vitro Sp1 or Sp3 and NF-Y, respectively, we first performed electrophoretic mobility shift assay (EMSA) with the corresponding radiolabeled oligonucleotides. Several DNA–protein complexes were formed in the presence of nuclear extracts from rat liver (Fig. 9 A, lanes 2 and 10). These complexes were sequence-specific because they disappeared in the presence of an excess of unlabeled homologous oligonucleotide (Fig. 9 A, lanes 3 and 11) but not in the presence of an excess of unlabeled mutated oligonucleotide (Fig. 9 A, lanes 4 and 12). To investigate if the retarded complexes result from the binding of Sp1/Sp3 and NF-Y, we performed EMSA in the presence of the specific antibodies. Incubation with the anti-Sp1 and/or anti-Sp3 antibodies resulted in specific supershifted complexes for both antibodies, indicating that the GC1 box binds Sp1 and Sp3 (Fig. 9 A, lanes 5–7). A supershift was also obtained with the anti–NF-YA antibody

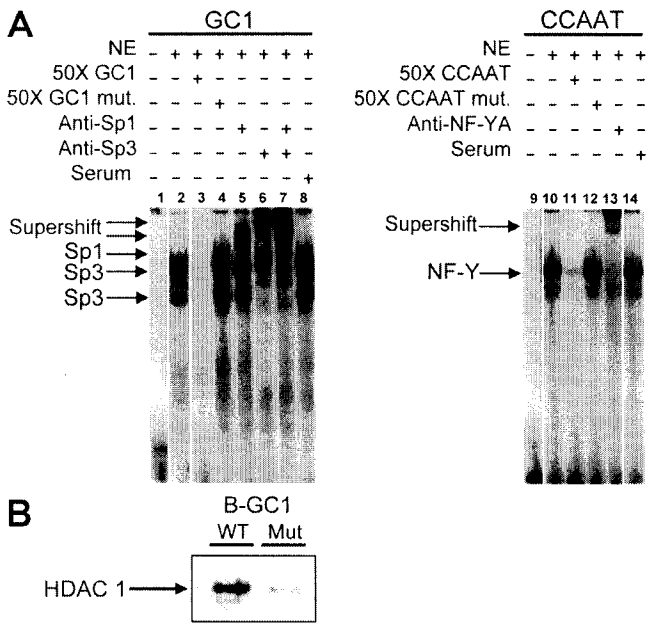

Figure 9. **Sp1/Sp3 and NF-Y bind to the GC1 and CCAAT boxes and HDAC1 is recruited through the GC1 box.** (A) EMSA was performed using the ^{32}P-labeled GC1 or CCAAT oligonucleotides with 10 μg of nuclear extracts (NE) from rat liver. Competition experiments were performed with a 50-fold molar excess of unlabeled oligonucleotides. Supershifts were performed using specific antibodies or serum for control. Retarded complexes are indicated. (B) DAPA was performed with the same nuclear extracts using the biotinylated normal or mutated GC1 oligonucleotide. Complexed proteins were resolved by SDS-PAGE and revealed by Western blot using an anti-HDAC1 antibody.

and the CCAAT probe (Fig. 9 A, lane 13), demonstrating that the CCAAT box binds NF-Y.

We further investigated by DNA affinity precipitation assay (DAPA) if the GC1 motif could be involved in the recruitment of HDAC1. We used the biotinylated oligonucleotides corresponding to the GC1 and mutated GC1 sequences used in EMSA. The presence of HDAC-1 was detected in the precipitated complexes obtained with the normal GC1 box but not with the mutated motif (Fig. 9 B). This finding indicates that HDAC-1 is recruited through interaction with the Sp1/Sp3 factors bound to the GC1 box of the *Abcd2* promoter.

Discussion

Because PBA induces peroxisome proliferation in human fibroblasts, PBA has been described as a new PP (Kemp et al., 1998). However, the fact that *AOX* and *PPARα* expression was unchanged in these cells indicates that PBA may induce peroxisome proliferation through a mechanism not shared by classical PPs such as fibrates. To clarify this point, we studied the effects of PBA in rodent tissues and cells. Induction of the *Abcd2* and *Aox* expression and of the peroxisome proliferation in the liver of rats was moderate and occurred only after a long-term (6–9-wk) treatment with high doses of PBA. The observed alterations in the shape (phi-bodies) and in the distribution (clusters and nearly touching organelles) of peroxisomes are reminiscent of PP-induced modifications already described in rat liver (Svoboda and Azarnoff, 1966; Baumgart et al., 1989; Gorgas and Krisans, 1989; Roels, 1991) and rat hepatoma cells (Duclos et al., 1997). It has been shown that overexpression of Pex11p in rodent or human cells causes peroxisome proliferation, characterized by initial conversion of peroxisomes from spherical vesicles into elongated tubules followed by appearance of numerous small vesicular peroxisomes (Passreiter et al., 1998; Schrader et al., 1998; Li and Gould, 2002). In the liver of rodents treated with PPs, peroxisome proliferation and peroxisomal gene induction occur early. In contrast, PBA had no effect when a short-term treatment (3 d) was given to rats, suggesting a different mode of action. However, the absence of effect could result from the rapid metabolism of PBA to phenylacetate leading to ineffective PBA plasma levels. Therefore, we exposed primary hepatocytes to high concentrations of PBA for 3 d and observed induction of the peroxisomal genes and peroxisome proliferation hardly higher than in vivo, indicating that PBA is a low-potent PP. It is well known that the peroxisome proliferation in the rodent liver due to classical PPs is totally suppressed in *PPARα* −/− mice (Lee et al., 1995). In contrast, the present work shows that the PBA-induced peroxisome proliferation is maintained in *PPARα* −/− hepatocytes. Both PBA and classical PPs induce *Pex11α* expression in mammals (Abe and Fujiki, 1998; Abe et al., 1998; Kemp et al., 1998; Schrader et al., 1998; Depreter et al., 2002). Surprisingly, Pex11α is dispensable for peroxisome proliferation mediated by PPARα activators, whereas Pex11α is required for peroxisome proliferation in response to PBA (Li et al., 2002). Furthermore, PBA but not fibrates induces peroxisome proliferation in nonhepatic cells (where PPARα expression is lower than in hepatocytes), namely fibroblasts (Kemp et al., 1998) and C6 cells (the present study). In summary, the requirement of PPARα and Pex11α for peroxisome proliferation and the cell type where peroxisome proliferation can occur are different for PBA and classical PPs. This finding indicates that the mechanism of peroxisome proliferation in response to PBA is distinct from that used by PPs.

X-ALD is characterized by demyelination in the brain. In the context of a pharmacological therapy based on the partial functional redundancy of the peroxisomal transporter ALDRP there is considerable interest to explore the effects of PBA in the brain. PBA is likely to cross the blood–brain barrier because it is effective in lowering VLCFA levels in the brain of *Abcd1* −/− mice (Kemp et al., 1998). Indeed, modifications at the peroxisomal level were detected in ependymal cells of the fourth ventricle in PBA-treated rats. Unfortunately, no induction in peroxisomal gene expression was seen in the brain examined as a whole. Nevertheless, the induction of *Abcd2* that we observed in PBA-treated glial cells might account for the restoration of VLCFA peroxisomal β-oxidation in the brain of PBA-treated *Abcd1* −/− mice described by Kemp et al. (1998).

The knowledge of the molecular mechanism underlying the PBA effects on *Abcd2* expression may provide leads in searching for new drugs for X-ALD therapy. We compared PBA with ciprofibrate or fenofibrate (classical powerful PPs) and with butyrate (an HDAC inhibitor) for their effects on peroxisomal gene expression in hepatic or nonhepatic cell cul-

tures. First, in fibroblasts and glial cells, fibrate was unable to induce *Abcd2*, suggesting that a cofactor of PPARα is missing or that the PPARα level is too low (Lemberger et al., 1996). In contrast, *Abcd2* was activated by PBA or butyrate in these cells, and we demonstrated that the activation is PPARα independent. Furthermore, in hepatocytes, *Abcd2* and *Aox* were induced by PBA, butyrate, and ciprofibrate, with some differences for the three compounds. We had observed that the induction of these genes by fibrate was completely abolished in the liver of *PPARα −/−* mice (Fourcade et al., 2001). Here, we show that PBA induction of *Abcd2* is only reduced in *PPARα −/−* hepatocytes, suggesting that part of the induction is PPARα dependent and that the other part would originate in the same mechanism underlying the activation of *Abcd2* by PBA and butyrate in nonhepatic cells. Similar conclusions can be drawn from our experiments on TSA-treated hepatocytes. Altogether, the results indicate that PBA and butyrate would mainly activate *Abcd2* by HDAC inhibition, whereas in hepatocytes an extra induction occurs through PPARα. This PPARα-dependent induction is in agreement with the relatively high level of PPARα in hepatocytes and the capacity of PBA to bind PPARα (Liu et al., 2002).

HDAC is known to interact with the transcription complex and the chromatin in a DNA region surrounding the transcription start, resulting in enhanced transcription rate (Nakayama and Takami, 2001). A basic promoter should be sufficient so that HDAC activity can take place. Support for this concept was obtained from our work demonstrating that the first 49 bp of the *Abcd2* promoter enable PBA and butyrate to activate a reporter gene and that the first 83 bp enable full induction. In transient transfection experiments, we demonstrated that the PBA-dependent induction and the basal level of expression of *Abcd2* depends on the GC1 and CCAAT boxes. Both motifs were shown to bind their cognate factors Sp1/Sp3 and NF-Y, respectively, and we demonstrated that HDAC-1 is recruited through the GC1 box in agreement with previous papers (Doetzlhofer et al., 1999). Expression of *Abcd2* probably results from the balanced action of HAT and HDAC activities. The CCAAT box, which binds NF-Y, likely allows HAT activity to be recruited and to antagonize the effect of HDAC-1 (Jin and Scotto, 1998). The recruitment of HAT activity may depend not only on NF-Y but also on Sp1, as it has already been described for the promoter of *HDAC1* for instance (Schuettengruber et al., 2003). It would explain why basal activity of the *Abcd2* promoter is reduced when the GC1 box is mutated, whereas it might have been expected that this mutation results in enhanced promoter activity because HDAC1 is not recruited anymore. This would also be in agreement with the up-regulation of HAT activity by physical interaction with Sp1 (Soutoglou et al., 2001). Besides, it was shown that the effect of PBA on *Abcd2* expression strictly depends on the presence of the GC1 box and consequently on the recruitment of HDAC1. However, full induction has been observed only when the CCAAT box is present, suggesting a synergistic effect of the two motifs. HDAC inhibition could increase recruitment of HAT to the CCAAT box as it has already been hypothesized for the *TβRII* gene (Park et al., 2002). Further work would be necessary to define more precisely the complexes containing HAT and HDAC activities and to show if other HDACs of the class I (Marks et al., 2003) can be involved in *Abcd2* expression.

We have shown that fibrates induce *Abcd2* expression in the liver of rodents in a PPARα-dependent way but not in the brain (Albet et al., 1997; Berger et al., 1999; Fourcade et al., 2001). It was believed that the absence of effects in brain was due to their inability to cross the blood–brain barrier. Actually, the present study revealed that fibrate, a powerful PP, has no effect in glial cells and fibroblasts. This lack of effect suggests that any drug, which requires PPARα, is likely to be ineffective in inducing *Abcd2* expression and in restoring VLCFA β-oxidation in the brain of *Abcd1 −/−* mice or X-ALD patients. PBA might be a better candidate for a pharmacological therapy of X-ALD because we showed that it can induce *Abcd2* expression in glial cells and cause peroxisome proliferation. An increased number of peroxisomes could contribute to improve VLCFA metabolism in X-ALD patients. However, it is still unclear whether or not the correction of VLCFA levels observed in the brain of *Abcd1 −/−* mice after PBA treatment (Kemp et al., 1998) results from enhanced *Abcd2* expression. A high effective dose and a decreased response in long-term studies are two stumbling blocks in using PBA for a therapy (McGuinness et al., 2001). In an effort to identify nontoxic agents effective at a low dose and with a long-term effect, we searched for the mechanism of pharmacological induction of *Abcd2* by PBA. We show that PBA acts at the peroxisomal level probably by inhibiting HDAC activity, like butyrate, suggesting that other HDAC inhibitors should be tested. Two compounds structurally related to PBA (styrylacetate and benzyloxyacetate) were shown to be as efficient as PBA in increasing VLCFA peroxisomal β-oxidation in *Abcd1 −/−* mice fibroblasts (McGuinness et al., 2001). It would be of great interest to assess the potential of these two analogues on *Abcd2* expression in oligodendrocytes, the myelin-forming cells.

There is a priori concern regarding the use of HDAC inhibitors because of their nonspecific effects on gene expression, but in clinical trials several HDAC inhibitors appeared to be well tolerated (Marks et al., 2003). Investigation of pharmacological agents acting through another molecular mechanism should also be considered. A more comprehensive understanding of the expression of the *Abcd2* gene is needed to identify other drugs for the development of an effective pharmacological therapy.

Materials and methods

Animals and treatments

Male Wistar rats of ~200 g (Charles River Laboratories) were kept at 22°C with equal periods of darkness and light and had free access to water and food. PBA (Sigma-Aldrich) was delivered to rats ($n = 6$) in their chow (7.5 g/kg) and water (10 g/L) corresponding to dose ×1 for 6–7 wk. A higher dose of PBA (dose ×1.5), corresponding to 11.3 g/kg of chow and 15 g/L of water, was also given to rats ($n = 4$) for 6–9 wk. The daily PBA uptake was estimated to be ~0.4–0.5 g per day per rat. The daily increase in body weight was significantly lower in treated animals (2.9 g) than in controls (5.3 g). Moreover, rats ($n = 3$) received 720 mg PBA per kilogram of body weight per day for 3 d via i.p. injections with an aqueous solution of PBA (40 mg/ml) twice a day. They were killed 12 h after the last injection.

Rats (400 g) were anesthetized with pentobarbital (60 mg/kg, i.p.). Drugs were administered at a delivery rate of 100 μl/h through a cannula stereotaxically implanted into the fourth ventricle. Rats received ei-

ther 2 mg of sodium ciprofibrate ($n = 4$) or 20 mg of PBA ($n = 4$) dissolved in a total volume of 100 μl of sterile water (pH adjusted at 7.3). Control rats ($n = 4$) received equiosmolar amounts of NaCl (100 μl). The rats were killed 48 h after injection.

Cell culture

Rat primary hepatocytes were prepared as described previously (Fourcade et al., 2001). Mouse primary hepatocytes were obtained according to Maslansky and Williams (1982), and a transfer on a cushion of Percoll yielded 90% viability. Differentiated CG4 rat glial cells, pure primary astocytes, and mixed primary culture of oligodendrocytes and astrocytes were obtained and cultured as described previously (Fourcade et al., 2003). Embryonic fibroblasts were prepared from 14-d-old fetuses of *PPARα* +/+ and −/− mice as described previously (Doetschman et al., 1985) and cultured in DME supplemented with 10% FCS. COS-7 cells were grown in DME supplemented with 10% FCS in the absence of antibiotics.

Northern blot analysis

Total RNA was extracted from rat tissues using a standard protocol. The GenElute Mammalian Total RNA kit (Sigma-Aldrich) was used to prepare RNA from cultured cells. Membranes containing 20 μg per lane of RNA were hybridized with α-[^{32}P]–labeled cDNA probe as described previously (Albet et al., 2001).

Semiquantitative RT-PCR

Total RNA was reverse-transcribed by random priming. To study *Aox* expression, PCR was performed as described previously (Fourcade et al., 2001). *Abcd2* cDNA was amplified using the forward (F) and reverse (R) primers 5′-GTGTATGCCACTGCTAAAG-3′ and 5′-TCAGCTCCAGAGGCCAGT-3′, respectively, for 27 cycles (30 cycles when RNA was extracted from primary hepatocytes) and 56°C as the annealing temperature. Amplification of *36b4* cDNA was performed using the primers 5′-AAYGTGGGCTCCAAGCAGATG-3′ (F) and 5′-GAGATGTTCAYCATGTTCAGCAG-3′ (R), for 17 cycles and 60°C as the annealing temperature. PCR products were analyzed on agarose gels and quantified by digital imaging, and the relative abundance of mRNA was determined by comparison with *36b4* mRNA level.

Microscopy

Rats were anesthetized and the tissues were fixed through intracardial perfusion with fixative. Peroxisomes were visualized by staining for catalase activity with DAB (Roels et al., 1995). Immunolocalization of AOX (antibody provided by A. Völkl, University of Heidelberg, Heidelberg, Germany) or catalase for LM or EM was performed according to Espeel and Van Limbergen (1995). LM images were photographed on film on an Aristoplan microscope (Leitz) using 63×, 1.4 NA, and 40×, 0.75 NA, oil immersion lenses (Leitz) for bright field and phase contrast and on an inverted microscope (model DMIRB; Leica) using a Leica PL Apo 63×, 1.32–0.6 NA oil immersion lens, and the Leica MPS-60 photoautomat for immunofluorescence. On randomly taken LM micrographs, the number of peroxisomes per cellular area was determined by counting catalase-stained peroxisomes and measuring cellular area excluding blood vessels with a semi-automatic image analysis system (Mini-Mop; Kontron). EM images were photographed on a transmission electron microscope (model JEM-100B; JEOL). Morphometry of peroxisomes was performed on random EM micrographs as described previously (Kerckaert et al., 1995). Gold particles per peroxisome were counted and organelle area was measured with the Mini-Mop apparatus. A nonparametric ranking test (Mann-Whitney) was used for statistical analysis of microscopy data. For publication, micrographs were scanned and imported into Adobe Photoshop.

Plasmid constructs

The first 83 bp of the rat *Abcd2* promoter (relative to the transcription start located at −194 from the translation start site) were cloned directionally into pGL3-Basic (Promega) to yield p277 as described previously (Fourcade et al., 2001). The p243 construct was prepared as p277 except that the inserted PCR fragment was amplified using forward primer 5′-ttagatcTGAGAAGCCTGGG-3′ containing a BglII site (underlined). The plasmids p277Δ5UTR and p243Δ5UTR were built as p277 and p243 using the reverse primer 5′-CTGaAGCTTGCTCAAACTCCACCGC-3′ (the HindIII site is underlined). The constructs were verified by sequencing with GL primer 2 (Promega). p277Δ1, p277Δ2, and p277Δ1,2 were obtained from the p277 plasmid by site-directed mutagenesis with the Quickchange site directed mutagenesis kit (Stratagene) according to the manufacturer's protocol using pairs of complementary oligonucleotides corresponding to the following sequences: GC1 mut, 5′-CCAATGAGAAGCCTGGG**GTTTG**GAGCCTGGCCAGC-3′; GC2 MUT, 5′-GGAGTCCAGGGTCTCA**AAGC**-**CC**ACGCAGCCAATGAG-3′ (the GC boxes are shown in bold and mutations are underlined).

Transient transfection experiments

COS-7 cells were transfected using Exgen 500 liposome (Euromedex) with 100 ng of pCMV-βGal (CLONTECH Laboratories, Inc.), 650 ng of pGLUC (a modified pGL2 vector) or empty pGL3-Basic or construct, and 250 ng of empty pSG5 (Stratagene) as previously described (Fourcade et al., 2001). The transfected cells were incubated with or without PBA or butyrate for 36 h and assayed for luciferase activity (Fourcade et al., 2001). Luciferase activity was corrected for transfection efficiency using β-galactosidase activity.

EMSA

The following pairs of oligonucleotides used as probes or competitors in EMSA were designed from the rat *ABCD2* promoter: GC1 (F, 5′-agcttCCTGGG**GGGTGG**AGCCTGG-3′; R, 5′-gatcCCAGGCT**CCACCC**CCCAGGa-3′), GC1 mut (F, 5′-agcttCCTGGG**GTTTGG**AGCCTGG-3′; R, 5′-gatcCCAGGCT**CCAAAC**CCCAGGa-3′), CCAAT (F, 5′-agcttCCACGCA-G**CCAAT**GAGAAGCCg-3′; R, 5′-gatccGGCTTCTC**ATTGG**CTGCGTGGa-3′), CCAAT mut (F, 5′-agcttCCACGCCC**CGTAT**TTGAAGCCg-3′; R, 5′-gatccGGCTTCAA**ATACG**GGGCGTGGa-3′) (GC1 and CCAAT boxes are shown in bold; mutations are underlined; lower case letters are modified nucleotides from the original sequence to create compatible ends for cloning and fill-in labeling). Labeling of probes and binding experiments in the presence of 10 μg of nuclear extracts from rat liver were performed as described previously (Fourcade et al., 2001). Competition and supershift experiments were performed by adding a 50-fold molar excess of unlabeled oligonucleotides or antibodies (Santa Cruz Biotechnology, Inc.; anti-Sp1, anti-Sp3, and anti–NF-YA) or a rabbit serum (control) 30 min before the addition of the radiolabeled probes. The samples were analyzed by electrophoresis at 4°C on 4% polyacrylamide gels in 0.5 × TBE (45 mM Tris-borate and 1 mM EDTA).

DAPA

Complementary oligonucleotides corresponding to the normal (5′-TGAGAAGCCTGGG**GGGTGG**AGCCTGGCCAG-3′) or mutated (5′-TGAGAAGCCTGGG**GTTTGG**AGCCTGGCCAG-3′) GC1 box were synthesized, biotinylated at their 5′ termini, and annealed. The DAPA was performed in a total volume of 400 μl by mixing 4 μg of biotinylated DNA probe with 50 μg of nuclear extracts from rat liver in binding buffer (20 mM Hepes, pH 7.9, 10% glycerol, 50 mM KCl, 0.2 mM EDTA, 1.5 mM $MgCl_2$, 10 μM ZnCl2, 1 mM DTT, and 0.25% Triton X-100). After a 30-min preincubation on ice, 50 μl of streptavidin-agarose beads (Novagen) were added and incubated for 2 h under agitation. Beads were collected by a brief centrifugation and washed twice in binding buffer. Proteins were eluted in 15 μl of SDS-PAGE loading buffer by heating for 5 min at 95°C. After centrifugation, the supernatant was loaded on SDS-PAGE and Western blot analysis was performed using anti-HDAC1 antibody (Santa Cruz Biotechnology, Inc.).

We dedicate this paper to the memory of Professor Maurice Bugaut, who initiated this project and who died on untimely death while the manuscript was being revised.

We thank Professor Alfred Völkl for acyl-CoA oxidase antibody. We also thank Betty De Prest, Dominique Jacobus, Hubert Stevens, Simonne Van Hulle, and Guido Van Limbergen (all from Ghent University) for their technical assistance.

This work was supported by grants from the European Association against Leukodystrophies (ELA) and the Regional Council of Burgundy. S. Fourcade and S. Leclercq were supported by a fellowship from ELA. S. Fourcade was also supported by a fellowship from Fondation pour la Recherche Médicale.

Submitted: 7 January 2005
Accepted: 3 March 2005

References

Abe, I., and Y. Fujiki. 1998. cDNA cloning and characterization of a constitutively expressed isoform of the human peroxin Pex11p. *Biochem. Biophys. Res. Commun.* 252:529–533.

Abe, I., K. Okumoto, S. Tamura, and Y. Fujiki. 1998. Clofibrate-inducible, 28-kDa peroxisomal integral membrane protein is encoded by PEX11. *FEBS Lett.* 431:468–472.

Albet, S., C. Causeret, M. Bentejac, J.L. Mandel, P. Aubourg, and M. Bugaut.

1997. Fenofibrate differently alters expression of genes encoding ATP-binding transporter proteins of the peroxisomal membrane. *FEBS Lett.* 405:394–397.

Albet, S., M. Bentejac, S. Savary, C. Gondcaille, A. Netik, J. Berger, C. Szpirer, N. Troffer-Charlier, and M. Bugaut. 2001. Rat adrenoleukodystrophy-related (ALDR) gene: full-length cDNA sequence and new insight in expression. *Biochim. Biophys. Acta.* 1517:257–269.

Baumgart, E., A. Volkl, T. Hashimoto, and H.D. Fahimi. 1989. Biogenesis of peroxisomes: immunocytochemical investigation of peroxisomal membrane proteins in proliferating rat liver peroxisomes and in catalase-negative membrane loops. *J. Cell Biol.* 108:2221–2231.

Berger, J., S. Albet, M. Bentejac, A. Netik, A. Holzinger, A.A. Roscher, M. Bugaut, and S. Forss-Petter. 1999. The four murine peroxisomal ABC-transporter genes differ in constitutive, inducible and developmental expression. *Eur. J. Biochem.* 265:719–727.

Braiterman, L.T., S. Zheng, P.A. Watkins, M.T. Geraghty, G. Johnson, M.C. McGuinness, A.B. Moser, and K.D. Smith. 1998. Suppression of peroxisomal membrane protein defects by peroxisomal ATP binding cassette (ABC) proteins. *Hum. Mol. Genet.* 7:239–247.

Davie, J.R. 2003. Inhibition of histone deacetylase activity by butyrate. *J. Nutr.* 133:2485S–2493S.

Depreter, M., J. Vandesompele, M. Espeel, F. Speleman, and F. Roels. 2002. Modulation of the peroxisomal gene expression pattern by dehydroepiandrosterone and vitamin D: therapeutic implications. *J. Endocrinol.* 175:779–792.

Doetschman, T.C., H. Eistetter, M. Katz, W. Schmidt, and R. Kemler. 1985. The in vitro development of blastocyst-derived embryonic stem cell lines: formation of visceral yolk sac, blood islands and myocardium. *J. Embryol. Exp. Morphol.* 87:27–45.

Doetzlhofer, A., H. Rotheneder, G. Lagger, M. Koranda, V. Kurtev, G. Brosch, E. Wintersberger, and C. Seiser. 1999. Histone deacetylase 1 can repress transcription by binding to Sp1. *Mol. Cell. Biol.* 19:5504–5511.

Duclos, S., J. Bride, L.C. Ramirez, and P. Bournot. 1997. Peroxisome proliferation and beta-oxidation in Fao and MH1C1 rat hepatoma cells, HepG2 human hepatoblastoma cells and cultured human hepatocytes: effect of ciprofibrate. *Eur. J. Cell Biol.* 72:314–323.

Espeel, M., and G. Van Limbergen. 1995. Immunocytochemical localization of peroxisomal proteins in human liver and kidney. *J. Inherit. Metab. Dis.* 18:135–154.

Flavigny, E., A. Sanhaj, P. Aubourg, and N. Cartier. 1999. Retroviral-mediated adrenoleukodystrophy-related gene transfer corrects very long chain fatty acid metabolism in adrenoleukodystrophy fibroblasts: implications for therapy. *FEBS Lett.* 448:261–264.

Fourcade, S., S. Savary, S. Albet, D. Gauthe, C. Gondcaille, T. Pineau, J. Bellenger, M. Bentejac, A. Holzinger, J. Berger, and M. Bugaut. 2001. Fibrate induction of the adrenoleukodystrophy-related gene (ABCD2): promoter analysis and role of the peroxisome proliferator-activated receptor PPARalpha. *Eur. J. Biochem.* 268:3490–3500.

Fourcade, S., S. Savary, C. Gondcaille, J. Berger, A. Netik, F. Cadepond, M. ElEtr, B. Molzer, and M. Bugaut. 2003. Thyroid hormone induction of the adrenoleukodystrophy-related gene (ABCD2). *Mol. Pharmacol.* 63:1296–1303.

Gartner, J., G. Jimenez-Sanchez, P. Roerig, and D. Valle. 1998. Genomic organization of the 70-kDa peroxisomal membrane protein gene (PXMP1). *Genomics.* 48:203–208.

Gorgas, K., and S.K. Krisans. 1989. Zonal heterogeneity of peroxisome proliferation and morphology in rat liver after gemfibrozil treatment. *J. Lipid Res.* 30:1859–1875.

Holzinger, A., S. Kammerer, and A.A. Roscher. 1997. Primary structure of human PMP69, a putative peroxisomal ABC-transporter. *Biochem. Biophys. Res. Commun.* 237:152–157.

Jin, S., and K.W. Scotto. 1998. Transcriptional regulation of the MDR1 gene by histone acetyltransferase and deacetylase is mediated by NF-Y. *Mol. Cell. Biol.* 18:4377–4384.

Kamijo, K., S. Taketani, S. Yokota, T. Osumi, and T. Hashimoto. 1990. The 70-kDa peroxisomal membrane protein is a member of the Mdr (P-glycoprotein)-related ATP-binding protein superfamily. *J. Biol. Chem.* 265:4534–4540.

Kemp, S., H.M. Wei, J.F. Lu, L.T. Braiterman, M.C. McGuinness, A.B. Moser, P.A. Watkins, and K.D. Smith. 1998. Gene redundancy and pharmacological gene therapy: implications for X-linked adrenoleukodystrophy. *Nat. Med.* 4:1261–1268.

Kerckaert, I., D. De Craemer, and G. Van Limbergen. 1995. Practical guide for morphometry of human peroxisomes on electron micrographs. *J. Inherit. Metab. Dis.* 18:172–180.

Lea, M.A., and V.M. Randolph. 1998. Induction of reporter gene expression by inhibitors of histone deacetylase. *Anticancer Res.* 18:2717–2722.

Lee, S.S.-T., T. Pineau, J. Drago, E.J. Lee, J.W. Owens, D.L. Kroetz, P.M. Fernandez-Salguero, H. Westphal, and F.G. Gonzalez. 1995. Targeted disruption of the alpha isoform of the peroxisome proliferator-activated receptor gene in mice results in abolishment of the pleiotropic effects of peroxisome proliferators. *Mol. Cell. Biol.* 15:3012–3022.

Lemberger, T., O. Braissant, C. Juge-Aubry, H. Keller, R. Saladin, B. Staels, J. Auwerx, A.G. Burger, C.A. Meier, and W. Wahli. 1996. PPAR tissue distribution and interactions with other hormone-signaling pathways. *Ann. NY Acad. Sci.* 804:231–251.

Li, X., and S.J. Gould. 2002. PEX11 promotes peroxisome division independently of peroxisome metabolism. *J. Cell Biol.* 156:643–651.

Li, X., E. Baumgart, G.-X. Dong, J.C. Morrell, G. Jimenez-Sanchez, D. Valle, K.D. Smith, and S.J. Gould. 2002. PEX11α is required for peroxisome proliferation in response to 4-phenylbutyrate but is dispensable for peroxisome proliferator-activated receptor α-mediated peroxisome proliferation. *Mol. Cell. Biol.* 22:8226–8240.

Liu, N., W. Qiang, X. Kuang, P. Thuillieer, W.S. Lynn, and P.K.Y. Wong. 2002. The peroxisome proliferator phenylbutyric acid (PBA) protects astrocytes from ts1 MoMuLV-induced oxidative cell death. *J. Neurovirol.* 8:318–325.

Lombard-Platet, G., S. Savary, C.O. Sarde, J.L. Mandel, and G. Chimini. 1996. A close relative of the adrenoleukodystrophy (ALD) gene codes for a peroxisomal protein with a specific expression pattern. *Proc. Natl. Acad. Sci. USA.* 93:1265–1269.

Lu, Y., and R. Lotan. 1999. Transcriptional regulation by butyrate of mouse galectin-1 gene in embryonal carcinoma cells. *Biochim. Biophys. Acta.* 1444:85–91.

Marks, P.A., T. Miller, and V.M. Richon. 2003. Histone deacetylases. *Curr. Opin. Pharmacol.* 3:344–351.

Maslansky, C.J., and G.M. Williams. 1982. Primary cultures and the levels of cytochrome P450 in hepatocytes from mouse, rat, hamster and rabbit liver. *In Vitro.* 18:683–693.

McCaffrey, P.G., D.A. Newsome, E. Fibach, M. Yoshida, and M.S. Su. 1997. Induction of gamma-globin by histone deacetylase inhibitors. *Blood.* 90:2075–2083.

McGuinness, M.C., H.P. Zhang, and K.D. Smith. 2001. Evaluation of pharmacological induction of fatty acid beta-oxidation in X-linked adrenoleukodystrophy. *Mol. Genet. Metab.* 74:256–263.

Moser, H.W., K.D. Smith, P.A. Watkins, J. Powers, and A.B. Moser. 2001. X-linked adrenoleukodystrophy. *In* The Metabolic & Molecular Bases of Inherited Disease, 8th edition. R. Scriver, A.L. Beaudet, W.S. Sly, and D. Valle, editors. McGraw-Hill Inc., New York. 3257–3301.

Mosser, J., A.M. Douar, C.O. Sarde, P. Kioschis, R. Feil, H. Moser, A.M. Poustka, J.L. Mandel, and P. Aubourg. 1993. Putative X-linked adrenoleukodystrophy gene shares unexpected homology with ABC transporters. *Nature.* 361:726–730.

Motojima, K. 1997. Peroxisome proliferator-activated receptor (PPAR)-dependent and -independent transcriptional modulation of several non-peroxisomal genes by peroxisome proliferators. *Biochimie.* 79:101–106.

Nakayama, T., and Y. Takami. 2001. Participation of histones and histone-modifying enzymes in cell functions through alterations in chromatin structure. *J. Biochem. (Tokyo).* 129:491–499.

Netik, A., S. Forss-Petter, A. Holzinger, B. Molzer, G. Unterrainer, and J. Berger. 1999. Adrenoleukodystrophy-related protein can compensate functionally for adrenoleukodystrophy protein deficiency (X-ALD): implications for therapy. *Hum. Mol. Genet.* 8:907–913.

Park, S.H, S.R. Lee, B.C. Kim, E.A. Cho, S.P. Patel, H.B. Kang, E.A. Sausville, O. Nakanishi, J.B. Trepel, B.I. Lee, S.J. Kim. 2002. Transcriptional regulation of the transforming growth factor beta type II receptor gene by histone acetyltransferase and deacetylase is mediated by NF-Y in human breast cancer cells. *J. Biol. Chem.* 15:277:5168-5174.

Passreiter, M., M. Anton, D. Lay, R. Frank, C. Harter, F.T. Wieland, K. Gorgas, and W.W. Just. 1998. Peroxisome biogenesis: involvement of ARF and coatomer. *J. Cell Biol.* 141:373–383.

Pineau, T., W.R. Hudgins, L. Liu, L.C. Chen, T. Sher, F.J. Gonzalez, and D. Samid. 1996. Activation of a human peroxisome proliferator-activated receptor by the antitumor agent phenylacetate and its analogs. *Biochem. Pharmacol.* 52:659–667.

Pujol, A., I. Ferrer, C. Camps, E. Metzger, C. Hindelang, N. Callizot, M. Ruiz, T. Pampols, M. Giros, and J.L. Mandel. 2004. Functional overlap between ABCD1 (ALD) and ABCD2 (ALDR) transporters: a therapeutic target for X-adrenoleukodystrophy. *Hum. Mol. Genet.* 13:2997–3006.

Roels, F. 1991. Peroxisomes: A Personal Account. VUB Press, Brussels. 151 pp.

Roels, F., B. De Prest, and G. De Pestel. 1995. Liver and chorion cytochemistry. *J. Inherit. Metab. Dis.* 18:155–171.

Schrader, M., B.E. Reuber, J.C. Morrell, G. Jimenez-Sanchez, C. Obie, T.A. Stroh, D. Valle, T.A. Schroer, and S.J. Gould. 1998. Expression of PEX11beta mediates peroxisome proliferation in the absence of extracellular stimuli. *J. Biol. Chem.* 273:29607–29614.

Schuettengruber, B., E. Simboek, H. Khier, and C. Seiser. 2003. Autoregulation of mouse histone deacetylase 1 expression. *Mol. Cell. Biol.* 23:6993–7004.

Soutoglou, E., B. Viollet, M. Vaxillaire, M. Yaniv, M. Pontoglio, and I. Talianidis. 2001. Transcription factor-dependent regulation of CBP and P/CAF histone acetyltransferase activity. *EMBO J.* 20:1984–1992.

Svoboda, D.J., and D.L. Azarnoff. 1966. Response of hepatic microbodies to a hypolipidemic agent, ethyl chlorphenoxyisobutyrate (CPIB). *J. Cell Biol.* 30:442–450.

Waddell, W.J., C. Marlowe, M.S. Rao, and J.K. Reddy. 1989. In vivo distribution of a carcinogenic hepatic peroxisome proliferator: whole-body autoradiography of [14C]ciprofibrate in the mouse. *Carcinogenesis.* 10:221–223.

Warrell, R.P.J., L.Z. He, V. Richon, E. Calleja, and P.P. Pandolfi. 1998. Therapeutic targeting of transcription in acute promyelocytic leukemia by use of an inhibitor of histone deacetylase. *J. Natl. Cancer Inst.* 90:1621–1625.

J. Parasitol., 93(3), 2007, pp. 694–700

SCRIPTAID AND SUBEROYLANILIDE HYDROXAMIC ACID ARE HISTONE DEACETYLASE INHIBITORS WITH POTENT ANTI–*TOXOPLASMA GONDII* ACTIVITY IN VITRO

Jeannine S. Strobl, Meredith Cassell, Sheila M. Mitchell*, Christopher M. Reilly, and David S. Lindsay*
Biomedical Sciences, Edward Via Virginia College of Osteopathic Medicine, Blacksburg, Virginia 24060. *e-mail: jstrobl@vcom.vt.edu*

ABSTRACT: *Toxoplasma gondii* is a well-recognized cause of disease in congenitally infected and immunocompromised individuals. Histone deacetylases (HDAC) comprise a family of enzymes that participate in the regulation of chromatin structure, gene expression, and cell signaling in eukaryotes. *Toxoplasma gondii* expresses a HDAC Class I enzyme homologous to human hdac3. Previous work showed that the histone deacetylase inhibitors (HDI) apicidin and valproic acid inhibit *T. gondii* infections in vitro. The present study compares the activity of hydroxamic-acid histone deacetylase inhibitors against the RH strain of *T. gondii* growing in HS68 human foreskin fibroblast cells. Nanomolar concentrations of suberoylanilide hydroxamic acid (SAHA), suberic bishydroxamic acid (SBHA), scriptaid, and trichostatin A (TSA) inhibited *T. gondii* tachyzoite proliferation. Scriptaid was the most potent hydroxamic acid inhibitor (IC_{50} = 39 nM). In comparison, the carboxylate histone deacetylase inhibitors sodium valproate, sodium butyrate, and 4-phenylbutyrate were less potent (IC_{50} range 1–5 mM). All of the inhibitors tested, except SBHA, completely protected the HS68 monolayers from *T. gondii* at concentrations 3–6 times greater than their respective IC_{50}. In contrast, nicotinamide, an inhibitor of NAD^+-dependent Class III HDAC, had minimal activity against *T. gondii* in our in vitro assays. We conclude that the hydroxamic acid class of histone deacetylase inhibitors exhibit potent anti–*T. gondii* activity in vitro.

Toxoplasma gondii is an intracellular protozoan parasite harbored by birds and mammals worldwide. There are several infectious stages in the *T. gondii* life cycle. The tachyzoites are a highly proliferative form that differentiate into less metabolically active bradyzoites that establish tissue cysts. The sporozoite form of *T. gondii* develops in the oocysts that are shed from definitive hosts. All feline species act as definitive hosts for *T. gondii*, and infections arise in these animals after ingestion of tissue cysts and, less frequently, oocysts. Transmission of *T. gondii* to humans may occur following contact with contaminated water and soil, or through ingestion of undercooked meat (Dubey et al., 2005). *Toxoplasma gondii* bradyzoites persist for years in the tissues of asymptomatic livestock and wildlife, and comprise a poorly controlled source of human infection.There is a growing awareness of the significance of *T. gondii* as a human zoonotic pathogen. In addition, toxoplasmosis is a recognized risk in organ transplant recipients, and transmission of *T. gondii* is sufficiently prevalent among heart transplant patients that toxoplasmosis chemoprophylaxis is recommended (Fricker-Hidaigo et al., 2005).

In humans, *T. gondii* manifests itself several ways. Women infected during pregnancy may transmit *T. gondii* tachyzoites transplacentally, resulting in congenital infections that may cause mental retardation and ocular disease in the child and young adults (Bonfioli and Orefice, 2005). Rapid multiplication of tachyzoites in HIV-infected persons and other immunocompromised patients can lead to diffuse disease involving lungs, liver, brain, heart, and retina, and may even result in death (Dubey and Lindsay, 2004). Newer studies show that *T. gondii* is also a source of disease in immunocompetent individuals. *Toxoplasma gondii* may cause lymphadenopathy, fever, muscle weakness, opthalmitis, and multiorgan infection in the general population. Most recently, human *T. gondii* infections were linked with cognitive impairments and susceptibility to personality disorders, including schizophrenia (McAllister, 2005). The knowledge implicating *T. gondii* in the etiology of a broader range of human disease conditions has stimulated the search for additional medical treatments.

The enzymes involved in chromatin remodeling pathways in *T. gondii* have been delineated recently, and include a known *T. gondii* drug target, histone deacetylase (Sullivan and Hakimi, 2006). Apicidin is a broad-spectrum antiprotozoal agent, and was the 1st histone deacetylase inhibitor discovered to have in vitro antiproliferative activity against the tachyzoite stage of *T. gondii* (Darkin-Rattray et al., 1996). Subsequently, valproic acid, another histone deacetylase inhibitor, was reported to reduce *T. gondii* tachyzoite numbers in vitro (Jones-Brando et al., 2003). Histone deacetylase is potentially a very important drug target in *T. gondii*. The latter drug was found to arrest tumor cell growth and promote tumor cell differentiation and apoptosis (reviewed in Ito et al., 2006; Kwon et al., 2006); many of these inhibitors have moved rapidly to the clinical testing stage. Preliminary clinical successes achieved with SAHA in cancer treatment trials (Kelly et al., 2005; O'Connor et al., 2006) are the basis for the present study, in which we compared the anti–*T. gondii* activity of various mammalian histone deacetylase inhibitors.

MATERIALS AND METHODS

Drugs

Trichostatin A, sodium valproate, 4-phenylbutyrate, and sodium butyrate were purchased from Sigma Chemical Company (St. Louis, Missouri). Scriptaid was purchased from BioMol International (Plymouth Meeting, Pennsylvania). TSA, SAHA, and scriptaid were dissolved in DMSO as 10 mM stocks and stored at −20 C. They were diluted into culture medium immediately prior to use. The concentration of DMSO solvent in these experiments did not exceed 0.1%. Fresh stock solutions of sodium valproate, phenylbutyrate, and sodium butyrate were prepared in sterile phosphate-buffered saline and diluted into culture medium for each experiment. Control-treated groups received an equal volume of DMSO or phosphate-buffered saline.

Parasite propagation

The RH strain of *T. gondii* was grown in bovine macrophage cells or HS68 human foreskin fibroblast cells obtained from the American Type Culture Collection (Rockville, Maryland). HS68 cells were grown in RPMI 1640 medium (Mediatech, Inc., Herndon, Virginia) plus 10% fetal bovine serum (Atlanta Biologicals, Lawrenceville, Georgia), 1 mM

Received 30 August 2006; revised 8 November 2006; accepted 14 November 2006.

* Department of Biomedical Sciences and Pathobiology, Virginia–Maryland Regional College of Veterinary Medicine, Virginia Polytechnic and State University, Blacksburg, Virginia 24061.

sodium pyruvate, and penicillin and streptomycin (100 U/ml). Parasites were harvested from infected cultures of HS68 cells growing in 75-cm^2 flasks. After the culture medium was removed, the cells were scraped into 5 ml of phosphate-buffered saline and a cell lysate obtained by passing through a 26-gauge needle. To purify the parasites, the cell lysate was passed through a 3-μm filter.

Proliferation assays

HS68 cells were replica plated in 48-well dishes, and grown to confluence prior to infection with 5 to 10 × 10^4 freshly purified *T. gondii* tachyzoites/well. After 2 hr, the media and noninfective tachyzoites were removed, and replaced with RPMI medium containing 2% fetal bovine serum plus 1 mM sodium pyruvate, penicillin (100 U/ml), streptomycin (100 U/ml), and a test agent or a vehicle control. The proliferation assays were terminated 48–72 hr postinfection (PI), when the untreated cells were heavily infected. All of the culture media were removed from the wells, and the tachyzoites in the media were fixed by dilution (1:1) into phosphate-buffered saline containing 10% formaldehyde. The tachyzoites were collected by brief centrifugation (30 sec at 80,000 g) at room temperature with the use of a tabletop microfuge. The tachyzoites were resuspended in 0.1 ml of phosphate-buffered saline, and duplicate aliquots were counted with the use of a hemocytometer. IC_{50} values, the concentrations of inhibitors necessary to decrease the number of tachyzoites in the medium by 50%, were determined for each experiment with the use of Prism GraphPad version 4.0 to fit the concentration-response data to a sigmoidal curve. In experiments in which low concentrations of the treatments increased tachyzoite numbers, only treatment concentrations that were inhibitory were used in the calculation of the IC_{50}. The monolayer of HS68 cells in each well was fixed and stained for 5 min with a solution of 50% ethanol, 5% formaldehyde, and 0.1% crystal violet in 0.85% sodium chloride, then rinsed with water and air dried. The minimum inhibitory concentration (MIC) of compounds that suppressed *T. gondii*–induced lysis of the HS68 cells was determined visually by counting the number of plaques/well in the monolayer.

Statistical analyses

Prism GraphPad version 4.0 was used to calculate experimental means and standard errors and to perform ANOVA. In the 1-way ANOVA analyses of the hydroxamic acid concentration–response curves, Dunnett's *t*-test, with $P < 0.05$ considered significant, was used to compare the effects of the histone deacetylase inhibitors with nontreated control samples.

RESULTS

Histone deacetylase inhibitors

The purpose of this study was to compare the anti–*T. gondii* activity of the hydroxamic acid and carboxylate human histone deacetylase enzyme inhibitors shown in Figure 1. The hydroxamic acids (Fig. 1a) and the carboxylates (Fig. 1b) are nonselective inhibitors of Class I and class II mammalian histone deacetylases. These compounds do not inhibit the Class III histone deacetylases, which are also known as the sirtuins that utilize NAD^+ as a cofactor and are inhibited by nicotinamide (Fig. 1b) (Sauve et al., 2006).

The histone deacetylase inhibitors in Figure 1 differ somewhat in their pharmacologic and biologic actions in mammalian cells. TSA (IC_{50} 20–40 nM) is the most potent inhibitor of mammalian hdac1, 2, and 3, followed by SAHA (IC_{50} 22–290 nM) (Furumai et al., 2001; Moradei et al., 2005). Su et al. (2000) and Hu et al. (2003) reported the biological activity of

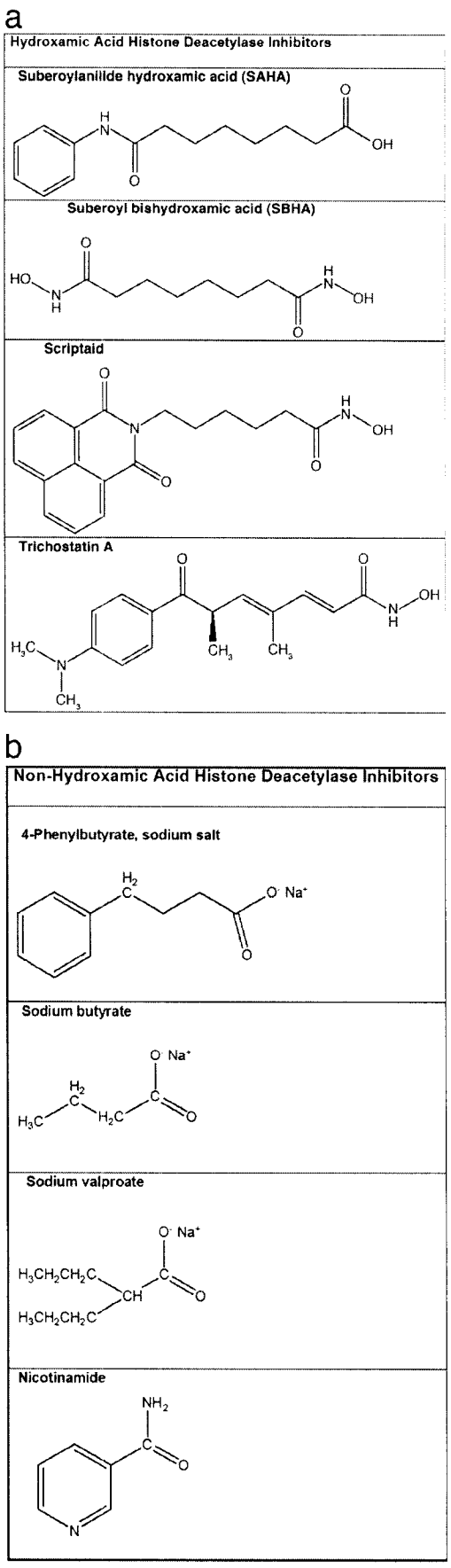

FIGURE 1. Structure of histone deacetylase inhibitors. (**a**) Hydroxamic acids. (**b**) Nonhydroxamic acids.

TABLE I. In vitro anti-*Toxoplasma* activity of histone deacetylase inhibitors. The IC_{50} values were derived by averaging the IC_{50} determined from n number of independent concentration-response curves. Data are mean ±SEM in n independent experiments conducted in triplicate at each concentration.

Agent	IC_{50} (μM) Tachyzoite count	MIC (μM) Plaque suppression	MIC/IC_{50}
HDAC Class I/II inhibitors			
Scriptaid	0.039 ± 0.011 n = 4	0.225 ± 0.025 n = 2	5.8
TSA	0.041 ± 0.001 n = 4	0.175 ± 0.025 n = 4	4.3
SAHA	0.083 ± 0.04 n = 5	0.400 ± 0.1 n = 4	4.8
SBHA	0.213 ± 0.11 n = 3	12.5 ± 5 n = 4	58.7
Sodium butyrate	1,000 ± 455 n = 6	4,200 ± 800 n = 6	4.2
Valproic acid	1,600 ± 1,116 n = 3	8,300 ± 1,000 n = 3	5.2
4-phenylbutyrate	5,350 ± 2,750 n = 2	16,700 ± 3,300 n = 3	3.1
HDAC Class III inhibitor			
Nicotinamide	> 50,000 n = 3	> 50,000 n = 3	ND

SAHA and scriptaid to be similar (Moradei et al., 2005). The carboxylates inhibit Class I and Class II hdacs and are at least 4,000 times less potent than TSA (Gurvich et al., 2004; Suzuki and Miyata, 2005). Carboxylates inhibit mammalian histone deacetylase enzyme activity in the following rank order of potency: sodium butyrate (IC_{50} 0.14–0.3 mM), 4-phenylbutyrate (IC_{50} 0.62 mM), and sodium valproate (IC_{50} 0.54–2.8 mM).

Hydroxamic acid inhibitors of *T. gondii* tachyzoites

Table I summarizes the in vitro activity of histone deacetylase inhibitors on the growth of *T. gondii* in cell cultures. Scriptaid and SAHA are potent anti–*T. gondii* compounds with low cytotoxicity. These agents reduced the number of tachyzoites released by infected cells with nanomolar IC_{50} levels. Scriptaid was more potent than SAHA. The average scriptaid IC_{50} calculated in 4 independent experiments was 39 nM. Scriptaid was nontoxic to the HS68 cells at 10 μM, the highest concentration tested (data not shown). SAHA reduced *T. gondii* tachyzoite numbers (IC_{50} = 81 nM, n = 5) with no discernable toxicity to HS68 cells at the highest concentration tested, which was 10 μM (data not shown). The anti–*T. gondii* in vitro activity of TSA (IC_{50} = 41 nM, n = 4) was similar to that of scriptaid. However, TSA was highly toxic to the HS68 cells. The HS68 cell monolayer was destroyed by a 48-hr exposure to 1 μM TSA, and apoptotic cells were evident after exposure to 500 nM TSA. Our results show that scriptaid and SAHA are more potent inhibitors of growth in *T. gondii* tachyzoites than tumor cells in vitro. In tests with a variety of human tumor cell lines growing in tissue culture, reductions in tumor cell numbers and activation of apoptosis in tumor cells contribute to the anticancer activity of 1 to 20 μM SAHA (Zhang et al., 2005; Komatsu et al., 2006; Sonnemann et al., 2006; Wilson et al., 2006). SAHA inhibited *T. gondii* tachyzoite growth with an IC_{50} value of 83 nM, indicating that tachyzoites are ~10–200 times more sensitive than human tumor cells to SAHA in vitro. The differential sensitivity of *T. gondii* tachyzoites to scriptaid is even greater than that of SAHA. Scriptaid IC_{50} levels between 3 and 60 μM (1–20 μg/ml) reduced tumor cell proliferation in vitro (Su et al., 2000; Keen et al., 2003; Takai et al., 2006). The scriptaid IC_{50} of 39 nM for *T. gondii* tachyzoites suggests that *T. gondii* tachyzoites are 80 to 1,500 times more sensitive to scriptaid than tumor cells.

Photomicrographs comparing *T. gondii*–infected cells (Fig. 2A) or control HS68 cells after 48 hr in culture (Fig. 2B) show complete destruction of the cell monolayer by the tachyzoite infection. In contrast, when *T. gondii*–infected cells were treated with either SAHA (Fig. 2C) or scriptaid (Fig. 2D) for 48 hr, the monolayer was completely intact. The results suggest that the hydroxamic acid inhibitor treatments suppressed *T. gondii* infection and proliferation and, even 7 days later, no evidence of residual *T. gondii* appeared as plaques in the HS68 cell monolayer. No other agent tested was as effective as scriptaid or SAHA in these assays.

Careful examination of the HS68 monolayers that were treated with SAHA showed evidence of a persistent, nonproliferating intracellular *T. gondii* zoite (Fig. 2E). There were no such zoites in the scriptaid-treated cells, pointing to a possible difference in the anti–*T. gondii* activity of scriptaid and SAHA.

Low concentrations of hydroxamic acid inhibitors stimulate *T. gondii* tachyzoites

TSA, SAHA, and scriptaid had atypical effects in *T. gondii*-infected HS68 cells in experiments where very low concentrations of hydroxamic acids were tested. As seen in Figure 3, a biphasic response in the number of the tachyzoites in the medium was observed. Figure 3 is a composite of all the TSA, SAHA, and scriptaid concentration-response curves. The stimulation of tachyzoite numbers with low TSA concentrations between 1 and 50 nM was reproducible, but not statistically significant ($P > 0.05$), because the magnitude of the response was highly variable. The dramatic decrease in tachyzoite numbers with TSA concentrations >100 nM was reproducible and statistically significant ($P < 0.05$). Tachyzoites and plaque formation were reproducibly eliminated by 200 nM TSA under our experimental conditions.

There was a small, statistically insignificant increase in tachyzoite numbers in response to low concentrations of SAHA and by 1–10 nM scriptaid. The basis for the variable increase in tachyzoites in response to levels of hydroxamic acid histone deacetylase inhibitors in the range of 1–50 nM is not known. However, we observed that plaque formation never increased in response to TSA, SAHA, or scriptaid in the wells containing increased tachyzoite numbers. These findings suggest that low nM concentrations of TSA, SAHA, and scriptaid potentially stimulate *T. gondii* tachyzoite proliferation and/or survival but suppress tachyzoite infectivity.

Comparison of histone deacetylase inhibitors on *T. gondii* IC_{50} and MIC

Table I reviews the anti–*T. gondii* activity of all the histone deacetylase inhibitors we tested. The IC_{50} and MIC values re-

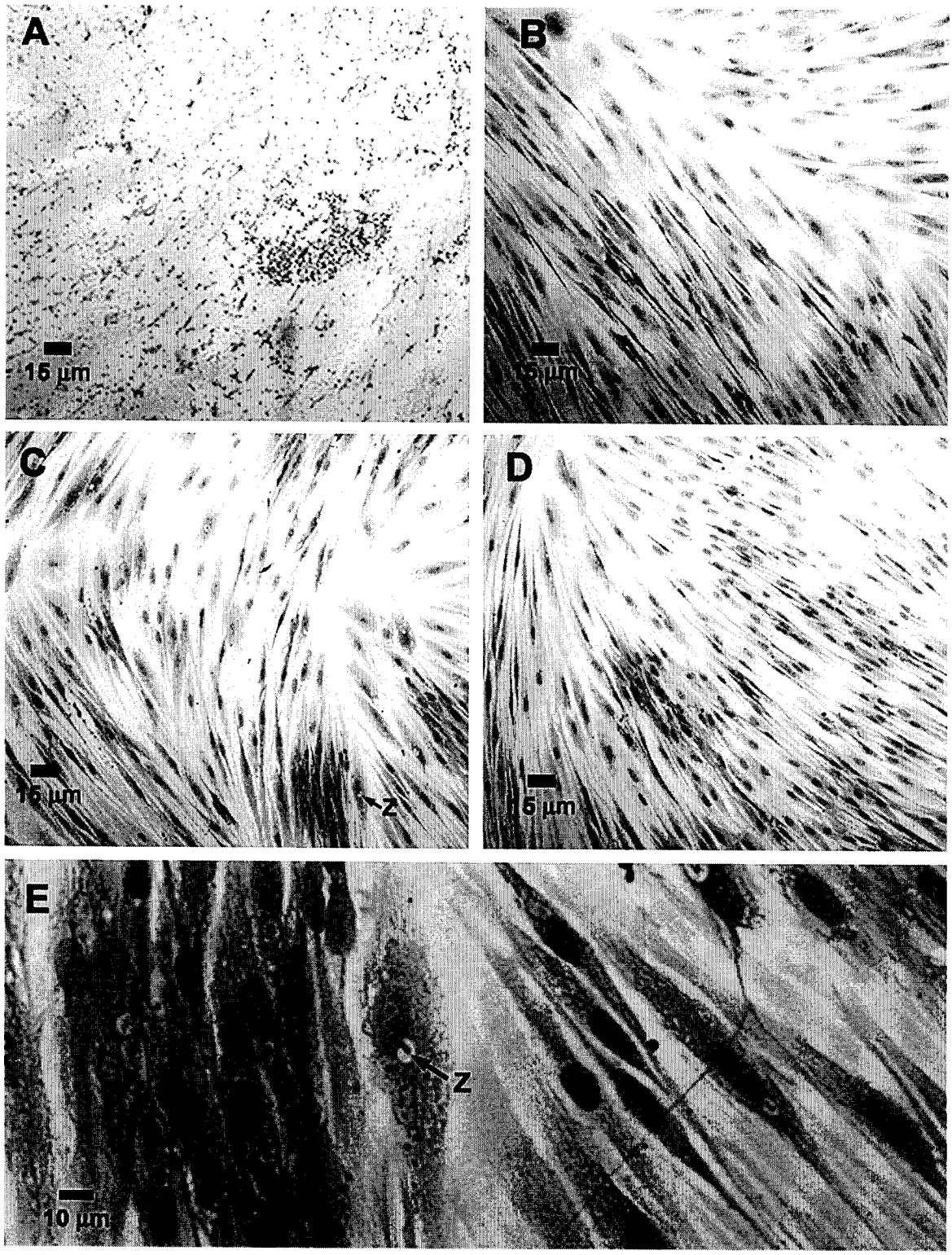

FIGURE 2. Photomicrographs of HS68 cell monolayers. (**A**) Forty-eight–hour postinfection with *T. gondii* tachyzoites (5–6 × 10^5 tachyzoites/35-mm^2 dish). (**B**) Uninfected cells. (**C**) Infected cells treated 48 hr with 1 µM SAHA. (**D**) Infected cells treated 48 hr with 1 µM scriptaid. (**E**) An enlargement of (**C**) to visualize the persistent zoite that is marked with an arrow and identified as "z."

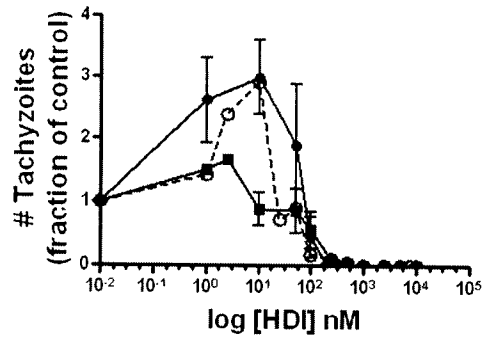

FIGURE 3. Concentration-response curves for inhibition of *T. gondii* tachyzoites by TSA (solid circles), SAHA (solid squares), and scriptaid (open circles). Data are the mean ± SEM of n = 4–5 experiments performed in triplicate. For clarity, the standard error bars for 10 nM scriptaid (± 1.9), which overlap those for TSA, were omitted.

ported in Table I specifically apply to the 48-well plate assay. Increasing or decreasing the number of tachyzoites used to infect the HS68 cells will shift the concentration-response curve to the right or left, respectively. Similarly, the MIC is dependent upon the tachyzoite numbers used in the infection, and higher inhibitor concentrations are needed to suppress plaque formation when more tachyzoites are used to infect the cells. At their MIC, the histone deacetylase inhibitors were not cytotoxic to the HS68 cells. In general, we found that the MIC for anti–*T. gondii* activity of the hydroxamic acid and carboxylate histone deacetylase inhibitors was 3–5 times higher than the respective IC_{50}.

The least potent hydroxamic acid inhibitor was SBHA. It showed good anti–*T. gondii* activity as measured by its ability to reduce tachyzoite numbers in the medium (IC_{50}), but unusually high concentrations of SBHA relative to its IC_{50} were required for suppression of plaque formation.

Carboxylate inhibitors of *T. gondii* tachyzoites

The carboxylates, sodium valproate, sodium butyrate, and 4-phenylbutyrate, are low-potency inhibitors of mammalian histone deacetylase enzymes, and we observed that all of these compounds were less potent than the hydroxamic acid inhibitors in reducing *T. gondii* tachyzoite numbers and plaque formation. The carboxylates are water soluble, and sufficiently high concentrations of all these compounds can be achieved in tissue culture to suppress *T. gondii* tachyzoite numbers and plaque formation in 48–72 hr assays. However, when experiments were extended to 5–7 days, tachyzoites appeared in the medium, eventually leading to reinfection of the cell monolayer.

DISCUSSION

Toxoplasma gondii is a widespread and significant cause of disease in humans and domesticated cats. Livestock and wildlife, including feral cats, serve as important reservoirs of the disease (Dubey and Lindsay, 2004). Antibiotics are effective treatments for the active phase of toxoplasmosis marked by rapid tachyzoite proliferation, but there is no method to eradicate the *T. gondii* bradyzoites once tissue cysts have formed (Bonfioli and Orefice, 2005). One approach to the control of *T. gondii* is to find pharmacologic agents that target tachyzoites and disrupt their conversion to bradyzoites. Histone deacetylase inhibitors exert pleiotropic effects in many cell types, and might alter survival and differentiation pathways in *T. gondii* to prevent bradyzoite formation (Saksouk et al., 2005; Sullivan and Hakimi, 2006; Verdin, 2006). The present work is focused upon the antiproliferative actions of histone deacetylase inhibitors in *T. gondii* tachyzoites.

The propagation of *T. gondii* tachyzoites in human fibroblast cells in tissue culture was fully suppressed by the hydroxamic acid histone deacetylase inhibitors, scriptaid, and SAHA. The carboxylate histone deacetylase inhibitors, sodium butyrate, sodium valproate, and 4-phenylbutyrate, displayed anti–*T. gondii* activity at higher concentrations than the hydroxamic acid inhibitors, consistent with their reduced potency for histone deacetylases. The results show that all 7 Class I/II histone deacetylase inhibitors tested reduced *T. gondii* tachyzoite numbers in HS68 fibroblast cultures, strongly implicating a role for histone deacetylase in tachyzoite survival.

We suggest that the *T. gondii* hdac3 gene product is a likely drug target contributing to the antiproliferative actions of histone deacetylase inhibitors in *T. gondii*. The RH *T. gondii* gene most closely related to human hdac3 (NM_003883.2) is the *T. gondii* hdac3 (DQ004745, AAY53803). The human hdac3 and *T. gondii* hdac3 share 83% nucleotide identity within the enzyme catalytic site and the known binding site for TSA and SAHA (Yang et al., 2002). Scriptaid and SAHA preferentially inhibit the Class I histone deacetylases, hdac1, 2, and 3; the prototypic protozoan histone deacetylase inhibitor, apicidin, is also a potent inhibitor of the Class I hdacs (Richon et al., 1998; Kwon et al., 2006). Furthermore, studies utilizing siRNA to knock down specific histone deacetylases showed that hdac1 and hdac3 are critically involved in mammalian cell growth regulation and apoptosis (Glaser et al., 2003; Wilson et al., 2006).

We now recognize that histone deacetylases control gene activation, as well as gene repression (Seto, 2006), and participate in many reactions that might impact tachyzoite proliferation and survival. Histone deacetylase inhibitors reduce expression of enzymes required for DNA synthesis (reviewed in Gabrielli, 2006), heat-shock chaperone proteins, and prosurvival proteins in mammalian cells (Takada et al., 2006). In *T. gondii*, functional inhibition of Hsp90 reduced tachyzoite invasiveness into host cells and disrupted tachyzoite proliferation within parasitophorous vacuoles (Ahn et al., 2003). These findings, as well as our results demonstrating reductions in tachyzoite numbers and protection of HS68 cells from *T. gondii* infection, implicate Hsp90 as a possible downstream target of the antiproliferative actions of SAHA and scriptaid in *T. gondii*.

Histone deacetylase inhibitors, TSA and SAHA, produce reactive oxygen species and cause DNA damage (Martirosyan et al., 2006); in tumor cells, failure of the G_2 checkpoint to halt progression of cells with damaged DNA through the cell cycle triggers apoptosis (Gabrielli, 2006). We suggest that the exquisite sensitivity of *T. gondii* tachyzoites to the hydroxamic acid histone deacetylase inhibitors might result from their high sensitivity to oxidative damage (Murray and Cohn, 1979) and the replication of *T. gondii* tachyzoites by an atypical eukaryotic cell cycle that lacks a G_2 phase (Radke et al., 2001; Khan et al., 2002).

There are additional histone deacetylases in *T. gondii* that

might critically influence tachyzoite survival or differentiation. Sullivan and Hakimi (2006) identified 5 *T. gondii* histone deacetylases in addition to hdac3, by searching the complete RH *T. gondii* genome sequence for homologs to known histone deacetylases (http://www.toxodb.org/toxo-release4-0/home.jsp) (Kissinger et al., 2003). Three of these genes are Class II histone deacetylase homologs to hdac7, 1 is a Class III Sir2 homolog, and 1 is a novel class XII gene. Clarification of the function of hdac7 in *T. gondii* biology will be important to our understanding of the therapeutic potential of histone deacetylase inhibitors in toxoplasmosis. The role of the *T. gondii* Class III Sir2 homolog is enigmatic. Although the sirtuins are known to modulate a diverse set of cellular functions in other organisms, including cell growth (reviewed in Verdin, 2006), we found that tachyzoite proliferation was unaffected by the Sir2 inhibitor, nicotinamide.

In conclusion, the sensitivity of *T. gondii* to histone deacetylase inhibitors was 1st recognized many years ago, but recent advances in drug discovery and *T. gondii* genomics have accelerated the pace of research and promise to delineate the role of histone deacetylases in toxoplasmosis and its treatment.

ACKNOWLEDGMENTS

The study was made possible by funds from a joint research state program between the Carillon Biomedical Institute, Virginia Polytechnic Institute and State University (Virginia Tech), and the University of Virginia. Christopher Reilly is supported by the Arthritis Foundation. The authors thank Aton Pharmaceuticals, Tarrytown, New York, for the gift of SAHA.

LITERATURE CITED

AHN, H.-J., S. KIM, AND H.-W. NAM. 2003. Molecular cloning of the 82-kDa heat shock protein (HSP90) of *Toxoplasma gondii* associated with the entry into and growth in host cells. Biochemical and Biophysical Research Communications **311:** 654–659.

BONFIOLI, A. A., AND F. OREFICE. 2005. Toxoplasmosis. Seminars in Opthalmology **20:** 129–141.

DARKIN-RATTRAY, S. J., A. M. GURNETT, R.W. MYERS, P. M. DULSKI, T. M. CRUMLEY, J. J. ALLOCCO, C. CANNOVA, P. T. MEINKE, S. L. COLLETTI, M. A. BEDNAREK, S. B. SINGH, M. A. GOETZ, A. W. DOMBROWSKI, J. D. POLISHOOK, AND D. M. SCHMATZ. 1996. Apicidin: A novel antiprotozoal agent that inhibits parasite histone deacetylase. Proceedings of the National Academy of Sciences USA **93:** 13143–13147.

DUBEY, J. P., D. E. HILL, J. L. JONES, A. W. HIGHTOWER, E. KIRKLAND, J. M. ROBERTS, P. L. MARCET, T. LEHMANN, M. C. B. VIANNA, K. MISKA, C. SREEKUMAR, O. C. H. KWOK, S. K. SHEN, AND H. R. GAMBLE. 2005. Prevalence of viable *Toxoplasma gondii* in beef, chicken, and pork from retail meat stores in the United States: Risk assessment to consumers. Journal of Parasitology **91:** 1082–1093.

———, AND D. S. LINDSAY. 2004. Biology of *Toxoplasma gondii* in cats and other animals. *In* World class parasites, Vol. 9, D. S. Lindsay and L. M. Weiss (eds.). Kluwer Academic, Boston, Massachusetts, p. 1–19.

FRICKER-HIDAIGO, H., J. P. BRION, M. DURAND, O. CHAVANON, M. P. BRENIER-PINCHART, AND H. PELLOUX. 2005. Disseminated toxoplasmosis with pulmonary involvement after heart transplantation. Transplantation and Infectious Disease **7:** 38–40.

FURUMAI, R., Y. KOMATSU, N. NISHINO, S. KHOCHBIN, M. YOSHIDA, AND S. HORINOUCHI. 2001. Potent histone deacetylase inhibitors built from trichostatin A and cyclic tetrapeptide antibiotics including trapoxin. Proceedings of the National Academy of Sciences USA **98:** 87–92.

GABRIELLI, B. G. 2006. Histone deacetylase inhibitors deliver their therapeutic benefit by targeting the cell cycle. *In* American Association for Cancer Research Education Book. Available: http://www.educationbook.aacrjournals.org. p. 318–321.

GLASER, K. B., J. LI, M. J. STAVER, R. Q. WEI, D. H. ALBERT, AND S. K. DAVIDSON. 2003. Role of class I and class II histone deacetylases in carcinoma cells using siRNA. Biochemical and Biophysical Research Communications **310:** 529–536.

GURVICH, N., O. M. TSYGANKOVA, J. L. MEINKOTH, AND P. S. KLEIN. 2004. Histone deacetylase is a target of valproic acid–mediated cellular differentiation. Cancer Research **64:** 1079–1086.

HU, E., E. DUL, C. M. SUNG, Z. CHEN, R. KIRKPATRICK, G. F. ZHANG, K. JOHANSON, R. LIU, A. LAGO, G. HOFMANN, R. MACARRON, M. DE LOS FRAILES, P. PEREZ, J. KRAWIEC, J. WINKLER, AND M. JAVE. 2003. Identification of novel isoform-selective inhibitors within class I histone deacetylases. Journal of Pharmacology and Experimental Therapeutics **307:** 720–728.

ITO, A., N. NISHINO, AND M. YOSHIDA. 2006. HDAC inhibitors: Discovery, development, and clinical impacts. *In* Histone deacetylases: Transcriptional regulation and other cellular functions, E. Verdin (ed.). Humana Press, Totowa, New Jersey, p. 271–297.

JONES-BRANDO, L., E. F. TORREY, AND R. YOLKEN. 2003. Drugs used in the treatment of schizophrenia and bipolar disorder inhibit the replication of *Toxoplasma gondii*. Schizophrenia Research **62:** 237–244.

KEEN, J. C., L. YAN, K. M. MACK, C. PETTIT, D. SMITH, D. SHARMA, AND N. E. DAVIDSON. 2003. A novel histone deacetylase inhibitor: Scriptaid, enhances expression of functional estrogen receptor α (ER) in ER negative human breast cancer cells in combination with 5-aza 2′-deoxycytidine. Breast Cancer Research and Treatment **81:** 177–186.

KELLY, W. K., O. A. O'CONNOR, L. M. KRUG, J. H. CHIAO, M. HEANEY, T. CURLEY, B. MACGREGORE-CORTELLI, W. TONG, J. P. SECRIST, L. SCHWARTZ, S. RICHARDSON, E. CHU, S. OLGAC, P. A. MARKS, H. SCHER, AND V. M. RICHON. 2005. Phase I study of an oral histone deacetylase inhibitor, suberoylanilide hydroxamic acid, in patients with advanced cancer. Journal of Clinical Oncology **23:** 3923–3931.

KHAN, F. J. T., C.-L. QIN, AND K. KIM. 2002. Cyclin-dependent kinase TPK2 is a critical cell cycle regulator in *Toxoplasma gondii*. Molecular Microbiology **45:** 321–332.

KISSINGER, J. C., B. GAJRIA, L. LI, T. PAULSEN, AND D. S. ROOS. 2003. ToxoDB: accessing the *Toxoplasma gondii* genome. Nucleic Acids Research **31:** 234–236.

KOMATSU, N., N. KAWAMATA, S. TAKEUCHI, D. YIN, W. CHIEN, C. W. MILLER, AND H. P. KOEFFLER. 2006. SAHA, a HDAC inhibitor, has profound anti-growth activity against non-small cell lung cancer cells. Oncology Reports **15:** 187–191.

KWON, P., M. HSU, D. COHEN, AND P. ATADJA. 2006. HDAC inhibitors: An emerging anticancer therapeutic strategy. *In* Histone deacetylases, transcriptional regulation and other cellular functions, E. Verdin (ed.). Humana Press, Totowa, New Jersey, p. 315–332.

MARTIROSYAN A., S. LEONARD, X. SHI, B. GRIFFITH, P. GANNETT, AND J. STROBL. 2006. Actions of a histone deacetylase inhibitor NSC3853 (5-nitroso-8-quinolinol) links reactive oxygen species to cell differentiation and apoptosis in MCF-7 human mammary tumor cells. Journal of Pharmacology and Experimental Therapeutics **317:** 546–552.

MCALLISTER, M. M. 2005. A decade of discoveries in veterinary protozoology changes our concept of "subclinical" toxoplasmosis. Veterinary Parasitology **132:** 241–247.

MORADEI, O., C. R. MAROUN, I. PAQUIN, AND A. VAISBURG. 2005. Histone deacetylase inhibitors: Latest developments, trends and prospects. Current Medical Chemistry of Anti-Cancer Agents **5:** 529–560.

MURRAY, H. W., AND Z. A. COHN. 1979. Macrophage oxygen-dependent antimicrobial activity. I. Susceptibility of *Toxoplasma gondii* to oxygen intermediates. Journal of Experimental Medicine **150:** 938–949.

O'CONNOR, O. A., M. L. HEANEY, L. SCHWARTZ, S. RICHARDSON, R. WILLIM, B. MACGREGOR-CORTELLI, T. CURLY, C. MOSKOWITZ, C. PORTLOCK, S. HORWITZ, A. D. ZELENETZ, S. FRANKEL, V. RICHON, P. MARKS, AND W. K. KELLY. 2006. Clinical experience with intravenous and oral formulations of the novel histone deacetylase inhibitor suberoylanilide hydroxamic acid in patients with advanced hematologic malignancies. Journal of Clinical Oncology **24:** 166–173.

RADKE, J. R., B. STRIEPEN, M. N. GUERINI, M. E. JEROME, D. S. ROOS, AND M. W. WHITE. 2001. Defining the cell cycle for the tachyzoite stage of *Toxoplasma gondii*. Molecular and Biochemical Parasitology **115:** 165–175.

RICHON, V. M., S. EMILIANI, E. VERDIN, Y. WEBB, R. BRESLOW, R. A. RIFKIND, AND P. A. MARKS. 1998. A class of hybrid polar inducers of transformed cell differentiation inhibits histone deacetylases. Proceedings of the National Academy of Sciences USA **95:** 3003–3007.

SAKSOUK, N., M. M. BHATTI, S. KIEFFER, A. T. SMITH, K. MUSSET, J. GARIN, W. J. SULLIVAN, JR., M.-F. CESBRON-DELAUW, AND M.-A. HAKIMI. 2005. Histone-modifying complexes regulate gene expression pertinent to the differentiation of the protozoan parasite *Toxoplasma gondii*. Molecular and Cellular Biology **25:** 10301–10314.

SAUVE, A. A., C. WOLBERGER, V. L. SCHRAMM, AND J. D. BOEKE. 2006. The biochemistry of sirtuins. Annual Review of Biochemistry **75:** 435–465.

SETO, E. 2006. The biology of HDAC3. *In* Histone deacetylases: Transcriptional regulation and other cellular functions, E. Verdin (ed.). Humana Press, Totowa, New Jersey, p. 61–86.

SONNEMANN, J., J. GANGE, S. PILZ, C. STOZER, R. OHLINGER, A. BELAU, G. LORENZ, AND J. F. BECK. 2006. Comparative evaluation of the treatment efficacy of suberoylanilide hydroxamic acid (SAHA) and paclitaxel in ovarian cancer cell lines and primary ovarian cancer cells from patients. BMC Cancer **6:** 183 (Epub).

SU, G. H., T. A. SOHN, B. RYU, AND S. E. KERN. 2000. A novel histone deacetylase inhibitor identified by high-throughput transcriptional screening of a compound library. Cancer Research **60:** 3137–3142.

SULLIVAN, W. J., JR., AND M. A. HAKIMI. 2006. Histone mediated gene activation in *Toxoplasma gondii*. Molecular and Biochemical Parasitology **148:** 109–116.

SUZUKI, T., AND N. MIYATE. 2005. Non-hydroxamate histone deacetylase inhibitors. Current Medical Chemistry **12:** 2867–2880.

TAKADA, Y., A. GILLENWATER, H. ICHIKAWA, AND B. B. AGGARWAL. 2006. Suberoylanilide hydroxamic acid potentiates apoptosis, inhibits invasion, and abolishes osteoclastogenesis by suppressing nuclear factor kappaB activation. Journal of Biological Chemistry **281:** 5612–5622.

TAKAI, N., T. UEDA, M. NISHIDA, K. NASU, AND H. NARAHAR. 2006. A novel histone deacetylase inhibitor, scriptaid, induces growth inhibition, cell cycle arrest and apoptosis in human endometrial cancer and ovarian cancer cells. International Journal of Molecular Medicine **17:** 323–329.

VERDIN, E. 2006. Histone deacetylases: Transcriptional regulation and other cellular functions. Humana Press, Totowa, New Jersey.

WILSON, A. J., D. S. BYUN, N. POPOVA, L. B. MURRAY, K. L'ITALLEN, Y. SOWA, D. ARANGO, A. VELCICH, L. H. AUGENLICHT, AND J. M. MARIADASON. 2006. Histone deacetylase 3 (HDAC3) and other class I HDACs regulate colon cell maturation and p21 expression and are deregulated in human colon cancer. Journal of Biological Chemistry **281:** 13548–13558.

YANG, W. M., S. C. TSAI, Y. D. WEN, G. FEJER, AND E. SETO. 2002. Functional domains of histone deacetylase-3. Journal of Biological Chemistry **277:** 9447–9454.

ZHANG, C., V. RICHON, X. NI, R. TALPUR, AND M. DUVIC. 2005. Selective induction of apoptosis by histone deacetylase inhibitor SAHA in cutaneous T-cell lymphoma cells: Relevance to mechanism of therapeutic action. Journal of Investigative Dermatology **125:** 1045–1052.

Antitumor histone deacetylase inhibitors suppress cutaneous radiation syndrome: Implications for increasing therapeutic gain in cancer radiotherapy

Yih-Lin Chung,[1] Ae-June Wang,[2] and Lin-Fen Yao[2]

[1]Department of Radiation Oncology, Koo Foundation Sun Yat-Sen Cancer Center, and School of Medicine, National Yang-Ming University, Taipei, Taiwan, Republic of China and [2]Drug Delivery Department, Biochemical Engineering Center, Industrial Technology Research Institute, Hsinchu, Taiwan, Republic of China

Abstract

Radiotherapy is an effective treatment for head and neck, skin, anogenital, and breast cancers. However, radiation-induced skin morbidity limits the therapeutic benefits. A low-toxicity approach to selectively reduce skin morbidity without compromising tumor killing by radiotherapy is needed. We found that the antitumor agents known as histone deacetylase (HDAC) inhibitors (phenylbutyrate, trichostatin A, and valproic acid) could suppress cutaneous radiation syndrome. The effects of HDAC inhibitors in promoting the healing of wounds caused by radiation and in decreasing later skin fibrosis and tumorigenesis were correlated with suppression of the aberrant expression of radiation-induced transforming growth factor β and tumor necrosis factor α. Our findings implicate that the inhibition of HDAC may provide a novel strategy to increase the therapeutic gain in cancer radiotherapy by not only inhibiting tumor growth but also protecting normal tissues. [Mol Cancer Ther. 2004;3(3):317–325]

Introduction

Radiotherapy is an effective modality for head and neck, breast, skin, and anogenital cancers. However, its therapeutic benefit is limited by radiation-induced skin injuries or cutaneous radiation syndrome (CRS), which includes acute reactions of swelling, dermatitis, desquamation, and ulceration, and long-term effects of fibrosis, necrosis, and the development of life-threatening sequelae of sarcoma, squamous, and basal cell carcinoma (1, 2). In fact, the skin is affected in every form of the external radiotherapy of internal organs. The topical application of steroidal or nonsteroidal anti-inflammatories is the most common treatment for CRS, yet the results are unsatisfactory. An approach to selectively reduce skin morbidity without compromising the tumor-killing effects of radiotherapy is a long-sought goal in radiation oncology.

After radiation injury, the release of cytokines [such as tumor necrosis factor (TNF-α)] and growth factors [such as transforming growth factor (TGF-β)] in irradiated tissues perpetuates and augments the inflammatory response, while promoting fibroblast recruitment and proliferation but inhibiting epithelial cell growth (3–10). The amplified injury response to radiation by the persistent secretion of TNF-α and TGF-β from epithelial, endothelial, and connective tissue cells, which is possibly caused by a modification in the genetic programming of cell differentiation and proliferation, leads to the histological modifications that characterize CRS (11–14). The chronic activation of TGF-β pathway also stimulates late tumorigenesis (15, 16). Thus, CRS and radiation-induced carcinogenesis could be regarded as a genetic disorder of the wound healing process after radiation exposure. This prompted us to propose whether there is a gene modulator that can simultaneously both reverse the skewed expression of TNF-α and TGF-β in irradiated skin and modulate the oncogenes or tumor suppressors in tumor cells.

A class compound of gene modulators, histone deacetylase (HDAC) inhibitors, such as short-chain fatty acids (phenylbutyrate and valproic acid) and hydroxamic acids (trichostatin A), activates and represses a subset of genes by remodeling the chromatin structure via the altered status in histone acetylation (17, 18). Histone hyperacetylation results in the up-regulation of cell-cycle inhibitors ($p21^{Cip1}$, $p27^{Kip1}$, and $p16^{INK4}$), the down-regulation of oncogenes (*Myc* and *Bcl*-2), the repression of inflammatory cytokines [interleukin (IL)-1, IL-8, TNF-α, and TGF-β], or no change [glyceraldehyde-3-phosphate dehydrogenase (GAPDH) and γ-actin] (17–27). HDAC inhibitors have exhibited properties in inducing cell-cycle arrest, cell differentiation, and apoptotic cell death in tumor cells and in decreasing inflammation and fibrosis in inflammatory diseases (17–32). Although the effects of HDAC inhibitors induce bulk histone acetylation, they result in apoptotic cell death, terminal differentiation, and growth arrest in tumor cells but no toxicity in normal cells (17, 21, 22, 33). In addition, the modulation of chromatin conformation by HDAC inhibitors can further radiosensitize tumors, the cells of which are intrinsically radioresistant (34–36).

Thus, on the basis of the potential possibility in simultaneously, coordinately, selectively, and epigenetically manipulating the expression of tumor suppressors, oncogenes, proinflammatory cytokines (TNF-α), and fibrogenic growth factors (TGF-β) by differentially remodeling the chromatins in normal and tumor cells, the use of HDAC

Received 8/8/03; revised 11/24/03; accepted 12/15/03.

The costs of publication of this article were defrayed in part by the payment of page charges. This article must therefore be hereby marked advertisement in accordance with 18 U.S.C. Section 1734 solely to indicate this fact.

Requests for Reprints: Yih-Lin Chung, Department of Radiation Oncology, Koo Foundation Sun Yat-Sen Cancer Center, No.125, Lih-Der Road, Pei-tou district, Taipei 112, Taiwan, Republic of China. Phone: 886-2-28970011 ext. 1306; Fax: 886-2-27020372. E-mail: ylchung@mail.kfcc.org.tw

inhibitors as topical agents to prevent systemic reactions warrants study, to test whether they can decrease radiation-induced skin damage and still exhibit antitumor effects. The present study may provide a novel strategy to maximize the therapeutic effectiveness of cancer radiotherapy.

Materials and Methods

Topical Drug Formulations and Preparation

The preparation of the topical HDAC inhibitors has been described elsewhere (37). In brief, different ratios of various amounts of sodium phenylbutyrate (Triple Crown America, Perkasie, PA), valproic acid (Sigma Chemical Co., St. Louis, MO) or trichostatin A (Sigma), white petrolatum, cetyl alcohol, paraffin, tefose, superpolystate, methylparaben, propylparaben, deionized water, Coster 5000, and Myriyol (all from Merck & Co., Whitehouse Station, NJ) were mixed, stirred at 400 rpm for 5 min at 70°C to form a paste, and then cooled at room temperature. Tests for skin permeation (using skin purchased from Ohio Valley Tissue & Skin Center, Cincinnati, OH), drug stability, skin irritation, and shelf life were performed at the Drug Delivery Department, Biochemical Engineering Center, Industrial Technology Research Institute, Hsinchu, Taiwan. Only the formulations with good stability, high skin penetration, low skin irritation, and long shelf life were selected for the study.

Generation of CRS, Treatment, and Evaluation of Skin Reactions

Skin over the gluteal area as large as 2 cm × 2 cm of adult female Sprague-Dawley rats weighing 150–175 g were irradiated by an electron beam with 6 MeV of energy on day 0 at 4 Gy/min up to 40 Gy to the prepared area after the rats were anesthetized. Vehicle, Vaseline (a negative control), madecassol (a positive control), or different HDAC inhibitors were applied topically at a dose of 200 mg/irradiated skin surface twice per day from Day 1 to Day 90. Acute skin reactions were evaluated and scored through 90 days after irradiation using the modified skin score system proposed elsewhere as follows: 0, normal; 0.5, slight epilation; 1.0, epilation in about 50% of the radiated area; 1.5, epilation in more than 50% of the area; 2.0, complete epilation; 2.5, dry desquamation in more than 50% of the area; 3.0, moist desquamation in a small area; and 3.5, moist desquamation in most of the area. Each point represents the mean of skin scores from five samples in the same group (38). Irradiated skins were subjected to RNase protection assays at the indicated times. After 90 days, skin reactions were evaluated by hematoxylin and eosin (H&E) histological testing, immunohistochemistry, and immunofluorescence. All experimental and surgical procedures performed on rats and mice were in accordance with the NIH guidelines outlined in the *Guide for Care and Use of Laboratory Animals* (NIH publication 85-23).

RNase Protection Assay

Levels of TGF-β1, TGF-β2, TGF-β3, and TNF-α mRNA were assessed using a multiple cytokine RNase protection assay kit (Riboquant; PharMingen, San Diego, CA) that contained a template set to allow for the generation of a ^{32}P-labeled antisense RNA probe set that hybridized with the target mRNA for TGF-β1, TGF-β2, TGF-β3, TNF-α, and internal control GAPDH. After hybridization of labeled probe to target RNA, unprotected RNA was digested by an RNase, and protected RNA fragments were resolved on a 6% polyacrylamide gel and recorded by phosphorimaging (Molecular Dynamics Corp., Sunnyvale, CA). Densitometry was used to quantify the amount of each mRNA species and was normalized to the internal control GAPDH.

Statistical Analysis

The means of skin scores for skin reactions from five rats in each group were calculated. The average levels of cytokine/growth factor mRNA from three skin samples in each group were normalized to the internal control GAPDH and expressed as a ratio to the average level in time-matched control groups. The Mann-Whitney test (Stata Statistical Software, College Station, TX) was used to determine statistical significance at the $P < 0.05$ level for differences in average skin scores and in average mRNA levels, respectively, between treated and control rats.

Histological, Immunohistochemical, and Immunofluorescence Tests

The samples were fixed in 10% formalin-buffered solution and embedded in paraffin wax. Serial 3-μm sections were cut, dewaxed, and stained with H&E-safranin. For immunohistochemical analyses, the paraffin sections were deparaffinized by xylene and rehydrated by sequential concentrated alcohols. The slides were subjected to microwave antigen retrieval (800 W, twice for 5 min each) in 0.01 M sodium citrate buffer (pH 6.0). The endogenous hydrogen peroxidase activity was blocked by 3% H_2O_2 for 10 min. The slides were incubated with a protein-blocking agent (Dako, Glostrup, Denmark) for 20 min and then treated with the rabbit polyclonal anti-TNF-α antibody (Santa Cruz Biotechnology, Santa Cruz, CA) for 1 h at room temperature, followed by the secondary anti-rabbit antibody incubation for 30 min, and then they were washed with PBS three times. The peroxidase reaction was visualized using AEC (3% 3-amino-9-ethylcarbazole in *N,N*-dimethylformamide) as chromagen for 3–10 min, and then the slides were counterstained with Mayer's hematoxylin and mounted. Because inflamed skin tends to bind antibodies nonspecifically, we also used an isotype-matched normal antibody as a control, to confirm positive TNF-α staining in the skin wound. For immunofluorescence analyses, the paraffin sections were treated using the same protocol as those for immunohistochemical testing, except for the use of primary goat anti-acetylated histone H3 and rabbit anti-TGF-β1 and TGF-β2 antibodies (all from Santa Cruz Biotechnology), and the secondary rhodamine-conjugated (red) anti-goat (Jackson ImmunoResearch, West Grove, PA) and FITC-labeled (green) anti-rabbit antibodies (Dako).

Northern Blot Assay

Total RNA was isolated from frozen skin samples using Trigent (Molecular Research Center Inc., Cincinnati, OH). Total RNA (30 μg) was electrophoresed in a

denaturing formaldehyde-agarose gel, blotted onto Hybond N (Amersham, Amersham, United Kingdom), and fixed by UV irradiation. The membrane was incubated with ^{32}P-labeled probes, as described below, in Rapid-hyb buffer (Amersham). To prepare probes for rat TGF-β1 and TGF-β2, their full-length coding sequences were amplified by reverse-transcription PCR using specific forward (TGF-β1, 5′-CGGGTGGCAGGCGAGAGC-3′ and TGF-β2, 5′-CATGCACTACTGTGTGCT-3′) and reverse (TGF-β1, 5′-GGAATTGTTGCTATATTTCTGC-3′ and TGF-β2, 5′-CCGAGGACTTTAGCTGCA-3′) primers. A template set of TNF-α and GAPDH from the RNase protection assay kit (Riboquant; PharMingen) was used to generate ^{32}P-labeled antisense RNA probes that hybridized with the mRNA for TNF-α and GAPDH.

Western Blot Assay

For the analysis of acetylated histones, collected irradiated skins, treated with or without phenylbutyrate were digested with 5 mg/ml collagenase (Sigma) and 1.5 mg/ml DNase (Sigma) and were passed through a wire mesh to prepare isolated cells. Nuclei were then isolated by lysis of the cells in a buffer that contained 10 mM Tris-HCl (pH 6.5), 50 mM sodium bisulfite, 1% Triton X-100, 10 mM $MgCl_2$, and 8.6% sucrose and a Dounce homogenizer was used. Histones were isolated by means of acid extraction, as described elsewhere (39). Isolated histones (5 μg) were then separated in 15% polyacrylamide-0.1% SDS minigels (Bio-Rad, Hercules, CA) and transferred to nitrocellular filters. The acetylated histones H3 were detected with anti-acetylated histone H3 (Santa Cruz Biotechnology). For analysis of $p21^{Cip1}$ in the cultured tumor cells treated with or without phenylbutyrate, cells were rinsed twice with PBS without Mg^{2+} and Ca^{2+} [PBS(−)] and lysed with PBS(−) supplemented with 1% NP40, 0.5% sodium deoxycholate, 0.1% SDS, 100 μg/ml phenylmethylsulfonyl fluoride, 3 trypsin inhibitor units/ml aprotinin, and 1 mM sodium orthovanadate (Sigma). The lysate was gently rotated for 60 min at 4°C and centrifuged at 15,000 × *g* for 30 min at 4°C. The supernatant, which contained 100 μg of proteins, was electrophoresed in 10% SDS-polyacrylamide gel and blotted onto polyvinylidene difluoride membranes (Millipore, Bedford, MA). The amount of $p21^{Cip1}$ was detected with the primary mouse monoclonal antibody $p21^{Cip1}$ (Santa Cruz Biotechnology) for 16 h at 4°C. The membranes were then incubated with the peroxidase-labeled secondary anti-mouse antibody (Amersham) for 1 h at room temperature. The membranes were rinsed, treated with enhanced chemiluminescent reagent (Amersham), and exposed to films.

Generation of Cutaneous Tumor Models and Treatment

The syngeneic carcinoma cells 1MEA7R.1 and CT-26 (purchased from American Type Culture Collection, Manassas, VA) were s.c. injected into the flank areas of female BALB/c mice. The tumor was allowed to a maximum dimension of 0.5 cm. Topical HDAC inhibitors or vehicle were applied at a dose of 200 mg/mouse to cover the whole tumor surface and surrounding skin twice per day for 4 weeks. The tumor size was calculated weekly with a caliper according to the formula $ab^2/2$, where *a* and *b* are the larger and smaller diameters (in centimeters), respectively.

Results

Topical Phenylbutyrate Treatment Induces Histone Hyperacetylation

Among the known HDAC inhibitors, phenylbutyrate, which is a natural low-toxic aromatic fatty acid purified from mammalian urine and plasma, has been approved by the US Food and Drug Administration for the treatment of inherited genetic diseases and malignancies (40–44). We prepared several topical formulations of phenylbutyrate to increase local concentrations, because a plasma level of phenylbutyrate above 0.5 mM (the minimal dose to induce histone hyperacetylation and antitumor effects) is difficult to maintain via the oral or i.v. routes (37, 45, 46). Among the different formulations, the phenylbutyrate cream (Tric- 02-3), which showed good stability, low rates of skin irritation, a long shelf life, and a high rate of skin penetration, was selected for the present study (37) (Fig. 1A). To determine what dosage of topical phenylbutyrate was suitable to treat irradiated skin, we used the amount of histone hyperacetylation in the nucleus as a marker to demonstrate the extent of drug penetration and to indicate whether the local drug concentration was enough to exert biological effects. Western blot analysis for acetylated histones in the irradiated skin 6 h after irradiation (40 Gy single fraction) showed that the acetylated form of histone H3 was mildly increased in the control and vehicle-treated groups but was markedly increased with the topical treatment of 1% phenylbutyrate cream at a dose of 200 mg/irradiated skin surface given immediately after irradiation (Fig. 1B). Immunofluorescence staining further demonstrated that histone hyperacetylation in irradiated skin was visually evident deep in the s.c. layer at 6 h after drug treatment (*i.e.*, coincident with the peak of the drug concentration in the skin test) (Fig. 1, A and C).

Topical Phenylbutyrate Treatment Suppresses CRS

The acute skin reaction after irradiation was scored to grade toxicity in five animals in each group receiving vehicle, phenylbutyrate, madecassol (a steroid-positive control), or Vaseline (a negative control) from Day 1 to Day 90 (Fig. 2). The skin score increased with a more severe skin reaction. The skin reactions in the phenylbutyrate group tended to be less marked than those in other groups. Transient skin erythema was noted within hours to the first 2 days in all groups. Depilation of the epidermis appeared earlier (at Day 5) in the phenylbutyrate group, but the scores in the Vaseline and vehicle control groups were higher within 11 days. By Day 21, the Vaseline and vehicle groups had progressed to wet desquamation in most areas, whereas in the madecassol and phenylbutyrate groups, wound healing in the epithelium had begun quickly.

After 90 days, the long-term effects of radiation in the skin were evaluated by histological testing. At Day 180, skin samples taken from the phenylbutyrate group showed

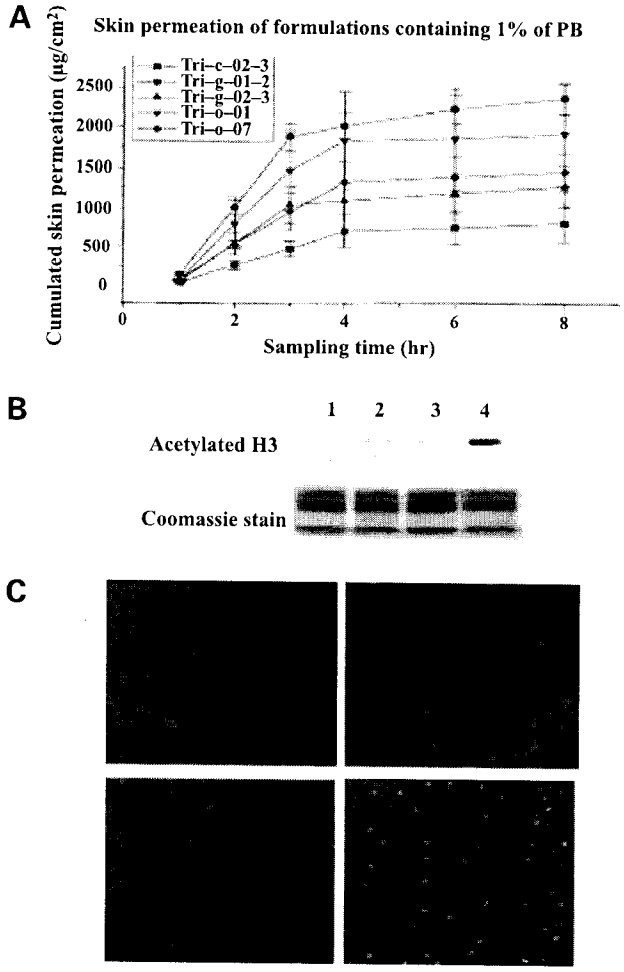

Figure 1. Induction of histone hyperacetylation in skin. **A,** pharmacokinetic studies of delivery of different phenylbutyrate formulations through the skin. Among them, the 1% phenylbutyrate (*PB*) cream (*Tri-c-02-3*) was used because of its stability and long shelf life. **B,** Western blot analysis for acetylated H3 in the irradiated skin (40 Gy single fraction) treated with or without phenylbutyrate cream for 6 h after irradiation. The Coomassie blue-stained gel sections demonstrate the equivalence of protein loading. *Lane 1,* normal skin without irradiation; *lane 2,* irradiated skin without any treatment; *lane 3,* irradiated skin treated with the vehicle; *lane 4,* irradiated skin treated with 1% phenylbutyrate cream. **C,** immunofluorescence staining of acetylated H3 in the irradiated skin treated with or without phenylbutyrate cream for 6 h after irradiation. The acetylated H3 in the nuclei was used as marker indicating the extent of drug penetration. *Left upper panel,* irradiated skin without any treatment; *right upper panel,* normal skin without irradiation; *left lower panel,* irradiated skin treated with 1% phenylbutyrate cream; and *right lower panel,* irradiated skin treated with the vehicle.

soft characteristics and less capillary bleeding, whereas skin samples taken from the vehicle group exhibited rigid characters and easily oozing. Histological sections were examined to provide a qualitative description of group differences in reepithelialization after irradiation and in the development of the dermal fibrosis (Fig. 3). The histology in the phenylbutyrate group at Day 180 showed a thicker epidermis with 10–30 cell layers, less subepithelial swelling, a thinner dermis with less collagen deposition, and few skin appendages, compared with the histological results in the vehicle group at Day 180 and with the control groups of normal skin and acute reaction at Day 7. These observations suggest that phenylbutyrate promotes epithelial healing in early radiation-induced skin damage and inhibits late, radiation-related proliferative dermal fibrosis.

Changes in Radiation-Induced Histology after Topical Phenylbutyrate Treatment Correlate with Suppression in Inflammatory and Fibrogenic Cytokine Expressions

Because the development of CRS has been attributed to radiation-induced temporal changes and the persistent up-regulation of proinflammatory cytokines such as TNF-α and fibrogenic growth factors such as TGF-β1 and β2(3–16), we next studied whether the suppression of CRS development by the topical phenylbutyrate treatment is correlated with the suppression of TNF-α and TGF-β.

The timing of the peak appearance of TGF-β1, TGF-β2, and TNF-α expression levels induced by radiation correlated with the progression in CRS development in all experimental groups (Figs. 2–Figs. 4). In the phenylbutyrate group, the highest surge of TGF-β1, TGF-β2, and TNF-α appeared at 6 h after irradiation, but levels were subsequently suppressed after Day 14. The suppression still persisted at 12 months, even when topical phenylbutyrate treatment was discontinued at Day 90. In the Vaseline and vehicle control groups, mRNA levels of TGF-β1, TGF-β2, and TNF-α in the irradiated skin increased and fluctuated above the nonirradiated control levels over a period of 1 year and reached the first peak of 2- and 3-fold above the nonirradiated control levels at 6 h after irradiation, the second peak of 10.5- to 16-fold around 14–28 days after irradiation, and the third peak of 13- to 14-fold at 9 months after irradiation; levels then declined to 2- to 3-fold normal levels by 12 months after irradiation. Although the mRNA levels of TGF-β1, TGF-β2, and TNF-α at the first peak at 6 h in the phenylbutyrate group were higher than those in the Vaseline and vehicle control groups, they decreased to the levels lower than those in the Vaseline and vehicle groups at Day 14 and returned to the nonirradiated control levels at Day 28–35.

TGF-β1 and TGF-β2 have similar cellular effects in inhibiting epithelial cell growth and promoting dermal

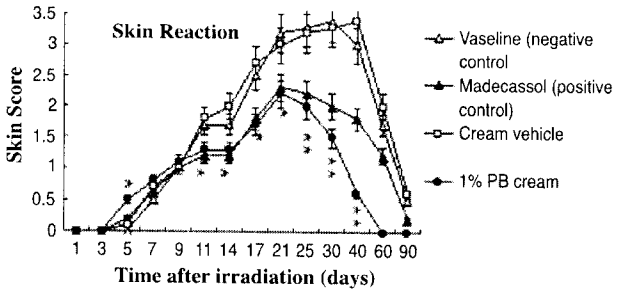

Figure 2. Evaluation of acute skin reactions after irradiation. Time course of the average skin score for the acute skin reaction after irradiation from Day 1 to Day 90. The skin score increases with more severe skin reaction. *, $P < 0.05$; **, $P < 0.001$, in comparison with the phenylbutyrate (*PB*)-treated and vehicle groups.

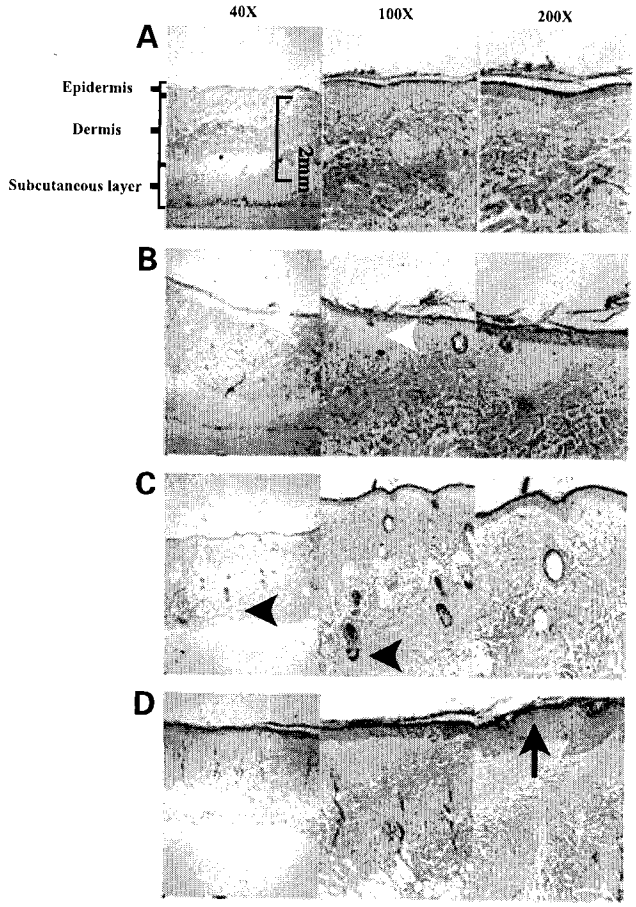

Figure 3. Histology of reaction after irradiation. Histological analysis by H&E stain of the skin damage. The histology in the phenylbutyrate-treated group at Day 180 (**D**) after skin irradiation showed thicker epidermis with 10–30 cell layers (*black arrow*), less subepithelial swelling, a thinner dermis with less collagen deposition, and few skin appendages compared with the histology in the vehicle group at Day 180 (**C**) and the control groups of normal skin at Day 0 (**A**) and acute reaction at Day 7 (**B**). The *black arrowheads* indicate that the s.c. fat layer in the vehicle group (**C**) was replaced by fibrous tissues and appendages. The *white arrowheads* indicate subepithelial swelling in the acute reaction group at Day 7 (**B**).

fibroblast proliferation, but TGF-β3 has the opposite effect (4, 10). Thus, we also studied the level change of TGF-β3 mRNA and found that it exhibited a slightly transient increase of 2-fold in all irradiated groups at 14 days then progressively decrease to the nonirradiated control level or lower. No significant differences in TGF-β3 mRNA levels were observed between the irradiated groups treated with Vaseline, vehicle, or phenylbutyrate.

Immunofluorescence staining further confirmed that TGF-β1 and β2 proteins were predominately present in the keratinocytes of the thinner epidermis and in myofibroblasts of the proliferative thicker dermis in the vehicle group, whereas the amount of TGF-β1 and β2 protein was low in both the thicker epidermis and the thinner dermis in the phenylbutyrate group, compared with the staining pattern in normal skin (Fig. 5).

Moreover, at Day 270, three of five rats in the Vaseline group and four of five rats in the vehicle group, compared with zero of five rats in the phenylbutyrate-treated group, showed chronic ulceration, necrosis, bullae formation, and inflammatory cell infiltration. The decrease in late radiation-induced skin damage by topical phenylbutyrate was consistent with the suppression of TNF-α expression (Fig. 6).

Topical Phenylbutyrate Treatment Both Prevents Late Radiation-Induced Skin Tumor Formation and Exhibits a Direct Antitumor Effect on Cutaneous Tumor Growth

Many studies have demonstrated that the chronic overexpression of TGF-β stimulates neoplastic growth (8, 15). Thus, the decrease of TGF-β expression caused by phenylbutyrate treatment might decrease the incidence of late radiation-induced tumorigenesis. We found that newly developed skin or cutaneous tumors increased with time after 50 weeks in the control group that did not receive phenylbutyrate treatment, but no tumors developed in the phenylbutyrate-treated group (Fig. 7). At 90 weeks, a cumulative tumor incident of 15% (6 of 39) was observed in the irradiated group without phenylbutyrate treatment, compared with 0% (0 of 42) in the irradiated groups with phenylbutyrate treatment. The histology of radiation-induced tumors included fibroma, spindle cell carcoma, basal cell carcinoma, and squamous cell carcinoma.

The topical phenylbutyrate formulation was further tested to assess whether it retained its antitumor effects. BNL 1MEA7R.1 and CT-26 carcinoma cells, which showed growth inhibition by phenylbutyrate *in vitro* by the up-regulation of $p21^{Cip1}$ (Fig. 8A), were inoculated into the back of syngeneic mice. Cutaneous tumors were allowed to grow to the largest dimension 0.5 cm, and phenylbutyrate was topically applied to the tumor surface at 200 mg/mouse twice per day. By 4 weeks, the tumor sizes of 1MEA7R.1 and CT-26 carcinomas in the placebo groups were almost 6- and 1.6-fold larger than those in the phenylbutyrate-treated groups, respectively (Fig. 8B). Cutaneous tumors in the phenylbutyrate-treated groups grew slowly, without skin ulceration, whereas tumors in the control or placebo group grew rapidly and showed a necrotic appearance and skin ulceration (Fig. 8C). After 5 weeks of treatment, withdrawal of topical phenylbutyrate resulted in a loss of tumor growth inhibition, and these tumors then reached the same size as those in the control or placebo groups within 2 weeks.

Similar Effects of Other Structurally Unrelated Antitumor HDAC Inhibitors in Treating CRS

In addition to phenylbutyrate, other structurally unrelated antitumor HDAC inhibitors, such as trichostatin A (an antifungal agent) and valproic acid (an antiseizure agent), also ameliorated the development of CRS and decreased the radiation-induced TGF-β1, TGF-β2, and TNF-α expression (Fig. 9, A and B).

Discussion

Although previous studies have demonstrated that HDAC inhibitors have effects in modulating multiple genes to

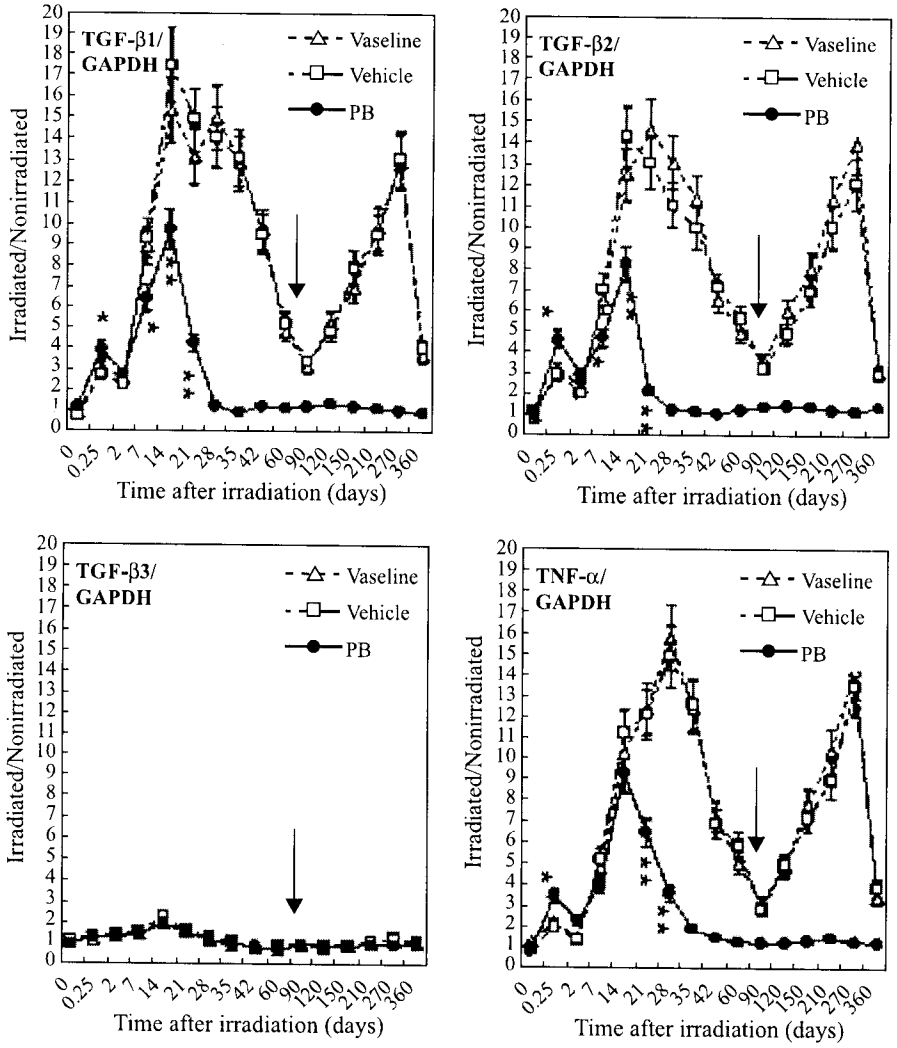

Figure 4. Expression levels of TGF-β and TNF-α after irradiation. Temporal variation in mRNA levels of TGF-β1, TGF-β2, TGF-β3, and TNF-α in skin after irradiation, normalized to the internal control GAPDH, and expressed as a ratio to levels in nonirradiated control samples. *Points,* mean of mRNA levels of five samples in the same group of Vaseline, vehicle, or phenylbutyrate (*PB*). The *arrow* indicates that the drug treatment was discontinued after Day 90 (*, $P < 0.05$; **, $P < 0.001$, in comparison with the phenylbutyrate-treated and vehicle groups).

inhibit tumor growth, reducing lipopolysaccharide induced circulating cytokines, affecting cytokine production to attenuate concanavalin A-induced hepatic injury, and reversing skewed cytokine expression in autoimmune inflammatory diseases (17, 18, 24, 26, 27), the present study appears to be the first to examine the cytokine- or gene-modulatory effects of the inhibition of HDAC in CRS and radiation-induced tumorigenesis. By virtue of reducing the levels of radiation-induced cytokines such as TNF-α and TGF-β, we found that HDAC inhibitors could be candidates

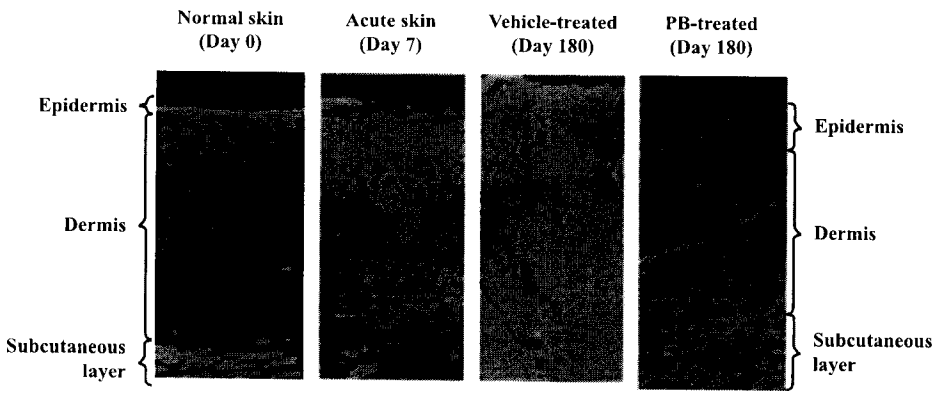

Figure 5. Immunofluorescence. TGF-β expression in the skin after irradiation. The expression level of TGF-β in the irradiated skin was high in the superficial dermis of acute reaction at Day 7 and in the thin epidermis and proliferative dermis in the vehicle group at Day 180 but was low in the hyperplastic epidermis and thinner dermis in the phenylbutyrate (*PB*) group at Day 180.

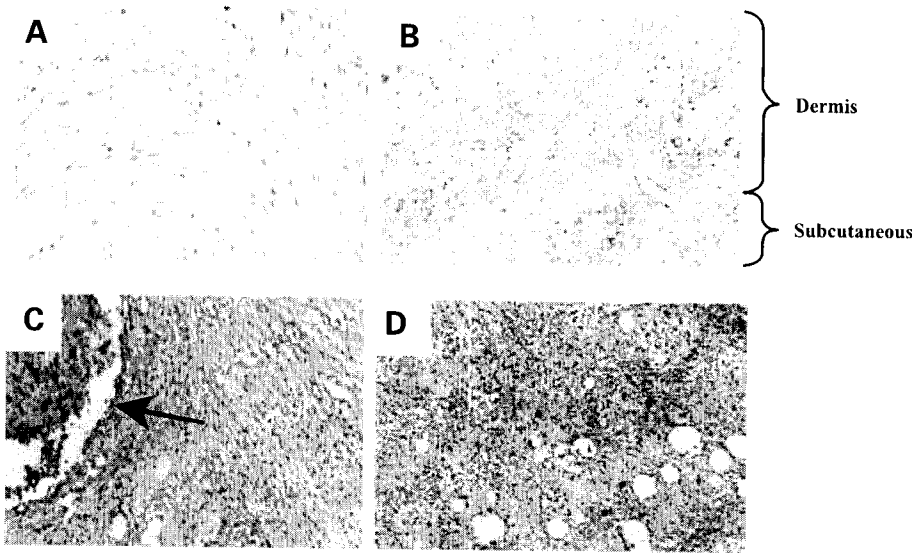

Figure 6. Immunohistochemistry. TNF-α expression in the long-term skin damage at Day 270 after irradiation. The expression levels of TNF-α in the normal skin and phenylbutyrate-treated group were low. In contrast, the high expression levels of TNF-α in the Vaseline and vehicle groups correlated with skin necrosis and heavy inflammatory infiltrates. **A,** normal skin; **B,** irradiated skin treated with the topical phenylbutyrate; **C,** irradiated skin treated with Vaseline (the *arrow* indicates the necrotic wound); and **D,** irradiated skin treated with vehicle.

for the treatment of CRS and the prevention of late tumorigenesis. Although the down-regulation of TNF-α and TGF-β by the inhibition of HDAC is likely to contribute to the effects observed in the present study, HDAC inhibitors may have another mechanisms, for example, the hyperacetylation of nonhistone proteins such as ribosomal S3 or the Rel-A subunit of NF-κB (47, 48). Moreover, as a consequence of nuclear hyperacetylation, which results in genetic reprogramming, HDAC inhibitors also up-regulate the cell cycle kinase inhibitor $p21^{Cip1}$, which, in part, accounts for their antitumor properties (21).

TGF-β is a pleiotropic growth factor that inhibits epithelial cell growth but promotes mesenchymal cell proliferation and neoplastic growth (8–10, 15, 16). In

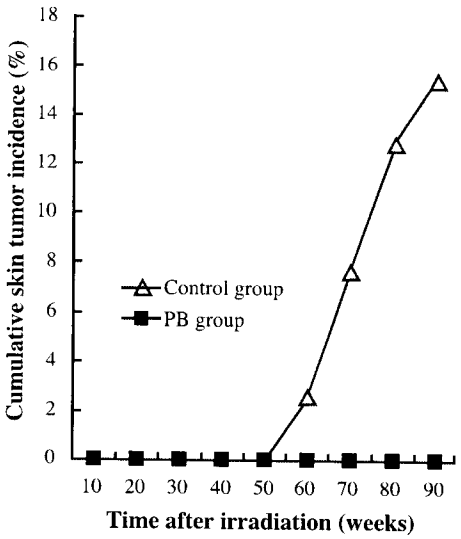

Figure 7. Skin tumorigenesis after irradiation. Cumulative skin tumor incidence after skin irradiation increased with time in the groups without the topical phenylbutyrate (*PB*) treatment.

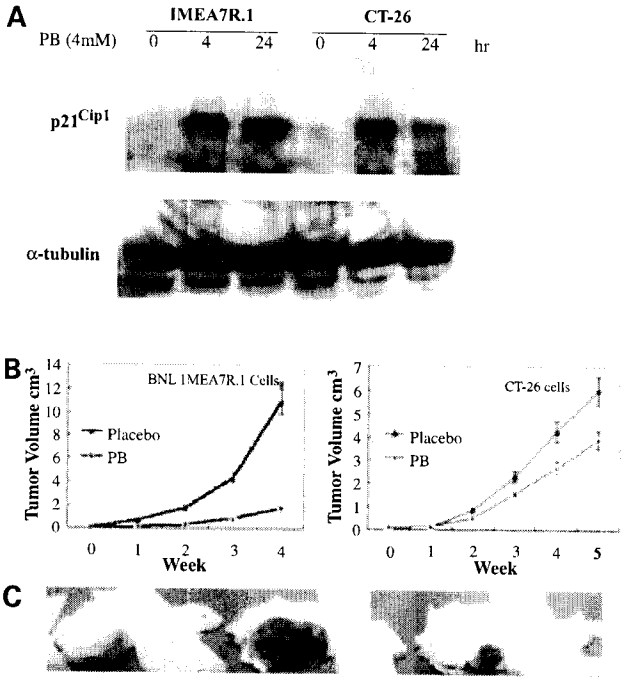

Figure 8. Phenylbutyrate inhibits tumor growth. **A,** time-course analysis of the up-regulated levels of $p21^{Cip1}$ protein in BNL 1MEA7R.1 and CT-26 carcinoma cells during treatment with 4 mM phenylbutyrate (*PB*). **B,** growth inhibition test *in vivo*. The cutaneous tumors (*BNL 1MEA7R.1* and *CT-26* carcinoma cells), grown to a size of 0.5 cm, were treated with the topical phenylbutyrate or vehicle at a dose of 200 mg/mouse, to cover the whole tumor surface and surrounding skin twice per day for 4 weeks. At the end of this period, the cutaneous tumor sizes of 1MEA7R.1 and CT-26 in mice in the placebo groups were almost 6- and 1.6-fold larger than those in the topical phenylbutyrate-treated groups, respectively. **C,** an initial tumor size of 1MEA7R.1 beneath the skin about 0.5 cm in dimension before treatment (*left*), a placebo- or vehicle-treated tumor at week 4 (*middle*), and a phenylbutyrate-treated tumor at week 4 (*right*).

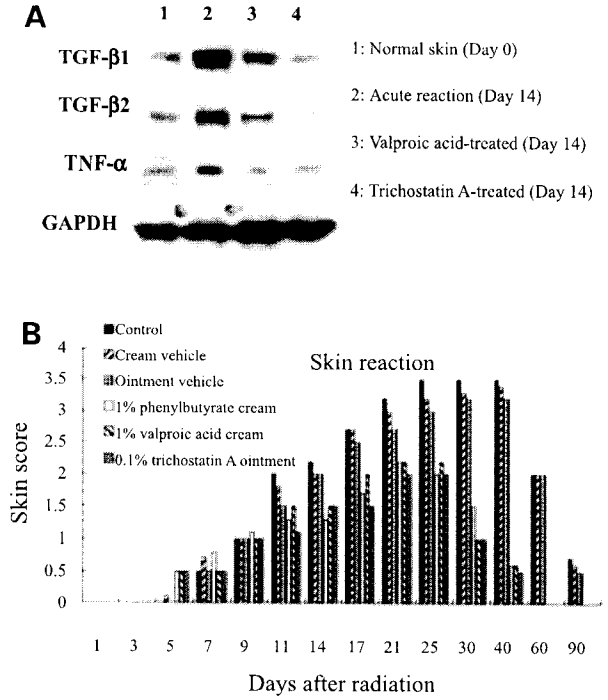

Figure 9. Effects of other structurally unrelated HDAC inhibitors in CRS. The different HDAC inhibitors (*trichostatin A* and *valproic acid*) also suppressed the radiation-induced levels of TGF-β1, TGF-β2, and TNF-α expression and ameliorated CRS. **A,** Northern blot assays for TGF-β1, TGF-β2, and TNF-α expressions. **B,** skin scores for skin reactions after radiation. The skin score increases with a more severe skin reaction.

the present study, the sustained high expression levels of TGF-β1 and -β2 in irradiated skin was significant in explaining the manifestation of thin epidermis and proliferative dermis in the vehicle group at Day 180 as well as the occurrence of tumor formation after 50 weeks. In contrast, the appearance of hyperplastic epidermis and a thinner dermis at Day 180, as well as no skin tumor development noted at Week 90 after irradiation in the phenylbutyrate-treated group, correlated with the early suppression of the chronic up-regulation of TGF-β1 and -β2 by phenylbutyrate. Although TGF-β is certainly a key growth factor, the development of CRS and the recovery from a perpetual wound might not depend on the modulation of a single factor. The wound healing process after irradiation involves a complex feedback network of interacting cytokines and growth factors, including platelet-derived growth factor, epidermal growth factor, basic fibroblast growth factor, granulocyte macrophage colony-stimulating factor, connective tissue growth factor, IL-1, IL-4, inhibiting growth factor-1, and TNF-α, and complex interactions among the parenchymal, epithelial, endothelial, and inflammatory cells (3, 12). Among them, TNF-α is implicated in triggering the recruitment of inflammatory cells through the expression of adhesion molecules on the vascular surface, as well as the stimulation of fibroblast proliferation (12, 49, 50). Thus, in addition to the down-regulation of long-term TGF-β activation, the simultaneous suppression of radiation-induced TNF-α in mesenchymal cells and macrophages should also contribute to the decrease in acute skin inflammation and the incidence of late skin necrosis and fibrosis seen in the present study.

Drugs that have previously been tested in the management of CRS include antioxidants (vitamin E and superoxide dismutase), anti-inflammatory agents (corticosteroids, colchicines, D-penicillamine, and TNF-α antagonist antibodies), and anti-fibrogenic agents (IFN, TGF-β antagonist, and angiotensin-converting enzyme inhibitors) (7). However, few of these are able to simultaneously ameliorate acute dermatitis, prevent the occurrence of fibrosis, and reduce late tumorigenesis; moreover, toxicities, side effects, tumor protection possibilities, and a lack of antitumor effects are troublesome. Rather than focusing on agents that act only on a few steps in the pathogenesis of CRS, our study provides a novel strategy to exert anti-inflammatory, anti-fibrogenic, and antitumor effects at one time by HDAC inhibitors to remodel chromatins and epigenetically regulate multiple genes involved in radiation-induced skin damage and tumor growth.

To our knowledge, this is the first time that the antitumor HDAC inhibitors have been shown to protect skin from radiation-induced damage and tumorigenesis. Our study warrants further clinical investigations into the combination of therapeutic radiation and HDAC inhibitors in increasing the therapeutic gain of cancer radiotherapy. Although TGF-β and TNF-α could be the targets of HDAC inhibitors, more cellular and molecular studies are needed to identify the precise mechanisms of HDAC inhibitors in both suppressing CRS and preventing tumorigenesis.

References

1. Peter RU. The cutaneous radiation syndrome. Advances in the treatment of radiation injuries. Oxford: Elsevier; 1996. p. 237 - 40.

2. Hopewell JW. The skin: its structure and response to ionizing radiation. Int J Radiat Biol, 1990;57:751 - 73.

3. Hill RP, Rodemann HP, Hendry JH, Roberts SA, Anscher MS. Normal tissue radiobiology: from the laboratory to the clinic. Int J Radiat Oncol Biol Phys, 2001;49:53 - 65.

4. Seong J, Kim SH, Chung EJ, Lee WJ, Suh CO. Early alteration in TGF-β mRNA expression in irradiated rat liver. Int J Radiat Oncol Biol Phys, 2000;46:639 - 43.

5. Wang J, Zheng H, Sung CC, Richter KK, Hauer-Jensen M. Cellular sources of transforming growth factor-β isoforms in early and chronic radiation enteropathy. Am J Pathol, 1998;153:1531 - 40.

6. Fedorocko P, Egyed A, Vacek A. Irradiation induces increased production of haemopoietic and proinflammatory cytokines in the mouse lung. Int J Radiat Biol, 2002;78:305 - 13.

7. Martin M, Lefaix J, Delanian S. TGF-β1 and radiation fibrosis: a master switch and a specific therapeutic target. Int J Radiat Oncol Biol Phys, 2000;47:277 - 90.

8. Randall K, Coggle JE. Long-term expression of transforming growth factor TGF β 1 in mouse skin after localized β-irradiation. Int J Radiat Biol, 1996;70:351 - 60.

9. Border WA, Noble NA. Transforming growth factor β in tissue fibrosis. N Engl J Med, 1994;331:1286 - 92.

10. Singer AJ, Clark RA. Cutaneous wound healing. N Engl J Med, 1999; 341:738 - 46.

11. Zhou D, Yu T, Chen G, et al. Effects of NF-κB (p50) targeted gene disruption on ionizing radiation-induced NF-κB activation and TNFα, IL-1α, IL-1β and IL-6 mRNA expression *in vivo*. Int J Radiat Biol, 2001;77: 763 - 72.

12. Skwarchuk MW, Travis EL. Changes in histology and fibrogenic cytokines in irradiated colorectum of two murine strains. Int J Radiat Oncol Biol Phys, 1998;42:169 – 78.

13. Sivan V, Vozenin-Brotons MC, Tricaud Y, et al. Altered proliferation and differentiation of human epidermis in cases of skin fibrosis after radiotherapy. Int J Radiat Oncol Biol Phys, 2002;53:385 – 93.

14. Delanian S, Martin M, Bravard A, Luccioni C, Lefaix JL. Abnormal phenotype of cultured fibroblasts in human skin with chronic radiotherapy damage. Radiother Oncol, 1998;47:255 – 61.

15. Wieser R. The transforming growth factor-β signaling pathway in tumorigenesis. Curr Opin Oncol, 2001;13:70 – 7.

16. Massague J, Blain SW, Lo RS. TGFβ signaling in growth control, cancer, and heritable disorders. Cell, 2001;103:295 – 309.

17. Marks PA, Richon VM, Rifkind RA. Histone deacetylase inhibitors: induction of differentiation or apoptosis of transformed cells. J Natl Cancer Inst, 2000;92:1210 – 6.

18. Kramer OH, Gottlicher M, Heinzel T. Histone deacetylase as a therapeutic target. Trends Endocrinol Metab, 2001;12:294 – 300.

19. Lagger G, O'Carroll D, Rembold M, et al. Essential function of histone deacetylase 1 in proliferation control and CDK inhibitor repression. EMBO J, 2002;21:2672 – 81.

20. Richon VM, O'Brien JP. Histone deacetylase inhibitors: a new class of potential therapeutic agents for cancer treatment. Clin Cancer Res, 2002; 8:662 – 7.

21. Richon VM, Sandhoff TW, Rifkind RA, Marks PA. Histone deacetylase inhibitor selectively induces p21WAF1 expression and gene-associated histone acetylation. Proc Natl Acad Sci USA, 2000;97:10014 – 9.

22. Van Lint C, Emiliani S, Verdin, E. The expression of a small fraction of cellular genes is changed in response to histone hyperacetylation. Gene Exp, 1996;5:245 – 53.

23. Huang N, Katz JP, Martin DR, Wu GD. Inhibition of IL-8 gene expression in Caco-2 cells by compounds which induce histone hyperacetylation. Cytokine, 1997;9:27 – 36.

24. Mishra N, Brown DR, Olorenshaw IM, Kammer GM. TSA reverses skewed expression of CD154, interleukin-10, and interferon-γ gene and protein expression in lupus T cells. Proc Natl Acad Sci USA, 2001;98: 2628 – 33.

25. Stockhammer G, Manley GT, Johnson R, Rosenblum MK, Samid D, Lieberman FS. Inhibition of proliferation and induction of differentiation in medulloblastoma- and astrocytoma-derived cell lines with phenylacetate. J Neurosurg, 1995;83:672 – 81.

26. Segain JP, Raingeard de la Bletiere D, Bourreille A, et al. Butyrate inhibits inflammatory responses through NFκB inhibition: implications for Crohn's disease. Gut, 2000;47:397 – 403.

27. Leoni F, Zaliani A, Bertolini G, et al. The antitumor histone deacetylase inhibitor suberoylanilide hydroxamic acid exhibits antiinflammatory properties via suppression of cytokines. Proc Natl Acad Sci USA, 2002;99: 2995 – 3000.

28. Warrell RP Jr, He LZ, Richon V, Calleja E, Pandolfi PP. Therapeutic targeting of transcription in acute promyelocytic leukemia by use of an inhibitor of histone deacetylase. J Natl Cancer Inst, 1998;90:1621 – 5.

29. Vigushin DM, Ali S, Pace PE, et al. Trichostatin A is a histone deacetylase inhibitor with potent antitumor activity against breast cancer *in vivo*. Clin Cancer Res, 2001;7:971 – 6.

30. Saunders N, Dicker A, Popa C, Jones S, Dahler A. Histone deacetylase inhibitors as potential anti-skin cancer agents. Cancer Res, 1999;59:399 – 404.

31. Gottlicher M, Minucci S, Zhu P, et al. Valproic acid defines a novel class of HDAC inhibitors inducing differentiation of transformed cells. EMBO J, 2001;20:6969 – 78.

32. Rombouts K, Niki T, Wielant A, Hellemans K, Geerts A. Trichostatin A, lead compound for development of antifibrogenic drugs. Acta Gastroenterol Belg, 2001;64:239 – 46.

33. Garber K. Silence of the genes: cancer epigenetics arrives. J Natl Cancer Inst, 2002;94:793 – 5.

34. Ferrandina G, Filippini P, Ferlini C, et al. Growth inhibitory effects and radiosensitization induced by fatty aromatic acids on human cervical cancer cells. Oncol Res, 2001;12:429 – 40.

35. Miller AC, Whittaker T, Thibault A, Samid D. Modulation of radiation response of human tumour cells by the differentiation inducers, phenylacetate and phenylbutyrate. Int J Radiat Biol, 1997;72:211 – 8.

36. Biade S, Stobbe CC, Boyd JT, Chapman JD. Chemical agents that promote chromatin compaction radiosensitize tumour cells. Int J Radiat Biol, 2001;77:1033 – 42.

37. Chung YL, Yen RL, Wang AJ, Yao LF. Treating radiation fibrosis. United States Patent 6,538,030. 2003.

38. Abe Y, Urano M. Fraction size-dependent acute skin reaction of mice after multiple twice-a-day doses. Int J Radiat Oncol Biol Phys, 1990;18: 359 – 64.

39. Richon VM, Emiliani S, Verdin E, et al. A class of hybrid polar inducers of transformed cell differentiation inhibits histone deacetylases. Proc Natl Acad Sci USA, 1998;95:3003 – 7.

40. Brusilow SW, Danney M, Waber LJ, et al. Treatment of episodic hyperammonemia in children with inborn errors of urea synthesis. N Engl J Med, 1984;310:1630 – 4.

41. Olivieri NF, Rees DC, Ginder GD, et al. Treatment of thalassaemia major with phenylbutyrate and hydroxyurea. Lancet, 1997;350:491 – 2.

42. Rubenstein RC, Zeitlin PL. A pilot clinical trial of oral sodium 4-phenylbutyrate (Buphenyl) in δF508-homozygous cystic fibrosis patients: partial restoration of nasal epithelial CFTR function. Am J Respir Crit Care Med, 1998;157:484 – 90.

43. Kemp S, Wei HM, Lu JF, et al. Gene redundancy and pharmacological gene therapy: implications for X-linked adrenoleukodystrophy. Nat Med, 1998;4:1261 – 8.

44. Gore SD, Weng LJ, Zhai S, et al. Impact of the putative differentiating agent sodium phenylbutyrate on myelodysplastic syndromes and acute myeloid leukemia. Clin Cancer Res, 2001;7:2330 – 9.

45. Gilbert J, Baker SD, Bowling MK, et al. A phase I dose escalation and bioavailability study of oral sodium phenylbutyrate in patients with refractory solid tumor malignancies. Clin Cancer Res, 2001;7: 2292 – 300.

46. Carducci MA, Gilbert J, Bowling MK, et al. A phase I clinical and pharmacological evaluation of sodium phenylbutyrate on an 120-h infusion schedule. Clin Cancer Res, 2001;7:3047 – 55.

47. Webb Y, Zhou X, Ngo L, et al. Photoaffinity labeling and mass spectrometry identify ribosomal protein S3 as a potential target for hybrid polar cytodifferentiation agents. J Biol Chem, 1999;274:14280 – 7.

48. Chen L, Fischle W, Verdin E, Greene WC. Duration of nuclear NF-κB action regulated by reversible acetylation. Science, 2001;293:1653 – 7.

49. Zhang K, Phan SH. Cytokines and pulmonary fibrosis. Biol Signals, 1996;5:232 – 9.

50. Van Deventer SJ. Tumor necrosis factor and Crohn's disease. Gut, 1997;40:443 – 7.

Differentiation (2004) 72:410–418

ORIGINAL ARTICLE

Karima Djabali · Angela M. Christiano

Hairless contains a novel nuclear matrix targeting signal and associates with histone deacetylase 3 in nuclear speckles

Received June 25, 2004; accepted August 10, 2004

Abstract Hair follicle cycling is a highly regulated and dynamic cellular process consisting of phases of growth, regression, and quiescence. The hairless (hr) gene encodes a nuclear factor that is highly expressed in the skin, where it appears to be an essential regulator during the regression in the catagen hair follicle. In hairless mice, as well as humans with congenital atrichia, the absence of hr protein initiates a premature and abnormal catagen due to defects in the signaling required for hair follicle remodeling. Here, we report that hr protein is a nuclear protein that is tightly associated with the nuclear matrix scaffold. Using a series of deletion constructs of the mouse hr gene, we monitored the subcellular localization of the recombinant protein by *in situ* immunolocalization and biochemical fractionation after nuclear matrix extraction of transiently transfected cells. We identified a novel nuclear matrix-targeting signal (NMTS) in the hr protein and mapped the domain to amino acid residues 111–186 of the mouse hr sequence. Furthermore, we provide evidence that this region not only mediates the interaction of hr with components of the nuclear architecture, but also specifies the sub-nuclear location of the hr protein to nuclear domains containing deacetylase activity. The N-terminal region directs hr to a speckled nuclear pattern that co-localizes with the histone deacetylase 3 (HDAC), but not with HDAC1 or HDAC7. Based on our findings, we propose that hr protein is part of a specific multiprotein repressor complex and that hr may be involved in chromatin remodeling.

Karima Djabali · Angela M. Christiano (✉)
Departments of Dermatology, and Genetics and Development
Columbia University
College of Physicians and Surgeons
New York, NY 10032, USA
Tel: (212) 305-9565
Fax: (212) 305-7391
E-mail: amc65@columbia.edu

Key words hairless · hair follicle · nuclear matrix · histone deacetylase · HDAC3

Introduction

The hair follicle is a dynamic structure that generates hair through a complex and tightly controlled cycle of growth and remodeling (Paus et al., 1999; Stenn and Paus, 2001). Mature follicles undergo a growth cycle consisting of growth (anagen), regression (catagen), and rest (telogen). Currently, very little is known about the molecular control of the signals that regulate progression through this cycle, although it is clear that at least some potentially influential regulatory molecules may play a role. Much of what is known about the hair cycle has emerged from the study of knock-out and transgenic mouse models, which sometimes correlates with naturally occurring mouse phenotypes (Nakamura et al., 2001). The most widely utilized model, the hairless mouse, has only recently gained prominence as a model for comparative analysis in the field of hair biology (Panteleyev et al., 1998a). The mouse hairless (hr) locus was later identified as the result of a spontaneous mutation caused by the insertion of an endogenous retrovirus between exons 6 and 7 of the hr gene on chromosome 14, and subsequently reduced mRNA levels (Cachon-Gonzalez et al., 1994). The rhino mutation (rh/rh) is allelic to hr/hr, and exhibits an exaggerated phenotype resulting from nonsense mutations in the hr gene, and therefore represents the true null mutation (Ahmad et al., 1998a, 1998b, 1998c).

The most striking phenotypic feature of all mice bearing mutations at the hr locus is the rapid onset of a complete and sharply demarcated postnatal wave of hair shedding, which follows a seemingly programmed time course (Panteleyev et al., 1998b). Histological studies of hairless mutants revealed normal development of the distal part of the hair follicle, including the infundibulum and sebaceous gland, but severe

U.S. Copyright Clearance Center Code Statement: 0301–4681/2004/7208–410 $ 15.00/0

malformation of the germinal, proximal portion of the follicle, leading to the lack of new hair development, follicular degeneration, and the formation of dermal cysts (Panteleyev et al., 1998a). The hairless phenotype in mice is allelic to the human disorder atrichia with papular lesions (APL; OMIM #209500), and is characterized by similar clinical and histological features.

At the cellular level, the function of the hairless protein remains largely unknown. We have previously characterized the sub-cellular localization of the hr gene product as being restricted to the nucleus (Djabali et al., 2001). Furthermore, we identified a novel bipartite nuclear localization signal (NLS) of the form KRA(X13)PKR at position 409–427 of the mouse sequence that is highly conserved in other species. In addition, we reported earlier that hr was tightly associated with the nuclear matrix (Djabali et al., 2001).

The nuclear matrix is the underlying scaffold structure that remains after the removal of nuclear chromatin. Because the transcriptional machinery is coordinated with the nuclear matrix architecture during cell growth and differentiation (Prince et al., 2000; Gniadecki et al., 2001), we investigated the mechanistic properties of the hr-NM interaction. Here, we report the characterization of the hr nuclear matrix-targeting signal (NMTS) that directs hr to the nuclear matrix compartment. The NMTS corresponds to amino acid residues 111–186 within the N-terminal region of the mouse hr sequence. Furthermore, we provide evidence that this region not only mediates the interaction of hr with components of the nuclear architecture, but also specifies the sub-nuclear location of the hr protein to nuclear domains containing deacetylase activity. The N-terminal region directs hr to a speckled nuclear co-localization coinciding with the histone deacetylase 3 (HDAC), but not with HDAC1 or HDAC7. We propose that hr protein may be part of a specific repressor multi-protein complex that contains HDAC3.

Methods

Cell culture and transfection

NIH3T3 and COS 7 cells were grown and cells transfected as described previously (Djabali et al., 2001). For immunofluorescence analysis, cells were grown on glass coverslips. After 24–48 hr, transfected cells were fixed in 3% paraformaldehyde in phosphate buffer saline (PBS) for 15 min, washed twice with PBS, and counterstained with 4,6-diamidino-2-phenylindole (DAPI). The sub-cellular location of green fluorescent protein (GFP) fusion proteins was determined by fluorescence microscopy.

Conventional indirect immunofluorescence microscopy

NIH3T3 cells were grown on glass coverslips and transfected as described above. Cells after fixation were incubated with anti-Flag monoclonal antibodies (Sigma, St. Louis, MO) (diluted 10 μg/ml) and anti-lamin B polyclonal antibodies (Chaudhary and Courvalin, 1993) for 30 min at room temperature. After appropriate washes, cells were further incubated with secondary antibodies: FITC-coupled goat anti-mouse antibodies or rhodamine-conjugated goat anti-rabbit (both from Silenus Laboratories, Hawthorn, Australia). Analysis of hairless and lamin B localization was carried out using the TCS40 (Leica Microsystems, Buffalo, NY) confocal imaging system. For each optical section, double fluorescence images were acquired simultaneously. The two images were merged to check the relative position of the two fluorochromes.

Nuclear matrix isolation

High-salt isolation of nuclear matrix was carried out as described (He et al., 1990). After transfection, cells were washed in PBS and extracted in cytoskeleton buffer (CSK; 10 mM PIPES, pH 6.8, 100 mM NaCl, 300 mM sucrose, 3 mM $MgCl_2$, 1 mM EGTA, supplemented with leupeptin, aprotinin, and pepstatin, 1 μg/ml each), 1 M DTT, and 0.5% Triton X-100. After 3 min at 4°C, the cytoskeleton frameworks were separated from soluble proteins by centrifugation at 600 g for 3 min.Chromatin was solubilized by DNA digestion with 1 mg/ml of RNAse-free DNAse I in CSK buffer plus proteinase inhibitors for 15 min at 37°C. Ammonium sulfate was added from a 1 M stock solution in CSK buffer to a final concentration of 0.25 M and after 5 min at 4°C, samples were pelleted at 5,000 g for 3 min.The pellet was further extracted with 2 M NaCl in CSK buffer for 5 min at 4°C, and then centrifuged as above. The remaining pellet was solubilized in urea buffer and represented the nuclear matrix fraction.

Green fluorescent protein-hairless constructs

The full-length cDNA for hairless (hr) was generated previously in the pAlter plasmid (Promega, Madison, WI; Djabali et al., 2001). PCR amplification of segments of hairless from pAlter-hr template was cloned in-frame into *Xho*I/*Eco*RI sites of pEGFP-C1 vector (Clontech, Palo Alto, CA). The primers used for amplification were as follows (all sequences 5′–3′): EGFP-1F CGCTCGAGCTATGGAGAGTATGCCC and CCGGAATTCGAGTGCTTGGCCAG GCC for EGFP-NT; CCGCTCGAGCTGGAGGGCCTGGC and CCGGAATTCGACCCCACAGCCGC for EGFP-CT. (A) First-step constructs: Δ1F oligo: CCGCTCGAGCTGGGCCGG CAT and Δ1R CCGGAATTCGAGCGTTTGGGAGCTGG for EGFP-Δ1; Δ2F CCGCTCGAGCTCGGAACATCCTCAGG and Δ1R oligo for EGFP-Δ2; Δ3F CCGCTCGAGCTAGGTGCCCATC TCC and Δ1R oligo for EGFP-Δ3. (B) Second-step constructs: Δ1.1F: CCGCTCGAGCTCTAGAGCGAGCTCCC and Δ1R for EGFP-Δ1.1; oligo Δ1.2F CCGCTCGAGCTGCCCCAAACC-CATGG Δ1R for EGFP-Δ1.2. (C) Third-step chimeric constructs: constructs for narrowing the NMTS was generated using the linearized vector EGFP-Δ41a generated previously (Djabali et al., 2001) containing amino acid residues 409–539 of mouse hr and therefore encoding the hr nuclear localization signal. Fragments containing the putative NMTS were inserted into the *Hind*III and *Eco*RI sites of the pEGFP-Δ41a. EGFP-NM111-214 corresponds to PCR-amplified region from amino acids 111–214 with oligo 112-F CCCAGAAGCTTCAGGGCCGGCATGC and 212-R CCGGAATTCGAGAGGATGTTCGG. EGFP-NM111-186 corresponded to residues 111–186 and was PCR amplified using oligo 112-F and 186-R CCGGAATTCGACCATGGGTTTGG. All recombinant plasmids were verified by DNA sequencing (Djabali et al., 2001).

Analysis of GFP-fusion proteins by Western blotting

Whole-cell extracts were harvested in urea buffer (8 M urea, 0.1 M $NaHPO_4$, 0.01 M Tris, pH 8) from the transiently transfected

NIH3T3 cells 48 hr after transfection. Total extracts were subjected to 10% SDS-polyacrylamide gel electrophoresis. After separation, Western blots were probed with the monoclonal anti-GFP antibody (Clontech), as described previously (Djabali et al., 1991).

Results

Hairless is associated with the nuclear matrix

To address the mechanism that directs hr to the nuclear matrix compartment, we initially assessed the sub-nuclear distribution of hr in transiently transfected NIH3T3 cells with the full-length hr cDNA (Djabali et al., 2001). We previously showed that hr resides in the nuclear compartment, and is tightly associated with components of the nuclear matrix (Djabali et al., 2001). As shown in Figure 1 (A1,A3), hr remains associated with the NM-IF scaffold following detergent extraction and chromatin removal as described in Methods (Fig. 1 A2,1A3).

Expression of the N-terminal region of hr (EGFP-NT1-551) and the full-length hr proteins exhibited identical localization patterns (Fig. 1B), and in addition, after DNAse digestion and high-salt extraction, the N-terminal region of hr remained associated with the nuclear matrix preparation (Fig. 1 B1, 1B3). Therefore, we concluded that the nuclear matrix-targeting signal of hr must be contained within the N-terminal region of the hr protein, between amino acid residues 1 and 551.

Delineation of the NMTS of hairless

To identify the region of hr responsible for nuclear matrix targeting, a series of N-terminal deletions was constructed and fused to the GFP reporter (Fig. 2A). We analyzed the *in situ* sub-nuclear localization of the N-terminal hr mutants in nuclear matrix preparations of NIH3T3 cells. When transiently expressed in NIH3T3 cells, EGFP-NT-Δ1 deletion mutants missing the first 111 amino acids of the N-terminal region (Fig. 2A), the recombinant protein localized similarly to the full-length hr protein and remained bound to the nuclear matrix (Fig. 1C1, 1C3). In contrast, deletion mutants missing the first 211 and 311 amino acids from the amino terminus as delineated in Figure 2A failed to remain associated with the nuclear matrix after extraction (Fig. 1D1,1D3 and 1E1,1E3, respectively). In order to confirm the *in situ* observation, we investigated how the different N-terminal truncated proteins behaved using a biochemical sequential extraction procedure as

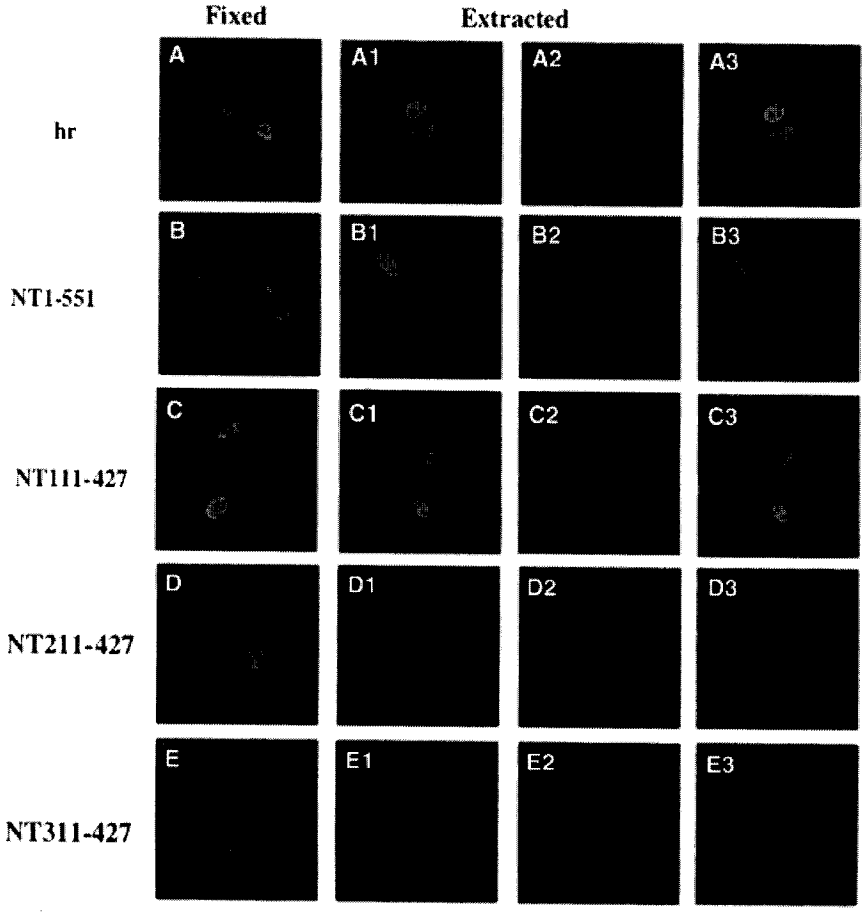

Fig. 1 Distribution of EGFP-hairless truncated proteins in transiently transfected NIH3T3 cells. For each construct, the amino acid numbers of the mouse hr fused to the EGFP protein are indicated. After 24 hr, transfected cells were directly fixed for (A)–(E) and the GFP signals were directly recorded. For (A1)–(E3), cells were treated for *in situ* nuclear matrix preparation and were processed for indirect immunofluorescence with anti-lamin B antibody. (A1)–(E1) correspond to the GFP signal, (A2)–(E2) correspond to the lamin B staining, and (A3)–(E3) correspond to the respective merge signal of the GFP and lamin B. Note that deletion of the first 211 amino acid residues abolishes the nuclear matrix association of the N-terminal region of the hr protein (D1, D2, D3).

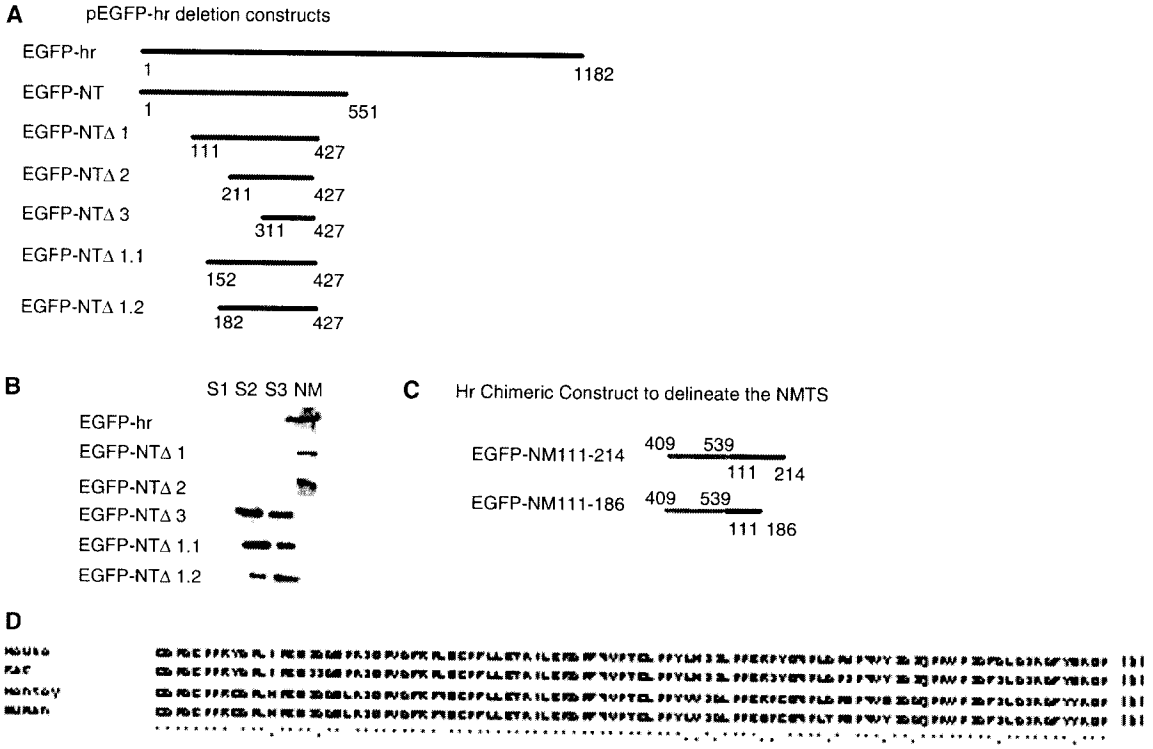

Fig. 2 (**A**) Schematic representation of deletion constructs of hairless fused to EGFP. All constructs were generated with EGFP at the amino terminus of the hairless coding region. A solid line represents the extent of the hairless coding region retained in each construct, and the position of the N- and C-terminal amino acids is indicated. (**B**) Sub-cellular partitioning of the hr deletion mutants from (A). NIH3T3 nuclear matrices were prepared using DNAse I digestion and high-salt extraction. Cells were transfected with the different deletion constructs and collected 48 hr later. Cells were sequentially extracted with 0.5% Triton X-100 (lane S1), DNAse I and 0.25 M $(NH_4)_2SO_4$ (lane S2), and 2 M NaCl (lane S3), and the remaining pellet of the nuclear matrix preparation was solubilized in 8 M urea buffer (lane NM). An equivalent aliquot of each step of the extractions was subjected to SDS-PAGE. The gels were immunoblotted with the anti-GFP antibody. (**C**) Chimeric constructs of hairless to narrow the hairless NMTS. Hairless fragment 409–539 containing the NLS sequence was fused to the putative hr NMTS (amino acids 111–214 or 111–186) and EGFP to follow the sub-cellular localization. (**D**) Amino acid sequence alignment from positions 111 to 211 of mouse and corresponding fragment in rat, monkey, and human hairless protein. Asterisks indicate identical residues.

described previously (He et al., 1990; Djabali et al., 2001). The full-length hr, the N-terminal half part of hr, and the N-terminal deletion construct missing the first 111 amino acids behaved similarly, as all proteins are detected in the final fraction corresponding to the nuclear matrix preparation (Fig. 2B). However, deletion constructs missing the first 211 and 311 amino acids were distributed in the chromatin and high-salt fraction, and not in the nuclear matrix preparation (Fig. 2B).

Based on the *in situ* immunolocalization and the biochemical sub-cellular fractionation, these results indicate that amino acids in the region between positions 111 and 211 contain critical determinants for association of hr with the nuclear matrix. In addition, this region is highly conserved between mouse, rat, monkey, and human as depicted in the sequence alignment (Fig. 2D). This 100 amino acid stretch showed 96% identity in rat, and 87% in monkey and human, when compared to the mouse sequence, with a homology of 97% in rat, 93% in monkey, and 91% in human.

Narrowing the NMTS from the N-terminal region of hairless

To precisely define the beginning of the NMTS, we generated two constructs by deleting amino acid residues within 111 and 211 from the amino terminus. The first construct started at amino acid 152 (EGFP-NT-Δ1.1) and the second started at position 182 (EGFP-NT-Δ1.2; Fig. 2A). We applied both *in situ* immunofluorescence (Fig. 3C–3F) and biochemical approaches (Fig. 2B) to delineate the specific amino acid sequences of hr necessary for nuclear matrix targeting and association. In comparison to the construct EGFP-NT111-427 ending just after the nuclear localization signal, NT152-427 and NT182-427 were distributed throughout the nuclear compartment and appeared rather diffuse in untreated cells (Fig. 3C, 3E). When cells were subjected to the different extractions, the signal of the GFP recombinant proteins was no longer detected (Fig. 3D, 3F), indicating that amino acids residues between positions 111 and 152 were critical for the interaction of hr with the nuclear matrix scaffold, because

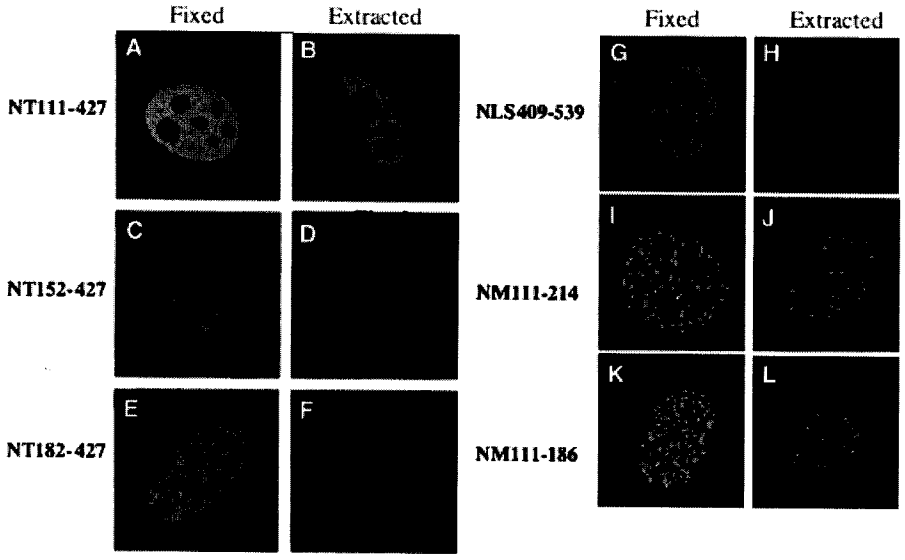

Fig. 3 Narrowing the NMTS of hairless. For each construct, the amino acid numbers of the mouse hr fused to the EGFP protein are indicated. After 24 hr, transfected cells were directly fixed for (**A**), (**C**), (**E**), (**G**), (**I**), and (**K**) and the GFP signals were directly recorded. For (**B**), (**D**), (**F**), (**H**), (**J**), and (**L**), cells were treated for *in situ* nuclear matrix preparation and were processed for direct immunofluorescence. Note that deletion of the first 152 amino acid residues abolished the nuclear matrix association (D).

their removal abolished the association. We also monitored the biochemical repartitioning of the recombinant protein from the deletion construct EGFP-NT152-427 and EGFP-NT-182-427 among the cytoplasmic, chromatin, and nuclear matrix compartments by Western blot analysis (Fig. 2B). Similar to the *in situ* localization, both recombinant proteins were detected in the chromatin and high-salt fraction, suggesting that these recombinant proteins do not contain the functional NMTS.

The NMTS of hr targets a heterologous protein to the nuclear matrix compartment

In order to narrow down the NMTS from the C-terminal region of hr starting from amino acid 427, we designed another set of chimeric constructs. The putative hr NMTS was fused to a GFP reporter gene and to the endogenous nuclear localization signal from hr (amino acids 409–539) in order to test whether the NMTS could target the recombinant protein to the nucleus.

We generated chimeric constructs encoding the GFP protein fused to amino acid residues 409–539 containing the endogenous hr NLS and fused directly to amino acid residues 111–214 (EGFP-NM111-214) or 111–186 (EGFP-NM111-186) of hr (Fig. 2C). Cells were transfected with the chimeric constructs, and the subnuclear distribution of these heterologous proteins was analyzed in whole-cell and NM-IF preparations by immunofluorescence microscopy (Fig. 3G–3L). The chimeric recombinant proteins were effectively translocated to the nucleus, consistent with the presence of the nuclear localization signal (Fig. 3G, 3I, 3K). The GFP-409–539 recombinant protein containing the hr NLS alone was localized in the nucleus, but appeared rather diffuse throughout the nuclear compartment in the whole-cell preparation (Fig. 3G). After the different extraction procedures, the GFP-409–539 was totally extracted, and no GFP signal could be detected in the nuclear matrix preparation (Fig. 3H), demonstrating that the NLS itself of hr is not responsible for the nuclear matrix attachment.

When cells were transfected with the chimeric constructs containing both the NLS and the NMTS, we observed a striking sub-nuclear distribution of the recombinant proteins (Fig. 3I–3L). Interestingly, the GFP signal was not diffuse, but instead organized into structures that gave a speckled or punctate-like distribution. Furthermore, after DNAse and high-salt extraction, these punctate speckles remained attached to the remnant nuclear matrix scaffold (Fig. 3J, 3L). Therefore, amino acid residues 111–186 are sufficient to target the GFP-fusion proteins to the nuclear matrix compartment. The hr NMTS is contained within amino acids residues 111–186, because this region is sufficient to mediate interactions with components of the nuclear architecture when fused to a chimeric protein. Our results established that the hr NMTS functions as an autonomous sub-cellular targeting signal.

Unexpectedly, we noted a specific pattern of distribution of the chimeric proteins that was not observed with the GFP fused to the NLS alone. We investigated the possibility that the NMTS-containing region might also be responsible for the unique speckled sub-nuclear location of the chimeric proteins.

Hr is localized in a nuclear domain with deacetylase activity

To address the mechanism that directs the chimeric protein to nuclear matrix-associated foci (Fig. 3I–3L), we systematically examined the distribution of hr in transiently transfected NIH3T3 cells with the full-length hr cDNA. We monitored each nucleus expressing the

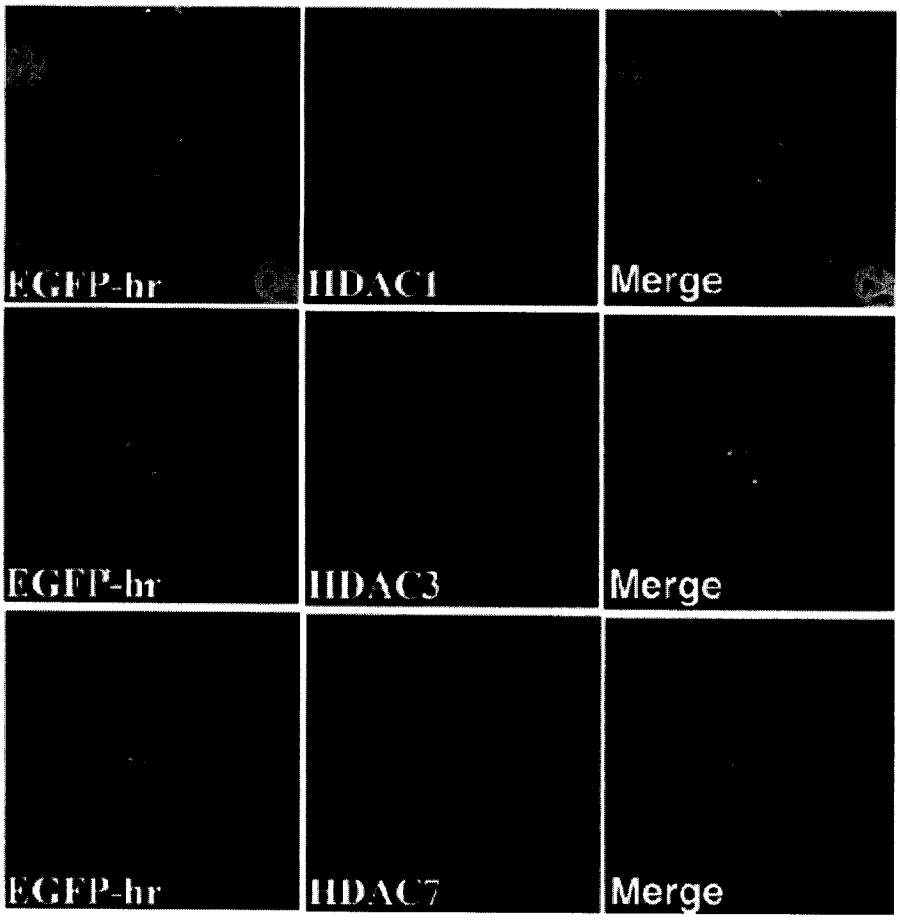

Fig. 4 Monitoring EGFP-hr speckle localization with HDAC1, 3, and 7. Cells were transfected with the EGFP-hr vector 24 hr after cells were fixed, and processed for indirect immunostaining of the endogenous HDAC proteins with anti-HDAC1, 3, or 7 as shown in panels HDAC1, 3, and 7, respectively. Note the co-localization of EGFP-hr and HDAC3 at sites of speckle formation (middle panel EGFP-hr, HDAC3, and merge).

hr-GFP protein, and found that the exogenous hr fusion protein distributed in sub-nuclear foci with a punctate appearance in 1% to 2% of the cells showing the lowest level of GFP signal (Fig. 4, EGFP-hr). We also recorded the number of nuclear speckles as varying from 2 to 10 spots. Interestingly, in cells transfected with the N-terminal region of hr corresponding to amino acid residues 1–551 or 111–427, the number of nuclei showing the punctate distribution was increased to more than 25% of the total number of transfected cells (data not shown).

Such nuclear speckles have previously been reported as containing numerous proteins and are implicated in transcriptional regulation. Therefore, we investigated whether the nuclear bodies containing hr were overlapping with a subset of endogenous HDAC proteins in NIH3T3 cells transiently transfected with the full-length hr cDNA. Using commercially available antibodies against HDAC1, 3, and 7, we monitored the distribution of these HDACs in comparison to the hr speckles by indirect immunofluorescence (Fig. 4). HDAC1 was localized throughout the nuclear compartment, exhibited a rather diffuse distribution, and was not co-localized with the hr speckles (Fig. 4, HDAC1). HDAC7 was localized in the cytoplasm in a punctate pattern at the perinuclear region and was not detectable in the nuclei (Fig. 4, HDAC7). HDAC3, however, was distributed within the nucleus with a very weak signal overall, suggesting a low level of endogenous HDAC3 expression in NIH3T3 cells. Notably, the HDAC3 signal appeared more concentrated at the hr speckles (Fig. 4, HDAC3, merge). When similar experiments were performed with the N-terminal half of hr, we observed a similar co-distribution with only HDAC3 (data not shown). Interestingly, when cells were transfected with the chimeric hr protein, we again observed no overlapping staining with HDAC1 and 7 (data not shown); however, we still observed a co-localization of HDAC3 with the chimeric protein (Fig. 5). Furthermore, as more speckles were formed with the chimeric protein, HDAC3 appeared to be recruited into the sub-nuclear bodies (Fig. 5).

Discussion

Localizing regulatory proteins to specialized sites within the nucleus involves nuclear import, *in situ* interactions with chromatin and transcriptional co-regulators, and sub-nuclear targeting. The mechanisms controlling nuclear import and interactions of transcription factors with DNA and co-regulators are well defined (Gorlich

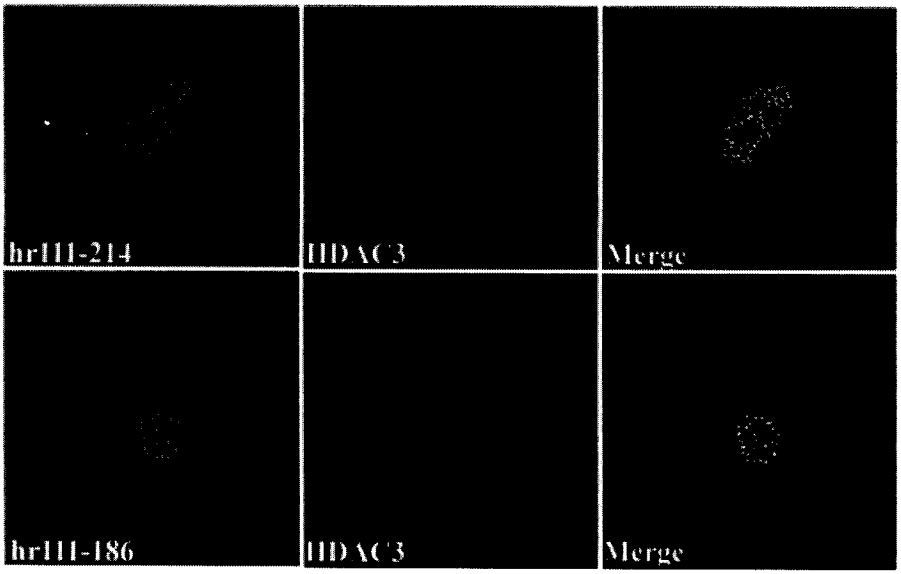

Fig. 5 The hr fragment 111–186 co-localized with HDAC3. Cells were transfected with the chimeric hr vector containing the hr NLS fused to amino acids 111–214 or 111–186. Twenty-four hours later, cells were processed for indirect immunofluorescence with anti-HDAC3 antibody. Note that the hr nuclear matrix region formed numerous speckles that co-localized with the HDAC3.

and Kutay, 1999; Lemon and Tjian, 2000). However, molecular determinants that target regulatory factors to specific sub-nuclear domains involved in transcription and chromatin remodeling remain to be identified.

Hairless has a novel NMTS and is localized in the N-terminal region

In this study, we report the determinants of sub-nuclear targeting for the hr regulatory complex. We demonstrate that hr is localized in distinct NM-associated sub-nuclear foci that are resistant to biochemical fractionation and chromatin removal from the nucleus. Using a panel of deletion mutants (Fig. 2A,2C), we find that amino acid sequence 111–186 of hr protein, designated the NMTS, is both necessary and sufficient for hr retention in sub-nuclear foci.

Analysis of the predicted hairless amino acid sequence does not show homology to any known protein. However, it disclosed a putative zinc-finger motif with homology to the GATA family of nuclear transcription factors (Arceci et al., 1993). The hr putative zinc-finger domain resides within a loop region at amino acids 590–620 in the mouse hr sequence and is comprised of a cluster of six cysteine residues with a novel spacing that is conserved among the rat, mouse, monkey, and human hr sequences (Ahmad et al., 1998b). Deletion constructs that removed the C-terminal half region of hr and therefore the zinc-finger domain did not alter the distribution of the N-terminal half of hr to the nuclear matrix compartment (Fig. 1). This observation suggested that deletion of the zinc-finger domain of hr and the rest of the C-terminal region were not required for retention of hr to the nuclear matrix scaffold. Strikingly, removal of amino acids within residues 111–186 does not influence competency for nuclear import, however, the sub-nuclear retention of this hr mutant is abrogated. Taken together, these results demonstrate that the sequences responsible for sub-nuclear distribution of hr are distinct from the zinc finger and that the determinants of sub-nuclear targeting reside in the N-terminal region of hr between positions 111 and 186 (Fig. 3). Importantly, the NMTS of hr functions autonomously, and can target a heterologous protein to sub-nuclear hr foci (Fig. 5).

The hr NMTS is a novel sequence

When the hairless sequence from amino acid residues 111–186 was aligned against protein sequences from the GenBank database using PSI-Blast from NCBI, the only sequences producing significant alignment corresponded to the hr sequence itself from different species as shown in Figure 2D. Interestingly, only one sequence that is not related to hairless was found to share sequence identity of 31% and homology of 41% within this region of hr. The protein sequence corresponded to a potential transcriptional repressor, Not-4, found in *S. cerevisiae*, mouse, and human with the accession numbers NM-016877, U71269, and AF180475, respectively. These results indicate that the NMTS of hairless is unique, and defines a new signal sequence that is not related to other proteins known to interact with the nuclear matrix scaffold.

Interestingly, sequence comparison of the hr NMTS did not reveal any similarities with other NMTSs reported to date. The number of NMTSs in the literature is very limited. For example, the bone-related Runx2 transcription factor was localized in distinct NM-associated sub-nuclear foci that are resistant to biochemical fractionation and chromatin removal from the nucleus (Zaidi et al., 2001), and a 38 amino acid sequence of Runx2 (amino acids 397–434) was designated as the

NMTS. Another transcription factor denoted YY1 was also shown to associate to the nuclear matrix compartment, and the YY1 NMTS was identified within the C-terminal domain at amino acid position 257–341 (McNeil et al., 1998). In the leukemia and bone-related AML/CBF-α transcription factor family, the NMTS resides within a 31 amino acid sequence and was localized at position 351–381 in AML-1B (Zeng et al., 1997). The fact that the different NMTSs reported so far do not share sequences similarities suggests that each signal sequence must govern the sub-nuclear distribution of the individual nuclear regulatory proteins.

In addition to the nuclear components described above, a number of steroid hormone receptors (glucocorticoid receptor, estrogen receptor, vitamin D receptor, androgen receptor) have also been reported as tightly associated to the nuclear matrix scaffold (Getzenberg and Coffey, 1990; Van Steensel et al., 1995a, 1995b; DeFranco and Guerrero, 2000). Furthermore, the histone deacetylases (HDAC) and acetyl transferases (HAT) have also been localized to the nuclear matrix compartment (Davie, 1998). The nuclear matrix is involved in gene localization and in the sub-nuclear concentration of regulatory factors (Blencowe et al., 1994; Mancini et al., 1994; Stein et al., 1994; Zaidi et al., 2001). A direct demonstration of the specificity of transcription factor-nuclear matrix interactions is supported by the different NMTS sequences identified so far, which indicate a possible role of the nuclear matrix in regulation of gene expression.

The regulatory consequences of hr NMTS-mediated sub-nuclear targeting may be significant for transactivation or repression of the hr-target genes in the skin. The conservation of the NMTS in hr proteins of different species suggests that intra-nuclear targeting represents a conserved function of hr. Additional characterization of mechanisms that control hr localization at sub-nuclear sites should contribute to a better understanding of hr function as well as its role in the development of the skin and hair phenotype in atrichia with papular lesions (APL).

Hairless is localized in nuclear speckles

In the course of this work, we noticed that the number of transfected cells showing speckle formation was dependent on the level of expression of the hr fusion protein. This observation suggested that at lower levels of expression, which probably mimicked the endogenous level of hr, expression was presumably localized at specific sites within the nuclear compartment. Such nuclear speckles have been reported to contain numerous proteins implicated in aspects of transcriptional regulation (activation or repression; Spector, 2001). Recently, it has been suggested that hr might function as a transcriptional co-repressor for thyroid hormone receptors (Potter et al., 2001). The co-repressors such as SMRT and N-CoR bind nuclear hormone receptors and act as platform proteins that recruit large protein complexes including class I and II histone deacetylases (HDACs; Downes et al., 2000). HDAC catalyzes removal of acetyl groups from hyperacetylated histone and this de-acetylation process leads to modification of nucleosome structure, resulting in transcriptional silencing (Kuo and Allis, 1998).

Therefore, we investigated whether the nuclear bodies containing hr also contained endogenous HDACs in NIH3T3 cells transiently transfected with hr cDNA. We found that HDAC3 co-localized with the hr speckles. When cells were transfected with the chimeric construct containing the NMTS of hr fused to GFP, we again obtained co-localization with HDAC3. These results demonstrate that more HDAC3 appeared to be recruited at the sites of nuclear speckle formation, suggesting that these foci are increasing the sites of interaction for HDAC3 protein. Taken together, these data suggest that there is a hierarchy of signals for protein localization within the nucleus. The NMTS region of hr (amino acids 111–186) not only mediated interactions with components of the nuclear matrix scaffold, but also specified the location of hr to functional multi-protein complexes by interacting or recruiting specific hr-associated proteins such as HDAC3.

In summary, our results are consistent with the notion that the sub-cellular localization of hr and/or its interactions with other nuclear matrix-associated regulatory factors may be determinants of hr-mediated transcriptional control within the context of nuclear architecture.

Acknowledgments We thank Dr. Burkhard Rost (Columbia University, http://cubic.bioc.columbia.edu/), for valuable advice on the hr NMTS identification. This work was supported in part by grants from the National Institutes of Health, NIAMS RO3AR4761 and KO1AR48594 to K.D. and RO147338 to A.M.C.

References

Ahmad, M., Panteleyev, A., Henson-Appollonio, V., Sundberg, J.P. and Christiano, A.M. (1998a) Molecular basis of a novel rhino (hr(rhchr)) phenotype: a nonsense mutation in the mouse hairless gene. Exp Dermatol 7:298–301.

Ahmad, W., Irvine, A.D., Lam, H., Buckley, C., Bingham, E.A., Panteleyev, A.A., Ahmad, M., McGrath, J.A. and Christiano, A.M. (1998b) A missense mutation in the zinc-finger domain of the human hairless gene underlies congenital atrichia in a family of Irish travelers. Am J Hum Genet 63:984–991.

Ahmad, W., Faiyaz ul Haque, M., Brancolini, V., Tsou, H.C., ul Haque, S., Lam, H., Aita, V.M., Owen, J., deBlaquiere, M., Frank, J., Cserhalmi-Friedman, P.B., Leask, A., McGrath, J.A., Peacocke, M., Ahmad, M., Ott, J. and Christiano, A.M. (1998c) Alopecia universalis associated with mutation in the human hairless gene. Science 279:720–724.

Arceci, R.J., King, A.A., Simon, M.C., Orkin, S.H. and Wilson, D.B. (1993) Mouse GATA-4: a retinoic acid-inducible

GATA-binding transcription factor expressed in endodermally derived tissues and heart. Mol Cell Biol 13:2235–2246.

Blencowe, B.J., Nickerson, J.A., Issner, R., Penman, S. and Sharp, P.A. (1994) Association of nuclear matrix antigens with exon-containing splicing complexes. J Cell Biol 127:593–607.

Cachon-Gonzalez, M.B., Fenner, S., Coffin, J.M., Moran, C., Best, S. and Stoye, J.P. (1994) Structure and expression of the hairless gene of mice. Proc Natl Acad Sci USA 91:7717–7721.

Chaudhary, N. and Courvalin, J.C. (1993) Stepwise reassembly of the nuclear envelope at the end of mitosis. J Cell Biol 122:295–306.

Davie, J.R. (1998) Covalent modifications of histones: expression from chromatin templates. Curr Opin Genet Dev 8:173–178.

DeFranco, D.B. and Guerrero, J. (2000) Nuclear matrix targeting of steroid receptors: specific signal sequences and acceptor proteins. Crit Rev Eukaryot Gene Expr 10:39–44.

Djabali, K., Portier, M.-M., Gros, F., Blobel, G. and Georgatos, S.D. (1991) Network antibodies identify nuclear lamin B as a physiological attachment site for peripherin intermediate filaments. Cell 64:109–121.

Djabali, K., Aita, V.M. and Christiano, A.M. (2001) Hairless is translocated to the nucleus via a novel bipartite nuclear localization signal and is associated with the nuclear matrix. J Cell Sci 114:367–376.

Downes, M., Ordentlich, P., Koa, H., Alavarez, J.G.A. and Evans, R. (2000) Identification of a nuclear domain with deacetylase activity. Proc Natl Acad Sci USA 97:10330–10335.

Getzenberg, R.H. and Coffey, D.S. (1990) Tissue specificity of the hormonal response in sex accessory tissues with nuclear matrix protein patterns. Mol Endocrinol 4:1336–1342.

Gniadecki, R., Olszewska, H. and Gajkowska, B. (2001) Changes in the ultrastructure of cytoskeleton and nuclear matrix during HaCaT keratinocyte differentiation. Exp Dermatol 10:71–79.

Gorlich, D. and Kutay, U. (1999) Transport between the cell nucleus and the cytoplasm. Annu Rev Cell Dev Biol 15:607–660.

He, D., Nickerson, A.N. and Penman, S. (1990) Core filaments of the nuclear matrix. J Cell Biol 110:569–580.

Kuo, M.H. and Allis, C.D. (1998) Roles of histone acetyltransferases and deacetylases in gene regulation. Bioessays 20:615–626.

Lemon, B. and Tjian, R. (2000) Orchestrated response: a symphony of transcription factors for gene control. Genes Dev 14:2551–2569.

Mancini, M.A., Shan, B., Nickerson, J.A., Penman, S. and Lee, W. (1994) The retinoblastoma gene product is a cell cycle-dependent, nuclear matrix-associated protein. Proc Natl Acad Sci USA 91:418–422.

McNeil, S., Guo, B., Stein, J.L., Lian, J.B., Bushmeyer, S., Seto, E., Atchison, M.L., Penman, S., van Wijnen, A.J. and Stein, G.S. (1998) Targeting of the YY1 transcription factor to the nucleolus and the nuclear matrix *in situ*: the C-terminus is a principal determinant for nuclear trafficking. J Cell Biochem 68:500–510.

Nakamura, M., Sundberg, J.P. and Paus, R. (2001) Mutant laboratory mice with abnormalities in hair follicle morphogenesis, cycling, and/or structure: annotated tables. Exp Dermatol 10:369–390.

Panteleyev, A.A., Paus, R., Ahmad, W., Sundberg, J.P. and Christiano, A.M. (1998a) Molecular and functional aspects of the hairless (hr) gene in laboratory rodents and humans. Exp Dermatol 7:249–267.

Panteleyev, A.A., Van der Veen, C., Rosenbach, T., Muller-Rover, S., Sokolov, V.E. and Paus, R. (1998b) Toward defining the pathogenesis of the hairless phenotype. J Invest Dermatol 110:902–907.

Paus, R., Muller-Rover, S. and Botchkarev, V.A. (1999) Chronobiology of the hair follicle: hunting the hair cycle clock. J Invest Dermatol 4:338–345.

Potter, G.B., Beaudoin, G.M.R., DeRenzo, C.L., Zarach, J.M., Chen, S.H. and Thompson, C.C. (2001) The hairless gene mutated in congenital hair loss disorders encodes a novel nuclear receptor corepressor. Genes Dev 15:2687–2701.

Prince, M., Banerjee, C., Javed, J., Green, J., Lian, J.B., Stein, G.S., Bodine, P.V.N. and Komm, B.S. (2000) Expression and regulation of Runx2/Cbfa1 and osteoblast phenotypic markers during the growth and differentiation of human osteoblasts. J Cell Biochem 80:424–440.

Spector, D.L. (2001) Nuclear domains. J Cell Sci 114:2891–2893.

Stein, G.S., van Wijnen, A.J., Stein, J.L., Lian, J.B., Bidwell, J.P. and Montecino, M. (1994) Nuclear architecture supports integration of physiological regulatory signals for transcription of cell growth and tissue-specific genes during osteoblast differentiation. J Cell Biochem 55:4–15.

Stenn, K.S. and Paus, R. (2001) Controls of hair follicle cycling. Physiol Rev 81:449–494.

Van Steensel, B., Brink, M., Van der Meuten, K., Van Binnendijk, E.P., Wansink, D.G., de Jong, L., de Kloet, E.R. and van Driel, R. (1995a) Localization of the glucocorticoid receptor in discrete clusters in the cell nucleus. J Cell Sci 108:3003–3011.

Van Steensel, B., Jenster, G., Damm, K., Brinkmann, A.O. and van Driel, R. (1995b) Domains of the human androgen receptor and glucocorticoid receptor involved in binding to the nuclear matrix. J Cell Biochem 57:465–478.

Zaidi, S.K., Javed, A., Choi, J.-Y., van Wijnen, A.J., Stein, J.L., Lian, J.B. and Stein, G.S. (2001) A specific targeting signal directs Runx2/Cbfa1 to subnuclear domains and contributes to transactivation of osteocalcin gene. J Cell Sci 114:3093–3102.

Zeng, C., van Wijnen, A.J., Stein, J.L., Meyers, S., Sun, W., Shopland, L., Lawrence, J.B., Penman, S., Lian, J.B., Stein, G.S. and Hiebert, S.W. (1997) Identification of a nuclear matrix targeting signal in the leukemia and bone-related AML/CBF-α transcription factors. Proc Natl Acad Sci USA 94:6746–6751.

Aromatic Sulfide Inhibitors of Histone Deacetylase Based on Arylsulfinyl-2,4-hexadienoic Acid Hydroxyamides

Charles M. Marson,*,† Pascal Savy,† Alphonso S. Rioja,† Thevaki Mahadevan,† Catherine Mikol,‡ Arthi Veerupillai,‡ Eva Nsubuga,‡ Angela Chahwan,‡ and Simon P. Joel‡

Department of Chemistry, University College London, Christopher Ingold Laboratories, 20 Gordon Street, London WC1H OAJ, U.K., and Department of Medical Oncology, St. Bartholomew's Hospital, London W12 ONN, U.K.

Received October 8, 2005

The synthesis of a novel series of potent inhibitors of histone deacetylases is described, based on arylsulfinyl-2,4-hexadienoic acid hydroxyamides and their derivatives. In vitro IC_{50} values down to 40 nM were obtained, and several compounds showed inhibition of CEM (human leukemic) cell viability with IC_{50} of ~1.5 μM, comparable to or better than that of suberoylanilide hydroxamic acid, an inhibitor of histone deacetylase currently in clinical trials.

Introduction

Inhibitors of histone deacetylase (HDAC) enzymes are emerging as a promising class of anticancer agents[1,2] able to regulate gene transcription[3−5] and inhibit cancer cell proliferation by induction of cell cycle arrest, differentiation, and/or apoptosis.[6−8] HDAC enzymes catalyze the deacetylation of ϵ-amino groups of lysine residues in the N-terminal tails of core histones in the nucleosome, resulting in an increased interaction of the protonated ϵ-amino lysine residues with DNA, leading to a compacted and less accessible chromatin structure.[9] Consequently, HDACs can act as repressors of gene transcription by mediating conformational changes in the nucleosome and altering the accessibility of transcription factors to DNA.[10,11] The inappropriate recruitment of HDAC enzymes by oncogenic proteins may alter gene expression in favor of arrested differentiation and/or excessive proliferation.[12] Accordingly, the hyperacetylation of chromatin induced by inhibitors of HDACs usually results in the relief of transcriptional repression of certain genes, e.g., the cyclin-dependent kinase inhibitor protein $p21^{WAF1/CIP1}$.[12,13] Relief of transcriptional repression is known to be central to the therapeutic mode of action of HDAC inhibitors in the treatment of several proliferative diseases, including a variety of leukemias.[14,15]

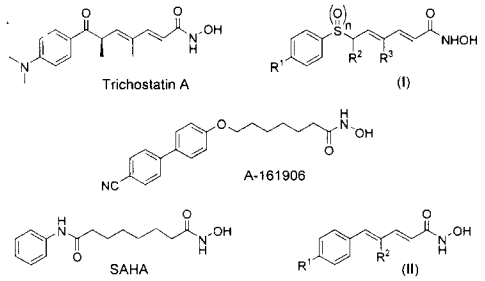

A number of small-molecule inhibitors of HDAC including trichostatin A (TSA)[16] and suberoylanilide hydroxamic acid (SAHA)[17] induce differentiation in cancer cell lines and suppress cell proliferation. Several HDAC inhibitors including SAHA, NVP-LAQ824,[5] MS-275,[18] and the cyclodepsipeptide FK-228[19] have entered clinical trials. The efficacy of such HDAC inhibitors is generally considered to depend on the presence of (1) a terminal group (hydroxamic acid in the present class of novel inhibitors) that can bind to the metal-containing active site of HDAC enzymes and is connected to (2) a chain of several atoms ("linker") that is linked to (3) an end moiety (or "cap") of sufficient bulk to occupy the cleft outside the pocket that leads to the active site. Such a model is in agreement with crystal structures of histone deacetylase-like protein (HDLP) to which is bound TSA or SAHA.[20]

As part of our anticancer program centered on therapy using small molecules, we have used the framework of trichostatin A to design novel HDAC inhibitors (**II**).[21] We have shown that HDAC inhibitory potency can be maintained (in vitro IC_{50} down to 50 nM)[21] by using a simplified carbon chain although it lacks the keto group and adjacent chiral center present in trichostatin A. As HDAC mimics of trichostatin A, a number of functionalities have been interposed between an aromatic ring and an alkyl or alkylene chain, especially numerous amides,[20,22−25] and recently an oxygen atom in the form of the aromatic ether designated A-161906, which showed potent in vitro HDAC inhibition (IC_{50} = 9 nM) but appeared to have correspondingly less satisfactory in vivo properties.[26] HDAC inhibitors based on aromatic thioethers were not reported and have the advantage of an adjustable oxidation level at sulfur for improving activity, possibly by means of a prodrug mode of action. Such replacement of carbon by sulfur was also structurally appealing since a sulfur isostere, the sulfoxide of **12**, could be prepared and evaluated in which a sulfoxide group replaced the inherently reactive carbonyl group of trichostatin A. Accordingly, we describe here the synthesis and preliminary biological evaluation of a new class of sulfur-containing HDAC inhibitors, principally of type **I**.

Chemistry

Few arylsulfanylhexa-2,4-dienoic acids are known,[27] and to our knowledge no arylsulfanylhexa-2,4-dienoic acid hydroxyamides have been previously reported. Reaction of methyl sorbate and *N*-bromosuccinimide in chlorobenzene at reflux and under irradiation with a sunlamp afforded methyl (2*E*,4*E*)-6-bromo-2,4-hexadienoate (**2**).[28] Ester **2** or the corresponding ethyl ester proved suitable for alkylation of a variety of aromatic thiols, typically in tetrahydrofuran and in the presence of triethylamine (1.0 equiv) at 20 °C or where the reaction was more sluggish

* To whom correspondence should be addressed. Phone: +44(0)20 7679 4712. Fax: +44(0)20 7679 7463. E-mail: c.m.marson@ucl.ac.uk.
† University College London.
‡ St. Bartholomew's Hospital.

10.1021/jm051010j CCC: $33.50
Published on Web 12/21/2005

Scheme 1[a]

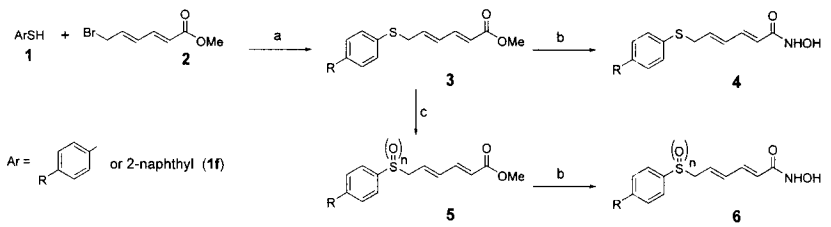

[a] Reagents: (a) Et_3N, Bu_4NI, THF; (b) aqueous NH_2OH; (c) $NaIO_4$. Key: (a) R = H (n = 1); (b) R = Cl (n = 1); (c) R = OMe (n = 1); (d) R = NMe_2 (n = 1); (e) R = H (n = 2); (f) Ar = 2-naphthyl.

Scheme 2[a]

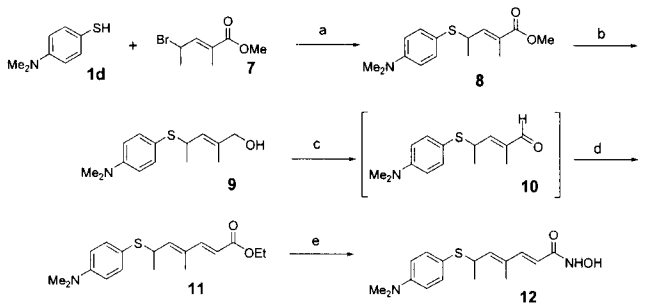

[a] Reagents: (a) Et_3N, Bu_4NI, THF; (b) DIBAL, THF; (c) pyridine–SO_3, Et_3N, DMSO; (d) $Ph_3P{=}CHCO_2Et$, CH_2Cl_2; (e) 50% aqueous NH_2OH, 1 M KOH in MeOH, THF.

Scheme 3[a]

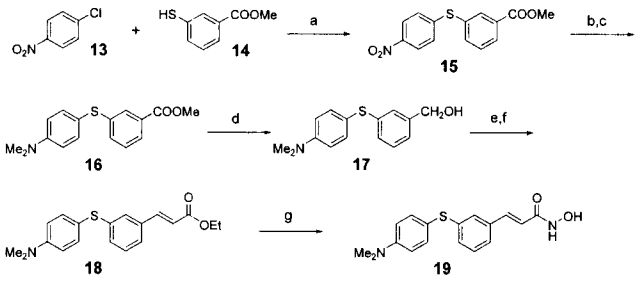

[a] Reagents: (a) NaOMe, MeOH, THF; (b) H_2, Pd/C; (c) 37% aqueous HCHO, $NaBH_3CN$, $ZnCl_2$, MeOH; (d) $LiAlH_4$, THF; (e) pyridine–SO_3, Et_3N, DMSO; (f) $Ph_3P{=}CHCO_2Et$, CH_2Cl_2; (g) 50% aqueous NH_2OH, 1 M KOH in MeOH, THF.

Scheme 4[a]

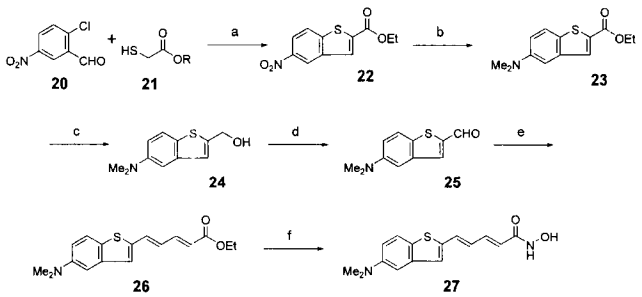

[a] Reagents: (a) NaH, DMF; (b) H_2, Pd/C, EtOAc, then 37% aqueous HCHO, $NaBH_3CN$, $ZnCl_2$, MeO; (c) $LiAlH_4$, THF; (d) pyridine–SO_3, Et_3N, DMSO; (e) $(EtO)_2P(O)CH_2CH{=}CHCO_2Et$, NaH, DME; (f) 50% aqueous NH_2OH, 1 M KOH in MeOH, THF.

by heating at reflux (Scheme 1). The resulting esters **3** were readily converted into the corresponding sulfoxides **5** (n = 1) by treatment with $NaIO_4$ (1.2 equiv) in aqueous methanol; the sulfone **5e** was prepared by reaction of methyl (2*E*,4*E*)-6-bromo-2,4-hexadienoate (**2**) with sodium benzenesulfinate. The thioethers **3** and the sulfoxides **5** (n = 1) were converted into their corresponding hydroxamic acids **4** and **6** by treatment of a solution of the appropriate ester in THF with 50% aqueous hydroxylamine (9 equiv) at 0 °C to which was subsequently added a solution of potassium hydroxide in methanol (1 M, 1.6 equiv) with stirring over ~30 min. The corresponding carboxylic acids of the thioethers **3** and the sulfoxides **5** (n = 1) could be prepared by hydrolysis with lithium hydroxide or sodium hydroxide.

Synthesis of the trichostatin thio analogue **12** (Scheme 2) required a sequence compatible with the sensitive nitrogen, sulfur, and dienic functionality. 4-Dimethylaminobenzenethiol (**1d**) was reacted with methyl (*E*)-4-bromo-2-methyl-2-pentenoate (**7**) in the presence of triethylamine to give the key thioether **8** in 95% yield. Ester **7** was prepared by reaction of methyl (*E*)-2-methylpent-2-enoate with *N*-bromosuccinimide in carbon tetrachloride at reflux and under irradiation with a sunlamp.[31] Reduction of ester **8** by diisobutylaluminum hydride (3 equiv) at 0 °C in toluene afforded the corresponding allylic alcohol **9** (88%), which was subjected to Moffatt oxidation (pyridine–sulfur trioxide complex in DMSO followed by addition of triethylamine) to give a solution from which the aldehyde **10** was extracted with diethyl ether; evaporation afforded the crude aldehyde **10**, which was reacted with ethyl (triphenylphosphoranylidene)acetate (1.1 equiv) in THF to give the ethyl ester **11** in 76% yield after purification by column chromatography. Treatment of ester **11** with 50% aqueous hydroxylamine (9 equiv) followed by a solution of potassium hydroxide in methanol gave the trichostatin thio analogue **12** in 52% yield.

Since the cinnamohydroxamic acid moiety was shown to be a favorable linker and terminus for HDAC inhibitors, the diarylthioether **19**, a benzannulated version of the 1,3-dimethyl-substituted hydroxamic acid **12**, was of considerable interest. The likely difficulty in forming an aryl ether linkage by reaction of thiol **1d** with an arene precursor that would be relatively unactivated suggested the reverse combination, i.e., a thiol component such as **14** for reaction with a displaceable halogen atom, as in *p*-chloronitrobenzene (**13**). Such an approach would necessitate conversion of the nitro group into the dimethylamino group present in diarylthioether **19**. The sequence in Scheme 3 proved to be effective; thus, treatment of the thiolate of ester **14** in methanol with *p*-chloronitrobenzene (**13**) first at 0 °C followed by heating at reflux for 2 h gave the thioether **15** (73%), which was reduced quantitatively to the corresponding amino compound, which was reductively aminated with aqueous 37% formaldehyde in the presence of $NaBH_3CN$ and $ZnCl_2$ to give the key *N,N*-dimethylamino intermediate **16** in 80% yield. The latter was then reduced quantitatively with $LiAlH_4$ to give the alcohol **17**, which was subjected to a sequence of Moffat oxidation, Wittig olefination, and hydroxamation, similar to that described above for alcohol **9** and resulting in the novel cinnamohydroxamic acid **19**.

In the quest for a more druglike compound (Scheme 4), a fused system, benzo[*b*]thiophene, was considered in which a methyl group in the chain was formally annealed to the aromatic

Scheme 5[a]

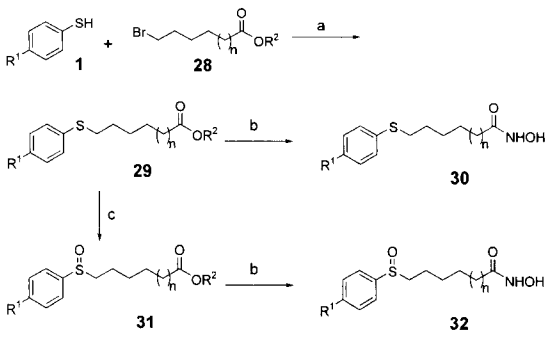

[a] Reagents: (a) Et_3N; (b) 50% aqueous NH_2OH, 1 M KOH in MeOH, THF; (c) $NaIO_4$. Key: (a) R^1 = H, R^2 = Me, n = 1; (b) R^1 = Cl, R^2 = Me, n = 1; (c) R^1 = Cl, R^2 = Et, n = 2; (d) R^1 = NMe_2, R^2 = Me, n = 1; (e) R^1 = p-$ClC_6H_4SO_2NH$, R^2 = Me, n = 1; (f) R^1 = NH_2, R^2 = Me, n = 1.

ring present in the previous compound types. The ready accessibility of the suitably functionalized benzo[*b*]thiophene **22**,[32] together with previously successful sequences of chain extension and hydroxamation permitted Scheme 4 to be realized. Thus, ester **22**, prepared from sodium hydride, ethyl 2-mercaptoacetate, and 2-chloro-5-nitrobenzaldehyde, was hydrogenated over 10% palladium on carbon to give the corresponding amine that after filtration was used directly in solution for the reductive amination with aqueous 37% formaldehyde in the presence of $NaBH_3CN$ and $ZnCl_2$ to give the key *N,N*-dimethylamino intermediate **23** in 60% yield. The latter was reduced with $LiAlH_4$ to give the alcohol **24**, which was subjected to a sequence of Moffat oxidation, Wittig olefination (differing from the above sequences by the use of triethyl phosphonocrotonate), and hydroxamation, similar to that described above for alcohols **9** and **1** and resulting in the novel cinnamohydroxamic acid **27**.

A variety of compounds containing a saturated chain (Scheme 5) were prepared using methods similar to those for the unsaturated ones shown in Scheme 1. Thus, thiolates **1** were reacted with ω-bromoesters **28** to give thioethers **29** that could be converted into the corresponding sulfoxides **31** using $NaIO_4$. Treatment of **29** and **31** with 50% aqueous hydroxylamine and potassium hydroxide, as described above, afforded the corresponding hydroxamic acids **30** and **32**. Treatment of sulfide **30b** with $NaIO_4$ afforded the sulfoxide **32b** in 68% yield. Upon treatment with *m*-CPBA, sulfoxide **32a** also underwent oxidation, affording the corresponding sulfone **33** in 54% yield. Such oxidations at sulfur in the presence of a hydroxamic acid group provide a useful alternative to establishing the desired oxidation level at sulfur prior to conversion into the hydroxamic acid.

Biology

Table 1 shows that most of the novel sulfur-containing compounds exhibited HDAC IC_{50} of <400 nM in the purified enzyme assay,[33] a promising result since the assay generally gives appreciably higher IC_{50} than assays involving release of tritiated acetic acid from an N-acylated peptide substrate.[4,5] The HPLC-based HDAC assay was modified to permit the determination of HDAC activity in intact cells at a single time-point, reflecting uptake of the compound by cells and inhibition of intracellular HDAC enzymes. Moreover, this measure of cellular HDAC inhibitory activity showed a better correlation with the concentration of inhibitor that induced a 50% reduction in cell viability in CEM cells after a 72 h incubation than with values from the liver HDAC assay (Spearman's rank correlation coefficient for liver IC_{50} vs % viability IC_{50} = −0.603, p = 0.017; cell IC_{50} vs % viability IC_{50} correlation coefficient = 0.82, p < 0.001). The cellular HDAC assay may therefore be a more accurate indication of the desired biological endpoint for further screening of HDAC inhibitors that show activity against partially purified enzyme.

Table 1. In Vitro Inhibition of Histone Deacetylase and CEM Cell Viability

Entry	Compound	Structure	HDAC inhibitory activity: Purified liver IC_{50} (μM)	HDAC inhibitory activity: CEM cells IC_{50} (μM)	50% Viability in CEM cells IC_{50} (μM)
1	**30a**	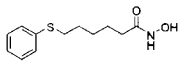	0.12±0.11	9.4±1.9	>25
2	**32a**	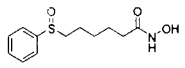	0.06±0.02	7.7±1.4	>25
3	**33**	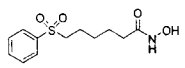	0.04±0.01	15.5±7.4	>25
4	**4a**	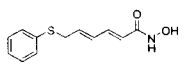	0.39±0.12	>25	ND[a]
5	**6a**	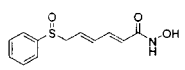	0.24±0.03	>25	ND
6	**30b**	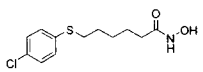	0.26±0.07	>25	>25
7	**32b**	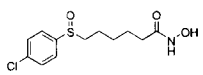	0.15±0.01	1.3±0.4	2.6±0.2
8	**32d**	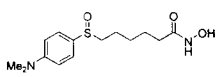	0.18±0.01	2.2±0.1	3.4±1.0
9	**32c**	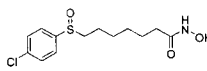	0.38±0.01	1.6±0.2	12.3±3.0
10	**30e**	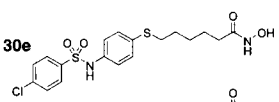	0.11±0.01	9.4±4	>25
11	**4b**	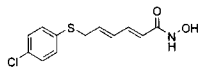	0.31±0.02	1.6±0.2	1.6±0.1
12	**4f**	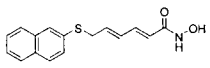	0.70±0.31	9.4±4.0	1.7±0.6
13	**12**	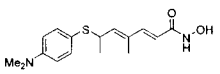	0.34±0.02	5.3±0.9	7.5±0.7
14	**6b**	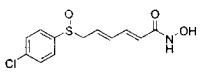	0.40±0.10	1.2±0.4	ND
15	**6c**	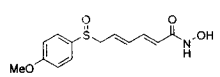	0.41±0.02	5.4±0.5	9.6±0.3
16	**19**	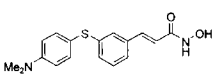	0.16±0.02	8.6±1.8	3.4±0.6
17	**27**	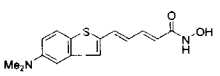	>25	ND	ND
18	**SAHA**	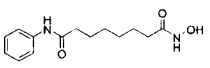	0.44±0.03	0.33±0.05	1.9±0.1

[a] ND = not determined.

The low IC_{50} value for CEM cell viability (1.6 μM) for **4b** encouraged a further study using a modification of the whole-cell assay to allow the determination of intracellular HDAC inhibitory activity after 1 and 24 h of incubation in CEM cells in culture media. The concentration of **4b** required to maintain 50% HDAC inhibition after 24 h was not different from the

concentration at 1 h (3.4 vs 3.4 μM). Additionally, similar studies with **32b** showed comparable stability to **4b** (2.9 μM at 1 h vs 3.4 μM at 24 h). This is in contrast to SAHA, which required a 65% increase in the concentration to achieve 50% HDAC inhibition at 24 h (0.9 vs 2.6 μM), and in marked contrast to TSA for which a >90% increase in concentration was required (0.03 vs 0.37 μM). Those data suggest an improved metabolic stability of **4b** in CEM cells.

All *S*-compounds in Table 1 except **32c** contain five carbon atoms between the sulfur atom and the carbon atom of the hydroxamic acid moiety, the additional methylene group in **32c** (compared with **32b**) conferring lower activity in all three assays and indicating that a linker of six methylene groups may be longer than optimal; that would be consistent with the additional length of ~0.8 Å arising from two carbon−sulfur bonds, compared with the two carbon−oxygen bonds present in A-161906. Both dienic and fully saturated chains were found to possess potent in vivo HDAC inhibitory activities. Potencies of the parent systems (entries 1−3) are high in the enzyme assay but low in both CEM cell assays, a pattern also found for the unsubstituted and unsaturated counterparts (entries 4 and 5). Of the para substituents examined, chloro was usually very effective (entries 7, 11, and 14) in the CEM cell assays. However, additional methyl groups as in **12** did not improve HDAC inhibitory activity, hydroxamic acid **12** showing an IC_{50} of 0.34 μM in the HDAC liver assay and 5.3 μM in CEM cells. Despite the sulfur atom of (±)-**12** being a replacement of the carbonyl group in trichostatin A, the latter (as a single enantiomer) has a much greater potency in the HDAC liver assay (IC_{50} = 0.015 μM) and the CEM cell asays (IC_{50} = 0.019 μM for HDAC inhibition and 0.12 μM for % viablility). In the compounds studied, the presence of a *p*-*N*,*N*-dimethylamino group was generally consistent with moderate but not outstanding potencies (entries 8, 13, and 17).

Although the sulfoxides were generally more potent than the corresponding sulfides in the enzyme assay (entries 1, 2; 4, 5; 6, 7 but contrast 11, 14), sulfide **4b** and sulfoxide **6b** were of comparable potency in the CEM cell HDAC assay. The sulfide **4f**, containing a hydrophobic capping region, is also of notable potency. The effect of sulfoxide **32b** on a further three cell lines was investigated; **32b** was shown to be cytotoxic to HCT116 (percentage viability IC_{50} ± SD: 3.9 ± 0.7 μM), SUD4 (7.5 ± 1.1 μM), and MCF-7 (6.1 ± 0.9 μM) cells. The concentration of **32b** that inhibited proliferation (cell number) by 50% in those cells was 0.9−2.7 μM. The saturated chain sulfides **30b** and **30e** showed potent activities using the purified enzyme assay but performed very poorly in the CEM cell assays; in contrast, the saturated chain sulfoxides **32b**−**d** typically showed good activities in all three assays. The striking difference in CEM cell activity between **30b** and **32b** may indicate the importance of a polar entity adjacent to the aromatic ring (such as the keto group in TSA) or may be associated with a more rapid cellular metabolism of the saturated chain sulfides. The additional hydrophobicity provided by the chlorophenyl terminus in **30e** was found, as expected,[21] to confer improved in vitro enzyme inhibition. While the cinnamohydroxamic acid type **19** provides tolerably good activities, such was not the case for **27** in which a fused ring system is present. Overall, these studies suggest that a sulfide or a sulfoxide linkage as part of an alkyl or possibly an alkylene chain, together with an extended hydrophobic capping region, could provide good potency and good antiproliferative properties with comparable or better metabolic stability than SAHA and much greater metabolic stability than TSA.

Summary

The efficacy of arylpenta-2,4-dienoic acid hydroxyamides indicates for the first time that aromatic thioether units can be present in a novel class of potent inhibitors of histone deacetylase. The sulfides tested, although structurally less similar to trichostatin A than the corresponding sulfones, were generally more potent than the latter, the sulfides probably exhibiting greater cellular uptake than the more polar sulfoxides (or sulfones). Sulfide **4b** was appreciably more metabolically stable than SAHA and far more so than trichostatin A. Since the rat liver assay[22] generally gives significantly higher in vitro IC_{50} than do assays based on deacetylation of tritiated histone-like substrates,[4,5] the present values of under 200 nM for several compounds are considered to be promising. Additionally, **32b** was shown to inhibit proliferation of three cell lines by 50% at 0.9−2.7 μM. One disadvantage of amidic HDAC inhibitors that have been clinically tested is their potential for cleavage by endogenous peptidases, a feature that is absent in most of the novel inhibitors of histone deacetylase herein described and that may confer improved in vivo stability over the more common amidic inhibitors such as SAHA.

Experimental Section

Chemistry. Melting points were determined on a microscope hot-stage apparatus and are uncorrected. IR spectra were recorded on a Perkin-Elmer PE-983 spectrophotometer. ^{1}H and ^{13}C NMR spectra were recorded on a Bruker AC300 instrument at 300 and 75 MHz, respectively; chemical shifts are reported in δ (ppm) relative to the internal reference tetramethylsilane. The homogeneity of the compounds was monitored by ascending thin-layer chromatography, performed on Merck 0.2 mm aluminum-backed silica gel 60 F_{254} plates and visualized using an alkaline $KMnO_4$ spray or by ultraviolet light. Flash column chromatography was performed using Merck 0.040−0.063 mm, 230−400 mesh silica gel. Elemental analysis (C, H, N, Cl, and S) results were obtained on a Perkin-Elmer 2400 CHN elemental analyzer, and all data were consistent with theoretical values (within ±0.4%) unless otherwise indicated. Mass spectra were obtained on a VG7070H mass spectrometer using Finigan Incos II. All solvents were reagent grade and, where necessary, were purified and dried by standard methods. Evaporation refers to the removal of solvent under reduced pressure. Flash column chromatography was performed using Sorbsil C60 40/60A silica gel. The following compounds were prepared according to the literature: (2*E*,4*E*)-6-phenylsulfanyl-2,4-hexadienoic acid,[27a] methyl (2*E*,4*E*)-6-phenylsulfanyl-2,4-hexadienoate,[39] methyl (2*E*,4*E*)-6-bromo-2,4-hexadienoate (**2**),[28] (2*E*,4*E*)-6-benzenesulfinyl-2,4-hexadienoic acid,[30] (2*E*,4*E*)-6-benzenesulfonyl-2,4-hexadienoic acid,[30] (2*E*,4*E*)-6-benzenesulfonyl-2,4-hexadienoic acid hydroxyamide,[30] 4-dimethylaminobenzenethiol (**1d**),[29,30] (*E*)-methyl 2-methyl-2-pentenoate,[35] with methyl 2(*E*)-4-bromo-2-methyl-2-pentenoate (**7**),[31] 5-nitrobenzo[*b*]thiophene-2-carboxylic acid ethyl ester (**22**),[32] methyl (2*E*,4*E*)-2,4-hexadienoate,[34] 3-mercaptobenzoic acid,[36] methyl 3-mercaptobenzoate (**14**),[37] methyl 6-bromohexanoate (**28a**),[38] ethyl 6-phenylsulfanyl hexanoate (**29a**),[39] *N*-(4methyl-7-coumarinyl)-*N*-ω-(*tert*-butyloxycarbonyl)-*N*-ω-acetyllysinamide (MAL),[33] (5-acetylamino-1-carbamoylpentyl)carbamic acid *tert*-butyl ester.[30]

(2*E*,4*E*)-6-(4-Chlorophenylsulfanyl)-2,4-hexadienoic Acid Hydroxyamide (4b). Procedure A. To a solution of methyl (2*E*,4*E*)-6-(4-chlorophenylsulfanyl)-2,4-hexadienoate (0.44 g, 1.64 mmol) in distilled THF (9.0 mL) containing 50% aqueous hydroxylamine (1.0 mL, 15.2 mmol) was added at 0 °C a solution of potassium hydroxide in methanol (1 M, 2.6 mL, 2.6 mmol) over 30 min. After the mixture was stirred at 0 °C for 1 h, distilled water (9.0 mL) was added and the mixture was made neutral by dropwise addition of 2 M HCl at 0 °C. The aqueous solution was extracted with ethyl acetate (3 × 30 mL), and the combined extracts were dried over anhydrous $MgSO_4$ and evaporated. The residue was recrystallized from acetone to give **4b** (0.21 g, 48%) as pale-brown microprisms,

mp 120−122 °C (dec). ^{1}H NMR ($CDCl_3$, 400 MHz) δ 10.63 (br s, 1H), 8.95 (br s, 1H), 7.34 (s, 4H), 6.98 (dd, J = 15.0, 11.2 Hz, 1H), 6.29 (dd, J = 15.0, 11.2 Hz, 1H), 6.07 (m, 1H), 5.75 (d, J = 15.2 Hz, 1H), 3.75 (d, J = 7.1 Hz, 2H); ^{13}C NMR ($CDCl_3$, 100 MHz) δ 162.7, 137.8, 135.1, 134.4, 131.1, 130.7, 130.4, 128.9, 122.0, 34.5. Anal. ($C_{12}H_{12}NClO_2S$) Calcd: C 53.43%, H 4.48%, N 5.19%. Found: C 52.88%, H 4.59%, N 5.08%.

(2*E*,4*E*)-6-(Naphthalen-2-ylsulfanyl)-2,4-hexadienoic Acid Hydroxyamide (4f). To a solution of methyl (2*E*,4*E*)-6-(naphthalen-2-ylsulfanyl)-2,4-hexadienoate (0.505 g, 1.78 mmol) in distilled THF (10 mL) containing 50% aqueous hydroxylamine (1.08 mL, 16.4 mmol) was added at 0 °C a solution of potassium hydroxide in methanol (1 M, 2.5 mL, 2.5 mmol) over 30 min. Continuation as in procedure A gave a residue that was recrystallized from ethyl acetate to give **4f** (0.315 g, 62%) as white microprisms, mp 141−142 °C. ^{1}H NMR ($CDCl_3$, 300 MHz) δ 7.82−7.43 (m, 7H), 7.37 (m, 1H), 6.28 (m, 2H), 5.97 (d, J = 15.4 Hz, 1H), 3.74 (d, J = 5.9 Hz, 2H); ^{13}C NMR ($CDCl_3$, 75 MHz) δ 167.5, 145.3, 142.8, 143.9, 139.3, 135.8, 133.8, 133.4, 132.6, 131.1, 129.5, 121.6, 51.9, 37.4. Anal. ($C_{16}H_{15}NO_2S$) C, H, N.

(2*E*,4*E*)-6-(4-Chlorobenzenesulfinyl)-2,4-hexadienoic Acid Hydroxyamide (6b). To a solution of methyl (2*E*,4*E*)-6-(4-chlorobenzenesulfinyl)-2,4-hexadienoate (0.80 g, 2.79 mmol) in distilled THF (15 mL) containing an aqueous solution of hydroxylamine (50%, 1.7 mL, 25.8 mmol) was added at 0 °C a solution of potassium hydroxide in methanol (1 M, 4.5 mL, 4.5 mmol) over 30 min. After the mixture was stirred at 0 °C for 1 h, distilled water (15 mL) was added and the mixture was made neutral by dropwise addition of 2 M HCl at 0 °C. Workup as for procedure A gave a residue that was recrystallized from acetone to give **6b** (0.45 g, 56%) as pale-brown microprisms, mp 159 °C (dec). ^{1}H NMR ($CDCl_3$, 300 MHz) δ 0.68 (br s, 1H), 9.21 (br s, 1H), 7.62 (s, 4H), 6.97 (dd, J = 15.0, 11.2 Hz, 1H), 6.23 (dd, J = 15.0, 11.2 Hz, 1H), 5.81 (d, J = 15.0 Hz, 1H), 5.79 (m, 1H), 3.88 (dd, J = 13.0, 7.7 Hz, 6H), 3.65 (dd, J = 13.0, 8.0 Hz, 1H); ^{13}C NMR ($CDCl_3$, 75 MHz) δ 162.5, 142.1, 137.4, 136.0, 135.6, 129.1, 127.1, 126.2, 123.0, 58.6. Anal. ($C_{12}H_{12}NClO_3S$) C, H, N, S.

6-Phenylsulfanylhexanoic Acid Hydroxyamide (30a). To a stirred solution of ethyl 6-phenylsulfanylhexanoate (0.40 g, 1.59 mmol) at 0 °C in anhydrous THF was added a solution of hydroxylamine (1 M, 16 mL) in methanol, followed immediately by dropwise addition of a solution of potassium hydroxide (1 M, 2.07 mL) in methanol. The mixture was warmed to 25 °C and stirred for 16 h. Ice was then added and the pH adjusted to 6−7 by addition of 2 M HCl. Workup as in procedure A gave a residue that was recrystallized from acetone to give **30a** (0.26 g, 68%) as white microprisms, mp 132−135 °C. ^{1}H NMR (300 MHz, DMSO-d_6) δ 10.03 (br s, 1H), 8.78 (br s, 1H), 7.41−7.30 (m, 5H), 2.90 (t, J = 7.1 Hz, 2H), 1.88 (t, J = 7.1 Hz, 2H), 1.50−1.32 (m, 4H), 1.27 (m, 2H); ^{13}C NMR (75 MHz, DMSO-d_6) δ 168.8, 136.1, 130.0, 129.3, 129.0, 32.3, 32.0, 28.7, 27.7, 24.7. Anal. ($C_{12}H_{17}NO_2S$) C, H, N.

6-(Benzenesulfinyl)hexanoic Acid Hydroxyamide (32a). To a stirred solution of ethyl 6-(benzenesulfinyl)hexanoate (0.50 g, 1.87 mmol) at 0 °C was added a solution of hydroxylamine (1 M, 18.7 mL) in methanol, followed immediately by dropwise addition of a solution of potassium hydroxide (1 M, 2.43 mL) in methanol. The mixture was warmed to 25 °C and stirred for 16 h. Ice was then added and the pH adjusted to 6−7 by addition of 2 M HCl. Workup as in procedure A gave a residue that was recrystallized from acetone to give **32a** (0.31 g, 65%) as white microprisms, mp 164−165 °C. ^{1}H NMR (300 MHz, DMSO-d_6) δ 10.09 (br s, 1H), 8.71 (br s, 1H), 7.60 (m, 5H), 3.02 (t, J = 7.2 Hz, 2H), 2.20 (t, J = 7.2 Hz, 2H), 1.47−1.35 (m, 4H), 1.28 (m, 2H); ^{13}C NMR (75 MHz, DMSO-d_6) δ 168.9, 136.4, 130.1, 129.8, 128.5, 54.1, 32.2, 29.4, 27.7, 25.0. Anal. ($C_{12}H_{17}NO_3S$) C, H, N.

6-(Benzenesulfonyl)hexanoic Acid Hydroxyamide (33). To a stirred solution of 6-(benzenesulfinyl)hexanoic acid hydroxyamide (0.31 g, 1.22 mmol) in anhydrous dichloromethane (6.0 mL) at 0 °C was added *m*-CPBA (0.21 g, 1.22 mmol) in small portions. The mixture was maintained at 0 °C for 1 h with stirring, after which the pH was adjusted to 6−7 by dropwise addition of aqueous 1 M NaOH. The organic layer was separated and washed with saturated aqueous ammonium chloride (10 mL) and then with brine (10 mL). The organic layer was dried over anhydrous $MgSO_4$, filtered, and evaporated. The oily residue was recrystallized from acetone to give **34** (0.18 g, 54%) as white microprisms, mp 184−186 °C. ^{1}H NMR (300 MHz, DMSO-d_6) δ 10.19 (br s, 1H, OH), 8.68 (br s, 1H, NH), 7.70−7.55 (m, 5H), 2.95 (m, 1H), 2.87 (m, 1H), 1.90 (t, J = 7.1 Hz, 2H), 1.70−1.20 (m, 6H); ^{13}C NMR (75 MHz, DMSO-d_6) δ 168.8, 143.2, 135.3, 129.2, 125.9, 55.1, 31.9, 27.4, 24.6, 21.0. Anal. ($C_{12}H_{17}NO_4S$) C, H, N.

Biology. HDAC Enzyme Assay. The procedure described in Hoffmann[33] was modified for use as described below and was further modified for use in the whole-cell HDAC activity assay.

Isolated Liver HDAC Activity Assay. The supernatant resulting from the high-speed centrifugation of rat liver homogenates was partially purified on a Q-Sepharose column using a sodium chloride gradient (10−500 mM), with a Tris (15 mM), EDTA (0.25 mM), glycerol (10%) buffer at pH 7.9. Fractions were collected and analyzed for HDAC activity using the method described herein. Those fractions containing HDAC activity were pooled and aliquots stored at −40 °C prior to use. The assay mixture comprised 100 μL of pooled HDAC enzyme, 100 μL of buffer (Tris-HCl (10 mM), NaCl (10 mM), $MgCl_2$ (15 mM), EGTA (0.1 mM), glycerol (10% v/v), and mercaptoethanol (0.007%), 100 μL of HDAC inhibitor (dissolved in DMSO and diluted with HEPES buffer (50 mM, pH 7.4) to working concentrations), and 100 μL of substrate (MAL, diluted to 20 μg/mL with 50 mM HEPES buffer, pH 7.4, 0.5 mL aliquots stored at −40 °C, diluted to 5 μg/mL for use in the assay). Samples were vortexed for 15 s and incubated at 37 °C for 60 min with gentle agitation every 15 min. Acetonitrile (100 μL) was then added to terminate the reaction, after which samples were centrifuged at 10 000 rpm for 10 min and then placed on ice prior to analysis by HPLC of substrate (MAL) and deacetylated product (ML) concentration in the supernatant.

Whole-Cell HDAC Activity Assay. The 1×10^6 CEM cells in RPMI medium (1 mL; Sigma Chemicals, Poole, Dorset U.K.) were exposed to HDAC inhibitors at six concentrations for 60 min at 37 °C, after which MAL (20 μg/mL final concentration) was added and the mixture incubated for a further 30 min. Cells were then rapidly washed with phosphate buffered saline at 4 °C and lysed by sonication. The reaction was stopped with acetonitrile (100 μL), and intracellular MAL and ML concentrations in the supernatant were determined by HPLC analysis.

Quantitation of MAL and ML by HPLC Analysis. Chromatographic separation of MAL and ML was carried out using a 15 cm Apex ODS 5 μm column with an acetonitrile/distilled water (40:60), 2% TFA (v/v) mobile phase at a flow rate of 1.2 mL/min. MAL and ML were quantified by fluorescence detection at excitation/emission wavelengths of 330/395 nm. The activity of each inhibitor was assessed at a minimum of five nonzero concentrations, determined from initial concentration studies. The peak heights of MAL and ML were used to derive the % MAL in the mixture as the ratio MAL/(MAL+ML). The % MAL in the absence of inhibitor (typically 22−25%) was taken as 100% HDAC activity, and the % HDAC activity at each inhibitor concentration was derived from $(100 - \%\,MAL_{DRUG})/(100 - \%\,MAL_{NODRUG}) \times 100$. These data (minimum of $n = 4$ at each concentration for each inhibitor) were fitted to a sigmoidal E_{MAX} model (Graphpad Prism, version 2.01) to derive the IC_{50} concentration for each compound.

Cytotoxicity Assay of HDAC Inhibitors. CEM (human leukemic) cells were exposed to HDAC inhibitors at a minimum of five nonzero concentrations for 3 days under standard cell culture conditions (RPMI medium, 37 °C, 5% CO_2 in a humidified atmosphere). Cell number and percentage viability were assessed by trypan blue staining. The % viability IC_{50} was determined using Graphpad Prism. For **32b** these studies were extended to include HCT116 (colorectal cancer), MCF-7 (breast cancer), and SUD4 (lymphoma) cells.

Acknowledgment. Financial support from the Lewis Family Charitable Trust, St. Bartholomew's and the Royal London Charitable Foundation, and the Nikki Taylor Memorial Fund is gratefully acknowledged.

Supporting Information Available: Experimental procedures, ^1H and ^{13}C NMR spectra for all new compounds, and microanalytical data. This material is available free of charge via the Internet at http://pubs.acs.org.

References

(1) Curtin, M. L. Current patent status of histone deacetylase inhibitors. *Expert Opin. Ther. Pat.* **2002**, *12*, 1375−1384.
(2) (a) Weinmann, H.; Ottow, E. Recent advances in medicinal chemistry of histone deacetylase inhibitors. *Annu. Rep. Med. Chem.* **2004**, *39*, 185−196. (b) Vigushin, D. M.; Coombes, R. C. Histone deacetylase inhibitors in cancer treatment. *Anti-Cancer Drugs* **2002**, *13*, 1−13.
(3) Jenuwein, T.; Allis, C. D. Translating the histone code. *Science* **2001**, *293*, 1074−1080.
(4) Taunton, J.; Hassig, C. A.; Schreiber, S. L. A mammalian histone deacetylase related to the yeast transcriptional regulator Rpd3p. *Science* **1996**, *272*, 408.
(5) Darkin-Rattray, S. J.; Gurnett, A. M.; Myers, R. W.; Dulski, P. M.; Crumley, T. M.; Allocco, J. J.; Cannova, C.; Meinke, P. T.; Colletti, S. L.; Bednarek, M. A.; Singh, S. B.; Goetz, M. A.; Dombromski, A. W.; Polishook, J. D.; Schmatz, D. M. Apicidin: A novel antiprotozoal agent that inhibits parasite histone deacetylase. *Proc Natl. Acad. Sci. U.S.A.* **1996**, *93*, 13143−13147.
(6) Johnstone, R. W. Histone deacetylase inhibitors: novel drugs for the treatment of cancer. *Nat. Rev. Drug Discovery* **2002**, *1* (4), 287−299.
(7) Marks, P. A.; Rifkind, R. A.; Richon, V. M.; Breslow, R.; Miller, T.; Kelly, W. K. Histone deacetylases and cancer: causes and therapies. *Nat. Rev. Cancer* **2001**, *1*, 194−202.
(8) Jung, M.; Brosch, G.; Kolle, D.; Scherf, H.; Gerhauser, C.; Loidl, P. Amide analogs of trichostatin A as inhibitors of histone deacetylase and inducers of terminal cell differentiation. *J. Med. Chem.* **1999**, *42*, 4669−4679.
(9) Hassig, C. A.; Schreiber, S. L. Nuclear histone acetylases and deacetylases and transcriptional regulation: HATs off to HDACs. *Curr. Opin. Chem. Biol.* **1997**, *1*, 300−308.
(10) Kouzarides, T. Histone acetylases and deacetylases in cell proliferation. *Curr. Opin. Genet. Dev.* **1999**, *9*, 40−48.
(11) Strahl, B. D.; Allis, C. D. The language of covalent histone modifications. *Nature* **2000**, *403*, 41−45.
(12) Sambucetti, L. C.; Fischer, D. D. Zabludoff, S.; Kwon, P. O.; Chamberlin, H.; Trogani, N.; Xu, H.; Cohen, D. Histone deacetylase inhibition selectively alters the activity and expression of cell cycle proteins leading to specific chromatin acetylation and antiproliferative effects. *J. Biol. Chem.* **1999**, *274*, 34940−34947.
(13) Archer, S. Y.; Meng, S.; Shei, A.; Hodin, R. A. p21(WAF1) is required for butyrate-mediated growth inhibition of human colon cancer cells. *Proc. Natl. Acad. Sci. U.S.A.* **1998**, *95*, 6791−6796.
(14) Redner, R. L.; Wang, J.; Liu, J. M. Chromatin remodeling and leukemia: new therapeutic paradigms. *Blood* **1999**, *94*, 417−428.
(15) Saha, V.; Young, B. D.; Freemont, P. S. Translocations, fusion genes, and acute leukemia. *J. Cell. Biochem. Suppl.* **1998**, *30/31*, 264−276.
(16) Yoshida, M.; Kijima, M.; Akita, M.; Beppu, T. Potent and specific inhibition of mammalian histone deacetylase both in vivo and in vitro by trichostatin A. *J. Biol. Chem.* **1990**, *265*, 17174−17179.
(17) Richon, V. M.; Emiliani, S.; Verdin, E.; Webb, Y.; Breslow, R.; Rifkind, R. A.; Marks, P. A. A class of hybrid polar inducers of transformed cell differentiation inhibits histone deacetylases. *Proc. Natl. Acad. Sci. U.S.A.* **1998**, *95*, 3003−3007.
(18) Saito, A.; Yamasita, T.; Mariko, Y.; Nosaka, Y.; Tsuchiya, K.; Ando, T.; Suzuki, T.; Tsuruo, T.; Nakanishi, O. A synthetic inhibitor of histone deacetylase, MS-27-275, with marked in vivo antitumor activity against human tumors. *Proc. Natl. Acad. Sci. U.S.A.* **1999**, *96*, 4592−4597.
(19) Nakajima, H.; Kim, Y. B.; Terano, H.; Yoshida, M.; Horinouchi, S. FR901228, a potent antitumor antibiotic, is a novel histone deacetylase inhibitor. *Exp. Cell Res.* **1998**, *241*, 126−133.
(20) Finnin, M. S.; Donigian, J. R.; Cohen, A.; Richon, V. M.; Rifkind, R. A.; Marks, P. A.; Breslow, R.; Pavletich, N. P. Structures of a histone deacetylase homologue bound to the TSA and SAHA inhibitors. *Nature* **1999**, *401*, 188−193.
(21) Marson, C. M.; Vigushin, D. M.; Rioja, A.; Coombes, R. C. Stereodefined and polyunsaturated inhibitors of histone deacetylase based on (2*E*,4*E*)-5-arylpenta-2,4-dienoic acid hydroxyamides. *Bioorg. Med. Chem. Lett.* **2004**, *14*, 2477−2481.
(22) Wittich, S.; Scherf, H.; Xie, C.; Brosch, G.; Loidl, P.; Gerhäuser, C.; Jung, M. Structure−activity relationships on phenylalanine-containing inhibitors of histone deacetylase: in vitro enzyme inhibition, induction of differentiation, and inhibition of proliferation in Friend leukemic cells. *J. Med. Chem.* **2002**, *45*, 3296−3309.
(23) Dai, Y.; Guo, Y.; Guo, J.; Pease, L. J.; Li, J.; Marcotte, P. A.; Glaser, K. B.; Tapang, P.; Albert, D. H.; Richardson, P. L.; Davidsen, S. K.; Michaelides, M. R. Indole amide hydroxamic acids as potent inhibitors of histone deacetylase. *Bioorg. Med. Chem. Lett.* **2003**, *13*, 1897−1901.
(24) Wada, C. K.; Frey, R. R.; Ji, Z.; Curtin, M. L.; Garland, R. B.; Holms, J. H.; Li, J.; Pease, L. J.; Guo, J.; Glaser, K. B.; Marcotte, P. A.; Richardson, P. L.; Murphy, S. S.; Bouska, J. J.; Tapang, P.; Magoc, T. J.; Albert, D. H.; Davidsen, S. K.; Michaelides, M. R. α-Keto amides as inhibitors of histone deacetylase. *Bioorg. Med. Chem. Lett.* **2003**, *13*, 3331−3335.
(25) Vanommeslaeghe, K.; Elaut, G.; Brecx, V.; Papeleu, P.; Iterbeke, K.; Geerlings, P.; Tourwé, D.; Rogiers, V. Amide analogues of TSA: synthesis, binding mode analysis and HDAC inhibition. *Bioorg. Med. Chem. Lett.* **2003**, *13*, 1861−1864.
(26) Glaser, K. B.; Li, J. L.; Aakre, M. E.; Morgan, D. W.; Sheppard, G.; Stewart, K. D.; Pollock, J.; Lee, P.; O'Connor, C. Z.; Anderson, S. N.; Mussatto, D. J.; Wegner, C. W.; Moses, H. L. Transforming growth factor beta mimetics: discovery of 7-[4-(4-cyanophenyl)-phenoxy]-heptanohydroxamic acid, a biaryl hydroxamate inhibitor of histone deacetylase. *Mol. Cancer Ther.* **2002**, *1*, 759−768.
(27) (a) Ma, G. X.; Batey, R. A.; Taylor, S. D.; Hum, G.; Jones, J. B. The synthesis of dienecarbamates as ADAPT prodrug models. *Synth. Commun.* **1997**, *27*, 2445−2453. (b) Cass, Q. B.; Jaxa-Chamiec, A. A.; Kunec, E. K.; Sammes, P. G. On the preparation and rearrangement of some vinylic sulfoxides. *J. Chem. Soc., Perkin Trans. 1* **1991**, 2683−2686.
(28) Durrant, G.; Green, R. H.; Lambeth, P. F.; Lester, M. G.; Taylor, N. R. Synthesis of some aromatic prostaglandin analogues. Part I. *J. Chem. Soc., Perkin Trans. 1* **1983**, 2211−2214.
(29) Gilman, H.; Webb, F. J. The relative reactivities of organometallic compounds. LXVI. The metalation of some sulfur-containing organic compounds. *J. Am. Chem. Soc.* **1949**, *71*, 4062−4066.
(30) Joel, S. P.; Marson, C. M.; Savy, P. Histone deacetylase inhibitors. PCT Int. Appl. WO 2004046094, 2004.
(31) Sydnes, L. K.; Skattebøl, L.; Chapleo, C. B.; Leppard, D. G.; Svanholt, K. L.; Dreiding, A. S. Preparation of mikanecic ester and its precursor, 1,3-butadiene-2-carboxylic ester. *Helv. Chim. Acta* **1975**, *58*, 2061−2073.
(32) Osuga, H.; Suzuki, H.; Tanaka, K. Practical synthesis of optically pure bifunctionalized heterohelicenes. *Bull. Chem. Soc. Jpn.* **1997**, *70*, 891−897.
(33) Hoffmann, K.; Brosch, G.; Loidl, P.; Jung, M. First non-radioactive assay for in vitro screening of histone deacetylase inhibitors. *Pharmazie* **2000**, *55*, 601−606.
(34) Lewis, F. D.; Howard, D. K.; Barancyk, S. V.; Oxman, J. D. Lewis acid catalysis of photochemical reactions. 5. Selective isomerization of conjugated butenoic and dienoic esters. *J. Am. Chem. Soc.* **1986**, *108*, 3016−3023.
(35) Palaty, J.; Abbott, F. S. Structure−activity relationships of unsaturated analogues of valproic acid. *J. Med. Chem.* **1995**, *38*, 3398−3406.
(36) Smiles, S.; Stewart, J. *m*-Dithiobenzoic acid. *J. Chem. Soc.* **1921**, *119*, 1792−1798.
(37) Boehm, H.-J.; Boehringer, M.; Bur, D.; Gmuender, H.; Huber, W.; Klaus, W.; Kostrewa, D.; Kuehne, H.; Luebbers, T.; Meunier-Keller, N.; Mueller, F. Novel inhibitors of DNA gyrase: 3D structure based needle screening, hit validation by biophysical methods, and 3D guided optimization. A promising alternative to random screening. *J. Med. Chem.* **2000**, *43*, 2664−2674.
(38) Swierczek, K.; Pandey, A. S.; Peters, J. W.; Hengge, A. C. A comparison of phosphonothioic acids with phosphonic acids as phosphatase inhibitors. *J. Med. Chem.* **2003**, *46*, 3703−3708.
(39) Yin, J.; Pidgeon, C. *Tetrahedron Lett.* **1997**, *38*, 5953−5954. A simple and efficient method for preparation of unsymmetrical sulfides.

JM051010J